

UNIVERSIDADE ESTADUAL DE CAMPINAS
FACULDADE DE ENGENHARIA QUÍMICA

LAURA PLAZAS TOVAR

*Modelagem e Simulação do Processo de Destilação Molecular
Centrífuga Reativa: Desenvolvimento, Avaliação e Aplicação
para o “Upgrading” de Frações Pesadas de Petróleo*

Tese de Doutorado apresentada à Faculdade de
Engenharia Química da Universidade Estadual de
Campinas para obtenção do título de Doutor em
Engenharia Química na área de concentração:
Desenvolvimento de Processos Químicos.

Prof^a. Dr^a. MARIA REGINA WOLF MACIEL
Orientadora

Este exemplar corresponde à versão final da Tese
defendida por Laura Plazas Tovar e orientada pela
Prof^a. Dr^a. Maria Regina Wolf Maciel



Prof^a. Dr^a. Maria Regina Wolf Maciel
Orientadora

Campinas, 2012

FICHA CATALOGRÁFICA ELABORADA PELA
BIBLIOTECA DA ÁREA DE ENGENHARIA E ARQUITETURA - BAE - UNICAMP

P699m Plazas Tovar, Laura
Modelagem e simulação do processo de destilação molecular centrífuga reativa: desenvolvimento, avaliação e aplicação para o “Upgrading” de frações pesadas de petróleo / Laura PlazasTovar. --Campinas, SP: [s.n.], 2012.

Orientador: Maria Regina Wolf Maciel.
Tese de Doutorado - Universidade Estadual de Campinas, Faculdade de Engenharia Química.

1. Destilação molecular. 2. Reação química. 3. Petróleo - Resíduos. 4. Modelagem matemática. 5. Simulação por computador. I. Maciel, Maria Regina Wolf. II. Universidade Estadual de Campinas. Faculdade de Engenharia Química. III. Título.

Título em Inglês: Modeling and simulation of the centrifugal reactive molecular distillation: development, assessment and application to upgrade high-boiling-point petroleum fractions

Palavras-chave em Inglês: Molecular distillation, Chemical reaction, Petroleum residue, Mathematical model, Computer simulation

Área de concentração: Desenvolvimento de Processos Químicos

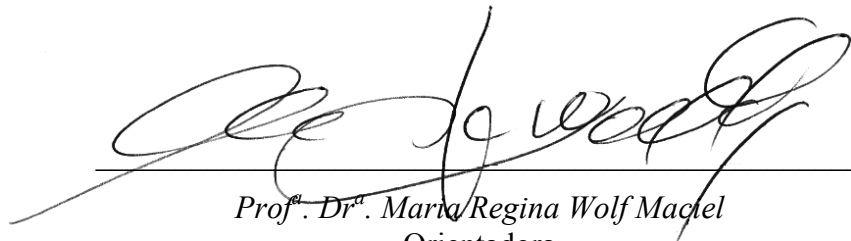
Titulação: Doutor em Engenharia Química

Banca examinadora: Antonio Souza de Araujo, Leonardo Vasconcelos Fregolente, Edvaldo Rodrigo de Moraes, Lamia Zuñiga Liñan

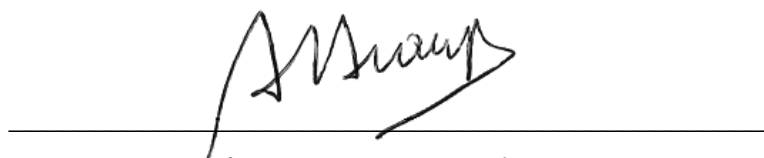
Data da defesa: 23-03-2012

Programa de Pós Graduação: Engenharia Química

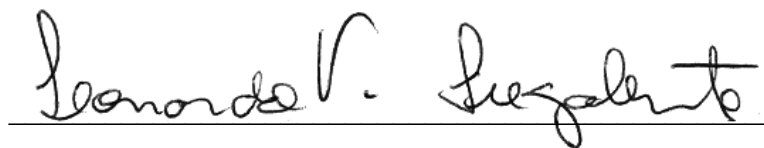
Tese de Doutorado defendida por Laura Plazas Tovar e aprovada em 23 de Março de 2012 pela
banca examinadora constituída pelos Doutores:



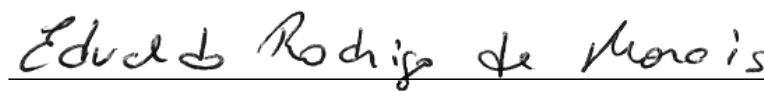
Prof. Dr. Maria Regina Wolf Maciel
Orientadora



Prof. Dr. Antonio Souza de Araujo
UFRGN – Membro Titular



Dr. Leonardo Vasconcelos Fregolente
REPLAN – Membro Titular

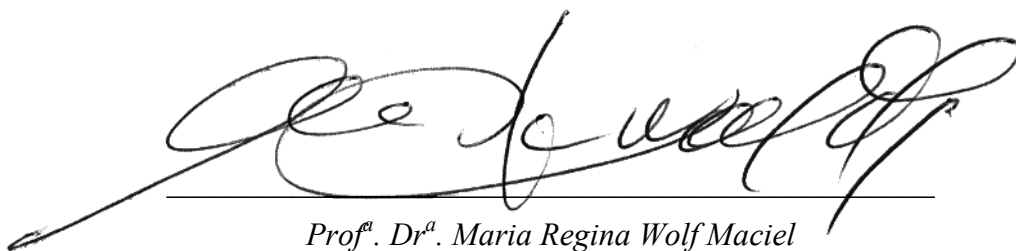


Dr. Edvaldo Rodrigo de Moraes
CTBE – Membro Titular



Dr. Lania Zuñiga Liñan
FEQ/UNICAMP – Membro Titular

Este exemplar corresponde à versão final da Tese defendida por Laura Plazas Tovar e orientada
pela Prof^a. Dr^a. Maria Regina Wolf Maciel

A handwritten signature in black ink, featuring a large, stylized 'M' and 'R' followed by 'Wolf Maciel'. The signature is written over a horizontal line.

Prof^a. Dr^a. Maria Regina Wolf Maciel
Orientadora

*A minha mãe Mirta de la Candelária
Tovar Gutiérrez, ao meu irmão Diego Armando
Plazas Tovar e a meu querido Diego Alonso
Fernández Merjildo, dedico este trabalho como
expressão de agradecimento a seus sentimentos
de amor, força e apoio abonados durante todos
os momentos significativos da minha vida.*

Agradecimentos

Profunda gratidão a **Deus** por ser o principal eixo da minha experiência de vida.

É um grande prazer reconhecer a todas as pessoas que me fizeram parte do caminho até hoje percorrido para a finalização deste trabalho de pesquisa e Tese de Doutorado. **Obrigada...**

...À minha família, pelo seu amor, compreensão, ajuda em todos os momentos, por me apoiar no meu crescimento pessoal e profissional. Suas recomendações, conselhos e sugestões sempre foram minha força para nunca parar e vencer as dificuldades.

...À Prof^a. Dr^a. Maria Regina Wolf Maciel pela oportunidade de trabalhar e aportar no seu grupo de pesquisa pertencente ao Laboratório de Desenvolvimento de Processos de Separação, da Universidade Estadual de Campinas (LDPS/UNICAMP). Grata por compartilhar sua experiência e conhecimento intelectual, pela segurança e apoio nos momentos que precisei e pelas oportunidades de participar no programa de estágio docente.

...Ao Prof. Dr. Rubens Maciel Filho por fazer parte do desenvolvimento de pesquisa e formação de valores. Grata pelas suas idéias e incentivos para estruturar e constituir o grande trabalho hoje apresentado.

...À Dra. Alessandra Winter e ao Dr. César Benedito Batistella, que com suas visões e experiências, me ajudaram na realização do projeto.

...À Engenheira Lilian Carmen Medina pelas contribuições e aportes no desenvolvimento do trabalho de pesquisa.

...Ao Prof. Dr. Antonio Carlos Luz Lisboa pela assistência e ajuda no desenvolvimento computacional e por compartilhar seus grandes conhecimentos na linguagem de programação em FORTRAN.

...Agradeço também aos membros da comissão julgadora por avaliar a Tese de Doutorado, suas considerações e sugestões foram muito apreciadas.

...À PETROBRAS (Petróleo Brasileiro S/A), CNPq (Conselho Nacional de Desenvolvimento Científico e Tecnológico de Brasil) e FINEP (Financiadora de Estudos e Projetos), pelas bolsas de estudo outorgadas.

...À Profa. Dra. Ana Silvia Prata Soares pela oportunidade de participar no programa estágio docente – PED A – da disciplina EU 600 Sistema de Fluido Térmico na Faculdade de Ciências Aplicadas – FCA/UNICAMP. Grande experiência para meu desenvolvimento pessoal e profissional.

...A meus amigos e os colegas dos laboratórios LDPS e LOPCA pelo apoio e contribuição, e principalmente, pela amizade. Meu agradecimento especial a Lamia Zuñiga Liñan, Nádson Murilo Nascimento Lima, Melvin Duran, Edgar Leonardo Martinez, Leandro Lody, Patrícia Fazzio Martins, Oscar Javier Celis Ariza, Sergio Andres Villalva, Henderson Iván Quintero Perez, Natalia Lorena Parada, Luisa Fernanda Rios Pinto, José Fernando Cuadros Bohórquez, Viktor Cárdenas, Cibelem Iribarrem Benites, Roniel Souza e Pablo Andres Alvarez, pela ajuda, contribuições nas etapas do trabalho e pela grande amizade. Aos professores e funcionários da UNICAMP, que de diversas maneiras contribuíram para a realização deste trabalho.

...Meus valiosos sentimentos de gratidão a Diego Alonso Fernandez Merjildo, por sua paciência e apoio no desenvolvimento desta Tese de Doutorado. Sempre será muito importante na minha vida e na conquista de grandes objetivos.

"Educar a inteligência é dilatar o horizonte dos seus desejos e das suas necessidades."

(James Russell Lowell)

Resumo

O processo de destilação molecular reativa, no qual ocorre o acoplamento de destilação molecular e reação química simultaneamente, pode ser qualificado como um processo híbrido e também como um processo intensificado, dada a configuração do equipamento e as condições operacionais que viabilizam a implementação de alto vácuo (<50 Pa), permitindo submeter o material a temperaturas adequadas num curto tempo operacional, garantindo um contato muito intenso da amostra com a superfície catalítica.

Este trabalho teve como finalidade desenvolver a modelagem matemática e simulação do processo de destilação molecular centrífuga reativa (DMCR – em catálise heterogênea) baseada na descrição matemática descrita para o processo de destilação molecular centrífuga de frações pesadas de petróleo. Para a simulação, foi considerado como caso de estudo o processamento do resíduo atmosférico “ATR-W” 673,15 K⁺ com grau API igual a 11,9 e massa molar igual a 2956 kg·kmol⁻¹. A modelagem e simulação foram realizadas nas condições de estado estacionário. O conjunto de (11+18N) equações diferenciais parciais e algébricas e (27+19N) variáveis foi incorporado no ambiente computacional, denominado DESTMOL-R, desenvolvido na linguagem FORTRAN-90 usando o compilador Compaq Visual Fortran (*professional edition 6.6*). O sistema de equações formuladas no filme, ao longo da superfície cônica do evaporador, foi resolvido numericamente através do método das linhas. Condições de temperatura do evaporador entre 473.15K e 523.15 K e de porcentagem de catalisador (catalisador zeolítico regenerado de uma unidade de FCC) entre 3 e 5% m/m foram avaliadas.

As variáveis de saída, tais como: a temperatura da superfície do filme (T_s), a espessura de filme (δ), a taxa de evaporação efetiva (G_E), o fluxo mássico de destilado (D), a velocidade radial (v_r), a concentração de pseudocomponente “a” (X_a) e a conversão (α) foram calculadas através da análise dos efeitos das condições operacionais definidas como sendo: a temperatura do evaporador (EVT), a vazão de alimentação (Q), a porcentagem de catalisador (%CAT), a temperatura de alimentação (T_{feed}), a temperatura do condensador (T_{cond}), a velocidade do rotor (RS) e a pressão do sistema (P_S).

Os resultados mostraram que as variáveis de entrada, tais como a temperatura do evaporador (EVT) e a porcentagem de catalisador (%CAT) são as condições operacionais de maior influência sobre a composição final do fluxo do condensado. A concentração do pseudocomponente “i” diminui nas direções $-s$ e $-r$, devido ao aumento da temperatura nas camadas internas do filme líquido. Por conseguinte, a espessura do filme diminui rapidamente ao longo da superfície do evaporador, enquanto que a quantidade de destilado aumenta continuamente ao longo do evaporador às condições operacionais seleccionadas. Resultados obtidos das simulações apresentaram uma conversão da carga de 65,6% no destilado e de 49,6% no resíduo, considerando uma porcentagem de 3% m/m de catalisador na carga inicial e uma temperatura de processo de 483,15 K. As predições oriundas da simulação foram comparadas com os dados experimentais e indicaram um desvio relativo percentual médio menor do que 6,82%; 9,39% e 14,92% para a taxa global de destilado, conversão na corrente de destilado e conversão na corrente de resíduo, respectivamente, o que é valioso, considerando-se a complexidade do processo e da mistura. Assim, o modelo desenvolvido mostrou-se adequado para descrever os processos de reação - separação na destilação molecular centrífuga reativa fornecendo orientação teórica para o desenvolvimento experimental e a futura otimização do processo.

Por fim, o salto tecnológico em matéria computacional e experimental da DMCR concluiu em um efetivo desempenho do processo obtendo produtos com características favoráveis para os processos de exploração, escoamento, transporte e refino desde que: (i) mudanças importantes na fração analítica $>613,15$ K foram reportadas nas correntes de destilado atingindo uma conversão do ATR-W 673,15 K⁺ superior a 64,3%, valores de grau API entre 19 e 21 e massa molar até 200 kg·kmol⁻¹, e (ii) foram observadas alterações significativas nas frações analíticas $>613,15$ K e $>813,15$ K nas correntes de resíduo, atingindo uma conversão do ATR-W 673,15 K⁺ entre 8,0% e 53,1%, valores de grau API aproximadamente iguais a 11,9 e massa molar entre 2570 kg·kmol⁻¹ - 2908 kg·kmol⁻¹.

Abstract

The reactive molecular distillation process, in which, the molecular distillation process and reactive process occur simultaneously can be characterized like an intensified and hybrid process due to the particular features on the equipment configuration which lead to use higher vacuum (<50 Pa), to keep the material inner the equipment with a short operational residence time, and to achieve a very intensive contact among the sample and catalytic surface.

This work focuses mainly on the mathematical modeling and numerical simulation of centrifugal reactive molecular distillation process (CRMD – using heterogeneous catalysis) based on mathematical description of the centrifugal molecular distillation from high-boiling-point petroleum fractions. The computational case study illustrated was a 673.15 K^+ high-boiling-point petroleum fraction of “W” crude oil (atmospheric residue ATR–W) with API gravity equals 11.9 and molar mass equals $2956\text{ kg}\cdot\text{kmol}^{-1}$. The model and simulations were described at the steady-state conditions. A set of $(11+18N)$ equations and $(27+19N)$ variables were processed by the computational program named DESTMOL–R developed in FORTRAN–90 language using Compaq Visual Fortran compiler (*professional edition 6.6*). The system equations formulated inner the thin liquid film, along the evaporator surface, was numerically solved by the numerical method of lines. The process temperature (evaporator temperature) from 473.15 K to 523.15 K and the influence of adding a zeolite-based catalyst (regenerated catalyst used for FCC technology) between 3 and 5 %wt were examined.

The output variables, such as the surface temperature (T_s), film thickness (δ), effective evaporation rate (G_E), distillate mass flow rate (D), radial velocity (v_r), concentration of pseudocomponent “a” (X_a) and the conversion degree (α) profiles, were computed by analyzing the effects of the operational conditions (the evaporator temperature (EVT), feed flow rate (Q), percent weight of catalyst (%CAT), feed temperature (T_{feed}), condenser temperature (T_{cond}), rotor speed (RS) and the system pressure (P_s)).

Results showed that the inlet variables such as the evaporator temperature (EVT) and the weight percent of catalyst (%CAT) are the most suitable operating conditions into the final composition of the condensate flow. The concentration of the pseudocomponent “i” shrinks in both s – and r – directions, due to the fast increase of the temperature in the thin liquid film. Consequently, the thickness of the film rapidly decreases in this region, whereas the amount of the distillate of the split molecules continuously increases along the evaporator at the selected operating conditions. Simulated data indicated a conversion equal to 49.6% of feedstock in the residue stream and 65.6% of feedstock in the distillate stream when considered 3 wt% of catalyst and an evaporator temperature (EVT) equals 483.15 K . The simulated results agree well with those obtained by the experimental study, indicating the accuracy and reliability of the mathematical model since the average percent error was no larger than 6.82%, 9.39% and 14.92% for the distillate flow rate, extent conversion in the distillate rate and in the residue stream, respectively.

It can be concluded that the mathematical model can describe the reaction – split processes in the CRMD process providing theoretical guidance for the further experimental runs and process optimization. Finally, the technological leap in the computational and experimental exercises of the CRMD process concluded in an effective performance of the process obtaining products with favorable characteristics for exploration, flow, transport and refining processes since: (i) important changes in the $>613.15\text{ K}$ analytical fraction were reported in the distillate stream reaching a conversion of the ATR–W 673.15 K^+ higher than 64.3%, values of API gravity between 19 – 21 and molar mass up $200\text{ kg}\cdot\text{kmol}^{-1}$, and (ii) significant changes were found in the $>613.15\text{ K}$ and $>813.15\text{ K}$ analytical fractions of the residue streams, reaching a conversion of the ATR–W 673.15 K^+ between 8.0 and 53.1%, values of API gravity approximately equal to 11.9 and molar mass between $2570\text{ kg}\cdot\text{kmol}^{-1}$ – $2908\text{ kg}\cdot\text{kmol}^{-1}$.

Sumário

Capítulo 1

Introdução e objetivos	1
1.1. Introdução.....	1
1.2. Objetivos.....	7
1.2.1. Objetivos específicos e etapas de desenvolvimento	7
1.3. Organização da Tese.....	10

Capítulo 2

Perspectivas na aplicação, modelagem e simulação do processo de destilação molecular reativa: processo híbrido e intensificado	15
2.1. Introdução.....	15
2.2. Generalidades do petróleo.....	16
2.3. Caracterização físico-química das misturas.....	17
2.3.1. Metodologias para representar o petróleo e suas frações.....	18
2.3.1.1. Conceito da mistura contínua para caracterização de frações de petróleo.....	20
2.3.1.2. Funções de distribuição utilizadas na termodinâmica contínua.....	20
2.4. Avanços nas tecnologias dos processos para o <i>upgrading</i> de óleos pesados e fundos.....	21
2.4.1. Processos não-catalíticos para o processamento de resíduos de petróleo.....	22
2.4.2. Processos catalíticos para o processamento de resíduos de petróleo.....	23
2.5. Opções tecnológicas não-convencionais.....	26
2.5.1. O processo de destilação molecular.....	26
2.5.1.1. Características operacionais de destilação molecular.....	26
2.5.1.2. O comportamento da fase vapor.....	27
2.5.2. O processo de destilação molecular reativa: processo híbrido e intensificado.....	27
2.5.2.1. Considerações teóricas sobre a destilação molecular centrífuga reativa.....	30
2.6. Considerações finais.....	32

Capítulo 3

Enfoque computacional para a caracterização físico-química de frações de petróleo visando à modelagem do processo de destilação molecular reativa.....	33
3.1. Introdução.....	33
3.2. Desenvolvimento.....	35
<i>Overview and computational approach for studying the physicochemical characterization of high-boiling-point petroleum fractions (350 °C⁺).....</i>	36
<i>Development & application of continuous thermodynamic to predict physicochemical properties of petroleum fractions.....</i>	82

3.3. Considerações finais.....	99
Capítulo 4	
Aplicações, considerações e fundamentos teóricos acerca da destilação molecular.....	101
4.1. Introdução.....	101
4.2. Desenvolvimento.....	102
<i>Molecular distillation High-Tech process: Knowledge-based understanding of mean free path and the Knudsen number applied to high-boiling-point petroleum fractions.....</i>	103
4.3. Considerações finais.....	142
Capítulo 5	
Análise do perfil de velocidade e do regime de fluxo na destilação molecular centrífuga.....	143
5.1. Introdução.....	143
5.2. Desenvolvimento.....	145
<i>CFD-Based analysis of the flow regime in the centrifugal molecular distillation of an atmospheric residue of petroleum.....</i>	146
5.3. Considerações finais.....	176
Capítulo 6	
Modelagem e simulação do processo de destilação molecular centrífuga de frações de petróleo	177
6.1. Introdução.....	177
6.2. Desenvolvimento.....	179
<i>Computational framework for the modeling and simulation of a centrifugal molecular distillation process for Brazilian high-boiling-point petroleum fractions (petroleum residues): Analysis of the parametric sensitivity of the process.....</i>	180
<i>Reliability-based optimization using surface response methodology to split heavy petroleum fractions by centrifugal molecular distillation process.....</i>	217
6.3. Considerações finais.....	257
Capítulo 7	
Aplicação da calorimetria exploratória diferencial no estudo da cinética de craqueamento em presença de catalisador de frações pesadas de petróleo.....	259
7.1. Introdução.....	259
7.2. Metodologia de análise.....	260
7.3. Desenvolvimento.....	260
<i>Kinetic study on catalytic cracking of Brazilian high-boiling-point petroleum fractions.....</i>	261
7.4. Considerações finais.....	291
Capítulo 8	
Destilação molecular reativa (tipo centrífuga): Modelagem e simulação.....	293
8.1. Introdução.....	293

8.2. Desenvolvimento.....	295
<i>Centrifugal reactive–molecular distillation: An intensified process–Part I. Mathematical modeling and simulation of the centrifugal reactive–molecular distillation process of high–boiling–point petroleum fractions (>623.15 K): Screening design using Plackett–Burman and 2_{IV}^{+1} factorial designs.....</i>	297
<i>Centrifugal reactive–molecular distillation: An intensified process–Part II. Key operating variables and their effects on the performance of the centrifugal reactive–molecular distillation process.....</i>	337
<i>Centrifugal reactive–molecular distillation: An intensified process–Part III. High–boiling–point petroleum fraction upgrading using the centrifugal reactive–molecular distillation process with a catalyst: high–temperature simulated distillation to evaluate the conversion products (distillate and residue streams).....</i>	359
8.3. Considerações finais.....	379
Capítulo 9	
Caracterização dos produtos obtidos por destilação molecular centrífuga reativa de um resíduo atmosférico de 673.15 K ⁺	381
9.1. Introdução.....	381
9.2. Desenvolvimento.....	382
<i>Characterization of converted products (distillate and residue streams) obtained from a petroleum residue upgrading using centrifugal reactive molecular distillation process: Rheological behavior, density, relative density and API gravity.....</i>	383
<i>Colloidal characterization of the fractions split using centrifugal reactive–molecular distillation of a Brazilian atmospheric residue 673.15 K⁺.....</i>	399
9.3. Considerações finais.....	420
Capítulo 10	
Conclusões e sugestões.....	421
10.1. Conclusões.....	421
10.2. Sugestões para trabalhos futuros.....	426
Capítulo 11	
Referências.....	429

Capítulo 1

Introdução e objetivos

1.1. Introdução

A *American Society for Testing and Materials*, ASTM D 4175 define o óleo cru ou petróleo como: uma mistura de ocorrência natural, consistindo predominantemente de hidrocarbonetos e derivados orgânicos sulfurados, nitrogenados e oxigenados, metais dentre outros (ASTM, 2009).

Sendo o petróleo um elemento de extrema importância para o mundo, pois dele são extraídas matérias-primas que irão atender diversos setores da indústria, no caso específico da indústria Brasileira, existem alguns aspectos para salientar:

1. Conforme apresentado nas Figuras 1a – 1c, tendo como base o ano 2001, as reservas provadas de petróleo nacional apresentaram um notável crescimento nos últimos dez anos quando comparado com o crescimento das reservas de outros países ou grupo econômico no mesmo período (ANP, 2011).
2. Em 2010, a produção brasileira de petróleo (Figura 1d), incluindo óleo cru e condensado, mas excluindo líquido de gás natural e óleo de xisto, chegou a 750 milhões de barris, o que elevou o Brasil à 12ª colocação no ranking mundial de produtores de petróleo (ANP, 2011).
3. Sendo a densidade °API (do inglês *API gravity* – ASTM D 4175 (2009)) um parâmetro de classificação através da qual o petróleo é considerado como extra-leve ($40 < ^\circ\text{API} < 45$), leve ($35 < ^\circ\text{API} < 40$), médio ($25 < ^\circ\text{API} < 35$), pesado ($20 < ^\circ\text{API} < 25$), ultra-pesado ($15 < ^\circ\text{API} < 20$) ou asfáltico ($^\circ\text{API} < 15$), os petróleos nacionais podem ser classificados como médio (16%), pesado (62%) e ultra-pesado (12%) somando um 90% da produção no Brasil em 2010, sendo um 10% classificado como petróleo leve, extra-leve e asfalto (Figura 2). Portanto, o panorama compreende uma predominância do petróleo pesado apresentando alta viscosidade e baixa mobilidade nos reservatórios, o que dificulta sua extração, bem como seu processamento (Guimarães e Pinto, 2007; Parisotto, 2007).

Logo, a ocorrência de petróleos pesados e ultra-pesados aponta para a necessidade de desenvolvimento de novas tecnologias que contribuam para o aprimoramento do processo de caracterização e processamento do petróleo e suas frações, sejam elas pesadas.

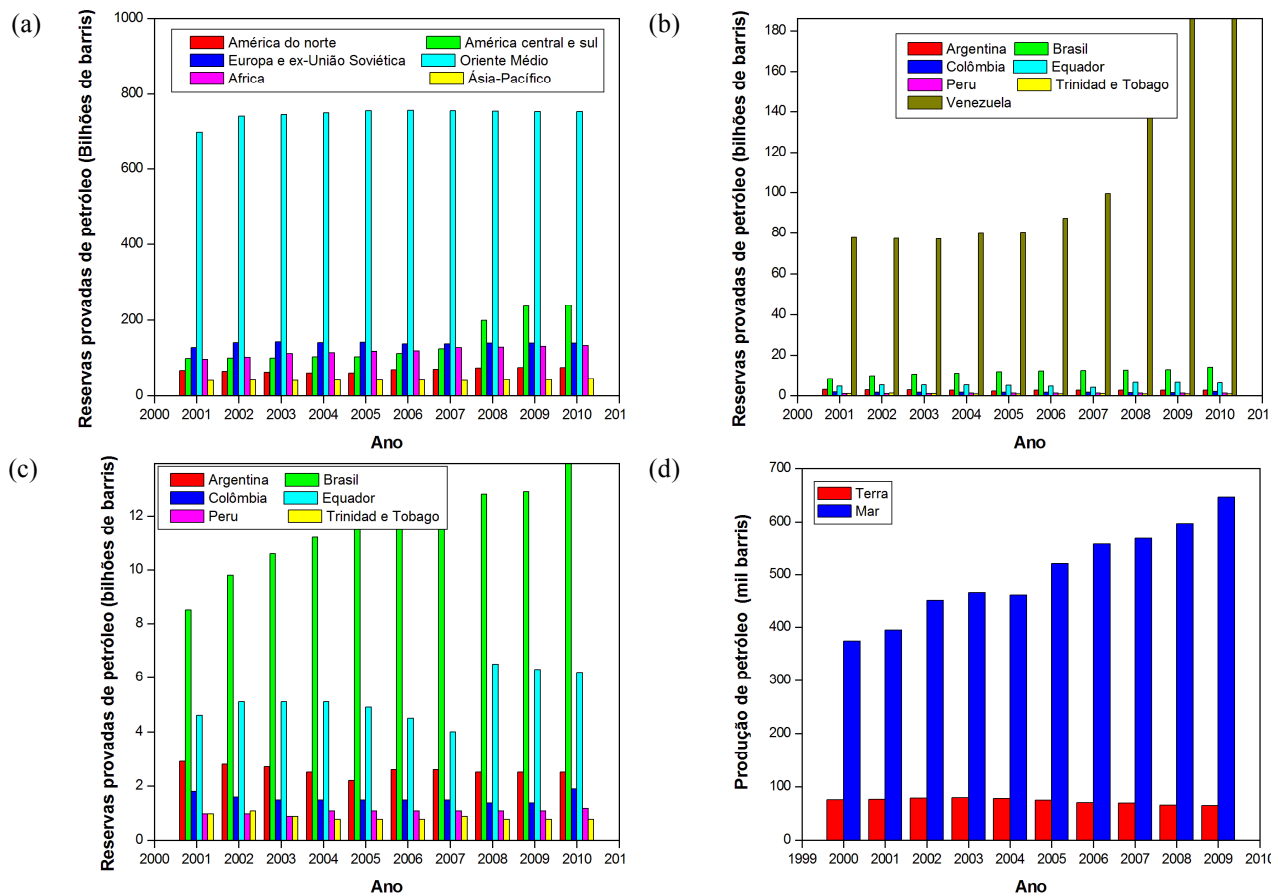


Figura 1. (a–c) Evolução das reservas provadas de petróleo, segundo regiões geográficas, países e blocos econômicos nos anos 2001–2010; (d) Produção de petróleo, por localização (terra e mar), 2001–2009 (Fonte: ANP, 2011)

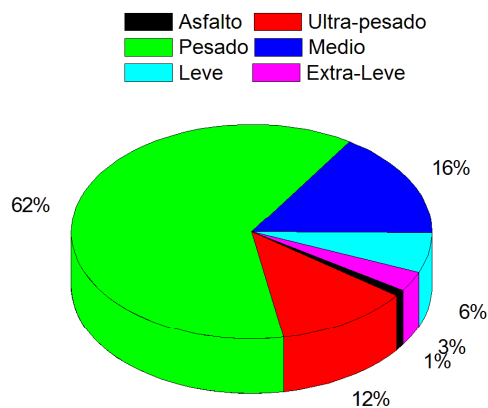


Figura 2. Produção de petróleo, em porcentagem, no Brasil por classificação do petróleo no ano de 2010 (Fonte: ANP, 2011).

Hoje são realizados investimentos em diferentes áreas da indústria de petróleo e pesquisa para o desenvolvimento de novas tecnologias com o objetivo de aprimorar e tornar mais ágil o processo de exploração, produção e caracterização do petróleo, frações, cortes e derivados. Os investimentos em tecnologia na área de petróleo vêm em alta e são imprescindíveis tanto para viabilizar a produção do petróleo disponível nas reservas brasileiras como para o refino desse petróleo com características físico-químicas diferentes dos petróleos encontrados em outras regiões. Esse crescimento levou à implantação de inúmeras empresas nesse setor e o desenvolvimento de projetos de pesquisa e engenharia, que apresentam um viés tecnológico, a fim de garantir uma melhora no rendimento e qualidade do óleo, aumentando a competitividade do setor petrolífero do Brasil.

A PETROBRAS que é movida pelos desafios, por incentivar o desenvolvimento e garantir o futuro da sociedade competitiva, vem enfrentando a tarefa de produzir combustíveis de alta qualidade, a partir do óleo pesado brasileiro produzido nos campos petrolíferos em quantidades consideráveis.

Tendo a empresa como objetivo imediato aumentar a conversão de resíduo, reduzir gastos com óleo importado e aumentar a produção de derivados de maior valor agregado a partir do petróleo pesado, muitos processos já foram desenvolvidos, aprimorados e/ou aperfeiçoados. Dentro deles, destaca-se o caso específico dos estudos realizados nos Laboratórios de Desenvolvimento de Processos de Separação (LDPS) e de Otimização, Projeto e Controle Avançado (LOPCA) da Faculdade de Engenharia Química (FEQ) da Universidade Estadual de Campinas (UNICAMP), em parceria com o órgão Financiador de Estudos e Projetos do Ministério da Ciência e Tecnologia (FINEP) e o Centro de Pesquisa CENPES/PETROBRAS que desenvolveram uma tecnologia, a destilação molecular, que permite obter cortes e resíduos pesados de petróleo a temperaturas superiores daquelas alcançadas pelos métodos padronizados ASTM D 2892 (2005) e ASTM D 5236 (2003). Resultados do desenvolvimento permitiram caracterizar de uma forma mais completa o petróleo, no que se refere à extensão da curva do Ponto de Ebulição Verdadeiro (PEV) a temperaturas próximas a 973,15 K (Tabela 1).

Tabela 1. Contribuições no desenvolvimento da destilação molecular de frações pesadas de petróleo.

Tipo de contribuição	Referência	Tipo de desenvolvimento		Configuração do equipamento
		Experimental	Modelagem/ Simulação	
Tese	Tovar, 2012	X	X	DMC
Tese	Zuñiga, 2009	X	X	DMFD
Dissertação	Hernández, 2009	X	-	DMFD
	Rocha, 2009	X	-	DMC/DMFD
	Lopes, 2008	X	-	DMFD
	Rocha, 2008	X	-	DMC/DMFD
	Winter, 2007	X	-	DMFD
Tese	Sbaite, 2005	X	-	DMFD
Artigo / periódico internacional	Tovar et al., 2012	X	X	DMC
	Lima et al., 2011	-	X	DMFD
	Zuñiga–Liñan et al., 2011	X	X	DMFD
	Rocha et al., 2011	X	-	DMFD
	Zuñiga et al., 2009	-	X	DMFD
	Zuñiga et al., 2009	X	-	DMFD
	Rocha et al., 2009a	X	-	DMFD
	Rocha et al., 2009b	X	-	DMFD
	Sbaite et al., 2006	X	-	DMFD
	Maciel–Filho et al., 2006	X	-	DMFD
	Batistella et al., 2002	X	X	DMC/DMFD
	Batistella et al., 2000	-	X	DMC/DMFD
	Batistella e Wolf–Maciel, 1996	-	X	DMC/DMFD
Artigo / anais de congresso	Hernández et al., 2008	X	-	DMFD
	Rocha et al., 2008	X	-	DMFD
	Liñan et al., 2007	X	-	DMFD
	Lopes et al., 2007	X	-	DMFD
	Rocha et al., 2007	X	-	DMFD
	Winter et al., 2007	X	-	DMFD
	Maciel–Filho et al., 2006	X	-	DMFD
	Winter et al., 2006	X	-	DMFD
	Sbaite et al., 2005	X	-	DMFD
	Winter et al., 2004	X	-	DMFD
	Sbaite et al., 2003	X	-	DMFD

DMC: Destilador molecular centrífugo; DMFD: Destilador molecular de filme descendente.

Hoje a realidade não mudou. A obtenção de alta conversão de óleo pesado vem se tornando um dos principais alvos das pesquisas e desenvolvimentos em matéria de processos de refino de frações pesadas de petróleo (Tovar et al., 2011; Martínez–Palou et al., 2011; de Lima e Schaeffer, 2011).

Baseado no que foi citado, foi feito no LOPCA/LDPS o desenvolvimento de uma metodologia para a realização do *upgrading* do óleo cru e/ou fração pesada de petróleo a qual compreende o conceito de um processo híbrido e intensificado, nomeado como destilação molecular reativa, no qual acontece o acoplamento da destilação molecular (alto vácuo) e

conversão reativa simultaneamente ou, em outras palavras, o craqueamento dos compostos mais complexos (de maior massa molar) e a destilação dos compostos mais leves formados, permitindo, assim, a transformação do óleo cru e/ou fração pesada e/ou ultra-pesada em óleo/fração mais leve, garantindo um melhor escoamento e processamento deste.

Desde o ponto de vista experimental uma das características mais importante deste avanço tecnológico em matéria de *upgrading* é a implementação de alto vácuo, permitindo submeter o material a temperaturas adequadas em um curto tempo operacional, e ter um contato muito intenso da amostra com a superfície catalítica sobre a superfície aquecida do evaporador. Assim, o potencial de aplicação desta nova técnica parece ser muito promissor, como já demonstrado por Winter (2011), cujos resultados evidenciaram um melhor aproveitamento das frações pesadas e ganhos na qualidade do produto final.

No cenário atual da indústria e dos processos, há uma forte tendência para a implantação de processos computacionais baseados na modelagem e na simulação de um sistema com o propósito de que informações significativas possam ser retiradas sobre sua dinâmica e/ou seu desempenho. Na destilação molecular reativa, informações sobre o perfil de temperatura, a espessura do filme, a taxa de evaporação efetiva e o perfil de conversão são importantes porque permitem determinar o rendimento e a pureza dos produtos convertidos, assim como definir o projeto das próximas operações no destilador molecular reativo. Entretanto, a avaliação direta destas variáveis do processo não é viável, estando sujeita ao desenvolvimento de um modelo matemático adequado que possa descrever o processo em função das variáveis operacionais e, assim, ser útil para a análise do mesmo.

Com esta finalidade e para abordar a modelagem do processo de destilação molecular reativa foram usadas neste trabalho de Tese equações de balanço (massa, energia e momento) que descrevem o comportamento do processo a partir das leis que regem seus fenômenos físicos e químicos. Também foram utilizadas equações algébrico-diferenciais gerando uma estrutura matemática (número e tipo de equações) chamada de modelo. Uma vez determinados os valores que as variáveis de saída tinham que adotar em diferentes condições de operação (variáveis de entrada), este procedimento foi chamado de simulação do processo; isto pode ser esquematizado na Figura 3.

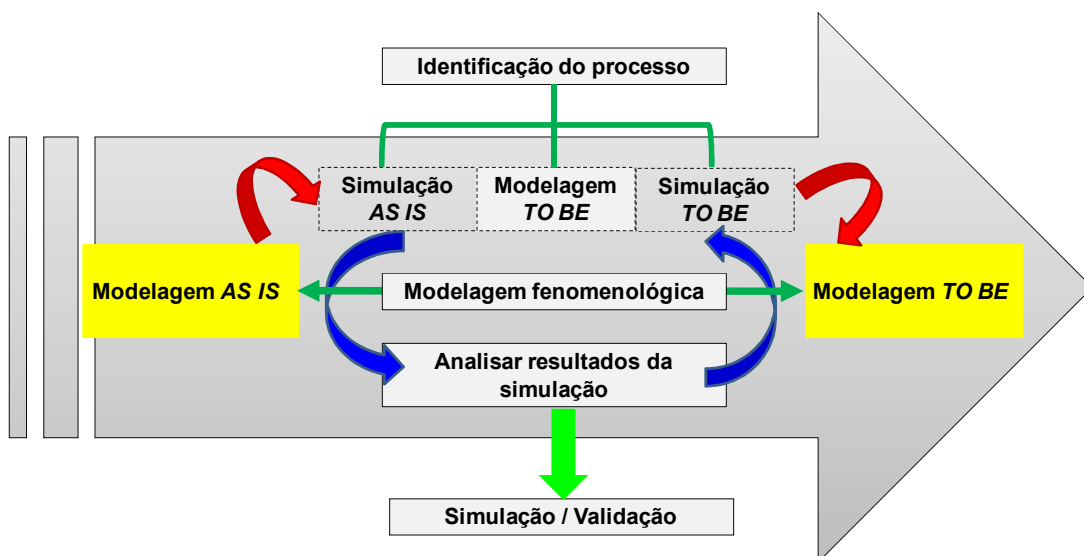


Figura 3. Forma de abordar a modelagem e simulação do processo de destilação molecular reativa.

Desta forma, a modelagem e a simulação formam uma ferramenta fundamental de auxílio na consolidação da tecnologia de destilação molecular reativa como processo híbrido e intensificado, no qual, através de simulações, considerando diferentes condições do processo foi possível obter informações rápidas e confiáveis sobre o desempenho do mesmo. Assim, o desenvolvimento desta ferramenta computacional permitiu entender como as variáveis operacionais características do processo (temperatura do evaporador, porcentagem de catalisador, pressão do sistema e vazão de alimentação), a composição da carga alimentada ao processo e as dimensões do evaporador (espaço entre a superfície do evaporador e a superfície do condensador e a distância radial da superfície do evaporador) influenciaram nas variáveis de saída: a espessura do filme, os perfis de temperatura e concentração no filme, a taxa de evaporação, a taxa de destilado produzido e a taxa de reação, parâmetros característicos dos processos de destilação molecular e destilação molecular reativa (tecnologia híbrida).

Além disso, os resultados provenientes das análises teóricas (simulações), apresentadas neste trabalho de Tese, permitiram o estabelecimento de novas condições operacionais visando à obtenção de um alto desempenho operacional da unidade em relação ao melhor rendimento de separação e da taxa de reação.

Finalmente, conseguiu-se dar um salto tecnológico, em matéria computacional e experimental, no processo de destilação molecular reativa, estabelecendo estratégias e condições operacionais que, concluíram em um efetivo aumento do desempenho técnico da unidade e

obtendo produtos com características favoráveis para exploração, escoamento, transferência, processamento primário e refino.

1.2. Objetivos

O objetivo geral deste trabalho foi desenvolver a modelagem matemática e simulação do processo de destilação molecular centrífuga reativa (DMCR), dando origem ao simulador DESTMOL-R, desenvolvido na linguagem FORTRAN-90 usando o compilador *Compaq Visual Fortran (professional edition 6.6)*, como contribuição e auxílio ao desenvolvimento de uma tecnologia para o processamento de óleo cru e frações pesadas obtendo produtos com características favoráveis para exploração, escoamento, transporte e refino. As etapas e sub-etapas no desenvolvimento estão esquematizadas na Figura 4.

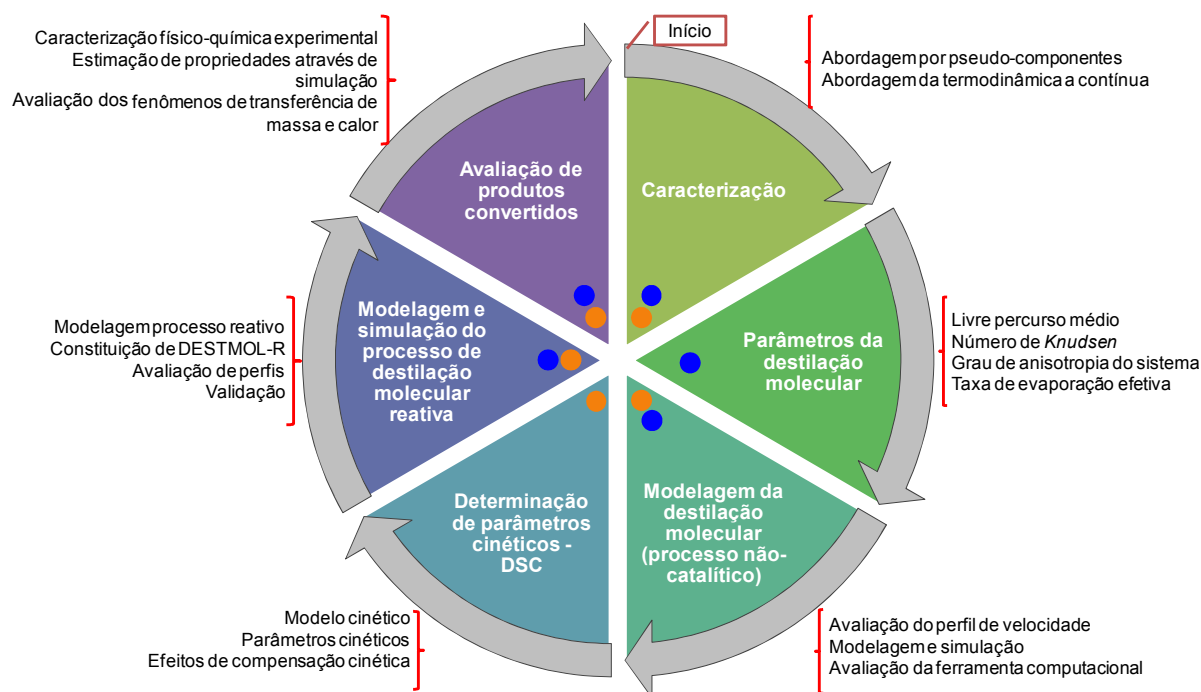


Figura 4. Esquema geral do desenvolvimento do trabalho de Tese. ● Desenvolvimento experimental, ● Desenvolvimento computacional.

1.2.1. Objetivos específicos e etapas de desenvolvimento

A seguir, são apresentados os objetivos específicos inerentes à pesquisa.

1. Desenvolver uma ferramenta computacional para estimar as propriedades físico-químicas das frações.
2. Realizar uma avaliação teórica das variáveis macroscópicas (livre percurso médio, MFP , número de *Knudsen*, Kn , e a taxa de evaporação efetiva, G_E) no contexto dos processos de destilação molecular (processo não catalítico) e destilação molecular centrífuga reativa (processo catalítico).
3. Desenvolver a modelagem do processo de destilação molecular centrífuga não reativa fundamentada nas equações de balanços de massa, energia e momento no filme formado escoando sobre a superfície do evaporador.
4. Determinar o perfil de decomposição térmica catalítica (3, 5 e 10 %m/m) dos sistemas em estudo (resíduos da destilação atmosférica de petróleo), através de curvas calorimétricas.
5. Desenvolver a modelagem e a simulação do processo de destilação molecular centrífuga reativa para obter informações sobre o perfil de temperatura, espessura do filme, taxa de evaporação efetiva, taxa de destilado e conversão.
6. Realizar ensaios experimentais de destilação molecular centrífuga reativa em função da análise das variáveis operacionais como a temperatura do evaporador (EVT) e a quantidade de catalisador (expressa como percentagem em massa de catalisador, %CAT); caracterizar os produtos obtidos da destilação molecular centrífuga reativa, mediante avaliação físico-química.

A seguir, estão descritas as etapas seguidas no desenvolvimento do trabalho.

Etapla 1: Caracterização dos sistemas em estudo

- Desenvolver uma ferramenta computacional (em linguagem FORTRAN-90) para estimar as propriedades físico-químicas das frações de petróleo em estudo utilizando a abordagens de pseudo-componentes e da termodinâmica contínua com a menor quantidade de dados de entrada necessários (densidade e curva PEV da fração).
- Determinar experimentalmente, utilizando metodologias padrões, propriedades físico-químicas das frações pesadas e ultra-pesadas de petróleo, contribuindo na modelagem e simulação do processo de destilação molecular centrífuga reativa.

Etapla 2: Estudo das considerações teóricas sobre a destilação molecular

- Realizar uma descrição teórica do processo de destilação molecular no contexto da estimativa de parâmetros teóricos (livre percurso médio, número de *Knudsen* e taxa de evaporação teórica e efetiva) envolvendo as condições operacionais da destilação molecular (temperatura do evaporador e pressão do sistema).

Etapa 3: Modelagem matemática e simulação do processo de destilação molecular centrífuga (processo não-catalítico)

- Desenvolver a modelagem do processo de destilação molecular centrífuga fundamentada nas equações de balanços de massa, energia e momento no filme formado escoando sobre a superfície do evaporador.
- Analisar o perfil de velocidade e o regime de fluxo (laminar e turbulento) na destilação molecular centrífuga de um resíduo atmosférico de petróleo utilizando a fluidodinâmica computacional.
- Desenvolver uma ferramenta computacional na linguagem FORTRAN-90 que englobe a modelagem e a simulação do processo de destilação molecular centrífuga para predizer informações sobre o perfil de temperatura, espessura do filme, taxa de evaporação efetiva e taxa de destilado.
- Realizar ensaios experimentais de destilação molecular centrífuga com o objetivo de validar a ferramenta computacional desenvolvida.

Etapa 4: Determinação do modelo cinético da reação de craqueamento

- Avaliar o perfil de decomposição térmica (sem catalisador) e catalítica (com catalisador – 3, 5 e 10 %m/m) dos sistemas em estudo (resíduos atmosféricos), através de curvas calorimétricas.
- Determinar o modelo cinético da reação de craqueamento (catalítico) e obter os parâmetros cinéticos: energia de ativação (E), fator pré-exponencial (A), ordem de reação (n) e constante de velocidade (k), visando sua introdução na modelagem da destilação molecular centrífuga reativa. Verificar a obediência dos parâmetros cinéticos com relação ao efeito de compensação cinética.

Etapa 5: Modelagem matemática e simulação do processo de destilação molecular centrífuga reativa

- Desenvolver a modelagem do processo de destilação molecular centrífuga reativa fundamentada nas equações de balanços de massa, energia e momento no filme formado sob a superfície do evaporador, tomando como base o modelo matemático desenvolvido para o processo não catalítico.
- Desenvolver uma ferramenta computacional na linguagem FORTRAN-90, que englobe a modelagem e a simulação do processo de destilação molecular centrífuga reativa para prever informações sobre o perfil de temperatura, espessura do filme, taxa de evaporação efetiva, taxa de destilado e taxa de reação.
- Realizar um mapeamento ou *screening* das variáveis significativas no processo de destilação molecular centrífuga reativa através do uso do planejamento fatorial avaliando a influência das variáveis operacionais (temperatura do evaporador, pressão do sistema e porcentagem de catalisador).
- Realizar ensaios experimentais de destilação molecular centrífuga reativa com o objetivo de validar a ferramenta computacional desenvolvida no item anterior, e avaliar os perfis característicos do processo através das variáveis de saída (taxa efetiva de evaporação, o perfil da taxa de destilado e a taxa de reação) em função da análise das variáveis operacionais como a temperatura do evaporador, a pressão do sistema e a porcentagem de catalisador.

Etapas 6: Caracterização das correntes obtidas da destilação molecular centrífuga reativa

- Caracterizar os produtos obtidos da destilação molecular centrífuga reativa, mediante avaliação físico-química.

1.3. Organização da Tese

As contribuições obtidas estão estruturadas em onze capítulos. O desenvolvimento do trabalho envolve tanto trabalho teórico e computacional quanto trabalho experimental. Cada capítulo é subdividido em três partes:

- I. A introdução contendo uma breve descrição do tópico.
- II. O desenvolvimento do tópico apresentado em forma de manuscrito (artigo aceito, submetido ou a ser submetido em periódico internacional e/ou congresso) apresentando em língua inglesa, contendo um resumo, uma introdução do tópico

a desenvolver no artigo, a metodologia, os resultados e discussões, referências e nomenclatura.

III. Por fim, apresentam-se as considerações e contribuições do capítulo. A síntese de todas as contribuições desta Tese de Doutorado é resumida no Capítulo 10.

Capítulo 2: Apresenta-se uma revisão dos principais tópicos a serem tratados nesta Tese de Doutorado. Discutem-se os conceitos da caracterização de misturas complexas como é o petróleo e suas frações, processos atuais utilizados no processamento de resíduos de petróleo, conceitos e fundamentos referentes ao desenvolvimento do processo de destilação molecular e se estabelece o marco conceitual do processo da destilação molecular reativa como um processo híbrido e intensificado no qual acontece o acoplamento de destilação molecular e reação química simultaneamente, permitindo submeter o material a temperaturas adequadas, num curto tempo operacional, garantindo um contato muito intenso da amostra com a superfície catalítica proporcionando alta cinética de reação e alta taxa de evaporação permitindo altas taxas de processamento.

Capítulo 3: Apresenta-se a metodologia de cálculo das propriedades físico-químicas, através de correlações empíricas reportadas na literatura, com sua comparação com as análises experimentais; visando seu acoplamento na modelagem matemática e na simulação do processo de destilação molecular centrífuga reativa. Foram utilizadas as abordagens de pseudo-componentes e da termodinâmica contínua constituindo ferramentas (independente cada uma delas) para o cálculo das respectivas propriedades. As respostas das metodologias desenvolvidas forneceram valores das propriedades básicas (temperatura de ebulição normal e densidade), propriedades termodinâmicas (composição mássica e molar, temperatura crítica, pressão crítica e fator acêntrico); e propriedades termofísicas (viscosidade cinemática, condutividade térmica, calor específico, entre outras).

Capítulo 4: A descrição teórica do processo de destilação molecular é apresentada, sendo de grande potencial o contexto do desenvolvimento dos parâmetros teóricos (livre percurso médio, número de *Knudsen* e taxa de evaporação efetiva) envolvendo as condições operacionais da destilação molecular (temperatura do evaporador e pressão do sistema).

Capítulo 5: Este capítulo contém o estudo fluidodinâmico do escoamento do filme líquido gerado na destilação molecular. A modelagem é fundamentada nas equações de balanços

de massa e momento no filme de líquido formado e escoando na superfície cônica do evaporador. Este trabalho tem como objetivo (i) investigar o efeito das diferentes condições de operação (vazão de alimentação e velocidade do rotor), com temperatura de evaporação constante (423,15 K), no perfil de velocidade do filme fino de líquido de um resíduo atmosférico de petróleo na superfície do evaporador de um destilador molecular centrífugo, e (ii) estudar os componentes da velocidade nas direções $-r$, $-\theta$ e $-\varphi$ (ou velocidade radial, angular e tangencial, respectivamente), considerando um estado bidimensional estacionário (no regime de fluxo laminar), onde o vetor velocidade perpendicular da superfície cônica (em direção $-\theta$) é ignorado, apenas vetores na direção radial (direção $-r$) e direção tangencial (direção $-\varphi$) foram considerados.

Capítulo 6: Neste capítulo se apresenta o desenvolvimento de uma ferramenta computacional para auxiliar na modelagem e a simulação do processo de destilação molecular centrífuga para estimar e avaliar os perfis característicos do processo através das variáveis de saída (o perfil de temperatura, o perfil de concentração do filme, o perfil da taxa efetiva de evaporação, o perfil da taxa de destilado e o perfil da espessura do filme) em função da análise das variáveis operacionais como temperatura da alimentação, a temperatura do evaporador, a pressão do sistema e os parâmetros geométricos do equipamento (distância entre o evaporador e o condensador, ângulo médio da superfície cônica e distância radial).

Também é apresentada a metodologia computacional e experimental implementada para a separação das frações constitutivas dos cortes pesados de petróleo. Por outro lado, através de uma análise estatística é feito um estudo das principais variáveis que influenciam no rendimento das frações de petróleo obtidas, definindo as melhores condições operacionais para o processamento destas amostras.

Capítulo 7: A análise termoanalítica – Calorimetria exploratória diferencial – do inglês DSC (*Differential scanning calorimeter*) foi usada com o objetivo de verificar as transições físico-químicas ocorridas no processo de craqueamento das frações de petróleo (resíduos da destilação atmosférica de petróleo). Assim, este estudo objetivou estudar a cinética do processo de craqueamento de frações pesadas de petróleo, permitindo avaliar a influência da quantidade de catalisador (3, 5 e 10% m/m) durante a reação de craqueamento.

Capítulo 8: Apresenta-se a modelagem e a simulação do processo de destilação molecular centrífugo reativo constituindo uma ferramenta fundamental no auxílio do

desenvolvimento experimental do processo, uma vez que informações sobre o perfil de temperatura, concentração, conversão de produtos, velocidade e taxa de destilado na superfície do filme permitem determinar o rendimento e eficiência do processo.

Para a modelagem e a simulação do processo, foi considerado como caso de estudo o *upgrading* do resíduo atmosférico 673,15 K⁺ do petróleo “W” no destilador molecular centrífugo reativo. A modelagem desenvolvida baseada no modelo matemático do processo de destilação molecular centrífuga junto com as modificações introduzidas pelo termo cinético relativo à reação *in-situ*. Por fim, as equações de balanço de massa e de energia foram resolvidas numericamente através do método das linhas.

Simultaneamente, neste capítulo, se descreve a metodologia experimental desenvolvida no estudo do processo de destilação molecular reativa, utilizando a unidade (de tipo centrífugo) construída pelos laboratórios de pesquisa LDPS/LOPCA/UNICAMP em parceria com os órgãos financiadores CENPES/PETROBRAS e FINEP.

Capítulo 9: É apresentado o procedimento de caracterização das frações convertidas (destilados e resíduos) obtidos do processo de destilação molecular centrífuga reativa. A caracterização realizada foi de tipo fracionamento preparativo, físico-químico e coloidal.

Capítulo 10: Neste capítulo se apresentam as conclusões e contribuições do trabalho.

Capítulo 11: Finalmente, se apresentam as referências mencionadas nas sessões introdutórias de cada capítulo.

Capítulo 2

Perspectivas na aplicação, modelagem e simulação do processo de destilação molecular reativa: processo híbrido e intensificado

2.1. Introdução

A intensificação de processos abrange novas e complexas tecnologias que substituem equipamentos grandes, caros e com grande consumo energético por plantas de menor custo, mais eficiente e de menor tamanho, contribuindo para um menor impacto ambiental (Keil, 2007). Na intensificação de processos podem ser utilizadas unidades de operação híbridas, as quais vinculam processos elementares tais como reação e separação, aumentando a produtividade e seletividade, além de facilitar a separação de subprodutos indesejáveis. A redução do número de etapas leva a um investimento reduzido e à redução significativa do gasto de energia. Além disso, a seletividade do produto conduz a uma diminuição do consumo de matéria-prima e consequentemente dos custos de operação (Keil, 2007).

Hoje, na indústria do petróleo, grandes esforços estão sendo dedicados no desenvolvimento de alternativas direcionadas a aumentar o grau API e reduzir a viscosidade dos óleos pesados e extra-pesados, favorecendo as propriedades de escoamento e transporte. Portanto, surge o desafio para os grupos de pesquisa e desenvolvimento de projetar e aperfeiçoar tecnologias que permitam o *upgrading* destes óleos pesados e extra-pesados aumentando seu valor de comercialização e atingindo uma produção de derivados de maior valor agregado. Assim, os Laboratórios de Desenvolvimento de Processos de Separação (LDPS) e de Otimização, Projeto e Controle Avançado (LOPCA) da Faculdade de Engenharia Química da Unicamp, em parceria com o órgão Financiador de Estudos e Projetos do Ministério da Ciência e Tecnologia (FINEP) e o Centro de Pesquisa CENPES/PETROBRAS, têm desenvolvido estratégias tecnológicas para a caracterização e processamento destes materiais usando o processo de destilação molecular. Hoje a meta destas entidades é garantir a competitividade e estimular

economicamente a área de processamento dos óleos crus pesados e das frações pesadas obtidas da destilação atmosférica e da destilação a vácuo. Assim sendo, o aprimoramento da tecnologia nomeada “Destilação Molecular Reativa”, no qual acontece o acoplamento de destilação molecular (alto vácuo) e conversão reativa (craqueamento) simultaneamente, é caracterizada como um processo híbrido – intensificado. As características particulares do processo de destilação molecular reativa levam a: viabilizar a implementação de alto vácuo, permitindo submeter o material a temperaturas adequadas, ter um curto tempo de residência (operacional), e a ter um contato muito intenso da amostra com a superfície catalítica permitindo altas taxas de processamento.

Portanto, este projeto propõe auxiliar a consolidação do sucesso tecnológico do processo de destilação molecular reativa, com o desenvolvimento de uma ferramenta computacional, sendo a modelagem e simulação um caminho disponibilizado pela área de pesquisa operacional estabelecendo cenários, a partir dos quais se pode: direcionar o processo de tomada de decisão, proceder a análises experimentais, avaliar o sistema como um conjunto de variáveis inter-relacionadas e propor soluções para a melhoria da *performance*. No caso específico do processo de destilação molecular centrífuga reativa, os principais ganhos serão: (a) a previsão de resultados na execução de experimentos, (b) a determinação de condições operacionais, (c) a identificação de problemas antes mesmo de suas ocorrências, (d) a eliminação/decisões de procedimentos extras que possa desagregar/agregar valor ao processo, (e) a realização de análises de sensibilidade e (f) a redução de custos com o emprego de recursos (Silva, 2010).

2.2. Generalidade do petróleo

O petróleo é uma mistura complexa de compostos formados em sua maioria por átomos de carbono e hidrogênio, chamados de hidrocarbonetos e outros átomos como oxigênio, enxofre, nitrogênio e metais (vanádio, níquel, ferro e cobre) (ASTM D 4175, 2009).

O petróleo contém apreciável quantidade de constituintes que são classificados como não hidrocarbonetos. Estes constituintes, considerados como impurezas, possuem elementos como enxofre, nitrogênio, oxigênio e metais que podem aparecer em toda faixa de destilação do petróleo, mas tendem a se concentrar nas frações mais pesadas (Thomas, 2004).

De acordo com a sua estrutura, os hidrocarbonetos presentes no petróleo, são classificados em saturados, insaturados e aromáticos (Tabela 1). Os hidrocarbonetos saturados, também denominados de alcanos, são aqueles cujos átomos de carbono são unidos somente por ligações simples entre si às de átomos de hidrogênio, constituído de cadeias lineares (parafinicos normais), ramificadas (iso–parafinicos) ou cíclicas (naftênicos). Os hidrocarbonetos insaturados, também denominados de olefinas, apresentam pelo menos uma dupla ou tripla ligação carbono–carbono, enquanto que os hidrocarbonetos aromáticos apresentam um anel de benzeno em sua estrutura (Thomas, 2004).

Tabela 1. Classificação dos hidrocarbonetos presentes no petróleo segundo Bueno (2004).

Constituintes	Características
Parafinicos	<ul style="list-style-type: none"> • Teor de parafinas maior que 75% m/m. • São petróleos leves, fluidos ou de alto ponto de fluidez, com baixa densidade e baixo teor de resinas e asfaltenos.
Naftênico–parafinico	<ul style="list-style-type: none"> • Contêm 50–70% m/m de parafinas e mais que 20% m/m de naftênicos. • Apresentam teor de resinas e asfaltenos entre 5 e 15% m/m, baixo teor de enxofre (menos que 1% m/m) e teor de naftênicos entre 25 e 40% m/m. • A densidade e a viscosidade apresentam valores maiores que os parafinicos, mas ainda são moderados.
Naftênicos	<ul style="list-style-type: none"> • Teor de naftênicos maior que 70% m/m. • Apresentam baixo teor de enxofre e se originam de alteração bioquímica de óleos parafinicos e parafinicos–naftênicos.
Aromáticos intermediários	<ul style="list-style-type: none"> • Teor de aromáticos maior que 50% m/m. • São óleos pesados, contendo de 10 a 30% m/m de asfaltenos e resinas e teor de enxofre acima de 1% m/m.
Aromático–naftênicos	<ul style="list-style-type: none"> • São óleos que sofreram um processo inicial de biodegradação, através do qual as parafinas são removidas. • São derivados dos óleos parafinicos e parafinicos–naftênicos, podendo ter mais de 25% m/m de resinas e asfaltenos e teor de enxofre entre 0,4 e 1% m/m.
Aromático–asfálticos	<ul style="list-style-type: none"> • São pesados e viscosos, geralmente resultantes da alteração dos óleos aromáticos intermediários. • O teor de asfaltenos e resinas é elevado.

2.3. Caracterização físico–química das misturas

Caracterizar físico–quimicamente substâncias significa definir seu comportamento físico–químico em processos, equipamentos industriais ou na aplicação de derivados como produtos sob diferentes condições operacionais, avaliando sua reatividade, incompatibilidade, estabilidade, solubilidade e facilidade para vaporizar, cristalizar e escoar. Tradicionalmente, a caracterização físico–química do petróleo é feita através de métodos convencionais que demandam tempo e conhecimento em diferentes técnicas analíticas, mas as metodologias analíticas já existentes sofrem adaptações ou novas precisam ser desenvolvidas para atender à

demanda de acompanhamento dos petróleos e/ou frações pesadas e ultra-pesadas. Assim, o conhecimento das principais propriedades destes materiais viabiliza a toma de decisão de forma rápida durante o processamento que visa o aumento da produção.

Misturas de composição definida podem ser caracterizadas pela identificação de sua composição conjugado com o uso de regras de mistura, usadas para calcular as propriedades da mistura através da contribuição ponderada de cada componente da mistura. Misturas de composição não-definida, como o petróleo, são caracterizadas utilizando-se abordagens diferentes, entre as quais se listam: (i) Representar toda a mistura por um conjunto de propriedades, calculadas a partir de equações que utilizam propriedades básicas da mistura e que foram determinadas experimentalmente; e (ii) decomposição de toda a mistura em um conjunto de componentes individuais denominados pseudo-componentes, que não são definidos por uma fórmula química e sim por suas propriedades físicas e termodinâmicas (Coats, 1985; Daubert et al., 2000). Entre essas propriedades, listam-se a densidade, temperatura de ebulição, viscosidade, temperatura e pressão crítica, fator acêntrico e massa molar.

2.3.1. Metodologias para representar o petróleo e suas frações

Os métodos de cálculos utilizados para a caracterização do petróleo e suas frações utilizam diferentes abordagens apresentadas a seguir:

- Representar todo o petróleo ou fração seja por um único componente caracterizado por um conjunto de propriedades, calculadas por correlações a partir de pelo menos duas propriedades básicas (temperatura normal de ebulição, T_b e gravidade específica (densidade relativa), SG). Esta abordagem tem como maior vantagem sua simplicidade, no entanto apresenta imprecisões pelo fato de considerar uma mistura complexa multicomponente como um único componente.
- Decompor o petróleo ou fração em um conjunto de número arbitrário pseudo-componentes, representados por constituintes não-identificados. Cada pseudo-componente é definido por suas propriedades termodinâmicas e físicas, tais como a densidade, temperatura de ebulição, viscosidade, temperatura e pressão críticas, fator acêntrico e massa molar, que devem estar disponíveis ou devem ser calculadas. De acordo com o método usado, pode ser necessário conhecer ainda a porcentagem dos tipos de hidrocarbonetos (Daubert et al., 2000).

A segunda abordagem, por pseudo-componente, pode estimar as propriedades termodinâmicas e físico-químicas por metodologias diferentes:

- Contribuição de grupos necessita conhecer a composição química da fração, em termos de estruturas, por tipo de átomo de carbono.
- Outra abordagem é através de modelos que utilizam componentes base (Hidrocarbonetos Parafínicos, Naftênicos e Aromáticos) (Quann e Jaffe, 1992; Hu e Zhu, 2001). Nesse caso, cada corte obtido através de uma destilação é representado por um conjunto de componentes fictícios (componentes base) de mesma massa molar (Riazi, 2004) ou mesmo número de átomos de carbono (Danesh, 1998).

Na Tabela 2 se apresentam algumas contribuições referentes às abordagens para representar a mistura complexa do petróleo em termos da geração de pseudo-componentes.

Tabela 2. Contribuição e desenvolvimento de metodologias para representar a mistura de componentes do petróleo.

Referência	Contribuição
Riazi e Al-Sahhaf, 1996	Foi desenvolvida uma correlação generalizada para as propriedades de varias series homologas de hidrocarbonetos em termos da massa molar. Pode-se aplicar para hidrocarbonetos acima de C ₅₀ .
Quann e Jaffe, 1992	Apresentaram um método que representa moléculas de hidrocarbonetos como um vetor de incrementos de grupos estruturais. Uma mistura de hidrocarbonetos (tal como petróleo ou suas frações) é representada por um grupo desses vetores, cada um com um determinado peso percentual (que equivaleria à sua influência nas propriedades da mistura). Segundo Quann e Jaffe (1992), a representação de moléculas por vetores oferece uma estrutura adequada para a construção de redes de reação de tamanho e complexidade variados, para desenvolver correlações de propriedades baseadas em moléculas e para incorporar métodos de contribuição de grupos existentes para a estimativa de propriedades termodinâmicas.
Miquel e Castells, 1993; 1994	Foi desenvolvido uma ferramenta computacional para caracterizar frações de petróleo em pseudo-componente. No trabalho um pseudo-componente é aquele que está definido por uma porção volumétrica da curva PEV, o qual está associado com uma temperatura normal de ebulição
Hu e Zhu, 2001	Aplicaram um método de modelagem composicional para correlacionar propriedades de frações de petróleo, semelhante ao trabalho apresentado por Quann e Jaffe (1992). O método usado por Hu e Zhu (2001) faz uso de matrizes de séries homólogas de tipo molecular, onde as linhas da matriz representam o número de átomos de carbono e as colunas representam as séries homólogas (n-parafinas, isoparafinas, naftênicos, etc.); cada elemento da matriz representa a fração mássica ou molar de uma molécula ou <i>lump</i> (por exemplo, para uma série homóloga de um anel aromático e oito (08) átomos de carbono, há quatro (04) moléculas possíveis: etil-benzeno, orto-xileno, meta-xileno e para-xileno, cujas propriedades físicas são semelhantes por serem moléculas com mesmo número de átomos de carbono e pertencentes à mesma série homóloga).
Eckert e Vaněk, 2005	Foi desenvolvida uma aproximação para a caracterização de misturas complexas baseada na representação da mistura original por um sistema de componentes. A nova mistura está completamente definida e caracterizada e as propriedades físicas podem ser obtidas de bases de dados.

2.3.1.1. Conceito de mistura contínua para caracterização de frações de petróleo

Um pouco mais complicado, mas com um tratamento das frações de petróleo mais preciso, é considerar esta mistura complexa de hidrocarbonetos como uma mistura contínua. Nesta aproximação, a mistura não é expressa em termos de um número finito de pseudo-componentes e suas propriedades estão dadas por uma função de distribuição contínua. Este método é equivalente à aproximação por pseudo-componentes, mas com um número infinito de componentes (Rätzsch e Kehlen, 1983). Nesta aproximação no lugar de especificar um componente i , este é expresso por um de seus parâmetros característicos (temperatura normal de ebulição, T_b ou massa molar, M).

A representação da composição química da mistura complexa, dada por uma série de valores discretos de concentrações dos componentes, pode ser substituída por uma função de distribuição contínua (FDC) $F(I)$, onde o índice contínuo (I) está definido em termos de uma ou mais propriedades macroscópicas de caracterização, tais como ponto de ebulição (T_b), massa específica (ρ) ou massa molar (M).

Uma mistura na qual as concentrações de alguns dos componentes são dadas por valores discretos e outros são descritos por FDCs é chamada de mistura semi-contínua. No caso do petróleo, a mistura complexa de componentes, é uma mistura semi-contínua, formada por componentes discretos (hidrocarbonetos leves e gases inorgânicos como CO_2 , N_2 , H_2 , etc.) e uma distribuição contínua, representando todos os demais componentes (componentes não identificados como hidrocarbonetos pesados e componentes identificados) (Cotterman e Prausnitz, 1985).

Os primeiros trabalhos em termodinâmica semi-contínua foram realizados por Cotterman et al. (1985) em sistemas com polímeros e petróleo, onde se compararam os resultados das distribuições contínuas com aqueles dos componentes discretos. Kehlen et al. (1985) analisaram matematicamente a termodinâmica contínua, enfatizando as facilidades da abordagem no tratamento de misturas contendo muitos componentes, pois são melhores descritas por funções de distribuição, do que através de frações molares para componentes discretos.

2.3.1.2. Funções de distribuição utilizadas na termodinâmica contínua

Existem diversas funções matemáticas que podem ser usadas na representação da distribuição de propriedades termodinâmicas de misturas complexas (Tabela 3). Podem-se citar

entre outras, as funções normais ou gaussianas, exponenciais e log-normal. No entanto, Riazi (1989) apresenta a função Gamma, obtendo bastante sucesso quando é aplicada na representação de misturas complexas de hidrocarbonetos derivados do petróleo. Um ponto crucial para o sucesso da uma modelagem termodinâmica, sob a hipótese de continuidade da mistura, é a escolha do índice contínuo (I). Alguns autores escolhem um índice mais usual, como a massa molar ou ponto de ebulição (Du e Mansoori, 1986). Outra tendência mais recente desenvolvida por Peixoto et al. (2000) é de escolher como índice continuamente distribuído, o número de grupos funcionais presentes na molécula.

Tabela 3. Resumo de funções de distribuição continua.

Função de distribuição continua	Equação	Equação de distribuição	Parâmetros	Referência
*Gamma	(1)	$F(I) = \frac{(I - \eta)^{\alpha-1} \exp\left[-(I - \eta) / \beta\right]}{\beta^{\alpha} \Gamma(\alpha)}$	α, β, η	Whitson, 1983
Gaussiana	(2)	$F(I) = \frac{1}{\sqrt{2\pi}\sigma} \exp\left(-\frac{(I - \theta)^2}{2\sigma^2}\right)$	θ, σ	Shibata et al., 1987
Exponencial	(3)	$F(I) = \frac{1}{\eta} \exp\left(-\frac{(I - \sigma)}{\eta}\right)$	η, σ	Mansoori et al., 1989
**Generalizada	(4)	$(I^*) = \left[\frac{A}{B} \ln\left(\frac{1}{x^*}\right) \right]^{1/B} \quad \text{onde } I^* = \frac{I - I_0}{I_0} \text{ e } x^* = 1 - x$	A, B, I_0	Vakili-Nezhaad et al., 2001; Riazi, 1989

* η : Corresponde ao valor mais baixo de I na mistura.

** x corresponde à fração mássica, molar ou volumétrica acumulada.

Para este trabalho, a composição química da mistura é melhor representada, naturalmente, pela distribuição de uma propriedade termodinâmica que esteja diretamente relacionada com a volatilidade dos componentes. Sendo assim, a temperatura de ebulição é usada como propriedade de caracterização da mistura. De acordo com Vakili-Nezhaad et al. (2001), essa consideração simplifica significativamente a modelagem de caracterização de misturas complexas de hidrocarbonetos.

2.4. Avanços nas tecnologias dos processos para o *upgrading* de óleos pesados e fundos

Nas unidades de destilação atmosférica e de vácuo são geradas basicamente duas correntes de fundo: resíduo atmosférico como aquele material de fundo da coluna de destilação

atmosférica, o qual apresenta uma temperatura atmosférica equivalente (TAE) de 616,15 K⁺. Este resíduo constitui a carga da coluna de vácuo. O resíduo de vácuo constitui o produto de fundo da destilação a vácuo (3,33–13,33 kPa), obtido a uma temperatura TAE de 838,15 K⁺ (Rana et al., 2007; Maciel-Filho et al., 2006).

Um resíduo atmosférico possui componentes com número de carbonos superiores a 25 (C₂₅) e densidade API menor do que 20, enquanto, o resíduo de vácuo apresenta componentes com número de carbonos maiores de 50 e massa molar superior a 800 kg·kmol⁻¹. Os resíduos de petróleo (ou produtos de fundo das destilações atmosféricas e a vácuo) apresentam uma estrutura complexa e esta complexidade é incrementada na medida em que aumenta sua temperatura de ebulição, a massa molar, a densidade, a viscosidade, o índice de refração (aromaticidade) e a polaridade (conteúdo de heteroátomos e metais). Estes produtos são ricos em componentes polares como resinas e asfaltenos, possuem também espécies químicas de diferente aromaticidade, heteroátomos funcionais e alto conteúdo de metais, quando comparados com o óleo cru, ou frações leves. As alternativas para processamento de resíduos são divididas em duas rotas principalmente como se apresenta na Tabela 4 e descritas na continuação.

Tabela 4. Alternativas para o processamento de resíduos de petróleo (Rana et al., 2007).

Processos não-catalíticos		Processos catalíticos	
Desasfaltação com solvente Térmicos	Gaseificação	Craqueamento catalítico fluidizado	
	Coqueamento retardado	Hidroprocessamento	Hidrotratamento de leito fixo
	Coqueamento fluido		Hidro craqueamento de leito fixo
	<i>Flexicoking</i>		<i>Slurry hydrocracking</i>
	Viscorredução		Hidrotratamento em leito fluidizado borbulhante

2.4.1. Processos não-catalíticos para o processamento de resíduos de petróleo

As principais condições operacionais para processos térmicos são resumidas na Tabela 5.

Tabela 5. Condições de operação das tecnologias de processamento de resíduos de petróleo.

Tecnologia	Condições de Operação		Referência
	Temperatura (K)	Pressão (MPa)	
Coqueamento retardado	753,15–788,15	0.61	Guo et al., 2008; Rana et al., 2007; Rodríguez-Reinoso et al., 1998
Viscorredução	723,15–783,15	0.34–2.0	Dente et al., 1997; Rana et al., 2007; Bozzano et al., 2005; Benito et al., 1995; Omole et al., 1999
Coqueamento fluido	753,15–838,15	0.07	Rana et al., 2007
<i>Flexicoking</i>	1103,15–1273,15	0.07	Rana et al., 2007; Furimsky, 2000;
Gaseificação	>1273,15	–	Rana et al., 2007

Estes processos são caracterizados pelo baixo investimento e custos operacionais de hidroprocessamento, mas o rendimento de produtos leves tende a ser menor e o valor agregado de seus produtos, portanto, é menor. Além disso, os produtos líquidos obtidos a partir de processos térmicos contêm S, N e metais (V, Ni, etc) que realmente precisam de purificação através de hidrotratamento como HDS (*hydrodesulfurization*), HDN (*hydrodenitrogenation*) e HDM (*hydrodemetallization*), respectivamente (Rana et al., 2007).

2.4.2. Processos catalíticos para o processamento de resíduos de petróleo

O craqueamento catalítico consiste nas reações de quebra catalítica de moléculas de cadeias carbônicas de compostos pesados, tais como, gasóleo e resíduos de outros processos do refino do petróleo (resíduos de fundo da destilação atmosférica e a vácuo). A presença de catalisador sólido particulado a alta temperatura acelera a quebra das cadeias, produzindo hidrocarbonetos mais leves e de maior valor comercial.

A seguir, se apresenta uma breve descrição dos processos catalíticos: craqueamento catalítico fluidizado e hidrocraqueamento.

Craqueamento catalítico fluidizado (FCC)

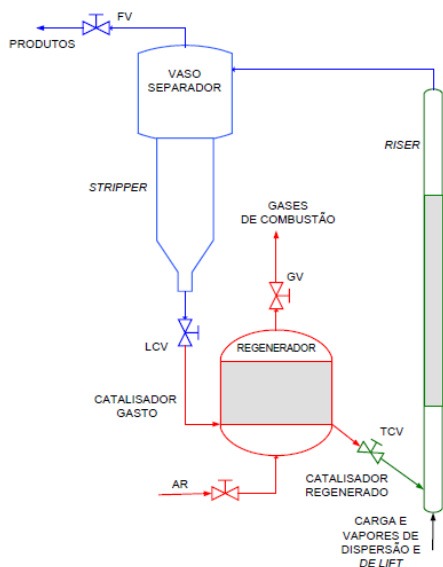
Este processo é utilizado nas refinarias para a conversão de produtos pesados em produtos mais leves, de maior valor agregado. Por exemplo, a produção de gasolina (iso-octano) e gás de cozinha (propano + butano) a partir do craqueamento catalítico dos gasóleos, e hoje, diesel (Pagani, 2009).

Características e vantagens

Fonte: Ribeiro, 2007; Vieira, 2002

- Ocorre em equipamentos chamados de conversores que são compostos basicamente de um tubo vertical (*riser*), um vaso separador/*stripper* e um regenerador.
- O FCC (Figura 1) é um processo utilizado para a conversão de hidrocarbonetos com massa molar mais elevada, tais como gasóleo (proveniente da unidade de destilação a vácuo) e resíduos do processo de refino do petróleo, em produtos mais leves e de maior valor comercial, através do contato com um catalisador pulverizado em condições apropriadas de processo.
- Grande flexibilidade, no sentido de ajustar sua produção às reais necessidades do mercado consumidor.
- Está ligado ao aspecto econômico das frações residuais, onde frações de baixo valor comercial são convertidas em derivados nobres de alto valor, tais como a gasolina e o GLP.

Descrição do processo



A carga de alimentação (gasóleo e resíduos), que é previamente aquecida, entra em contato com o catalisador (material sólido à base de sílica e alumina) a alta temperatura, provocando sua vaporização quase que instantânea.

Devido à ação da temperatura e das propriedades catalíticas do meio, as moléculas da carga são quebradas principalmente em compostos separados por três frações distintas: gás combustível, moléculas contendo 1 a 2 átomos de carbono, C1 e C2, de 3 a 12 átomos de carbono GLP (gás liquefeito de petróleo) e nafta de craqueamento (gasolina automotiva) de 5 a 12 átomos de carbono, C5 a C12 (LCO e óleo decantado).

Algumas destas correntes podem passar por processos de tratamento químico onde são reduzidos os teores de enxofre. No craqueamento também é formando o coque que consiste primordialmente de cadeias carbônicas não craqueadas, metais pesados e compostos aromáticos com características próximas a do grafite, que é o responsável tanto geração de energia quanto pela desativação do catalisador.

Fonte: Equipe Petrobras, 2002; Erthal, 2003; Ribeiro, 2007

Figura 1. Processo de craqueamento catalítico fluidizado. Fonte: (Erthal, 2003)

Hidrocraqueamento

O hidrocraqueamento (Figura 2) é um processo em 2 estágios, combinando o craqueamento catalítico e a hidrogenação.

Características e vantagens

Fonte: Equipe Petrobras, 2002

- Os produtos deste processo são hidrocarbonetos saturados; dependendo das condições de reação (temperatura, pressão, atividade catalítica), estes produtos variam de etano e GLP aos hidrocarbonetos pesados compostos principalmente de isoparafinas. Hidrocraqueamento normalmente é facilitado por um catalisador bifuncional que é capaz de reorganizar e quebrar cadeias de hidrocarbonetos assim como a adição de hidrogênio a aromáticos e olefinas para produzir naftenos e alcanos.
- Este processo emprega altas pressões, altas temperaturas, um catalisador e hidrogênio.
- A grande vantagem do hidrocraqueamento é sua extrema versatilidade. Pode operar com cargas que variam, desde nafta, até gasóleos pesados ou resíduos leves, maximizando a fração que desejar o refinador.
- Outra grande vantagem constatada é a qualidade das frações no que diz respeito a contaminantes.
- Diante das severíssimas condições em que ocorrem as reações, praticamente todas as impurezas, como compostos de enxofre, nitrogênio, oxigênio e metais, são radicalmente reduzidas ou eliminadas dos produtos.
- A desvantagem do processo consiste nas drásticas condições operacionais. Elevadas pressões e temperaturas são usadas, o que obriga a utilização de equipamentos caros e de grande porte, com elevado investimento.

Descrição do processo

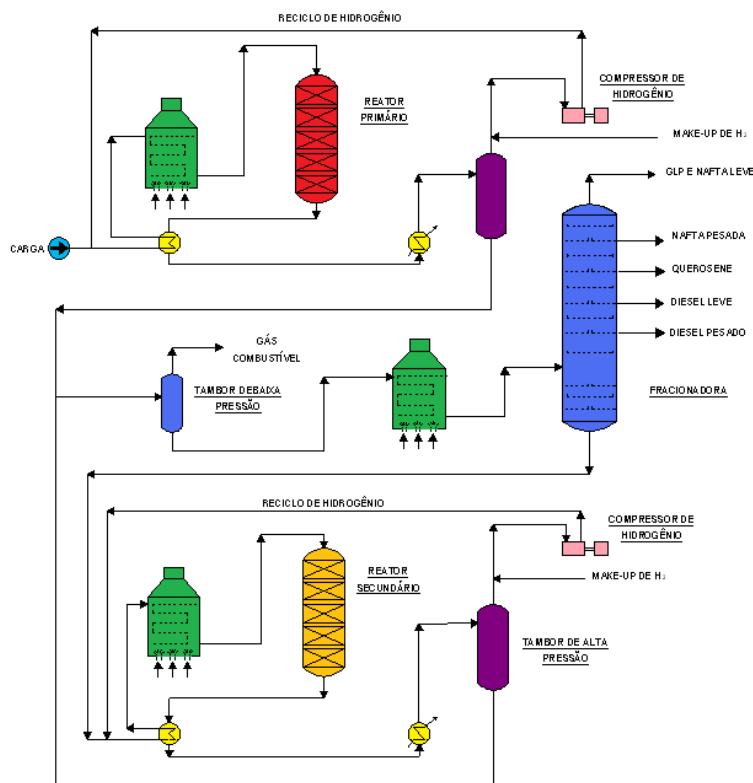


Figura 2. Processo de hidrocraqueamento.

Fonte: Equipe Petrobras. 2002

- No primeiro estágio, a carga pré-aquecida é misturada com um reciclo de hidrogênio e enviada para o primeiro estágio do reator, onde o catalisador converte os compostos de enxofre e nitrogênio em sulfeto de hidrogênio e amônia.
- Após os hidrocarbonetos deixarem o primeiro estágio, estes são resfriados e liquefeitos e em seguida passam por um separador. O hidrogênio é reciclado para voltar a misturar com a carga fresca. Dependendo dos produtos desejados (gasolina, combustível de aeronaves e gasóleo), o fracionador é ajustado para separar os produtos em uma determinada faixa.
- Os resíduos de fundo do fracionador são misturados com hidrogênio e enviados ao segundo estágio desde que esta material também esteja sujeito a hidrogenação e reforma. As operações do segundo estágio são mais severas (altas temperaturas e pressões) já que vai craquear resíduos mais pesados. Os produtos oriundos do segundo estágio são então enviados a coluna fracionadora.

Fonte: Souza et al., 2008; Equipe Petrobras. 2002; Souza. 2001.

2.5. Opções tecnológicas não-convencionais

2.5.1. O processo de destilação molecular

O processo de destilação molecular teve seu desenvolvimento, inicialmente, nos Estados Unidos e Europa na década de 30 para permitir a purificação de produtos termicamente sensíveis. Na América Latina, os trabalhos de Destilação Molecular foram iniciados no Brasil com os trabalhos realizados no LDPS/LOPCA/UNICAMP com o trabalho de Batistella (1996) na área de química fina e com posteriores trabalhos na área de óleos lubrificantes e frações de petróleo (Tovar et al., 2011; Zuñiga-Liñan et al., 2011; Tovar et al., 2010; Medina et al., 2010; Zuñiga, 2009; Zuñiga et al., 2009; Zuñiga et al., 2009; Hernández, 2009; ; Winter et al., 2009; Rocha, 2009; Hernández et al., 2008; Lopes, 2008; Rocha, 2008; Rocha et al., 2008; Fregolente et al., 2007; Liñan et al., 2007; Lopes et al., 2007; Rocha et al., 2007; Winter, 2007; Winter et al., 2007; Martins et al., 2006; Martins et al., 2006; Sbaite et al., 2006; Maciel-Filho et al., 2006; Moraes et al., 2006; Winter et al., 2006; Fregolente et al., 2005; Sbaite, 2005; Winter et al., 2004; Sbaite et al., 2003; Batistella et al., 2002; Batistella et al., 2000; Batistella e Wolf-Maciel, 1998, 1996). A destilação molecular constitui um tipo de processo de vaporização a baixas pressões e, portanto, baixas temperaturas, que apresenta utilidade na separação e purificação de materiais com baixa volatilidade, bem como para aqueles que apresentam sensibilidade térmica (Tovar et al., 2011; Zuñiga-Liñan et al., 2011; Tovar et al., 2010; Zuñiga et al., 2009).

O interesse atual sobre o processo de destilação molecular é crescente devido às suas vantagens industriais e sua aplicabilidade nas indústrias de cosméticos, alimentos, farmacêutica, química, petroquímica, plásticos entre outras, para a recuperação, purificação e concentração de substâncias (Catálogo UIC GmbH, 2010).

2.5.1.1. Características operacionais de destilação molecular

A destilação molecular se caracteriza por tempos de residência curtos, cujos valores variam entre 1 e 10 s (Lutišan e Cvengroš, 1995) e, em alguns casos, pode chegar até a 0,2 s (Holló et al., 1971), apresentar alta taxa de evaporação ($20\text{--}40\text{ g}\cdot\text{m}^{-2}\cdot\text{s}^{-1}$) (Cvengroš et al., 2000) e empregar baixa pressão ($0,13\text{ Pa} - 0,0133\text{ Pa}$) (Batistella, 1996). O uso de baixa pressão, além de eliminar a oxidação que pode acontecer na presença de ar (Burrows, 1973), permite a utilização de temperaturas mais brandas na separação quando comparado aos processos convencionais de

destilação e evaporação, fato que, juntamente com o pequeno tempo de residência, minimiza as perdas por decomposição térmica.

2.5.1.2. O comportamento da fase vapor

Lutišan e Cvengroš (1995) descreveram a fase vapor a partir das variáveis macroscópicas do processo de destilação molecular apresentadas na Tabela 6.

Tabela 6. Variáveis macroscópicas do processo de destilação molecular.

Variável macroscópica	Relação no processo de destilação molecular	Formulação matemática	Equação
Velocidade de evaporação	<p>↓, com o aumento de colisões mútuas das moléculas evaporadas.</p> <p>↓, pelas colisões das moléculas evaporadas com as moléculas do gás residual.</p> <p>↑, com o incremento de calor ao sistema, gera-se um aumento de temperatura, induzindo a um incremento na pressão de vapor.</p>	$\dot{G}_q = P_q^{vap} \sqrt{\frac{M_q}{2\pi R_g T_s}}$	(5)
Densidade das moléculas	<p>↑, com o aumento da temperatura do condensador Este comportamento se apresenta porque as moléculas já condensadas na superfície do condensador voltam a evaporar em consequência do incremento da temperatura, fenômeno este conhecido como re-vaporização.</p>	$n = \frac{N_c}{V_c}$	(6)
O livre percurso médio	Corresponde à média das distâncias percorridas por uma molécula entre duas colisões sucessivas com moléculas do mesmo tipo ou com moléculas de outro componente.	$MFP = \frac{1}{(4/3)\pi\delta^2 N}$	(7)

↑ Corresponde ao aumento da variável macroscópica no processo de destilação molecular; ↓ Corresponde à diminuição da variável macroscópica no processo de destilação molecular; P_q^{vap} é Pressão de vapor do componente na superfície do filme; M_q é a massa molar do componente q; R_g é a constante universal dos gases; T_s é a temperatura na superfície do filme; n é o número de moléculas por metro cúbico de gás; N_c é o número de moléculas no volume V_c ; n é a densidade da molécula; δ é o diâmetro da molécula e N é o número de moléculas por unidade de volume.

2.5.2. O processo de destilação molecular reativa: processo híbrido e intensificado

A intensificação de processos é uma abordagem revolucionária para processar, implementar e desenvolver processos, proporcionando desafios e oportunidades inovadoras para as indústrias, a fim de aumentar a produtividade, flexibilidade, segurança e, diminuir o consumo de energia, geração de resíduos e custo operacional sem prejudicar a qualidade do produto, seguindo uma das rotas descritas por Keil (2007) na Figura 3.

Outras definições apresentadas no livro autorado por Keil (2007) são:

Cross e Ramshaw (1986) definem a intensificação de processos como: “Um termo usado para descrever a estratégia de redução de tamanho da planta de produtos químicos necessários para atingir um objetivo de produção determinado”.

Stankiewicz e Moulijn (2002) definiram a intensificação de processos como: “Qualquer desenvolvimento na engenharia química que permita uma tecnologia limpa e energeticamente mais eficiente”.

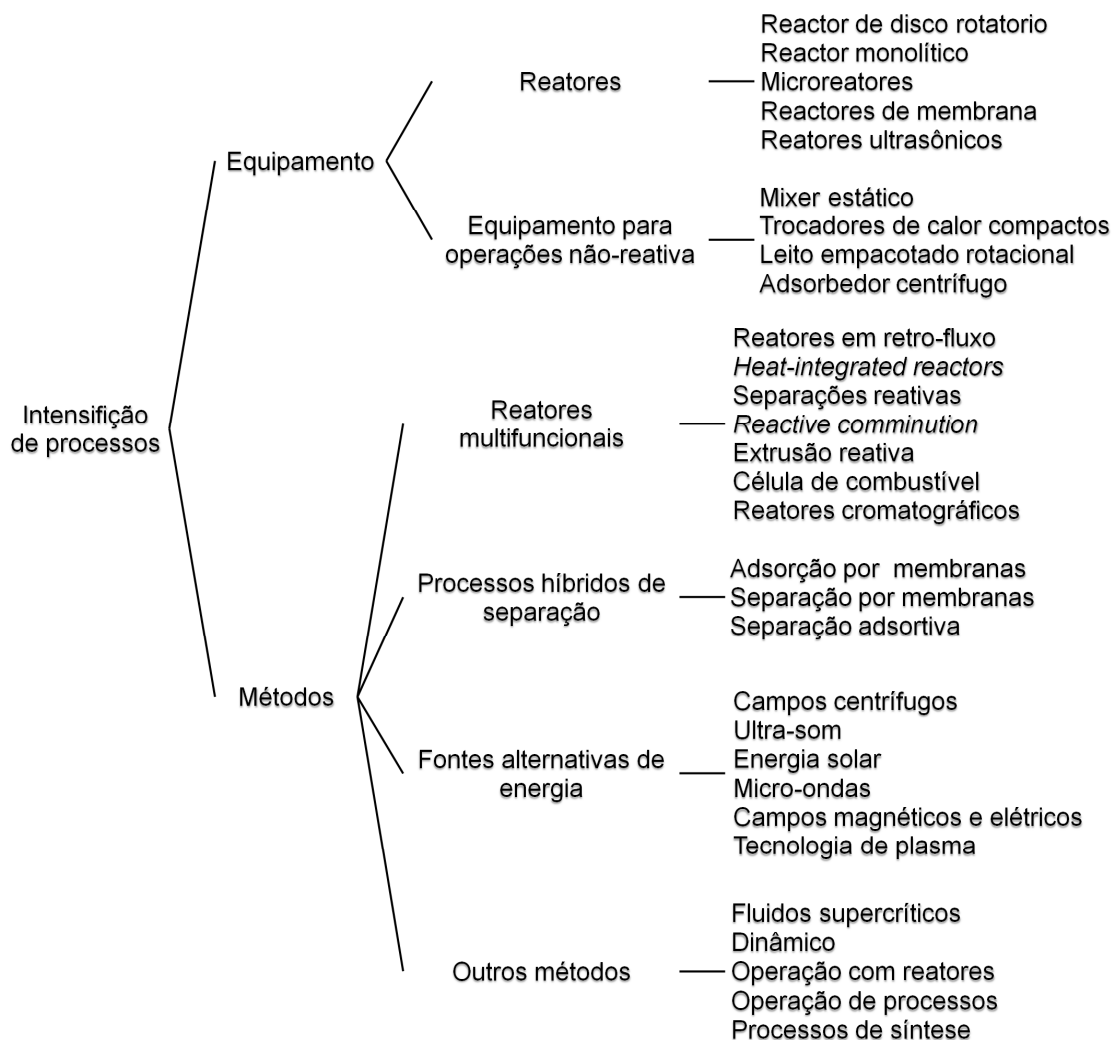


Figure 3. Intensificação de processo. Adaptado: Keil, 2007.

Em resumo, a intensificação do processo consiste no desenvolvimento de novos equipamentos, métodos, processos e técnicas na área de engenharia química, que quando comparado com a atual, traz melhoras na produção, diminuindo substancialmente o tamanho do equipamento sem prejudicar a capacidade de produção (redução dos investimentos e dos custos das matérias-primas), com a diminuição do consumo de energia (redução dos custos), e/ou diminuição da produção de resíduos. Por conseguinte, as vantagens que oferece a intensificação

de processos na engenharia química e na engenharia de processo chegam a ser resumidas em seis elementos principais: custos, segurança, compactação, condições controladas, eficiência e tempo (Stankiewicz e Moulijn, 2002).

Portanto, a Tese de Doutorado abrange o desenvolvimento em nível computacional (modelagem e simulação) e experimental do processo de destilação molecular reativa, no qual acontece o acoplamento de destilação molecular e conversão (reação química) simultaneamente, podendo ser qualificado como um processo híbrido e também como um processo intensificado, dado a configuração do equipamento e as condições operacionais, que viabilizam a implementação de alto vácuo, permitindo submeter o material a temperaturas adequadas, num curto tempo operacional, garantindo um contato muito intenso da amostra com a superfície catalítica. Estes fatores devem proporcionar alta cinética de reação e alta taxa de evaporação permitindo altas taxas de processamento.

Assim sendo, com o desenvolvimento do processo de destilação molecular reativa obtêm-se ganhos em termos de conversões e separação de produtos, apresentando por sua vez características vantajosas e favoráveis à intensificação de processos, seguindo a classificação de Keil (2007) tais como:

- Condições experimentais de temperatura e pressão mais afáveis com o processamento da carga favorecendo a reação de craqueamento, que levam a um melhor controle dos produtos convertidos numa única etapa de processo.
- Maior contato dos reagentes (alimentação) com a superfície do catalisador o que permite um incremento na taxa de transferência de massa dadas as condições de processo.
- Abordagem multidisciplinar, que considera as oportunidades para melhorar a tecnologia de processo de forma simultânea com o acoplamento de dois processos separação/craqueamento.

Com respeito à modelagem do destilador molecular reativo, esta está baseada na modelagem desenvolvida para o processo de destilação molecular. Ela foi devidamente adaptada, com objetivo de fazer estudos de predição e também de avaliação do processo, levando à condução de trabalhos experimentais em condições já otimizadas e mesmo possibilitando, a priori, a verificação dos resultados que seriam conseguidos com uma aplicação experimental.

Equações de balanço de massa, de energia e momento, foram consideradas nesta modelagem. A taxa de evaporação considerada foi a de evaporação efetiva de Langmuir, levando em consideração os efeitos da fase vapor e o grau de anisotropia do sistema.

O termo cinético reativo foi incorporado ao modelo. A equação da cinética de reação foi aplicada para determinar a conversão química através das concentrações de cada componente na superfície do evaporador.

2.5.2.1. Considerações teóricas sobre a destilação molecular centrífuga reativa

Durante a destilação molecular centrífuga reativa (Figura 4), o líquido a ser processado flui ao longo da superfície cônica do evaporador devido à força centrífuga e gravitacional e é distribuído homogeneamente na superfície do evaporador na forma de um filme muito fino com uma espessura que depende da viscosidade da mistura e das condições operacionais de vazão de alimentação e velocidade do rotor.

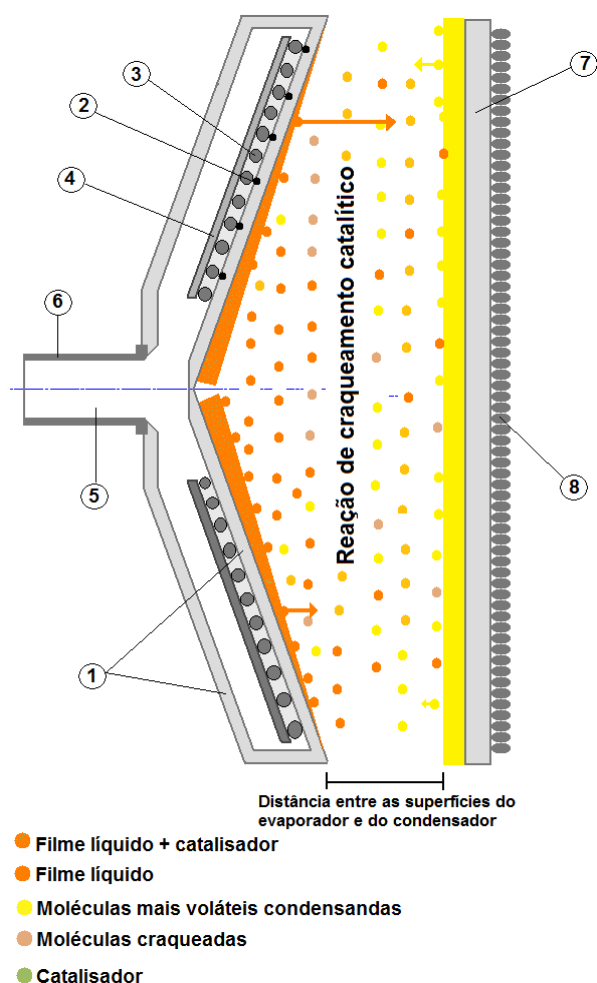


Figura 4. Vista lateral esquemática do processo de destilação molecular centrífuga reativa. 1. Superfície do evaporador 2. Termopar; 3. Resistência elétrica; 4. Suporte da resistência; 5. Furo do eixo; 6. Eixo 7. Superfície do condensador; 8. Serpentina de arrefecimento.

A reação de craqueamento e a separação dos componentes da mistura no destilador molecular centrífugo reativo ocorrem basicamente em cinco (05) etapas:

- *Etapa 1:* Reação catalítica nas camadas internas do filme que escoam sobre a superfície do evaporador (Figura 5a).
- *Etapa 2:* Transporte das moléculas craqueadas nas camadas internas do filme e evaporadas desde a mistura líquida até a superfície livre do filme.
- *Etapa 3:* Destilação da mistura (componentes de alta massa molar e componentes de menor massa molar quando comparado com a alimentação) desde a superfície livre do filme.
- *Etapa 4:* Transporte das moléculas evaporadas na superfície livre do filme através do espaço da destilação (distância entre a superfície de evaporação e a superfície de condensação).
- *Etapa 5:* condensação da(s) molécula(s) evaporada(s) mais volátil(eis).

Assim, para a simulação, foi considerado como caso de estudo o processamento de um resíduo atmosférico do petróleo “W” (ATR–W) 673,15 K⁺, em um destilador molecular centrífugo reativo aquecido, onde a superfície do evaporador constitui uma superfície cônica. O resíduo atmosférico total foi dividido em 02 pseudo–componentes, os quais foram caracterizados utilizando dados de propriedades físico–químicas geradas pelo simulador desenvolvido por Tovar et al. (2011).

Em relação ao desenvolvimento experimental, ensaios foram desenvolvidos entre 473.15 e 523.15 K considerando na carga do processo 1, 3 e 5% m/m de catalisador, constituindo um processo em catálise heterogênea (termo que descreve a catálise quando o catalisador está em uma fase diferente (ou seja sólido) aos reactantes). Como resultados foram obtidos quinze cortes de destilados e quinze de resíduos do processo de destilação molecular centrífuga reativa, cujas propriedades de massa molar, viscosidade, massa específica e °API foram avaliadas utilizando técnicas cromatográficas (SEC do inglês size–exclusion chromatography), análises reológicas e métodos padronizados (ASTM D 4052, ASTM D 5002 e ASTM D 70).

2.6. Considerações finais

Neste capítulo foi apresentada uma breve revisão dos principais conceitos envolvidos no petróleo, sua composição, tecnologias catalíticas e não-catalíticas para o processamento de resíduos pesados, assim como opções tecnológicas para o processamento destas matérias-primas. Também foi apresentado o processo de destilação molecular reativa, objeto de estudo nesta Tese de Doutorado, como um processo híbrido e intensificado.

De acordo com os objetivos e delineamentos do processo de destilação molecular reativa, o óleo cru pesado e as frações pesadas de petróleo constituíram a matéria-prima para o sistema de separação – reacional não-convencional, representando um considerável avanço no sistema de análise desses materiais e proporcionando um melhor aproveitamento destes materiais, além de ganhos na qualidade e rendimento dos produtos finais.

A modelagem e a simulação da destilação molecular reativa constituem uma ferramenta fundamental de auxílio na consolidação da tecnologia de destilação molecular reativa como processo híbrido e intensificado, no qual, através de simulações, considerando diferentes condições do processo, será possível obter informações rápidas e confiáveis sobre o desempenho do mesmo.

Além disso, os resultados provenientes do desenvolvimento computacional (modelagem e simulação) do processo de destilação molecular centrífuga reativa de óleo cru pesado e frações pesadas permitirão o estabelecimento de novas condições operacionais à escala piloto, visando à obtenção de um alto desempenho operacional da unidade, como: a redução do consumo de energia e utilidades, a minimização da quantidade de resíduos e o melhor rendimento de separação, características de um processo intensificado.

Finalmente, um salto tecnológico está sendo dado, em matéria de modelagem, simulação e experimentação, no processo de fracionamento, separação e conversão do petróleo e suas frações pesadas obtidos das destilações atmosféricas e de vácuo, pois com uma melhor conversão do petróleo através da proposta tecnológica, poderão ser estabelecidas estratégias e condições operacionais que, seguramente, favorecerá a cadeia produtiva do petróleo.

Capítulo 3

Enfoque computacional para a caracterização físico-química de frações de petróleo visando à modelagem do processo de destilação molecular reativa

3.1. Introdução

O petróleo constitui uma mistura complexa de hidrocarbonetos formados na rocha sedimentar como consequência da conversão de componentes orgânicos em hidrocarbonetos (parafinas, oleofinas, naftênos e aromáticos), os quais são encontrados como gases (gás natural), líquidos (óleo cru), semi-sólidos (betumem), ou sólidos (asfalto) (Riazi, 2004).

Atualmente, os investimentos em tecnologia na área de petróleo estão em ascensão, sendo esses imprescindíveis, tanto para viabilizar a sua produção, disponível nas reservas brasileiras como, também, para o refino desse, que possui características físico-químicas diferentes dos petróleos encontrados em outras regiões. Esse crescimento levou à implantação de inúmeras empresas nesse setor e o desenvolvimento de projetos de pesquisa e engenharia, que apresentam um viés tecnológico, a fim de garantirem uma melhora no rendimento e qualidade do óleo, aumentando, com isso, a competitividade na área do petróleo no Brasil.

Em se tratando de misturas indefinidas, métodos particulares para sua caracterização são necessários. Essa caracterização, experimentalmente, é obtida através das normas ASTM e curvas de destilação, que visa modelar o comportamento do petróleo, das correntes das frações pesadas e ultra-pesadas. Um artifício usado é a caracterização das frações como um conjunto de pseudo-componentes, em número suficiente para descrever as propriedades físico-químicas de interesse.

A proposta deste capítulo compreende o desenvolvimento de uma metodologia teórica baseada em abordagens de pseudo-componentes discretos e contínuos. Este procedimento constitui uma tentativa para prever o comportamento de tais misturas com a menor quantidade de dados de entrada necessários.

Na literatura existem aproximações que representam as propriedades dos petróleos em estudo. Uma delas é a aproximação por contribuição de grupos. Essa metodologia necessita conhecer a composição química, em termos de estruturas, por tipo de átomo de carbono. Uma das suas desvantagens é a de apresentar desvios acentuados, especialmente para frações pesadas, e por essa razão, não tem sido utilizada com frequência.

Outra abordagem são os modelos que utilizam como componentes bases (hidrocarbonetos Parafínicos, Naftênicos e Aromáticos) (Quann e Jaffe, 1992 e Hu e Zhu, 2001). Nesse caso, o óleo cru, fração ou corte obtido através de uma destilação é representado por um conjunto de componentes fictícios (componentes base) de mesma massa molar (Riazi, 2004) ou mesmo número de átomos de carbono (Danesh, 1998).

Indistintamente, Coats (1985) fez uma contribuição importante ligada à simulação computacional, criando um agrupamento de componentes, que ficou conhecida como “pseudoização”. Essa contribuição teve como objetivo reduzir o número de elementos necessários para a representação de um fluido, com consequente redução do processamento computacional.

Um pseudo-componente está primeiramente definido por sua (pseudo) temperatura de ebulição e por alguns parâmetros, principalmente, gravidade específica, massa molar ou viscosidade. As propriedades físicas restantes (sendo elas as propriedades termodinâmicas e termofísicas) precisam ser estimadas. Em Miquel e Castells (1993 e 1994) é apresentada uma metodologia computacional para a previsão das propriedades onde se caracterizaram e se agruparam os compostos da mistura, formando uma série de pseudo-componentes baseada na premissa de um fator de caracterização (Kw) constante.

Dessa forma, a metodologia descrita por Miquel e Castells (1993 e 1994) foi adotada no trabalho com modificações nas sub-rotinas de cálculo e nas correlações das estimativas das propriedades básicas e termodinâmicas.

Mais uma abordagem analisada no trabalho utiliza o conceito da termodinâmica de misturas contínuas ou semi-contínuas, a qual é chamada por muitos autores de termodinâmica contínua (Cotterman e Prausnitz, 1985; Cotterman et al., 1985; Rätzsch e Kehlen, 1983; Shibata et al., 1987). A distribuição contínua ou termodinâmica contínua é usada para descrever uma mistura complexa de componentes (não identificados, como hidrocarbonetos pesados, e

componentes identificados), através de uma função de distribuição, seja analítica ou numérica. Esse método relaciona uma ou mais variáveis mensuráveis, tais como, a massa molar ou a temperatura de ebulição com a composição da mistura.

A resposta das metodologias desenvolvidas fornecerá valores das propriedades básicas (temperatura de ebulição normal e densidade), e das propriedades termodinâmicas (composição mássica e molar, temperatura crítica, pressão crítica e fator acêntrico) para cada pseudo-componente. Todas essas informações são obtidas a partir da entrada de dados experimentais das propriedades (curva de destilação PEV e densidade da fração completa), que tradicionalmente são medidas em laboratórios.

Frente ao exposto, torna-se claro o destaque que os temas relacionados à caracterização e a determinação das propriedades físico-químicas das frações do petróleo têm no desenvolvimento de estudos teóricos e experimentais de técnicas de processamento dessas amostras. Dessa forma, os resultados provenientes desta primeira fase permitirão a obtenção das propriedades físico-químicas, através das correlações empíricas reportadas na literatura, através da sua comparação com as análises experimentais; Visa-se, assim, a sua inserção na modelagem matemática e na simulação do processo da destilação molecular reativa.

3.2. Desenvolvimento

O desenvolvimento deste capítulo é apresentado a seguir, nos manuscritos intitulados:

- *Overview and computational approach for studying the physicochemical characterization of high-boiling-point petroleum fractions (350 °C⁺)*, a ser publicado no periódico internacional *Oil & Gas Science and Technology – Revue d'IFP Energies nouvelles* (aceptado para publicação em 24 de Agosto de 2011, doi:10.2516/ogst/2011150).
- *Development & application of continuous thermodynamics to predict physicochemical properties of petroleum fractions*, publicado nos anais, respectivamente, do *Distillation Absorption 2010 (DA2010)*, September 12–15 2010, Eindhoven, The Netherlands / Ed. A.B. de Haan, H. Kooijman, A. Górak. – Eindhoven, The Netherlands : DA2010, 2010. – ISBN 978-90-386-2215-6. – p. 503–508.

Source: From Tovar L. P., Wolf Maciel M. R., Maciel Filho R., Batistella C. B., Ariza O. C., Medina L. C. (2011) Overview and computational approach for studying the physicochemical characterization of high-boiling-point petroleum fractions (350 °C+). Oil Gas Sci. Technol. – Rev. IFP doi:10.2516/ogst/2011150.

Copyright notice: The content of this manuscript is licensed under the Ethical Guidelines to Publication of Oil & Gas Science and Technology – Revue d'IFP Energies nouvelles. Please contact credited rights holders directly for permission to reproduce material.

Overview and computational approach for studying the physicochemical characterization of high-boiling-point petroleum fractions (350 °C⁺)

Abstract

The processing and upgrading of high-boiling-point petroleum fractions (350 °C⁺), containing a large number of components from different groups (paraffins, olefins, naphthenes, aromatics) require an in-depth evaluation. In order to characterize them, their thermodynamic and thermophysical properties must be determined. This work presents a computational approach based on the breakdown of the petroleum fraction into pseudocomponents defined by a trial-and-error exercise in which the mass- and molar- balance errors were minimized. Cases studies are illustrated to three heavy residues 400°C⁺ of “W, Y and Z” crude oil. This procedure requires the boiling point distillation curve and the density of the whole fraction as the input bulk properties. The methods proposed according to available correlations in the literature and standard industrial methods were mainly used to estimate properties that include the basic properties (normal boiling point, density and Watson factor characterization), the thermodynamic properties (molar mass and critical properties) and the thermophysical and transport properties (kinematic viscosity, thermal conductivity, specific heat capacity and vapor pressure). The methodology developed has shown to be a useful tool for calculating a remarkably broad range of physicochemical properties of high-boiling-point petroleum fractions with good accuracy when the bulk properties are available, since computational approach gave an overall absolute deviation lower than 10% when compared with the experimental results obtained in the research laboratories LDPS /LOPCA / UNICAMP.

Keywords: Computational approaches, pseudocomponent breakdown, high-boiling-point petroleum fractions, property estimations

Contents

1. Introduction
 - 1.1. Pseudoization method for the characterization
2. Overview of the estimation of the physicochemical properties
 - 2.1.1. Characterization of the average boiling points
 - 2.1.2. Characterization factor
 - 2.2. Estimation of the thermodynamic properties
 - 2.3. Methods for estimating the thermophysical and transport properties
 - 2.3.1. Estimation of transport properties
 - 2.3.1.1. Generalized viscosity correlations
 - 2.3.1.2. Thermal conductivity–temperature correlations
 - 2.3.2. Estimation of thermal properties
 - 2.3.2.1. Specific heat capacity
 - 2.3.2.2. Vapor pressure
3. Computational framework
 - 3.1. High–boiling–point petroleum fractions samples and data requirements
 - 3.2. Pseudocomponent breakdown methodology
 - 3.3. Correlations and predictive technique availability
 - 3.3.1. Computational procedure description
4. Experimental data
 - 4.1. Thermal analyses: differential scanning calorimetry (DSC)
 - 4.2. Rheological measurements
5. Results and discussion
 - 5.1. Simulated boiling point data and pseudocomponent distribution
 - 5.2. Determination of the basic and thermodynamic properties
 - 5.2.1. Density and molar mass distributions in the pseudocomponents
 - 5.2.2. Critical properties
 - 5.2.2.1. Reliable critical property correlations
 - 5.2.2.2. Data for the pseudocritical properties of high–boiling–point petroleum fractions
 - 5.3. Thermophysical properties of the whole fractions
 - 5.3.1. Transport properties
 - 5.3.1.1. Kinematic Viscosity
 - 5.3.1.2. Thermal Conductivity
 - 5.3.2. Thermal properties
 - 5.3.2.1. Specific heat capacity
 - 5.3.2.2. Predicted vapor pressure
6. Conclusions
- Acknowledgements
- Nomenclature
- References

1. Introduction

Investment in technology in the petroleum industry is increasing and this is essential both to enable the use of available oil reserves worldwide, and to refine petroleum with different

physical and chemical characteristics. This growth has led to the establishment of numerous companies in this sector and the development of research and engineering projects with technological bias, in order to ensure improvement in petroleum yield and quality, increasing competitiveness in this sector.

Petroleum fractions are undefined mixtures of hydrocarbon compounds with a limited boiling point range, and their properties depend on their compositions and types of hydrocarbon present in the mixture (aromatics, paraffins, olefins, and naphthenes). Subsequently, in the field of production, refining, processing and upgrading technologies for petroleum fractions, the values of the basic, thermodynamic and thermophysical properties must be available (Merdrignac and Espinat, 2007).

In general, three classes of predictive correlations are published in the open literature: (i) One class contains the group contribution method, but it can not be used for mixtures of unknown structure and composition (e.g. high-boiling-point petroleum fractions); (ii) another approach is via models using basic components (paraffinic hydrocarbons and naphthenic compounds) (Hu and Zhu, 2001; Quann and Jaffe, 1992). In this case, the crude oil, fraction or cut obtained by distillation, is represented by a set of hypothetical components (basic components) of the same molar mass (Riazi, 2004) or even with the same number of carbon atoms (Danesh, 1998). (iii) The last class comprises a pseudoization approach, where the properties are estimated from their basic properties, such as the boiling point (T_b), specific gravity (SG) and Watson factor characterization (K_w) (Daubert and Danner, 1997).

Hence, this work presents an accurate computational approach used for evaluating and estimating the physicochemical properties of three (03) petroleum fractions (high-boiling-point petroleum fractions). The petroleum fraction was broken down into pseudocomponents based on the knowledge of their global properties such as the boiling point distillation data (BP) of the whole fraction and the specific gravity (SG). The methodology adopted in this work was based on the procedure presented by Miquel and Castells (1993, 1994). The aim of the work consisted of two parts. (i) The first part consisted of the estimation of the basic properties and the thermodynamic properties (such as molar mass (M), density (ρ) and critical properties (critical temperature (T_c), critical pressure (P_c), critical volume (V_c) and acentric factor (ω_{ac})) based on a route for the minimization of the error, depending on the type of correlation set used; and (ii) the

second part consisted of the estimation of the thermophysical properties (kinematic viscosity (ν), thermal conductivity (λ), specific heat capacity (C_p) and vapor pressure (P_{vap})). The characterization procedure was carried out for each whole fraction and for the set of pseudocomponents (NPSE), identifying each physicochemical property with a subscript NPSE. The choice of correlation depends on: (a) the use of the specific property or the input data to predict another property; and (b) the accuracy and range of applicability of the property. The reliability of the data estimated by the computational approach (pseudoization method) was determined by comparison with the experimental information. Taking into account that the modeling approach is not exact, but approximate, its inaccuracy was evaluated by approximation regarding to experimental data. Results estimated in order to retry the basic properties of the entire fractions were evaluated in terms of the minimization of mass– and molar– balance error. On the other hand, thermophysical and transport properties, in the temperature range between 350 K and 600 K, were evaluated in terms of average absolute deviation ($AAD\%$) which is define as a relation among the absolute deviation of estimating a quantity divided by its experimental value ($y_{i,ref}$). The absolute deviation is defined as the difference between the observed value ($y_{i,ref}$) and the response predicted by the modeling approach at each operating condition ($y_{i,cal}$) as follows:

$$AAD\% = (1 / m) \sum_{i=1}^m \frac{|y_{i,cal} - y_{i,ref}|}{y_{i,ref}} * 100 \quad (1)$$

1.1. Pseudoization method for the characterization

The pseudoization approach for petroleum fractions was developed in several research projects, independent of the kind of compound.

Coats (1985) made an important contribution to connected computer simulation by creating a grouping of dummy components. This approach is known as pseudoization, and it aims to reduce the number of elements necessary to represent a fluid, reducing the computational effort. A pseudocomponent was defined primarily by its (pseudo) normal boiling temperature and by some other parameters, specifically the specific gravity (SG) and molar mass (M) or kinematic viscosity (ν).

Schlijper (1986) developed a method in which a pseudocomponent represented a mixture of components, and thus the thermodynamic behavior of the mixture was determined from the equation–of–state.

Miquel and Castells (1993, 1994) presented a computational methodology for predicting the properties of components of a mixture based on the hypothesis of constant Watson's characterization factor, K_w , for all the pseudocomponents of the mixture.

Beer (1994) described a method for the characterization of petroleum fractions and for the breakdown of pseudocomponents. This approach requires an inspection of the ASTM analyses or TBP (True Boiling Point) distillation curves as the input data.

Riazi and Al-Sahhaf (1996) developed a generalized correlation for the properties of several homologous series of hydrocarbons in terms of their molar mass. This approach can be applied to hydrocarbons up to C_{50} .

Eckert and Vaněk (2005) presented a brief description of the pseudoization approach for the characterization of petroleum fractions.

Nichita et al. (2008) proposed an approach for the modeling of wax precipitation from hydrocarbon mixtures. The modeling requires extended compositional data for the high-boiling-point petroleum fractions. The method is based on lumping into pseudocomponents, which reduces the dimensionality of the phase equilibrium calculations without affecting the location of the solid phase transitions.

Satyro and Yarranton (2009) suggested a procedure based on the representation of the mixture of real components that boil within a certain boiling point interval, by hypothetical components that boil at the average normal boiling temperature. This procedure is advantageous, since it is completely general and is not based on a specific thermodynamic model for the mixture.

2. Overview of the estimation of the physicochemical properties

The physicochemical properties are perhaps one of the most important factors in both experimental and theoretical researches, since they are needed to predict the performance of the process, the behavior of the material under the operating conditions and the modeling and the simulation of the industrial processes.

However, important limitations in the use of the methods are present, such as the availability of the input parameters e.g. some critical property of the petroleum fractions and the range of applicability of the methods. Thus, an inadequate estimation of the physicochemical

properties of the high-boiling-point petroleum fractions may result in low reliability of the prediction of the performance process under study (Riazi, 2004). Hence, specific methods for the estimation of the basic, thermodynamic, thermophysical and transport properties are given in the following sections.

2.1. Prediction of the basic properties

2.1.1. Characterization of the average boiling points

High-boiling-point petroleum fractions, being mixtures of several compounds, present an average boiling point, which is inappropriate from the physical point of view, since volatility is associated with a single boiling point. However, even though it is considered inadequate to define the average boiling point of a mixture, this is the usual practice, because it allows the estimation of the properties of the petroleum fractions and petroleum cuts by standard industrial methods and for a correlation with values cited in the literature. Thus, Watson et al. (1935) proposed methods to calculate the so-called average boiling point of the whole mixture, as presented in Equations (2) – (6) from Table 1.

Table 1. Summary of average boiling points for a multicomponent mixture.

Average boiling point	Correlation	Equation
Volumetric average boiling point (<i>VABP</i>)	$VABP = \sum_{i=1}^n x_{vi} T_{bi}$	(2)
Molar average boiling point (<i>MABP</i>)	$MABP = \sum_{i=1}^n x_{mi} T_{bi}$	(3)
Weight average boiling point (<i>WABP</i>)	$WABP = \sum_{i=1}^n x_{wi} T_{bi}$	(4)
[‡] Cubic average boiling point (<i>CABP</i>)	$CABP = \left(\frac{1}{1.8} \right) \left[\sum_{i=1}^n x_{vi} (1.8 T_{bi} - 459.67)^{1/3} \right]^3 + 255.37$	(5)
[‡] Mean average boiling point (<i>MeABP</i>)	$MeABP = \frac{MABP + CABP}{2}$	(6)

[‡]Riazi, 2004

n : Number of components (or pseudocomponents); *i* : Component (or pseudocomponent); *x_{vi}* : Volume fraction of component (or pseudocomponent *i*); *x_{mi}* : Mole fraction of component (or pseudocomponent *i*); *x_{wi}* : Weight fraction of component (or pseudocomponent *i*); *T_{bi}* : Normal boiling point of pseudocomponent *i* in Kelvin.

2.1.2. Characterization factor

The Watson characterization factor (*K_w*) or Universal Oil Products Company (UOP) characterization factor (*K_{OUP}*) is the ratio of the cube root of the absolute boiling point (of a pure

component) or the average normal boiling point for petroleum cuts to the specific gravity. It is used as an approximate index of the paraffinicity of a petroleum cut, thus a high value for this index indicates a high percent of saturated pure components and paraffin components (Gharagheizi and Fazeli, 2008; Watson and Nelson, 1933).

The K_w is defined as follows:

$$K_w = K_{OUP} = \frac{\sqrt[3]{1.8T_b}}{SG} \quad (7)$$

$$SG = \frac{\rho}{\rho_{water}} \quad (8)$$

Where, T_b is the normal boiling point; and for whole petroleum fraction is the mean average boiling point ($MeABP$) (in Kelvin). Therefore, the SG is the ratio of its density (ρ) to the density of the water (ρ_{water}) at 288.15 K (15.6 °C or 60 °F).

2.2. Estimation of the thermodynamic properties

The critical properties (T_c , P_c , V_c and ω_{ac}) of unknown mixtures can be estimated as a function of T_b and SG (Boozarjoomehry et al., 2005). The critical properties are parameters commonly used by process simulators in the design of unit operations and in the estimation of the thermophysical properties. Several methods have been proposed and some are presented in Equations (9) – (17) from Table 2. For estimating M , the methods available are very similar to those used in the determination of the critical properties, and use T_b and SG as the input parameters.

Table 2. Summary of correlations to estimate T_c , P_c and M of high-boiling-point petroleum fractions.

Source	Correlation	Input data	Range of applicability	Equation
Winn, 1955	$\ln(T_c) = -0.58779 + 4.2009(T_b^{0.08615})(SG^{0.04614})$	T_b, SG	NA	(9)
	$P_c = 10^5 \left[6.148341 \times 10^7 (T_b^{-2.3177})(SG^{24853}) \right]$	T_b, SG	NA	(10)
	$M = 2.70579 \times 10^{-5} (T_b^{2.4966})(SG^{-1.174})$	T_b, SG	NA	(11)
Riazi and Daubert, 1980	$T_c = 35.9413 \left[\exp(-6.9 \times 10^{-4} T_b - 1.4442(SG) + 4.91 \times 10^{-4} (T_b SG)) \right] T_b^{0.7293} SG^{1.2771}$	T_b, SG	$M > 280 \text{ kg} \cdot \text{kmol}^{-1}$	(12)
	$P_c = 10^5 \left\{ 6.9575 \left[\exp(-1.35 \times 10^{-2} T_b - 0.3129(SG) + 9.174 \times 10^{-3} (T_b SG)) \right] T_b^{0.6791} SG^{-0.6807} \right\}$	T_b, SG	$M > 280 \text{ kg} \cdot \text{kmol}^{-1}$	(13)
	$M = 42.965 \left[\exp(2.097 \times 10^{-4} T_b - 7.78712(SG) + 2.08476 \times 10^{-3} (T_b SG)) \right] T_b^{1.26007} SG^{4.98308}$	T_b, SG	70 – 700 $\text{kg} \cdot \text{kmol}^{-1}$ 300 – 850 K	(14)
Kesler and Lee, 1976	$T_c = 189.8 + 450.6(SG) + [0.4244 + 0.1174(SG)](T_b) + \frac{[0.1441 - 1.0069(SG)]10^5}{T_b}$	T_b, SG	$T_b > 923 \text{ K}$; 70 – 700 $\text{kg} \cdot \text{kmol}^{-1}$	(15)
	$\ln(P_c) = 10^5 \left[\left(5.689 - \frac{0.0566}{SG} - \left(0.43639 + \frac{4.1216}{SG} + \frac{0.21343}{(SG)^2} \right) 0.001(T_b) + \left(0.47579 + \frac{1.182}{SG} + \frac{0.15302}{(SG)^2} \right) \times 10^{-6} (T_b)^2 - \left(2.4505 + \frac{9.9099}{(SG)^2} \right) \times 10^{-10} (T_b)^3 \right]$	T_b, SG	$T_b > 923 \text{ K}$; 70 – 700 $\text{kg} \cdot \text{kmol}^{-1}$	(16)
	$M = -12272.6 + 9486.4(SG) + \left(8.3741 - \frac{5.9917}{SG} \right) T_b + [1 - 0.77084(SG) - 0.02058(SG)^2] \left(0.7465 - \frac{222.466}{T_b} \right) \frac{10^7}{T_b} + [1 - 0.80882(SG) - 0.02226(SG)^2] \left(0.3228 - \frac{17.335}{T_b} \right) \frac{10^{12}}{(T_b)^3}$	T_b, SG	$T_b < 750 \text{ K}$	(17)

T_c : Critical Temperature (or T_{cNPSE} : pseudocritical temperature) (K); P_c : critical pressure (or P_{cNPSE} : pseudocritical critical) (Pa); M : molar mass (or M_{NPSE} : molar mass of pseudocomponents) ($\text{kg} \cdot \text{kmol}^{-1}$); T_b : Boiling point (T_{bi} : normal boiling point of pseudocomponent i or $MeABP$: mean average boiling point of whole fraction) (K); SG : specific gravity; NA: Not available.

On the other hand, the critical volume (V_c) and acentric factor (ω_{ac}) are parameters that are not measured directly and can be obtained from accurate values for T_c and P_c using methods available in the literature described in Equations (18) – (20) from Table 3.

Table 3. Summary of correlations to estimate V_c and ω_{ac} of high-boiling-point petroleum fractions.

Source	Correlation	Input data	Range of applicability	Equation
Edmister, 1958	$\omega_{ac} = \left(\frac{3}{7}\right) \left(\frac{T_{br}}{1 - T_{br}}\right) \left[\log_{10} \left(\frac{P_c}{101325} \right) \right] - 1$	T_b, T_c, P_c	NA	(18)
Lee and Kesler, 1975	$\omega_{ac} = \frac{-\ln P_i - 5.92714 + 6.09648/T_{br} + 1.28862 \ln T_{br} - 0.169347 T_{br}^6}{15.2518 - 15.6875/T_{br} - 13.4721 \ln T_{br} + 0.43577 T_{br}^6}$	T_b, T_c, K_w	$T_{br} < 0.8$	(19)
Kesler and Lee, 1976	$\omega_{ac} = -7.904 + 0.1352 K_w - 0.007465 K_w^2 + 8.359 T_{br} + \frac{1.408 - 0.01063 K_w}{T_{br}}$	T_b, T_c, K_w	$T_{br} > 0.8$	
Daubert and Danner, 1997).	$V_c = (10^{-6}) \left\{ \frac{83.14 T_c}{P_c [3.72 + 0.26(\alpha_R - 7.00)]} \right\}$ $\alpha_R = 5.811 + 4.919 \omega_{ac}$	T_c, P_c, ω_{ac}	NA	(20)

V_c : Critical volume (or V_{cNPSE} : pseudocritical volume) ($\text{m}^3 \cdot \text{mol}^{-1}$); T_c : Critical Temperature (or T_{cNPSE} : pseudocritical temperature) (K); P_c : critical pressure (or P_{cNPSE} : pseudocritical critical) (bar); ω_{ac} : Acentric factor (or ω_{acNPSE} : pseudoacentric factor); T_{br} : reduced boiling point; T_b : Boiling point (T_{bi} : normal boiling point of pseudocomponent i or $MeABP$: mean average boiling point of whole fraction) (K); SG : specific gravity; NA: Not available.

2.3. Methods for estimating the thermophysical and transport properties

In this section, methods available for estimating transport properties such as the kinematic viscosity (ν) and thermal conductivity (λ), and thermal properties such as the specific heat capacity (C_p) and vapor pressure (P_{vap}) of petroleum fractions are presented in Equations (21) – (29). These properties are essential for energy balances involved in chemical process unit and in the design of heat transfer equipment.

2.3.1. Estimation of transport properties

2.3.1.1. Generalized viscosity correlations

Numerous estimation methods have been presented by researchers to show the effect of temperature on the kinematic viscosity (ν). A review of viscosity estimation methods is given by Mehrotra et al. (1996) and some correlations with the use of SG and T_b as input data as in the present work, are presented in Equations (21) – (23) from Table 4.

Table 4. Summary of correlations to estimate ν of high-boiling-point petroleum fractions.

Source	Correlation	Input data	Range of applicability	Equation
Moharam et al. 1995	$\ln[\nu(10^{-6})] = A \exp\left[\left(\frac{T_b}{T}\right)(SG)^B\right] + C$ $A = 1.0185; B = \frac{T_b}{305.078} - 0.55526; C = -3.2421$	T_b, SG, T	323 – 823 K	(21)
Mehrotra, 1995	$\log \log [\nu(10^{-6}) + 0.8] = a_1 + a_2 \log(T)$ $a_1 = 5.489 + 0.148(T_b)^{0.5}$ $a_2 = -3.7$	T_b, T	323 – 823 K	(22)
Aboul-Seoud and Moharam, 1999a	$\ln \ln [\nu(10^{-6}) + 0.8] = a_1 + a_2 \ln(T)$ $a_1 = 4.3414(T_b SG)^{0.2} + 6.6913$ $a_2 = -3.7$	T_b, SG, T	323 – 823 K	(23)

ν : Kinematic viscosity ($\text{m}^2 \cdot \text{s}^{-1}$); T_b : Boiling point (T_{bi} : normal boiling point of pseudocomponent i or $MeABP$: mean average boiling point of whole fraction) (K); SG : specific gravity; T : temperature (K).

2.3.1.2. Thermal conductivity–temperature correlations

As in the case of kinematic viscosity (ν), the thermal conductivity (λ) of high-boiling-point petroleum fractions (and its approach using the pseudoization method) is required in the thermal balance equations. The procedures suggested in this work comprises reliable correlations for predicting λ values based on the input data and in the range of applicability of the property, as presented in Equations (24) – (26) from Table 5.

Table 5. Summary of correlations to estimate λ of high-boiling-point petroleum fractions.

Source	Correlation	Input data	Equation
Riazi and Faghri, 1985	$\lambda = \frac{(1.11 / M^{1/2}) \left[3 + 20 \left(1 - \frac{T}{T_c} \right)^{2/3} \right]}{3 + 20 \left(1 - \frac{T_b}{T_c} \right)^{2/3}}$	T_b, T_c, M, T	(24)
Lakshmi and Prasad, 1992	$\lambda = 0.0655 - 0.00005T + \frac{(1.3855 - 0.00197T)}{M^{0.5}}$	M, T	(25)
Aboul-Seoud and Moharam, 1999b	$\lambda = 2.540312 \left(\frac{SG}{T} \right)^{0.5} - 0.014485$	SG, T	(26)

λ : Thermal conductivity ($\text{W} \cdot \text{m}^{-1} \cdot \text{K}^{-1}$); T_c : Critical Temperature (or T_{cNPSE} : pseudocritical temperature) (K); T_b : Boiling point (or T_{bi} : normal boiling point of pseudocomponent i or $MeABP$: mean average boiling point of whole fraction) (K); SG : specific gravity; M : molar mass; T : temperature (K); NA: not available.

2.3.2. Estimation of thermal properties

2.3.2.1. Specific heat capacity

The specific heat capacity (C_p) (of liquid phase) is required when modeling based on mass, momentum and energy balances is to be carried out. It is sensitive to temperature variations and depends mainly on the type of molecular structure of the compounds involved.

A summary of the calculation procedures used to estimate C_p (of liquid phase) is presented in Equations (27) – (28) from Table 6. The input parameters are K_w and SG .

Table 6. Summary of correlations to estimate C_p of high-boiling-point petroleum fractions.

Source	Correlation	Input data	Range of applicability	Equation
Watson and Nelson, 1933	$C_p = (10^3) \left(0.28299 + 0.23605 K_w \right) \left[\frac{0.645 - 0.05959(SG) + (2.32056 + 0.94752(SG)) \left(\frac{T}{1000} - 0.25537 \right)}{1} \right]$	K_w, SG, T	NA	(27)
Kesler and Lee, 1976	$C_p = A_1 + A_2 T + A_3 T^2$ $A_1 = \left[\frac{-4.90383 + (0.099319 + 0.104281 SG) K_w + 4.81407 - 0.194833 K_w}{SG} \right] (10^3)$ $A_2 = (10^{-1}) \left(7.53624 + 6.214610 K_w \right) \left(1.12172 - \frac{0.27634}{SG} \right)$ $A_3 = -(10^{-4}) \left(1.35652 + 1.11863 K_w \right) \left(2.9027 - \frac{0.70958}{SG} \right)$	K_w, SG, T	$T_{br} < 0.8$	(28)

C_p : Specific heat capacity ($\text{J} \cdot \text{kg}^{-1} \cdot \text{K}^{-1}$); SG : specific gravity; T : temperature (K); T_b : Boiling point (or T_{bi} : normal boiling point of pseudocomponent i or $MeABP$: mean average boiling point of whole fraction) (K). NA: Not available.

2.3.2.2. Vapor pressure

Methods for calculating the vapor pressure (P_{vap}) of pure compounds or mixtures with known components are available in the book “The Properties of Gases and Liquids” (Poling et al., 2001) and in “The Design Institute for Physical Property Data – DIPPR” (Daubert et al., 2000), using predictive correlations developed from experimental data, such as the Antoine or Wagner equations. Most of the procedures used for petroleum fractions were suggested for a narrow boiling range or are applicable to mixtures with a known composition (Panteli et al., 2006). Nevertheless, a simple method for estimating the vapor pressure (P_{vap}) of high-boiling-point petroleum fractions is presented in Equation (29) (Riazi, 2004).

$$\log_{10} (1 \times 10^5 P_{vap}) = 3.2041 \left[1 - 0.998 \left(\frac{T_b - 41}{T - 41} \right) \left(\frac{1393 - T}{1393 - T_b} \right) \right] \quad (29)$$

Where, P_{vap} is the vapor pressure (Pa); T_b is the boiling point (T_{bi} : normal boiling point of pseudocomponent i or $MeABP$: mean average boiling point of the whole fraction) (K); and T is the temperature (K).

3. Computational framework

3.1. High-boiling-point petroleum fractions samples and data requirements

High-boiling-point petroleum fractions are characterized by their SG or API gravity and BP curve, parameters well established in the ASTM D 287 (2006), ASTM D 1298 (2005) and ASTM D 2892 (2005) standard methods, respectively. Three Brazilian crude oils with different API gravities (16 – 25 °API), obtained from separate sources, and distilled by conventional atmospheric distillation (ASTM D 2892, 2005), providing three atmospheric distillation residues (ATR–W, ATR–Y and ATR–Z), were studied in the present work. The BP curves were obtained in the Petrobras Research and Development Center (CENPES–Brazil) and are represented by pairs of points of accumulated distilled volume versus temperature as presented in Table 7.

Table 7. Boiling point curve and the density of the whole high-boiling-point petroleum fractions.

ATR–W 952.2 kg·m ⁻³		ATR–Y 914.4 kg·m ⁻³		ATR–Z 903.8 kg·m ⁻³	
Accumulate volume of distillate (%v/v)	Boiling temperature (K)	Accumulate volume of distillate (%v/v)	Boiling temperature (K)	Accumulate volume of distillate (%v/v)	Boiling temperature (K)
3.31	459.1	38.21	653.2	3.5	377.15
10.70	551.2	41.45	680.2	4.2	398.15
19.87	647.2	42.79	693.2	5.4	423.15
24.80	670.2	46.41	700.2	7.5	448.15
30.83	693.2	47.36	706.2	10.9	493.15
34.13	710.2	49.69	716.2	14.1	519.15
31.98	720.2	52.88	723.2	14.6	523.15
35.29	733.2	56.86	726.2	18.0	546.15
38.54	748.2	61.75	733.2	21.0	566.15
40.81	768.2	66.32	746.2	24.7	589.15
42.66	773.2	70.89	762.2	27.8	611.15
45.03	790.2	72.33	773.2	30.9	633.15
47.38	801.2			33.9	653.15
49.65	810.2			37.0	673.15
51.36	813.2			39.9	692.15
51.93	818.2			42.7	705.15
60.59	818.4			45.5	711.15
62.35	846.3			46.2	713.15
65.24	880.0			49.0	728.15
69.62	920.3			51.7	743.15
73.81	967.9			54.4	753.15
				56.9	763.15
				58.6	778.15
				61.5	788.15
				63.6	807.15
				65.9	823.15
				68.7	837.15
				71.3	839.15

3.2. Pseudocomponent breakdown methodology

The range of the BP curve was cut in order to obtain non-overlapping temperature intervals, continuously covering the temperature range according to the integral mean temperature of the corresponding interval of the distilled fraction (Eckert and Vaněk, 2005).

Whitson and Brulé (2000) and Eckert and Vaněk (2005) pointed out that it is sufficient to use about 15 K for normal boiling points up to 700 K, about 30 K for between 700 and 950 K and about 50 K for higher boiling point mixtures. Thus, each temperature interval represents one pseudocomponent with a normal boiling point, defined by the integral mean temperature over the corresponding interval of the distilled fraction, as described in Equations (30) – (31) (Eckert and Vaněk, 2005; Miquel and Castells, 1993; Beer, 1994).

$$T_{bi} = \frac{T_{TBP}(x_{vi}^{R_s}) + T_{TBP}(x_{vi}^{L_s})}{2} \quad (30)$$

$$T_{bi} = \frac{1}{x_{vi}^{R_s} - x_{vi}^{L_s}} \int_{x_{vi}^{L_s}}^{x_{vi}^{R_s}} T_{TBP}(x_v) dx_v \quad (31)$$

Where i is the component (or pseudocomponent); x_{vi} is the volume fraction of the component (or pseudocomponent i) on the left side (L_s) and on the right side (R_s) in the boiling range; and T_{bi} is the normal boiling point of pseudocomponent i in Kelvin.

3.3. Correlations and predictive technique availability

In this study, a pseudoization method is presented to relate the basic properties (boiling point (T_b), specific gravity (SG) and Watson factor characterization (K_w)), to the thermodynamic properties (critical temperature (T_c), critical pressure (P_c), critical volume (V_c) and acentric factor (ω_{ac})) and to thermophysical and transport properties (thermal conductivity (λ), specific heat capacity (C_p), kinematic viscosity (ν) and vapor pressure (P_{vap})) of high-boiling-point petroleum fractions.

The development of the pseudocomponent approach presented in this work was based on the procedure suggested by Lion and Edmister (1975) and Miquel and Castells (1994, 1993), assuming K_w to be constant, that is, the same for each pseudocomponent and calculated using Equation (7). Thus, the liquid density (ρ_i) (at 288.75 K) of each pseudocomponent (NPSE) could be estimated using Equation (32) (Miquel and Castells, 1994; 1993).

$$\rho_i = \rho_{NPSE_i} = 1215.253 \frac{T_{bi}^{1/3}}{K_w} \quad (32)$$

In the computational approach, an optimization subroutine was introduced to estimate the best set of thermodynamic properties (T_c , P_c and M) based on minimization of the material balance error as described in the next section.

3.3.1. Computational procedure description

The computational tool used to develop the pseudoization computational approach and to analyze the physicochemical properties of the high-boiling-point petroleum fractions was built up in FORTRAN-90 language using Compaq Visual Fortran compiler (professional edition 6.6). It is organized in seven (07) environments as presented in Figure 1 and described as follows from items (a) to (f):

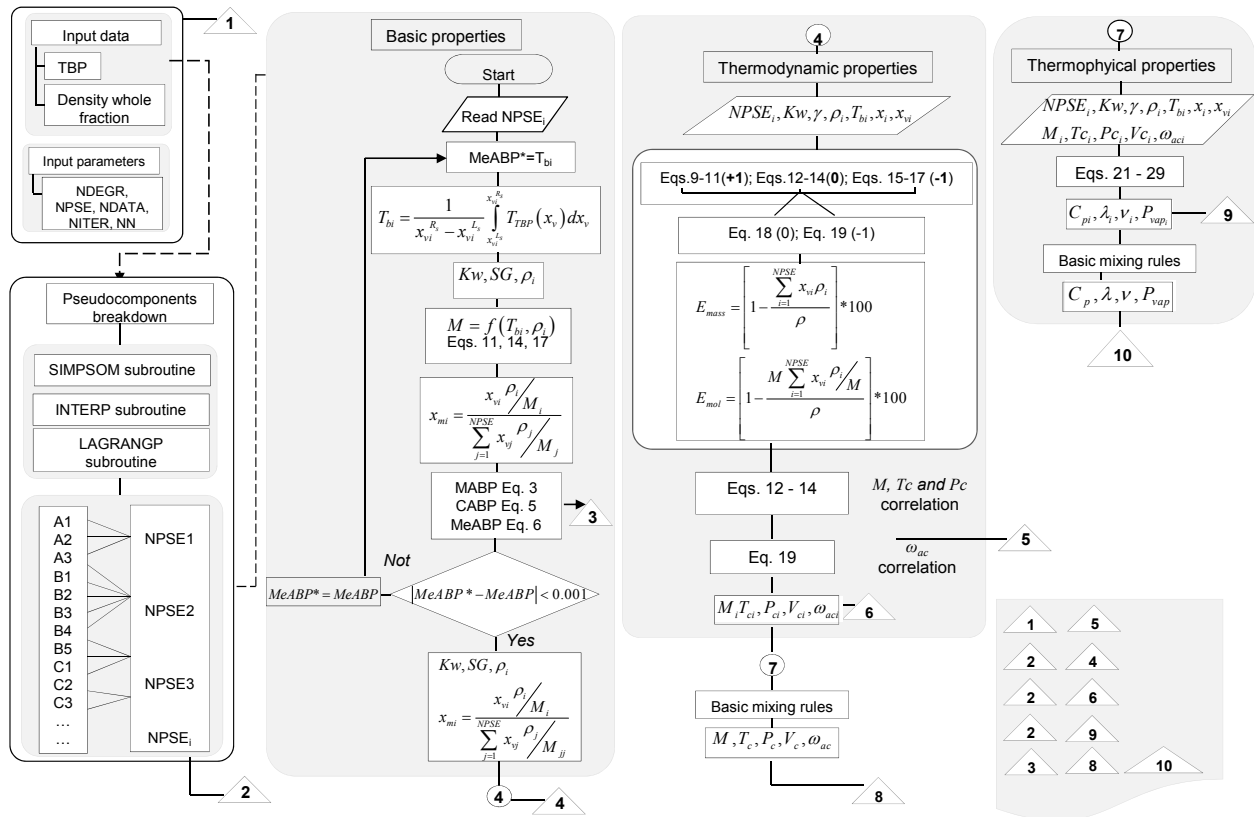


Figure 1. Computational environment to estimate the basic, the thermodynamic and the thermophysical properties of heavy petroleum fractions.

(a) High-boiling-point petroleum fractions data environment–Input data

The user has to introduce the BP distillation data and the whole fraction density.

(b) Internal procedures data environment–Input parameter

Within the computational framework some information is required in order to apply the numerical methods for interpolation, obtain the trial-and-error numerical solution and present information in the output report. Hence, the input parameter required are: Degree of lagrange's interpolation polynomial (NDEGR) based on the fact that a polynomial fitting lower than third order defining the BP curve is recommended as a procedure to estimate the accumulated distilled volume values for each distilling temperature (Pasquini and Bueno, 2007); number of pseudocomponents (NPSE); number of input data for the BP data (NDATA), maximum number of iterations (NITER), total interpolated data on BP curve to be presented in output report (NN).

(c) Pseudocomponent breakdown environment

This environment computes the integral boiling point (T_{bi}) using Equation (31). It consists of three subroutines called: SIMPSON, INTERP and LAGRANP (Miquel and Castells, 1994, 1993).

(d) Basic characterization environment

The procedure for estimating the basic properties is described in Miquel and Castells (1993) as follows.

Stage 1: Compute the T_{bi} of each pseudocomponent predefined in the input data parameters environment, using Equation (31).

Stage 2: This subroutine requires a starting value for the mean average boiling point ($MeABP$) as follows:

$$MeABP^* = T_{bi} \quad (33)$$

Stage 3: Estimate K_w (Equation 7) and the pseudocomponent liquid density (ρ_i) (Equation 32) based on the starting value for $MeABP^*$.

Stage 4: Calculate the molar (x_{mi}) fraction of each pseudocomponent (i) using the correlation in Equation (34) as follows:

$$x_{mi} = \frac{x_{vi} \rho_i / M_i}{\sum_{j=1}^{NPSE} x_{vj} \rho_j / M_{jj}} \quad (34)$$

Stage 5: Calculate the molar-, cubic- and mean-average boiling points ($MABP$, $CABP$ and $MeABP$) of the whole fraction using Equations (3), (5) – (6) in Table 1.

Stage 6: If the absolute difference between the $MeABP$ value obtained in stage 5 and stage 1 is larger than 0.001, assign the new value for $MeABP$ obtained in stage 5 and go back to step stage 1; on convergence, then proceed to stage 7.

Stage 7: Assign the normal boiling point (T_{bi}), density (ρ_i), volume, and molar concentrations (x_{vi} and x_{mi} , respectively) to each pseudocomponent.

(e) Thermodynamic characterization environment

The thermodynamic properties (M , T_c and P_c) and acentric factor (ω_{ac}) are estimated from correlations shown in Tables 2 – 3, which are denoted according to the coded numbers: **-1**, **0** or **1** for M , T_c and P_c , respectively, and **-1** or **0** for the ω_{ac} correlations (Table 8).

Table 8. Coded correlations for estimation of thermodynamic properties.

Thermodynamic property	Coded number	Correlation
Critical properties set (T_c , P_c , M)	-1	Kesler and Lee, 1976
	0	Riazi and Daubert, 1980
	1	Winn, 1955
Acentric factor (ω_{ac})	-1	Kesler and Lee, 1976; Lee and Kesler, 1975
	0	Edmister, 1958

Aiming to obtain the best set of correlations, an optimization subroutine for minimization of the mass- and molar- balance errors was included. Hence, based on a set of twenty five (25) pseudocomponents, all possible combinations between these correlations were defined (see Figure 2). From the subroutine for basic properties estimation, assigned the normal boiling point (T_{bi}), density (ρ_i), volume, and molar concentrations (x_{vi} and x_{mi} , respectively) to each pseudocomponent, compute critical properties (T_{ci} and P_{ci}), acentric factor (ω_{aci}), molar mass (M_i) and Watson's characterization factor (K_w) of the pseudocomponent and compute whole fraction critical properties (T_c and P_c), acentric factor (ω_{ac}) and molar mass (M) using $MeABP$ and ρ . Subsequent, compute the pseudocomponent-breakdown mass- and molar- balance error using Equations (35) – (36) (Beer, 1994; Miquel and Castells, 1994, 1993) as follows:

$$E_{mass} = \left[1 - \frac{\sum_{i=1}^{NPSE} x_{vi} \rho_i}{\rho} \right] * 100 \quad (35)$$

$$E_{mol} = \left[1 - \frac{M \sum_{i=1}^{NPSE} x_{vi} \rho_i / M}{\rho} \right] * 100 \quad (36)$$

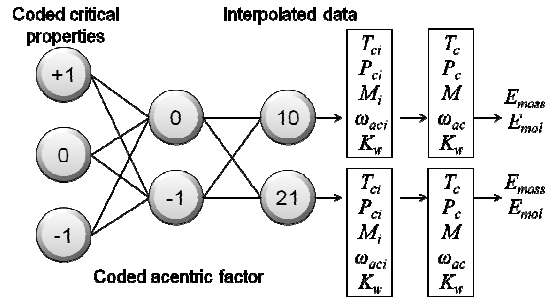


Figure 2. Sketch for optimization procedure to estimate the thermodynamic properties of the pseudocomponents (T_{ci} , P_{ci} , M_i , ω_{aci} and K_w) and whole fraction (T_c , P_c , M , ω_{ac} and K_w).

At this stage, the solution was reached when the mass– and molar– balance errors were minimized. Table 9 presents the result obtained for the ATR–W and analogous data were obtained for ATR–Y and ATR–Z.

Table 9. Mass– and molar– balance errors calculated from optimization procedure using coded critical properties and coded acentric factor.

Case study: ATR–W					
Coded critical property	coded ω_{ac}	Interpolated data	E_{mass}	E_{mol}	
-1	-1	21	1.37	27.45	
-1	0	21	1.37	27.45	
-1	-1	10	1.40	26.94	
-1	0	10	1.40	26.94	
0	-1	21	2.73	8.60	
0	0	21	2.73	8.60	
0	-1	10	2.71	8.52	
0	0	10	2.71	8.52	
1	-1	21	3.09	10.08	
1	0	21	3.09	10.08	
1	-1	10	3.07	9.97	
1	0	10	3.07	9.97	

ω_{ac} : Acentric factor; E_{mass} : Error in mass balance; E_{mol} : Error in molar balance.

On the other hand, mass– and molar– balance error were analyzed. Hence, the results for the mass– and molar– balance errors (E_{mass} and E_{mol}) presented in Table 9 for the ATR–W case study showed that the choice of ω_{ac} correlation appears to have no influence on the reliability of the thermodynamic properties. Following, considering the Kesler and Lee (1976) and Lee and Kesler (1975) correlation, coded with **–1**, for the estimation of ω_{ac} , analyses were performed establishing the possible combinations among the set of correlations to estimate the

thermodynamic properties (M , T_c and P_c) and the number of interpolated data on the BP curve (input data) being ten (10) or twenty one (21).

In order to accomplish the best set of correlations, data from E_{mass} and E_{mol} constituted an array of two vectors (called *mass_vector* and *molar_vector*) which were used in a subroutine to choose the minimum value in the arrays.

(f) Thermophysical and transport characterization environment

A final subroutine estimates the thermal conductivity (λ), the specific heat capacity (C_p) the kinematic viscosity (ν) and the vapor pressure (P_{vap}) of each pseudocomponent as a function of the temperature (T), using the normal boiling point (T_{bi}) (for pseudocomponents) or *MeABP* (for whole fractions) as the input data. The methods presented in Equations (21) – (28) from Tables 4 – 6 and Equation (29) are included in this module.

(g) Reliability of the pseudoization approach environment

The success of the method is based on the accuracy of the empirical or semi-empirical correlations in the literature and the standard industrial methods. Hence, the reliability of the basic and thermodynamic properties is calculated from the mass and molar balance equations (Equations 35 – 36) (Beer, 1994; Miquel and Castells, 1994, 1993). The thermophysical properties were compared with the experimental data obtained in the research laboratories using the methods described in the next section. Data computed were evaluated in terms of average absolute deviation (*AAD%*) which is define as a relation among the absolute deviation of estimating a quantity divided by its experimental value ($y_{i,ref}$) as presented in Equation (1).

4. Experimental data

4.1. Thermal analyses: differential scanning calorimetry (DSC)

The DSC experiments were carried out on the high-boiling-point petroleum fractions using a Mettler-Toledo DSC 823e thermal analysis system (Mettler Toledo GmbH, Germany), and liquid nitrogen was used for cooling. The DSC module was calibrated with indium standard (It had a certified fusion temperature of 156.6 ± 0.3 °C and heat flow calibration of 28.45 ± 0.6 J·g⁻¹). The experiments were carried out with a sample size of ~10 mg. The samples were weighed into open aluminum pans, hermetically sealed and then placed in the sample chamber of the DSC module. The reference was an identical, empty pan, with an equal weight

matched within ± 0.1 mg. A linear heating rate of $25 \text{ K} \cdot \text{min}^{-1}$ was used over the temperature range from 350 to 600 K, with a nitrogen flow of $50 \text{ mL} \cdot \text{min}^{-1}$ controlled by a gas control system (Mettler–Toledo TS0800GC1). The STAR^e (V 9.01) software was used to provide an estimate of the enthalpy (ΔH), the heat flow and specific heat capacity.

In order to evaluate the repeatability of the measurement, the relative standard deviation (%RSD) with respect to the mean signal of each measurement, calculated over three (03) consecutive repetitions of Indium standard was examined. The value obtained was lower than 8.53%.

4.2. Rheological measurements

The rheological analyses were carried out in a Thermo Scientific Haake Rheostress 6000 rotational rheometer (Gebrüder HAAKE GmbH, Germany) interfaced with an electric cone heating system UTCE/C, using 2 parallel plates of 0.035 m and setting the gap set at 1.0×10^{-3} m.

Two measuring techniques were applied. The first rheological measurements refers to the analyses of transition between pseudoplastic and Newtonian flow obtained from an analysis of the flow curve prepared using the controlled rate mode at 383.15 and 363.15 K and at the shear rate range from 10 to 700 s^{-1} with measurements being made every 10 s^{-1} . The flow behavior and dynamic viscosity (μ) of the ATR–W, ATR–Y and ATR–Z was investigated over a wide range of shear rates at 383.15 K (for ATR–W) and 363.15 K (for ATR–Y and ATR–Z). Three runs were done for each material, and the resulting shear stress was the three experimental averages values. The results were recorded and fitted to the Newtonian models.

The experimental data were evaluated and fitted according to the rheological Newtonian model, using the average shear stress (τ) value for each shear rate (σ). High-boiling-point petroleum fractions found to follow Newtonian behavior based on the yield stress of the oils (Table 10). It can be observed that the shear stress is proportional to the shear rate (Newtonian behavior) which mean that the dynamic viscosity (μ) is constant and independent from the shear rate at constant temperature (test temperature).

The other rheological measurement was focus on the sweep measurements in the temperature range from 473.15 K to 343.15 K with the heating rates of $2 \text{ K} \cdot \text{min}^{-1}$ at constant frequency and constant shear stress (100 s^{-1}). The temperature was controlled, in both cases, to

allow a maximum deviation of ± 0.5 K. All experiments were carried out under an oxidizing atmosphere using air.

Table 10. Yield stress (τ) and dynamic viscosity (μ) measurements of ATR-W at 383.15 K, and ATR-Y and ATR-Z at 363.15 K as functions of shear rate (σ).

σ (s^{-1})	ATR-W		ATR-Y		ATR-Z	
	τ (Pa)	μ (Pa·s)	τ (Pa)	μ (Pa·s)	τ (Pa)	μ (Pa·s)
10.0	6.4	0.639	5.6	0.561	3.4	0.340
20.0	12.8	0.639	11.2	0.560	6.8	0.339
30.0	19.2	0.639	16.8	0.560	10.2	0.339
40.0	25.6	0.640	22.4	0.560	13.6	0.339
50.0	32.0	0.639	27.9	0.559	17.0	0.340
60.0	38.1	0.636	33.6	0.559	20.4	0.340
70.0	44.5	0.636	39.2	0.560	23.9	0.342
80.0	51.0	0.637	44.8	0.560	27.4	0.342
90.0	57.2	0.635	50.4	0.560	30.9	0.343
100.0	63.4	0.634	56.0	0.560	34.4	0.344
110.0	69.6	0.633	61.5	0.559	37.9	0.345
120.0	75.7	0.631	67.1	0.560	41.4	0.345
130.0	82.0	0.631	72.7	0.559	44.9	0.346
140.0	88.3	0.630	78.3	0.559	48.4	0.345
150.0	94.5	0.630	84.0	0.560	51.9	0.346
160.0	101.1	0.632	89.5	0.559	55.5	0.347
170.0	107.4	0.632	95.2	0.560	59.0	0.347
180.0	114.3	0.635	101.0	0.561	62.6	0.348
190.0	121.0	0.637	106.5	0.560	66.2	0.348
200.0	127.5	0.637	112.0	0.560	69.5	0.348
210.0	133.9	0.638	117.7	0.560	72.9	0.347
220.0	140.5	0.639	123.3	0.561	76.5	0.348
230.0	146.7	0.638	128.9	0.561	80.1	0.348
240.0	152.7	0.636	134.5	0.561	83.6	0.348
250.0	159.3	0.637	140.2	0.561	87.1	0.348
260.0	166.0	0.638	146.0	0.562	90.5	0.348
270.0	173.0	0.641	151.8	0.562	94.2	0.349
280.0	179.0	0.639	157.2	0.562	97.7	0.349
290.0	185.4	0.639	162.8	0.562	101.1	0.349
300.0	192.5	0.642	168.5	0.562	104.7	0.349
310.0	199.0	0.642	174.0	0.561	108.2	0.349
320.0	204.6	0.639	179.9	0.562	111.6	0.349
330.0	210.5	0.638	185.8	0.563	115.3	0.349
340.0	216.2	0.636	191.4	0.563	118.9	0.350
350.0	222.6	0.636	197.3	0.564	122.1	0.349
360.0	229.1	0.636	202.6	0.563	125.7	0.349
370.0	234.5	0.634	208.0	0.563	129.3	0.350
380.0	240.7	0.633	214.0	0.564	132.9	0.350
390.0	246.6	0.632	219.5	0.563	136.5	0.350
400.1	252.5	0.631	224.7	0.562	139.8	0.350
410.0	260.6	0.636	230.1	0.562	143.3	0.350
420.0	267.2	0.636	235.5	0.561	146.9	0.350
430.0	273.0	0.635	240.7	0.560	150.3	0.350
440.0	279.4	0.635	246.4	0.561	153.8	0.350
450.0	285.9	0.635	251.9	0.560	157.7	0.351
460.0	293.0	0.637	257.2	0.560	161.1	0.350
470.0	298.5	0.635	262.9	0.560	164.4	0.350
480.0	306.2	0.638	268.0	0.559	168.2	0.351
490.0	312.4	0.638	273.6	0.559	171.6	0.350
500.0	318.1	0.636	279.6	0.560	175.5	0.351
510.0	324.1	0.635	285.1	0.560	178.9	0.351
520.0	331.0	0.637	290.6	0.559	182.0	0.350
529.9	336.5	0.635	295.8	0.559	185.7	0.351
539.9	342.9	0.635	300.8	0.558	189.1	0.350

Table 10 continued. Yield stress (τ) and dynamic viscosity (μ) measurements of ATR-W at 383.15 K, and ATR-Y and ATR-Z at 363.15 K as functions of shear rate (σ).

σ (s ⁻¹)	ATR-W		ATR-Y		ATR-Z	
	τ (Pa)	μ (Pa·s)	τ (Pa)	μ (Pa·s)	τ (Pa)	μ (Pa·s)
549.9	349.7	0.636	306.3	0.557	192.5	0.350
559.9	354.7	0.634	312.1	0.558	196.7	0.351
570.0	360.2	0.632	317.4	0.557	200.0	0.351
580.0	365.2	0.630	323.1	0.558	202.9	0.350
590.0	370.3	0.628	328.9	0.558	206.6	0.350
600.0	376.1	0.627	333.7	0.557	210.2	0.351
610.0	381.9	0.626	339.2	0.557	213.5	0.350
620.0	389.7	0.629	345.0	0.557	216.7	0.350
629.9	396.5	0.629	350.0	0.556	220.2	0.350
639.9	403.7	0.631	355.2	0.556	223.8	0.350
649.8	410.0	0.631	360.0	0.555	227.1	0.350
659.9	416.5	0.631	365.1	0.554	230.4	0.349
669.9	423.2	0.632	370.7	0.554	234.0	0.350
679.8	430.3	0.633	375.7	0.554	237.3	0.349
689.8	434.6	0.630	380.4	0.552	240.5	0.349
699.8	439.5	0.628	386.2	0.553	244.2	0.349

5. Results and discussion

5.1. Simulated boiling point data and pseudocomponent distribution

The pseudocomponents were selected considering the need to represent the behavior of the mixture over the entire computational effort and availability of the input data. The most advantageous number of pseudocomponents to satisfactorily fit the data was determined by the trial-and-error exercise through applying a sensibility procedure in which the mass- and molar-balance errors were minimized. In this sense, Table 11 summarizes the sensibility exercise and establishes that twenty five (25) pseudocomponents are required to avoid excessive computational effort but guaranteeing the accuracy to estimate physicochemical properties of petroleum fractions.

Table 11. Summary of trial-and-error exercise for optimizing the number of pseudocomponents.

NPSE	ATR-W		ATR-Y		ATR-Z	
	E_{mass}	E_{mol}	E_{mass}	E_{mol}	E_{mass}	E_{mol}
5	4.76	12.71	3.02	4.63	2.79	3.80
10	4.10	10.37	2.78	3.25	2.27	3.41
15	3.26	9.04	2.39	2.91	2.00	3.01
20	2.84	8.55	1.27	2.22	1.76	2.92
25	2.73	8.60	0.71	2.03	1.12	2.92
30	2.69	8.60	0.71	1.99	1.12	2.92
50	2.66	8.60	0.70	1.99	1.12	2.92

The results in Figure 3 are presented to show the response of the computational approach using the pseudoization method with twenty five (25) pseudocomponents, in relation to

the representation of the input data. Figure 3 shows the comparison between the simulated BP curve and the experimental data obtained from CENPES–PETROBRAS. The initial and final boiling points were set from 300 to 1300 K for ATR–W, from 650 to 800 K for ATR–Y, and from 350 and 850 K for ATR–Z, respectively.

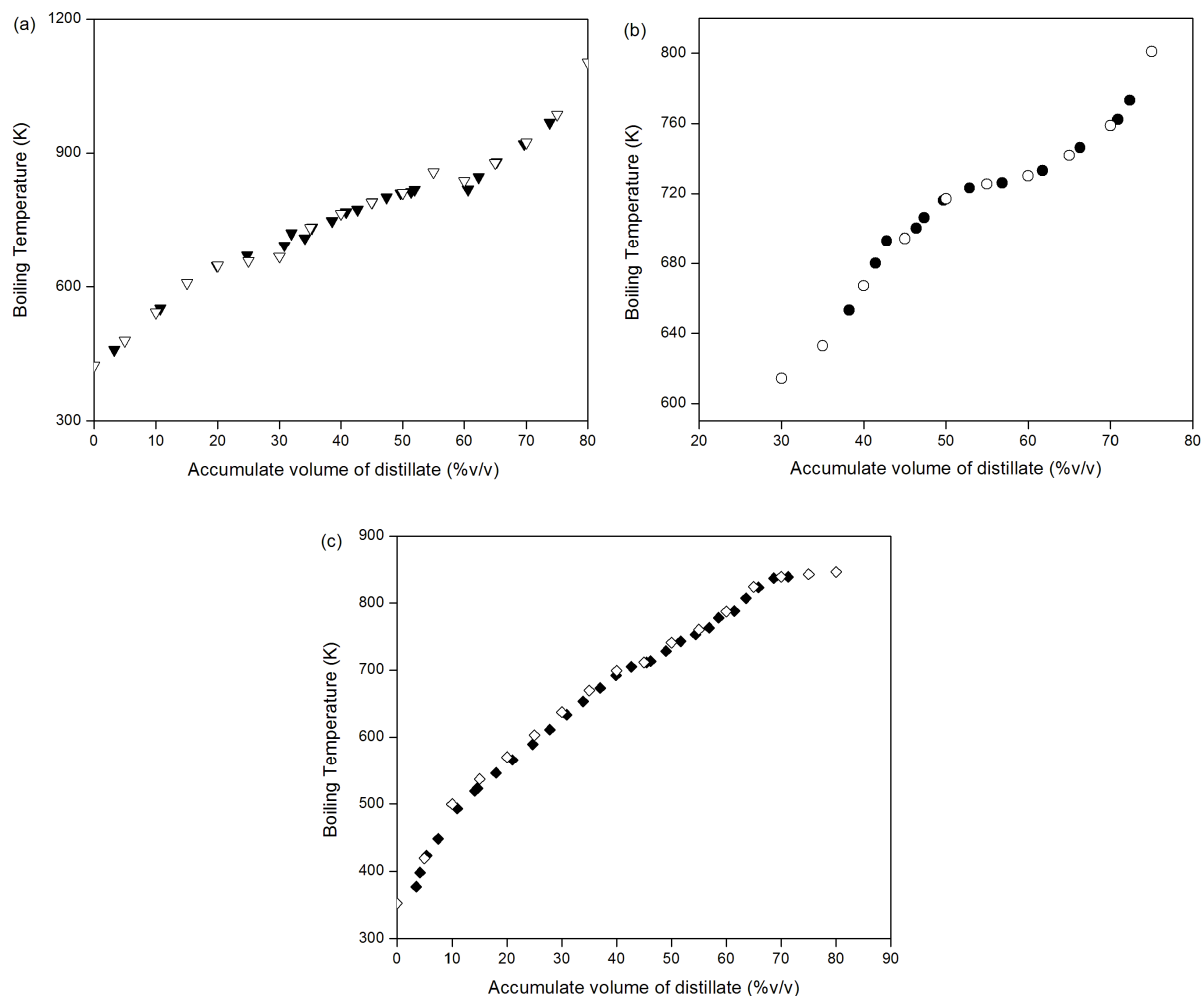


Figure 3. Boiling point curve of a) ATR–W (▼–Cenpes/Petrobras boiling point; ▽–Simulated boiling point); b) ATR–Y (●–Cenpes/Petrobras boiling point; ○–Simulated boiling point), and c) ATR–Z (◆–Cenpes/Petrobras boiling point; ◇–Simulated boiling point).

The boiling point temperatures were evaluated in terms of average absolute deviation ($AAD\%$) where the absolute deviation was defined as the difference between the experimental value ($y_{i,ref}$) obtained from Petrobras Research and Development Center (CENPES–Brazil) and the response predicted by the modeling approach ($y_{i,cal}$) with the interpolation method, divided by its experimental value ($y_{i,ref}$). Figure 3 shows that with twenty five (25) pseudocomponents (each

representing average boiling point ranges of 40 K, 6 K and 20 K for ATR–W, ATR–Y and ATR–Z, respectively) good agreement was obtained reporting an *AAD%* of just 1.74, 0.89 and 1.75% for ATR–W, ATR–Y and ATR–Z, respectively (Table 12).

It is of interest to note in Figure 3 that the simulated and experimental BP values, based on the chemical analysis, are effectively identical up to approximately 80% v/v distillation. Hence, the boiling temperature curve above 80% v/v and below 3% v/v of distillation, represented an extrapolation, and some possible deviations could occur, since there are no data to match them up. However, it can be seen that the results of the extrapolation still show the cubic polynomial trend of the experimental data provided by CENPES–PETROBRAS, the volume fractions being arranged in a cumulative distribution of the volume fraction, as expected.

Table 12. Predicted boiling temperature and absolute deviations percent (%) calculated by computational pseudocomponent approach for ATR-W, ATR-Y and ATR-Z.

ATR-W 952.2 kg·m ⁻³				ATR-Y 914.4 kg·m ⁻³				ATR-Z 903.8 kg·m ⁻³			
Accumulate volume of distillate (%v/v)	Boiling temperature (K)		Absolute deviations percent (%)	Accumulate volume of distillate (%v/v)	Boiling temperature (K)		Absolute deviations percent (%)	Accumulate volume of distillate (%v/v)	Boiling temperature (K)		Absolute deviations percent (%)
	Experimental (<i>y_{ref}</i>)	Predicted (<i>y_{cal}</i>)			Experimental (<i>y_{ref}</i>)	Predicted (<i>y_{cal}</i>)			Experimental (<i>y_{ref}</i>)	Predicted (<i>y_{cal}</i>)	
3.31	459.1	494.30	7.67	38.21	653.2	663.65	1.60	3.5	377.15	357.45	5.22
10.70	551.2	557.03	1.06	41.45	680.2	677.60	0.38	4.2	398.15	366.38	7.98
19.87	647.2	620.94	4.06	42.79	693.2	683.45	1.41	5.4	423.15	380.72	10.03
24.80	670.2	653.34	2.52	46.41	700.2	699.55	0.09	7.5	448.15	403.81	9.89
30.83	693.2	692.51	0.10	47.36	706.2	703.86	0.33	10.9	493.15	437.88	11.21
34.13	710.2	714.03	0.54	49.69	716.2	714.58	0.23	14.1	519.15	467.70	9.91
31.98	720.2	699.99	2.81	52.88	723.2	718.05	0.71	14.6	523.15	472.23	9.73
35.29	733.2	721.65	1.58	56.86	726.2	726.90	0.10	18.0	546.15	502.32	8.02
38.54	748.2	743.16	0.67	61.75	733.2	738.48	0.72	21.0	566.15	528.16	6.71
40.81	768.2	758.39	1.28	66.32	746.2	750.21	0.54	24.7	589.15	559.48	5.04
42.66	773.2	770.96	0.29	70.89	762.2	763.10	0.12	27.8	611.15	585.51	4.20
45.03	790.2	787.31	0.37	72.33	773.2	767.47	0.74	30.9	633.15	611.50	3.42
47.38	801.2	803.83	0.33					33.9	653.15	636.76	2.51
49.65	810.2	820.13	1.23					37.0	673.15	674.52	0.20
51.36	813.2	832.65	2.39					39.9	692.15	687.05	0.74
51.93	818.2	836.88	2.28					42.7	705.15	699.35	0.82
60.59	818.4	847.91	3.61					45.5	711.15	711.89	0.10
62.35	846.3	860.39	1.66					46.2	713.15	715.07	0.27
65.24	880.0	881.75	0.20					49.0	728.15	727.99	0.02
69.62	920.3	916.59	0.40					51.7	743.15	740.79	0.32
73.81	967.9	953.49	1.49					54.4	753.15	753.99	0.11
								56.9	763.15	766.61	0.45
								58.6	778.15	775.45	0.35
								61.5	788.15	791.07	0.37
								63.6	807.15	802.86	0.53
								65.9	823.15	816.31	0.83
								68.7	837.15	833.56	0.43
								71.3	839.15	850.59	1.36
AAD%= 1.74				AAD%= 0.79				AAD%= 1.75			

$$AAD\% = (1/m) \sum_{i=1}^m \frac{|y_{i,cal} - y_{i,ref}|}{y_{i,ref}} * 100$$

Where *m* equals 21 for ATR-W, 12 for ATR-Y and 28 for ATR-Z.

The methodology for distributing the complex bulk liquid into pseudocomponent compositions is shown in Figure 4. The results show that most of the components are concentrated in the first-cuts for ATR-W and ATR-Y (Figure 4a – 4b), and in the end-cut for ATR-Z (Figure 4c).

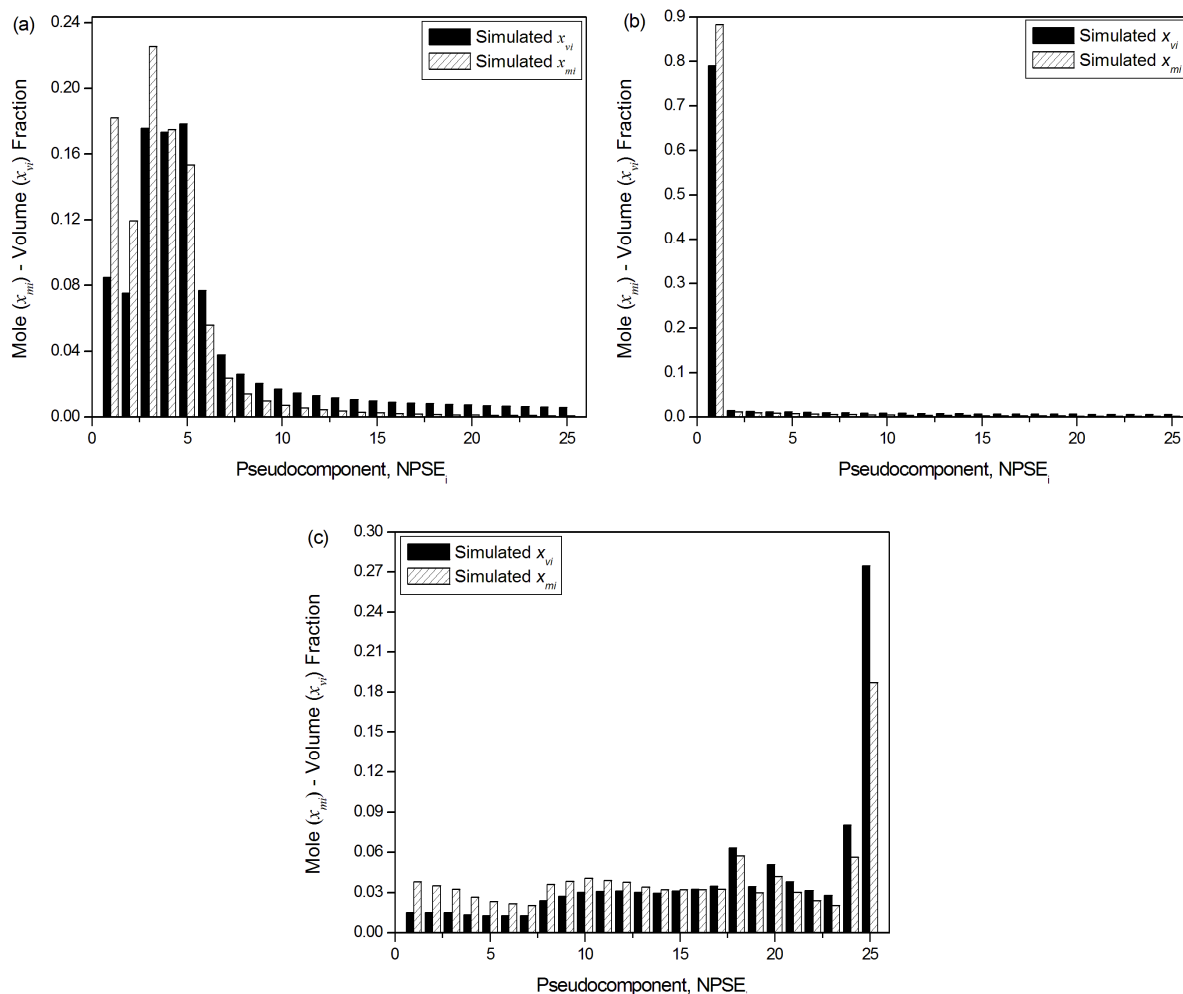


Figure 4. Pseudocomponent mol (x_{mi}) – volume (x_{vj}) fraction distributions of a) ATR-W; b) ATR-Y, and c) ATR-Z.

5.2. Determination of the basic and thermodynamic properties

Properties of high-boiling-point petroleum fractions are estimated based on the computational procedure presented in this work, where the BP curve and the density of the whole fraction are the input bulk properties. The determination of the basic properties of the high-boiling-point petroleum fractions involved the cube of the average boiling point (*CABP*), the mean average boiling point (*MeABP*), the molar average boiling point (*MABP*) and the Watson

characterization factor (K_w) (Table 13). The K_w is an approximate index of the paraffinicity of a petroleum fraction. The high values obtained for this index for ATR-W, ATR-Y and ATRZ ($K_w=11.94$, $K_w=12.18$ and $K_w=11.79$, respectively) indicated a high percent of pure saturated components and paraffin components.

Table 13. Average basic and thermodynamic properties of petroleum fractions.

Average basic properties	ATR-W	ATR-Y	ATR-Z
CABP (K)	888.8	783.1	697.1
MABP (K)	750.7	750.1	651.3
MeABP (K)	819.7	766.6	674.2
K_w	11.94	12.18	11.79
ω_{ac}	1.2188	1.1348	0.8546
T_c (K)	971.2	920.1	849.6
P_c (MPa)	0.905	0.962	1.260
V_c (m ³ ·mol ⁻¹)	1.796x10 ⁻³	1.636 x10 ⁻³	1.245 x10 ⁻³

K_w : Watson characterization factor; *CABP*: Cubic average boiling point; *MeABP*: Mean average boiling point; M : Molar mass; P_c : Critical pressure; T_c : Critical temperature; V_c : Critical volume.

Comparing the values of the average boiling points (Table 13), it appears that the *MeABP* was always lesser than the *CABP*, since the relationship between the density and molar mass increased as the boiling point decreased. This implies in an increase in the relative importance of the fractions with lower boiling points and lower average molar masses, reducing the value of the *MeABP*. Conversely, *MeABP* was larger than *MABP*, and thus there was a relative increase in the importance of the fractions with higher boiling points due to the increase in density with increase in boiling point. Moreover, it is important to estimate the average boiling points, and specifically the *MeABP*, for use in the correlations used to estimate the various thermodynamic and thermophysical properties.

5.2.1. Density and molar mass distributions in the pseudocomponents

On the other hand, both the molar mass (M) and the density (ρ) are fundamental physical properties that can be used in conjunction with other physical properties to characterize the ATR-W, ATR-Y and ATR-Z petroleum fractions. Figure 5 presents the values for molar mass (M_{NPSE}) and density (ρ_{NPSE}) as a function of the normal boiling point (T_{bi}) for the pseudocomponents. From Figure 5a, it is evident that, in the case of ATR-W, both these properties increase with an increment in T_{bi} .

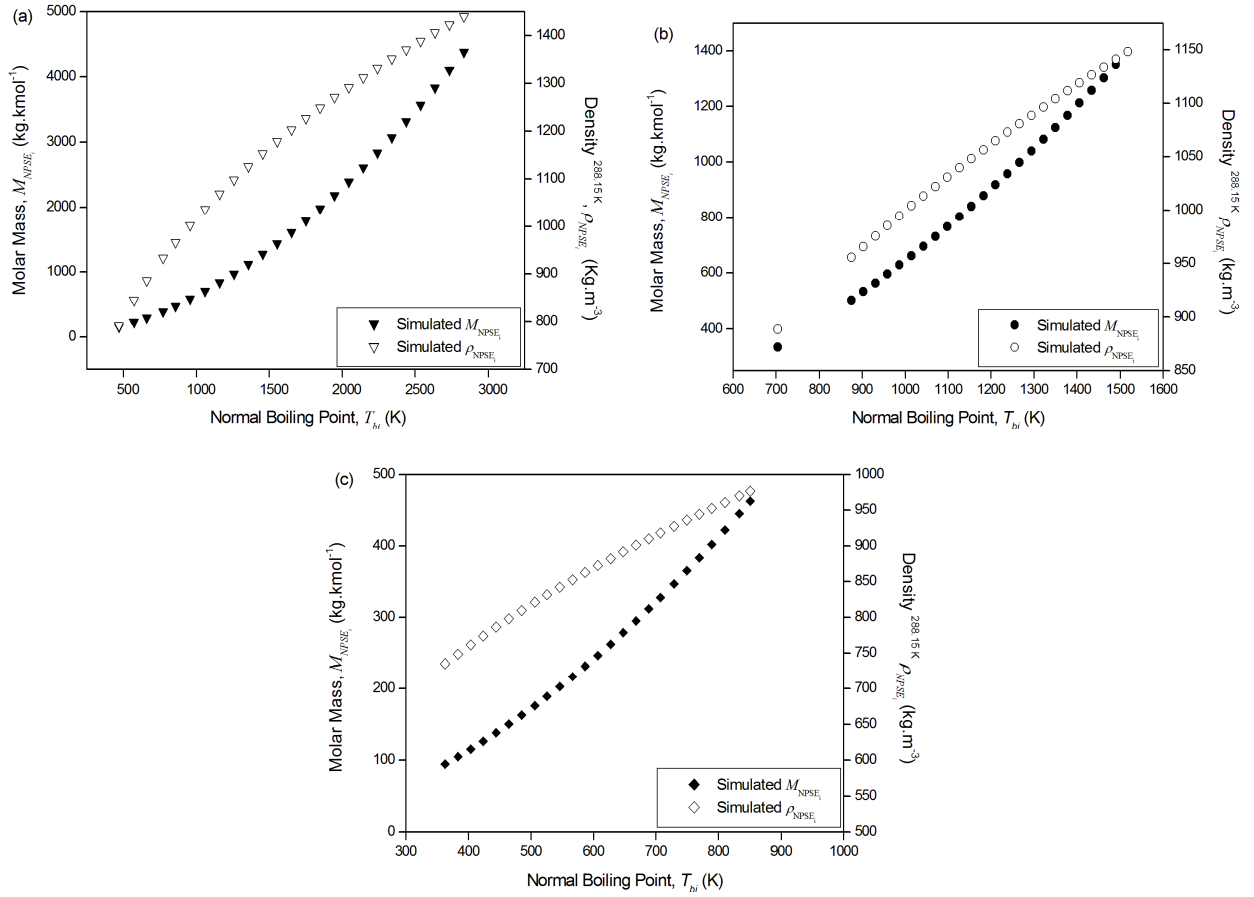


Figure 5. Density at 288.15 K ($\rho_{NPSE_i}^{288.15 K}$) and molar mass (M_{NPSE_i}) distribution of a) ATR-W; b) ATR-Y, and c) ATR-Z.

However, Figure 5 also shows that the value for M_{NPSE} decreases significantly as the API gravity ($^{\circ}\text{API}$) of the fraction increases, which is followed by a more gradual change in M_{NPSE} with the increase in ρ_{NPSE} . Such behavior is to be expected, since, as T_{bi} increases M_{NPSE} and ρ_{NPSE} rise correspondingly.

5.2.2. Critical properties

The availability of critical data for complex mixtures such as high-boiling-point petroleum fractions is insufficient, due to the experimental conditions required and the fact that they can not be measured directly (Korsten, 1998). In this study, a computational framework was presented with respect to reliable methods for predicting the critical properties based on the mass and molar balance errors (Equations 35 – 36).

5.2.2.1. Reliable critical property correlations

Table 14 presents the available correlations introduced in this work, to estimate the critical properties (Equations 9 – 17 from Table 2) by means of a computational environment using the pseudocomponent approach, based on the fact that in predicting the ω_{ac} , the choice of correlation appears to have no influence on the reliability of the thermodynamic properties. Hence, the results for the mass and molar balance errors (E_{mass} and E_{mol}) presented in Table 14 for the ATR–W, ATR–Y and ATR–Z case studies, are for a set of twenty five (25) pseudocomponents obtained using the correlation presented by Kesler and Lee (1976) and Lee and Kesler (1975), and coded with **-1** for the estimation of ω_{ac} . Table 14 established that the number of interpolated data used to predict the BP curve appeared to have no influence, since the variation between the balance errors was minimal when considering ten (10) and twenty one (21) data.

Table 14. Mass– and molar– balance errors for assaying the reliability of thermodynamic properties considering coded acentric factor correlation (**-1**).

Coded critical property set	ω_{ac}	Interpolated data	ATR–W		ATR–Y		ATR–Z	
			$E_{mass}(\%)$	$E_{mol}(\%)$	$E_{mass}(\%)$	$E_{mol}(\%)$	$E_{mass}(\%)$	$E_{mol}(\%)$
-1	-1	21	1.37	27.45	0.64	4.86	1.32	3.99
-1	-1	10	1.40	26.94	0.64	4.84	1.32	3.99
0	-1	21	2.73	8.60	0.71	2.03	1.12	2.92
0	-1	10	2.71	8.52	0.71	2.02	1.12	2.92
1	-1	21	3.09	10.08	0.80	2.33	1.34	3.36
1	-1	10	3.07	9.97	0.80	2.32	1.34	3.35

ω_{ac} : Acentric factor; E_{mass} : Material balance error and E_{mol} : Molar balance error.

Thus for the system adopted using twenty one (21) interpolated points, the combination of the correlations of Kesler and Lee (1976) and Lee and Kesler (1975), coded with **-1**, for the estimation of ω_{ac} , and of Riazi and Daubert (1980), coded with **0**, for the prediction of M , T_c , P_c , represents a great choice in the estimation of the thermodynamic properties of high-boiling-point petroleum fractions, when the values for the boiling point and density of the fraction as input data are available, since the errors in mass balance were 2.73% for ATR–W, 0.71% for ATR–Y and 1.12% for ATR–Z, and the errors in molar balance were 8.60% for ATR–W; 2.03% for ATR–Y and 2.92% for ATR–Z.

5.2.2.2. Data for the pseudocritical properties of high-boiling-point petroleum fractions

The critical temperature (T_c), critical pressure (P_c), critical volume (V_c) and acentric factor (ω_{ac}) represent four widely used constants in physicochemical characterizations, process modeling and unit operation studies. These critical constants are very important properties in the physicochemical characterization of petroleum fractions, since almost all the thermophysical properties are estimated from the boiling point and critical constant data.

In the present work, the term *pseudocritical properties* were introduced to identify the effective values for the critical properties (such as temperature, pressure and volume) of the multicomponent chemical systems, ATR-W, ATR-Y and ATR-Z. Thus, the pseudocritical properties refer to the estimation of the critical properties of a set of pseudocomponents. However, the true critical properties are those calculated using the associated mixing rules.

It can be seen in Figure 6 that the pseudocritical temperature (T_{CNPSE}) increased with the increase in the value for T_{bi} , but the pseudocritical pressure (P_{CNPSE}) (Figure 7) and the density (ratio between molar mass (M_{NPSE}) and critical volume (V_{CNPSE})) decreased (Figure 8) as the M_{NPSE} and ρ_{NPSE} increased.

On the other hand, ω_{ac} is a concept that was introduced by Pitzer et al. (1955) and has proved to be important in the physicochemical characterization of petroleum fractions (Shouzhi et al., 2005). The value for ω_{ac} is said to be a measure of the non-sphericity (acentricity). Values for ω_{ac} can be determined from the T_c , P_c and T_{bi} data. In the present work, the Edmister (Edmister, 1958) and Lee-Kesler (Kesler and Lee, 1976; Lee and Kesler, 1975) methods were evaluated, but only the Lee-Kesler approach was reported (Figure 9). Figure 9 illustrates the dependence of ω_{ac} on T_{bi} and ρ_i for the set of twenty five (25) pseudocomponents of ATR-W, ATR-Y and ATR-Z. A nearly linear variation of this property with the increasing number of carbons can be seen, since the value for T_{bi} increased, and consequently the value for ρ_i rose. Therefore, as confirmed by Ourique and Telles (1997), it is reasonable to state that the estimation of ω_{ac} must be a function of the structural and functional groups, but correlations to relate the structures and ω_{ac} are often limited to specific hydrocarbon compounds.

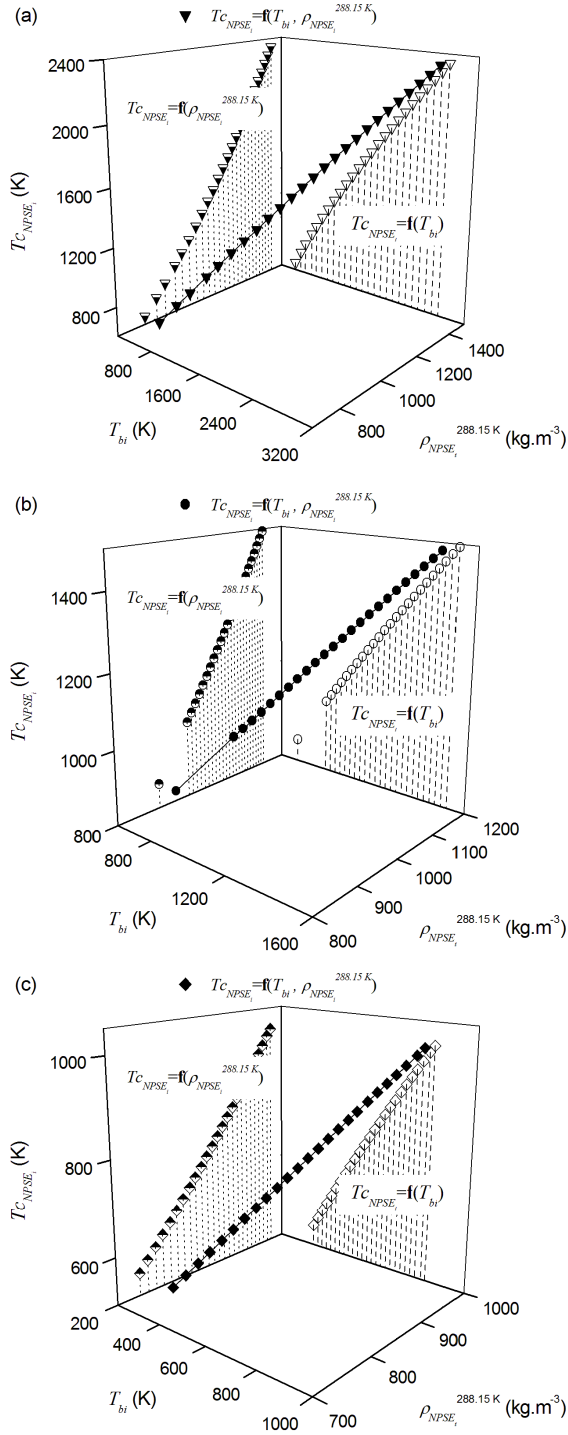


Figure 6. Pseudocritical temperature ($T_{c_NPSE_i}$) as a function of normal boiling point (T_{bi}) and density at 288.15 K (ρ_{NPSE_i}) of a) ATR-W, b) ATR-Y and c) ATR-Z.

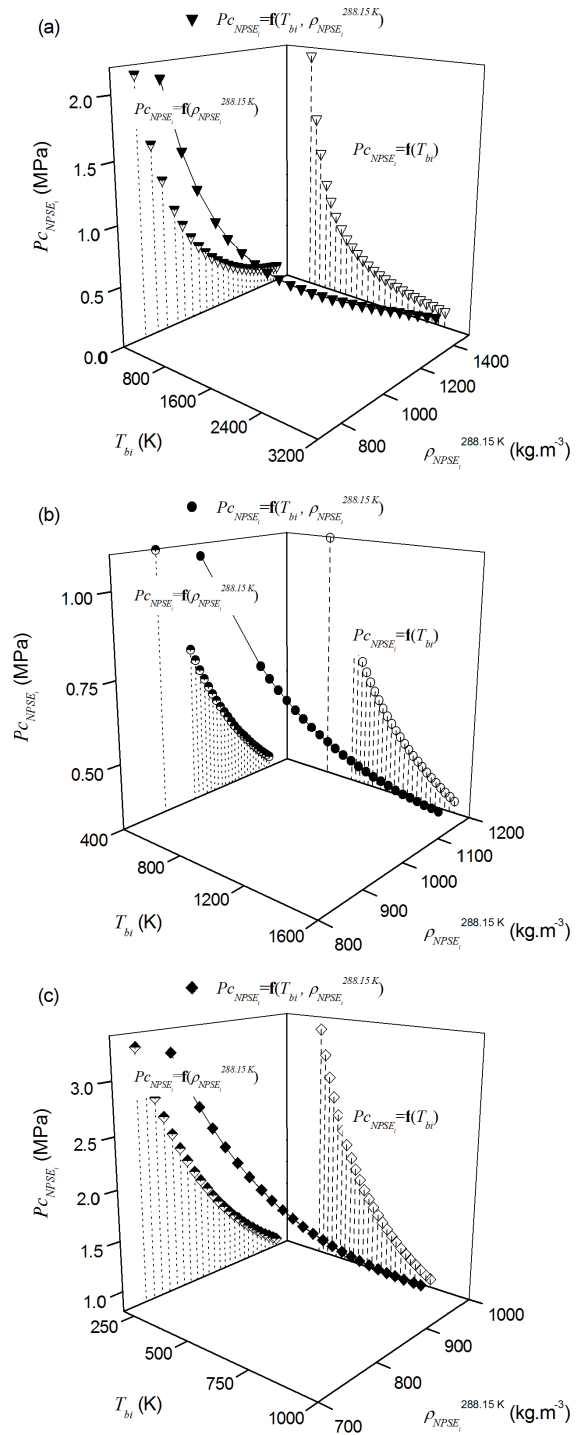


Figure 7. Pseudocritical pressure ($P_{c_NPSE_i}$) as a function of normal boiling point (T_{bi}) and density at 288.15 K (ρ_{NPSE_i}) of a) ATR-W, b) ATR-Y and c) ATR-Z.

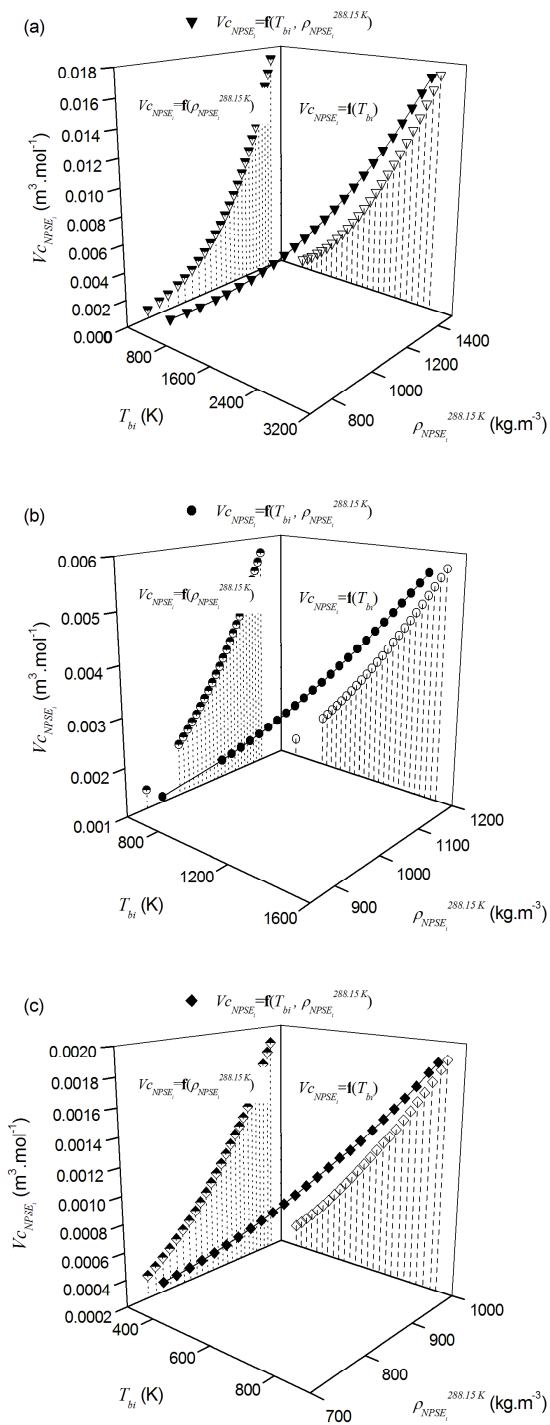


Figure 8. Pseudocritical volume ($V_{c_{NPSE_i}}$) as a function of normal boiling point (T_{bi}) and density at 288.15 K ($\rho_{NPSE_i}^{288.15 K}$) of a) ATR-W, b) ATR-Y and c) ATR-Z.

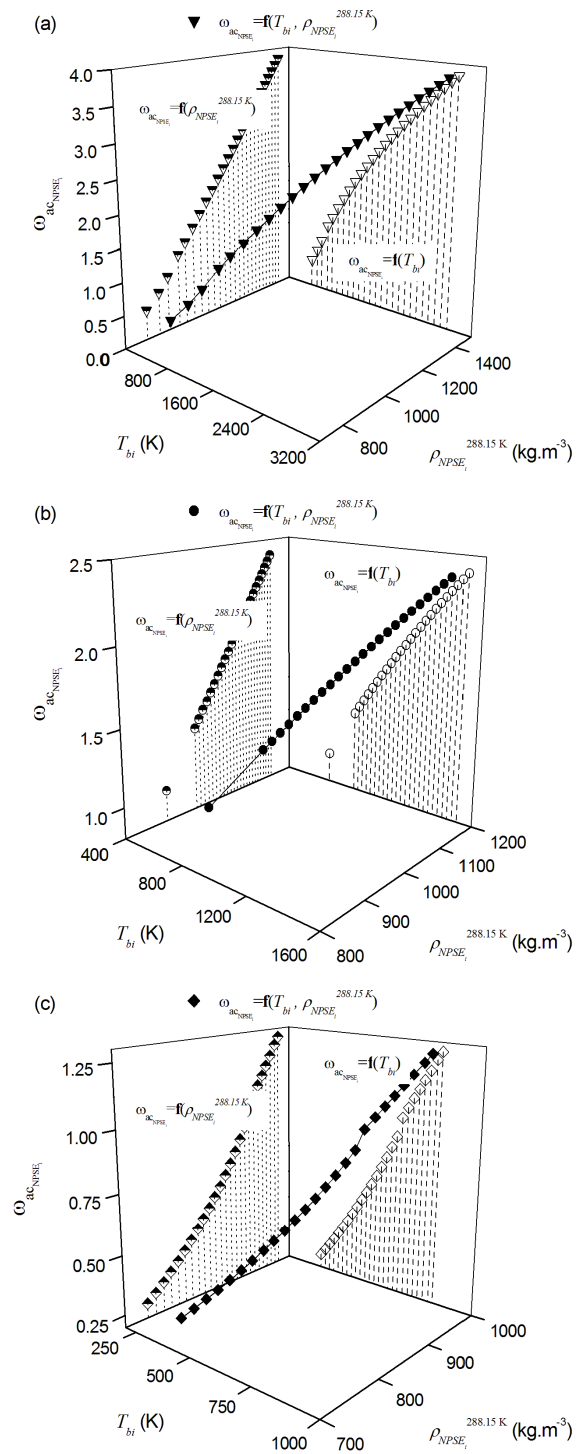


Figure 9. Pseudocritical acentric factor ($\omega_{ac_{NPSE_i}}$) as a function of normal boiling point (T_{bi}) and density at 288.15 K ($\rho_{NPSE_i}^{288.15 K}$) of a) ATR-W, b) ATR-Y and c) ATR-Z.

5.3. Thermophysical properties of the whole fractions

Figures 10 – 13 present the thermophysical properties for the three Brazilian high-boiling-point petroleum fractions (ATR-W, ATR-Y and ATR-Z), calculated in a temperature range from 350 to 600 K according to the semi-theoretical method mentioned in Equations (21) – (29). Data computed were compared with the experimental data.

5.3.1. Transport properties

5.3.1.1. Kinematic Viscosity

The estimation of kinematic viscosity (ν) was carried out using two correlations (Equations 22 and 23) aiming to compare the methods with respect to the experimental data (Figure 10 and Table 15). Thus, the methods employed varied with the type of fraction analyzed. The comparison of these different methods showed that they produced consistent results with each other.

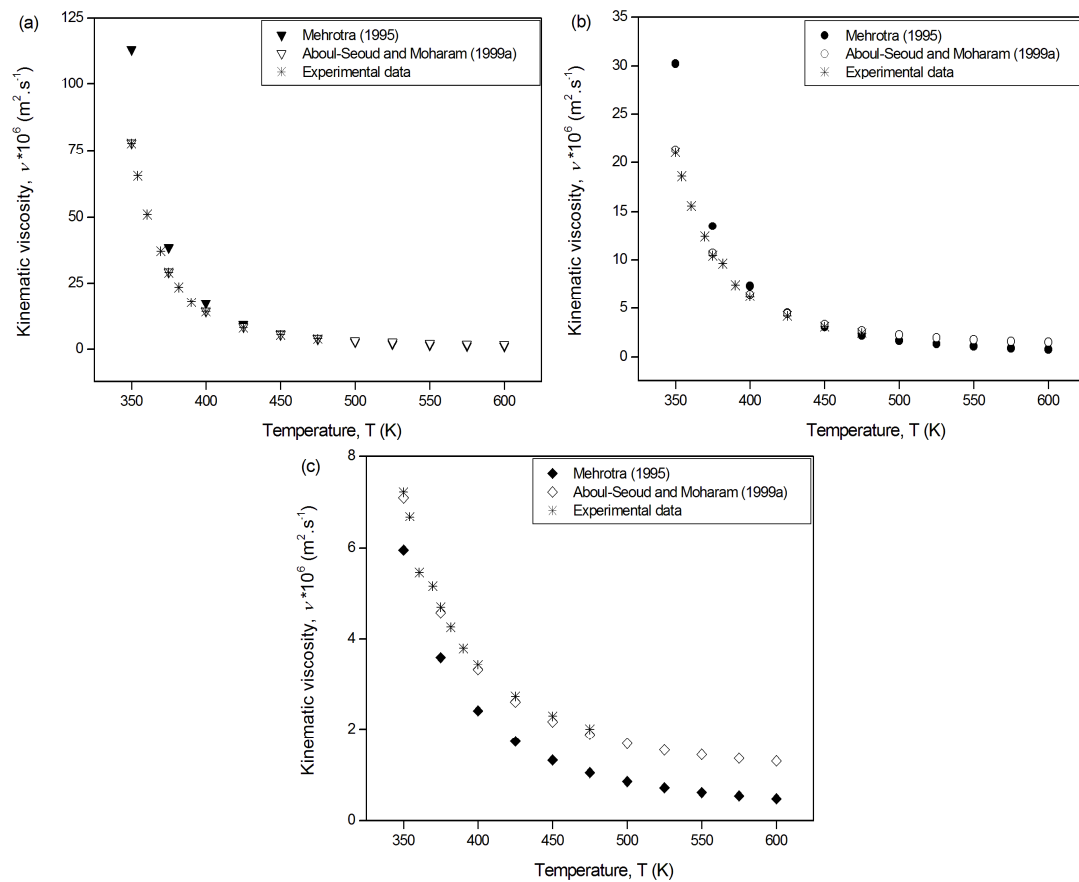


Figure 10. Kinematic viscosity (ν) as function of temperature (T) for a) ATR-W, b) ATR-Y and c) ATR-Z and comparison with experimental data (*).

Several factors are responsible for the viscosity of oil and its fractions. In the specific case study approached here, the viscosity showed a general trend to decrease with increasing temperature and increase with increasing pressure and density, and it also depended on the molecular structure of the hydrocarbons. According to this, it was found that the value for ν increased for pseudocomponents with the high molar mass. This was because the flow was facilitated by the possibility of larger flexibility or deformation of molecules that have a smaller number of carbons in their compositions. With respect to this question, the presence of certain functional groups capable of forming hydrogen bonds leads to an increase in the intermolecular size, even resulting in an increase in ν , such as, for example, in the ATR–Y case study, since it is rich in asphaltene chains.

Reliable correlations that are capable of estimating the value of ν for undefined high-boiling-point petroleum fractions (ATR–W, ATR–Y and ATR–Z), using the minimum input information, were used. Simulated data were compared with experimental data obtained in the research laboratories. The Aboul–Seoud and Moharam (1999a) correlation (Equation 23) gives overall average absolute deviation percents (*AAD%*) of 2.54%, 3.78% and 3.71% for ATR–W, ATR–Y and ATR–Z, respectively, in comparison with the method of Mehrotra (1995) (Equation 22) that gave values of 25.64%, 22.52% and 27.64%, respectively, for the average absolute deviation percentages (*AAD%*). Thus, Equation (23) provides more accurate results than Equation (22) as proposed by Mehrotra (1995), since Equation (23) requires more input information and the improvement in *AAD%* justifies the endeavor to introduce the *SG* as an input parameter, especially when it is readily available, together with the *MeABP* (for the whole fraction) and T_{bi} (for the pseudocomponents), to characterize the undefined high-boiling-point petroleum fractions and its pseudocomponents.

Table 15. Predicted kinematic viscosity and absolute deviations percent (%) calculated by Equations (22) and (23) at various temperatures for ATR-W, ATR-Y and ATR-Z.

Feedstock	Temperature (K)	Kinematic viscosity, $\nu \cdot 10^6 \text{ (m}^2 \cdot \text{s}^{-1}\text{)}$				
		Predicted data (y_{cal})		Experimental data (y_{ref})	Absolute deviations percent (%)	
		Equation (22)	Equation (23)		Equation (22)	Equation (23)
ATR-W	350.0	113.242	77.898	77.694	45.754	0.263
	354.2	92.150	64.544	65.454	40.786	1.390
	360.6	68.713	49.411	51.067	34.555	3.243
	369.7	47.041	35.044	37.011	27.100	5.315
	375.0	38.430	29.199	28.995	32.540	0.704
	381.8	30.181	23.502	23.444	28.737	0.247
	390.3	22.883	18.358	17.700	29.282	3.718
	400.0	17.193	14.259	14.055	22.327	1.451
	425.0	9.267	8.360	8.156	13.622	2.501
	450.0	5.682	5.577	5.373	5.751	3.797
	475.0	3.819	4.084	3.880	1.572	5.258
	500.0	2.746	3.202	—	—	—
	525.0	2.077	2.642	—	—	—
	550.0	1.634	2.266	—	—	—
	575.0	1.327	2.002	—	—	—
	600.0	1.105	1.809	—	—	—
					AAD%=25.64	AAD%=2.54
ATR-Y	350.0	30.230	21.297	21.063	43.522	1.111
	354.2	25.953	18.663	18.602	39.517	0.328
	360.6	20.870	15.470	15.589	33.876	0.763
	369.7	15.727	12.154	12.423	26.596	2.165
	375.0	13.512	10.692	10.457	29.215	2.247
	381.8	11.260	9.180	9.6333	16.886	4.706
	390.3	9.125	7.718	7.4334	22.757	3.829
	400.0	7.332	6.463	6.229	17.707	3.757
	425.0	4.537	4.442	4.208	7.818	5.561
	450.0	3.079	3.343	3.109	0.965	7.527
	475.0	2.233	2.686	2.451	8.894	9.588
	500.0	1.704	2.264	—	—	—
	525.0	1.352	1.978	—	—	—
	550.0	1.106	1.776	—	—	—
	575.0	0.929	1.628	—	—	—
	600.0	0.796	1.516	—	—	—
					AAD%=22.52	AAD%=3.78
ATR-Z	350.0	5.953	7.105	7.226	17.617	1.675
	354.2	5.419	6.528	6.688	18.974	2.392
	360.6	4.731	5.788	5.466	13.447	5.891
	369.7	3.957	4.959	5.170	23.462	4.081
	375.0	3.592	4.568	4.689	23.395	2.581
	381.8	3.193	4.142	4.255	24.959	2.656
	390.3	2.783	3.707	3.791	26.589	2.216
	400.0	2.407	3.308	3.429	29.805	3.529
	425.0	1.738	2.601	2.722	36.150	4.445
	450.0	1.325	2.168	2.289	42.114	5.286
	475.0	1.053	1.884	2.005	47.481	6.035
	500.0	0.866	1.689	—	—	—
	525.0	0.731	1.549	—	—	—
	550.0	0.631	1.445	—	—	—
	575.0	0.556	1.367	—	—	—
	600.0	0.497	1.306	—	—	—
					AAD%=27.64	AAD%=3.71

$$AAD\% = (1/m) \sum_{i=1}^m \frac{|y_{i,cal} - y_{i,ref}|}{y_{i,ref}} * 100$$

Where m equals 11.

5.3.1.2. Thermal Conductivity

Thermal conductivity (λ) is an important property of high-boiling-point petroleum fractions and it is defined from the quantity of heat transmitted due to a unit temperature gradient in a unit area under steady state conditions. It is of large importance, since heat-transfer coefficients are usually computed using correlations that require thermal conductivity data. In process engineering, a number of methods have been published for estimating the thermal conductivity of high-boiling-point petroleum fractions at normal pressure. In this study, two methods have been investigated and compared with the experimental data (Figure 11).

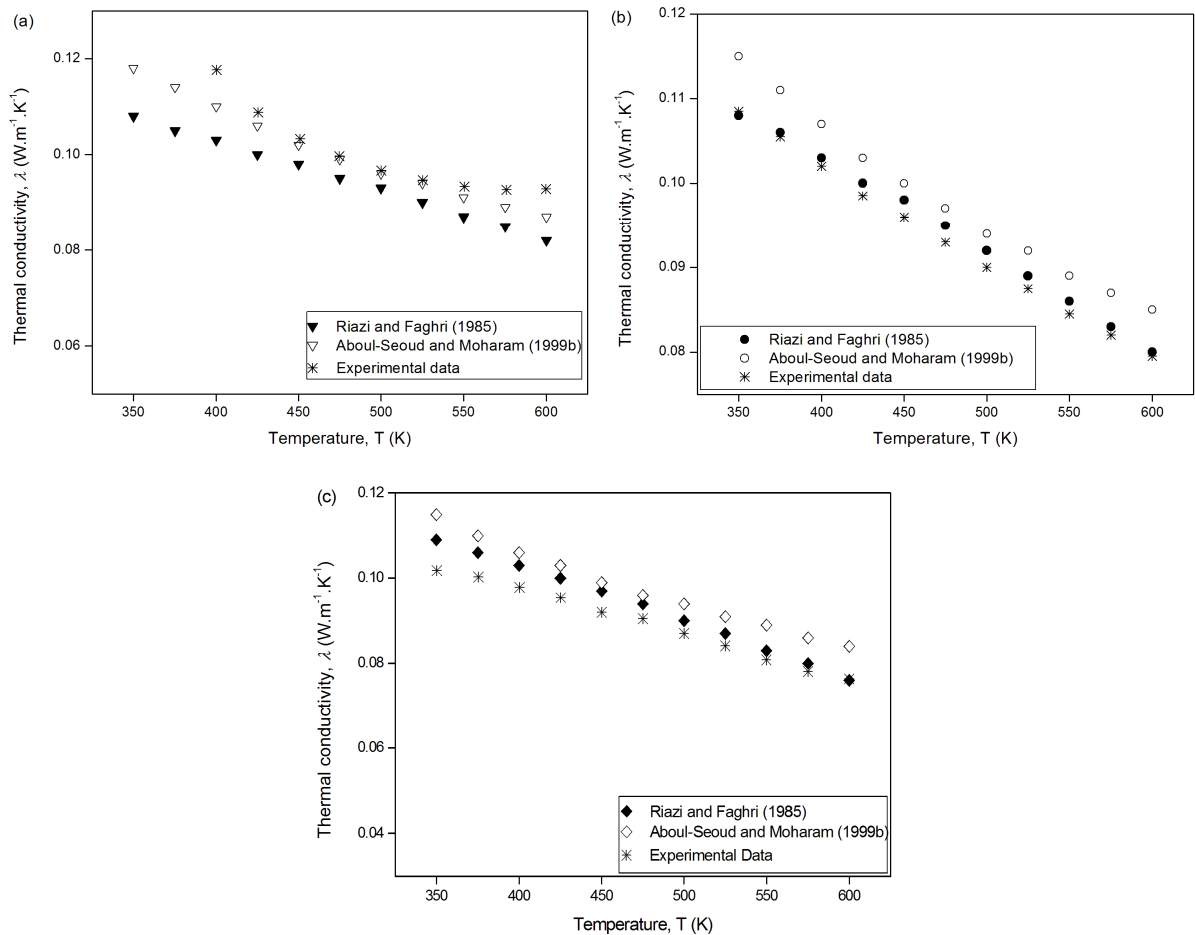


Figure 11. Thermal conductivity (λ) as function of temperature (T) for a) ATR-W, b) ATR-Y and c) ATR-Z and comparison with experimental data (*).

Figure 11 shows the λ plot using both the Riazi and Faghri (1985) (Equation 24 from Table 5) and also Aboul-Seoud and Moharam (1999b) (Equation 26 from Table 5) methods. It

was showed that the second method provided better correspondence and it can be considered more accurate than the other correlations for the ATR–Y and ATR–Z fractions. In Figure 11, a comparison was made with the data for λ obtained for the high-boiling-point petroleum fractions by DSC experiments. Using the method of Aboul-Seoud and Moharam (1999b), values of 5.84, 5.19 and 9.01 *AAD%*, were obtained for ATR–W, ATR–Y and ATR–Z, respectively, when compared with the values of 10.73, 1.39 and 4.05 *AAD%* for ATR–W, ATR–Y and ATR–Z obtained using the Riazi and Faghri (1985) method (Table 16).

5.3.2. Thermal properties

5.3.2.1. Specific heat capacity

The specific heat capacities (C_p) for ATR–W, ATR–Y and ATR–Z were plotted in Figure 12 for a temperature range between 350 and 600 K. For these samples, a strong temperature dependence of the C_p was observed in the range considered. It is apparent from Figure 12 that the C_p of the fractions increased linearly with an increase in temperature for all the fractions. The difference in C_p amongst the high-boiling-point petroleum fractions was due to differences in the chemical composition. In general, the specific heat capacity might have a general effect on density and on the nature of the compounds in the mixture.

The specific heat capacities (C_p) data were evaluated in terms of average absolute deviation (*AAD%*) where the absolute deviation was defined as the difference between the experimental value ($y_{i,ref}$) obtained from experimental studies and the data predicted by the computational approach ($y_{i,cal}$) (Table 16). Moreover, the results predicted were entirely consistent with those obtained experimentally in the research laboratories (LDPS/LOPCA), in which conventional differential scanning calorimetry (DSC) was employed. For ATR–W, the method of Kesler and Lee (1976) gave an overall average absolute deviation (*AAD%*) of 2.61%, as compared to 8.65% for the Watson and Nelson (1933) method; for ATR–Y the method of Kesler and Lee (1976) gave 9.72 % as compared to 12.19% for the Watson and Nelson (1933) method, and for ATR–Z the method of Kesler and Lee (1976) gave 8.58 % *AAD* as compared to 13.00% for the Watson and Nelson (1933) method (Table 16).

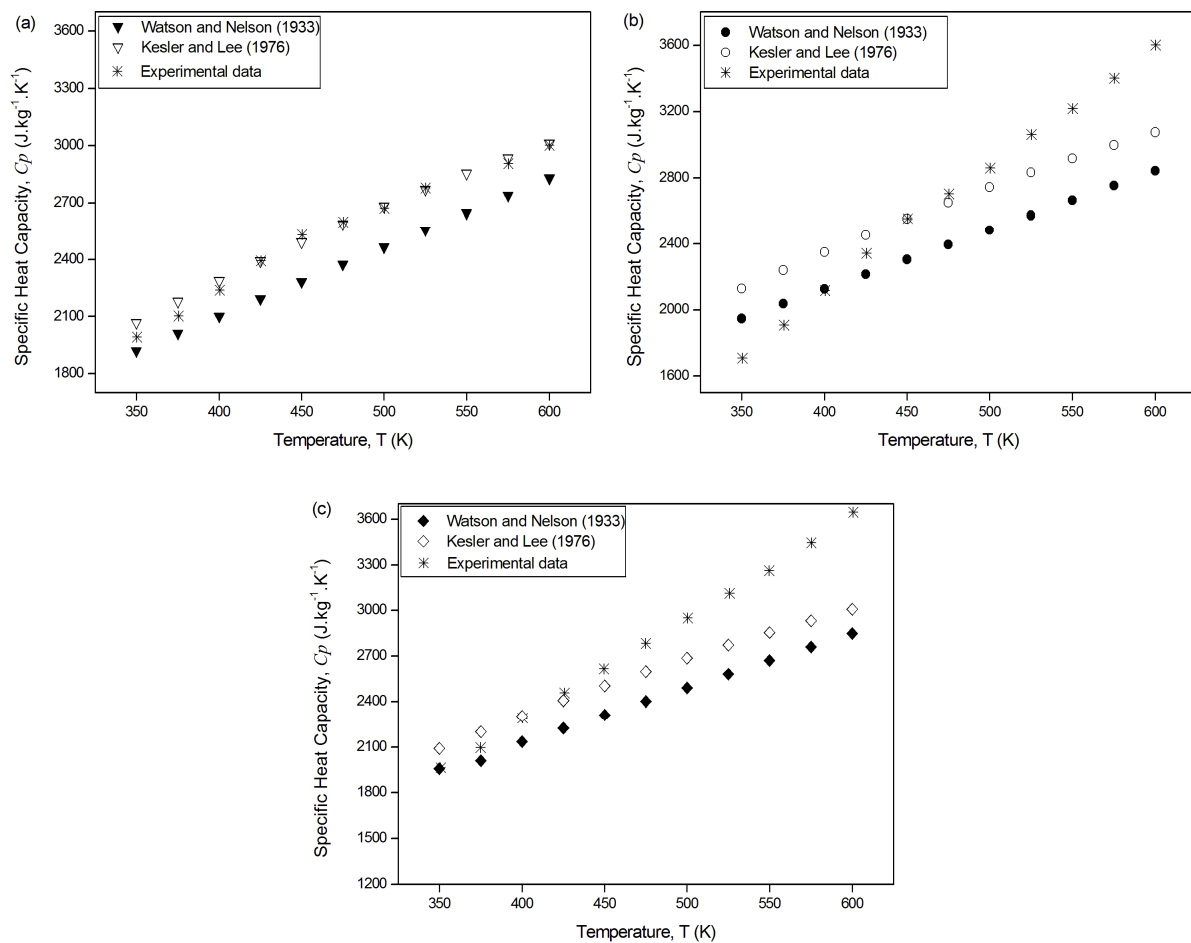


Figure 12. Specific heat capacity (C_p) as function of temperature (T) for a) ATR-W, b) ATR-Y and c) ATR-Z and comparison with experimental data (*).

Table 16. Predicted thermal conductivity and specific heat capacity and absolute deviations percent (%) calculated by Equations (24) and (26) and Equations (27) – (28), respectively, at various temperatures for ATR–W, ATR–Y and ATR–Z.

Feedstock	Temperature (K)	Thermal conductivity, λ (W·m ⁻¹ ·K ⁻¹)					Specific heat capacity, [†] C_p (J·kg ⁻¹ ·K ⁻¹)						
		Predicted data (y_{cal})		Experimental data (y_{ref})	Absolute deviations percent (%)		Predicted data (y_{cal})		Experimental data (y_{ref})	Absolute deviations percent (%)			
		Equation (24)	Equation (26)		Equation (24)	Equation (26)	Equation (27)	Equation (28)		Equation (27)	Equation (28)		
ATR-W	350.0	0.108	0.118	0.158	31.507	25.165	1919.753	2067.381	1992.520	3.652	3.757		
	375.0	0.105	0.114	0.132	20.653	13.852	2010.757	2179.767	2599.990	22.663	16.162		
	400.0	0.103	0.110	0.118	12.460	6.510	2101.761	2288.186	2238.840	6.123	2.204		
	425.0	0.100	0.106	0.109	8.071	2.556	2192.765	2392.636	2394.470	8.424	0.077		
	450.0	0.098	0.102	0.103	5.149	1.278	2283.769	2493.119	2531.910	9.801	1.532		
	475.0	0.095	0.099	0.100	4.733	0.722	2374.773	2589.633	2599.990	8.662	0.398		
	500.0	0.093	0.096	0.097	3.777	0.673	2465.777	2682.180	2671.380	7.697	0.404		
	525.0	0.090	0.094	0.095	4.953	0.729	2556.781	2770.758	2777.950	7.962	0.259		
	550.0	0.087	0.091	0.093	6.752	2.465	—	—	—	—	—		
	575.0	0.085	0.089	0.093	8.287	3.971	2738.789	2936.010	2906.220	5.761	1.025		
	600.0	0.082	0.087	0.093	11.666	6.280	2829.793	3012.685	3002.760	5.760	0.331		
					AAD%=10.73	AAD%=5.84						AAD%=8.65	AAD%=2.61
ATR-Y	350.0	0.108	0.115	0.109	0.461	5.991	1948.240	2129.018	1708.270	14.048	24.630		
	375.0	0.106	0.111	0.106	0.474	5.213	2037.856	2241.586	1909.220	6.738	17.408		
	400.0	0.103	0.107	0.102	0.980	4.902	2127.472	2350.178	2118.540	0.422	10.934		
	425.0	0.100	0.103	0.099	1.523	4.569	2217.088	2454.796	2344.720	5.443	4.695		
	450.0	0.098	0.100	0.096	2.083	4.167	2306.705	2555.437	2556.170	9.759	0.029		
	475.0	0.095	0.097	0.093	2.151	4.301	2396.321	2652.104	2704.310	11.389	1.930		
	500.0	0.092	0.094	0.090	2.222	4.444	2485.937	2744.795	2861.710	13.131	4.085		
	525.0	0.089	0.092	0.088	1.714	5.143	2575.553	2833.510	3063.130	15.918	7.496		
	550.0	0.086	0.089	0.085	1.775	5.325	2665.169	2918.251	3218.340	17.188	9.324		
	575.0	0.083	0.087	0.082	1.220	6.098	2754.786	2999.015	3401.150	19.004	11.824		
	600.0	0.080	0.085	0.080	0.629	6.918	2844.402	3075.805	3600.330	20.996	14.569		
					AAD%=1.39	AAD%=5.19						AAD%=12.19	AAD%=9.72
ATR-Z	350.0	0.109	0.115	0.102	7.083	12.978	1956.379	2091.286	1963.850	0.380	6.489		
	375.0	0.106	0.110	0.100	5.683	9.671	2010.757	2200.268	2096.020	4.068	4.974		
	400.0	0.103	0.106	0.098	5.306	8.373	2134.818	2305.400	2291.720	6.846	0.597		
	425.0	0.100	0.103	0.095	4.789	7.933	2224.038	2406.684	2456.070	9.447	2.011		
	450.0	0.097	0.099	0.092	5.435	7.609	2313.258	2504.118	2615.840	11.567	4.271		
	475.0	0.094	0.096	0.091	3.833	6.042	2402.477	2597.704	2784.670	13.725	6.714		
	500.0	0.090	0.094	0.087	3.401	7.996	2491.697	2687.440	2951.740	15.585	8.954		
	525.0	0.087	0.091	0.084	3.436	8.192	2580.917	2773.328	3112.240	17.072	10.890		
	550.0	0.083	0.089	0.081	2.710	10.135	2670.136	2855.368	3261.120	18.122	12.442		
	575.0	0.080	0.086	0.078	2.446	10.129	2759.356	2933.556	3646.810	24.335	19.558		
	600.0	0.076	0.084	0.076	0.445	10.034	2848.576	3007.897	3646.810	21.889	17.520		
					AAD%=4.05	AAD%=9.01						AAD%=13.00	AAD%=8.58

$$AAD\% = (1/m) \sum_{i=1}^m \frac{|y_{i,cal} - y_{i,ref}|}{y_{i,ref}} * 100 \quad \text{Where } m \text{ equals 11. } ^{\dagger} m \text{ equals 10 to compute } AAD\% \text{ by Equations (27) – (28) in order to estimate specific heat capacity for ATR–W.}$$

5.3.2.2. Predicted vapor pressure

Vapor pressure (P_{vap}) predictions as a function of temperature were carried out using Equation (29). As a general trend, the relation between P_{vap} and temperature is non-linear. The P_{vap} of the samples, at a given temperature, increases as the value for $MeABP$ increases. This is illustrated in the vapor pressure chart that shows graphs of P_{vap} versus temperature for ATR-W, ATR-Y and ATR-Z (Figure 13). For example, at a given temperature (at 450 K), the ATR-W sample showed the highest vapor pressure as compared to the other samples in the chart. It also had the highest $MeABP$, equal to 819.7 K.

However, the vapor pressure of a liquid increases as the temperature increases in a non-linear relation as shown in Figure 13 for ATR-W, ATR-Y and ATR-Z, respectively. As the temperature increased, the molecular kinetic energy of the molecules increased, and thus more molecules can escape from the liquid phase to the vapor phase. Accordingly, as the temperature increased, so did the P_{vap} .

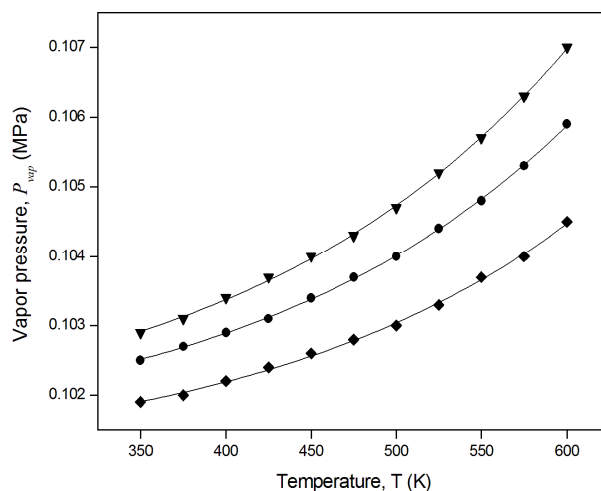


Figure 13. Vapor pressure (P_{vap}) of whole fraction as a function of temperature (T). ATR-W (\blacktriangledown), ATR-Y (\bullet) and ATR-Z (\blacklozenge).

At constant temperature and pressure, existing inter-molecular forces of the substance are the determining factors of the P_{vap} . The effect of M on P_{vap} is depicted in Figure 13. At a given temperature (at 400 K) the vapor pressures for ATR-W, ATR-Y and ATR-Z differed due to differences in the length of their hydrocarbon chains and the type of intermolecular forces, namely London dispersion forces. This type of intermolecular force is related to the molecular size and has some connection with the molar mass (M).

Nevertheless, possible non-polar pseudocomponents present in ATR-W and ATR-Y have relatively small intermolecular forces (no hydrogen bonding and/or dipole-dipole forces), and thus these samples have a relatively high P_{vap} when compared with the ATR-Z fraction.

6. Conclusions

The computational approach has shown to be a powerful and efficient tool to predict the physicochemical properties of petroleum fractions. The method requires a boiling point curve and the specific gravity as the input data information. This method focuses specifically on high-boiling-point petroleum fractions and the selection of the right characterization method has an important effect on the properties calculated. Moreover, the computational procedure can be combined with or incorporated into petroleum process simulations or assist studies about petroleum processing by providing an easy and accurate method for characterization of petroleum fraction properties with lower computational effort.

The critical properties were assayed by way of an optimization exercise to obtain the best set of correlations for estimating the molar mass (M), critical properties (T_c , P_c) and acentric factor (ω_{ac}). Accordingly, a set established by Equations (12) – (14) (coded by **0**) and Equation (19) (coded by **-1**) comprised the correlations with which it was possible to obtain the lowest mass and molar balance errors.

The critical properties such as critical temperature (T_c) and critical pressure (P_c) were sensitive to the normal boiling point (T_{bi}) and density (ρ_i) of the pseudocomponents. For higher values of T_{bi} , the value for T_{CNPSE} increased, but the value for P_{CNPSE} and the ratio between M_{NPSE} and V_{CNPSE} decreased. This result reflects the relationship between the thermodynamic properties and the amount of hydrocarbons and type of chains amongst them.

A set of reliable correlations can be used to estimate the thermophysical and transport properties with a minimal number of input data such as the *MeABP* (mean average boiling point), in the case of a whole petroleum fraction or T_{bi} (normal boiling point) for each pseudocomponent, together the *SG* (specific gravity). The proposed method seems to be simple and flexible. The data computed were in good agreement with the experimental data obtained in the research laboratories, since the *ADD%* was lower than 10%. Hence, the model of Aboul-Seoud and Moharam (1999b) for the prediction of the thermal conductivity (λ) of high-boiling-point petroleum fractions, which requires as input information the value of T_b , was evaluated in this

work and compared with that of Riazi and Faghri (1985). The model of Aboul-Seoud and Moharam (1999b) provided satisfactory results, which were much better than those obtained with the second model since good agreement between the predicted and experimental values has been found, with an overall absolute deviation of 5.84, 5.19 and 9.01 % for ATR–W, ATR–Y and ATR–Z, respectively.

Aboul-Seoud and Moharam (1999a) method, Equation (23), showed the lowest standard deviation (below 5%) for predicting the kinematic viscosity (ν) values of the analyzed high-boiling-point petroleum fractions in the Newtonian range from 350 to 600 K, when compared with the Mehrotra (1995) method (Equation 22).

The results obtained for the specific heat capacity (C_p) for the selected high-boiling-point petroleum fractions (ATR–W, ATR–Y and ATR–Z) provided reliable data using the correlation proposed by Kesler and Lee (1976), since the values for the $AAD\%$ were 2.61%, 9.72% and 8.58% for ATR–W, ATR–Y and ATR–Z, respectively.

In this work, a simple correlation was used for the estimation of the vapor pressure (P_{vap}) of the high-boiling-point petroleum fractions, where only the boiling point (T_b) and the temperature (T) are required.

Acknowledgements

This research was supported by the Brazilian National Council for Technological and Scientific Development (CNPq), the Petrobras Research and Development Center (PETROBRAS/CENPES) and the Brazilian Study and Project Financing Institution (FINEP).

Nomenclature

C_p	Specific heat capacity of whole fraction	$[J \cdot kg^{-1} \cdot K^{-1}]$
$CABP$	Cube of the average boiling point	$[K]$
E_{mass}	Material balance error	$[-]$
E_{mol}	Molar balance error	$[-]$
K_{OUP}	Universal Oil Products Company characterization factor	$[-]$
K_w	Watson characterization factor	$[-]$
M	Molar mass	$[kg \cdot kmol^{-1}]$
$MABP$	Molar average boiling point	$[K]$
$MeABP$	Mean average boiling point	$[K]$
$MeABP^*$	Starting value of the mean average boiling point	$[K]$
M_{NPSE}	Molar mass of pseudocomponent	$[kg \cdot kmol^{-1}]$
n	Number of pseudocomponent	$[-]$

P_c	Critical pressure	[Pa]
$P_{c_{NPSE}}$	Pseudocritical pressure	[Pa]
P_{vap}	Vapor pressure of whole fraction	[Pa]
SG	Specific gravity	[-]
T	Temperature	[K]
T_b	Boiling point	[K]
T_{bi}	Normal boiling point	[K]
T_{b_r}	Reduced boiling point $T_{b_r} = T_b / T_c$	[-]
T_c	Critical temperature	[K]
$T_{c_{NPSE}}$	Pseudocritical temperature	[K]
$VABP$	Volumetric average boiling point	[K]
V_c	Critical volume	[m ³ ·mol ⁻¹]
$V_{c_{NPSE}}$	Pseudocritical volume	[m ³ ·mol ⁻¹]
$WABP$	Weight average boiling point	[K]
x_{mi}	Molar fraction of pseudocomponent	[-]
x_{vi}	Volume fraction of pseudocomponent	[-]
x_{wi}	Weight fraction of pseudocomponent	[-]
<i>Greek letters</i>		
λ	Thermal conductivity of whole fraction	[W·m ⁻¹ ·K ⁻¹]
μ	Dynamic viscosity of whole fraction	[Pa·s]
ν	Kinematic viscosity of whole fraction	[m ² ·s ⁻¹]
ρ	Density of whole fraction	[kg·m ⁻³]
ρ_i, ρ_{NPSE}	Density of pseudocomponent i	[kg·m ⁻³]
ρ_{water}	Density of water (at 288.15 K)	[kg·m ⁻³]
σ	Shear rate	[s ⁻¹]
τ	Yield stress	[Pa]
ω_{ac}	Acentric factor	[-]
$\omega_{ac_{NPSE}}$	Acentric factor of pseudocomponent	[-]
<i>Subscript</i>		
i	Pseudocomponent i	
$NPSE$	Pseudocomponent	
<i>Superscript</i>		
L_s	Left side	
R_s	Right side	
$*$	Starting value	
<i>Acronyms</i>		
ATR	Residue from conventional atmospheric distillation (ASTM D 2892, 2005)	
BP	Boiling Point distillation data	
CENPES	Petrobras Research and Development Center	
NDATA	Number of input data for the BP data	
NDGER	Degree of lagrange's interpolation polynomial	
NITER	Maximum number of iterations	
OUP	Universal Oil Products Company	
TBP	True boiling point	
W, Y, Z	Dummy names for ATR fractions	

References

- Aboul-Seoud A.-L., Moharam H. M. (1999a) Short communication – A generalized viscosity correlation for undefined petroleum fractions, *Chemical Engineering Journal* **72**, 3, 253–256.
- Aboul-Seoud A.-L., Moharam H. M. (1999b) A simple thermal conductivity–temperature correlation for undefined petroleum and coal liquid fractions, *Chemical Engineering Research and Design* **77**, 3, 248–252.
- American Society for Testing Materials, ASTM D 287: Standard test method for API gravity of crude petroleum and petroleum products (Hydrometer method). West Conshohoken, (Pennsylvania): ASTM International, 1992. 3p, [Reapproved 2006].
- American Society for Testing Materials, ASTM D 1298. Standard test method for density, relative density (specific gravity), or API gravity of crude petroleum and liquid petroleum products by hydrometer method. West Conshohoken, (Pennsylvania): ASTM International, 1999. 6p, [Reapproved 2005].
- American Society for Testing Material, ASTM D 2892. Standard test method for distillation of crude petroleum (15–Theoretical plate column). West Conshohoken, (Pennsylvania): ASTM International, 2005. 32p.
- Beer E. (1994) Petroleum fractions characterization and breakdown into pseudocomponents, *Nafta* **45**, 12, 617–627.
- Boozarjomehry R. B., Abdolahi F., Moosavian M. A. (2005) Characterization of basic properties for pure substances and petroleum fractions by neural network, *Fluid Phase Equilibria* **231**, 2, 188–196.
- Coats K. H. (1985) Simulation of gas condensate reservoir performance, *Journal of Petroleum Technology* **37**, 10, 1870–1886.
- Danesh A. (1998) PVT and phase behavior of reservoir fluids, in: *Developments in Petroleum Science*, Elsevier Science, New York.
- Daubert T. E., Danner R. P., Sibul H. M., Stebbins C. C., Oscarson J.L., Zundel N., Marshal T.L., Adams M. E., Wilding W. V. (2000). *Physical and Thermodynamic Properties of Pure Chemicals: DIPPR: Data Compilation*, (10thed.). Taylor and Francis.

- Daubert T. E., Danner R. P. (1997) *API Technical Data book–petroleum refining*, (6th ed.), American Petroleum Institute (API), Washington, D.C.
- Eckert E., Vaněk T. (2005) New approach to the characterisation of petroleum mixtures used in the modelling of separation processes, *Computers & Chemical Engineering* **30**, 2, 343–356.
- Edmister W. C. (1958) Applied hydrocarbon thermodynamics, Part 4: Compressibility factors and equations of state, *Petroleum Refiner* **37**, 4, 173–179.
- Gharagheizi F., Fazeli A. (2008) Prediction of the Watson characterization factor of hydrocarbon components from molecular properties, *QSAR & Combinatorial Science* **27**, 6, 758–767.
- Hu S., Zhu F. X. X. (2001) A general framework for incorporating molecular modelling into overall refinery optimisation, *Applied Thermal Engineering* **21**, 13–14, 1331–1348.
- Kesler M. G., Lee B. I. (1976) Improve Prediction of enthalpy of fractions, *Hydrocarbon Processing* **55**, 3, 153–158.
- Korsten H. (1998) Critical properties of hydrocarbon systems, *Chemical Engineering & Technology* **21**, 3, 229–244.
- Lakshmi D. S., Prasad D. H. L. (1992) A rapid estimation method for thermal conductivity of pure liquids, *The Chemical Engineering Journal* **48**, 3, 211–214.
- Lee B. I., Kesler M. G. (1975) A generalized thermodynamic correlation based on three-parameter corresponding states, *AIChE Journal* **21**, 3, 510–527.
- Lion A. R., Edmister W. C. (1975) Make equilibrium calculations by computer; *Hydrocarbon Processing* **54**, 8, 119–122.
- Mehrotra A. K. (1995) A simple equation for predicting the viscosity of crude oil fractions, *Chemical Engineering Research and Design* **73**, 1, 87–90.
- Mehrotra A. K.; Monnery W. D.; Svrcek, W. Y. (1996) A review of practical calculation methods for the viscosity of liquid hydrocarbons and their mixtures, *Fluid Phase Equilibria* **117**, 1–2, 344–355.
- Merdrignac I., Espinat D. (2007) Physicochemical characterization of petroleum fractions: The state of the art, *Oil & Gas Science and Technology* **62**, 1, 7–32.

- Miquel J., Castells F. (1993) Easy characterization of petroleum fractions (part 1), *Hydrocarbon Processing* **72**, 12, 101–105.
- Miquel J., Castells F. (1994) Easy characterization of petroleum fractions (part 2), *Hydrocarbon Processing* **73**, 1, 99–103.
- Moharam H. M., Al-Mehaideb R. A., Fahim M. A. (1995) New correlation for predicting the viscosity of heavy petroleum fractions, *Fuel* **74**, 12, 1776–1779.
- Nichita D. V., Pauly J., Montel F., Daridon J.-L. (2008) Pseudocomponent delumping for multiphase system with waxy solid phase precipitation, *Energy & Fuels* **22**, 2, 775–783.
- Ourique J. E., Telles A. S. (1997) Estimation of properties of pure organic substances with group and pair contributions, *Brazilian Journal of Chemical Engineering* **14**, 2, 1–17.
- Panteli E., Voutsas E., Magoulas K., Tassios D. (2006) Prediction of vapor pressures and enthalpies of vaporization of organic compounds from the normal boiling point temperature, *Fluid Phase Equilibria* **248**, 1, 70–77.
- Pasquini C., Bueno A. F. (2007) Characterization of petroleum using near-infrared spectroscopy: Quantitative modeling for the true boiling point curve and specif gravity, *Fuel* **86**, 12–13, 1927–1934.
- Pitzer K. S., Lippmann D. Z., Curl Jr. R. F., Huggins C. M., Petersen D. E. (1955) The Volumetric and thermodynamic properties of fluids. II. Compressibility factor, vapor pressure and entropy of vaporization¹, *Journal of the American Chemical Society* **77**, 13, 3433–3440.
- Poling B. E., Prausnitz J. M., O’Connel J. P. (2001) *The Properties of Gases and Liquids*, (5th ed.), McGraw–Hill, New York.
- Quann R. J., Jaffe S. B. (1992) Structure-oriented lumping: Describing the chemistry of complex hydrocarbon mixtures, *Industrial & Enginnering Chemistry Research* **31**, 11, 2483–2497.
- Riazi M. R. (2004) *Characterization and properties of petroleum fractions*, ASTM International Standards Worldwide, Kuwait.
- Riazi M. R., Al-Sahhaf T. A. (1996) Physical properties of heavy petroleum fractions and crude oils, *Fluid Phase Equilibria* **117**, 1–2, 217–224.

- Riazi M. R., Daubert T. E. (1980) Simplify property predictions, *Hydrocarbon Processing* **59**, 3, 115–116.
- Riazi M. R., Faghri A. (1985) Thermal conductivity of liquid and vapor hydrocarbon system: Pentanes and heavier at low pressures, *Industrial & Engineering Chemistry Process Design and Development* **24**, 2, 398–401.
- Satyro M. A., Yarranton H. (2009) Oil Characterization from simulation of experimental distillation data, *Energy & Fuels* **23**, 8, 3960–3970.
- Schlijper A. G. (1986) Simulation of compositional processes: The use of pseudocomponents in equation-of-state calculations, *SPE Reservoir Engineering* **1**, 5, 441–452.
- Shouzhi Y., Yuanyuan J., Peisheng M. (2005) Estimation of acentric factor of organic compounds with corresponding states group contribution method, *Chinese Journal of Chemical Engineering* **13**, 5, 709–712.
- Watson K. M., Nelson E. F. (1933) Improved methods for approximating critical and thermal properties of petroleum fractions, *Industrial & Engineering Chemistry* **25**, 8, 880–887.
- Watson K. M., Nelson E. F.; Murphy G. B. (1935) Characterization of petroleum fractions, *Industrial & Engineering Chemistry* **27**, 12, 1460–1464.
- Whitson C. H., Brulé M. R. (2000) *Phase Behavior. SPE Monograph series*, Richardson: Society of Petroleum Engineers, Inc., Texas.
- Winn W. (1955) Physical properties by nomogram, *Petroleum Refiner* **36**, 2, 157–159.

Source: From Tovar L. P., Wolf Maciel M. R., Batistella C. B., Maciel Filho R., Gomes A. de O., Medina L. C. (2010) Development & application of continuous thermodynamics for studying physicochemical properties of petroleum fractions. Proceedings of Distillation Absorption 2010 (DA2010), September 12–15 2010, Eindhoven, The Netherlands / Ed. A.B. de Haan, H. Kooijman, A. Górak. – Eindhoven, The Netherlands : DA2010, 2010. – ISBN 978–90–386–2215–6. – p. 503–508.

Copyright notice: The content of this manuscript is licensed under the Ethical Guidelines to Publication of Proceedings of Distillation Absorption 2010 (DA2010). Please contact credited rights holders directly for permission to reproduce material.

Development & application of continuous thermodynamic to predict physicochemical properties of petroleum fractions

Abstract

In studies to predict the physicochemical properties of petroleum fractions (mixture of hydrocarbons), the general practice in the petroleum industry is divided mathematically this fractions into a group of narrow boiling range which enables to assign properties to these pseudocomponents. However, the tracking of all pseudocomponents, which are more than 20.000, of petroleum fractions would involve enormous computational efforts.

This work presents an approach for characterizing the petroleum fractions as a continuous distribution functions. Calculations by continuous thermodynamics approach are developed where distilled volume data and the specific gravities are the input data; normal boiling point is the distribution variable and the distribution function is the boiling point curve that already had the temperature experimental data converted to atmospheric equivalent temperature – AET. Thermodynamic, transport and thermophysical properties are related to boiling point by well-established petroleum methods proposed by available correlations and industry standard methods.

The computational results indicated that the continuous thermodynamic method is an accurate technique for predicting the physicochemical properties of petroleum fractions. Continuous thermodynamics provides a potentially useful tool for petroleum industry to increase the computational speed and accuracy because it is not necessary to characterize various families of hydrocarbons which may be present in the petroleum fraction.

Keywords: Continuous thermodynamics, continuous mixture, generalized distribution function, petroleum fractions characterization.

Contents

1. Introduction
 - 1.1. Distribution function
 2. Modeling of continuous mixture
 - 2.1. Petroleum fractions and data requirements
 - 2.2. Development Method
 - 2.3. Adjustment and optimization of model parameters
 - 2.4. Physical properties studied
 3. Results and discussion
 - 3.1. Evaluation of the proposed method
 - 3.2. Parameters for the continuous distribution functions
 - 3.3. Distribution functions for the boiling point of petroleum fractions
 - 3.4. Thermodynamic characterization of petroleum fractions
 - 3.5. Thermophysical and transport properties of petroleum fractions
 4. Conclusions
- Acknowledgements
Nomenclature
References

1. Introduction

A complex mixture is defined as one in which various families of compounds, with diverse molar mass, are present (Manafi et al., 1999). Petroleum fraction is a hydrocarbon mixture of unknown composition and of a wide boiling range. Hence, petroleum fractions may present some difficulties in the estimation of its physicochemical properties because: (i) The computation time increases when it is considered a great number of pseudocomponents (Shibata et al., 1987); (ii) The information about the type of the mixture (e.g. paraffinic or aromatic), or the type of some of its components (e.g. polar or non-polar) could not be easily utilized (Shibata et al., 1987; Vakili-Nezhaad et al., 2001) and (iii) The characterization of the mixture could be incomplete (Shibata et al., 1987).

In the present work, an accurate and efficient computational method, which reduces significantly the difficulties mentioned above, is presented for estimation of petroleum fractions physicochemical properties. Such approach is defined as thermodynamic of continuous mixture in which, a function of measurable property, such normal boiling point (T_b), specific gravity (SG) or molar mass (M), is introduced to describe composition of multicomponent mixtures.

1.1. Distribution function

The formulation of the continuous thermodynamic based on functional analysis, has been developed by several researchers in their works about description of the composition of multicomponent mixtures occurring in petroleum processes (or any other complex mixture); representation of physicochemical properties and phase equilibrium calculations of mixtures where number of chemical species is very large (Manafi et al., 1999; Vakili-Nezhaad et al., 2001; Cotterman et al., 1985; Cotterman and Prausnitz, 1985; Kehlen et al., 1985; Fang and Lei, 2003; Riazi, 1989; Briesen and Marquardt, 2003, 2004). Complex mixtures may be represented by: (i) Continuous and discrete components, which is usually called semicontinuous mixture (Lage, 2007; Koral et al., 1993), and, (ii) Continuous mixture which composition of all chemical species are described by continuous distribution functions.

In continuous thermodynamics, a distribution function, instead of mole or weight fraction, is used to represent the composition of complex mixture (Vakili-Nezhaad et al., 2001; Riazi, 1989). Some of the well-known equations for continuous description are presented in Table 1, where I is the distribution variable and $\alpha, \beta, \eta, \theta, \sigma, A, B, I_0$ are adjustable model parameters.

Table 1. Distribution functions for continuous thermodynamics description.

	Distribution Function	Adjustable parameters	Source	Equation
Gamma	$F(I) = [\beta^\alpha \Gamma(\alpha)]^{-1} (I - \eta)^{\alpha-1} \exp\left[\frac{(I - \eta)}{\beta}\right]$	α, β, η	Whitson, 1983	(1)
Gaussian	$F(I) = \left[\frac{1}{\sqrt{2\pi}\sigma}\right] \exp\left[\frac{-(I - \theta)^2}{2\sigma^2}\right]$	θ, σ	Shibata et al., 1987	(2)
Exponential decay	$F(I) = \left(\frac{1}{\eta}\right) \exp\left(\frac{-(I - \sigma)}{\eta}\right)$	η, σ	Mansoori et al., 1989	(3)
Generalized	$(I^*) = \left[\left(\frac{A}{B}\right) \ln\left(\frac{1}{1-x}\right)\right]^{1/B}$ where $I^* = (I - I_0) / I_0$	A, B, I_0	Riazi, 1989; Riazi et al., 2004	(4)

I : is the distribution variable; x : represents the cumulative volume fraction and $\alpha, \beta, \eta, \theta, \sigma, A, B, I_0$ are adjustable model parameters.

2. Modeling of continuous mixture

2.1. Petroleum fractions and data requirements

Three different petroleum fractions (ATR–W, ATR–Y and ATR–Z) have been studied. The API gravity degrees of those samples were between 16 – 25. These information were provided by the Petrobras Research and Development Center (CENPES–Brazil).

2.2. Development Method

The generalized relation proposed by Riazi has been applied for representing the boiling point distribution and it has the following form (Riazi et al., 2004; Riazi, 1989):

$$(I^*) = \left[\left(A / B \right) \ln \left(1 / (1 - x) \right) \right]^{1/B} \quad (4)$$

Where $I^* = (I - I_0) / I_0$; I is the absolute boiling point (T_b) and parameter x represents the cumulative volume fraction. x is defined by the following equation:

$$x = \int_0^{I^*} F(I^*) dI^* \quad (5)$$

Therefore, the distribution function has the property that:

$$\int_0^{\infty} F(I^*) dI^* = 1 \quad (6)$$

Rearranging and differentiating with respect to I^* Equation (4), the probability density function ($F(I^*)$) for distribution functions was defined by the following expression:

$$F(I^*) = \left(B^2 / A \right) I^{*B-1} \exp \left[- \left(B / A \right) I^{*B} \right] \quad (7)$$

Average value can be obtained from the following relation:

$$I_{av}^* = \int_0^{\infty} I^* F(I^*) dI^* = \left(A / B \right)^{1/B} \Gamma(1 + 1 / B) \quad (8)$$

Where $\Gamma(1 + 1 / B)$ is the gamma function and it can be calculated through the following relation (Riazi et al, 2004):

$$\Gamma(1 + 1 / B) = 0.992814 - 0.504242B^{-1} + 0.696215B^{-2} - 0.27293B^{-3} + 0.08836B^{-4} \quad (9)$$

Once I_{av}^* has been known, the average property of the mixture is obtained as:

$$I_{av} = I_0(1 + I_{av}^*) \quad (10)$$

2.3. Adjustment and optimization of model parameters

Equation (4) has three distribution parameters (A , B and I_0), where A and I_0 are parameters specific for each property and each sample; and B is the parameter specific for each property but the same for all samples (these value is $B_T=1.5$) (Riazi et al., 2004). The adjustable model parameters (A and I_0) were estimated by the FORTRAN subroutine RNLIN, available from IMSL MATH/LIBRARY. It uses a modified Levenberg–Marquardt method. For obtaining a suitable initial guess, of the A and I_0 , has been used PIKAIA sub-routine which is a genetic–algorithm–based optimization sub-routine developed at the High Altitude Observatory, and available in the public domain (Metcalf and Charbonneau, 2003). The genetic algorithm is capable of a much faster search than might be expected, when compared to classical (analytical or numerical) methods. Furthermore, it is reasonably simple to develop and represent a global search method. The typical objective function $C(x)$ is presented as follows:

$$\max C(x) = \max \left\{ \frac{1}{\text{error}(x)} \right\} \quad (11)$$

Where,

$$\text{error}(x) = \left[I_{T_b}(x) - \left\{ I_0 + I_0 \left[(A/1.5) \ln(1/(1-x)) \right]^{1/15} \right\} \right]^2 \quad (12)$$

The interval in which the optimum is searched is:

For ATR–W and $450 \leq T_b(K) \leq 820$, $3.31 \leq x \leq 51.93$

For ATR–W and $820 \leq T_b(K) \leq 1000$, $51.93 \leq x \leq 73.81$

For ATR–Y and $650 \leq T_b(K) \leq 720$, $3821 \leq x \leq 52.88$

For ATR–Y and $720 \leq T_b(K) \leq 800$, $52.88 \leq x \leq 72.33$

For ATR–Z and $370 \leq T_b(K) \leq 660$, $3.5 \leq x \leq 51.7$

For ATR–Z and $660 \leq T_b(K) \leq 840$, $51.7 \leq T_b \leq 71.3$

The maximum number of generations over which solution is to evolve is set at 2000. Initial population includes 120 individuals. The initial mutation rate, defined as the probability that any one gene locus will mutate in any one generation, is set at 0.005. In addition, the

crossover probability equals 0.85 and elitist function is not employed. After 2000 generations, the optimal solution of the suitable initial guess for the adjustable parameters of Equation (4) (A and I_0) is obtained and estimated parameters are shown in Table 4.

2.4. Physical properties studied

Table 2 present the physical properties investigated in this study by continuous thermodynamics and pseudocomponent (considering 25 discrete pseudocomponents). Column reference indicates the specific method applied to each one.

It is important let clear that thermal conductivity (λ) and specific heat capacity (C_p) were determined experimentally too, by standard methodologies.

Table 2. Properties used for characterizing ATR-W, ATR-Y and ATR-Z.

Type	Property	Methodology / Reference
		Pseudocomponent
Thermodynamic	Molar mass (M)	Riazi and Daubert, 1980
	Critical Temperature (T_c) and pressure (P_c)	Riazi and Daubert, 1980
Transport	Kinematic viscosity (ν)	Aboul-Seoud and Moharam, 1999a
	Thermal Conductivity (λ)	Aboul-Seoud and Moharam, 1999b
Thermophysical	Specific heat capacity (C_p)	Kesler and Lee, 1976

M : Molar mass; P_c : Critical pressure; T_c : Critical temperature; λ : Thermal conductivity; and ν : Kinematic viscosity.

3. Results and discussion

3.1. Evaluation of the proposed method

The distribution model proposed by Riazi (Riazi et al., 2004; Riazi, 1989) was examined with different distribution functions represented by Equations (1) – (3). These equations were used for estimating the normal boiling point curve of petroleum fractions studied. The absolute average deviation, often expressed as a percentage ($AAD\%$), it is shown in Table 3. The absolute deviation (Equation 13) is defined as the difference between the observed value ($y_{i,ref}$) and the response predicted by the distribution functions at each operating condition ($y_{i,cal}$) into the interval input data reported in Table 4 defined by the deflection exhibited in the boiling point curves obtained in the Petrobras Research and Development Center (CENPES–Brazil) represented by pairs of points of accumulated distilled volume versus temperature.

$$AAD\% = (1/m) \sum_{i=1}^m \frac{|y_{i,cal} - y_{i,ref}|}{y_{i,ref}} * 100 \quad (13)$$

From these evaluations, it is clear that Equation (4) had the minimum %ADD compared with Equations (1) – (3). Accordingly, the distribution function from Equation (4) was used in this work.

Table 3. Evaluation of the distribution functions for continuous description of normal boiling point.

Distribution Function	%AAD		
	ATR–W	ATR–Y	ATR–Z
Equation (2)	4.52	2.17	2.98
Equation (1)	3.38	2.76	4.03
Equation (4)	1.74	0.58	1.14

%AAD: absolute average deviation, often expressed as a percentage.

3.2. Parameters for the continuous distribution functions

All adjustable parameters of Equation (4) (A and I_0) were calculated by the regression analysis method. Table 4 shows results for the estimation of the adjustable model parameters. Statistical analyses were determined with 95% confidence interval on the regression parameters.

Table 4. Estimation of parameter for distribution functions.

Fraction	Interval input data, T_b (K)	Adjustable model parameters	95% Confidence Intervals		
			Estimate	Lower limit	Upper limit
ATR–W	450–820	I_0	443.88	416.99	470.78
		A	1.71	1.32	2.09
	820–1000	I_0	463.29	457.52	469.05
		A	1.22	0.50	1.94
ATR–Y	650–720	I_0	473.23	467.93	478.53
		A	0.80	0.21	1.38
	720–800	I_0	602.75	588.55	616.95
		A	0.17	0.07	0.27
ATR–Z	370–660	I_0	337.39	319.54	355.24
		A	3.45	2.74	4.17
	660–840	I_0	487.17	473.83	500.51
		A	0.77	0.69	0.86

A , I_0 : They are adjustable model parameters of Equation (4).

3.3. Distribution functions for the boiling point of petroleum fractions

Since, the chemical composition of the petroleum fractions is well represented and related to the volatility of the components; the normal boiling point was used as a distribution variable. Figure 1 shows the boiling point distribution from Equation (4) and Figure 2 shows the probability density function for the normal boiling point from Equation (7).

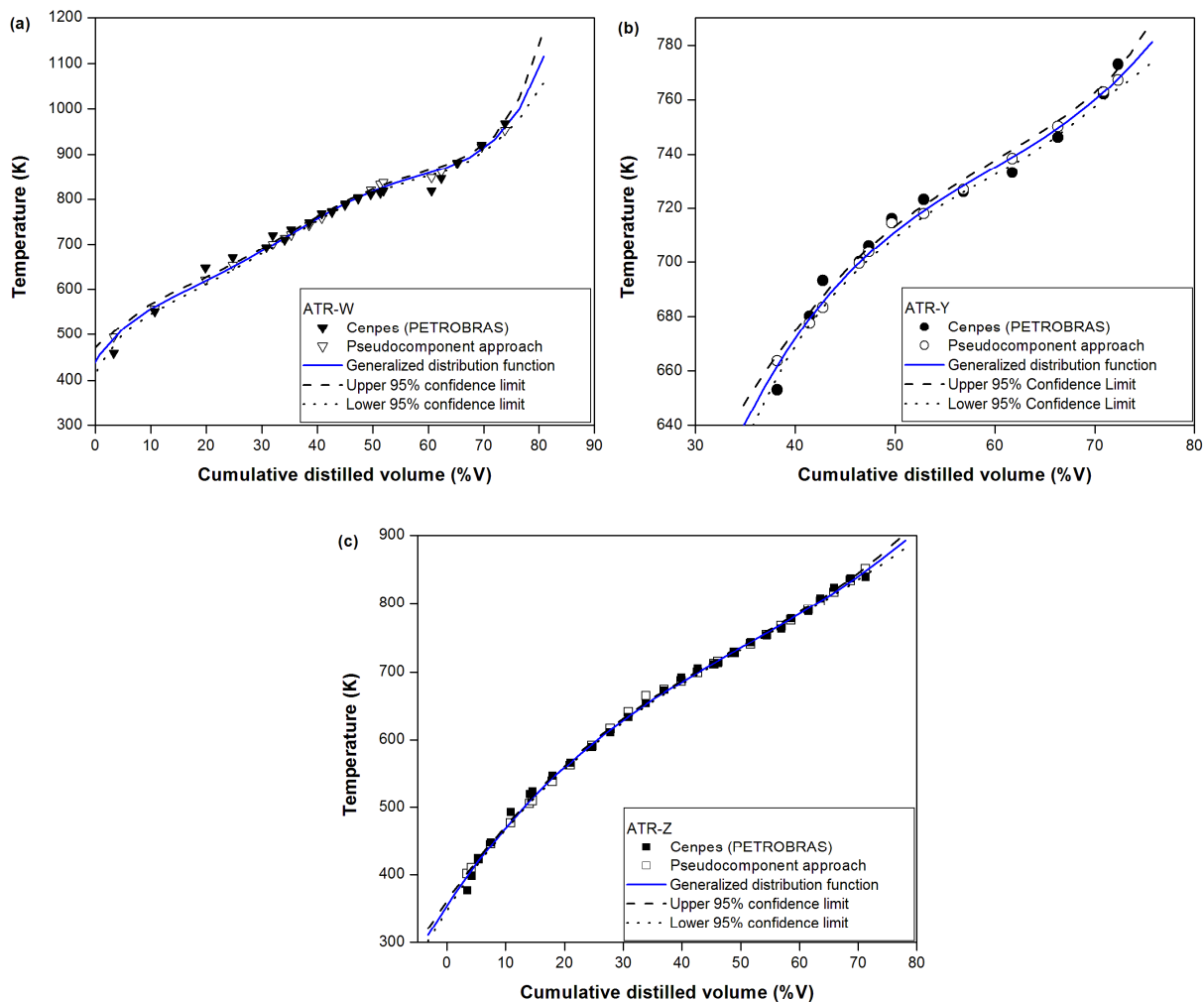


Figure 1. Distribution function for boiling point. a) ATR-W; b) ATR-Y and c) ATR-Z.

Results obtained using continuous thermodynamic indicated that normal boiling point distribution was consistent with those data provided by CENPES–Brazil and it was more accurate than pseudocomponent approach, once the %AADs estimated were 1.74%, 0.58% and 1.14% for ATR-W, ATR-Y and ATR-Z, respectively, in comparison with 8.06%, 2.03% and 2.92%, in that order, when pseudocomponent method was used.

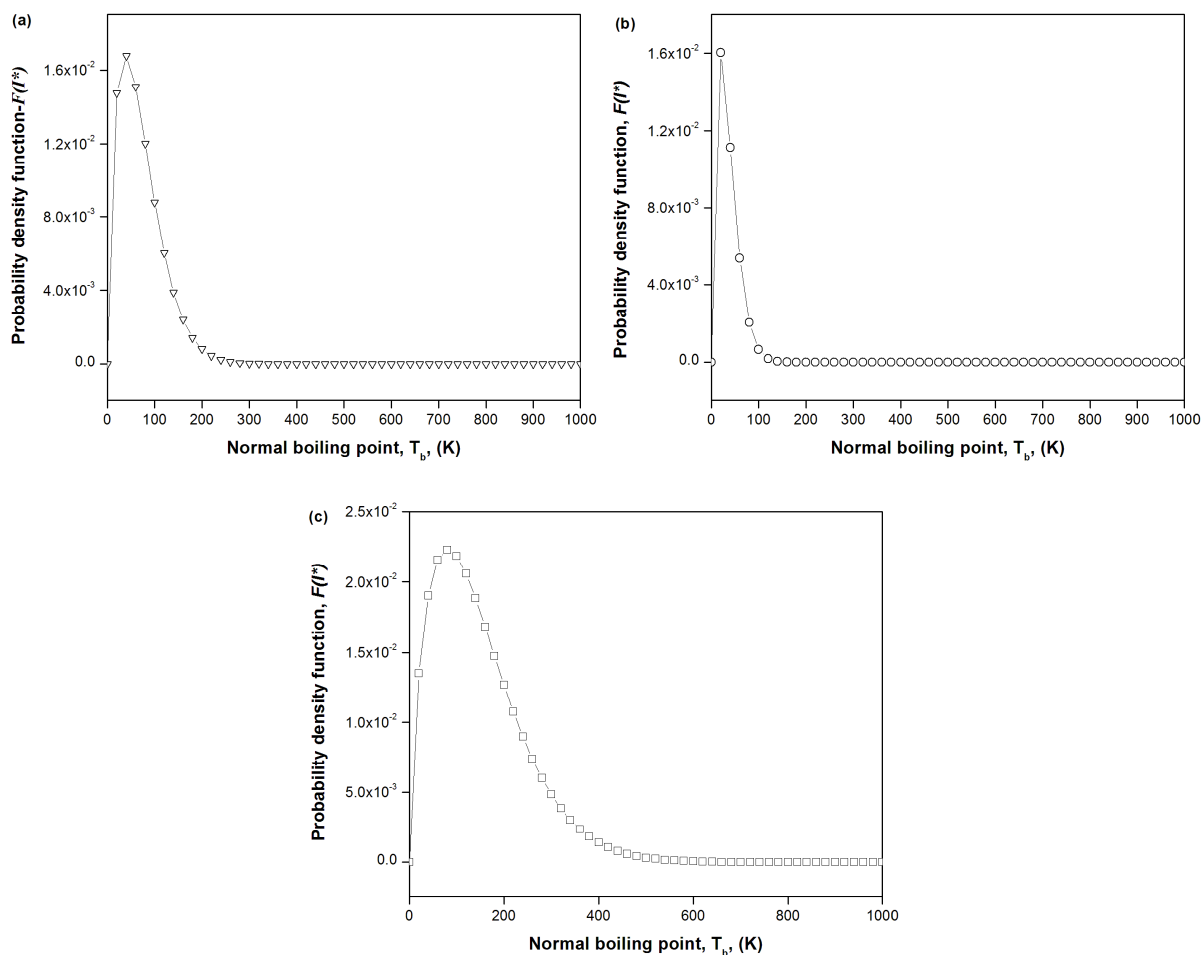


Figure 2. Probability distribution function. a) ATR-W; b) ATR-Y and c) ATR-Z.

3.4. Thermodynamic characterization of petroleum fractions

As described by Korsten (Korsten, 1998), both, critical properties and molar mass are two necessary parameters in the prediction of molecular-type analysis (paraffin, naphthenic or aromatic content) as a function of normal boiling point (Figures 3 – 5).

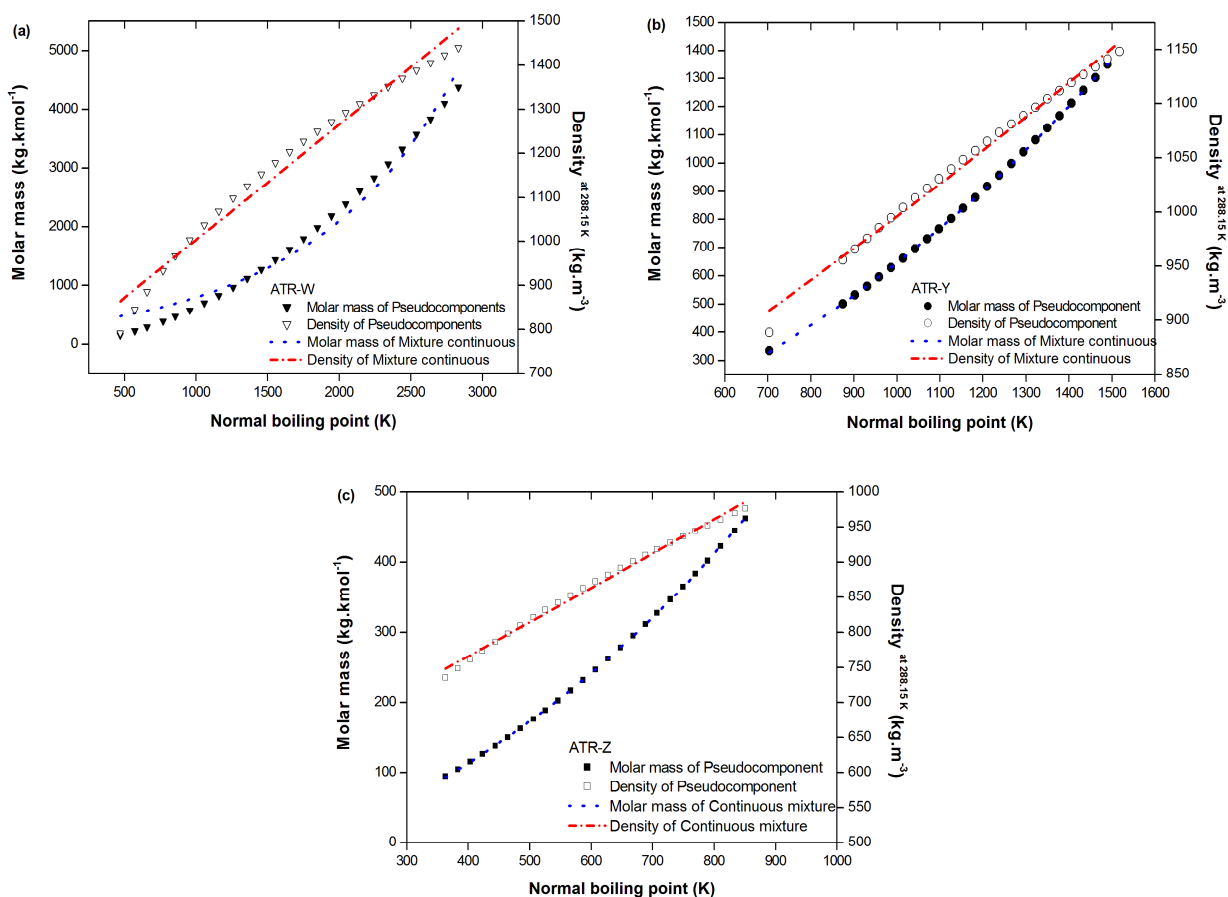


Figure 3. Probability distribution function. a) ATR-W; b) ATR-Y and c) ATR-Z.

Once normal boiling point distribution for whole mixture was known, it was possible to obtain the properties through correlations presented in Table 2. Bulk properties (Figure 3) and critical properties (Figures 4 – 5), are required for predicting the thermophysical properties. In Figures 3 – 5 the molar mass distribution and critical properties were compared with the pseudocomponents approach. Inside the normal boiling point range, the deviations between all the predicted values are not much large.

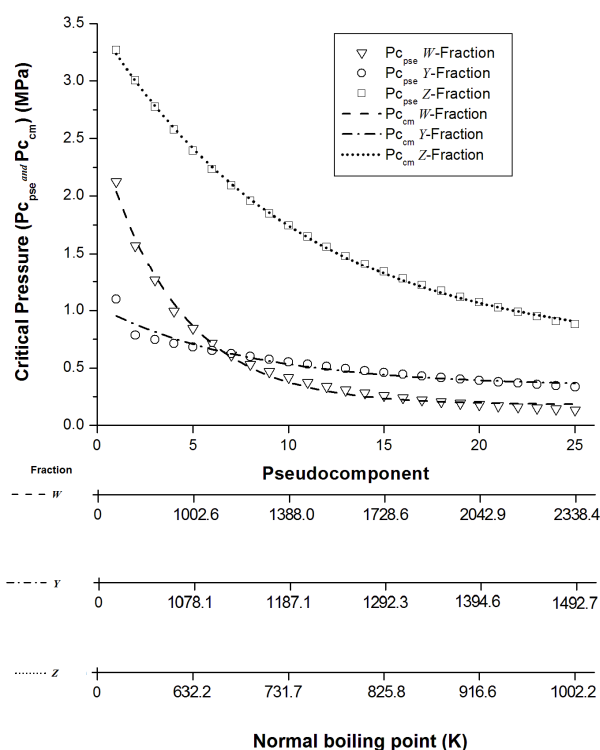


Figure 4. Estimation of critical pressure.

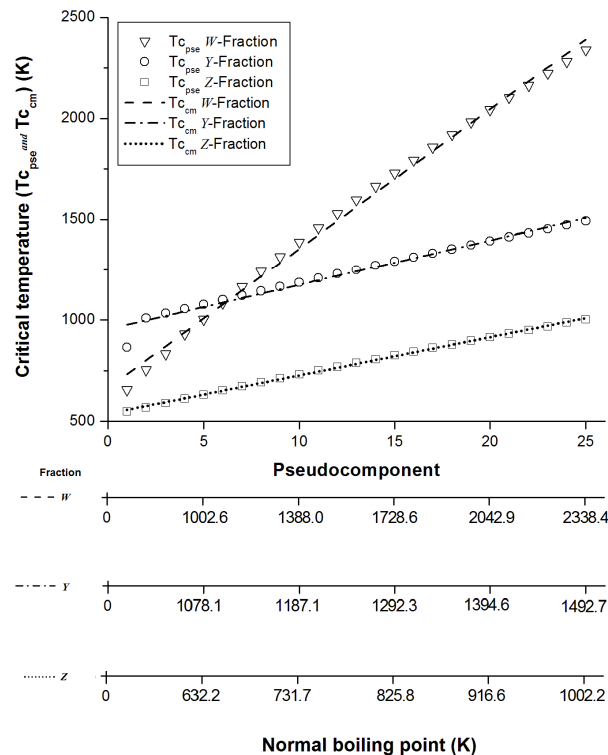


Figure 5. Estimation of critical temperature.

3.5. Thermophysical and transport properties of petroleum fractions

Thermophysical and transport properties (ν , λ and C_p) were calculated at temperature range from 350 to 600 K (Figures 6 – 8).

Figure 6 shows the plots of kinematic viscosity (ν) of samples, over a wide temperature range compared with the pseudocomponents approach. The temperature effect upon ν was important. From Figure 6, it follows that the maximum variation of ν with temperature was given for ATR–W, while lower variation of ν was observed for ATR–Z with 24.9 of API gravity. Such variation in ν behavior may be ascribed to variation in the distribution of molar mass within the normal boiling point range for every fraction.

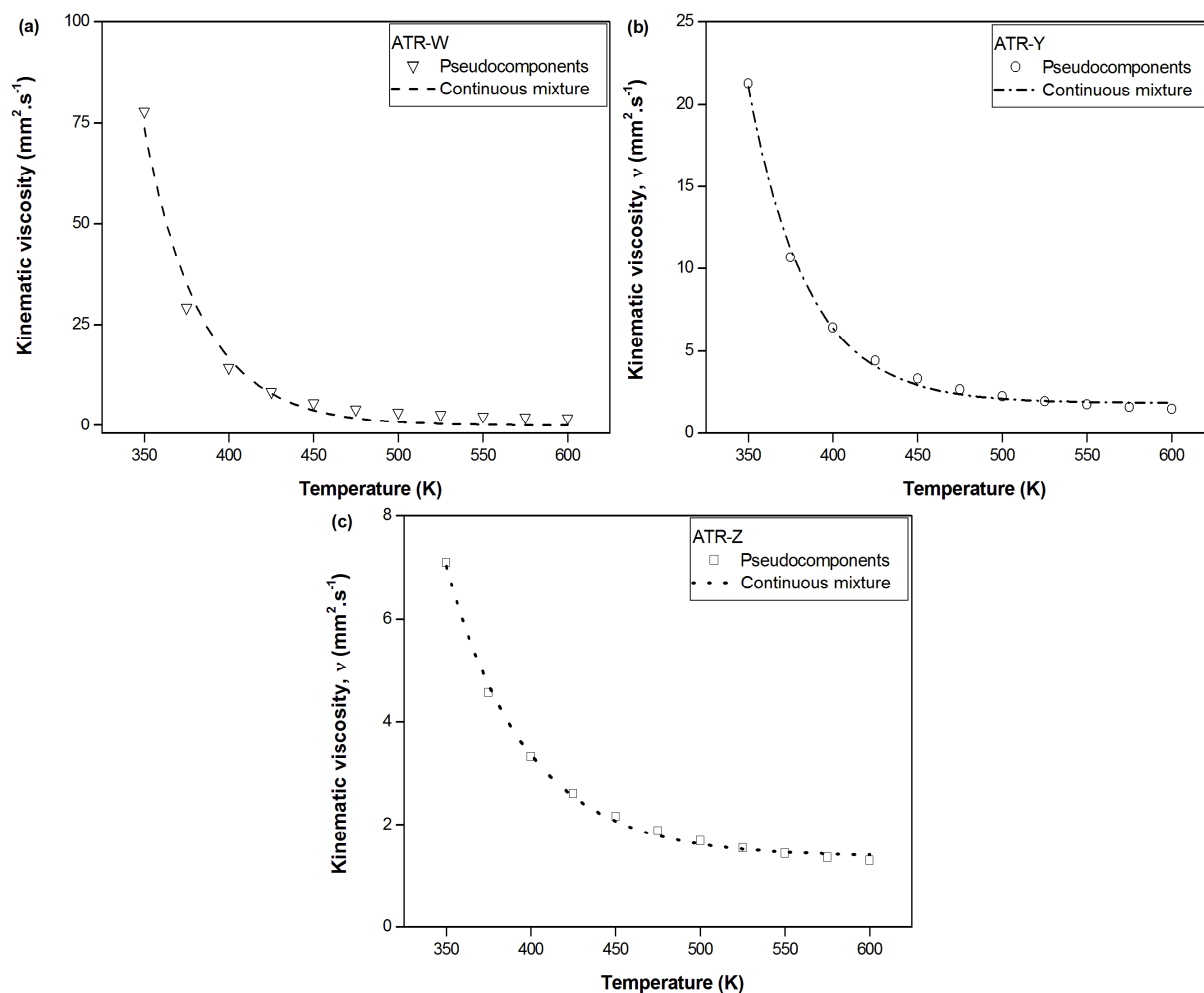


Figure 6. Estimation of viscosity. a) ATR-W; b) ATR-Y and c) ATR-Z.

The thermal conductivity (λ) of the samples was a function of density and of the nature of them (Figure 7). At higher API gravity and boiling points, petroleum fractions tend to be less paraffinic and have higher values of density than light fractions with low boiling point, thus the λ tends to decrease. In comparison with experimental data, the %AAD is estimated to be $< 2\%$ (0.49% for ATR-W, 0.22% for ATR-Y and 1.08% for ATR-Z).

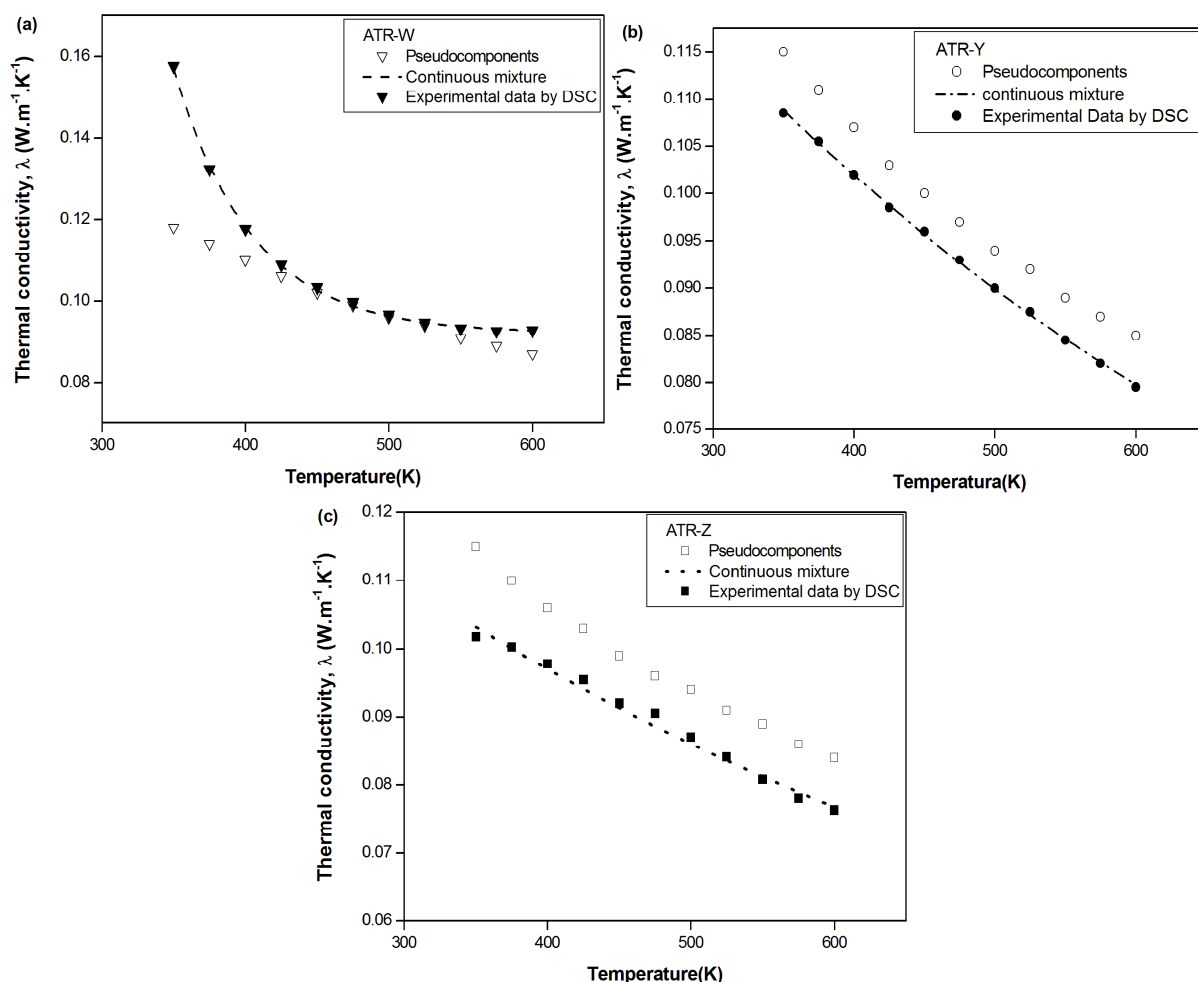


Figure 7. Estimation of thermal conductivity. a) ATR-W; b) ATR-Y and c) ATR-Z.

The results of the specific heat capacity (C_p), plotted in Figure 8, showed that the C_p increased with the raise in temperature. The variation in the rising trend of the C_p , among the mixtures, is due to the differences in chemical composition. Estimated values of C_p using the function distribution of normal boiling point were compared with experimental data obtained in our laboratory by DSC experiments. The %AADs for fitted C_p regarding to the experimental values were 1.88% for ATR-W, 9.36% for ATR-Y and 7.48% for ATR-Z.

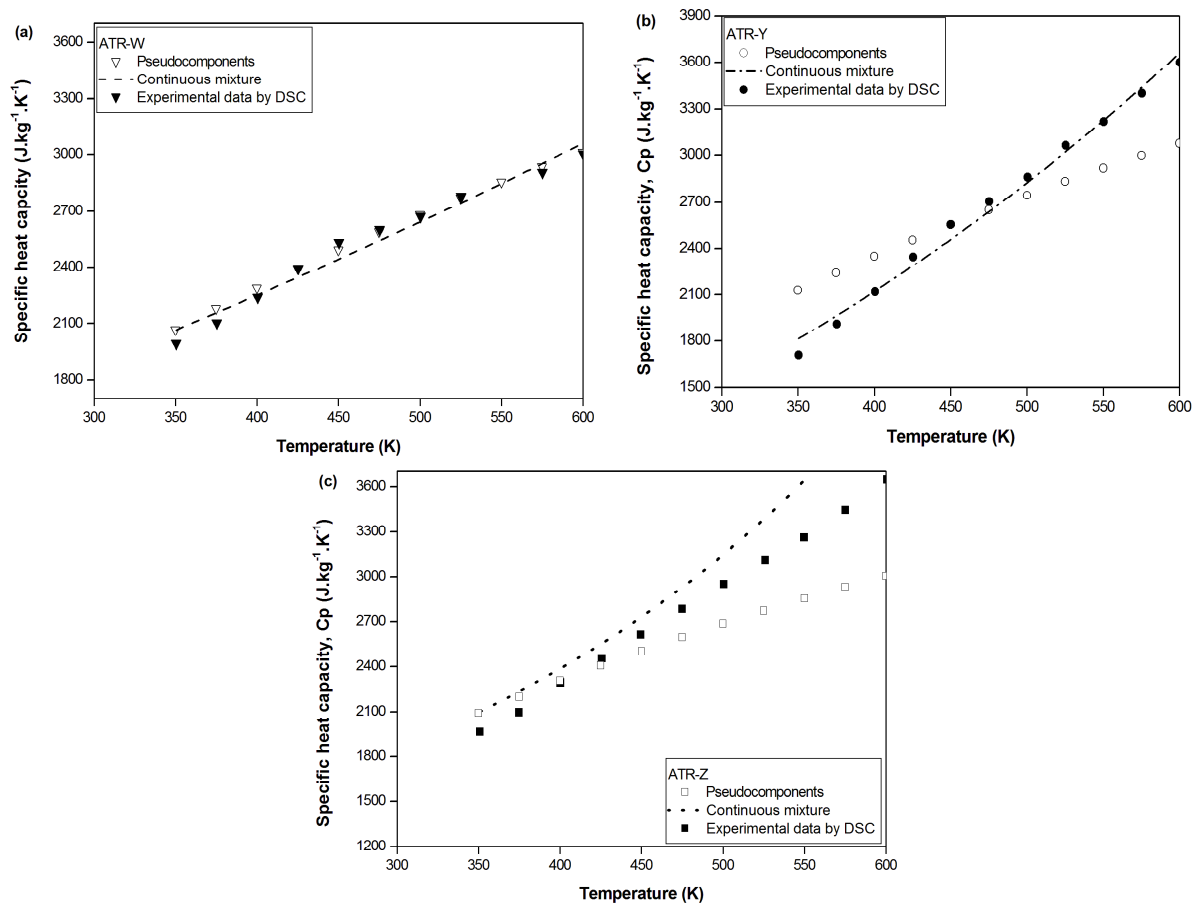


Figure 8. Estimation of specific heat capacity. a) ATR-W; b) ATR-Y and c) ATR-Z.

4. Conclusions

A generalized distribution function (Equation 4) with two adjustable parameters was used for modeling cumulative distilled volume where the normal boiling point was the distribution variable. Therefore, modeling of continuous mixture was a versatile method to be applied to multicomponent systems such as petroleum fractions because it reduces the computer time considerably while it keeps the accuracy of the properties predictions. According to the absolute average deviations, results obtained for property predictions, by mean of continuous thermodynamic approach, showed better agreement, to the experimental data, than that attained by pseudocomponent approach.

Acknowledgements

This research was supported by the Brazilian National Council for Technological and Scientific Development (CNPq), the Petrobras Research and Development Center (PETROBRAS/CENPES) and the Brazilian Study and Project Financing Institution (FINEP).

Nomenclature

A	Parameter in Equations (4), (7) and (8)	[–]
B	Parameter in Equations (4), (7) – (9)	[–]
C_p	Specific heat capacity	[J·kg ⁻¹ ·K ⁻¹]
F	Distribution function	[–]
I	Distribution variable	[–]
I^*	Dimensionless parameter defined by Equation (4) as $[=(I-I_0)/I_0]$	[–]
I_0	Initial value of property I at $x=0$	[–]
M	Molar mass	[kg·kmol ⁻¹]
P_c	Pseudocritical pressure	[MPa]
T_c	Pseudocritical temperature	[K]
T_b	Boiling point	[K]
x	Continuous mixture	[–]
<i>Acronyms</i>		
AAD	Absolute average deviation	
DSC	Differential Scanning Calorimetric	
<i>Greek Letters</i>		
α	Parameter in Equation (1)	
β	Parameter in Equation (1)	
Γ	Gamma function Equation (1) and (9)	
η	Parameter in Equation (1) and (3)	
λ	Thermal conductivity	[W·m ⁻¹ ·K ⁻¹]
θ	Parameter in Equation (2)	
σ	Parameter in Equation (2) and (3)	
ν	Kinematic viscosity	[mm ² ·s ⁻¹]
<i>Subscripts</i>		
av	Average value for a property	
T	Boiling point parameter	
cm	Continuous mixture	
pse	Pseudocomponent	

References

- Aboul-Seoud A.–L., Moharam H. M. (1999a) A generalized viscosity correlation for undefined petroleum fractions, *Chemical Engineering Journal* **72**, 3, 253–256.
- Aboul-Seoud A.–L., Moharam H. M. (1999b) A simple thermal conductivity–temperature correlation for undefined petroleum and coal liquid fractions, *Chemical Engineering Research and Design* **77**, 3, 248–252.

- Briesen H., Marquardt W. (2003) An adaptive multigrid method for steady-state simulation of petroleum mixture separation processes, *Industrial & Engineering Chemistry Research* **42**, 11, 2334–2348.
- Briesen H., Marquardt W. (2004) New approach to refinery process simulation with adaptive composition representation, *AIChE Journal* **50**, 3, 633–645.
- Cotterman R. L., Prausnitz J. M. (1985) Flash calculations for continuous or semicontinuous mixtures using an equation of state, *Industrial & Engineering Chemistry Process Design and Development* **24**, 2, 434–443.
- Cotterman R. L., Bender R., Prausnitz J. M. (1985) Phase equilibria for mixtures containing very many components. Development and application of continuous thermodynamics for chemical process design, *Industrial & Engineering Chemistry Process Design and Development* **24**, 1, 194–203.
- Fang W., Lei Q. (2003) Continuous thermodynamic correlation and calculation of vapor pressure and vapor–liquid equilibrium, *Fluid Phase Equilibria* **213**, 1–2, 125–138.
- Kehlen H., Rätzsch M. T., Bergmann J. (1985) Continuous thermodynamics of multicomponent systems, *AIChE Journal* **31**, 7, 1136–1148.
- Kesler M. G., Lee B. I. (1976) Improve prediction of enthalpy of fractions, *Hydrocarbon Processing* **55**, 3, 153–158.
- Koral S. L., Sayegh S. G., George A. E. (1993) Phase equilibria of crude oils using the continuous thermodynamics approach, *The Canadian Journal of Chemical Engineering* **71**, 1, 130–140.
- Korsten H. (1998) Critical properties of hydrocarbon systems, *Chemical Engineering & Technology* **21**, 3, 229–244.
- Lage P. L. C. (2007) The quadrature method of moments for continuous thermodynamics, *Computer & Chemical Engineering* **31**, 7, 782–799.
- Manafi H., Mansoori G. A., Ghotbi S. (1999) Phase behavior prediction of petroleum fluids with minimum characterization data, *Journal of Petroleum Science and Engineering* **22**, 1–3, 67–93.

- Mansoori G. A., Du P. C., Antoniadis E. (1989) Equilibrium in multiphase polydisperse fluids, *International Journal of Thermophysics* **10**, 6, 1181–1204.
- Metcalfe T., Charbonneau P. (2003) Stellar structure modeling using a parallel genetic algorithm for objective global optimization, *Journal of Computational Physics* **185**, 1, 176–193.
- Riazi M. R. (1989) Distribution model for properties of hydrocarbon-plus fractions, *Industrial & Engineering Chemistry Research* **28**, 11, 1731–1735.
- Riazi M. R., Daubert T. E. (1980) Simplify property predictions, *Hydrocarbon Processing* **59**, 3, 115–116.
- Riazi M. R., Al-Adwani H. A., Bishara A. (2004) The impact of characterization methods on properties of reservoir fluids and crude oils: options and restrictions, *Journal of Petroleum Science and Engineering* **42**, 2–4, 195–207.
- Shibata S. K., Sandler S. I., Behrens R. A. (1987) Phase equilibrium calculations for continuous and semicontinuous mixtures, *Chemical Engineering Science* **42**, 8, 1977–1988.
- Vakili-Nezhaad G. R., Modarress H., Mansoori G. A. (2001) Continuous thermodynamics of petroleum fluids fractions, *Chemical Engineering and Processing* **40**, 5, 431–435.
- Whitson C. H. (1983) Characterizing hydrocarbon plus fractions, *SPE Journal* **23**, 4, 683–694.

3.3. Considerações finais

As propriedades físico-químicas (propriedades básicas, termodinâmicas e térmicas) foram estimadas através das correlações reportadas na literatura e comparadas com os resultados obtidos das análises experimentais realizadas, no laboratório de pesquisa (LDPS/LOPCA/UNICAMP), visando seu acoplamento na modelagem matemática e a simulação do processo de destilação molecular reativa.

A caracterização adequada das frações pesadas de petróleo é uma informação indispensável para o desenvolvimento de estudos teóricos e experimentais das técnicas de processamento destas frações. Baseado no conceito da termodinâmica contínua, o modelo da função de distribuição contínua generalizada, com dois parâmetros, proposto por Riazi (1989), foi utilizado para a estimativa de propriedades básicas e termodinâmicas das frações de petróleo.

As propriedades críticas, de maneira geral, são utilizadas no cálculo de outras propriedades que, são necessárias para o processo de simulação da destilação molecular reativa. As correlações utilizadas para estimar o fator acêntrico não apresentam influência significativa na estimativa das outras propriedades termodinâmicas, dado que os desvios obtidos com os diferentes conjuntos de correlações foram menores do que 10%.

As propriedades críticas de temperatura e pressão são sensíveis à temperatura de ebulição. Com o aumento da temperatura de ebulição aumenta a temperatura crítica, mas a pressão crítica e a densidade crítica diminuem. Esse resultado reflete em uma relação entre essa propriedade e a quantidade de componentes pesados que se encontram nas frações em estudo.

Para o desenvolvimento da modelagem matemática da destilação molecular reativa é necessária a existência de uma relação entre a temperatura de operação e o calor específico. As equações avaliadas correlacionam o calor específico com a temperatura operacional (exemplo: 300 – 600 K), apresentando um aumento com essa variável. A massa específica e densidade relativa das frações estudadas (ATR-W, ATR-Y e ATR-Z) não apresentam influência significativa na determinação do calor específico destas frações.

Capítulo 4

Aplicações, considerações e fundamentos acerca da destilação molecular

4.1. Introdução

O desenvolvimento da destilação molecular para a caracterização de frações pesadas de petróleo realizado pelo grupo de pesquisa do LDPS/FEQ/UNICAMP representa um considerável avanço na metodologia de análise dessas frações que, proporciona um melhor aproveitamento do óleo cru e ganhos na qualidade do produto final (Zuñiga–Liñan et al., 2011; Rocha et al., 2011; Zuñiga, 2009; Zuñiga et al., 2009; Zuñiga et al., 2009; Hernández, 2009; Rocha, 2009; Winter et al., 2009; Hernández et al., 2008; Lopes, 2008; Rocha, 2008; Rocha et al., 2008a; Rocha et al., 2008b; Liñan et al., 2007; Lopes et al., 2007; Rocha et al., 2007; Winter, 2007; Winter et al., 2007; Sbaite et al., 2006; Maciel–Filho et al., 2006; Winter et al., 2006; Sbaite, 2005; Winter et al., 2004; Sbaite et al., 2003; Batistella et al., 2002; Batistella et al., 2000; Batistella e Wolf–Maciel, 1998, 1996).

A destilação molecular usada em vários processos da indústria química, farmacêutica, de alimentos e de petróleo é um caso particular de evaporação, a qual ocorre em pressões extremamente baixas, de modo que, o efeito do vapor gerado sobre o líquido praticamente não influencia a taxa de evaporação. Portanto, a superfície de evaporação e a superfície de condensação devem estar separadas entre si por uma distância de ordem de grandeza do livre percurso médio das moléculas evaporadas, ou seja, as moléculas evaporadas atingirão o condensador facilmente, uma vez que encontrarão um percurso relativamente desobstruído.

Os tópicos aqui abordados englobam uma revisão dos seguintes conceitos quando considerada a configuração de um destilador molecular centrífugo:

- Livre percurso médio ou caminho livre médio molecular, definido como a distância ou espaço entre duas colisões sucessivas das moléculas na fase vapor. Normalmente, na destilação molecular, o valor do livre percurso médio é da ordem de 0,02 a 0,05 m para pressões de processo de 0,13 Pa, ou seja, valores próximos à média da distância entre o

evaporador e o condensador, exigência para que a destilação ocorra eficientemente (Lutišan e Cvengroš, 1995; Holló et al., 1971).

- O número de *Knudsen*, um número adimensional, definido como a razão entre o comprimento do caminho livre médio molecular e uma escala de comprimento fisicamente representativa (distância entre a superfície do evaporador e o condensador). O número de *Knudsen* é muito útil para determinar se a formulação da mecânica estatística ou da mecânica do contínuo deve ser usada: Se o número de *Knudsen* é próximo ou maior que um, o caminho médio livre de uma molécula é comparável a escala de comprimento do problema e a consideração de continuidade da mecânica dos fluidos não é mais uma boa aproximação (Kawala e Dakiniewicz, 2002; Barber e Emerson, 2002).
- A taxa de evaporação efetiva ou velocidade de evaporação é representada pela equação de Langmuir–Knudsen (Langmuir, 1913; Lutišan et al., 2002; Badin e Cvengroš, 1992; Inuzuka et al., 1989; Inuzuka et al., 1986). Portanto, a velocidade de evaporação diminui tanto pelas colisões mútuas das moléculas evaporadas como pelas colisões das moléculas evaporadas com as moléculas do gás residual. No entanto, quando é incrementado o calor do sistema gera-se um aumento de temperatura, induzindo a um incremento na pressão de vapor, que resultará em um aumento da velocidade de evaporação.

Contudo, a consideração de todos os aspectos anteriores na *performance* do processo da destilação molecular de frações de petróleo constitui a segunda fase deste estudo.

4.2. Desenvolvimento

O desenvolvimento deste capítulo é apresentado a seguir, no manuscrito intitulado: *Molecular distillation High-Tech process: Knowledge-based understanding of mean free path and the Knudsen number applied to high-boiling-point petroleum fractions*, submetido ao periódico internacional *Vacuum* e atualmente em fase de revisão.

Source: From Tovar L. P., Wolf Maciel M. R., Maciel Filho R., Batistella C. B., Medina L. C. (submitted in 2011 Manuscript ID: VAC-D-11-00772) Molecular distillation High-Tech process: Knowledge-based understanding of mean free path and the Knudsen number applied to high-boiling-point petroleum fractions. Vacuum.

Molecular distillation High-Tech process: Knowledge-based understanding of mean free path and the Knudsen number applied to high-boiling-point petroleum fractions

Abstract

A theoretical study on the principles of molecular distillation (non-conventional High-Tech process) such as: mean free path (MFP), effective evaporation rate (G_E) and the influence of the Knudsen number (Kn) on the hydrodynamic development on an evaporating surface, was carried out under different conditions of evaporator temperature (423.15 K – 623.15 K) and pressure system (0.1 Pa – 1 Pa). In this study, the modeling and simulation were based on the kinetic theory and Langmuir-Knudsen equation for a set of twenty five (25) pseudocomponents in three high-boiling-point petroleum fractions (atmospheric petroleum residues W, Y and Z) with different API gravities. Numerical simulations showed that the main features of the principles of molecular distillation are linked with the distance between the evaporator and condenser surface (distillation gap) and pressure system. Thus, the MFP of evaporating molecules indicated that the anisotropic degree of the vapor phase, in a low pressure system with a relatively high evaporator temperature, is an essential condition in the molecular distillation process. Moreover, results of simulations have demonstrated that when it was considered a distance between the evaporator and condenser of 0.08 m and 0.05 m intermediate range values for the Kn (0.01 – 3.00) elucidated a flow pattern with the characteristics of molecular flow, and allowed one to estimate consistent values for the G_E .

Keywords: Molecular distillation; mean free path; Knudsen number; distillation gap; molecular flow; pressure system.

Contents

1. Introduction
 - 1.1. Research and development
 2. Molecular distillation in petroleum industry
 - 2.1. Process principles and operational advantages
 - 2.1.1. Boiling temperature and pressure system
 - 2.1.2. Residence time
 - 2.1.3. Mean free path: Principle of molecular distillation
 - 2.1.4. Anisotropic condition and effective rate of evaporation
 - 2.2. Molecular distiller units for processing high-boiling-point petroleum fractions
 3. Computational development
 - 3.1. Chemical systems: High-boiling-point petroleum fractions
 4. Results and discussion
 - 4.1. Effect of pressure system on the mean free path
 - 4.2. The influence of the Knudsen number on the hydrodynamic in the distillation gap
 - 4.3. The effective evaporation rate
 5. Conclusions
- Acknowledgments
Nomenclature
References

1. Introduction

In recent years, more efforts have been made to widen technology and develop the necessary procedures to reduce thermal hazards in the separation and purification of thermally unstable compounds and substances with low volatility, ensuring their quality for the required applications. In this context it is important to develop a chemical industry based on safe-efficient technology. Many materials such as oils, chemicals, medicines and natural foods, healthcare products, fatty acids, petroleum fractions etc, are viscous, high boiling and/or heat sensitive. To separate and/or purify them while maintaining their good quality, a non-conventional process is required at a low boiling temperature or even below it, with a short residence time, in order to minimize thermal degradation and allow for parallel reactions. In view of this, molecular distillation (MD) is a innovative separation technology that could be used in an attempt to secure separation, efficiency and quality aspects in a single process.

MD is a high-tech thermal separation technique operating at pressures in the range from 0.1 to 10 Pa. The potential of MD is due to the fact that it is appropriate for the separation and purification of thermally unstable materials without the hazard of thermal decomposition, as in

the case of many vitamins, essential oils, heat sensitive and high boiling point materials, since the process occurs under high vacuum with lower temperatures [1 – 8]. In the MD process, the vapor molecules must find a free path between the evaporator and the condenser, the pressure must be low and the width of the distillation gap must be comparable with the mean free path of the evaporating molecules. Under these conditions, theoretically, the evaporation rate should only be governed by the rate of escape of the molecules from the liquid surface, and therefore phase equilibrium does not exist [9].

1.1. Research and development

Experimental procedures and theoretical studies have been developed since the early twentieth century. These studies involved the design and construction of equipment on a pilot and laboratory scale, experimental studies with different feedstock (animal oils, vegetable oils, petroleum fraction etc.), the determination of the operating conditions, the development of mathematical models and the simulation of the molecular distillation process. Hence, the development of a separation process for thermally unstable materials was one of the most promising research and development areas in separation processes during the last decade, and this was reflected in the papers in specialized scientific journals and international conferences concerning non-conventional separation processes [10 – 48] (see Tables 1 – 2).

Table 1. Overview of experimental research on MD process from different feedstock and operating conditions.

Feedstock	Application	Operating conditions			Equipment	Source
		Pressure system (Pa)	Evaporator temperature (K)	Feed flow (mL·min ⁻¹)		
Deodorized oil from the squid <i>Illex argentinus</i>	Recovery of ω -3 fatty acid ethyl esters	40	273.15 and 393.15 K (1 st stage) and 393.15 and 413.15 K (2 nd stage)	NA		[1]
Cymbopogon citratus essential oil	Purification/ Extraction	5.00	333.15 – 393.15	1.5 – 6.0	CMD	[3–4]
Fast pyrolysis of biomass	Separation	60.00	343.15 – 403.15	1.0	FFMD	[10]
Rapeseed soapstock	Acidification	2.66	323.15 and 393.15	N.A.	FFMD	[11]
Pyrolysis oil	Separation	60.00	323.15	1	FFMD	[12]
Palm oil	Purification	0.10	493.15 – 523.15	[†] 0.5 – 1	FFMD	[13]
Vegetable oils	Purification	2.7–3.3	393.15 – 513.15	3.0	CMD	[14]
Decanoic acid in cuphea fatty acids	Purification	0.08–0.40	313.15 – 383.15	[†] 0.03 – 0.1122	CMD	[15]
Octacosanol extract from rice bran waxn	Purification	66.66	363.15	3.0	FFMD	[16]
Monoglycerides	Concentration	16.00	423.15 – 523.15	5.0 – 10.0	CMD	[17]
Grape seed oil	Recovery and deacidification	1.25	469.15 – 497.15	0.3 – 1.7	FFMD	[18]
Wheat germ oil	Purification	1.00	453.15 – 503.15	1.0	FFMD	[19]
Palm fatty acid distillates	Extraction tocotrienols	0.13	393.15 (3 rd stage) and 433.15 (4 th stage)	[†] 0.25	FFMD	[20]
Palm oil distillates	Extraction tocotrienols	0.13	383.15 – 433.15	[†] 0.1 – 0.4	FFMD	[21]
Olive Tree	Isolation	150–200	343.15 – 463.15	15.0	FFMD	[22]
Rapeseed oil deodorizer distillate (product of vegetable refining edible oil)	Recovered tocopherol and fatty acid methyl esters	NA	443.15 – 503.15	30 – 150	FFMD	[23]
Distillates of the vegetable oil deodorization	Purification and deacidification	NA	373.15 – 453.15	[†] 0.09 – 1.38	FFMD	[24]
Distillates of the vegetable oil deodorization	Purifying and deacidification	0.10	393.15 and 458.15 (1 st strategy) and 398.15 and 468.15 (2 nd strategy)	[†] 0.3	FFMD	[25]
Heavy oils (Brazilian vacuum residue)	Characterization oil	0.10	508.15 – 613.15	8.33	FFMD	[26]
Gamma-linolenic acid/soybean oil	Enrichment and recovery	16.00 / 9.99x10 ⁻²	Up to BP / 373.15 – 413.15	[†] 0.1 – 0.7	CMD/ FFMD	[27]
Soybean oil	Recovery	13.30	413.15 – 493.15	[†] 0.3 – 0.9	CMD	[28]
Petroleum	Modeling	0.10	353.15 – 613.15	5.8 and 10.83	FFMD	[29]
Soya oil	Separation	0.10	373.15 – 433.15	[†] 0.1 – 0.7	FFMD	[30]
Octacosanol extract from rice bran wax	Purification	39.06–227.58	449.01–477.29	3.0	FFMD	[31]
Commercial monoglyceride	Concentration	16.00	373.15–573.15	5–15	CMD	[32]
3-hydroxypropionitrile	Purification	0.50–1.50	298.15 and 308.15	1.5–3.0	FFMD	[33]
Butterfat	Fractionation/Production	0.10	353.15–433.15	3.33–4.17	FFMD	[34]
Fat milk	Fractionation	1.07–1.87	373.15–523.15	[†] 0.594	FFMD	[35]
Mixture of rapeseed oil and capric acid	Deacidification	0.10	313.15–373.15	66.66	FFMD	[36]
Paraffin wax	Fractionation	40–70	393.15–443.15		FFMD	[37]

CMD: Centrifugal Molecular Distiller; FFMD: Falling Film Molecular Distiller

[†]: Feed flow rate in kg·h⁻¹; N.A.: Not available

Table 2. Overview of theoretical research on MD process.

Focus on	Equation type	Equipment	Flow patterns	Source
Film thickness, evaporation rate, temperature profile, concentration profiles and amount of distillate	Heat and material balances	FFMD	Laminar	[2]
Flow rate and molar composition at the evaporating and condensing surfaces; surface temperature, velocity and film thickness profile	Balance equations	FFMD	Laminar	[6]
Thin-film thickness	—	FFMD,CMD	N.A.	[38]
Effect of feed temperature and condenser temperature on film thickness, film surface temperature and concentration, degree of evaporation and concentration of distillate	Navier–Stokes equations and balance equations	FFMD	Laminar	[39]
Temperature, concentration, density and velocity profiles	Balance equations	FFMD	Laminar	[5]
Velocity profile	Continuous and momentum equations	FFMD	Turbulent	[40]
Distance between the discs and rate of distillation	Distribution of temperature in the distillate and Langmuir equation	CMD	N.A.	[41]
Liquid flow, evaporation degree, surface temperature, film thickness and surface composition	Balance equations	FFMD	Laminar/Turbulent	[42]
Residence time distribution	Residence time distribution	FFMD	Laminar/Turbulent	[43]
Short-path distillation in an evaporator with a divided condenser	Boltzman and Navier–Stokes equations	FFMD	N.A.	[44]
Vapor phase pressure and mean free path	Monte Carlo and Boltzmann equation	N.A.	Laminar	[45]
Concentration and temperature profile, evaporation degree and film thickness	Boltzmann, Navier–stokes and thermal balance equations	FFMD	Laminar	[46]
Temperature profile, evaporation degree and position on sieve	Balance equations and Monte Carlo method	FFMD	N.A.	[47]
Effect of variation in concentration in a wiped film short path distiller in a stationary regime on the separation capacity	Langmuir–Knudsen equation and balance equations	FFMD	Turbulent	[48]

CMD: Centrifugal Molecular Distiller; FFMD: Falling Film Molecular Distiller

N.A. Not available

In this work, a theoretical study on the principles of molecular distillation such as: mean free path, effective evaporation rate and the influence of the Knudsen number on the hydrodynamic development on an evaporating surface, was carried out under three different conditions of evaporator temperature (423.15 K, 523.15 K and 623.15 K) and pressure system (0.1 Pa, 0.13 Pa and 1 Pa) when it was considered a centrifugal molecular distiller.

In this study, the modeling and simulation were based on the kinetic theory and Langmuir–Knudsen equation for a set of twenty five (25) pseudocomponents in three atmospheric petroleum residues (high-boiling-point petroleum fractions) with different API gravities.

2. Molecular distillation in petroleum industry

Petroleum includes the presence of heavy oil but there is a demand for lighter products in the oil industry, and therefore the refineries tend to convert part of their residues into light fractions. In the case of Brazilian oil, the difference in the quantity and quality of the residues from the vacuum column requires further development in order to raise their value and also to meet the demand. A detailed characterization is necessary and important before the optimized processing routes can be fixed. The term petroleum or crude oil includes petroleum-based substances comprising a complex blend of hydrocarbons, mainly paraffins (also called alkanes), olefins (alkenes), cycloparaffins (cycloalkanes), and aromatics; compounds containing nitrogen, sulfur and oxygen, such as the resins and asphaltenes and metallic species [49].

The research petroleum groups, Separation Process Development Laboratory (LDPS) and Laboratory of Optimization and Advanced Control (LOPCA) of the State University of Campinas have developed studies, methodologies and procedures to characterize the petroleum fractions from the extension of the true boiling point curve to approximately 973.15 K. In this context, experiments were carried out in a molecular distiller (wiped film short path distillers) using heavy Brazilian oil fractions with different API gravities and under different operating conditions [2, 26, 29]. The cuts and residues obtained in the molecular distillation process were collected, quantified and characterized. These studies showed the potential for molecular distillation in characterizing petroleum fractions, since it was possible to extend the TBP curve and obtain gains in final product quality.

Therefore, such research emphasized the importance of the MD process in converting the heavier oil fractions into lighter products. Thus, MD of high-boiling-point petroleum fractions basically separates the molecules according to the differences in their vapor pressures, which generally decrease with increasing molar mass, carbon number and boiling point.

2.1. Process principles and operational advantages

Distillation under high vacuum, where the condensing surface is very close to the surface of the evaporating liquid, enables one to operate in a different pressure range, such as under moderate vacuum (equilibrium phase), where the pressure range is above 133 Pa [50]; unobstructed path distillation, where there is free transfer of the molecules [50, 51]; and molecular distillation, where the distance between the evaporator and condenser surface is comparable with the mean free path of the evaporating molecules [41,50].

2.1.1. Boiling temperature and pressure system

The temperature at which a liquid boils depends on the pressure system. Therefore high-vacuum distillation shows the benefit of evaporating and condensing the molecules at low pressure (0.1–10 Pa), and consequently in a low operating temperature range (evaporator temperature), obtaining a reduction in the distillation temperatures [44, 52, 53]. Furthermore, Catalogue UIC–GmbH [54] has introduced the concept of fine vacuum as related to the mean free path (*MFP*), that is, the pressure system (*P*) is in the range between 0.1 Pa and 100 Pa, such that the *MFP* of the molecules is a few centimeters, comparable to the distillation gap between the evaporator and condenser surfaces, and the flow on the evaporator surface is in the free molecular flow regime.

2.1.2. Residence time

In MD the residence time of the material in the distillation gap at the evaporator temperature is to the order of seconds [8] i.e. typically less than one minute [54]. As a consequence, the residence time relies mainly on the viscosity of the material, the film thickness and the geometry of the evaporator. The most important advantage of MD is the minimal thermal load on the material to be distilled, and also the period of the thermal load has an influence on the degree of separation efficiency and thermal degradation [7, 45, 54]. In order to avoid any

negative effect on process quality, a short contact time of the liquid with the evaporator surface should be avoided [8]; and lengthy heating of the material to be distilled should be minimized.

2.1.3. Mean free path

The MD process is characterized by the following features: short residence time in the distillation gap; low operating temperatures because of the reduced pressure, and a characteristic mechanism of mass transfer in the gap between the evaporating and condensing surfaces.

In addition to the operating conditions (pressure system and temperature) being low, the condenser surface should be separated from the evaporator surface by a distance comparable with the mean free path of the evaporating molecules. Thus the mean free path (*MFP*) or average distance moved by the free molecules is the mean distance of the molecule from other moving particles, that is, the vapor molecules reach the condenser surface without intermolecular collisions. As a consequence, the *MFP* is a very important reference data in the design of a molecular distiller and in the MD process [51,53].

According to the theory of kinetics, the *MFP* of a molecule can be estimated by considering the number density (number of molecules per unit volume) and the volume swept out by a molecule per unit time as it travels. Accordingly, the separation principle of molecular distillation is based on the difference in molecular *MFP* defined by the theory of the kinetics of ideal gases, as follows [53,55, 56]:

$$MFP = \frac{1}{\sqrt{2}\pi\sigma^2 N_m} = \frac{kT}{\sqrt{2}\pi\sigma^2 P} = \frac{RT}{\sqrt{2}\pi\sigma^2 N_A P} \quad (1)$$

$$N_m = \frac{N_A P}{RT} \quad (2)$$

$$\sigma = 8.09 \times 10^{-11} V_c^{1/3} \quad (3)$$

Where *MFP* is the mean free path (m); σ is the molecule diameter (m); N_m is the number density – number of molecules per unit volume of vapor phase (m^{-3}); k is the Boltzmann constant ($1.38 \times 10^{-23} \text{ J} \cdot \text{K}^{-1}$); T is the temperature (or evaporator temperature) (K); P is the pressure system (Pa); R is the universal gas constant ($8.314 \text{ J} \cdot \text{K}^{-1} \cdot \text{mol}^{-1}$), N_A is the Avogadro constant ($6.023 \times 10^{23} \text{ mol}^{-1}$); V_c is the critical volume ($\text{cm}^3 \cdot \text{mol}^{-1}$) and σ is the molecule diameter (m).

2.1.4. Anisotropic condition and effective rate of evaporation

The evaporation rate is an important factor in evaluating the efficiency of the MD process. Evaporation proceeds at a different rate and the vapor phase presents different physical properties as consequences of the fact that the gas behaves like a collection of independent particles. Thus, the appropriate vapor phase dynamic regime is determined by means of the Knudsen number (Kn), Equation (4), which expresses the ratio of the mean free path (MFP) of the vapor phase to a characteristic length (L), such as the boundary layer thickness, or a molecular distiller device dimension (the distance between the evaporator and the condenser surface) [41,57].

$$Kn = \frac{MFP}{L} \quad (4)$$

In the case of a MD process, $Kn > 0.1$ explains the fact that the vapor phase shows anisotropic behavior, which means that, at $Kn > 0.1$ intermolecular collisions in the region of interest (space between the evaporator and the condenser surfaces) are much less frequent than molecular interactions [41, 58]. In the other cases, the Knudsen number (Kn) is less than 0.1, and thus the vapor has isotropic properties and behaves as continuous matter, such that the number of collisions between the molecules increases and the molecules can reach the condenser, but can also return to the evaporator surface and attain equilibrium; not a valid state in the MD process [41].

Nevertheless, with short distances between the evaporator and the condenser and a low number of collisions, evaporation of the molecules proceeds at the maximal rate described by the Langmuir–Knudsen equation (Equation 5) [42, 59, 60].

$$G_T = P_{vap} \sqrt{\frac{M}{2\pi RT_s}} \quad (5)$$

Where G_T is the theoretical rate of evaporation, R is the universal gas constant (8314 J·K⁻¹ ·kmol⁻¹), P_{vap} is the equilibrium vapor pressure at the absolute temperature T_s , M is the molar mass of the compound, and R is the universal gas constant.

Therefore the MD process is a function of the molecular species and the surface temperature, that is, the molecular distillation process is a surface phenomenon [61].

The effective rate of evaporation (G_E) of each component is calculated using a modified Langmuir–Knudsen equation [62], where conditions in the vapor phase, above the thin evaporating liquid film, influence the effective mean free path of the molecules, as described by Equation (6) [41, 62]:

$$G_E = G_T f \quad (6)$$

Where the coefficient f represents the fraction of vaporized molecules that reach the condenser and is expressed as follows [41]:

$$f = \left[1 - (1 - F) \left(1 - e^{k^* K n} \right)^{n'} \right] \quad (7)$$

Kawala and Stephan [62] stated that the best value for n' is equal to 5, and the degree of anisotropy k^* of the vapor phase in the space between the evaporator and the condenser is given by:

$$\log k^* = 0.2F + 1.38(F + 0.1)^4 \quad (8)$$

Where F describes the curvature of the evaporation surface [41]:

$$F = \frac{d_e - 2L}{2d_e - 2L} \quad (9)$$

Where d_e is the diameter of the evaporation surface curvature and L is the distance between the evaporator and the condenser. Hence, the effective rate of the evaporation surface takes into account the anisotropic effect of the vapor phase.

2.2. Molecular distiller units for processing high-boiling-point petroleum fractions

The Separation Process Development Laboratory (LDPS) and the Optimization, Project and Advanced Control Laboratory (LOPCA) of the Chemical Engineering School of State University of Campinas (UNICAMP), sponsored by the Petrobras Research Center (CENPES/Petrobras, Brazil) and Brazilian Study and Project Financing Institution (FINEP), projected and built molecular distiller units (pilot plants) and aimed at enhancing the performance of the heavy petroleum fractions and heavy petroleum crude oil. Molecular distillers show two principal designs: Falling film molecular distillers (FFMD) (with two (02)

configurations: wiped film short path distillers and thin falling evaporators); or centrifugal molecular distillers (CMD). The principal characteristics among them are described in Table 3.

Table 3. Comparative characteristics of molecular distiller units available at the research laboratory of the Separation Processes Development (LDPS) and the Optimization, Project and Advanced Control Laboratory (LOPCA) sectors at the State University of Campinas (UNICAMP) aiming at enhancing the performance of the heavy petroleum fractions and heavy petroleum crude oil.

Molecular distiller type	Wiped Film short path		Centrifugal
Construction project	LDPS/LOPCA/UNICAMP/CENPES (PETROBRAS) Sponsored by Brazilian agencies	KDL 5–Mini Pilot Plant/UIC–GmbH [54]	LDPS/LOPCA/UNICAMP/CENPES (PETROBRAS) Sponsored by Brazilian agencies
Molecular distiller units	Pilot plant	Lab scale	Pilot plant
Configuration design	Agitated thin film by a rotating roller wiper basket		Distributed film of liquid over evaporator surface
Agitation system	With		Without
Distribution onto the inner surface of the evaporator	Centrifugal and gravity forces		Centrifugal force
Design	Batch/Continuous		Batch/Continuous
Throughout Capacity	10 L/h	0.3 L/h – 2 L/h	40 L/h – 50 L/h
Evaporator	Cylindrical body with a heating jacket	Vertical double-jacketed cylinder	Central rotational heated disk
Evaporator surface	0.11 m ²	0.05 m ²	0.19 m ²
Operating temperature range	298 K – 623 K	298 K – 623 K	298 K – 623 K
Condenser	External/internal	Internal	External
Vapor Flow	Countercurrent		–
Material construction	316 Stainless steel	Borosilicate glass	Mostly stainless steel so there is little glass to break.
Distillation gap	0.10 m	0.02 m	0.08 cm
Flow Pattern	Turbulent	Turbulent	Laminar
Vacuum system	A combination of several vacuum pumps in series (a mechanical pump and a diffusion Langmuir pump)		
Ultimate Pressure	0.3 Pa	0.1 Pa	0.4 Pa
Operating Pressure	0.3 Pa – 50 Pa	0.1Pa – 10.0 Pa	0.4 Pa – 50 Pa

3. Computational development

3.1. Chemical systems: High-boiling-point petroleum fractions

In this study, Brazilian crude oils with different API gravities (16–25 °API), obtained from several sources, were distilled by conventional atmospheric distillation [63], resulting in three atmospheric distillation residues (ATR–W, ATR–Y and ATR–Z). The high-boiling-point petroleum fraction samples used as the feedstock were specifically selected in this study to cover a very broad range of properties. The BP curves were obtained in the Petrobras Research and Development Center (CENPES–Brazil) (Table 4).

Table 4. Properties of the atmospheric distillation residues studied.

Feedstock	ATR–W		ATR–Y		ATR–Z	
API gravity	11.9		N.A.		18.0	
Asfalthene content (%wt)	9.15		9.40		5.26	
True Boiling Point	Accumulate volume of distillate (%v/v)	Boiling temperature (K)	Accumulate volume of distillate (%v/v)	Boiling temperature (K)	Accumulate volume of distillate (%v/v)	Boiling temperature (K)
	3.31	459.1	38.21	653.2	3.5	377.15
	10.70	551.2	41.45	680.2	4.2	398.15
	19.87	647.2	42.79	693.2	5.4	423.15
	24.8	670.2	46.41	700.2	7.5	448.15
	30.83	693.2	47.36	706.2	10.9	493.15
	34.13	710.2	49.69	716.2	14.1	519.15
	31.98	720.2	52.88	723.2	14.6	523.15
	35.29	733.2	56.86	726.2	18.0	546.15
	38.54	748.2	61.75	733.2	21.0	566.15
	40.81	768.2	66.32	746.2	24.7	589.15
	42.66	773.2	70.89	762.2	27.8	611.15
	45.03	790.2	72.33	773.2	30.9	633.15
	47.38	801.2			33.9	653.15
	49.65	810.2			37.0	673.15
	51.36	813.2			39.9	692.15
	51.93	818.2			42.7	705.15
	60.59	818.4			45.5	711.15
	62.35	846.3			46.2	713.15
	65.24	880.0			49.0	728.15
	69.62	920.3			51.7	743.15
	73.81	967.9			54.4	753.15
					56.9	763.15
					58.6	778.15
					61.5	788.15
					63.6	807.15
					65.9	823.15
					68.7	837.15
					71.3	839.15

N.A. Not available

In order to characterize the fluid properties (Tables 5 – 6), the ATR–W, ATR–Y and ATR–Z were modeled as in previous physicochemical studies [64].

Table 5. Average properties of the atmospheric distillation residues.

Property Type	Properties	EVT (K)	System		
			ATR–W	ATR–Y	ATR–Z
Basic	Kw		11.94	12.16	11.79
	$MeABP$ (K)		819.7	750.1	674.2
	$MABP$ (K)		750.7	766.6	651.3
Thermodynamic	Pc (MPa)		0.905	0.962	1.260
	Tc (K)		971.2	920.1	849.6
	V_c (cm ³ ·mol ⁻¹)		1795.917	1636.008	1245.002
	ω_{ac}		1.2188	1.1348	0.8546
Thermophysical	Cp (J·kg ⁻¹ ·K ⁻¹)				
		423.15	2388.03	2449.30	2401.00
		523.15	2767.57	2829.54	2769.03
		623.15	3083.57	3146.12	3075.43
	λ (W·m ⁻¹ ·K ⁻¹)				
		423.15	0.106	0.104	0.103
		523.15	0.094	0.092	0.091
		623.15	0.085	0.083	0.082
	ν (mm ² ·s ⁻¹)				
		423.15	86.947	26.917	19.632
		523.15	7.642	3.748	3.151
		623.15	2.447	1.465	1.304
	P_{vap} (MPa)				
		423.15	0.1052	0.1044	0.1034
		523.15	0.1037	0.1031	0.1024
		623.15	0.1027	0.1023	0.1017

ρ : Density at evaporator temperature; Kw : Watson characterization factor; $MeABP$: Mean average boiling point; M : Molar mass; Pc : Critical pressure; Tc : Critical temperature; Vc : Critical volume; ω_{ac} : acentric factor; Cp : Specific heat capacity; λ : Thermal conductivity; ν : Kinematic viscosity; P_{vap} : Vapor pressure; EVT : Evaporator temperature.

Table 6. Basic properties of each pseudocomponent [64].

NPSE _i	ATR-W					ATR-Y					ATR-Z				
	x_v	x_m	Tb_i	M_{NPSE} (kg·kmol ⁻¹)	ρ_i at 298.15 K (kg·m ⁻³)	x_v	x_m	Tb_i	M_{NPSE} (kg·kmol ⁻¹)	ρ_i at 298.15 K (kg·m ⁻³)	x_v	x_m	Tb_i	M_{NPSE} (kg·kmol ⁻¹)	ρ_i at 298.15 K (kg·m ⁻³)
1	0.0850	0.1823	470.9	156.0	791.5	0.7903	0.8825	703.7	335.2	888.7	0.0153	0.0381	362.8	94.9	735.2
2	0.0753	0.1195	573.3	224.9	845.2	0.0148	0.0119	874.8	502.3	955.6	0.0153	0.0351	383.2	105.0	748.6
3	0.1758	0.2254	659.7	292.0	885.7	0.0135	0.0103	902.8	532.5	965.6	0.0153	0.0324	403.5	115.6	761.7
4	0.1734	0.1750	772.1	391.0	933.4	0.0125	0.0091	930.7	563.6	975.5	0.0134	0.0265	423.5	126.5	774.0
5	0.1785	0.1535	857.3	475.0	966.5	0.0116	0.0081	958.7	595.4	985.2	0.0127	0.0233	444.2	138.2	786.5
6	0.0770	0.0560	957.0	582.6	1002.6	0.0109	0.0073	986.7	628.1	994.7	0.0127	0.0218	464.6	150.2	798.3
7	0.0379	0.0236	1059.2	703.4	1037.1	0.0103	0.0066	1014.6	661.5	1004	0.0127	0.0204	484.9	162.7	809.8
8	0.0261	0.0142	1159.1	831.6	1068.7	0.0098	0.0060	1042.6	695.8	1013.1	0.0241	0.0362	506.3	176.2	821.5
9	0.0204	0.0098	1258.2	968.5	1098.4	0.0094	0.0055	1070.5	730.9	1022.1	0.0272	0.0386	525.6	188.9	831.8
10	0.0170	0.0072	1357.0	1114.5	1126.4	0.0090	0.0051	1098.5	766.7	1030.9	0.0303	0.0406	546.0	202.8	842.5
11	0.0146	0.0056	1455.6	1269.7	1153.1	0.0087	0.0047	1126.5	803.3	1039.6	0.0308	0.039	566.4	217.0	852.8
12	0.0130	0.0045	1554.2	1433.9	1178.5	0.0084	0.0044	1154.4	840.8	1048.1	0.0313	0.0376	586.7	231.7	862.9
13	0.0117	0.0037	1652.7	1607.3	1202.9	0.0081	0.0041	1182.4	879.0	1056.5	0.0301	0.0343	606.9	246.7	872.7
14	0.0107	0.0031	1751.2	1789.8	1226.4	0.0079	0.0038	1210.3	917.9	1064.8	0.0296	0.0321	627.4	262.4	882.4
15	0.0099	0.0026	1849.8	1981.4	1248.9	0.0076	0.0036	1238.3	957.7	1072.9	0.0312	0.0322	647.7	278.5	891.8
16	0.0092	0.0023	1948.2	2181.8	1270.7	0.0074	0.0034	1266.2	998.2	1080.9	0.0326	0.0321	668.3	295.1	901.2
17	0.0087	0.0020	2046.6	2390.8	1291.8	0.0072	0.0032	1294.2	1039.6	1088.8	0.0347	0.0326	688.4	311.8	910.1
18	0.0082	0.0017	2145.0	2608.7	1312.1	0.0071	0.0030	1322.1	1081.6	1096.6	0.0634	0.0573	707.2	327.8	918.3
19	0.0077	0.0015	2243.5	2835.5	1331.9	0.0069	0.0029	1350.1	1124.5	1104.3	0.0346	0.0298	729.1	346.9	927.7
20	0.0074	0.0014	2341.9	3071.0	1351.1	0.0067	0.0027	1378.0	1168.1	1111.8	0.0507	0.0419	749.7	365.4	936.4
21	0.0070	0.0012	2440.4	3315.1	1369.8	0.0066	0.0026	1406.0	1212.5	1119.3	0.0380	0.0302	769.6	383.6	944.6
22	0.0067	0.0011	2538.8	3567.8	1388.0	0.0065	0.0024	1433.9	1257.7	1126.7	0.0315	0.0240	789.4	402.1	952.6
23	0.0065	0.0010	2637.2	3828.8	1405.7	0.0063	0.0023	1461.9	1303.6	1133.9	0.0278	0.0204	810.5	422.3	961.0
24	0.0062	0.0009	2735.6	4098.4	1422.9	0.0062	0.0022	1489.8	1350.2	1141.1	0.0802	0.0564	833.7	445.0	970.1
25	0.0060	0.0008	2834.0	4376.4	1439.8	0.0061	0.0021	1517.8	1397.7	1148.2	0.2747	0.1871	851.2	462.5	976.8

Finally, considering just the liquid film on the wall of the evaporator surface, the values for MFP (Equations 1 – 3), the Kn (Equation 4) and G_E (Equations 6 – 9) for the 25 pseudocomponents from the high-boiling-point petroleum fractions under the different operating conditions (evaporator temperature ranging from 423.15 to 623.15 K and pressure ranging from 0.1 to 1 Pa) were estimated.

The computational tool used to develop the pseudoization computational approach and to estimate the MFP , Kn and G_E of the high-boiling-point petroleum fractions was built up in FORTRAN-90 language using Compaq Visual Fortran compiler (professional edition 6.6) [64].

4. Results and discussion

The study on molecular distillation parameters was based on knowledge-based understanding of mean free path (MFP) and the Knudsen number (Kn) values applied to high-boiling-point petroleum fractions, as the important parameters in the description of the process taking place in a distillation gap with a width equal to 0.08 m (a centrifugal molecular distiller – pilot plant module) and 0.05 and 0.02 m (lab scale module). The operating conditions (evaporator temperature and pressure system) and dimension parameter (distance between evaporator and condenser) were analyzed.

4.1 Effect of pressure system on the mean free path

Computational data derived from Equations (1) – (3) are presented in Figures 1 – 3, showing the values for the MFP of the high-boiling-point petroleum fractions molecules under different operating conditions (evaporator temperature and pressure system) at a distance of 0.08 m from the surface of evaporation to the condenser surface.

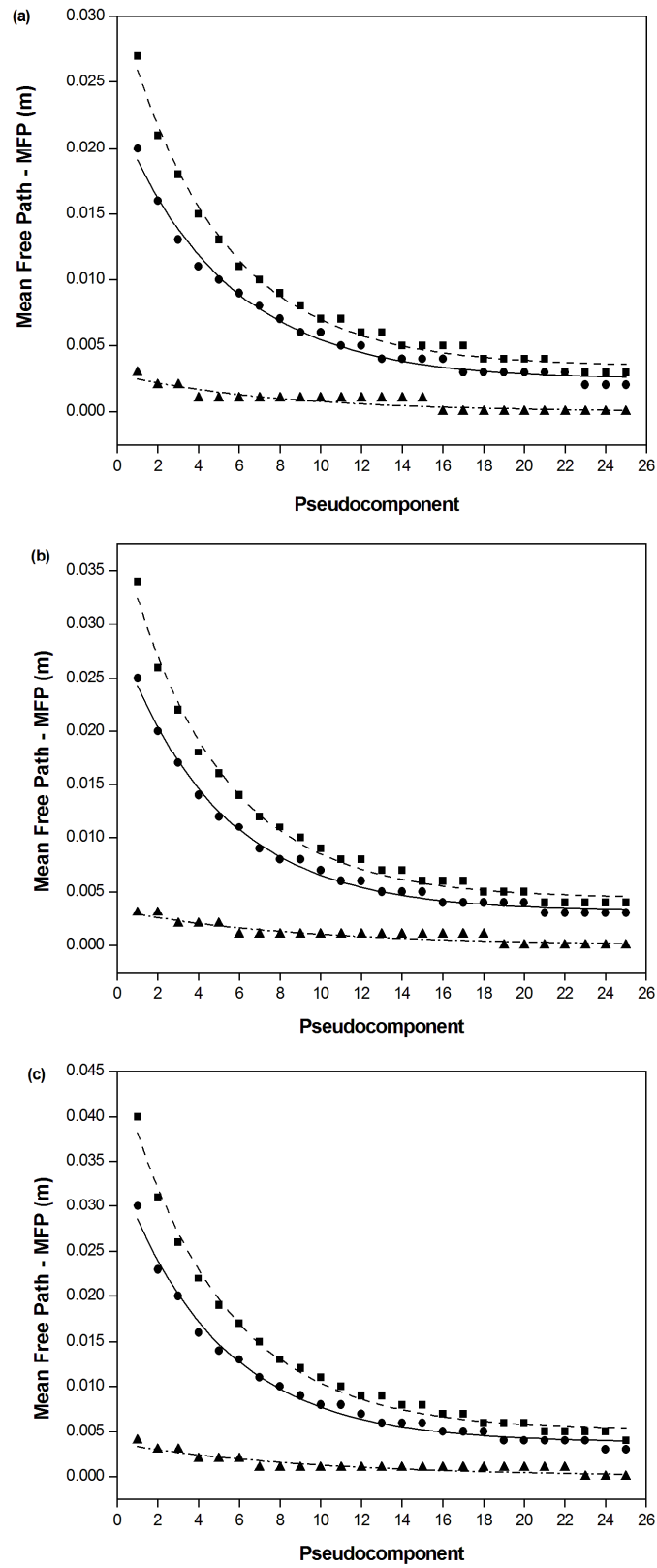


Figure 1. Mean free path for each pseudocomponent of the ATR-W high-boiling-point petroleum fraction as a function of the operating conditions: Evaporator temperature: a) 423.15 K, b) 523.15 K and c) 623.15 K; and vacuum system at ■ 0.1 Pa, ● 0.13 Pa and ▲ 1 Pa at a distance between the evaporator and condenser surfaces of $L=0.08$ m.

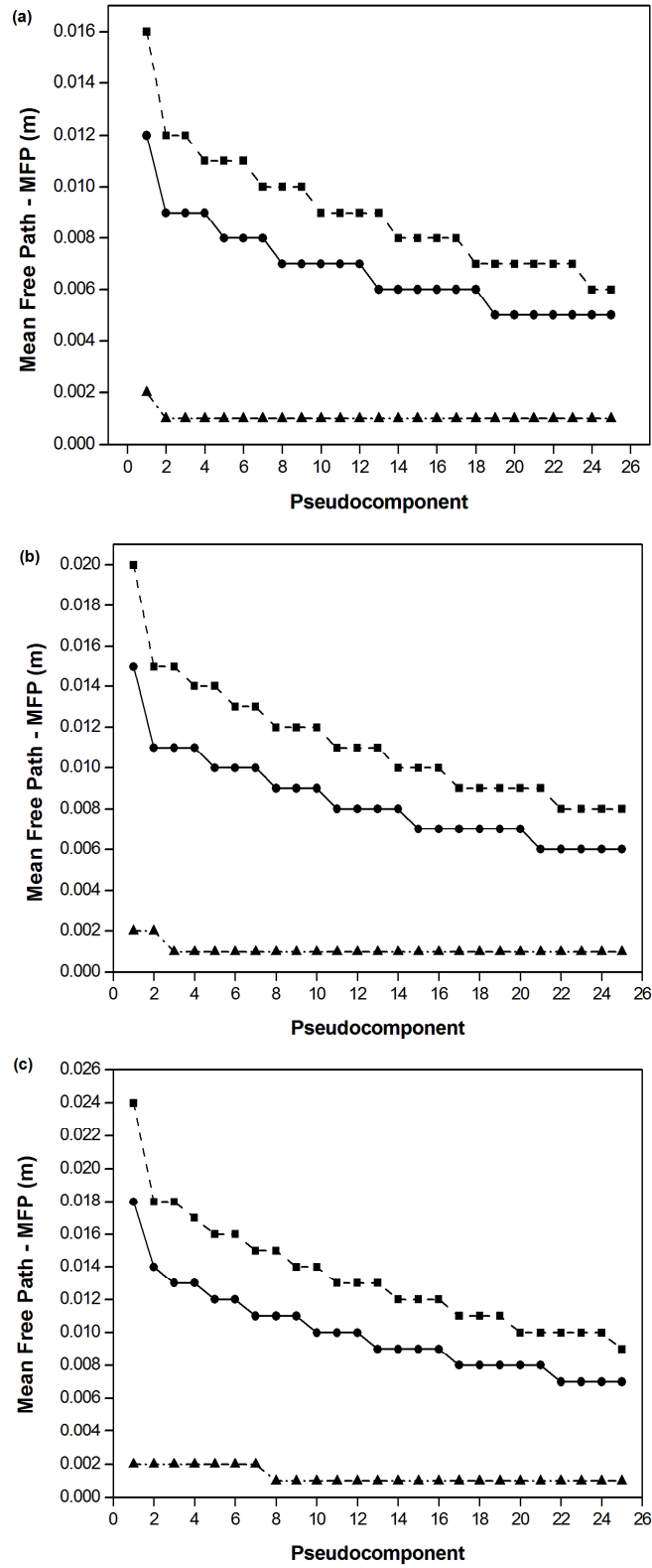


Figure 2. Mean free path for each pseudocomponent of the ATR-Y high-boiling-point petroleum fraction as a function of the operating conditions: Evaporator temperature: a) 423.15 K, b) 523.15 K and c) 623.15 K; and vacuum system at ■ 0.1 Pa, ● 0.13 Pa and ▲ 1 Pa at a distance between the evaporator and condenser surfaces of $L=0.08$ m.

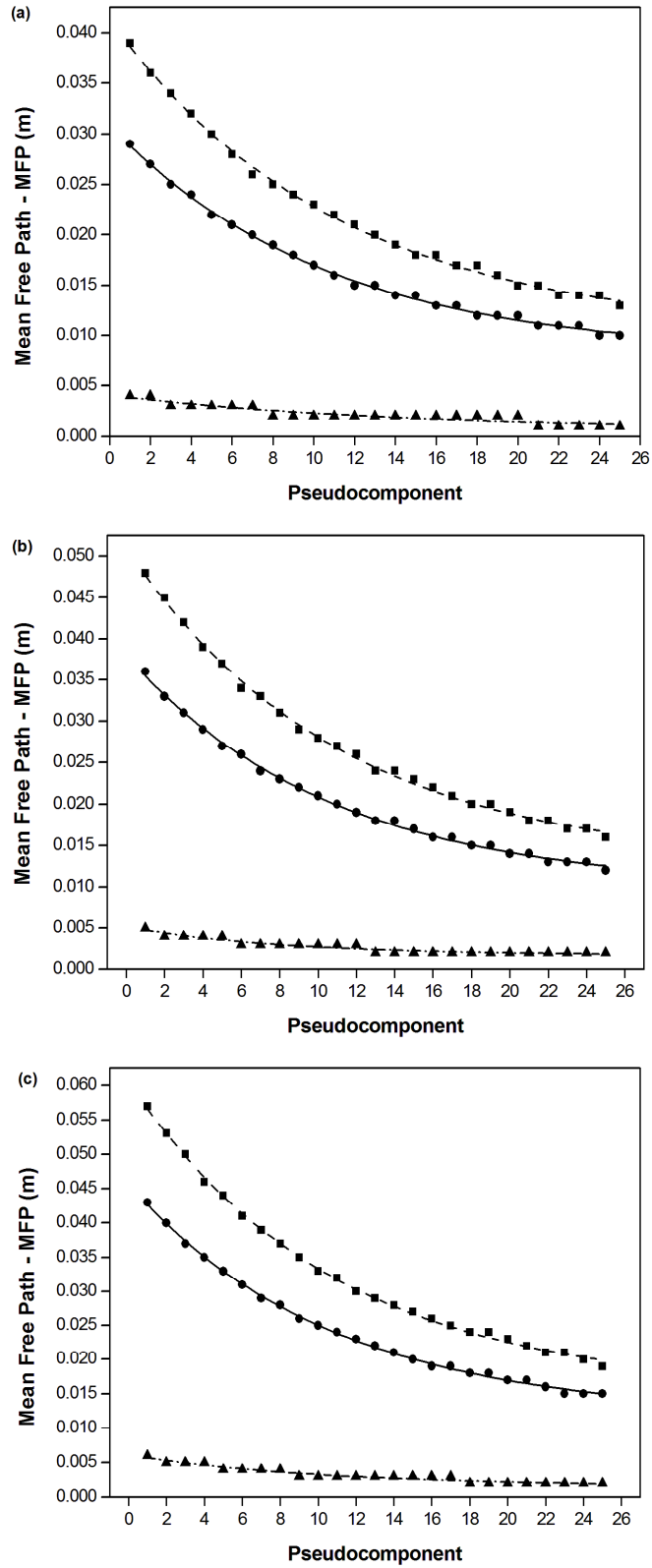


Figure 3. Mean free path for each pseudocomponent of the ATR-Z high-boiling-point petroleum fraction as a function of the operating conditions: Evaporator temperature: a) 423.15 K, b) 523.15 K and c) 623.15 K; and vacuum system at ■ 0.1 Pa, ● 0.13 Pa and ▲ 1 Pa at a distance between the evaporator and condenser surface of $L=0.08$ m.

As can be seen in Figure 1, the *MFP* depends on the pressure system more than on the evaporator temperature, although both operating variables are important. An increase in evaporator temperature and a decrease in the pressure system (understood as the lowest value of the pressure system in the range studied) led to an increase in the *MFP* values for each pseudocomponent. Therefore, in order to take advantage of the *MFP*, the evaporator temperature must be kept at the highest trial level and the pressure system at the lowest level. Thus the greatest *MFP* appears to be near 623.15 K (between the range studied and the operational limit of the equipment) and the pressure equal to 0.1 Pa.

With a higher pressure system, low *MFP* values were obtained, because the density of the molecules rises in the distillation gap, and the motion of the particles in the distillation gap causes isotropic behavior. Furthermore, *MFP* values equal to zero were reported, at the highest value of the pressure system (1 Pa), which means that the separation process does not occur. Figure 1 shows the effect of the evaporator temperature when it is increased from 423.15 to 623.15 K. Under these conditions, the evaporation rate of the molecule with the lowest vapor pressure was higher than the evaporation rate of the molecules with higher vapor pressures, and as a consequence, a greater evaporation rate caused a larger molecule density.

The separation and split principle in molecular distillation is based on the pressure system enabling the molecules to evaporate from the evaporator to the condenser in the distillation gap (distance between the evaporator and condenser), and a small distance between these elements. Thus the concept of anisotropy in the distillation gap, introduced when it was analyzed with a lower pressure system (e.g. 0.1 Pa), refers to the motion of molecules implying heterogeneity in all directions.

Figures 2 – 3 show the *MFP* values of the ATR–Y high-boiling-point petroleum fraction with a high asphaltene content, and of ATR–Z, with the highest API gravity of all the samples, representing the trials carried out with $L=0.08$ m, evaporator temperature ranges between 423.15 and 623.15 K and pressure systems ranging between 0.1 – 1 Pa. It can be seen that, in the simulation of the results, the difference between the *MFP* for the ATR–W molecules and that for the ATR–Z molecules, under the defined operational conditions, was to the order of 60%, whereas in the simulations carried out with the ATR–Y high-boiling-point petroleum fraction, the *MFP* values were very close to the specific range of the pseudocomponent, and thus

the *MFP* calculated for the ATR–Y molecules was also related to the asphaltene content, showing the highest isotropic behavior under a high pressure system (e.g. 1 Pa) when compared to 0.13 and 0.1 Pa.

As shown before (Figure 1), the effect of the pressure system was very relevant under the conditions analyzed, presenting an effect of about 33.33%, which means that, on average, the *MFP* increased 33.33% when the values for the pressure were decreased from 0.13 Pa to 0.1 Pa.

Figure 3 shows the *MFP* of the ATR–Z high-boiling-point petroleum fraction molecules as a function of the pseudocomponent number, pressure system and evaporator temperature. Under the operational conditions explored, there was a decrease in the *MFP* values ranging from 0.040 to 0.012 m (when the pressure system was maintained at 0.1 Pa), from 0.029 to 0.010 m (when the pressure system was maintained at 0.13 Pa) and from 0.005 to 0.001 (when the pressure system was maintained at 1 Pa) for 423.15 K. At 523.15 K, the *MFP* ranged from 0.047 to 0.015 m (when the pressure system was maintained at 0.1 Pa), from 0.035 to 0.013 m (when the pressure system was maintained at 0.13 Pa) and from 0.005 to 0.002 (when the pressure system was maintained at 1 Pa). Finally, at 623.15 K, the *MFP* ranged from 0.056 to 0.019 m (when the pressure system was maintained at 0.1 Pa), from 0.048 to 0.015 m (when the pressure system was maintained at 0.13 Pa) and from 0.006 to 0.002 (when the pressure system was maintained at 1 Pa). However, it appears that both the operating conditions of evaporator temperature and pressure system, and also the chemical composition of the samples (volatiles content and asphaltene content) present a great influence on the *MFP* values for the molecules of the high-boiling-point petroleum fractions.

Since the *MFP* of the molecules of the light pseudocomponent (low volatility) decreased sharply as the distilling pressure increased, so more and more molecules failed to reach the condenser, and hence, there were less and less volatile components in the distillates. In the same way, when the distilling pressure increased to 1 Pa (low vacuum pressure), most of the heavier molecules with a larger molar mass as compared to the volatile components, failed to reach the condenser, resulting in isotropic behavior and/or continuous flow.

The *MFP* values of the molecules calculated using the Equations (1) – (3) for ATR–W, ATR–Y and ATR–Z at 0.1 Pa and 0.13 Pa (in the whole evaporator temperature range) were in good agreement with the molecular distillation process, since they were quite comparable with

the distillation gap width (space between the evaporator and the condenser surface i. e. 0.08 m) and few intermolecular collisions would have been expected during the passage of the molecules from the evaporator surface to the condenser surface.

Limiting the working pressure to a certain low level in order to be able to distill at the lowest possible temperature must be considered. This low level must be reached with a specifically dimensioned pressure system instead of an over-dimensioned system below this physical limit, or otherwise condensable molecules will not condense on the condenser surface, but will be carried over from the molecular distillation module to the succeeding vacuum system. In order to consider the distance between the evaporator and condenser surface as a design parameter, the role of the Knudsen number on the hydrodynamic development in the distillation gap must be examined.

4.2. The influence of the Knudsen number on the hydrodynamic in the distillation gap

The Knudsen number (Kn) represents the relationship between the MFP and the characteristic dimension of the flow geometry (in the case studied, this corresponds to the distance between the evaporator and condenser surfaces). Figures 4 – 6 display the Kn parameter for each pseudocomponent, showing the effect of the pressure system ($0.1 < P < 1$ Pa) and evaporator temperature ($423.15 < EVT < 623.15$ K) as the operating conditions, and the distance between the evaporator and the condenser ($0.02 < L < 0.08$ m) as a mechanical design parameter, on the degree of rarefaction of the vapor phase.

The validity of the continuum flow assumption and the rarefaction of the vapor phase are described by the Knudsen number (Kn), and the main effects of the two operational variables studied (EVT and P) and of the design parameter (distance between the evaporator and condenser surfaces, L) on the Kn are shown in Figures 4 – 6 for a set of 25 pseudocomponent numbers, and are therefore related to the boiling point of the pseudocomponent.

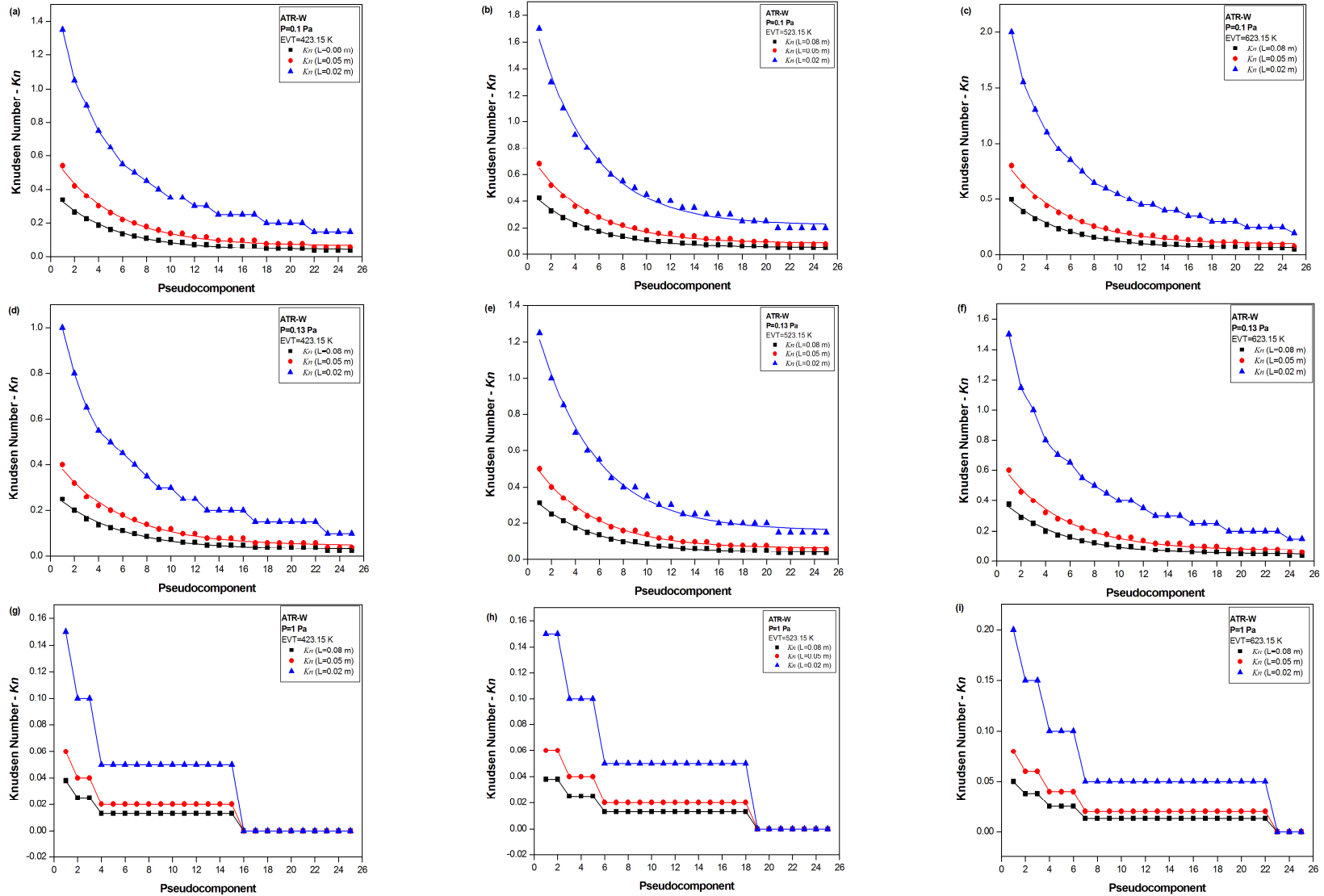


Figure 4. Non-dimensionalised length (Kn) for rarefied vapor phase in the distilled gap for each pseudocomponent of the ATR-W at a) $P=0.1$ Pa and $EVT=423.15$ K; b) $P=0.1$ Pa and $EVT=523.15$ K; c) $P=0.1$ Pa and $EVT=623.15$ K; d) $P=0.13$ Pa and $EVT=423.15$ K; e) $P=0.13$ Pa and $EVT=523.15$ K; f) $P=0.13$ Pa and $EVT=623.15$ K; g) $P=1$ Pa and $EVT=423.15$ K; h) $P=1$ Pa and $EVT=523.15$ K and i) $P=1$ Pa and $EVT=623.15$ K as a function of L equals $\blacktriangle 0.02$ m, $\bullet 0.05$ m and $\blacksquare 0.08$ m.

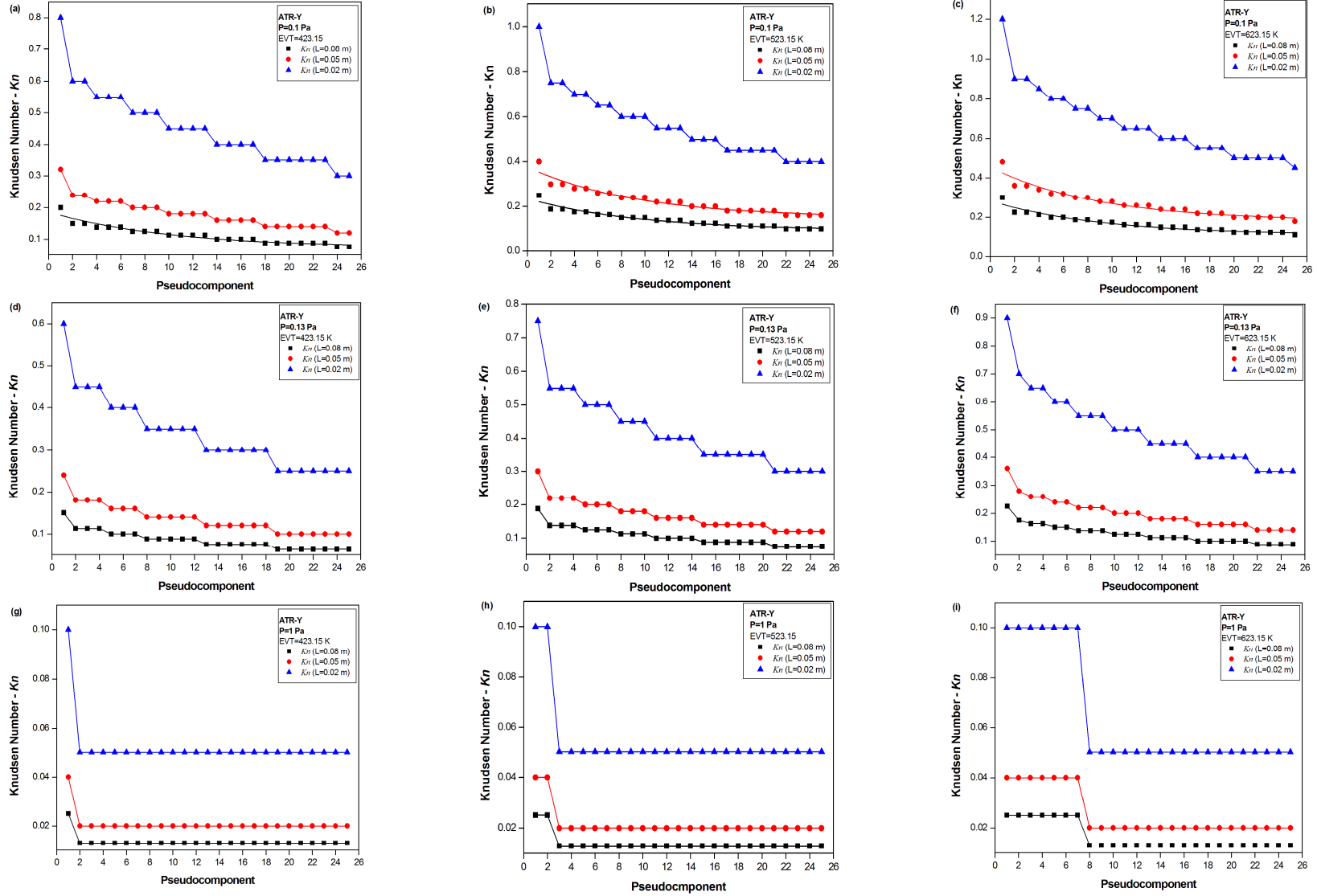


Figure 5. Non-dimensionalised length (Kn) for rarefied vapor phase in the distilled gap for each pseudocomponent of the ATR-Y at a) $P=0.1$ Pa and $EVT=423.15$ K; b) $P=0.1$ Pa and $EVT=523.15$ K; c) $P=0.1$ Pa and $EVT=623.15$ K; d) $P=0.13$ Pa and $EVT=423.15$ K; e) $P=0.13$ Pa and $EVT=523.15$ K; f) $P=0.13$ Pa and $EVT=623.15$ K; g) $P=1$ Pa and $EVT=423.15$ K; h) $P=1$ Pa and $EVT=523.15$ K and i) $P=1$ Pa and $EVT=623.15$ K as a function of L equals $\blacktriangle 0.02$ m, $\bullet 0.05$ m and $\blacksquare 0.08$ m.

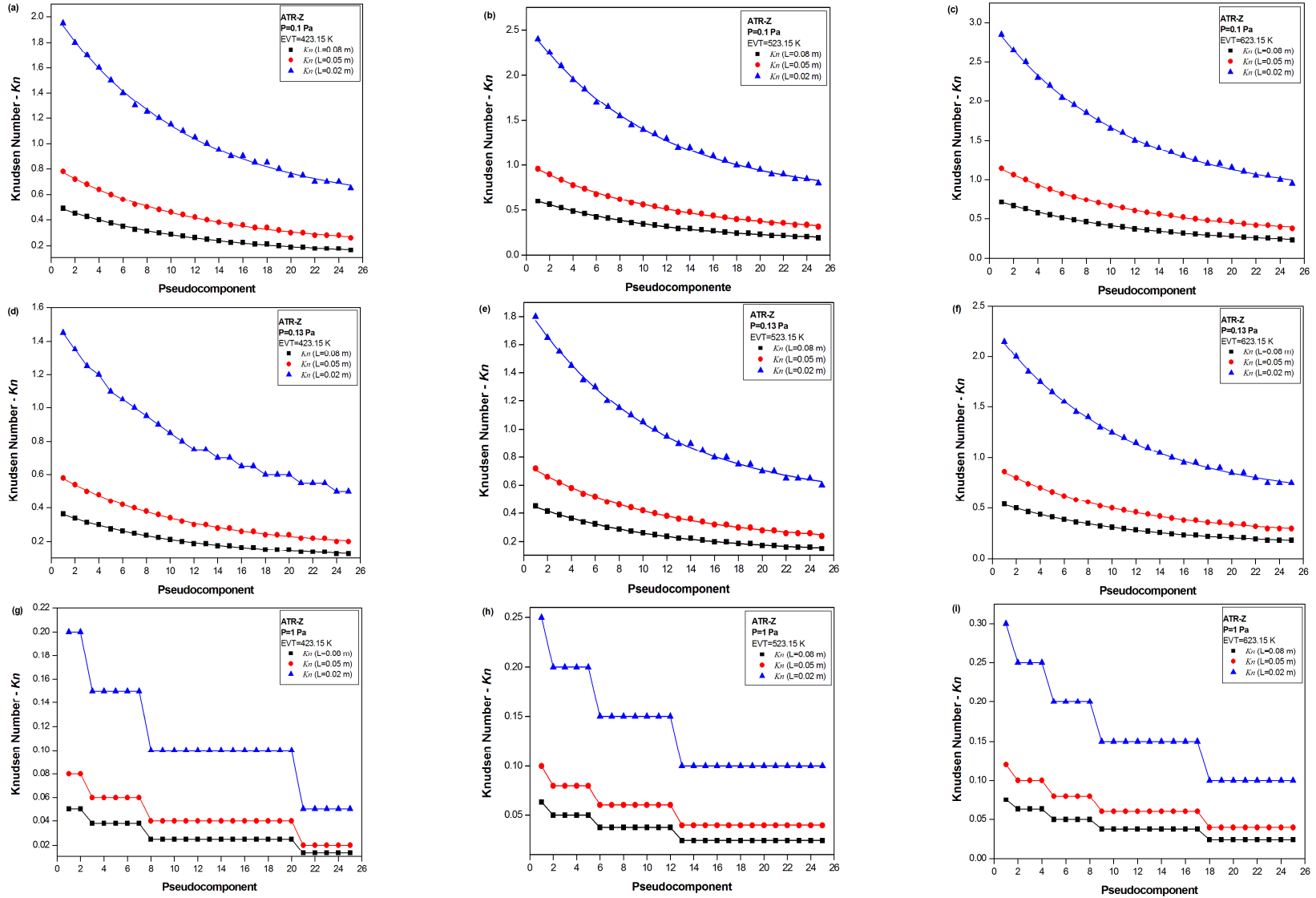


Figure 6. Non-dimensionalised length (Kn) for rarefied vapor phase in the distilled gap for each pseudocomponent of the ATR-Z at a) $P=0.1$ Pa and $EVT=423.15$ K; b) $P=0.1$ Pa and $EVT=523.15$ K; c) $P=0.1$ Pa and $EVT=623.15$ K; d) $P=0.13$ Pa and $EVT=423.15$ K; e) $P=0.13$ Pa and $EVT=523.15$ K; f) $P=0.13$ Pa and $EVT=623.15$ K; g) $P=1$ Pa and $EVT=423.15$ K; h) $P=1$ Pa and $EVT=523.15$ K and i) $P=1$ Pa and $EVT=623.15$ K as a function of L equals ▲ 0.02 m, ● 0.05 m and ■ 0.08 m.

Case study 1: ATR–W and ATR–Z

Figures 4 and 6 present the results of simulations for the Kn values with respect to the distribution of the components in the heavy petroleum fractions of ATR–W and ATR–Z. It was noted that the Kn values ranged between $0.01 < Kn < 3.00$ under the ranges of evaporator temperature and pressure systems tested as the operating conditions. Hence, the effects of the two operating conditions must be analyzed as a function of the distance between the evaporator and the condenser surfaces.

- Analyzing the distance between the evaporator and the condenser distance equaled 0.08, 0.05 and 0.02 m, when the EVT was increased from 423.15 K to 623.15 K (at 0.1 Pa), on average, the Kn increased 49.61% for each pseudocomponent.

In the data set of Kn values obtained at low vacuum pressure (that is, relatively high pressure system e.g. 1 Pa), Kn values equal to zero were obtained (not compromising the conclusions of the analyses) and isotropic behavior, since the Kn values did not change from pseudocomponent to pseudocomponent, maintaining an approximately constant value as shown in Figures 4g–4i and 6g–6i.

- When the pressure system increased from 0.1 Pa to 1 Pa (at 423.15 K), on average the Kn decreased 92.34% for each pseudocomponent, analyzing the distance between the evaporator and the condenser between 0.08 m and 0.02 m.

Considering the high evaporator temperature used ($EVT=623.15$ K) in the range studied (from 0.1 Pa to 1 Pa), on average, the Kn decreased 89.19% for each pseudocomponent.

Case study 2: ATR–Y with high asphaltene content

Figures 5a – 5c show that the anisotropic condition was obtained at 0.1 Pa with evaporator temperatures equal to 423.15 K, 523.15 K and 623.15 K and values for Kn ranging between $0.1 < Kn < 0.2$ with L equal to 0.08 m; $0.15 < Kn < 0.32$ with L equal to 0.05 m; and $0.371 < Kn < 0.8$ with L equal to 0.02 m.

Furthermore, the effect of the two operational parameters was evaluated as follows:

- When the EVT increased from 423.15 K to 623.15 K (at 0.1 Pa, Figures 5a – 5c), on average, the value for Kn increased 48.57% for every pseudocomponent, analyzing distances

between the evaporator and condenser equal to 0.08, 0.05 and 0.02 m. Considering a pressure system of 1 Pa in the *EVT* range studied from 423.15 K to 623.15 K (Figures 5d – 5f), on average, the value for Kn increased 24%. Nevertheless, it is evident that the effect of pressure is more significant than the effect of evaporator temperature, since in the *EVT* range studied from 423.15 K to 623.15 K at 1 Pa (Figures 5g – 5i) profiles of Kn number showed an isotropic behavior because of it shows unchanged from pseudocomponent to pseudocomponent.

- When the pressure system increased from 0.1 Pa to 1 Pa (at 423.15 K), on average, the value for Kn decreased 88% for every pseudocomponent, analyzing distances between the evaporator and condenser equal to 0.08, 0.05 and 0.02 m. Similarly, considering the high *EVT* used (623.15 K) in the range of pressure system studied, on average the Kn value decreased 90.48% analyzing distances between the evaporator and condenser equal to 0.08, 0.05 and 0.02 m.

As a general overview, besides having a great impact on the design parameters of molecular stills, the parameter Kn is essential in the field of modeling and simulation of the molecular distillation process. The estimated values for Kn modeled the rarefaction effects of the vapor phase on the distillation gap, that it is understood as the beginning of the influence on the evaporating film flow, representing the slip-flow regime ($0.01 < Kn < 0.5$) and anisotropic behavior ($Kn > 0.5$), where the Navier –Stokes equations can only be employed if one has tangential slip-velocity boundary conditions along the walls of the flow domain [58]. In this situation, the vapor molecules seldom collide with each other, and they can reach the condenser surface by way of distillation in an unobstructed path. This type of flow is known as free-molecule flow (molecular flow regime) and it is characteristic of the molecular distillation process. However, comparing Figures 5a – 5i, it can be seen that the high-boiling-point petroleum fraction molecules of ATR-Y exhibit the greatest isotropic behavior for each pseudocomponent and for every operating condition studied, due to the higher asphaltene content.

4.3. The effective evaporation rate

Figures 7 – 9 depict the effective evaporation rate (G_E) on the evaporator surface in a molecular distiller with distillation gap widths equal to 0.08 (corresponding to a pilot plant module) and to 0.05 and 0.02 m (corresponding to a lab scale module). The effective evaporation

rates were estimated in a temperature range from 423.15 to 623.15 K using a modification of the Langmuir – Knudsen expression (Equations 6 – 9) and taking the anisotropic effect into account. In the cases studied where multi-component mixtures were analyzed, the results showed that the more volatile components evaporated faster than the others, explaining the fact that their quantities in the feed diminished and the effective evaporation rates decreased as shown in Figures 7 – 9.

The effective evaporation rate (G_E) taking place at the evaporator surface was evaluated in a temperature range. In Figures 7a – 7i, the G_E of the ATR–W high-boiling-point petroleum fraction is shown as a Gaussian distribution function following the distribution fraction of the pseudocomponents. For three different values of distillation gap width, the simulations showed that the G_E decreased when that distance decreased. Nevertheless, when distance decreased to 0.02, values were obtained for the effective evaporation rate, which had no physical meaning (negative values), which means that, theoretical studies could lead to over-dimensioned devices and the results will not be in good agreement with the process.

Figures 8a – 8i show the G_E for the ATR–Y high-boiling-point petroleum fractions for twenty five pseudocomponents. Considerable changes can be seen in the profiles when one considers the high asphaltene contents present in samples such ATR–Y. In general, under the operating conditions studied, a fast decrease in the G_E was observed for the first pseudocomponents, with minimum variation being caused by the rest of the set of pseudocomponents.

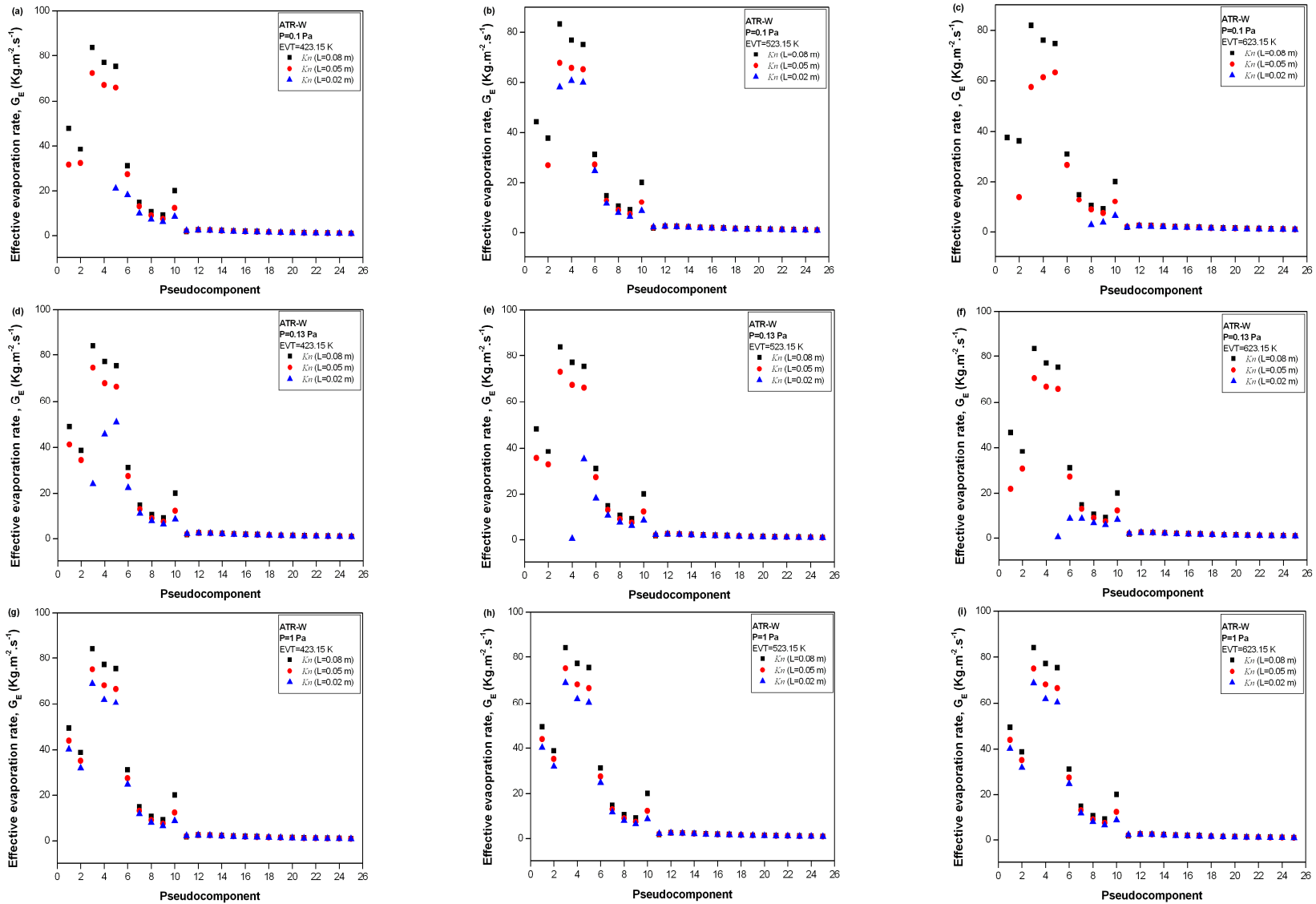


Figure 7. Effective evaporation rate of multicomponent mixture (set of twenty five pseudocomponents) of the ATR–W high-boiling-point petroleum fraction at a) $P=0.1$ Pa and $EVT=423.15$ K; b) $P=0.1$ Pa and $EVT=523.15$ K; c) $P=0.1$ Pa and $EVT=623.15$ K; d) $P=0.13$ Pa and $EVT=423.15$ K; e) $P=0.13$ Pa and $EVT=523.15$ K; f) $P=0.13$ Pa and $EVT=623.15$ K; g) $P=1$ Pa and $EVT=423.15$ K; h) $P=1$ Pa and $EVT=523.15$ K and i) $P=1$ Pa and $EVT=623.15$ K as a function of L equals \blacktriangle 0.02 m, \bullet 0.05 m and \blacksquare 0.08 m.

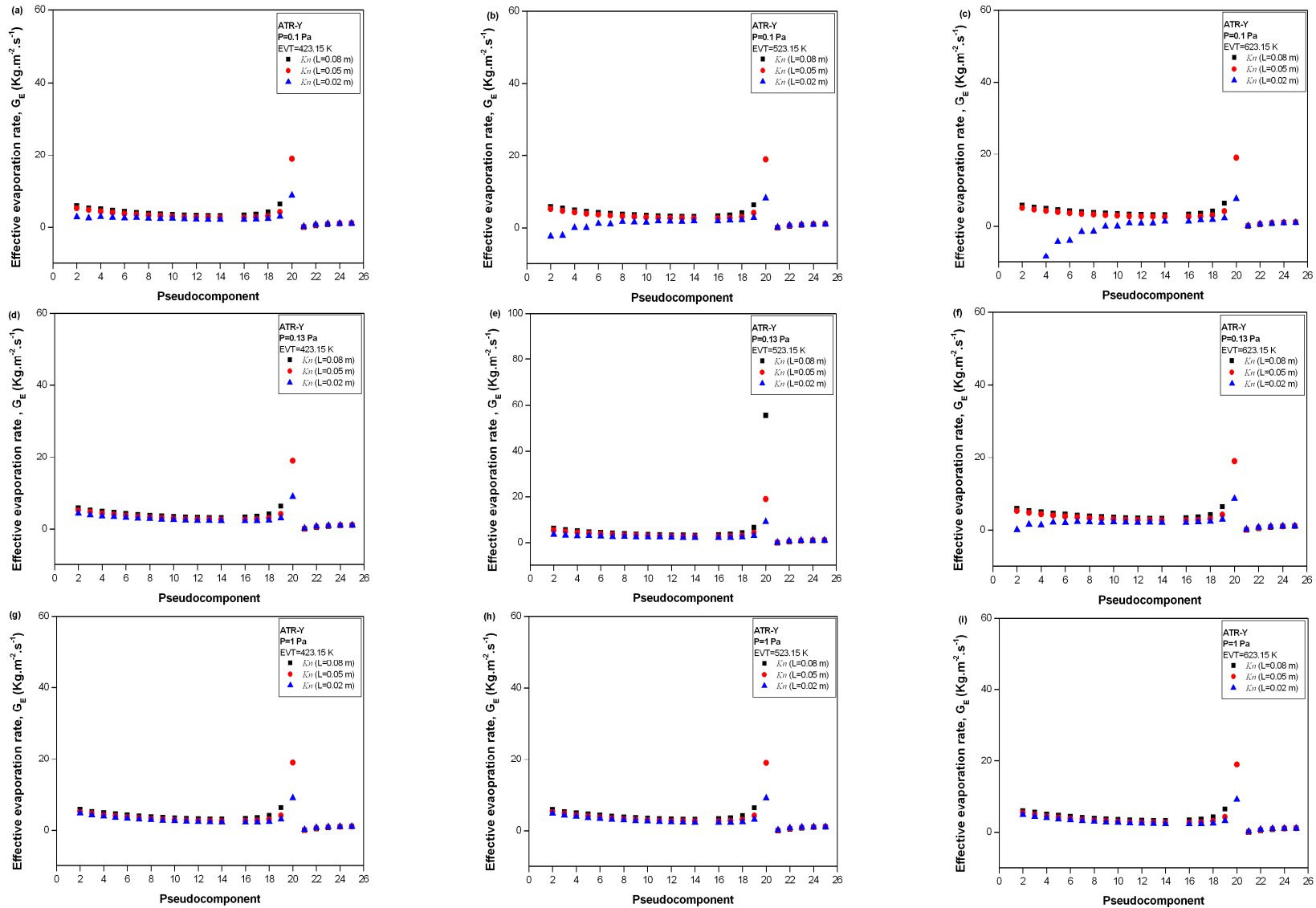


Figure 8. Effective evaporation rate of multicomponent mixture (set of twenty five pseudocomponents) of the ATR-Y high-boiling-point petroleum fraction at a) $P=0.1$ Pa and $EVT=423.15$ K; b) $P=0.1$ Pa and $EVT=523.15$ K; c) $P=0.1$ Pa and $EVT=623.15$ K; d) $P=0.13$ Pa and $EVT=423.15$ K; e) $P=0.13$ Pa and $EVT=523.15$ K; f) $P=0.13$ Pa and $EVT=623.15$ K; g) $P=1$ Pa and $EVT=423.15$ K; h) $P=1$ Pa and $EVT=523.15$ K and i) $P=1$ Pa and $EVT=623.15$ K as a function of L equals $\blacktriangle 0.02$ m, $\bullet 0.05$ m and $\blacksquare 0.08$ m.

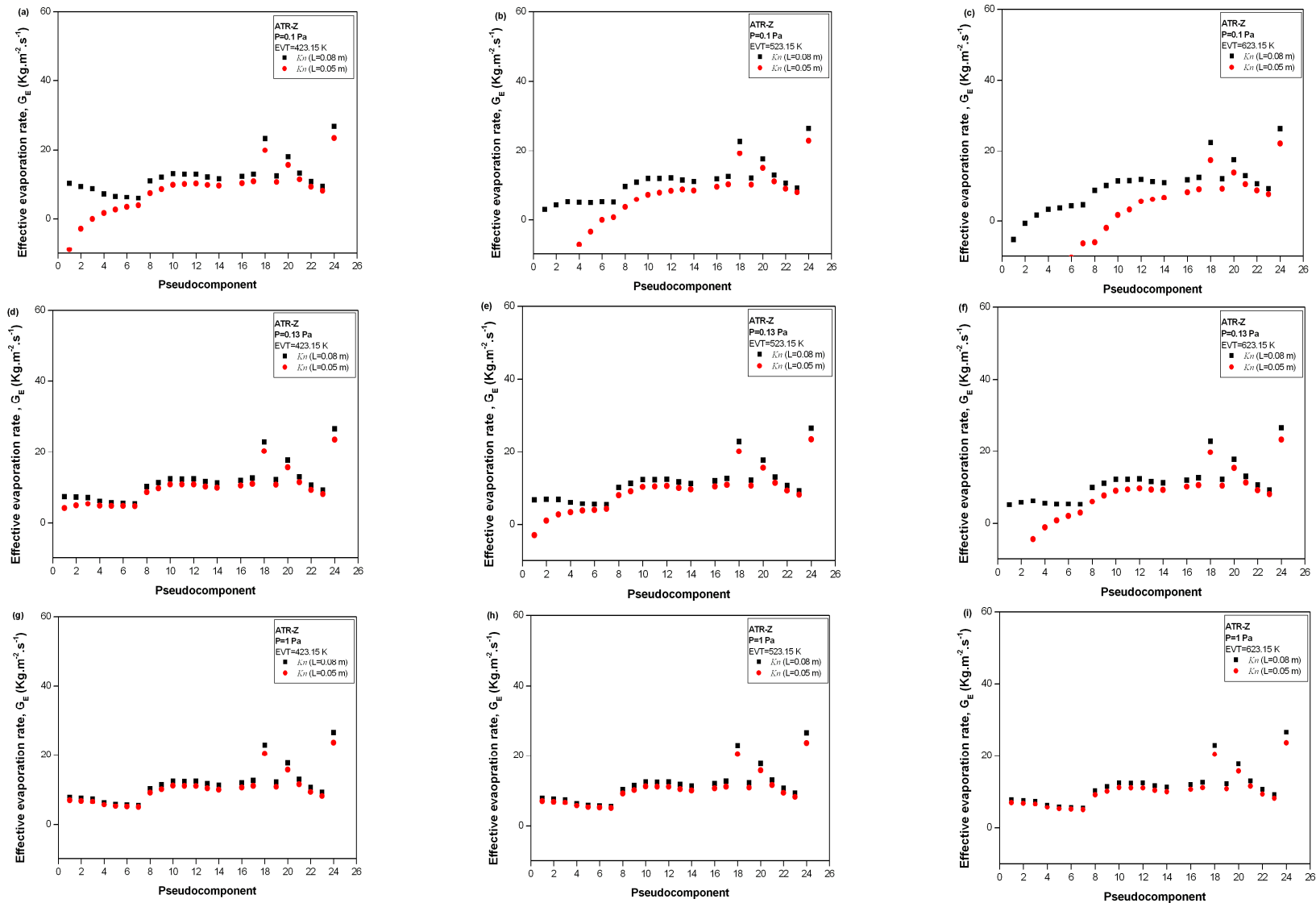


Figure 9. Effective evaporation rate of multicomponent mixture (set of twenty five pseudocomponents) of the ATR-Z high-boiling-point petroleum fraction at a) $P=0.1$ Pa and $EVT=423.15$ K; b) $P=0.1$ Pa and $EVT=523.15$ K; c) $P=0.1$ Pa and $EVT=623.15$ K; d) $P=0.13$ Pa and $EVT=423.15$ K; e) $P=0.13$ Pa and $EVT=523.15$ K; f) $P=0.13$ Pa and $EVT=623.15$ K; g) $P=1$ Pa and $EVT=423.15$ K; h) $P=1$ Pa and $EVT=523.15$ K and i) $P=1$ Pa and $EVT=623.15$ K as a function of L equals \bullet 0.05 m and \blacksquare 0.08 m.

Figures 9a – 9i present the evaporation rate for the ATR–Z mixture plotted against the 25 pseudocomponents under different operating conditions, comparing the parameter of the different distances between the evaporator and the condenser surfaces. Different distillation gap widths (distance between the evaporator and condenser equal to 0.08 m and 0.05 m), low asphaltene contents and low API gravities caused increases in the G_E of the pseudocomponents with high molar mass, carbon number and boiling point, when compared with the effective evaporation rates of the ATR–W and ATR–Y, maintaining a continuous distribution of the set of pseudocomponents without any defined trend for increase or decrease.

Figures 7 – 9 showed that the changes in the G_E were greatly affected by the low value of the length, $L=0.02$ m, where a negative evaporation rate was obtained, showing that overdimensioning can generate results with no physical meaning from the point of view of the molecular distillation process.

The results obtained, analyzing different operating conditions for the evaporator temperature and pressure system, will allow one to define the operating ranges to carry out modeling and simulation analyses, such as those analyzed in this work, where the changes in the evaporation rate are greatly affected by the initial operating temperature (evaporator wall temperature or evaporator temperature) and the distillation gap width, showing great changes in the inlet region of the evaporator–condenser devices.

5. Conclusions

The examination of the principles of molecular distillation applied to high-boiling-point petroleum fractions, such as the mean free path, Knudsen number and effective evaporating rate at the evaporator surface, was based on kinetic theory (mean free path) and the Langmuir–Knudsen equation (effective evaporation rate) for a set of pseudocomponents from three high-boiling-point petroleum fractions. Three different conditions of evaporator temperature (423.15 K, 523.15 K and 623.15 K) and pressure system (0.1 Pa, 0.13 Pa and 1 Pa) were analyzed.

The mean free path of the molecules, as a significant parameter in the molecular distillation process, indicated heterogeneous values for each pseudocomponent of the high-boiling-point petroleum fractions as a function of the operating conditions and dimension parameter (distillation gap width). Thus when the pressure system increased, the mean free path

of the molecules tended to be lower, when compared with the simulated data obtained at 0.13 Pa and 1 Pa. Therefore, the mean free path attains its lowest value for pseudocomponents with high molar mass, carbon number and boiling point, meaning that they cannot easily reach the condenser surface.

A great influence of the gap width on the Knudsen number was observed, and consequently on the effective evaporation rate. In this sense, it is important to assess the dimension parameter of the distance between the evaporator and the condenser in both theoretical and experimental studies, since this can lead to an over-dimensioning of the gap width. Accordingly, low values for this variable (e.g. 0.02 m), could lead to results with no physical meaning (negative values) for the effective evaporation rate.

One can also conclude that the Knudsen number can characterize the flow through the distillation gap from the ratio of the mean free path to the characteristic length of the distillation gap, where by means of the data obtained during the simulation, Knudsen numbers of above 0.01 were estimated for the set of pseudocomponents from high-boiling-point petroleum fractions, establishing a characteristic fluid flow called Knudsen flow, where the continuum assumption begins to break down to achieve the anisotropic status with Knudsen number greater than 0.5.

Analogous to the above parameters, the effective evaporation rate was strongly influenced by both operating conditions (evaporator temperature and pressure system) and the dimension parameter, distance between the evaporator and the condenser surfaces for the ATR-W and ATR-Z high-boiling-point petroleum fractions. As the evaporator temperature increased and the pressure system decreased, so the Knudsen number increased and consequently, so did the anisotropic behavior. Therefore it was reported that by including these effects in the evaporation rate, the Knudsen number was affected in the same direction.

In summary, the numerical simulation of the principles of molecular distillation allowed one to investigate the effect on evaporation rate for each pseudocomponent, where the rarefaction effects are important and must be included in the evaporation rate equation. The numerical data indicated that for outlooks work the flow could be modeled using the Navier-Stokes equations, but including the slip-velocity boundary conditions along the wall of evaporator.

Acknowledgments

The authors acknowledge the financial support received from the National Counsel for Technological and Scientific Development (CNPq) and from the National Plan of Science and Technology for the Petroleum and Natural Gas Sector (CTPETRO).

Nomenclature

C_p	=	Specific heat capacity	$[\text{J} \cdot \text{kg}^{-1} \cdot \text{K}^{-1}]$
d_e	=	Diameter of evaporation surface curvature	$[\text{m}]$
EVT	=	Evaporator temperature	$[\text{K}]$
f	=	Fraction of vaporized molecules	$[-]$
F	=	Surface ratio	$[-]$
G_E	=	Effective evaporation rate	$[\text{kg} \cdot \text{m}^{-2} \cdot \text{s}^{-1}]$
G_T	=	Theoretical evaporation rate	$[\text{kg} \cdot \text{m}^{-2} \cdot \text{s}^{-1}]$
k	=	Boltzmann Constant ($1.38 \times 10^{-23} \text{ J} \cdot \text{K}^{-1}$)	$[\text{J} \cdot \text{K}^{-1}]$
Kn	=	Knudsen number	$[-]$
K_w	=	Watson factor characterization	$[-]$
k^*	=	Anisotropy of vapor phase	$[-]$
L	=	Distance between evaporator and condenser surfaces	$[\text{m}]$
M	=	Molar mass	$[\text{kg} \cdot \text{kmol}^{-1}]$
$MABP$	=	Molar average boiling point	$[\text{K}]$
$MeABP$	=	Mean average boiling point	$[\text{K}]$
MPF	=	Mean free path	$[\text{m}]$
n'	=	Number of intermolecular collisions before the vapor reaches the isotropic state ($n'=5$)	$[-]$
N_m	=	Number of molecules per volume unit of vapor phase	$[\text{m}^{-3}]$
N_A	=	Avogadro constant ($6.023 \times 10^{23} \text{ mol}^{-1}$)	$[\text{mol}^{-1}]$
P	=	Pressure system	$[\text{Pa}]$
P_c	=	Critical pressure	$[\text{Pa}]$
P_{vap}	=	Equilibrium vapor pressure	$[\text{Pa}]$
R	=	Universal gas constant ($8.314 \text{ J} \cdot \text{K}^{-1} \cdot \text{mol}^{-1}$)	$[\text{J} \cdot \text{K}^{-1} \cdot \text{mol}^{-1}]$
T_c	=	Critical temperature	$[\text{K}]$
T_s	=	Film Surface temperature	$[\text{K}]$
V_c	=	Critical volume	$[\text{cm}^3 \cdot \text{mol}^{-1}]$
x_{mi}	=	Mole fraction of pseudocomponent	$[-]$
x_{vi}	=	Volume fraction of pseudocomponent	$[-]$
Greek Letter			
λ	=	Thermal conductivity	$[\text{W} \cdot \text{m}^{-1} \cdot \text{K}^{-1}]$
ν	=	Kinematic viscosity	$[\text{mm}^2 \cdot \text{s}^{-1}]$
ρ_i	=	Density of pseudocomponent i	$[\text{kg} \cdot \text{m}^{-3}]$
σ	=	Molecule diameter	$[\text{m}]$
Subscripts			
i	=	Component	
$NPSE$	=	Pseudocomponent	
Acronyms			
ATR	=	Residue from conventional atmospheric distillation	

CMD	=	Centrifugal molecular distiller
EVT	=	Evaporator temperature
FFMD	=	Falling film molecular distiller
MD	=	Molecular distillation
W, Y, Z	=	Dummy names for ATR petroleum fractions

References

- [1] Rossi PC, Pramparo MC, Gaich MC, Grosso NR, Nepote V. Optimization of molecular distillation to concentrate ethyl esters of eicosapentaenoic (20:5 ω -3) and docosahexaenoic acids (22: 6 ω -3) using simplified phenomenological modeling. *J Sci Food Agric* 2011; 91: 1452–8.
- [2] Zuñiga-Liñan L, Nascimento-Lima NM, Manenti F, Wolf-Maciel MR, Maciel Filho R, Medina LC. Experimental campaign, modeling, and sensitivity analysis for the molecular distillation of petroleum residues 673.15 K+. *Chem Eng Res Des*; doi:10.1016/j.cherd.2011.07.001.
- [3] Tovar LP, Pinto GMF, Wolf-Maciel MR, Batistella CB, Maciel-Filho R. Short-path-distillation process of lemongrass essential oil: Physicochemical characterization and assessment quality of the distillate and the residue products. *Ind Eng Chem Res* 2011; 50: 8185–8194.
- [4] Tovar LP, Wolf-Maciel MR, Ferreira-Pinto GM, Maciel-Filho R, Gomes DR. Factorial design applied to concentrate bioactive component of cymbopogon citratus essential oil using short path distillation. *Chem Eng Res Des* 2010; 88: 239–244.
- [5] Xubin Z, Chunjian X, Ming Z. Modeling of falling film molecular distillator. *Sep. Sci. Technol* 2005; 40:1371–86.
- [6] Sales-Cruz M, Gani R. Computer-Aided modelling of short-path evaporation for chemical product purification, analysis and design. *Chem Eng Res Des* 2006; 84: 583–94.
- [7] Batistella CB, Moraes EB, Maciel Filho R, Wolf Maciel MR. Molecular distillation: Rigorous modeling and simulation for recovering vitamin E from vegetal oils. *Appl Biochem Biotechnol* 2002; 98–100: 1187–206.

- [8] Cvengroš J, Badin V, Pollák S. Residence time distribution in a wiped liquid film. *The (Chem Eng J Biochem Eng J)* 1995; 59: 259–63.
- [9] Hickman KCD. High–vacuum Short–path Distillation–A Review. *Chemical Review* 1994; 34: 51–106.
- [10] Wang S, Gu Y, Liu Q, Yao Y, Guo Z, Luo Z, Cen K. Separation of bio–oil by molecular distillation. *Fuel Process Technol* 2009; 90: 738–45.
- [11] Shao P, He J, Sun P, Jiang S. Process optimisation for the production of biodiesel from rapeseed soapstock by a novel method of short path distillation. *Biosyst Eng* 2009; 102: 285–90.
- [12] Guo Z –G, Wang S –R., Zhu Y –Y, Luo Z –Y, Cen K –F. Separation of acid compounds for refining biomass pyrolysis oil. *J Fuel Chem Technol* 2009; 37: 49–52.
- [13] Lin SW, Yoo CK. Short–path distillation of palm olein and characterization of products. *Eur J Lipid Sci Technol* 2009; 111: 142–7.
- [14] Compton DL, Laszlo JA, Eller FJ, Taylor SL. Purification of 1,2–diacylglycerols from vegetable oils: Comparison of molecular distillation and liquid CO₂ extraction. *Ind Crop Prod* 2008; 28: 113–21.
- [15] Cermak SC, John AL, Evangelista RL. Enrichment of decanoic acid in cuphea fatty acids by molecular distillation. *Ind Crop Prod* 2007; 26: 93–9.
- [16] Chen F, Wang Z, Zhao G, Liao X, Cai T, Guo L, Hu X. Purification process of octacosanol extracts from rice bran wax by molecular distillation. *J Food Eng* 2007; 79: 63–8.
- [17] Fregolente LV, Fregolente PBL, Chicuta AM, Batistella CB, Maciel–Filho R, Wolf–Maciel MR. Effect of operating conditions on the concentration of monoglycerides using molecular distillation. *Chem Eng Res Des* 2007; 85: 1524–8.
- [18] Martinello M, Hecker G, Pramparo MC. Grape seed oil deacidification by molecular distillation: Analysis of operative variables influence using the response surface methodology. *J Food Eng* 2007; 81: 60–4.
- [19] Martinello MA, Villegas M, Pramparo MC. Retaining maximum antioxidative potency of wheat germ oil refined by molecular distillation. *J Sci Food Agric* 2007; 87: 1559–63.

- [20] Posada LR, Shi J, Kakuda Y, Xue SJ. Extraction of tocotrienols from palm fatty acid distillates using molecular distillation. *Sep Purif Technol* 2007; 57: 220–9.
- [21] Shi J, Posada LR, Kakuda Y, Xue SJ. Molecular distillation of palm oil distillates: Evaporation rates, relative volatility and distribution coefficients of tocopherols and other minor components. *Sep Purif Technol* 2007; 42: 3029–48.
- [22] Rada M, Guinda A, Cayuela J. Solid/liquid extraction and isolation by molecular distillation of hydroxytyrosol from *Olea europaea* L. leaves. *Eur J Lipid Sci Technol* 2007; 109: 1071–6.
- [23] Jiang ST, Shao P, Pan LJ, Zhao YY. Molecular distillation for recovering tocopherol and fatty acid methyl esters from rapessed oil deodoriser distillate. *Biosyst Eng* 2006; 93: 383–91.
- [24] Martins PF, Ito VM, Batistella CB, Maciel MRW. Free fatty acids separation from vegetables oil deodorizer distillate using molecular distillation process. *Sep Purif Technol* 2006; 48: 78–84.
- [25] Martins PF., Batistella CB., Maciel-Filho R, Wolf-Maciel MR. Comparison of two different strategies for tocopherols enrichment using a molecular distillation process. *Ind Eng Chem Res* 2006; 45: 753–8.
- [26] Sbaite P, Batistella CB, Winter A, Vasconcelos CJ, Wolf-Maciel MR, Maciel-Filho R, Gomes A, Medina L, Kunert R. True boiling point extended curve of vacuum residue through molecular distillation. *Petrol Sci Tech* 2006; 24: 265–74.
- [27] Fregolente LV, Moraes EB, Martins PF, Batistella CB, Wolf Maciel MR, Afonso AP, Reis MHM. Enrichment of natural products using an integrated solvent-free process: Molecular distillation. *ICHEME Symposium series* 2006; 152; 648–56.
- [28] Ito VM, Martins PF, Batistella CB, Maciel-filho R, Wolf-Maciel MR. Natural Compounds obtained through centrifugal molecular distillation. *Appl Biochem Biotechnol* 2006; 131: 716–26.
- [29] Maciel-Filho R, Batistella CB, Sbaite P, Winter A, Vasconcelos CJ, Wolf-Maciel MR, Gomes A, Medina L, Kunert R. Evaluation of atmospheric and vacuum residues using molecular distillation and optimization. *Petrol Sci Tech* 2006; 24: 275–83.

- [30] Moraes EB, Martins PF, Batistella CB, Alvarez ME, Maciel-Filho R, Wolf-Maciel MR. Molecular distillation: A powerful technology for obtaining tocopherols from soya sludge. *Appl Biochem Biotechnol* 2006; 129–132: 1066–76.
- [31] Chen F, Cai T, Zhao G, Liao X, Guo L, Hu X. Optimizing conditions for the purification of crude octacosanol extract from rice bran wax by molecular distillation analyzed using response surface methodology *J Food Eng* 2005; 70: 47–53.
- [32] Fregolente LV, Batistella CB, Maciel-Filho R, Wolf-Maciel MR. Response surface methodology applied to optimization of distilled monoglycerides production. *J Am Oil Chem Soc* 2005; 82: 673–8.
- [33] Xu S, Xiang A, Ying A. Purification of 3-hydroxypropionitrile by wiped molecular distillation. *Sci China Ser B-Chem* 2004; 47: 521–7.
- [34] Yang T, Zhang H, Mu H, Sinclair AJ, Xu X. Diacylglycerols from butterfat: Production by glycerolysis and short-path distillation and analysis of physical properties. *J. Am. Oil Chem. Soc.* 2004; 81: 979–87.
- [35] Campos RJ, Litwinenko JW, Marangoni AG. Fractionation of milk fat by short-path distillation. *J Dairy Sci* 2003; 86: 735–44.
- [36] Xu X, Jacobsen C, Nielsen NS, Heinrich MT, Zhou D. Purification and deodorization of structured lipids by short path distillation. *Eur J Lipid Sci Technol* 2002; 104: 745–55.
- [37] Crause JC, Nieuwoudt I. Fractionation of paraffin wax mixtures. *Ind Eng Chem Res* 2000; 39: 4871–6.
- [38] Lee E. Simulation of the thin-film thickness distribution for an OLED thermal evaporation process. *Vacuum* 2009; 83: 848–52.
- [39] Shao P, Jiang ST, Ye K. Influences of feed and condenser temperature on molecular distillation of ideal binary mixtures. *J Sci Ind Res* 2007; 66: 37–46
- [40] Xiang A, Xu S. Comparison of two turbulent models in simulating evaporating liquid film in a wiped molecular distillator. *Sci China Ser B-Chem* 2005; 48: 183–8.
- [41] Kawala Z, Dakiniewicz P. Influence of evaporation space geometry on rate of distillation in high-vacuum evaporator. *Sep Sci Technol* 2002; 37: 1877–1895.

- [42] Lutišan J, Cvengroš J, Micov M. Heat and mass transfer in the evaporating film of a molecular evaporator. *Chem Eng J* 2002; 85: 225–34.
- [43] Cvengroš J, Pollák S, Micov M, Lutišan J. Film wiping in the molecular evaporator. *Chem Eng J* 2001; 81: 9–14.
- [44] Cvengroš J, Lutišan J, Micov M. Feed temperature influence on the efficiency of a molecular evaporator. *Chem Eng J* 2000; 78: 61–7.
- [45] Batistella CB., Maciel MRW, Maciel Filho R. Rigorous modeling and simulation of molecular distillators: Development of a simulator under conditions of non ideality of the vapor phase. *Comput Chem Eng* 2000; 24: 1309–15.
- [46] Cvengroš J, Micov M, Lutišan J. Modelling of fractionation in a molecular evaporator with divided condenser. *Chem Eng Process* 2000; 39: 191–9.
- [47] Lutišan J, Micov M, Cvengroš J. The influence of entrainment separator on the process of molecular distillation. *Sep Sci Technol* 1998; 33: 83–96.
- [48] Nguyen AD, Goffic FL. Limits of wiped film short-path distiller. *Chem Eng Sci* 1997; 52: 2261–6.
- [49] Pasquini C, Bueno AF. Characterization of petroleum using near-infrared spectroscopy: Quantitative modeling for the true boiling point curve and specific gravity. *Fuel* 2007; 86: 1927–34.
- [50] Liu D, Shi J, Posada LR, Kakuda Y, Xue SJ. Separating tocotrienols from palm oil by molecular distillation. *Food Rev Int* 2008; 24: 376–91.
- [51] Eckles AJ, Benz PH. The basics of vacuum processing. *Chem Eng* 1992; 99: 78–86.
- [52] Lutišan J, Cvengroš J. Effect of inert gas pressure on the molecular distillation process. *Sep Sci Technol* 1995; 30: 3375–89.
- [53] Lutišan J, Cvengroš J. Mean free path of molecules on molecular distillation. *The (Chem Eng J Biochem Eng J)* 1995; 56: 39–50.
- [54] Catalogue UIC GmbH, 2010. Available in: < <http://www.UIC-GmbH.de/>>. Accessed in: December 10th. 2010.

- [55] Whitman JR, Aranovich GL, Donohue MD. Anisotropic mean free path in simulations of fluids traveling down a density gradient. *J Chem Phys* 2010; 132: 224302–1–224302–7.
- [56] Einwohner T, Alder BJ. Molecular dynamics. VI. Free-path distributions and collision rates for hard–sphere and square-well molecules. *J Chem Phys* 1968; 49: 1458–73.
- [57] Barber RW, Sun Y, Gu XJ, Emerson DR. Isothermal slip flow over curved surfaces. *Vacuum* 2004; 76: 73–81.
- [58] Barber RW, Emerson DR. The influence of Knudsen number on the hydrodynamic development length within parallel plate micro–channels. In: *Advances in Fluid Mechanics IV, Advances in fluid mechanics series* (p. 207–216). WIT Press, Southampton: UK, 2002.
- [59] Langmuir I. The vapor pressure of metallic tungsten. *Phys Rev* 1913; 2: 329–42.
- [60] Badin V, Cvengroš J. Model of temperature profiles during condensation in a film in a molecular evaporator. *The (Chem Eng J)* 1992; 49: 177–80.
- [61] Greenberg DB. A theoretical and experimental study of the centrifugal molecular still. *AIChE J* 1972; 18: 269–76.
- [62] Kawala Z, Stephan K. Evaporation rate and separation factor of molecular distillation in a falling film apparatus. *Chem Eng Technol* 1989; 12: 406–413.
- [63] American Society for Testing Material, ASTM D 2892. Standard Test Method for Distillation of Crude Petroleum (15–Theoretical Plate Column). West Conshohoken, (Pennsylvania): ASTM International, 2005. 32p.
- [64] Tovar LP, Wolf Maciel MR, Maciel Filho R, Batistella CB, Ariza OC, Medina LC. Overview and computational approach for studying the physicochemical characterization of high–boiling–point petroleum fractions (350 °C+). *Oil Gas Sci Technol*; doi:10.2516/ogst/2011150.

4.3. Considerações finais

Nesse capítulo foi apresentada uma ampla revisão de estudos realizados ao redor do mundo e, especialmente, nos Laboratórios de Desenvolvimento de Processos de Separação (LDPS) e de Otimização, Projeto e Controle Avançado (LOPCA) da Faculdade de Engenharia Química da Unicamp, que em parceria com o órgão Financiador de Estudos e Projetos do Ministério da Ciência e Tecnologia (FINEP) e o Centro de Pesquisa CENPES/PETROBRAS desenvolveram uma metodologia – a destilação molecular – que permite caracterizar e separar cortes e resíduos pesados de petróleo a temperaturas superiores daquelas alcançadas pelos métodos padronizados ASTM D 2892 (2005) e ASTM D 5236 (2003).

Considerações e aspectos teóricos, o livre percurso médio, o número de *Knudsen* e a taxa de evaporação efetiva, foram estudados. Com isso foi possível concluir que a eficiência da destilação molecular para separar frações pesadas de petróleo baseia-se em condições operacionais especiais de alto vácuo (entre 0,1 – 1 Pa) e temperatura do evaporador (entre 423,15 – 623,15 K). Com a relação entre o livre percurso médio das moléculas presentes nas frações pesadas de petróleo (ATR-W, ATR-Y e ATR-Z), e a longitude característica do sistema (a distância entre a superfície do evaporador e a superfície do condensador), obteve-se um número adimensional denominado número de *Knudsen*. Com o número de *Knudsen* calculado foi descrito o comportamento da fase vapor sob a superfície do evaporador, para o qual é admissível estabelecer que para números de *Knudsen* maiores do que 0,5 descreveu-se um fluxo tal, que nestas condições, as colisões intermoleculares, na região de interesse, são menos frequentes que as colisões das moléculas com a superfície do condensador, satisfazendo uma das condições necessárias para atingir a separação no processo de destilação molecular (de tipo centrífugo).

Outro aspecto estudado foi a taxa de evaporação sob o processo de destilação molecular, a qual é controlada pela taxa que as moléculas escapam da superfície livre do evaporador e atingem o condensador. Portanto, os resultados apresentaram que o condensador deve estar na imediata vizinhança da superfície do evaporador entorno de 0,05 a 0,08 m para os sistemas estudados (ATR-W, ATR-Y e ATR-Z).

Capítulo 5.

Análise do perfil de velocidade e do regime de fluxo na destilação molecular centrífuga

5.1. Introdução

A caracterização do escoamento do filme líquido, bem distribuído na parede interna da superfície de evaporador, é de essencial importância para a dinâmica do fluido no desempenho do processo da destilação molecular (processo não catalítico) e da destilação molecular reativa (processo catalítico).

Alguns autores têm introduzido análises de características específicas da modelagem para misturas binárias, considerando evaporadores adiabáticos, sendo algumas dessas características a temperatura de alimentação, a pressão do sistema, as diferentes configurações de equipamentos e os efeitos da fase vapor. A modelagem resulta, então, num sistema de equações diferenciais parciais, que pode ser resolvido por métodos numéricos comumente descritos na literatura.

Neste capítulo, é apresentado um estudo fluidodinâmico do escoamento do líquido gerado na destilação molecular. Para a simulação, foi considerado como caso de estudo o processamento de um resíduo atmosférico do petróleo “W” (ATR–W) $673,15\text{ K}^+$, em um destilador molecular centrífugo aquecido, onde a superfície do evaporador constitui uma superfície cônica. O resíduo atmosférico total foi dividido em 25 pseudo–componentes, os quais foram caracterizados utilizando dados de propriedades físico–químicas geradas pelo simulador desenvolvido por Tovar et al. (2011), e através de equações de predição, em função da temperatura média de ebulição e da densidade dos pseudo–componentes.

A modelagem é fundamentada pelas equações de balanço de massa e de momento no filme líquido formado e escoando na superfície cônica do evaporador. A modelagem do processo descrita neste capítulo assume que:

- O material apresenta um comportamento característico dos fluidos newtonianos.

- Considerou-se nas simulações deste trabalho um sistema monofásico, no qual o fluido simulado tem propriedades físicas correspondentes à média ponderada entre os componentes da mistura.
- O filme líquido é considerado incompressível, distribuído uniformemente na superfície do evaporador garantindo uma boa transferência de massa.
- A espessura do filme é considerada muito menor que o raio da superfície cônica.
- Com a tentativa de obter a solução numérica para o fluxo em estado estacionário sobre a superfície do evaporador, a força gravitacional é desprezível em comparação com a força centrífuga.
- A superfície cônica gira a velocidade angular ω , e o fluxo apresenta simetria axial em relação à coordenada φ , o que implica que a velocidade na direção $-\theta$ (velocidade angular) é muito menor do que a velocidade na direção $-\varphi$ (velocidade tangencial) e a velocidade na direção $-r$ (velocidade radial)).
- Tendo em conta a finalidade deste trabalho e para a simplificação do processo de computação, a transferência de calor é ignorada.

O desenvolvimento desta etapa do trabalho de Tese de Doutorado utiliza a técnica de CFD (do Inglês *Computational fluid dynamics*) para estudar, analisar e visualizar o comportamento fluidodinâmico do filme líquido sobre a superfície do evaporador. Este trabalho tem como objetivo (i) investigar o efeito das diferentes condições de operação (vazão de alimentação e velocidade do rotor), com temperatura de evaporação constante (423,15 K), no perfil de velocidade do filme fino de líquido de um resíduo atmosférico de petróleo escoando sobre a superfície do evaporador de um destilador molecular centrífugo, e (ii) estudar as componentes da velocidade nas direções $-r$, $-\theta$ e $-\varphi$, considerando um estado bidimensional estacionário (no padrão de fluxo laminar), onde o vetor velocidade, perpendicular à superfície cônica (em direção $-\theta$), é ignorado. Apenas vetores na direção radial (direção $-r$) e direção tangencial (direção $-\varphi$) foram considerados.

As equações do modelo foram resolvidas no software comercial ANSYS CFX (de Ansys Inc., EUROPE) baseadas nas equações de continuidade de Navier–Stokes e nas equações de modelo de turbulência (k – ϵ e *Shear Stress Transport* k – ω ’).

5.2. Desenvolvimento

O desenvolvimento deste capítulo é apresentado a seguir, no manuscrito intitulado:

CFD–Based analysis of the flow regime in the centrifugal molecular distillation of a petroleum atmospheric residue.

Esse trabalho é a versão estendida que compreende dois trabalhos:

CFD-based analysis of the flow regime in the centrifugal molecular distillation of a petroleum atmospheric residue. Publicado nos anais, respectivamente do *2010 AIChE Annual Meeting, 10AIChE; Salt Lake City, UT; 7–12 November 2010. ISBN/ISSN: 978-081691065-6, 185j – ePaper.*

Study of velocity distribution in evaporating liquid film of a petroleum fraction on the evaporator surface of a centrifugal molecular distiller using computational fluid dynamics. Publicado nos anais, respectivamente do *XVIII Congresso Brasileiro de Engenharia Química 2010 (COBEQ2010), September 19–22 2010, Foz de Iguaçu, PR–Brazil / Ed. n.a – Foz de Iguaçu, PR–Brazil: COBEQ2010, 2010. - ISSN 2178–3659. – p. 8684–8694.*

Source: From Medina L. C., Tovar L. P., Wolf Maciel M. R., Batistella C. B., Maciel Filho R. (2010) CFD-based analysis of the flow regime in the centrifugal molecular distillation of a petroleum atmospheric residue. Conference Proceedings; 2010 AIChE Annual Meeting, 10AIChE; Salt Lake City, UT; 7-12 November 2010. ISBN/ISSN: 978-081691065-6, 185j – ePaper.

Copyright notice: The content of this manuscript is licensed under the Ethical Guidelines to Publication of American Institute of Chemical Engineers, AIChE. Please contact credited rights holders directly for permission to reproduce material.

Source: From Tovar L. P., Wolf Maciel M. R., Batistella C. B., Maciel Filho R., Medina L. C. (2010) Study of velocity distribution in evaporating liquid film of a petroleum fraction on the evaporator surface of a centrifugal molecular distiller using computational fluid dynamics. Proceedings of XVIII Congresso Brasileiro de Engenharia Química 2010 (COBEQ2010), September 19-22 2010, Foz de Iguaçu, PR-Brazil / Ed. n.a - Foz de Iguaçu, PR-Brazil: COBEQ2010, 2010. - ISSN 2178-3659. - p. 8684-8694.

Copyright notice: The content of this manuscript is licensed under the Ethical Guidelines to Publication of XVIII Congresso Brasileiro de Engenharia Química 2010, COBEQ2010. Please contact credited rights holders directly for permission to reproduce material.

CFD–Based analysis of the flow regime in the centrifugal molecular distillation of an atmospheric residue of petroleum

Abstract

The characterization of the flow in the evaporating liquid film, well distributed on the inner wall of the evaporator surface, is of paramount importance to the fluid dynamics within the molecular distillation process performance. This work aims (i) to investigate the effect of the different operating conditions (feed flow rate and rotor speed) at constant evaporator temperature (423.15 K) on the velocity profile in the thin liquid film of a residue from atmospheric distillation of petroleum on the evaporator surface of a centrifugal molecular distiller; and (ii) to study the components of velocity in r , θ and φ –directions considering a two–dimensional steady state model (in laminar flow pattern), where the perpendicular velocity vector of the conical surface (in θ –direction) was ignored, only tangential (φ –direction) and radial (r –direction) vectors were considered and the effect of gravity on flow was negligible in comparison with the centrifugal force.

The analyses were carried out using computational fluid dynamics (CFD) simulations, making use of the commercial software ANSYS CFX 11.0 (of Ansys Inc., EUROPE) based on the finite volume method.

A laminar flow model and two turbulence flow models (the standard $k-\varepsilon$ and the SST $k-\omega$ ' turbulence models) were considered. A comprehensive model based on the Navier–Stokes and continuity equations represented the computational model.

The simulations showed an overall good agreement with the molecular distillation process, based on the fact that the feed flow rate at the inlet of the device has an important effect on the velocity distribution. Results suggest that the $k-\varepsilon$ and SST $k-\omega$ ' turbulence models are suitable for simulating evaporating liquid film in centrifugal molecular distiller. Nevertheless, small differences between the results obtained with turbulence and laminar models were found. Hence, laminar flow model is enough for modeling centrifugal molecular distillation process.

About velocity components, the results from this computational study showed the radial velocity component is higher than the tangential velocity component in respect to the conical surface. The usefulness of the above information obtained from the CFD simulation and analysis will be elucidated for modeling of a centrifugal molecular distillation process.

Keywords: Molecular distillation, flow regime, computational fluid dynamics, velocity components and operating variables.

Contents

1. Introduction
 - 1.1. Centrifugal molecular distillation
2. Physical modeling, governing equations and computational method
 - 2.1. Computational fluid approach: Numerical framework
 - 2.2. Turbulence models
 - 2.2.1. Standard $k-\varepsilon$ turbulence model
 - 2.2.2. Shear stress transport $k-\omega$ ' model
 - 2.3. CFD modeling: Pre-processing
 - 2.3.1. Geometry details and modeling of computational flow domain
 - 2.3.2. Flow domain
 - 2.3.2.1. Study cases
 - 2.4. Boundary conditions and solution domain
3. Results and discussion
 - 3.1. Modeling laminar flow of thin liquid film on evaporator surface: Overall effects of operating conditions
 - 3.2. Modeling turbulent flow of thin liquid film on evaporator surface: Overall effects of operating condition
 - 3.2.1. Turbulence kinetic energy
 - 3.3. Study of components of velocity in evaporating liquid film of a petroleum fraction on the evaporator surface
 - 3.3.1. Effect of evaporator temperature on velocity distribution

3.3.2. Effect of feed flow rate and rotor speed on velocity distribution

4. Conclusions

Acknowledgment

Nomenclature

References

1. Introduction

Molecular distillation is acknowledged as a continuous separation process operating under high vacuum conditions (Lin and Yoo, 2009; Cvengroš et al., 2000). It is a thermal purification and separation process for thermally unstable materials, liquids with low vapor pressure, high boiling points and elevated molar masses from the fields of chemical, pharmaceutical, petrochemical and food industries. This process is characterized by short exposure of the distilled liquid to elevated temperatures (short residence time) and low evaporation temperatures to cause a minimum thermal hazard to the distilled product (Tovar et al., 2010; Sales–Cruz and Gani, 2006; Xubin et al., 2005; Micov et al., 1997).

Numerous theoretical and numerical investigations have been carried out to understand the molecular distillation characteristics, the effect of various parameters on their performance and process modeling. Several authors have published works concerning the modeling of the molecular distillation process for binary and multicomponent mixtures. Greenberg (1972), Rees (1980), and Inuzuka et al. (1986) developed a mathematical model of the centrifugal molecular distillation process based on a fully developed profile (but for the first two works, negligible normal and tangential velocity components were considered). In their works the authors analyzed thermal gradients, liquid film thickness and rates of evaporation.

Bhandarkar and Ferron (1988) studied the liquid–phase transfer in high–vacuum distillation on a rotating evaporator surface using the mass, momentum and energy balance equations. Micov et al. (1997) and Xubin et al. (2005) presented a mathematical formulation which considers the liquid film flowing over the evaporator surface and vapor phase under the assumption that the distilled liquid consists of two components. The first authors presented a model described by the Boltzmann equation for mass transfer in the vapor phase, the Navier–Stokes equations for liquid film, a diffusion equation and a thermal balance equation. They showed results on different operating conditions (laminar isothermal and non–isothermal films) where the difference in those regimes was clearly shown in the volume and composition of the

residual liquid. The second authors considered different operating conditions (i.e. feed flow rate, evaporation temperature, and inert gas pressure) in order to obtain the profile of temperatures, the concentration of the film and the profiles of density.

On the other hand, some authors have previously studied specific issues. For instance, Kawala and Stephan (1989) and, Kawala and Dakiniewicz, (2002) studied the process in which the falling film was considered in an adiabatic regime. Batistella and Maciel (1996) compared the performance of two equipment configurations (centrifugal and falling film) for binary mixtures based on the model proposed by Kawala and Stephan (1989). Cvengroš et al. (2000) analyzed the effect of the inlet feedstock temperature on the evaporation rate considering the mixture as a single component.

Additionally, some works related to the hydrodynamic behavior on the evaporator surface have been developed recently. Non-conventional techniques or methods have been fully established in the literature to evaluate the flow behavior and/or quality of thin film on an evaporator surface in the centrifugal and falling film molecular distillers. Analyses include flow visualization and flow partners (laminar or turbulent) that take place in the thin liquid film.

Computational fluid dynamics (CFD) has become a very powerful tool in the research and development of industry processes which attempt to understand, analyze and predict behavior under specific operating conditions. Several new works related to the hydrodynamic behavior on the evaporator surface have been developed recently. Xiang and Xu (2005) analyzed the velocity distribution of evaporating liquid film in a wiped molecular distiller considering two turbulent models.

Centrifugal molecular distillation process is one kind of molecular distillation, and its modification from others is in the centrifugal force by which the evaporating liquid film is formed. It has a fast rotating spinning cone, to create a fast spreading and moving film of liquid. When the rotating cone is heated, distillation takes place.

The aim of this study was to evaluate different operating conditions (feed flow rate (Q) and rotor speed (RS)), at a constant evaporator temperature (423.15 K), on the flow pattern in thin liquid film for specific feedstock (a residue from atmospheric distillation of petroleum, ATR-W) when considered two turbulence flow models (the standard $k-\varepsilon$ and SST $k-\omega$ ' turbulence models) on the evaporator surface of a centrifugal molecular distiller (CMD).

In the same system, but now considering different operating conditions for evaporator temperature (*EVT*), was investigate the components of velocity in r , θ , and φ –directions (v_r , v_θ and v_φ , respectively) on the velocity profile on the thin liquid film over the evaporator surface considering a laminar flow model.

The effect of operating conditions on the velocity profile, including flow visualization and flow partners (laminar or turbulent), was investigated by the Computational Fluid Dynamics (CFD) using the commercial software package, ANSYS CFX (of Ansys inc., EUROPE). The study is projected to (i) serve as a powerful tool for characterizing the flow formed in the thin film during molecular distillation processes and, (ii) provide information about the velocity profile based on the choice of operating conditions to be used in the mathematical modeling of the centrifugal molecular distillation process. Therefore, this work will serve as a novel method to study the flow and hydrodynamic behavior of liquid film on an evaporator surface in a centrifugal molecular distiller by means of CFD simulation.

1.1. Centrifugal molecular distillation

The layout of the centrifugal molecular distiller is shown in Figures 1a– 1b.

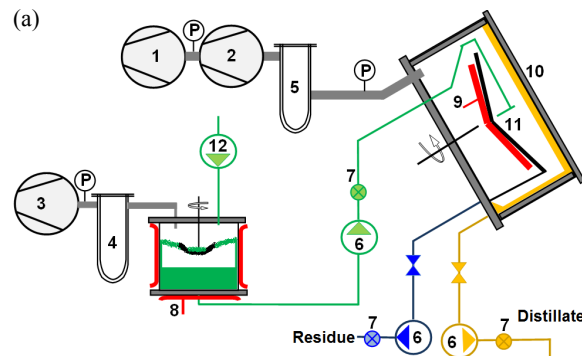


Figure 1a. Schematic diagram of CMD.
1. Backing/Roughing vacuum pump (chamber); 2. Diffusion (high vacuum) pump; 3. Rough vacuum pump (degasser); 4. Trap (degasser); 5. Trap (chamber); 6. Liquid transfer pump; 7. Check valve; 8. Degasser heater; 9. Rotor heater; 10. Vacuum chamber/ condenser; 11. Rotor; 12. Variable speed liquid transfer pump; P: Vacuum pressure gauge (Myers–Vacuum, 2010).

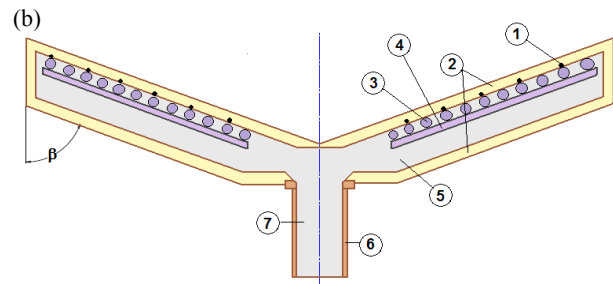


Figure 1b. Schematic diagram of evaporator of CMD. 1. Thermocouple; 2. Evaporator surface; 3. Electrical resistance; 4. Support resistance; 5. Region of electrical cables and thermocouples; 6. Axis; and 7. Shaft hole.

The material is pumped from the customer supplied supply/feed tank by a variable speed feed pump (12) into the degasser. A feed pump (6) moves the degassed material to the center of the heart of a centrifugal molecular distiller, the evaporator (Figure 1b), described as a conical spinning surface (11) housed in a high vacuum chamber (10). The centrifugal force spreads the material rapidly over the hot surface (9), where distillation takes place and the material expands out on the radius of the disc. Distillate condenses upon the inner surface of the cooled condenser dome (10), and by gravity, passes through the bottom of the base plate to the distillate collector vessel (6–7), while the unevaporated molecules, which did not reach the condenser surface, slides into a gutter surrounding the rotor and then carried to a collector vessel (6 –7). Therefore, the objective of separation has been reached.

2. Physical modeling, governing equations and computational method

Numerical simulations were performed with a commercially available CFD software ANSYS CFX 11.0 (of Ansys inc., EUROPE). A sketch of the coordinate system is depicted in Figure 2, and it uses spherical polar coordinates (r, θ, ϕ) with corresponding velocity components (v_r, v_θ, v_ϕ). The origin is at the apex of the cone, the axis is along $\theta=0$.

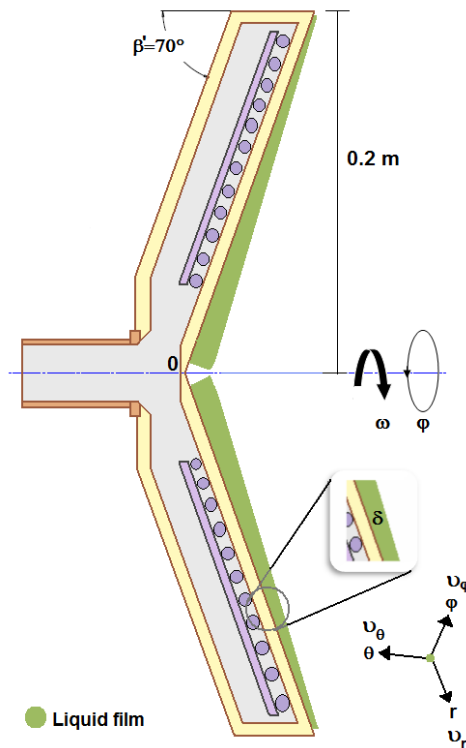


Figure 2. Sketch of the thin liquid film on the surface of a spinning cone.

In this study some assumptions are made:

- As a simple constitutive equation, material is assumed to be a Newtonian fluid.
- The distilled liquid is considered like a single component and the physicochemical properties are not dependent on the evaporator temperature.
- The liquid film (fluid domain for CFD study) is considered to be incompressible, uniformly distributed on the evaporator wall guarantying an excellent mass transfer, and the film thickness is considered much smaller than the radius of the conical surface.
- As attempt to obtain numerical solution for the steady-state flow over the evaporator surface, the gravitational force is negligible in comparison with the centrifugal force onto the heated evaporator wall.
- The conical surface rotates at a fixed angular velocity ω ; and the flow shows axial symmetry with respect to the coordinate φ , it implies that the velocity in the θ -direction is much smaller than both, the velocity in φ -direction and the velocity in the r -direction.
- Taking into account the purpose of this work and for simplifying the computing process, heat transfer is ignored.

2.1. Computational fluid approach: Numerical framework

The present model is based on the procedure suggested by Hinze and Milborn (1950), Bruin (1969), Rees (1980), Bhandarkar and Ferron (1988); and Batistella and Maciel (1996) involving a thin liquid film on a surface of a spinning truncated cone. The Navier–Stokes equations and the continuity equation for the liquid film in Figure 2 are given by Equations (1) – (4):

$$\nu_r \frac{\partial \nu_r}{\partial r} + \frac{\nu_\theta}{r} \frac{\partial \nu_r}{\partial \theta} - \frac{(\nu'_\varphi)^2}{r} - \omega^2 \sin^2 \beta' + 2\omega \nu'_\varphi \sin \beta' = \frac{\nu}{r^2} \frac{\partial^2 \nu_r}{\partial \theta^2} \quad (1)$$

$$-\nu_r \frac{\partial \nu'_\varphi}{\partial r} - \frac{\nu_\theta}{r} \frac{\partial \nu'_\varphi}{\partial \theta} - \frac{\nu_r \nu'_\varphi}{r} + 2\omega \nu_r \sin \beta' = -\frac{\nu}{r^2} \frac{\partial^2 \nu'_\varphi}{\partial \theta^2} \quad (2)$$

$$-(\nu'_\varphi)^2 \frac{\cot \beta'}{r} - \omega^2 r \sin \beta' \cos \beta' + 2\omega \nu'_\varphi \cos \beta' = \frac{\nu}{r^2} \left[\frac{\partial^2 \nu_\theta}{\partial \theta^2} + 2 \frac{\partial \nu_r}{\partial \theta} \right] \quad (3)$$

$$\frac{\partial v_r}{\partial r} + 2\frac{v_r}{r} + \frac{1}{r}\frac{\partial v_\theta}{\partial \theta} = 0 \quad (4)$$

Where, $v'_\phi = -v_\phi + \omega r \sin \beta'$ is an analogous coordinate system, wherein the system rotates at ω (Bruin, 1969).

The boundary conditions are:

$$v_r = v_{r_0} \text{ at } r = r_0 \text{ (that corresponds to feed location)} \quad (5)$$

$$v_\theta = 0 \text{ and } v_\phi = \omega r \text{ at } \theta = 0 \quad (6)$$

$$\frac{\partial v_r}{\partial \theta} = 0, \quad \frac{\partial v_\phi}{\partial \theta} = 0 \text{ at } \theta = \delta \text{ (at the free surface)} \quad (7)$$

2.2. Turbulence models

2.2.1. Standard k - ε turbulence model

A transport equation for the fluctuating vorticity, and thus the dissipation rate, can be derived from the Navier Stokes equations. It includes two extra transport equations to represent the turbulent properties of the flow. The first transported variable is turbulent kinetic energy, k , which determines the energy in the turbulence (Equation 8). The second transported variable is the turbulent dissipation, ε (Equation 9), which determines the scale of the turbulence (Rapley et al., 2008; El-Beherly and Hamed, 2009; Singhal and Spalding, 1981).

The equations involved in the standard k - ε model for turbulence energy and turbulence dissipation rate are given as (El-Beherly and Hamed, 2009; Rapley et al., 2008; Yakhot et al., 1992):

$$\frac{\partial}{\partial t}(\rho k) + \frac{\partial}{\partial x_i}(\rho k v_i) = \frac{\partial}{\partial x_j} \left[\left(\mu + \frac{\mu_t}{\sigma_k} \right) \frac{\partial k}{\partial x_j} \right] + P_k + P_b - \rho \varepsilon - Y_M \quad (8)$$

$$\frac{\partial}{\partial t}(\rho \varepsilon) + \frac{\partial}{\partial x_i}(\rho \varepsilon v_i) = \frac{\partial}{\partial x_j} \left[\left(\mu + \frac{\mu_t}{\sigma_\varepsilon} \right) \frac{\partial \varepsilon}{\partial x_j} \right] + C_{1\varepsilon} \frac{\varepsilon}{k} (P_k + C_{3\varepsilon} P_b) - C_{2\varepsilon} \rho \frac{\varepsilon^2}{k} \quad (9)$$

Turbulent viscosity is modeled as:

$$\mu_t = \rho C_\mu \frac{k^2}{\varepsilon} \quad (10)$$

In these equations, P_k represents the generation of turbulent kinetic energy due to the mean velocity gradients. P_b is the generation of turbulent kinetic energy due to buoyancy. Y_M represents the contribution of the fluctuating dilatation in compressible turbulence to the overall dissipation rate. In the above equations C_μ , σ_k , σ_ε , $C_{1\varepsilon}$ and $C_{2\varepsilon}$ are all taken to be constants and are respectively given the values 0.09; 1.0; 1.3; 1.44 and 1.92 (Launder and Spalding, 1974).

2.2.2. Shear stress transport k - ω ' model

In the CFD software ANSYS CFX 11.0 (of Ansys inc., EUROPE), the shear stress transport k - ω ' model (SST k - ω ') combines advantages of both the standard k - ε model and the k - ω ' model. It automatically switches to the k - ω ' model in the near region and the standard k - ε model when away from the walls. The SST k - ω ' model has a similar form to the standard k - ω ' model (El-Behery and Hamed, 2009; Rapley et al., 2008):

$$\frac{\partial}{\partial t}(\rho k) + \frac{\partial}{\partial x_i}(\rho k v_i) = \frac{\partial}{\partial x_j} \left[\Gamma_k \frac{\partial k}{\partial x_j} \right] + \tilde{P}_k - Y_k + S_K \quad (11)$$

$$\frac{\partial}{\partial t}(\rho \omega') + \frac{\partial}{\partial x_i}(\rho \omega' v_i) = \frac{\partial}{\partial x_j} \left[\Gamma_{\omega'} \frac{\partial \omega'}{\partial x_j} \right] + P_{\omega'} - Y_{\omega'} + D_{\omega'} + S_{\omega'} \quad (12)$$

In these equations, \tilde{P}_k represents the generation of turbulence kinetic energy due to the mean velocity gradients. $P_{\omega'}$ represents the generation of ω' . $\Gamma_{\omega'}$ represents the effective diffusivity of k and ω' . $Y_k, Y_{\omega'}$ represent the dissipation of k and ω' due to turbulence. $D_{\omega'}$ represents the cross-diffusion term.

2.3. CFD modeling: Pre-processing

The 3-D CFD analysis presented in this study was developed using the ANSYS CFX 11.0 (of Ansys Inc., EUROPE). The ANSYS CFX package was used to model the fluid phase (liquid thin film) through a system of governing equations in the steady state for the fluid flow on the evaporator surface of the centrifugal molecular distiller.

2.3.1. Geometry details and modeling of computational flow domain

Flow predictions were carried out to study the performance of thin liquid film on an evaporator surface. Figures 3a – 3c shows the details of the geometry of the evaporator surface used in the flow investigation. The studied geometry involves a cone with a constant vertex angle rotating with a constant rotational velocity.

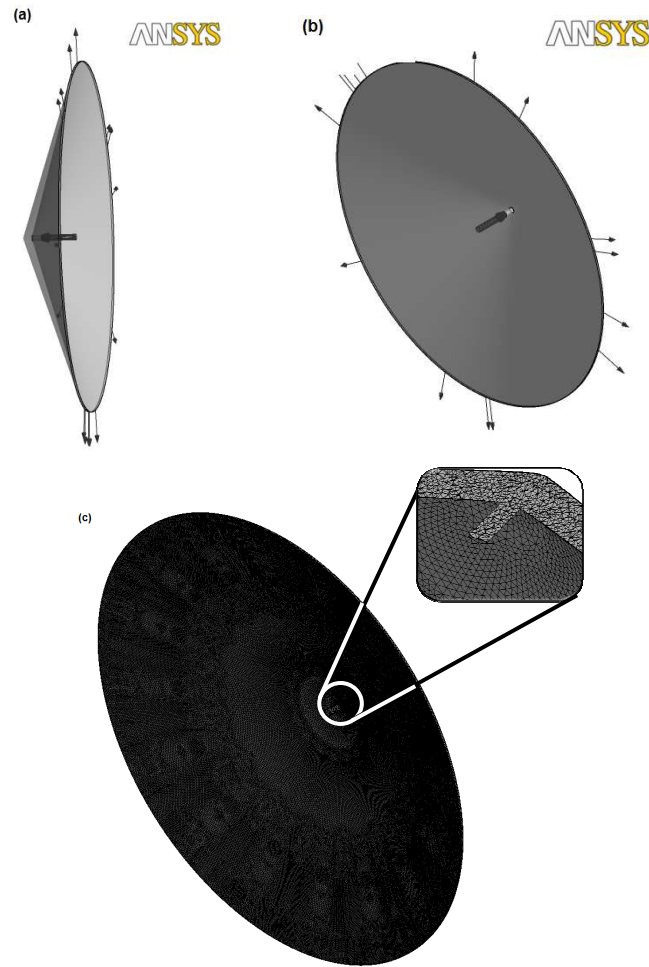


Figure 3. Geometry (a – b) and mesh (c) of the numerical model used CFD simulations.

The mesh (Figure 3c) was obtained for the geometry of the thin liquid film on the evaporator surface and was used in the case simulations as described in Figure 4. A mesh composed of 2,226,399 (428,607 nodes) tetrahedral, prismatic and pyramidal elements was used (Figure 3c). The grid was tested with different grid densities in order to verify that the solution was grid-independent. Therefore, the prismatic elements are located adjacent to the walls and ensure that the boundary layer is properly resolved.

Simulations were considered converged when the normalized root mean square (RMS) residuals for the velocities were below 1×10^{-4} . The residuals for different equations are given as (Singh et al., 2010):

$$\frac{\sum_{i=1}^M |R_{rs}|^2}{S_{N_\psi}} \leq 10^{-4} \quad (13)$$

Where, $|R_{rs}|^2$ is the sum of the absolute residuals for a dependent variables ψ for the nth iteration and S_{N_ψ} is the corresponding normalizing factor.

2.3.2. Flow domain

Conventional atmospheric distillation (ASTM D 2892, 2005) from Brazilian crude oil from API gravity around 18 °API provided an atmospheric distillation residue (ATR–W). It was supplied by the Petrobras Research and Development Center (CENPES–Brazil). The atmospheric residue was used as the operating fluid. In order to characterize fluid properties (Table 1), the ATR–W was modeled in previous physicochemical study (Tovar et al., 2011).

Table 1. Liquid petroleum residue properties used at CFD simulations (Tovar et al., 2011).

Property	EVT (K)		
	423.15	523.15	623.15
C_p (J·kg ⁻¹ ·K ⁻¹)	2388.03	2767.57	3083.57
λ (W·m ⁻¹ ·K ⁻¹)	0.106	0.094	0.085
ν (mm ² ·s ⁻¹)	0.0133	0.0025	0.0011
M (kg·kmol ⁻¹)		437.0	
ρ (kg·m ⁻³)		952.2	
MeABP (K)		819.7	

EVT: Evaporator temperature; M : Molar mass; C_p : Specific heat capacity; λ : Thermal conductivity; ν : Kinematic viscosity; ρ : Density at evaporator temperature; and MeABP: Mean average boiling point.

2.3.2.1. Study cases

Different operating conditions were analyzed. The computational flow domain was modeled according to the physical cases described in Figure 4a and Figure 4b for patter flow study and visualization of components of velocity in laminar flow, respectively.

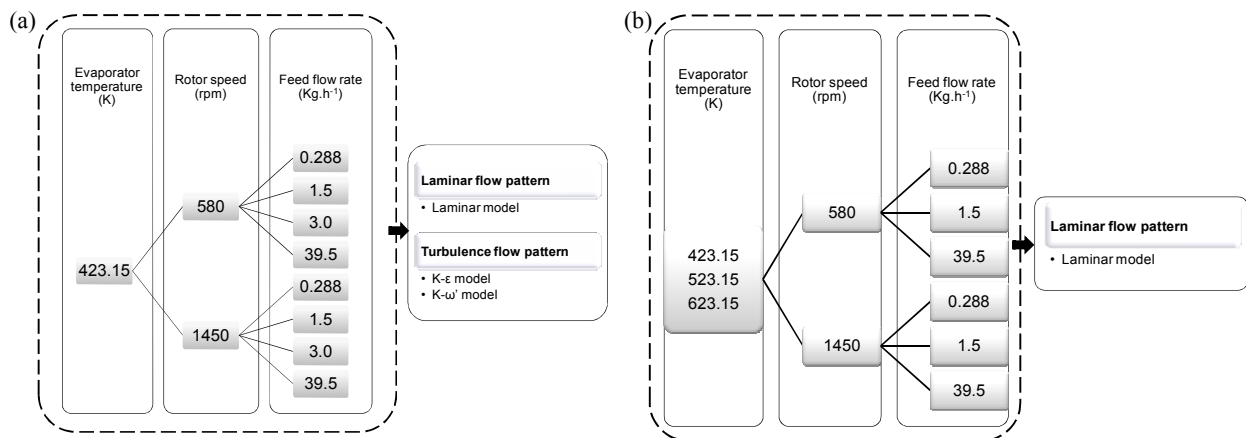


Figure 4. Conditions for CFD simulation in: (a) the pattern flow study and (b) visualization of components of velocity study.

2.4. Boundary conditions and solution domain

Flow simulations were carried out using the commercial CFD software package CFX version 11 and were based on a finite volume approach to solve the governing equations. All boundary conditions used in the simulations are given in Table 2.

Table 2. Computational domain and boundary conditions used in CFD simulations.

Domain	Boundary condition
Inlet/outlet	Mass flow rate: Figure 4a – 4b Flow direction: Normal to a boundary conditions Relative pressure: 0 Pa Reference pressure: 101,325 Pa Uniform velocity profile. The initial value of both, tangential and radial velocity was $0.00 \text{ m}\cdot\text{s}^{-1}$
Section1 (Evaporator surface)	Wall influence on flow: No slip. Wall velocity rotating wall: 580 and 1450 rpm. Rotating axis: ϕ -direction
Section 2 (Thin liquid film)	Wall influence on flow: Free slip.

3. Results and discussion

3.1. Modeling laminar flow of thin liquid film on evaporator surface: Overall effects of operating conditions

Simulated velocity profile plots of the flow (the thin liquid film of the ATR–W) produced by the molecular distillation process using the laminar flow pattern are presented in Figures 5a – 5d and 6a – 6d. Different operating conditions of the Q (at 0.288, 1.5, 3.0 and $39.5 \text{ kg}\cdot\text{h}^{-1}$) and the RS (at 580 and 1450 rpm) at 423.15 K as the EVT were analyzed.

In both conditions of the *RS* (580 and 1450 rpm), results showed that a high flow region was formed in the r -direction along the evaporator surface through the spinning cone from $r=0.000$ m to $r=0.213$ m. When outward flow was analyzed, the maximum upward velocity magnitude was about $28.700 \text{ m}\cdot\text{s}^{-1}$ (at 0.288 , 1.5 and $3.0 \text{ kg}\cdot\text{h}^{-1}$ and 1450 rpm); $17.640 \text{ m}\cdot\text{s}^{-1}$ (at $39.5 \text{ kg}\cdot\text{h}^{-1}$ and 1450 rpm); $9.500 \text{ m}\cdot\text{s}^{-1}$ (at 0.288 , 1.5 and $3.0 \text{ kg}\cdot\text{h}^{-1}$ and 580 rpm); $12.038 \text{ m}\cdot\text{s}^{-1}$ (at $39.5 \text{ kg}\cdot\text{h}^{-1}$ and 580 rpm) near $r=0.213$ m. Hence, the thin liquid film on the evaporator surface spreads outside since the vector of velocity distribution is moving in the r -direction, describing symmetrical velocity distributions.

Nevertheless, the plots generally show similar flow patterns, with a strong primary circulation for creating a strong vortex flow in the center of the spinning cone. However, some slight differences can be noticed when Q is increased, keeping *RS* constant (at 580 rpm or 1450 rpm). As a result, the circulation of the vortex flow predicted by this study is situated slightly lower in the inlet section. Results reported that a vortex, below the inlet section, was entrapped between the inner cone (the evaporator surface) and the flow domain (the thin liquid film). As the rate of Q is increased, the size of the vortex seems to increase, with its center traveling away from the inlet (in the positive axial direction) to the r -direction. Accordingly, similar results have been obtained by Rapley et al. (2008) and Pereira and Sousa (1999) on a rotating cone geometry where streamlines show a vortex to be located near the inlet pipe.

Nonetheless, Figures 5 – 6 shows that the predicted flow patterns are generally in good agreement, quantitatively and qualitatively, with the studied process. However, simulated data of the liquid flow on the evaporator surface allowed the identification of a limiting situation related to Q as an operating variable in which, at high values of Q might affect the mass transfer in the molecular distillation process.

However, the operating condition in which Q equals $39.5 \text{ kg}\cdot\text{h}^{-1}$, requires special attention. The simulation results showed a profile velocity magnitude of about $12.038 \text{ m}\cdot\text{s}^{-1}$ at 580 rpm and $17.640 \text{ m}\cdot\text{s}^{-1}$ at 1450 rpm near the outlet section. Therefore, a swirling region below the inlet section was observed and the flow assumptions made in the laminar model suggest analyses about turbulence approach in this region.

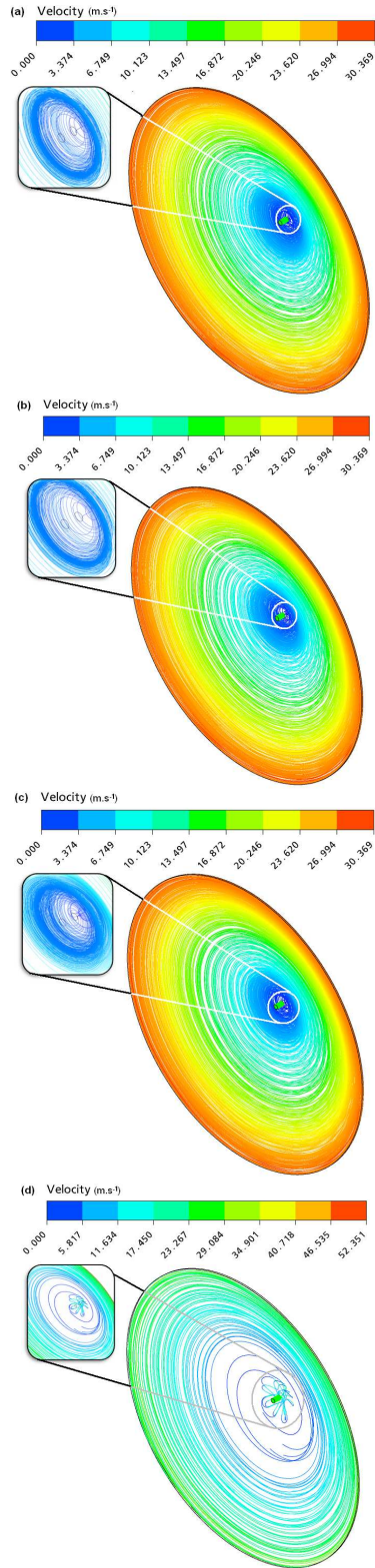


Figure 5: Velocity profile of thin liquid film in evaporator device at feed flow rates equal to a) 0.288 kg·h⁻¹, b) 1.5 kg·h⁻¹, c) 3.0 kg·h⁻¹ and d) 39.5 kg·h⁻¹; keeping *EVT* and *RS* equal 423.15 K and 1450 rpm, respectively, and considering laminar flow pattern.

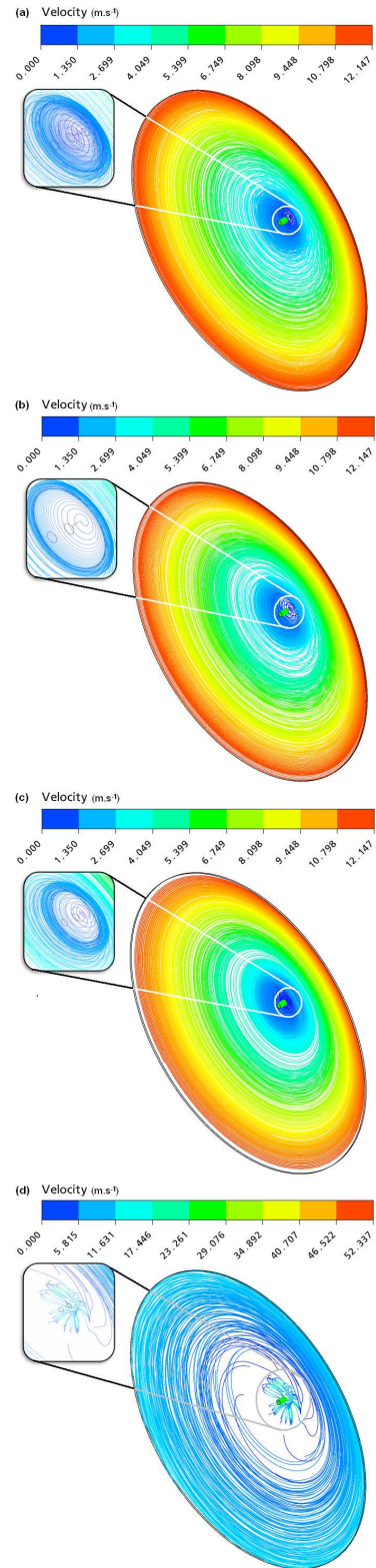


Figure 6: Velocity profile of thin liquid film in evaporator device at feed flow rates equal to a) 0.288 kg·h⁻¹, b) 1.5 kg·h⁻¹, c) 3.0 kg·h⁻¹ and d) 39.5 kg·h⁻¹; keeping *EVT* and *RS* equal 423.15 K and 580 rpm, respectively, and considering laminar flow pattern.

3.2. Modeling turbulent flow of thin liquid film on evaporator surface: Overall effects of operating condition

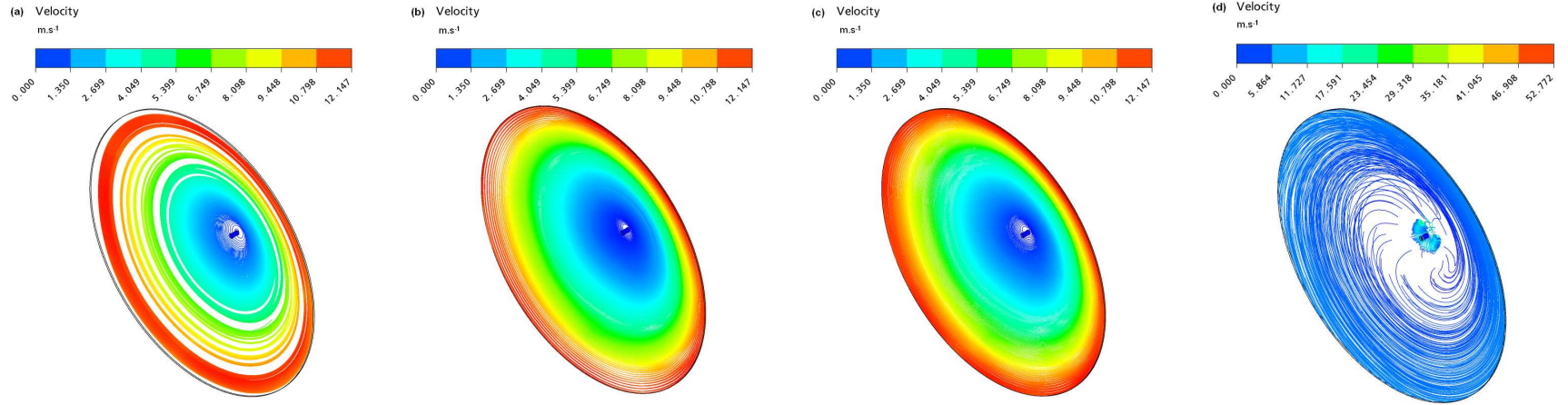
The effect of the turbulence model was investigated using an isotropic eddy viscosity model (the standard $k-\varepsilon$ turbulence model) and the shear-stress transport model $k-\omega'$ model (SST $k-\omega'$ model). Convergence was based on the behavior of the transport equation residuals. The iterative convergence history showed that both models had good convergence. However, a large amount of numerical noise in the behavior of the turbulent kinetic energy, with the $k-\varepsilon$ turbulence model approach, was observed. It could be damped by choosing the SST $k-\omega'$ turbulence model which increases the computational effort and the solver robustness.

The stream lines plots using the standard $k-\varepsilon$ and the SST $k-\omega'$ models (Figures 7 – 8) are compared with those of the reference case in Figures 5 – 6, corresponding to laminar flow pattern. In a general aspect, the two turbulence models give flow patterns that are very alike. Some small differences were noticed however in the inlet and in the outlet section of the system. At the center of the spinning cone, when simulations were carried out using SST $k-\omega'$ model, there appeared to be a slight reverse flow in regards to the flow predicted by the laminar flow pattern, which was not observed with the standard $k-\varepsilon$ model.

In the internal distance ($r=0.030$ m), the velocity magnitude, predicted by the standard $k-\varepsilon$ model, were slightly higher than the value predicted by the SST $k-\omega'$ model. This small discrepancy could be due to the fact that the velocity distribution in this region is better modeled by the SST $k-\omega'$ model for modeling swirling flows. Thus, the SST $k-\omega'$ model showed more sensitivity to this upstream boundary condition than the standard $k-\varepsilon$ model.

Nevertheless, both CFD simulations predicted the same trend for velocity distribution as the thin liquid film flows away from the evaporator surface, when compared with simulations carried out with laminar flow pattern approach. Smaller differences between the simulation results can be found in the outlet section of the evaporator surface, especially in the region near to $r=0.213$ m leading edge. The simulation with the SST $k-\omega'$ turbulence model captures the velocity distribution better, while the simulation with the standard $k-\varepsilon$ turbulence model showed some discrepancies at the region near $r=0.030$ m.

Rotor Speed at 580 rpm



Rotor speed at 1450 rpm

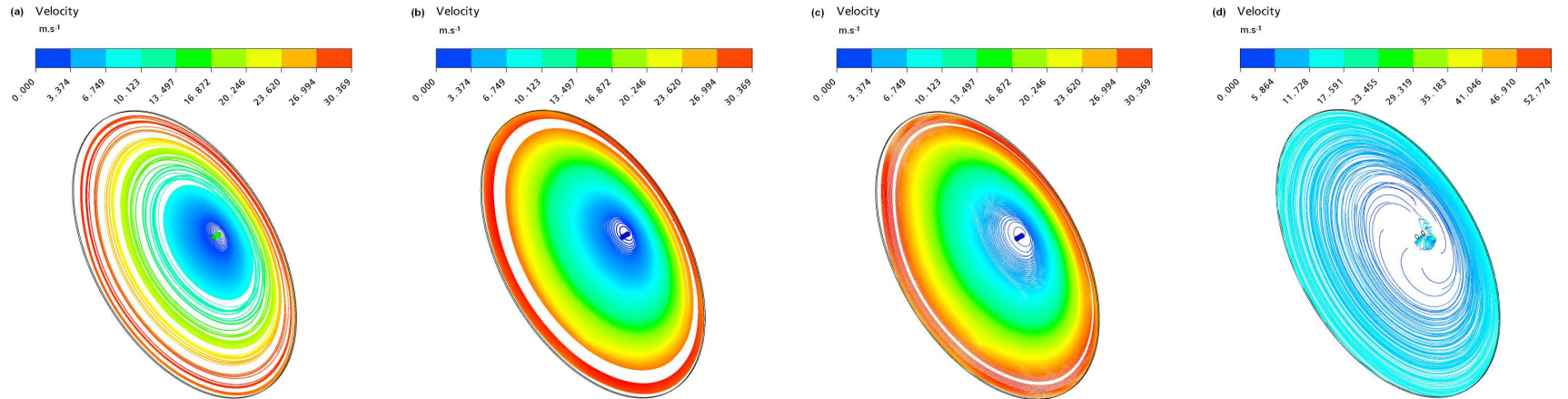
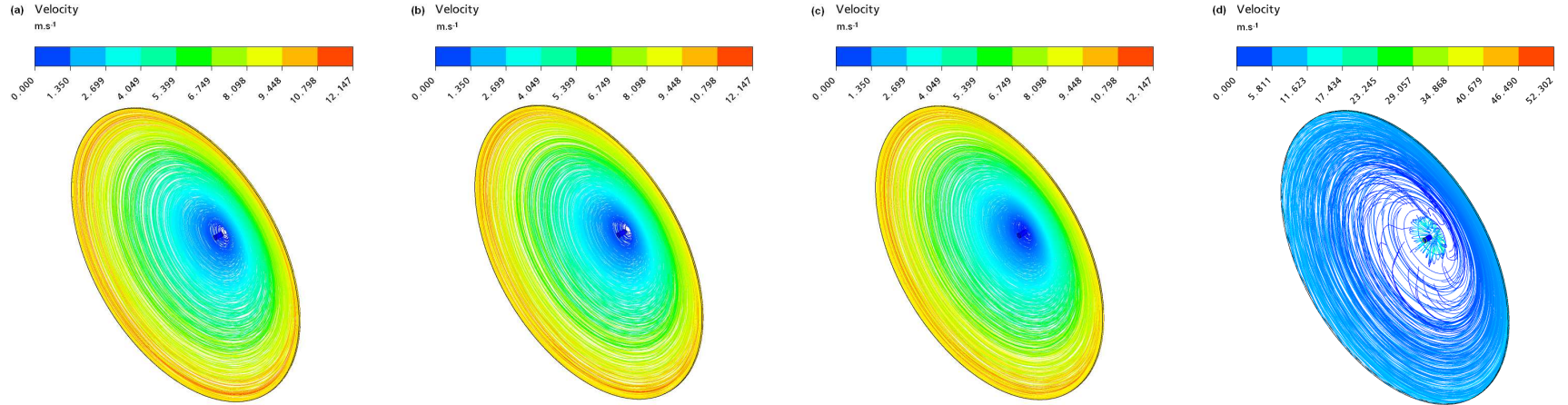


Figure 7. Velocity profile of thin liquid film in evaporator device at feed flow rates equal to a) 0.288 kg·h⁻¹, b) 1.5 kg·h⁻¹, c) 3.0 kg·h⁻¹ and d) 39.5 kg·h⁻¹; keeping evaporator temperature at 423.15 K and rotor speed at 580 and 1450 rpm, respectively, and considering $k-\epsilon$ turbulence model.

Rotor Speed at 580 rpm



Rotor speed at 1450 rpm

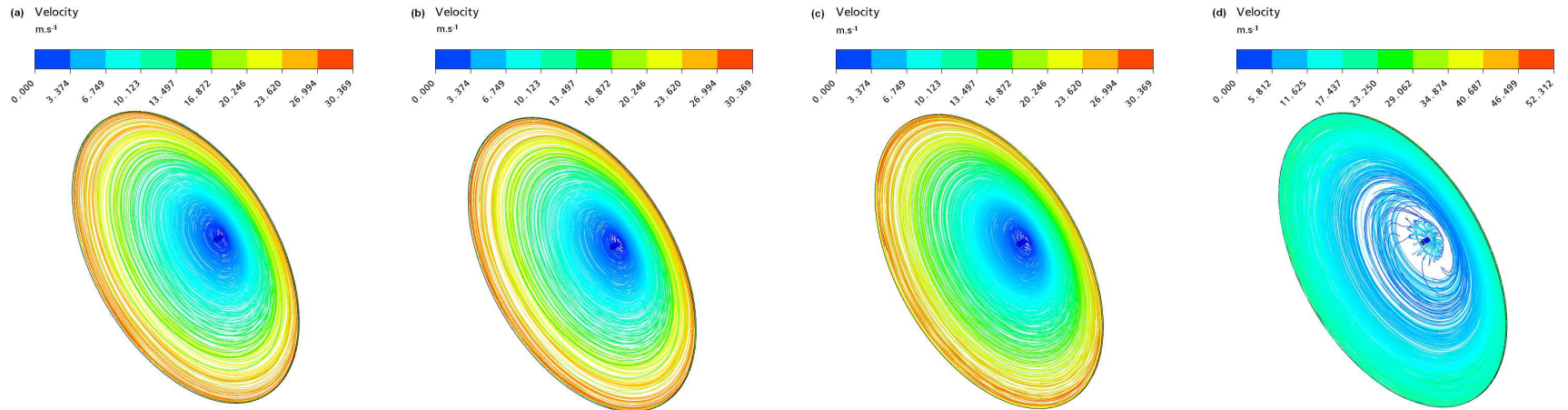


Figure 8. Velocity profile of thin liquid film in evaporator device at feed flow rates equal to a) 0.288 kg·h⁻¹, b) 1.5 kg·h⁻¹, c) 3.0 kg·h⁻¹ and d) 39.5 kg·h⁻¹; keeping evaporator temperature at 423.15 K and rotor speed at 580 and 1450 rpm, respectively, and considering $k-\omega$ turbulence model.

3.2.1. Turbulence kinetic energy

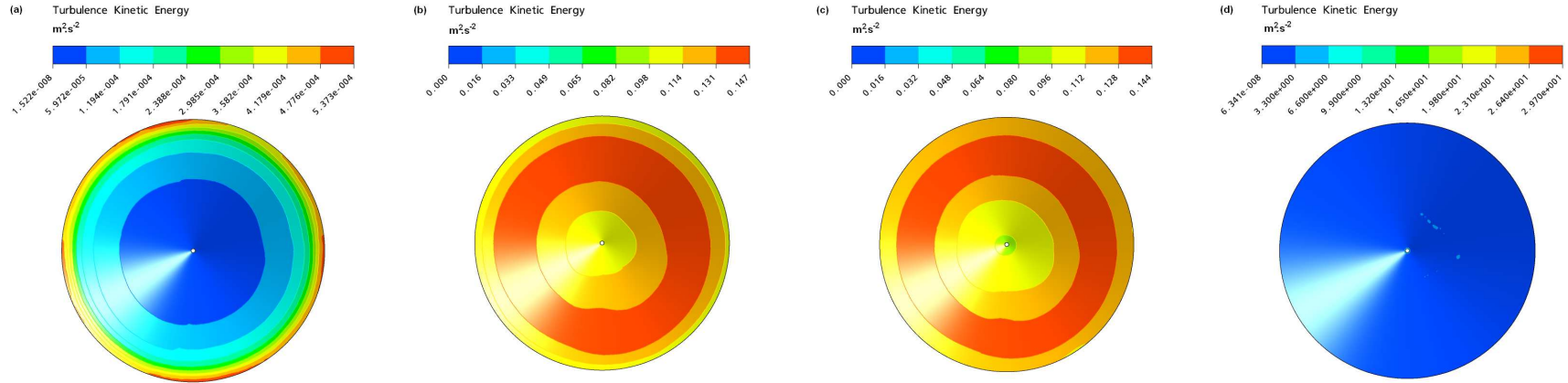
Figures 9 – 10 shows the contour graph of the turbulence kinetic energy field in the $r-\phi$ plane and at the operating conditions of Q (at 0.288, 1.5, 3.0 and 39.5 kg·h⁻¹) and RS (at 580 and 1450 rpm) at 423.15 K for the standard $k-\varepsilon$ and SST $k-\omega$ ' turbulence models, respectively.

Qualitatively, a number of features of the flow in the inlet section were correctly predicted by these models. Figures 9 – 10 shows the radial profile of the turbulent kinetic energy for the thin film on the evaporator surface. Based on the simulated data, it was observed that the standard $k-\varepsilon$ model is not able to predict the turbulent kinetic energy anywhere nears the inlet region, and the SST $k-\omega$ ' model showed comparatively better agreements with the process objective. These deviations could be explained on the basis that the standard $k-\varepsilon$ model is based on isotropic assumptions where the turbulent kinetic energy formulation is constructed with a limitation that all the normal components of stresses are equal to each other as described in Aubin et al. (2004). In this way, due to the inaccuracy of the isotropic turbulence model (the standard $k-\varepsilon$ model) in predicting anisotropic turbulent flows, the SST $k-\omega$ ' model was able to simulate some of the turbulence anisotropy near from evaporator wall at the region below inlet section.

On the other hand, using the standard $k-\varepsilon$ model, results concerning to the production of turbulent kinetic energy, due to flow velocity distribution, reported that values of Q less than 3.0 kg·h⁻¹ may, in fact, be enough to form a uniform thin film on the evaporator surface. Hence, taking into account the standard $k-\varepsilon$ model, the turbulence kinetic energy values at feed flow rates < 3.0 kg·h⁻¹ (Figures 9a – 9d) were lower than 0.147 m²·s⁻² (at 580 rpm) and 2.873×10⁻³ m²·s⁻² (at 1450 rpm) in comparison with values obtained with the Q operating condition at 39.5 kg·h⁻¹ reaching values of 9.897 m²·s⁻² at both, 580 rpm and 1450 rpm.

However, using the SST $k-\omega$ ' approach (Figures 10a – 10d), it was noted that the system showed higher effectiveness than performance of process developed with the standard $k-\varepsilon$ model, since the turbulent kinetic energy production was approximately 0.000 m²·s⁻².

Rotor Speed at 580 rpm



Rotor speed at 1450 rpm

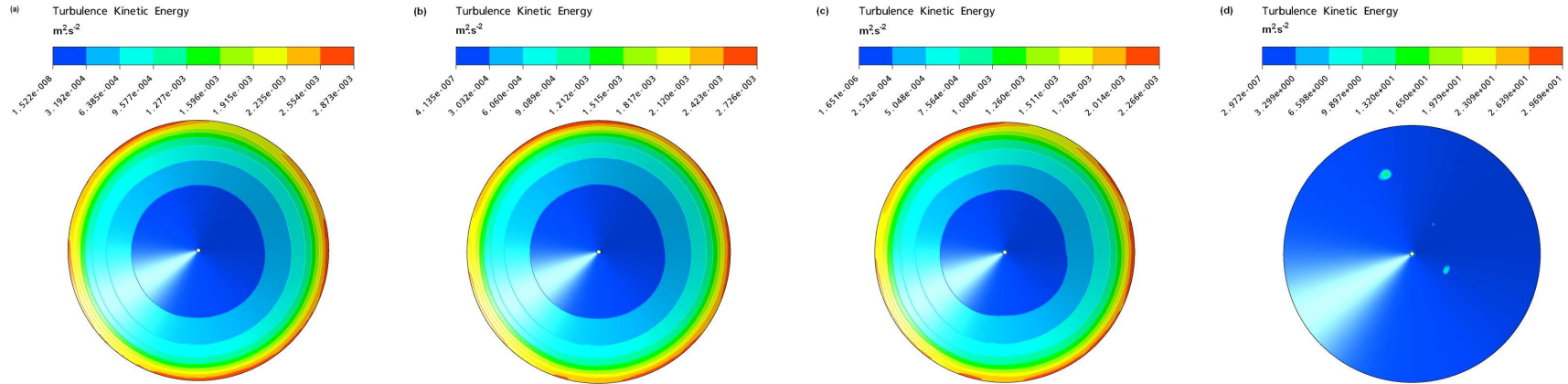
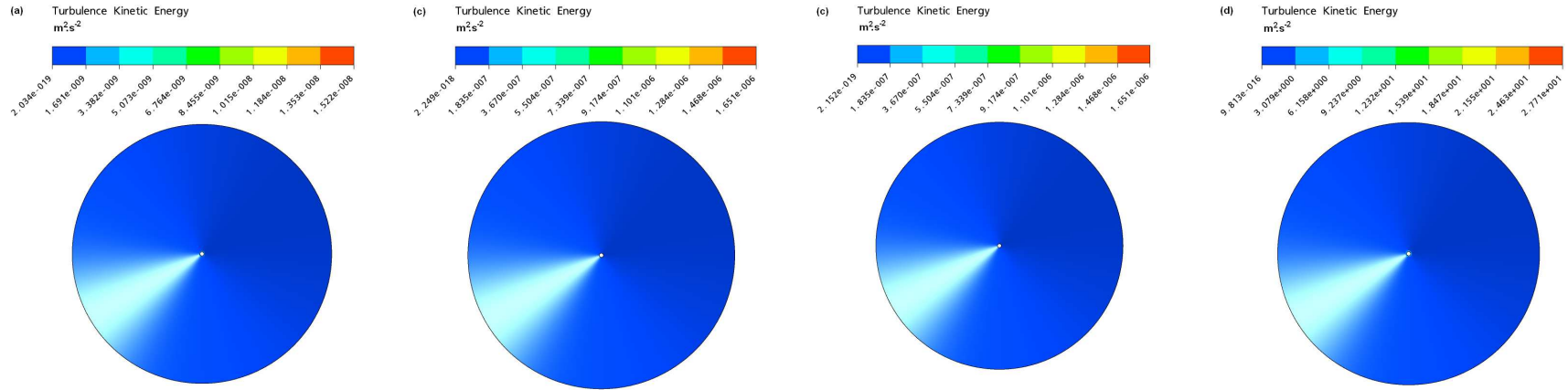


Figure 9. Turbulence kinetic energy distribution in the thin liquid film in evaporator device at feed flow rates equal to a) 0.288 kg·h⁻¹, b) 1.5 kg·h⁻¹, c) 3.0 kg·h⁻¹ and d) 39.5 kg·h⁻¹; keeping evaporator temperature at 423.15 K and rotor speed at 580 and 1450 rpm, respectively, and considering $k-\varepsilon$ turbulence model.

Rotor Speed at 580 rpm



Rotor speed at 1450 rpm

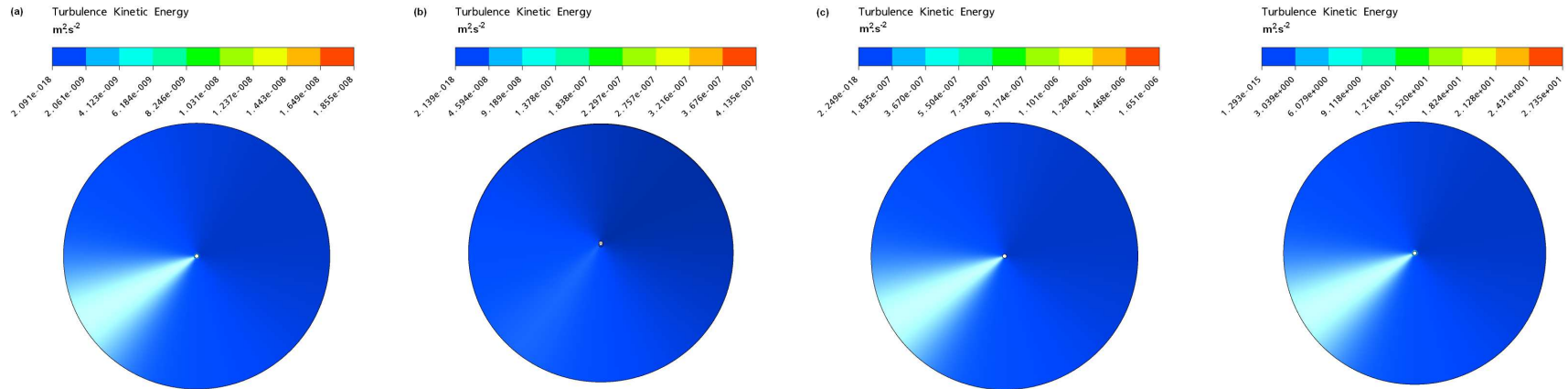


Figure 10. Turbulence kinetic energy distribution in the thin liquid film in evaporator device at feed flow rates equal to a) 0.288 kg·h⁻¹, b) 1.5 kg·h⁻¹, c) 3.0 kg·h⁻¹ and d) 39.5 kg·h⁻¹; keeping evaporator temperature at 423.15 K and rotor speed at 580 and 1450 rpm, respectively, and considering $k-\omega$ turbulence model.

3.3. Study of components of velocity in evaporating liquid film of a petroleum fraction on the evaporator surface

The 3-D simulation by means of ANSYS CFX software package provided the velocity profile developed in the evaporating liquid film. Using the contour graph, the velocity profiles along the thin film are given in Figures 11 – 13 at different operating conditions. In this section, results will be presented in two sub-sections, describing the quantitative and qualitative influence of the operating variables (EVT , Q and RS).

3.3.1. Effect of evaporator temperature on velocity distribution

To illustrate the influence of EVT on velocity distribution, simulations were carried out as shown in Figure 11a–c – 13a–c. In the simulations, different EVT values were studied at fixed Q (equals 0.288 kg.h^{-1}) and RS (equals 1450 rpm) values. For all these runs, maximum magnitudes of velocity, at 423.15 , 523.15 and 623.15 K , were kept around 28.747 , 24.306 and 26.981 m.s^{-1} , respectively (considering a radial distance equals 0.213 m). In the same way, the maximum magnitudes of radial velocity components, at 423.15 , 523.15 and 623.15 K , were 28.544 , 24.305 and 26.980 m.s^{-1} respectively and, the magnitudes of the tangential velocity component at 423.15 , 523.15 and 623.15 K , were 0.086 , 0.192 and 0.207 m.s^{-1} respectively (considering a radial distance equals 0.213 m).

In general, it can be observed that an increase in the EVT causes an increase in the vorticity moment below the inlet section. Due to this, below the inlet section, the tangential velocity component on the conical evaporator surface attains negative values; and is known as the *transition path* between the inlet flow through the feed pipe and the entrance region of the flow on the evaporator surface. Therefore, the centrifugal force generated by high rotational velocity of the rotor creates a tangential gradient across the inlet section that results in the generation of a vortice flow. Hence, the existence of the vortice flow leads to flow distortion in the cross-sectional plane of the conical surface.

However, based on the results obtained by analyzing the effect of EVT on the velocity profile, two important facts were elucidated: (i) the tangential velocity component can be considered negligible when compared with the radial component; and (ii) the velocity profile of flow in the thin film varies significantly because of the EVT and RS effect.

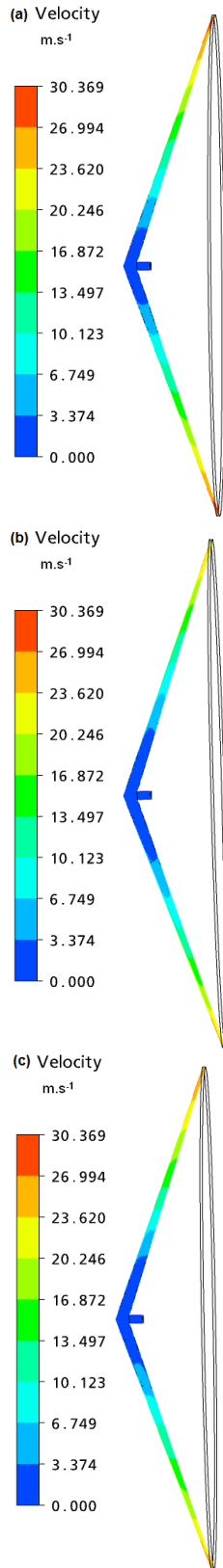


Figure 11. Velocity profile of thin liquid film in evaporator device at a) 423.15 K, b) 523.15 K and c) 623.15 K; keeping Q and RS equal 0.288 kg.h⁻¹ and 1450 rpm.

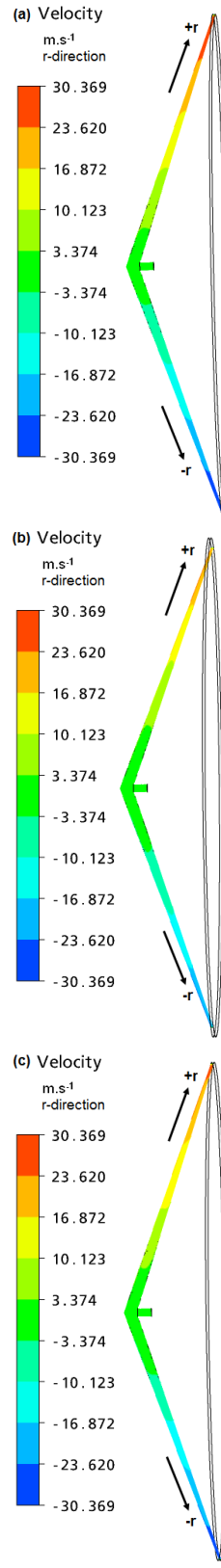


Figure 12. Velocity in r -direction of thin liquid film in evaporator device at a) 423.15 K, b) 523.15 K and c) 623.15 K; keeping Q and RS equal 0.288 kg.h⁻¹ and 1450 rpm.

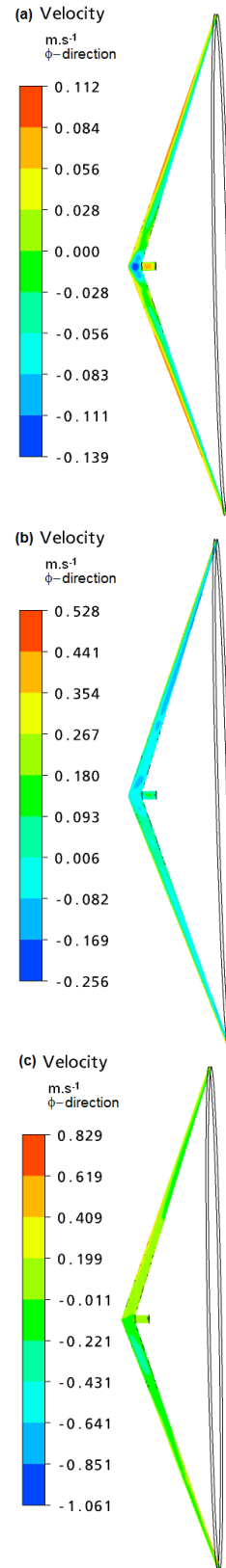


Figure 13. Velocity in ϕ -direction of thin liquid film in evaporator device at a) 423.15 K, b) 523.15 K and c) 623.15 K; keeping Q and RS equal 0.288 kg.h⁻¹ and 1450 rpm.

Nevertheless, it is known that *EVT* plays an important role in the molecular distillation process from the viewpoint of both the mass ratio of the distillate and residue streams and the evaporation rate. However, taking into account the purpose of this work, heat transfer in the thin film was still ignored.

3.3.2. Effect of feed flow rate and rotor speed on velocity distribution

Analyses related to the Q and RS effects on the velocity visualization in r and φ -directions components inner the thin liquid film over the evaporator surface were carried out using CFD and they are presented in Figures 14 – 19. A reasonable agreement can be observed between principles of the CMD process and simulated data, except below the inlet section when it is considered a high value of Q (e.g. $39.5 \text{ kg}\cdot\text{h}^{-1}$). Figures 14a–c – 16a–c present the dependence of the velocity profile with Q and RS . It can be observed that the effect of RS is higher at elevated Q values. Therefore, in the CFD approach, different Q values were studied at fixed *EVT* (equals 423.15) and RS (equal 580 and 1450 rpm) values. For all these runs, keeping RS at 580 rpm (Figures 14 – 16), maximum magnitudes of velocity, around 9.460, 9.813 and $12.038 \text{ m}\cdot\text{s}^{-1}$, were reached at $0.288 \text{ kg}\cdot\text{h}^{-1}$, $1.5 \text{ kg}\cdot\text{h}^{-1}$ and $39.5 \text{ kg}\cdot\text{h}^{-1}$ respectively (considering a radial distance equals 0.213 m). In the same way, the maximum magnitudes of radial velocity component, at $0.288 \text{ kg}\cdot\text{h}^{-1}$, $1.5 \text{ kg}\cdot\text{h}^{-1}$ and $39.5 \text{ kg}\cdot\text{h}^{-1}$, were 9.456, 9.813 and $11.890 \text{ m}\cdot\text{s}^{-1}$ respectively (considering a radial distance equals 0.213 m). In addition, the magnitudes of the tangential velocity component at $0.288 \text{ kg}\cdot\text{h}^{-1}$, $1.5 \text{ kg}\cdot\text{h}^{-1}$ and $39.5 \text{ kg}\cdot\text{h}^{-1}$, were 0.265, 0.096 and $1.88 \text{ m}\cdot\text{s}^{-1}$ respectively (considering a radial distance equals 0.213 m).

Comparing the results obtained in which *EVT* and RS were kept constant at 423.15 K and 580 rpm, Figures 17a–c – 19a–c show that the CFD modeling approach predicts velocity profiles that are generally in good agreement, quantitatively and qualitatively, with the process, once it was analyzed the *EVT* and RS at 423.15 K and 1450 rpm, respectively. Analyzing the maximum magnitudes of velocity at $0.288 \text{ kg}\cdot\text{h}^{-1}$, $1.5 \text{ kg}\cdot\text{h}^{-1}$ and $39.5 \text{ kg}\cdot\text{h}^{-1}$, they were predicted around 28.544, 28.785 and $17.640 \text{ m}\cdot\text{s}^{-1}$, respectively (considering a radial distance equals 0.213 m). In the same way, the maximum magnitudes of radial velocity components, at $0.288 \text{ kg}\cdot\text{h}^{-1}$, $1.5 \text{ kg}\cdot\text{h}^{-1}$ and $39.5 \text{ kg}\cdot\text{h}^{-1}$, were 23.714, 23.785 and $16.934 \text{ m}\cdot\text{s}^{-1}$, respectively (considering a radial distance equals 0.213 m); and the tangential velocity components at $0.288 \text{ kg}\cdot\text{h}^{-1}$, $1.5 \text{ kg}\cdot\text{h}^{-1}$ and $39.5 \text{ kg}\cdot\text{h}^{-1}$, were 0.026, 0.023 and $0.293 \text{ m}\cdot\text{s}^{-1}$, respectively.

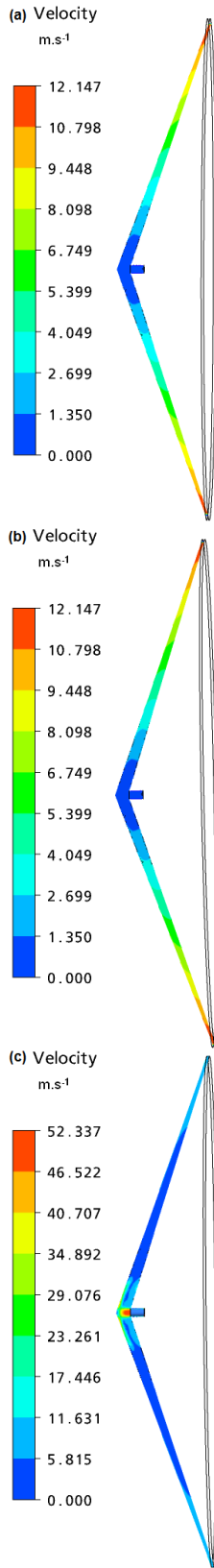


Figure 14. Velocity profile of thin liquid film in evaporator device at Q equal a) $0.288 \text{ kg.h}^{-1} \text{ K}$, b) $1.5 \text{ kg.h}^{-1} \text{ K}$ and c) 39.5 kg.h^{-1} ; keeping EVT and RS equal 423.15 K and 580 rpm .

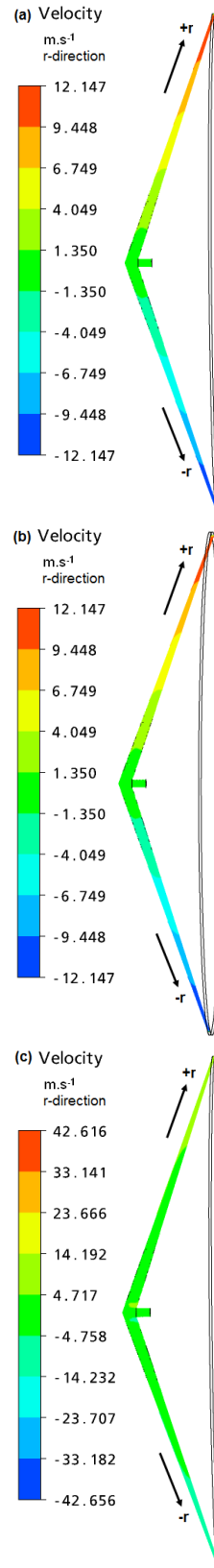


Figure 15. Velocity in r -direction of thin liquid film in evaporator device at Q equal a) $0.288 \text{ kg.h}^{-1} \text{ K}$, b) $1.5 \text{ kg.h}^{-1} \text{ K}$ and c) 39.5 kg.h^{-1} ; keeping EVT and RS equal 423.15 K and 580 rpm .

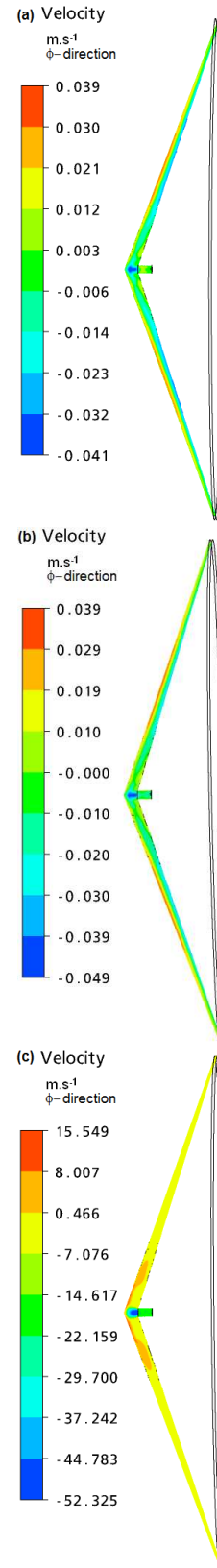


Figure 16. Velocity in ϕ -direction of thin liquid film in evaporator device at Q equal a) $0.288 \text{ kg.h}^{-1} \text{ K}$, b) $1.5 \text{ kg.h}^{-1} \text{ K}$ and c) 39.5 kg.h^{-1} ; keeping EVT and RS equal 423.15 K and 580 rpm .

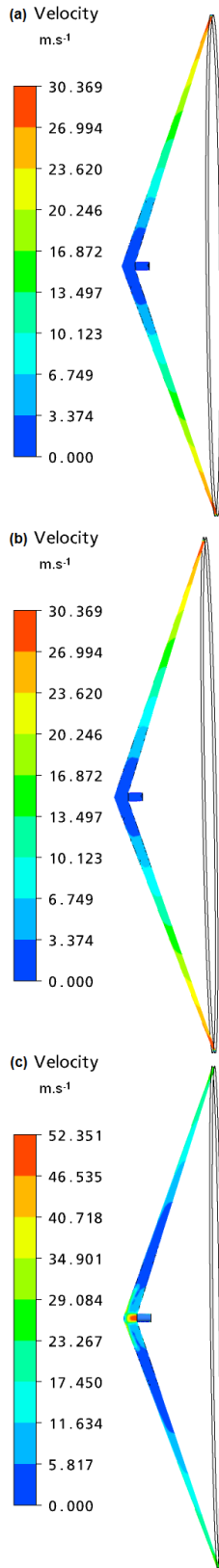


Figure 17. Velocity profile of thin liquid film in evaporator device at Q equal a) 0.288 kg.h⁻¹ K, b) 1.5 kg.h⁻¹ K and c) 39.5 kg.h⁻¹; keeping EVT and RS equal 423.15 K and 1450 rpm.

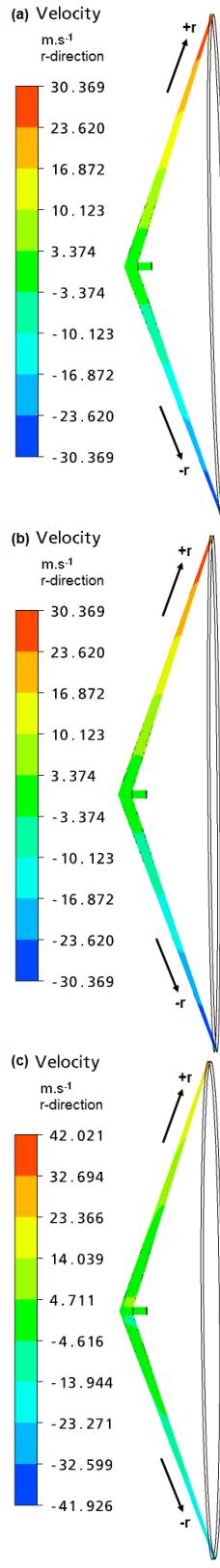


Figure 18. Velocity in r-direction of thin liquid film in evaporator device at Q equal a) 0.288 kg.h⁻¹ K, b) 1.5 kg.h⁻¹ K and c) 39.5 kg.h⁻¹; keeping EVT and RS equal 423.15 K and 1450 rpm.

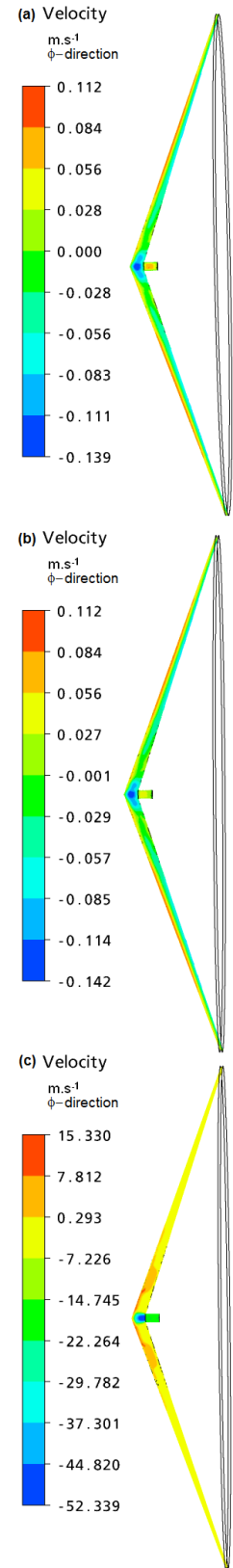


Figure 19. Velocity in ϕ -direction of thin liquid film in evaporator device at Q equal a) 0.288 kg.h⁻¹ K, b) 1.5 kg.h⁻¹ K and c) 39.5 kg.h⁻¹; keeping EVT and RS equal 423.15 K and 1450 rpm.

In Figures 14 – 16 (at 580 rpm) and in Figures 17 – 19 (at 1450 rpm), it can be observed that the increasing of the Q values caused an increase in the vorticity moment below the inlet, as was described when it was considered the *EVT* effect. From this, the tangential velocity component was negative for at least the first fourth part of the conical surface, whereas after the *transition path*, the tangential velocity component was positive along the follow radial distance.

The effect of Q and RS on visualization of the components of velocity in φ -direction is marked by the positive values for the tangential velocity component which imply that the flow it is rotating slightly faster or at the same rotational speed than the cone, but if it is negative, the flow is rotating slower than the cone, thus it will be retarding the flow, which will create greater vortices about the cone surface inlet than the flow domain. Finally, Q and RS will become important variables in the centrifugal molecular process because at high values of this operating conditions, the residence time of the molecules on the evaporator surface will be shorter, thus, the mass transfer is affected and the evaporation rate might not be high enough to produce a considerable amount of the desired stream (distillate or residue).

4. Conclusions

CFD simulations of the flow generated on an evaporator surface by centrifugal molecular distillation have been carried out. The investigations have focused on the analyses of pattern flow, both laminar and turbulent, and on velocity distribution. Overall, the results, using both approaches, are in very good agreement with the molecular distillation process.

The turbulence pattern flow simulations expressed that these two turbulent models, the standard $k-\varepsilon$ and SST $k-\omega'$, are suitable for simulating evaporating liquid film in a molecular centrifugal distiller. Nevertheless, the CFD simulations conducted for this work with the turbulence models did not reflect significant changes on the velocity distribution in the upward flow on the evaporator surface regarding to laminar flow. Thus, the velocity distribution of the thin film on the evaporator surface can be modeled by the laminar pattern flow in order to simplify the computing process.

Based on the results obtained in the theoretical work through CFD simulation, Q (feed flow rate) and RS (rotor speed) presented important effects on visualization of the velocity profile. The liquid flow pattern on the evaporator surface indicated the laminar flow of thin film is governed by the radial velocity component and, consequently, the tangential velocity

component may be negligible. The liquid flow on the evaporator surface allowed the identification of a limiting situation related to feed flow rate (Q) as an operating variable, in which, at high values of Q might affect the mass transfer in the molecular distillation process.

The results presented in this work are useful for broadening the application of CFD as a tool for simulating the flow of complex mixtures, such as a petroleum atmospheric residue, on an evaporator surface in centrifugal molecular distillers.

The CFD simulations were validated for this study corresponding to a framework analysis of a centrifugal molecular distillation. Though the CFD results in the present study have not been experimentally validated, these results provided useful information on the flow dynamics (the flow regime and components of velocity distribution in thin liquid film) of the thin liquid film (of the ATR–W) along the evaporator surface. Therefore, the CFD analyses will be used as an intermediate step towards the modeling flow during the process.

Acknowledgment

This research was supported by the Brazilian National Council for Technological and Scientific Development (CNPq), the Petrobras Research and Development Center (PETROBRAS/CENPES) and the Brazilian Study and Project Financing Institution (FINEP).

Nomenclature

C_p	=	Specific heat capacity	$[\text{J}\cdot\text{kg}^{-1}\cdot\text{K}^{-1}]$
C_μ	=	Constant in Equation (10) ($C_\mu = 0.09$)	$[-]$
$C_{1\varepsilon}$	=	Constant in Equation (9) ($C_{1\varepsilon} = 1.44$)	$[-]$
$C_{2\varepsilon}$	=	Constant in Equation (9) ($C_{2\varepsilon} = 1.92$)	$[-]$
$D_{\omega'}$	=	Represents cross-diffusion	$[\text{kg}\cdot\text{m}^{-1}\cdot\text{s}^{-3}]$
EVT	=	Evaporator temperature	$[\text{K}]$
k	=	Turbulent kinetic energy	$[\text{m}^2\cdot\text{s}^{-2}]$
M	=	Mass molar	$[\text{kg}\cdot\text{kmol}^{-1}]$
$MeABP$	=	Mean average boiling point	$[\text{K}]$
P_b	=	Generation of k due to buoyancy in k – ε turbulence model	$[\text{kg}\cdot\text{m}^{-1}\cdot\text{s}^{-3}]$
\tilde{P}_k	=	Generation of k due to the velocity gradients in k – ω' turbulence model	$[\text{kg}\cdot\text{m}^{-1}\cdot\text{s}^{-3}]$
P_k	=	Generation of k due to the velocity gradients in k – ε turbulence model	$[\text{kg}\cdot\text{m}^{-1}\cdot\text{s}^{-3}]$
$P_{\omega'}$	=	Generation of ω' in k – ω' turbulence model	$[\text{kg}\cdot\text{m}^{-1}\cdot\text{s}^{-3}]$
Q	=	Feed flow rate	$[\text{kg}\cdot\text{h}^{-1}]$
r	=	Radial position	$[\text{m}]$
r_0	=	Feed location	$[\text{m}]$
RS	=	Rotor Speed	$[\text{rpm}]$
R_{rs}	=	Root mean residuals	$[-]$
S_k	=	User-defined source terms	$[\text{kg}\cdot\text{m}^{-1}\cdot\text{s}^{-3}]$

$S_{\omega'}$	= User-defined source terms	$[\text{kg}\cdot\text{m}^{-1}\cdot\text{s}^{-3}]$
$S_{N_{\psi}}$	= Normalizing factor	$[-]$
T	= Temperature	$[\text{K}]$
v_r	= Radial velocity	$[\text{m}\cdot\text{s}^{-1}]$
v_{r_0}	= v_r at feed location	$[\text{m}\cdot\text{s}^{-1}]$
v_{θ}, v_{ϕ}	= Meridional and Tangential velocity	$[\text{m}\cdot\text{s}^{-1}]$
Y_M	= Represents the contribution of the fluctuating dilatation in compressible turbulence to the overall dissipation rate	$[\text{kg}\cdot\text{m}^{-1}\cdot\text{s}^{-3}]$
Y_k	= Represents the dissipation of k	$[\text{kg}\cdot\text{m}^{-1}\cdot\text{s}^{-3}]$
$Y_{\omega'}$	= Represents the dissipation of ω'	$[\text{kg}\cdot\text{m}^{-1}\cdot\text{s}^{-3}]$
<i>Greek letters</i>		
β'	= Cone half-angle	$[-]$
ε	= rate of dissipation of turbulent kinetic energy in the k - ε turbulence model	$[\text{m}^2\cdot\text{s}^{-3}]$
ϕ	= Tangential direction in spherical coordinates	$[-]$
λ	= Thermal conductivity	$[\text{W}\cdot\text{m}^{-1}\cdot\text{K}^{-1}]$
δ	= Local film thickness	$[\text{m}]$
ΔH	= Heat of evaporation	$[\text{J}\cdot\text{mol}^{-1}]$
μ	= Dynamic viscosity	$[\text{kg}\cdot\text{m}^{-1}\cdot\text{s}^{-1}]$
μ_t	= Turbulent viscosity	$[\text{kg}\cdot\text{m}^{-1}\cdot\text{s}^{-1}]$
ν	= Kinematic viscosity	$[\text{m}^2\cdot\text{s}^{-1}]$
σ_k	= Prandtl number for k for k - ε turbulence model ($\sigma_k = 1.0$)	$[-]$
σ_{ε}	= Prandtl number for ε for k - ε turbulence model ($\sigma_{\varepsilon} = 1.3$)	$[-]$
ρ	= Density of liquid fluid	$[\text{kg}\cdot\text{m}^{-3}]$
ω	= Angular velocity of evaporator surface	$[\text{s}^{-1}]$
ω'	= Rate of dissipation of turbulent kinetic energy in the SST k - ω' turbulence model	$[\text{m}^2\cdot\text{s}^{-3}]$

References

- American Society for Testing Material, ASTM D 2892. Standard Test Method for Distillation of Crude Petroleum (15–Theoretical Plate Column). West Conshohocken, (Pennsylvania): ASTM International, 2005. 32p.
- Aubin J., Fletcher D. F., Xuereb C. (2004) Modeling turbulent flow in stirred tanks with CFD: The influence of the modeling approach, turbulence model and numerical scheme, *Experimental Thermal and Fluid Science* **28**, 5, 431–445.
- Batistella C. B., Maciel M. R. W. (1996) Modeling, simulation and analysis of molecular distillators: Centrifugal and falling film, *Computers & Chemical Engineering* **20**, supplement 1, S19–S24.
- Bhandarkar M., Ferron J. R. (1988) Transport processes in thin liquid films during high-vacuum distillation, *Industrial & Engineering Chemistry Research* **27**, 6 1016–1024.

- Bruin S. (1969) Velocity distributions in a liquid film flowing over a rotating conical surface, *Chemical Engineering Science* **24**, 11, 1647–1654.
- Cvengroš J., Lutišan J., Micov M. (2000) Feed temperature influence on the efficiency of a molecular evaporator, *Chemical Engineering Journal* **78**, 1, 61–67.
- El-Behery S. M., Hamed M. M. (2009) A comparative study of turbulence models performance for turbulent flow in a planar asymmetric diffuser, *Computer & Fluids* **44**, 1, 248–257.
- Greenberg D. B. (1972) A theoretical and experimental study of the centrifugal molecular still, *AIChE Journal* **18**, 2, 269–276.
- Hinze J. O., Milborn H. (1950) Atomization of liquid by means of a rotating cup, *Journal of Applied Mechanics* **17**, 2, 145–153.
- Inuzuka M., Sugiyama R., Saito I., Yamada I., Hiraoka S., Ishikawa H., Banno, I. (1986) Analysis of heat and mass transfer in a centrifugal molecular still, *Journal of Chemical Engineering of Japan* **19**, 1, 14–20.
- Kawala Z., Dakiniewicz P. (2002) Influence of evaporation space geometry on rate of distillation in high-vacuum evaporator, *Separation Science and Technology* **37**, 8, 1877–1895.
- Kawala Z., Stephan K. (1989) Evaporation rate and separation factor of molecular distillation in a falling film apparatus, *Chemical Engineering & Technology* **12**, 1, 406–413.
- Launder B. E., Spalding D. B. (1974) The numerical computation of turbulent flows, *Computer Methods in Applied Mechanics and Engineering* **3**, 2, 269–289.
- Lin S. W., Yoo C. K. (2009) Short-path distillation of palm olein and characterization of products, *European Journal of Lipid Science and Technology* **111**, 2, 142–147.
- Micov M., Lutišan J., Cvengroš J. (1997) Balance equations for molecular distillation. *Separation Science and Technology* **32**, 18, 3051–3066.
- Myers–Vacuum, 2010. Available in: < <http://www.myers-vacuum.com/index.shtml> >. Accessed in: November 10th. 2010.
- Pereira J. C., Sousa J. M. (1999) Confined vortex breakdown generated by a rotating cone, *Journal of Fluid Mechanics* **385**, 1, 287–323.

- Rapley S., Eastwick C., Simmons K. (2008) Computational investigation of torque on coaxial rotating cones, *Journal of Fluids Engineering* **130**, 6, 061102_1–1061102_14.
- Rees G. J. (1980) Centrifugal molecular distillation – I: Fluid dynamics, heat transfer and surface evaporation, *Chemical Engineering Science* **35**, 4, 837–840.
- Sales–Cruz M., Gani R. (2006) Computer–Aided modelling of short–path evaporation for chemical product purification, analysis and design, *Chemical Engineering Research and Design* **84**, 7, 583–594.
- Singh R. K., Singh S. N., Seshadri V. (2010) CFD prediction of the effects of the upstream elbow fittings on the performance of cone flowmeters, *Flow Measurement and Instrumentation* **21**, 2, 88–97.
- Singhal A. K., Spalding, D. B. (1981) Predictions of two dimensional boundary layers with the aid of the *k-epsilon* model of turbulence, *Computers Methods in Applied Mechanics and Engineering* **25**, n.a., 365–383.
- Tovar L. P., Wolf–Maciel M. R., Ferreira–Pinto G. M., Maciel–Filho R., Gomes D. R. (2010) Factorial design applied to concentrate bioactive component of *cymbopogon citratus* essential oil using short path distillation, *Chemical Engineering Research and Design* **88**, 2, 239–244.
- Tovar L. P., Wolf Maciel M. R., Maciel Filho R., Batistella C. B., Ariza O. C., Medina L. C. (2011) Overview and computational approach for studying the physicochemical characterization of high-boiling-point petroleum fractions (350 °C+). *Oil & Gas Science and Technology*; doi:10.2516/ogst/2011150.
- Xiang A., Xu S. (2005) Comparison of two turbulent models in simulating evaporating liquid film in a wiped molecular distillator, *Science in China Series B. Chemistry* **48**, 3, 183–188.
- Xubin Z., Chunjian X., Ming Z. (2005) Modeling of falling film molecular distillator, *Separation Science and Technology* **40**, 6, 1371–1386.
- Yakhot V., Orszag S. A., Thangam S., Gatski T. B., Speziale C. G. (1992) Development of turbulence models for shear flows by a double expansion technique, *Physics of Fluids A* **4**, 7, 1510–1520.

5.3. Considerações finais

Neste trabalho, a fluidodinâmica computacional, CFD (do inglês *Computational Fluid Dynamics*), mostrou-se como uma abrangente ferramenta computacional para a simulação de escoamento, que envolve o filme líquido sob a superfície do evaporador. A versatilidade na obtenção de distribuições das velocidades ou das características do escoamento, em qualquer região da superfície do evaporador, tornou amplo o emprego dessa técnica.

Nesse capítulo, foi apresentado o estudo dos efeitos das condições operacionais: temperatura do evaporador, vazão de alimentação e velocidade do rotor, sob o comportamento fluidodinâmico. As equações do fluxo líquido foram resolvidas e as características e a estrutura do campo de fluxo, em regime laminar e turbulento (considerando $k-\varepsilon$ e *Shear Stress Transport* $k-\omega'$, como modelos de turbulência) foram analisadas.

As simulações de escoamento do filme de líquido sobre a superfície do evaporador num destilador molecular centrífugo em regime turbulento reportaram que os dois modelos de turbulência estudados, $k-\varepsilon$ e SST $k-\omega'$, são apropriados para simular a distribuição de velocidades. No entanto, as simulações conduzidas neste trabalho com os modelos de turbulência não refletem alterações significativas na distribuição de velocidade do fluxo sobre a superfície do evaporador em relação ao sistema em regime laminar. Assim, a distribuição de velocidade do filme de líquido sobre a superfície do evaporador pode ser modelada em regime laminar, a fim de simplificar o processo de computação.

Ao estudar os componentes da velocidade nas direções $-r$, $-\theta$ e $-\varphi$, considerando um estado bidimensional estacionário (no padrão de fluxo laminar), apenas o vetor da velocidade na direção radial (direção $-r$) apresenta variação apreciável com as condições operacionais do processo da destilação molecular.

Capítulo 6.

Modelagem e simulação do processo de destilação molecular centrífuga de frações de petróleo

6.1. Introdução

Em estudos realizados nos laboratórios de pesquisa, Laboratórios de Desenvolvimento de Processos de Separação (LDPS) e de Otimização, Projeto e Controle Avançado (LOPCA) da Faculdade de Engenharia Química (FEQ) da Universidade Estadual de Campinas (UNICAMP), em parceria com o órgão Financiador de Estudos e Projetos do Ministério da Ciência e Tecnologia (FINEP) e o Centro de Pesquisa CENPES/PETROBRAS foi desenvolvida uma metodologia, a destilação molecular, para caracterizar os resíduos pesados de petróleo a temperaturas superiores daquelas alcançadas pelos métodos padronizados ASTM D 2892 (2005) e ASTM D 5236 (2003) (Zuñiga–Liñan et al., 2011; Rocha et al., 2011; Zuñiga, 2009; Zuñiga et al., 2009; Zuñiga et al., 2009; Hernández, 2009; Rocha, 2009; Winter et al., 2009; Hernández et al., 2008; Lopes, 2008; Rocha, 2008; Rocha et al., 2008a; Rocha et al., 2008b; Liñan et al., 2007; Lopes et al., 2007; Rocha et al., 2007; Winter, 2007; Winter et al., 2007; Sbaite et al., 2006; Maciel–Filho et al., 2006; Winter et al., 2006; Sbaite, 2005; Winter et al., 2004; Sbaite et al., 2003; Batistella et al., 2002; Batistella et al., 2000; Batistella e Wolf–Maciel, 1998, 1996).

Para se ter um panorama abrangente do processo de destilação molecular, informações sobre o perfil da temperatura, o da concentração do filme, o da taxa efetiva de evaporação, o da taxa de destilado e o da espessura do filme são importantes, pois esses dados permitem avaliar o rendimento do processo, a pureza do produto da destilação e definir condições ótimas de operação. No entanto, a obtenção experimental desses perfis resulta em um trabalho difícil. Para tanto, na indústria pode-se propor a utilização de modelos matemáticos para descrever o comportamento dos sistemas, como uma via rápida de baixo custo e eficiente.

A modelagem do processo da destilação molecular, e nesse caso específico da destilação molecular centrífuga, foi baseada nas equações de balanço de massa, energia e momento para o

filme líquido escoando pela superfície cônica do evaporador. Trabalhos apresentados pelos pesquisadores formulam modelos baseados num processo em não-equilíbrio, desprezando o fenômeno de re-evaporação e considerando um filme de líquido newtoniano, altamente viscoso, e com número de Reynolds pequenos, característicos de fluidos em regime laminar.

Outra contribuição dos trabalhos teóricos é apresentada neste capítulo, é o desenvolvimento de uma ferramenta computacional para auxiliar na modelagem e simulação do processo de destilação molecular centrífuga. Essa contribuição serve para estimar e avaliar os perfis característicos do processo através das variáveis de saída como: da temperatura, da concentração do filme, da taxa efetiva de evaporação, da taxa de destilado e da espessura do filme. Esses perfis são função das análises das variáveis operacionais tais como: temperatura da alimentação, temperatura do evaporador, pressão do sistema e parâmetros geométricos do equipamento que por sua vez dizem respeito à distância entre o evaporador e o condensador, ao ângulo médio da superfície cônica e à distância radial da superfície do evaporador.

A modelagem apresentada neste capítulo é constituída de um sistema de equações diferenciais parciais, resolvida pelo método das linhas. Para a simulação, foi considerado como caso de estudo o processamento de três resíduos da destilação atmosférica dos petróleos “W”, “Y” e “Z” (ATR-W, ATR-Y e ATR-Z, respectivamente) $673,15\text{ K}^+$, em um destilador molecular centrífugo aquecido, onde a superfície do evaporador constitui uma superfície cônica. Os resíduos atmosféricos foram dividido em 25 pseudo-componentes, os quais foram caracterizados, em cada caso de estudo, utilizando dados de propriedades físico-químicas geradas pelo simulador desenvolvido por Tovar et al. (2011). Os resultados provenientes deste estudo permitirão estabelecer apropriadas condições operacionais para a condução de experimentos visando, com isso à obtenção de um alto desempenho operacional do equipamento e um melhor rendimento da separação. Foram realizados experimentos de destilação molecular com o objetivo de validar a ferramenta computacional das simulações. Os experimentos foram definidos a partir de um planejamento de dois níveis do tipo composto central rotacional, onde as variáveis de entrada ou independentes para a análise foram: a vazão da alimentação ($1,473 - 4,418\text{ kg}\cdot\text{h}^{-1}$) e a temperatura do evaporador ou temperatura da destilação ($423,15\text{ K} - 603,15\text{ K}$). Como variável resposta do planejamento foi considerada o rendimento do destilado. Variáveis operacionais de entrada (como a agitação na alimentação, a temperatura do condensador e as temperaturas das linhas de destilado e do resíduo) foram consideradas constantes no planejamento, pois, estas

variáveis não desempenham um efeito significativo sobre a variável rendimento de destilado (Sbaite, 2005; Winter, 2007).

6.2. Desenvolvimento

O desenvolvimento deste capítulo é apresentado a seguir, nos manuscritos intitulados:

- *Computational framework for the modeling and simulation of a centrifugal molecular distillation process for Brazilian high-boiling-point petroleum fractions (petroleum residues): Analysis of the parametric sensitivity of the process*, a ser submetido no periódico internacional *Chemical Engineering Science*.
- *Reliability-based optimization using surface response methodology to split heavy petroleum fractions by centrifugal molecular distillation process*, a ser publicado no periódico internacional *Separation Science and Technology* (aceptado para publicação em 23 de Novembro de 2011, doi: 10.1080/01496395.2011.644612).

Computational framework for the modeling and simulation of a centrifugal molecular distillation process for Brazilian high-boiling-point petroleum fractions (petroleum residues): Analysis of the parametric sensitivity of the process

Abstract

In the case of liquids with low vapor pressure and high molar mass, the molecular distillation process presents significant advantages by working in high vacuum and short exposure of distilled liquid to elevated temperatures. This study intends to expand the understanding of the mechanism of liquid film flowing and evaporating over the evaporator surface of a centrifugal molecular distiller. A theoretical and mathematical description of the liquid-phase transfer processes in centrifugal molecular distillation is presented for three (03) high-boiling-point petroleum fractions divided into twenty five (25) pseudocomponents. The thin liquid film over conical evaporator surface is modeled by the mass, momentum, and energy balance equations. The theoretical analyses are based on the Langmuir–Knudsen equation derived from the kinetic theory of the ideal gas to describe the effective evaporation rate. The equations are included in a computational framework for solving by the method of lines. The simulations were carried out at the steady-state setting conditions, where the effects of the process variables such as the evaporator temperature, the feed flow rate, the rotor speed and the pressure system upon the distillation rates, liquid film profile temperature, effective evaporation rate and film liquid thickness were computed and discussed. The procedure made possible to relate operating conditions and to determine profiles of surface temperature, total distillate flow rate and liquid film thickness. The results presented that the inlet parameters influence significantly the output variables. It was shown that the temperature profiles change sharply through the layer next to the evaporator surface. Along the length of the conical evaporator (radius), the temperature profile inner the liquid film on evaporator surface reached an asymptotic temperature in relaxation length behavior as evaporator temperature increases. Therefore, the effective evaporation rate and consequently the distillate flow rate increase as well.

Keywords: Centrifugal molecular distillation, computational environment in FORTRAN, Physical modeling, simulation, heavy petroleum fractions.

Contents

1. Introduction
 - 1.1. Overview of centrifugal molecular distillation modeling
 - 1.2. Centrifugal molecular distillation description
 2. Physical modeling and governing equations
 - 2.1. Mathematical description
 - 2.2. Dimensionless governing equations
 - 2.2.1. Pseudoanalytical approximate solution
 - 2.3. Physical modeling
 3. Computational framework
 4. Results and discussion
 - 4.1. Effect of EVT on output variables
 - 4.2. Effect of Q on output variables
 - 4.3. Effect of RS on output variables
 5. Conclusions
- Acknowledgment
Appendix A
Nomenclature
References

1. Introduction

The trend in information about the Hi-Tech thermal processes, as molecular distillation process, over gentle separation process of thermally unstable mixtures, liquids with low vapor pressure and high molar mass, is very interesting due to the significant potential in processing the materials and in obtaining products with many advantages.

During the molecular distillation process, the distilled liquid flows over the heated evaporator surface along the characteristic distance (the radial length in centrifugal molecular distillation or the length along the cylinder in falling film molecular distillation processes). Therefore, the molecular distillation process must be satisfying the following statements: (i) the pressure system must be sufficiently low; (ii) the mean free path of molecules must be comparable to the size of the equipment (distillation gap) and, (iii) the condenser temperature must be lower than the evaporator temperature. Consequently, evaporated molecules can pass through the unobstructed distillation gap to the condenser surface without thermal hazard at a reduced distillation temperature, and with short residence time of the distilled liquid on the heated surface (Lutišan et al., 2002).

Moreover, the molecular distillation process performance requires the information about the thin liquid film related to the temperature profile (T_s), the velocity profile (v_r) and the film thickness (δ) to determine yield and purity of the distilled product as a function of inlet parameters such as evaporator temperature (EVT), feed flow rate (Q), rotor speed (RS), pressure system (P_s) as described in Sales–Cruz and Gani (2006). Therefore, the development of a mathematical model of the molecular distillation process is important to characterize the liquid film on evaporator surface at high vacuum conditions and to describe the separation process efficiency through the film profiles. Several studies have presented the modeling of a molecular distillation process using two equipment configurations: falling molecular distiller and / or centrifugal molecular distiller. Most of the developed models have been reported for binary mixtures, based on mass, momentum and energy balance equations. Other works have concentrated on specific design issues such residence time, feed temperature, and anisotropic properties of the vapor phase, as it is presented in Table 1.

Table 1. Summary of researches developed on the modeling of molecular distillation process.

Source	System	Equation type	Equipment type
Zuñiga-Liñan et al., 2011	Heavy petroleum cuts	Energy and material balances	FFMD
Sales-Cruz and Gani, 2006	Glycerol and caprylic esters in the form of caprylic mono-, di- and triglycerides	Energy and material balances	FFMD
Shao et al., 2007	DBP–DBS	Navier–Stokes equations and balance equations	FFMD
Batistella et al., 2006	Carotenoids recovery from palm oil	Energy and material balances	CMD
Xubin et al., 2005	EHP–EHS	Energy and material balances	FFMD
Xiang and Xu, 2005	NA	Computational fluid dynamics (Continuous and momentum equations)	FFMD
Martinello et al., 2003	Glycerine – propyleneglycol	Energy and material balances	FFMD
Kawala and Dakiniewicz, 2002	DBP–DBS	Distribution of temperature in the distillate and Langmuir equation	CMD
Lutišan et al., 2002	EHP–EHS	Energy and material balances	FFMD
Cvengroš et al., 2001	NA	Residence time distribution	FFMD
Batistella et al., 2000	DBP	Monte Carlo and Boltzmann equation	NA
Cvengroš et al., 2000	DBP	Boltzmann, Navier–stokes and heat balance equations	FFMD
Lutišan et al., 1998	DBP–DBS	Balance equations and Monte Carlo method	FFMD
Nguyen and Goffic, 1997	Ethyl myristate/ethyl palmitate and caprylic acid/lauryl alcohol	Langmuir–Knudsen equation and balance equations	FFMD

Table 1 continued. Summary of researches developed on the modeling of centrifugal molecular distillation process.

Source	System	Equation type	Equipment type
Micov et al., 1997	DBP-DBS	Boltzmann; Navier-Stokes; balance equations and diffusion equation	FFMD
Batistella and Maciel, 1996	DBP-DBS	Energy and material balances	CMD, FFMD
Lutišan and Cvengroš, 1995	DBP	Langmuir-Knudsen equation for rate of molecular evaporation, and no-time-counter direct simulation Monte Carlo method	FFMD, CMD
Badin and Cvengroš, 1992	Glycerol	Navier-Stokes equation	FFMD
Bhandarkar and Ferron, 1991	EHP-EHS and DBP-DBS	Monte Carlo method	NA
Kawala and Stephan, 1989	DBP-DBS	Langmuir-Knudsen equation for rate of molecular evaporation and balance equations	FFMD
Bhandarkar and Ferron, 1988	EHP-EHS	Energy and material balances	CMD
Ferron, 1986		Maxwell-Boltzmann equations	NA
Inuzuka et al., 1986,1989	DBP-EHP-EHS	Energy and material balances	CMD
Kaplon et al., 1986	DBP	Navier-Stokes equation and Langmuir-Knudsen equation	CMD
Bose and Palmer, 1984	EHP-EHS-NOP	Energy and material balances	CMD
Rees, 1980	TDD-PTT	Energy and material balances	CMD
Burrows, 1973	NA	Clausius Clapeyron	NA
Greenberg, 1972	EHP-EHS	Balance equations	CMD

FFMD: Falling film molecular distiller

CMD: Centrifugal molecular distiller

NA: Not available

DBP-DBS: di-butyl-phthalate (DBP) – di-butyl-sebacate (DBS)

EHP-EHS: di-(ethylhexyl)-phthalate (EHP) and di-(ethylhexyl)-sebacate (EHS)

NOP: Normal Octyl

TDD-PTT: Tetraphenyl-dimethyl-disiloxane (TDD) – Pentafenyl-trimethyl-trisiloxane (PTT)

1.1. Overview of centrifugal molecular distillation modeling

Centrifugal molecular distillation (CMD) process constitutes a multivariable process, based on principles of molecular distillation described before, where it is important to define the operating strategy (operating conditions and the interactions among them) focused on the desired products and the high performance operation. Several authors have previously suggested the modeling of the centrifugal molecular distillation process and the description of the liquid-phase transfer processes in high-vacuum condition.

Batistella et al. (2006) based the design of centrifugal molecular distiller with industrial dimensions on the simulation and operational strategy developed for small scale equipment from the results obtained from carotenoids recovery from palm oil system.

Kawala and Dakiniewicz (2002) proposed a design of a evaporator surface based on the theoretical framework of the three major ranges of high-vacuum distillation (molecular distillation, intermediate range and equilibrium distillation) in which the characteristic quantity for each of the ranges was the Knudsen number which expresses a ratio of the mean free path of vapor particles to the distance between the evaporator and the condenser surface.

Batistella and Maciel (1996) suggested a mathematical model for falling film and centrifugal molecular distillers. The equations that characterized both processes were the mass, energy and momentum balances and the Langmuir equation in order to define the rate of evaporation. It was analyzed the effect of operating parameters on the distillation rate. The performance of the processes was analyzed for binary systems (dibutyl-phthalate and dimethyl-sebacate (DBP-DBS)) and they were compared with results presented in Kawala and Stephan (1989).

Bhandarkar and Ferron (1988) presented a theoretical study to the heat and mass transport processes in the liquid over the evaporator surface under high vacuum conditions. Results allowed comparing the geometrical parameters and the inlet variables such EVT and Q . It was presented an extensively discussion about the influence of the material preheated on the performance of the process. The principal assumption in the model was that the evaporation process is independent of the vapor-phase properties and the condenser behavior under high vacuum is highly efficient.

Inuzuka et al. (1986) and Inuzuka et al. (1989) developed a mathematical model of heat and mass transfer in the liquid film on the centrifugal molecular still comparing with the accuracy of approximate solutions with the numerical solutions. The model was based on model suggested by Hinze and Milborn (1950). The validity of the mathematical model was reported in 1989 for the systems DBP-EHP and EHP-EHS under high vacuum conditions (0.1 Pa). Experiments showed good agreements to the numerical solution at evaporator temperature equal to 403 K and 413 K.

Kaplon et al. (1986) presented a model based on balance equations and the Langmuir-Knudsen equation to describe the evaporation rate. The model described the temperature distribution in the liquid evaporating film over the rotating disc in high vacuum condition and allowed to estimate the surface area of disc required to obtain a desired yield of condensate. The

results showed that the distillate flow rate is related to the initial liquid temperature and the feed flow rate.

Bose and Palmer (1984) developed a theoretical model, as a function of process variables, for predicting the separation factor and the evaporation rate of a binary mixture, DBP–DBS, into a partial vacuum taking into account the transport resistances on separation factor. It was also analyzed the coupling between interfacial cooling and surface depletion of the most volatile component. The results showed that the surface depletion is the dominant factor responsible for the reduction in separation factor as the temperature increases.

Rees (1980) suggested a mathematical model based on Emslie et al. (1958) and Greenberg (1972) models and the theoretical evaporation rate described by Langmuir (1916). The mathematical model described that there is a thermal gradient along radial positions to obtain changes in the film thickness and evaporation rate profiles.

In Greenberg (1972) was presented a mathematical model using the approach suggested by Emslie et al. (1958). Result showed that predicted film thickness and thermal gradients were consistent with values reported in Hickman (1944) for the binary system EHP and EHS.

Emslie, et al. (1958) presented a study on a Newtonian liquid fluid over a rotating disk. It was showed that centrifugal force exerted on a fluid liquid film does not disturb the uniformity and it is keeping as a thin layer.

Hinze and Milborn (1950) proposed a model for the radial velocity profile and thickness of the liquid film flowing over a rotating conical surface. It was based on the assumptions that tangential velocity component is very small with respect to the radial component, implying that the path described by liquid film is practically straight and in radial direction.

The present work suggests a theoretical study base on a mathematical centrifugal molecular distillation model that describes the process of the heat and mass transfer in the evaporating liquid film over the evaporator surface from three (03) high-boiling-point petroleum fractions (atmospheric distillation residues named as ATR–W, ATR–Y and ATR–Z) from Brazilian crude oils with different API gravities (16 – 25 °API) that were distilled by conventional atmospheric distillation (ASTM D 2892, 2005).

The effects of operating conditions such as EVT , Q , RS and P_s on the distillate mass flow rate (D), the effective evaporation rate (G_E), the film thickness (δ), the surface temperature (T_s) profiles in the liquid film were investigated and computed along the radial distance (RD). In this regard, it has been defined a model to characterize the steady-state flow over the evaporator surface driven by the rotation of conical surface in a centrifugal molecular distiller. At this time, we focus on the thin liquid film cross-sectional spinning cone as the first solution attempt. The study is expected to provide information on the choice of adequate operation conditions for an outlook work referred to experimental work with a unique chosen system based on availability sample.

1.2. Centrifugal molecular distillation description

The centrifugal molecular distiller consists on a chamber under high vacuum conditions which contains the evaporator surface and condenser surface in which it is formed the evaporating film (Figure 1a). The surfaces are kept at constant evaporator temperature (EVT) and condenser temperature, respectively. In this configuration, it is used close temperature control through thermocouples.

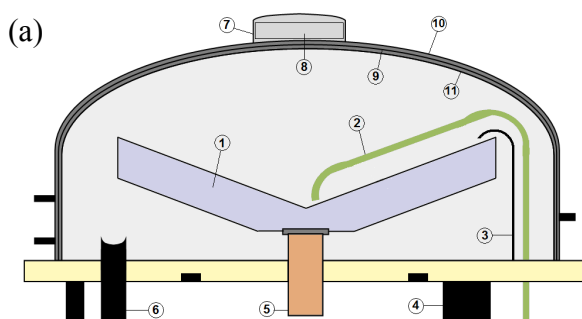


Figure 1a. Simplified scheme of a centrifugal molecular distiller. 1. Evaporator device; 2. Feeding tube; 3. Gutter; 4. Vacuum tube; 5. Axis; 6. Pipe connection; 7. Flange; 8. Viewfinder; 9. Dome camera; 10. Cooling camera; 11. Dome.

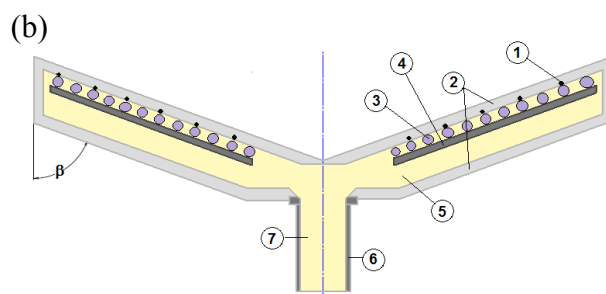


Figure 1b. Schematic diagram of evaporator surface. 1. Thermocouple; 2. Evaporator surface; 3. Electrical resistance; 4. Support resistance; 5. Region of electrical cables and thermocouples; 6. Axis; and 7. Shaft hole.

The load fed to be processed is pumped into the center of the heated rotating evaporator surface housed in a vacuum chamber (Figure 1b). The feed material is spread due to the centrifugal force forming a thin liquid film along the evaporator in radial direction. Thus, the film thickness profile of the most volatile compound or compounds (pseudocomponents) decrease monotonically in the same direction to attain a minimum value for the film thickness as the

surface temperature profile increases. The lighter fraction (the most volatile compound or compounds) of the load leaves from the heated surface, evaporates, and reaches the cooled surface (condenser surface) and condenses, which constitutes the distillate stream. Meanwhile, the heavier fraction or unevaporated molecules goes off the chamber into a collecting vessel called the residue stream. In this instance, the objective of the molecular distillation process has been reached.

2. Physical modeling and governing equations

In Figure 2 the flow over the evaporator surface is presented where the coordinate s instead of θ is introduced as follows:

$$-ds = r d\theta \quad (1)$$

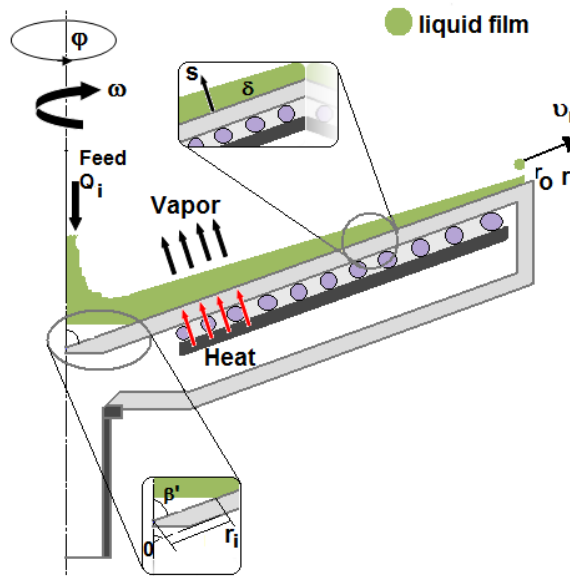


Figure 2. Sketch of the evaporator surface and its coordinate system.

2.1. Mathematical description

The model developed by Inuzuka et al. (1986), Inuzuka et al. (1989) and Batistella and Maciel (1996) has been taken for developing a generalized two-dimensional steady state model for centrifugal molecular distillation process following the above assumptions:

- Spherical coordinates system is well-matched to the developed model.
- The CMD process is in steady state.

- The liquid film over the evaporator surface is considered to be incompressible, uniformly distributed and the film thickness is much smaller than the radius of the conical surface.
- It is assumed Newtonian fluid and the flow over the evaporator surface is in laminar regime.
- Re-evaporation, splashing phenomena and diffusional process in θ -direction are neglected (Sales-Cruz and Gani, 2006).
- Gravitational force is negligibly in comparison with the centrifugal force.
- The conical surface rotates at a fixed angular velocity ω . Velocity components (in θ -direction and φ -directions, respectively) are neglected when compared with the radial velocity component (in r -direction).
- Thermophysical properties (specific heat capacity, thermal conductivity, kinematic viscosity, vapor pressure, effective evaporation rate and evaporation enthalpy are function of the EVT (at evaporator wall) and surface temperature (T_s) profile inner the thin liquid film.

Based on the above assumptions the mass, momentum and energy balances, the mathematical model is described next.

Momentum balance

A momentum balance is used below to derive a general differential equation that can be then employed to solve thin film flowing over conical evaporator surface in spherical coordinates. For this, an incompressible liquid film fluid in laminar regime inner a system of radial length, which is at an angle β' to the vertical, is considered (Figure 2).

The continuity equation can be written as follows:

$$\rho \frac{d\dot{Q}}{dr} + 2\pi r G_E (\sin \beta') = 0 \quad (2)$$

The velocity profile in the liquid film is assumed to be fully developed on the rotating evaporator surface, as presented by Hinze and Milborn (1950) and Inuzuka et al. (1986).

$$\mu \frac{\partial^2 v_r}{\partial s^2} + \rho (\sin^2 \beta') r \omega^2 = 0 \quad (3)$$

The boundary conditions for \dot{Q} and v_r are given as:

$$\dot{Q} = \dot{Q}_i \quad \text{At} \quad r = r_i \quad (4)$$

$$v_r = 0 \quad \text{At} \quad s = 0 \quad \text{At wall} \quad (5)$$

$$\frac{\partial v_r}{\partial s} = 0 \quad \text{At} \quad s = \delta(s) \quad \text{At free surface} \quad (6)$$

The volumetric flow rate \dot{Q} is related to the thickness of liquid film δ , as described by Inuzuka et al. (1986):

$$\dot{Q} = \int_0^\delta 2\pi r v_r (\sin \beta') ds \quad (7)$$

Mathematically, taking into account the velocity profile in the liquid film expressed by Equation (3) and from integration of Equation (7) it is possible to obtain an expression for determining the velocity profile as a function of thickness of liquid film in s -direction as follows:

$$v_r = \frac{\omega^2 \sin^2 \beta'}{\nu} r \left(\delta s - \frac{s^2}{2} \right) \quad (8)$$

Effective evaporation rate

The effective evaporation rate (G_E) is calculated through a modified Langmuir–Knudsen equation described by Equation (9) (Tovar, 2012; Kawala and Dakiniewicz, 2002; Kawala and Stephan, 1989; Langmuir, 1913; Lutišan et al., 2002):

$$G_E = \left(P_{vap} \sqrt{\frac{M}{2\pi R T_s}} \right) \left[1 - \left(1 - \left(\frac{d_e - 2L}{2d_e - 2L} \right) \right) (1 - e^{k^* Kn})^{n'} \right] \quad (9)$$

Where, P_{vap} is the equilibrium vapor pressure at absolute temperature T_s , M is the mass molar of the compound, Kn is the Knudsen defined as a ratio of the mean free path (MFP) of vapor phase to the characteristic length ($L=0.08$ m), R is the universal gas constant and n' represents the number of intermolecular collisions before the vapor reaches isotropic state ($n'=5$) (Kawala and Stephan, 1989) and the degree of anisotropy k^* of the vapor phase in the space between the evaporator and the condenser is given by (Kawala and Dakiniewicz, 2002):

$$\log k^* = 0.2 \left[\frac{d_e - 2L}{2d_e - 2L} \right] + 1.38 \left[\left(\frac{d_e - 2L}{2d_e - 2L} \right) + 0.1 \right]^4 \quad (10)$$

Where d_e is the diameter of evaporation surface curvature and L is the distance between the evaporator and the condenser (equals 0.08 m). Hence, the effective evaporation rate surface takes into account the anisotropic effect of the vapor phase.

The mean free path (MFP) is defined as (Lutišan and Cvengroš, 1995):

$$MFP = \frac{1}{\sqrt{2}\pi\sigma^2 N_m} \quad (11)$$

$$\text{Where, } N_m = \frac{N_A P_s}{RT} \quad (12,13)$$

$$\sigma = 8.09 \times 10^{-11} V_c^{1/3} \quad (\text{Poling et al., 2004})$$

Where MFP is the mean free path (m); σ is the molecule diameter (m); N_m is the number density – number of molecules per unit volume of vapor phase (m^{-3}); R is the universal gas constant ($8.314 \text{ J}\cdot\text{K}^{-1}\cdot\text{mol}^{-1}$); N_A is the Avogadro constant ($6.023 \times 10^{23} \text{ mol}^{-1}$); T is the temperature (or evaporator temperature) (K); P_s is the pressure system (Pa); V_c is the critical volume ($\text{cm}^3 \cdot \text{mol}^{-1}$) and σ is the molecule diameter (m).

Thermal energy balance

The thermal balance in an element of the thin liquid film on the evaporator surface is written with the equation of conservation of energy as (Inuzuka et al., 1986):

$$\frac{d}{dr} \int_0^\delta \rho C_p r v_r T (\sin \beta') ds = \sin \beta' [q_w - (\Delta H + C_p T_s) G_E] r \quad (14)$$

With the follows boundary conditions:

$$T = T_i \quad \text{at} \quad r = r_i \text{ and } 0 \leq s \leq \delta \quad (15)$$

$$-\lambda \frac{\partial T}{\partial s} = q_w = \text{const} \quad \text{at} \quad r_i \leq r \leq r_o \text{ and } s = 0 \quad (16)$$

$$-\lambda \frac{\partial T}{\partial s} = \Delta H G_E \quad \text{at} \quad r_i \leq r \leq r_o \text{ and } s = \delta \quad (17)$$

Film thickness

Substituting Equation (8) into volumetric flow rate equation (Equation 7) and solving the continuity equation with corresponding boundary conditions (Equation 2), the film thickness is given as expression from Equation (18) (Inuzuka et al., 1986):

$$\delta = \left[\frac{3\nu}{2\pi\omega^2 r^2 (\sin^3 \beta')} \left(\dot{Q}_i - \frac{1}{\rho} \int_{r_i}^r 2\pi r G_E (\sin \beta') dr \right) \right]^{1/3} \quad (18)$$

2.2. Dimensionless governing equations

Dimensionless form of above equations is more convenient to identify a group of dimensionless variables which affect the performance of the process. Hence, it is introduced characteristic quantities as listed in Equations (19) – (31), where superscript asterisk stands for corresponding dimensionless parameters (Inuzuka et al., 1986).

$$\xi = \frac{S}{\delta} \quad (19)$$

$$r^* = \frac{r}{r_i} \quad (20)$$

$$\delta^* = \frac{\delta}{\delta_i} \quad (21)$$

$$T^* = \frac{T}{T_i} \quad (22)$$

$$\nu_r^* = \frac{\nu}{\omega^2 (\sin^2 \beta') r_i \delta_i^2} \nu_r \quad (23)$$

$$G_E^* = \frac{G_E}{P_{vap(T_i)} \sqrt{\frac{M}{2\pi R T_i}}} \quad (24)$$

$$D^* = (\sin \beta') G_{E_i}^+ \int_1^{r^*} r^* G_E^* dr^* \quad (25)$$

The dimensionless parameter used in dimensionless model and are listed below (Inuzuka et al., 1986):

$$G_{E_i}^+ = \frac{P_{vap}}{\rho [\omega \nu]^{1/2} (\sin^2 \beta')} \sqrt{\frac{M}{2\pi R T_i}} \quad (26)$$

$$\dot{Q}_i^+ = \frac{\dot{Q}_i}{2\pi (r_i \sin \beta')^2 [\omega \nu]^{1/2}} \quad (27)$$

$$\delta_i^+ = \delta_i \left(\frac{\omega}{\nu} \right)^{1/2} = \left(\frac{3\dot{Q}_i^+}{\sin \beta'} \right)^{1/3} \quad (28)$$

$$q_w^+ = \frac{q_w}{\rho C_p T_i (\omega \nu)^{1/2} (\sin^2 \beta')} \quad (29)$$

$$\Delta H^+ = \frac{\Delta H}{C_p T_i} \quad (30)$$

$$\text{Pr} = \frac{C_p \mu}{\lambda} \quad (31)$$

Then, dimensionless form Equations (8), (14) and (18) could be stated as (Inuzuka et al., 1986):

$$\nu_r^* = r^* \delta^{*2} \left(\xi - \frac{\xi^2}{2} \right) \quad (32)$$

$$\delta^* = \left(\frac{Q_i^+ - D^*}{Q_i^+} \right)^{1/3} r^{*-2/3} \quad (33)$$

$$\frac{3\dot{Q}_i^+}{\sin \beta'} \frac{d}{dr^*} \left(r^* \delta^{*2} \int_0^1 \nu_r^* T^* d\xi \right) = \left[q_w^* - (\Delta H^+ + T_s^*) G_{E_i}^+ G_E^* \right] r^* \quad (34)$$

with the corresponding boundary conditions

$$\delta^* = 1 \quad \text{at} \quad r^* = 1 \quad (35)$$

$$T^* = 1 \quad \text{at} \quad r^* = 1 \quad \text{and} \quad 0 \leq \xi \leq 1 \quad (36)$$

$$\frac{\partial T^*}{\partial \xi} = -(\sin^2 \beta') q_w^+ \delta_i^+ \text{Pr} \delta^* \quad \text{at} \quad 1 \leq r^* \leq \frac{r_o}{r_i} \quad \text{and} \quad \xi = 0 \quad (37)$$

$$\frac{\partial T^*}{\partial \xi} = -(\sin^2 \beta') \Delta H^+ G_{E_i}^+ \delta_i^+ \text{Pr} G_E^* \delta^* \quad \text{at} \quad 1 \leq r^* \leq \frac{r_o}{r_i} \quad \text{and} \quad \xi = 1 \quad (38)$$

2.2.1. Pseudoanalytical approximate solution

For the temperature profile in the liquid film is assumed fully developed. Inuzuka et al. (1986) proposed a derivation of approximate solutions based on a quadratic equation, which satisfies both boundary conditions of Equations (37) – (38) (Inuzuka et al., 1986).

Thus, Equation (39) gives the final solution of the dimensionless surface temperature profile:

$$\frac{3\dot{Q}_i^+}{\sin \beta'} \frac{d}{dr^*} (r^{*2} \delta^{*3} T_s^*) = \left[q_w^* - (\Delta H^+ + T_s^*) G_{E_i}^+ G_E^* \right] r^* \quad (39)$$

Applying dimensionless forms to Equation (2), the equation for $\frac{dD^*}{dr^*}$ is written as Equation (40):

$$\dot{Q}_i^+ \frac{d(r^{*2} \delta^{*3})}{dr^*} = -\frac{dD^*}{dr^*} = -G_{E_i}^+ G_E^* r^* (\sin \beta') \quad (40)$$

Substituting Equations (33) and (40) into Equation (39) it is possible to obtain a dimensionless temperature profile inner the thin liquid film as:

$$\left(\frac{\dot{Q}_i^+ - D^*}{\sin \beta'} \right) \frac{dT_s^*}{dr^*} = r^* (q_w^+ - \Delta H^+ G_{Et}^+ G_E^*) \quad (41)$$

2.3. Physical modeling

The mathematical model includes mass and heat transfer in the thin liquid film in the centrifugal molecular distillation process under the operating condition such EVT , Q , RS and P_s . In Table 2, it is presented a summarized list of variables and parameter needy in the model.

Table 2. Variables used in mathematical model of centrifugal molecular distillation.

Variable	Type of variable
<i>Constants</i>	
Avogadro Constant	Known
Universal gas constant	Known
Pi	Known
<i>Geometrical parameters</i>	
Evaporator radius	Known /Parameter
Distillation gap	Known /Parameter
Half angle of apex of cone radius	Known /Parameter
<i>Model parameters</i>	
Number of intermolecular collisions	Parameter
Mean free path	Explicit
Distance from apex at which liquid enters cone	Parameter
Diameter of evaporation surface curvature	Parameter
Anisotropy degree of vapor phase	Explicit
Number of molecules per volume unit of vapor phase	Explicit
<i>Physicochemical properties</i>	
Molar mass	Explicit /Parameter
Thermal conductivity	Explicit /Parameter
Specific heat capacity	Explicit /Parameter
Vapor pressure	Explicit /Parameter
Kinematic viscosity	Explicit /Parameter
Dynamic viscosity	Explicit/Parameter
Density	Explicit /Parameter
Heat of evaporation	Explicit /Parameter
<i>Operating condition</i>	
Evaporator temperature	Known/ Parameter
Pressure system	Known/ Parameter
Rotor speed	Known/ Parameter
Feed flow rate	Known/ Parameter
Feed composition of each compound	Known/ Parameter
<i>Output variables</i>	
Temperature profile	Dependent
Velocity profile	Dependent
Distillate flow rate	Dependent
Effective evaporation rate	Dependent
Split ratio	Dependent
Liquid film thickness	Dependent

3. Computational framework

The computational framework allows to know the performance of the centrifugal molecular distillation process, from ATR–W, ATR–Y and ATR–Z, by a parametric sensitivity analysis over the output variables due to changes in operating variables (EVT , Q , RS and P_s) as inlet parameters as shown in Table 3.

Table 3. Parameters and percentage changes of inlet operating conditions.

Parameter	Value			
Distance from apex at which liquid enters cone (r_i)	0.03095 m			
Radial position which liquid leaves (r_o)	0.26620 m			
Half angle of apex of cone radius (β')	70°			
Distance between evaporator and condenser surfaces (L)	0.08 m			
Number of intermolecular collisions before the vapor reaches isotropic state (n')	5			
Feed temperature (T_{feed})	393.15 K			
Sensitivity	Variables			
	EVT (K)	Q (kg·h ⁻¹)	RS (rpm)	P_s (Pa)
-30%	296.21	1.050	700	0.0910
-20%	338.52 ^{††}	1.200	800	0.1040
-10%	380.84	1.350	900	0.1170
-5%	401.99 [†]	1.425	950	0.1235
0%	423.15	1.500	1000	0.1300
+5%	444.31	1.575	1050	0.1235
+10%	465.47	1.650	1100	0.1430
+20%	507.78	1.800	1200	0.1560
+30%	550.10 [‡]	1.950	1300 [*]	0.1690

EVT : Evaporator temperature; Q : Feed flow rate, RS : Rotor speed and P_s : Pressure system.

* For ATR–Y was not possible to simulate above +28% of RS (1280 rpm).

† For ATR–Y was not possible to simulate below -4% of EVT (406.22 K).

‡ For ATR–Z was not possible to simulate above +20% of EVT .

†† For ATR–Z was not possible to simulate above -20% of EVT .

The general framework for the integration of computational approach and analysis of simulation data provided important aspects related to the quality of model, reliability and the most sensitive output variables.

The computational tool was developed in FORTRAN–90 language using Compaq Visual Fortran compiler (professional edition 6.6) and organized in ten (10) environments as presented in Figure 3 and described as follows:

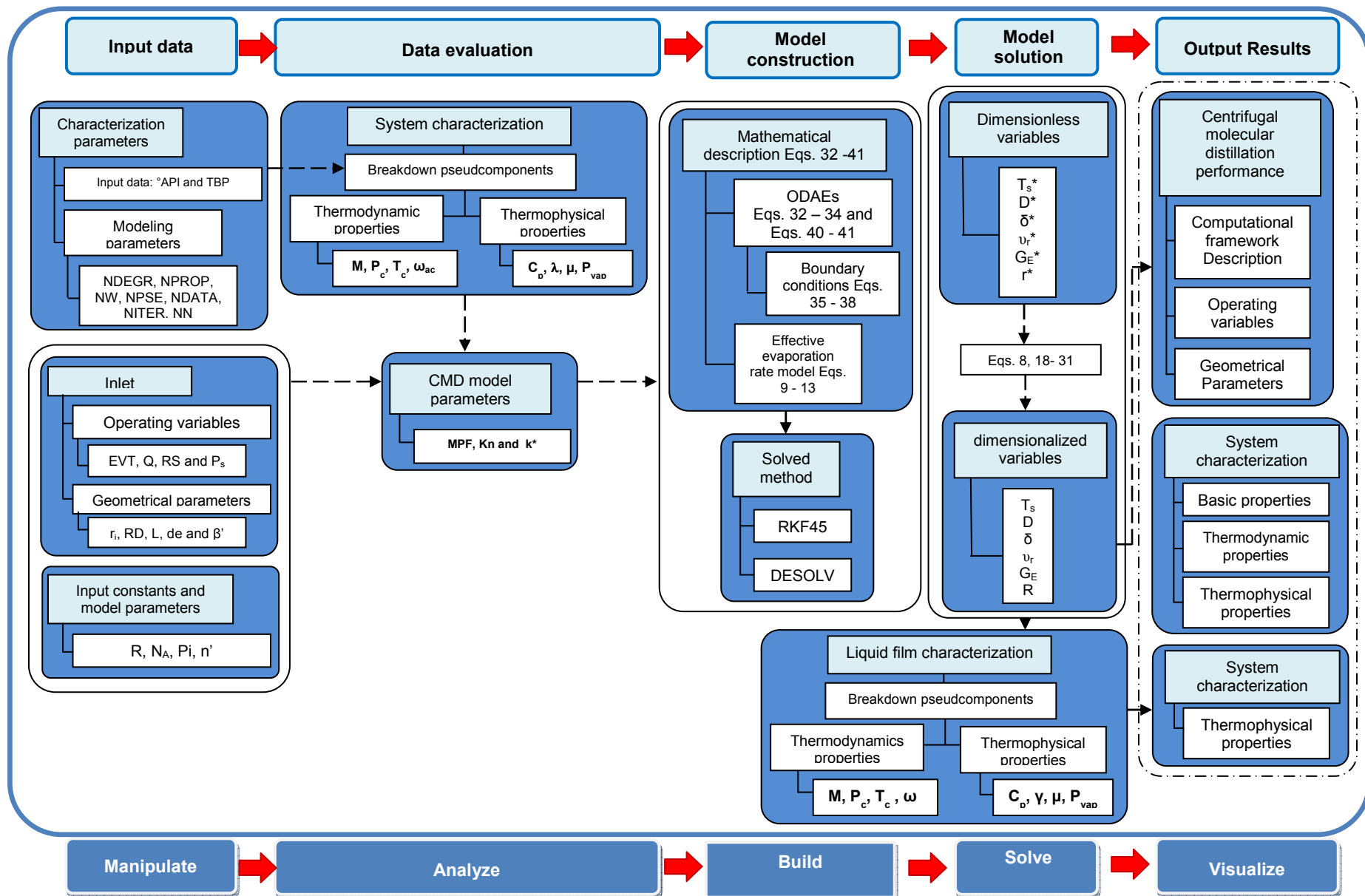


Figure 3. CMD Computational aided environment for numerical approach.

- Input parameters for system characterization: The procedure requires as input bulk properties: Boiling Point distillation curve (BP) and whole-fraction density (Tovar et al., 2011).
- Input parameters for mathematical model: The computational aided requires fixed parameters: The universal gas constant, Avogadro constant and Pi value (π). The geometrical parameters such as evaporator radius ($r_o=0.2662$ m), radial distance from entrance load ($r_i=0.03095$ m), half angle of apex of cone radius ($\beta'=70^\circ$) and distillation gap space ($L=0.08$ m). About process conditions, EVT , Q , RS and P_s are required which play an important role in order to analyze the effect of a percent variation on output variables. Regarding to the specific model parameters is required the number of intermolecular collisions n' equals five (5) defined by Kawala and Stephan (1989).
- Subroutine for physicochemical characterization of load material: It contains three subroutines for estimating the basic properties (normal boiling point, density and Watson factor characterization), the thermodynamic properties (molar mass, density and critical properties) and thermophysical properties (viscosity, thermal conductivity, heat capacity and enthalpy of evaporation) (Tovar et al., 2011).
- Subroutine for modeling centrifugal molecular distillation principles: It is estimated the mean free path (MFP), the effective evaporation rate (G_E), the Knudsen number (Kn) and anisotropic degree of the pseudocomponents (k^*).
- Subroutine for numerical solution of system equations: The partial differential algebraic equations system (PDAEs) comprising the effective evaporation rate model described by Equations (9) – (13), and the momentum, mass and energy balances written by Equations (32) – (38) and Equations (40) – (41). The PDAEs were solved by a computer aided tool with options for analysis of the operating condition, the geometrical parameters, the characterization system parameters and the solution of the mathematical model equations. The goal of the computational framework was to find the numerical solutions to a model with reliable and efficient results. In order to compute a numerical approximation for the solution of the boundary condition problem, a subroutine related to the method of lines was the numerical method for solving PDEs using centered finite difference relationships for the

spatial derivative (Schiesser, 1991). In addition, for the resulting system, it was included the fourth–fifth order Runge–Kutta–Fehlberg (RKF45) subroutine (Mathews and Fink, 2004).

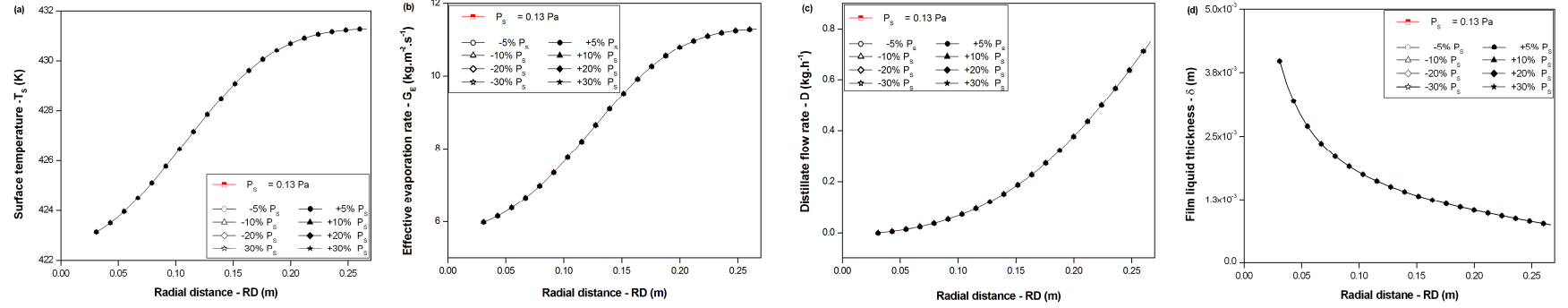
- Subroutine for linking dimensionless parameter with real variables: In dimensional analysis, dimensionless quantities were defined as a product and/or ratio of quantities that might have units individually as written in Equations (19) – (31). The computational aided allowed to carry out percentage changes in the operating variables in order to obtain the resulting variation in dimensionless variables (r^* , T_s^* , D^* , G_E^* and δ^*); and by means of Equations (19) – (31) it was possible to obtain the responses in the output variables T_s , D , G_E and δ as function of RD .
- Subroutine for physicochemical characterization of the thin liquid film: It refers to a subroutine for estimating the thermophysical properties of the thin liquid film over the evaporator surface and distillate stream (reach in volatile compounds) as a function of the T_s as RD increases. The subroutine is based on the code developed in the physicochemical characterization of the loads materials (Tovar et al., 2011).

4. Results and discussion

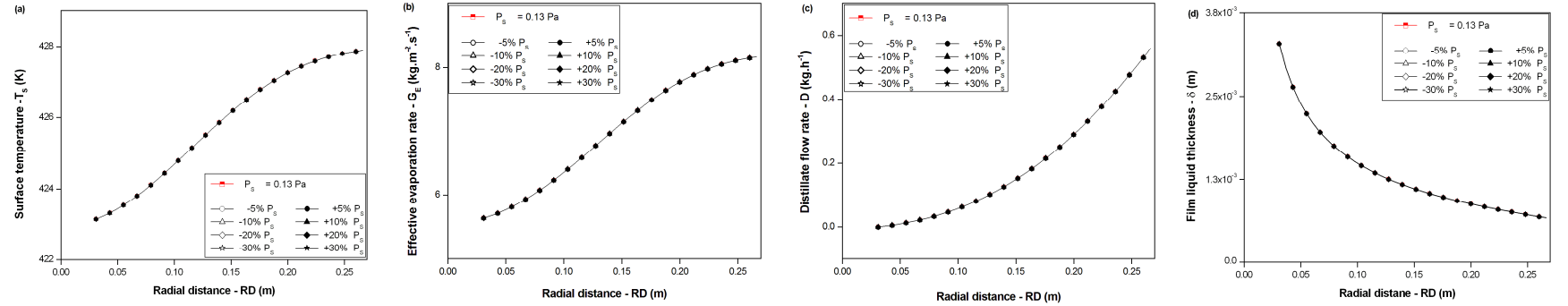
Numerical results of surface temperature (T_s), effective evaporation rate (G_E), distillate flow rate (D) and liquid film thickness (δ) profiles have been analyzed from simulated data obtained with the computational environment through the mathematical model developed by Inuzuka et al. (1986) and modified, using the effective evaporation rate. Therefore, it was adopted for discussing the effect of operating condition on output variables. Typical results from these calculations are presented in Figures 4 – 13 for ATR–W, ATR–Y and ATR–Z as follows.

The centrifugal molecular distillation mathematical model allowed to predict the entire T_s profile along the radial position (RD) showing a continuous variation, which means that the G_E is highly affected by the EVT . However, the effect of P_s was not very noticeable in any of the studied output variables (Figure 4). Nevertheless, from the simulated data it was found that the main operating characteristic was the P_s range from 0.1 to 0.13 Pa. Under these conditions, the volatility of the components increases satisfying the principle of molecular distillation based on the MFP of the evaporating molecules as discussed in Tovar (2012).

ATR-W



ATR-Y



ATR-Z

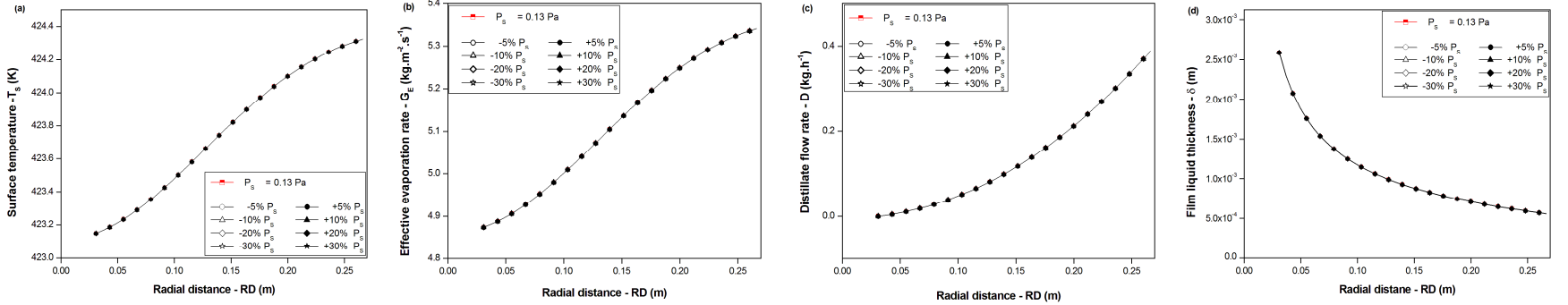


Figure 4. Simulated effect of P_s on T_s , G_E , D and δ at $EVT=423.15$ K, $Q=1.5$ $\text{kg} \cdot \text{h}^{-1}$, and $RS=1000$ rpm.

4.1. Effect of *EVT* on output variables

In Figures 5 – 7, for ATR–W, ATR–Y and ATR–Z, respectively, T_s of the liquid film is shown as a function of the RD along the evaporator surface. As shown in Equation (41), the dimensionless surface temperature is determined by a differential equation of dimensionless parameters T_s^* , which is associated to the fluid properties, geometric parameters and processing conditions. Therefore, once D^* (Equation 40) and T_s^* (Equation 41) were evaluated it was rather simple to determine the T_s of the film by solving the nonlinear Equations (20) – (25).

The *EVT* is the most important governing condition in the evaporating flow, linked with the phenomena related to how fast the front of liquid film flow advances along the evaporator surface and how the fluid flow changes into the vapor state over the evaporator surface.

For the study of the *EVT* effect, it was extensively carried out computational simulations for nine (09) possible combinations of operating conditions in the range of *EVT* at fixed Q , RS and P_s . In Figures 5a , 6a and 7a, considering a reference value of *EVT* equals 423.15 K, if *EVT* increase, the T_s increases along of RD and it approaches to an upper limit value corresponding to the asymptotically behavior; except in cases in which critical operating conditions were found as described later. For ATR–W, the upper values asymptotically reached were 451.88 K (at +5% of *EVT*), 472.35 K (at +10% of *EVT*), 512.65 K (at +20% of *EVT*) and 551.97 K (at +30% of *EVT*) (Figure A1 in appendix A). Whereas, if *EVT* decreases, the T_s profile decreases relatively slowly but keeping the asymptotical tend forward with upper limit as 410.54 K (at –5% of *EVT*), 389.72 K (at –10% of *EVT*), 347.78 K (at -20% of *EVT*) and 305.58 K (at -30% of *EVT*) (Figure A1 in appendix A).

Furthermore, results showed that the radial thermal gradients inner the thin liquid film produced a significantly change in the G_E and D . Figures 5b – 5c, 6b – 6c, and 7b –7c showed that the G_E and D varied strongly after the center of evaporator surface. Based on statements that the G_E is greatly influenced by *EVT*, the concept of relaxation length was applied for understand the effect on this output variable. The relaxation length concept refers to the radial position at which a given parameter (T_s and G_E) reaches asymptotic value (Cvengroš et al., 2000). Therefore, in reference to the G_E at 0.2662 m, for the ATR–W case study, the upper limits were 12.46 kg·m⁻²·s⁻¹ (at +5% of *EVT*), 13.76 kg·m⁻²·s⁻¹ (at +10% of *EVT*), 16.86 kg·m⁻²·s⁻¹ (at +20% of *EVT*) and 21.06 kg·m⁻²·s⁻¹ (at +30% of *EVT*). In contrast, if the *EVT* decreases (in reference to

$EVT=423.15$ K), the G_E of the most volatile pseudocomponents reaches asymptotic values, at relaxation length of 0.2500 m, of $10.22 \text{ kg}\cdot\text{m}^{-2}\cdot\text{s}^{-1}$ (at -5% of EVT), $9.22 \text{ kg}\cdot\text{m}^{-2}\cdot\text{s}^{-1}$ (at -10% of EVT), $7.41 \text{ kg}\cdot\text{m}^{-2}\cdot\text{s}^{-1}$ (at -20% of EVT) and $5.76 \text{ kg}\cdot\text{m}^{-2}\cdot\text{s}^{-1}$ (at -30% of EVT) as shown in Figure 5b.

On the other hand, for ATR–Y and ATR–Z cases studies, it was possible to identify some critical operating conditions for the centrifugal molecular distillation process, where the G_E is not enough for evaporating molecules and the amount of distillate flow rate became insignificant. Thus, when EVT decreases, G_E is lower, regarding to the value at entrance of liquid film on evaporator surface, and G_E reaches lower asymptotic limits (at relaxation length 0.2500 m).

For ATR–Y case study, as shown in Figures 6b, at EVT values higher than 423.15 K, the upper limits of the G_E were: $8.98 \text{ kg}\cdot\text{m}^{-2}\cdot\text{s}^{-1}$ (at +5% of EVT), $10.34 \text{ kg}\cdot\text{m}^{-2}\cdot\text{s}^{-1}$ (at +10% of EVT), $12.98 \text{ kg}\cdot\text{m}^{-2}\cdot\text{s}^{-1}$ (at +20% of EVT) and $13.37 \text{ kg}\cdot\text{m}^{-2}\cdot\text{s}^{-1}$ (at +30% of EVT). On the contrary, if the EVT is lower than 423.15 K, the G_E decreases reaching asymptotic values of $7.17 \text{ kg}\cdot\text{m}^{-2}\cdot\text{s}^{-1}$ (at -5% of EVT) and $6.24 \text{ kg}\cdot\text{m}^{-2}\cdot\text{s}^{-1}$ (at -10% of EVT). For ATR–Z case study (Figure 7b), the upper limits of the G_E were $6.28 \text{ kg}\cdot\text{m}^{-2}\cdot\text{s}^{-1}$ (at +5% of EVT), $7.28 \text{ kg}\cdot\text{m}^{-2}\cdot\text{s}^{-1}$ (at +10% of EVT) and $9.56 \text{ kg}\cdot\text{m}^{-2}\cdot\text{s}^{-1}$ (at +20% of EVT). In contrast, if EVT is lower than 423.15 K, the G_E decreases. Thus, at -5%, -10% and -20% of EVT , the G_E goes from 4.75, 4.63 and $4.41 \text{ kg}\cdot\text{m}^{-2}\cdot\text{s}^{-1}$ (at $RD=0.03095$ m), respectively, to 4.44, 3.56 and $2.36 \text{ kg}\cdot\text{m}^{-2}\cdot\text{s}^{-1}$ (at $RD=0.2662$ m and -5%, -10% and -20% of EVT , respectively). At -30% of EVT , it was not possible to analyze this operating condition due to the fact that the volatile compounds do not attain the enough temperature for evaporating and travels in the distillation gap.

Related to T_s profiles along the evaporator surface, results for ATR–Y in Figure 6a (and in Figure A2 appendix A) and for ATR–Z in Figure 7a (and in Figure A3 appendix A) showed a limiting and critical operating condition, where as EVT decreases, the T_s decreases along of the evaporator surface and it approaches to the lower limit value where the temperature is not enough for evaporating. In consequence, G_E and D of the most volatile compounds become vary slightly along the flow pathway over the evaporator surface.

It was evident that the centrifugal molecular distillation process is strongly influenced by the EVT . Accordingly, as the EVT is raised, G_E and D increase when the amount of the more

volatile component decrease because the molecules move more vigorously and increasing the energy to escape from the evaporator surface and reached the condenser surface. However, the EVT effects on G_E , D and δ at constant Q , RS and P_s allowed bringing to a close that if it is desired to distill more undesired components out, the EVT should be lower. Contrarily, when the distillate flow is desired, the EVT should be appropriately high to prevent more undesired components are distilled, and subsequently, the distillate flow rate is increased.

In Figures 5d, 6d and 7d (for ATR–W, ATR–Y and ATR–Z, respectively) is presented the δ profile for different values of EVT in the range of 296.21 K (-30% of EVT) to 550.10 K (+30% of EVT). The radial distance, RD , is plotted on the abscissa and the film thickness, δ , on the ordinate. It can be seen that the greatest changes in the film thickness profile occurred in the region between 0.03095 m to 0.1500 m corresponding to the entrance section of the feed material and center section of the evaporator surface.

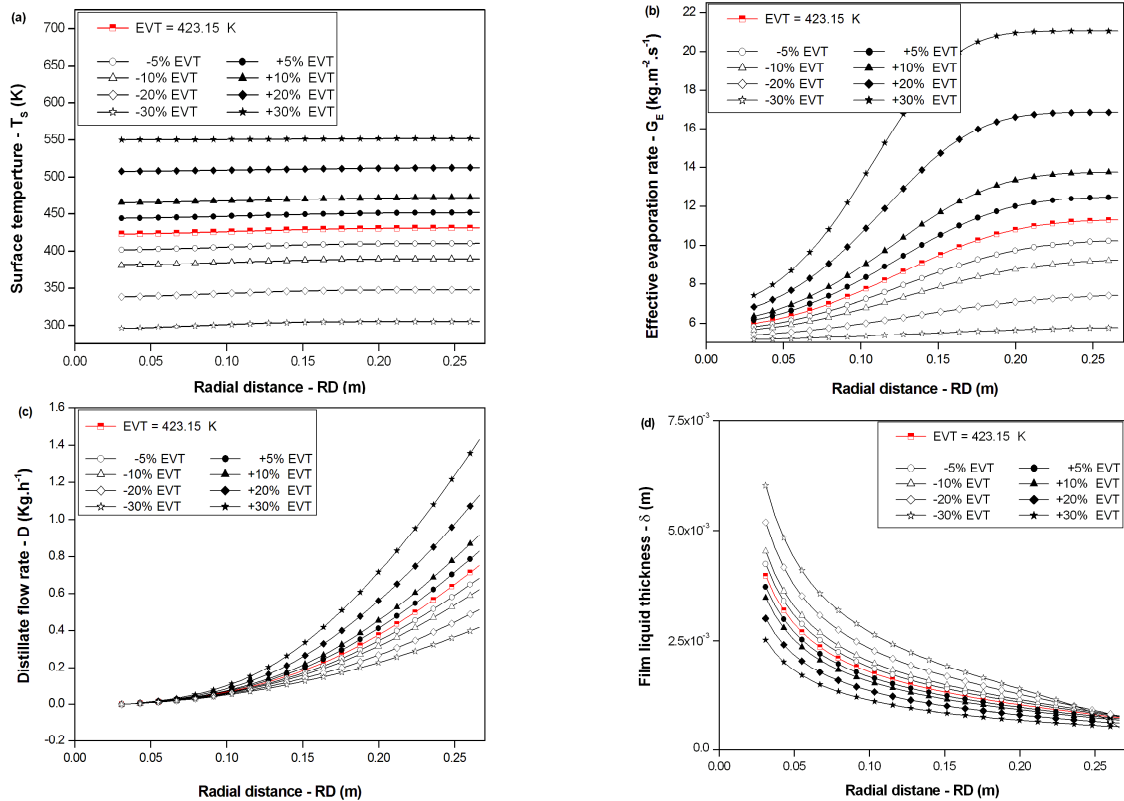


Figure 5. Effect of EVT on: (a) T_s ; (b) G_E ; (c) D , (d) δ at $Q=1.5 \text{ kg} \cdot \text{h}^{-1}$, $RS=1000 \text{ rpm}$ and $P_s=0.13 \text{ Pa}$ during centrifugal molecular distillation process from ATR–W.

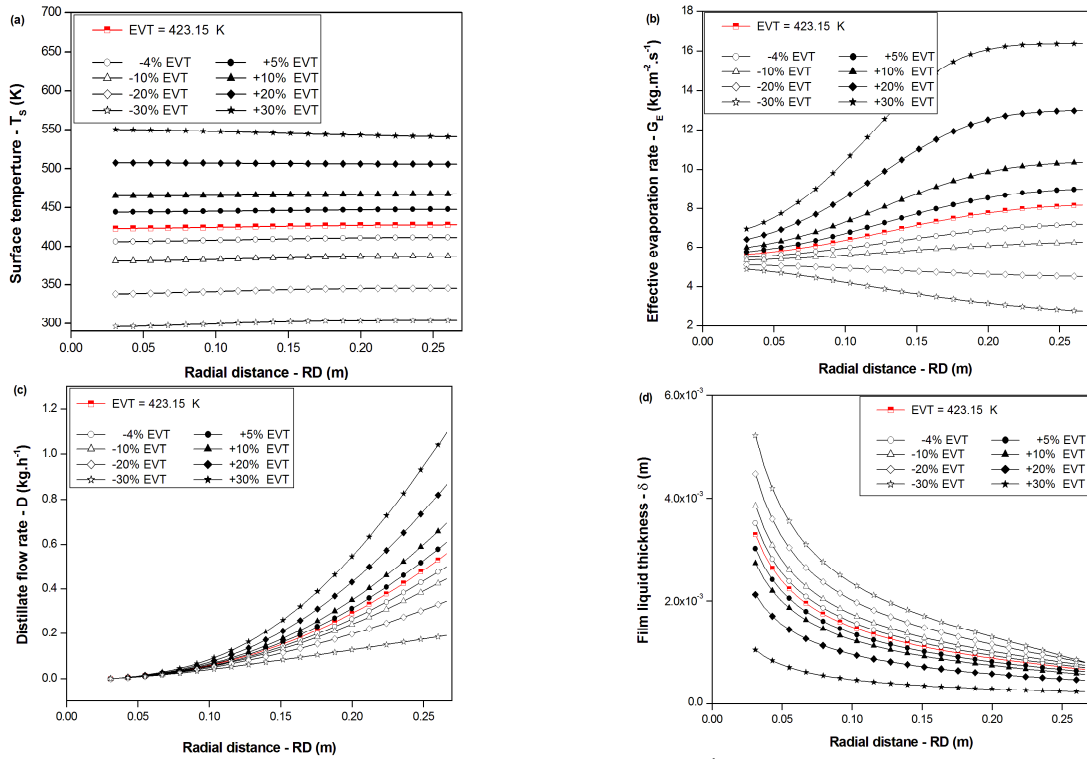


Figure 6. Effect of EVT on: (a) T_s ; (b) G_e ; (c) D ; (d) δ at $Q=1.5 \text{ kg}\cdot\text{h}^{-1}$, $RS=1000 \text{ rpm}$ and $P_s=0.13 \text{ Pa}$ during centrifugal molecular distillation process from ATR-Y.

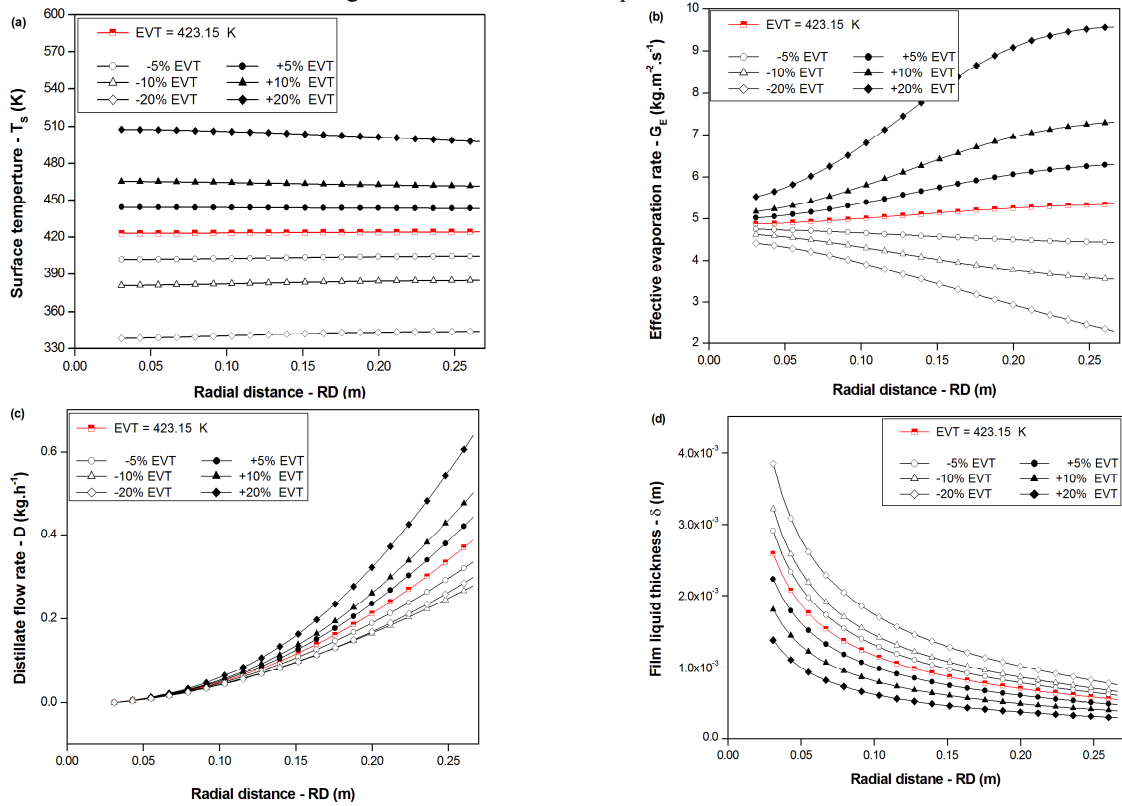


Figure 7. Effect of EVT on: (a) T_s ; (b) G_e ; (c) D ; (d) δ at $Q=1.5 \text{ kg}\cdot\text{h}^{-1}$, $RS=1000 \text{ rpm}$ and $P_s=0.13 \text{ Pa}$ during centrifugal molecular distillation process from ATR-Z.

Analyzing the highest and the lowest conditions of EVT , it was depicted a continuous decrease of the thin liquid film as RD increases as follows: (i) at the highest EVT condition (at +30% of EVT for ATR–W and ATR–Y, and at +20% of EVT for ATR–Z), the δ decreases as RD increases and does so rapidly from 2.52×10^{-3} m to 5.39×10^{-4} for ATR–W, from 1.04×10^{-3} to 2.38×10^{-4} for ATR–Y and from 1.38×10^{-3} to 3.06×10^{-4} for ATR–Z. (ii) When it was considered the lowest EVT condition, (at -30% of EVT for ATR–W and ATR–Y, and at -20% of EVT for ATR–Z), the δ decreases so rapidly from 6.03×10^{-3} m to 7.75×10^{-4} for ATR–W, from 5.23×10^{-3} to 8.04×10^{-4} for ATR–Y and from 3.98×10^{-3} to 8.35×10^{-4} for ATR–Z.

Hence, when a thin liquid film of a multicomponent flows over a heated evaporator surface, under vacuum conditions (i.e. 0.13 Pa), evaporation phenomenon at the free surface, leads to depletion of the most volatile component or components in the liquid phase, forming a thin liquid film that, evenly, might to condense along the condenser surface. As a result, the distillate flow rate increases as consequence of: (i) The elevated film surface temperature; (ii) the decrease of the film thickness on the evaporator surface and, (iii) advantageous operating conditions on the centrifugal molecular distillation process.

4.2. Effect of Q on output variables

In order to provide a qualitative and quantitative physical insight inner the evaporating liquid film over the evaporator surface device, it was extensively performed the parametric studies on the flow behavior in terms of the T_s , G_E , D and δ , as functions of Q at EVT , RS and P_s fixed.

In Figures 8 – 10, the relationship of T_s , G_E , D and δ versus RD is shown with Q as parameter sensitivity. In Figures 8a, 9a and 10a as Q increases, T_s profiles reach asymptotic values in correspondence with the rises of the relaxation length. In the studied range of Q , the temperature difference in the radial direction was very small. These relatively small radial gradients might be ascribed to the low thermal conductivity, about $1.22 \text{ W} \cdot \text{m}^{-1} \cdot \text{K}^{-1}$ for ATR–W, $1.13 \text{ W} \cdot \text{m}^{-1} \cdot \text{K}^{-1}$ for ATR–Y and $0.85 \text{ W} \cdot \text{m}^{-1} \cdot \text{K}^{-1}$ for ATR–Z, to conduct heat transferred from the evaporator surface to the inner of the liquid film.

The slight rise of T_s (Figures 8a, 9a and 10a) and G_E (Figures 8b, 9b and 10b) as Q decreases is related mainly to the good mass transfer over the evaporator surface and,

consequently, to the increase of evaporation of volatile compounds. In addition, the liquid film at lower Q values had lower relaxation length that means, at Q values between $1.000 \text{ kg}\cdot\text{h}^{-1}$ and $1.500 \text{ kg}\cdot\text{h}^{-1}$, the relaxation length was around 0.2000 m ; while at Q values between $1.500 \text{ kg}\cdot\text{h}^{-1}$ and $2.000 \text{ kg}\cdot\text{h}^{-1}$, the relaxation length was around 0.2500 m . Therefore, Q parameter influenced directly on the liquid film thickness and mass transfer, once values of Q lower than $1.000 \text{ kg}\cdot\text{h}^{-1}$ may not be high enough to efficient mass and heat transfers. On the other hand, for Q values higher than $2.000 \text{ kg}\cdot\text{h}^{-1}$, the system might operate with low effectiveness because the residence time of the molecules on the evaporator might be too low.

Figures 8d, 9d and 10d show the development of the δ along the evaporator length in r -direction for various liquid loads. The δ profile was affected by the change of Q condition. Thus, it is noted that lower δ values were reached at low values of Q , which is the same trend as the analyses reported for *EVT* effects, confirming in these conditions, that a uniform thin film promotes high efficiency in the mass and in the energy transfers.

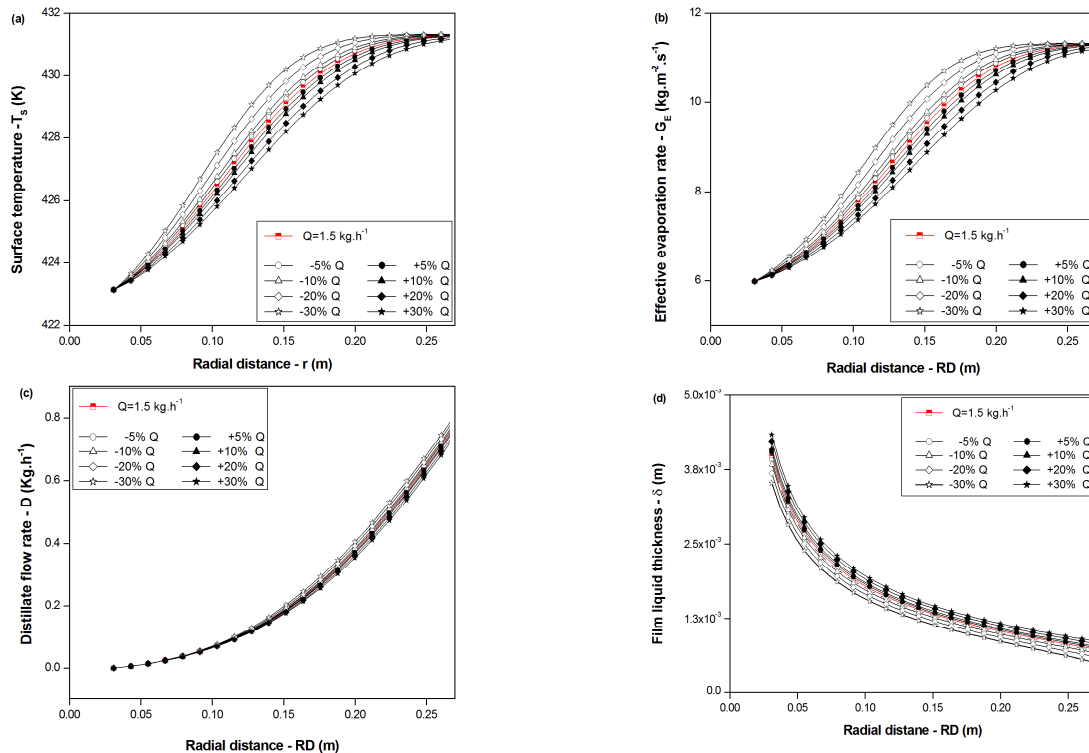


Figure 8. Effect of Q on: (a) T_s ; (b) G_E ; (c) D , (d) δ at $EVT=423.15 \text{ K}$, $RS=1000 \text{ rpm}$ and $P_s=0.13 \text{ Pa}$ during centrifugal molecular distillation process from ATR-W.

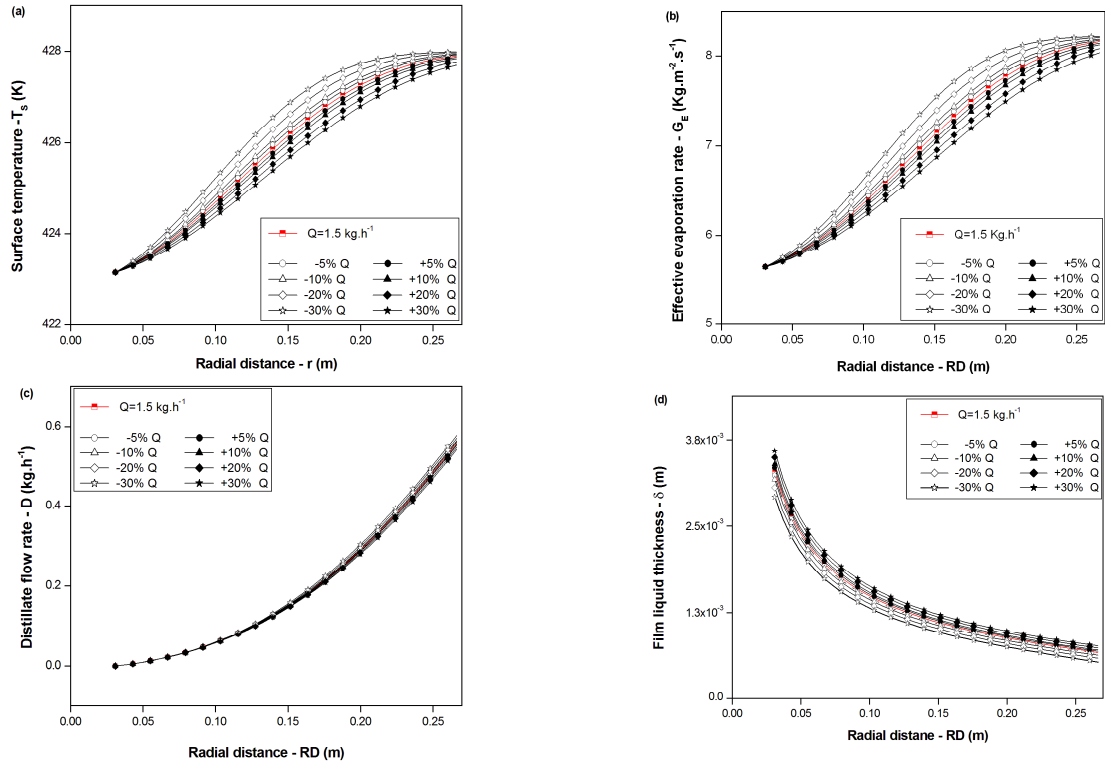


Figure 9. Effect of Q on: (a) T_s ; (b) G_E ; (c) D ; (d) δ at $EVT=423.15 \text{ K}$, $RS=1000 \text{ rpm}$ and $P_s=0.13 \text{ Pa}$ during centrifugal molecular distillation process from ATR-Y.

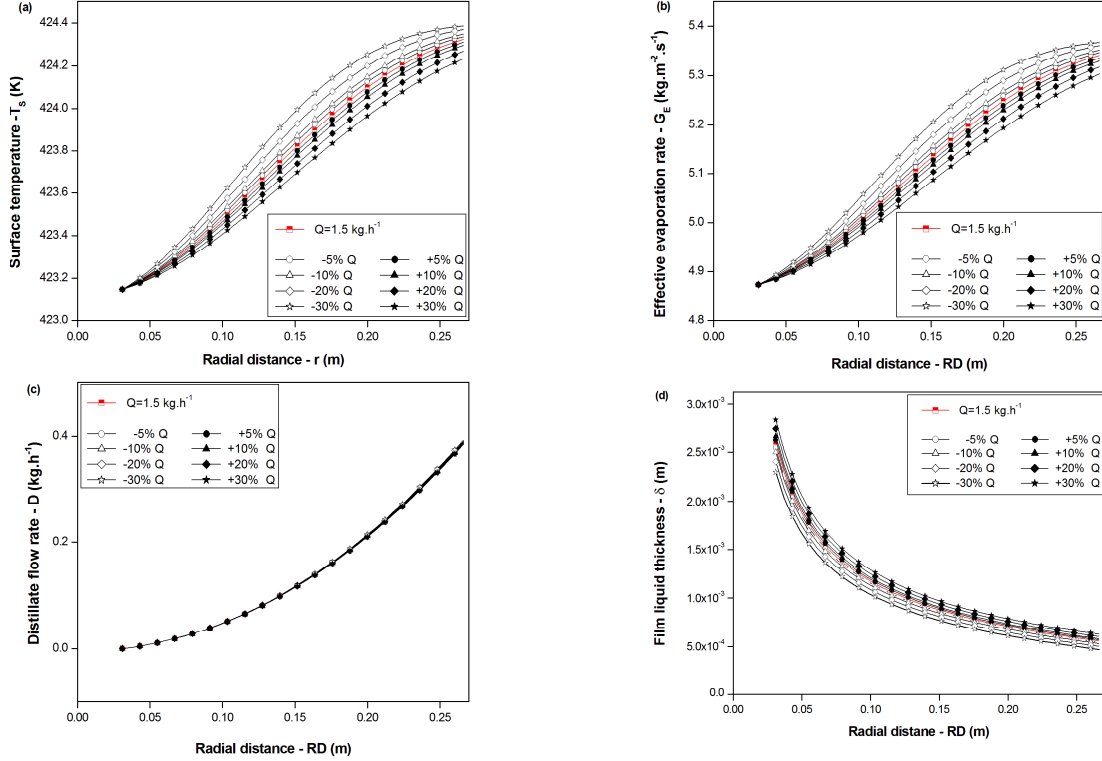


Figure 10. Effect of Q on: (a) T_s ; (b) G_E ; (c) D ; (d) δ at $EVT=423.15 \text{ K}$, $RS=1000 \text{ rpm}$ and $P_s=0.13 \text{ Pa}$ during centrifugal molecular distillation process from ATR-Z.

4.3. Effect of RS on output variables

The aim of this section is to determine the profiles of T_s , G_E , and δ along the RD of the evaporator in dependence on RS parameter at constant EVT , Q and P_s . As mentioned in the analyses of EVT and Q effects, G_E and δ profiles represent the determining factor for the centrifugal molecular distillation process. With respect to the heat transfer, two regions can be elucidated: (i) the temperature profile at the entrance section of conical evaporator surface from 0.03095 m to 0.1000 m and, (ii) a fully developed T_s profile from 0.1000 m to 0.2662 m.

In Figures 11a, 12a and 13a for ATR-W, ATR-Y and ATR-Z, respectively, it can be seen that as the RS increases, the first region presented a uniform T_s profile increasing monotonically with a gradient of $0.05 \text{ K}\cdot\text{m}^{-1}$ to RD about 0.1000 m as RS increases. In the first section, evaporation of liquid was negligible in comparison with the section between 0.100 m and 0.2662 m. In contrast, the second section was characterized by the developed T_s profile inner the liquid film. For high values of RS , G_E increases rapidly and, in consequence, the efficiency of centrifugal molecular distillation process increased exponentially along the RD , resulting in the correspondingly exponential increase of D due to the increase of the induced centrifugal force, which is known as the flow driving force in the system.

Figures 11b, 12b and 13b for ATR-W, ATR-Y and ATR-Z, respectively, show that G_E strongly increases as the RS increases, due to T_s dependence and RS conditions that affected the viscosity of film on evaporator surface. Using the concept to relaxation behavior, different relaxation lengths for G_E were confirmed. Thus, as RS and RD increase, G_E reached asymptotic values in 0.2200 m for ATR-W, 0.2400 m for ATR-Y and 0.2500 m for ATR-Z.

In Figures 11c, 12c and 13c is presented D profiles which are more sensitively affected by the change of RS than Q due to the fact that the RS is proportional to the generated centrifugal force inner the system and, in front of that, the δ profile is affected.

In Figures 11d, 12d and 13d, δ profiles are plotted as a function of RD with RS as parameter. In this sense, when RS increases up to 1300 rpm (+30% of RS), δ of evaporating liquid film decreases and reaches 6.08×10^{-4} m for ATR-W, 5.58×10^{-4} m for ATR-Y and 4.63×10^{-4} m for ATR-Z.

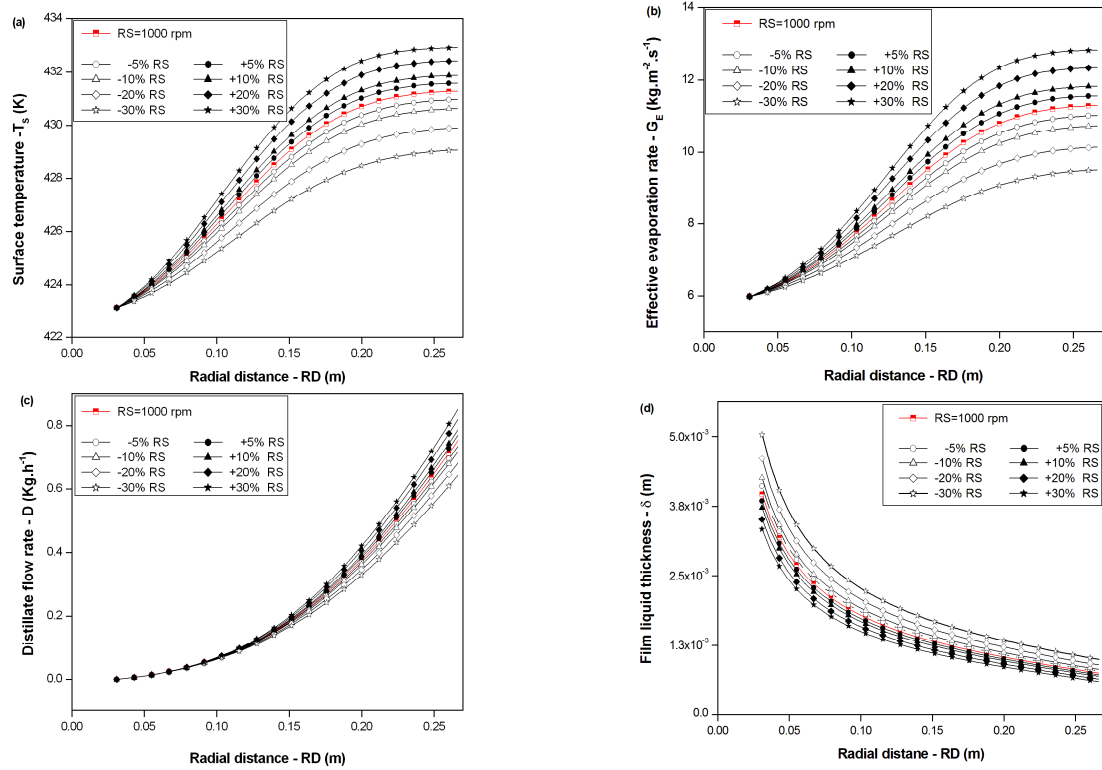


Figure 11. Effect of RS on: (a) T_s ; (b) G_E ; (c) D , (d) δ at $Q=1.5 \text{ kg} \cdot \text{h}^{-1}$, $EVT=423.15 \text{ K}$ and $P_s=0.13 \text{ Pa}$ during centrifugal molecular distillation process from ATR-W.

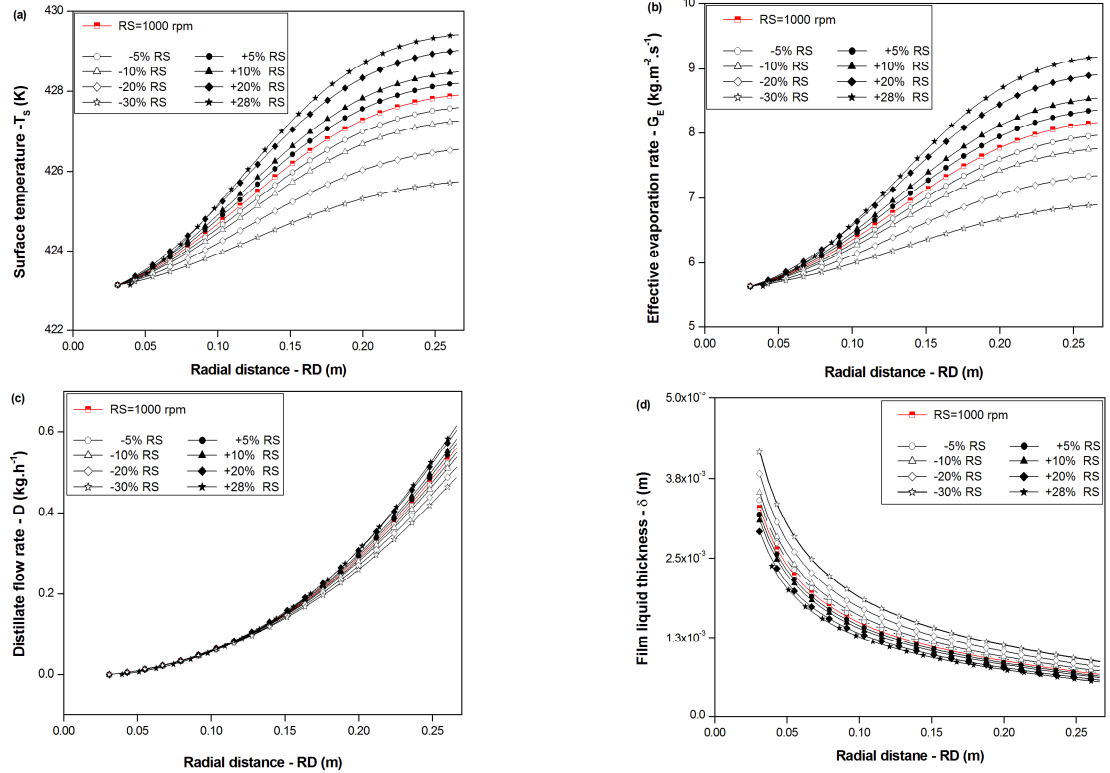


Figure 12. Effect of RS on: (a) T_s ; (b) G_E ; (c) D , (d) δ at $Q=1.5 \text{ kg} \cdot \text{h}^{-1}$, $EVT=423.15 \text{ K}$ and $P_s=0.13 \text{ Pa}$ during centrifugal molecular distillation process from ATR-Y.

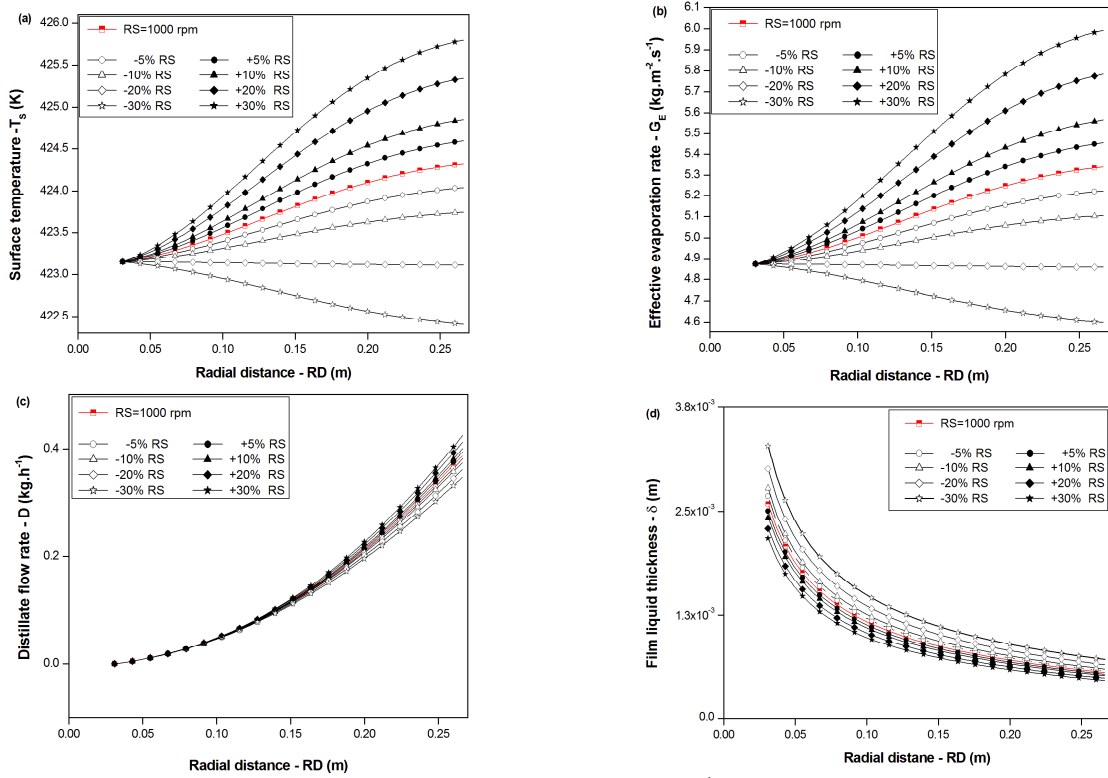


Figure 13. Effect of RS on: (a) T_s ; (b) G_E ; (c) D , (d) δ at $Q=1.5 \text{ kg}\cdot\text{h}^{-1}$, $EVT=423.15 \text{ K}$ and $P_s=0.13 \text{ Pa}$ during centrifugal molecular distillation process from ATR–Z.

Furthermore, the effect of RS showed the existence of large temperature gradients along the evaporator surface, and for this reason, G_E gradients were rather pronounced. Accordingly, the low resistance to mass and heat transfer in the evaporating film is advantageous for the centrifugal molecular distillation process once, the distillate stream, the desired product, apparently increases as RS increases. This engages to the fact that the distillation speed increases when the liquid film over the evaporator surface becomes more uniform when RS is increased ensuring the short residence time of the liquid load over the evaporator surface and the distributing in the form of a thin liquid film.

5. Conclusions

A mathematical model of the thin liquid film flowing over the evaporator surface in the centrifugal molecular distillation process was presented based on the model proposed by Inuzuka et al. (1986) including the modified Knudsen–Langmuir equation for representing the effective evaporation rate. The mathematical description was built up in FORTRAN–90 language using Compaq Visual Fortran compiler (professional edition 6.6) comprising a computational

environment for analyzing the heat and mass transfers in the liquid film of ATR–W, ATR–Y and ATR–Z on the rotating evaporator surface of a centrifugal molecular distiller. Therefore, the mathematical model presented in this work allows a reasonable theoretical approach for prediction of the centrifugal molecular distillation performance from atmospheric petroleum residue.

The computational framework allowed carrying out qualitative and quantitative sensitivity analyses from different operating condition, such as EVT , Q and RS , in percent variation, on output variables such as surface temperature (T_s), distillate flow rate (D), effective evaporation rate (G_E) and film thickness profiles (δ) as a function of radial distance (RD) from the apex of the conical surface to the external distance at which the liquid film is completely evaporated. Hence, it is suggested that the main operating variables for this particular process were EVT and RS , which marked some limiting conditions for carrying out future theoretical and experimental works.

The simulations data reported that the liquid film thickness is affected by the evaporator temperature, rotor speed, liquid viscosity and the difference in temperature between the evaporator wall and the evaporating liquid. Thus, the effectiveness of molecular distillation process from ATR–W, ATR–Y and ATR–Z was evaluated by minimum film thickness, high distillate flow rate and high effective evaporation rate as consequence of the depletion phenomenon of the most volatile compound or compounds (pseudocomponents) and efficient mass and heat transfers inner the evaporating liquid film over the evaporator surface device.

Acknowledgements

This research was supported by the Brazilian National Council for Technological and Scientific Development (CNPq), the Petrobras Research and Development Center (PETROBRAS/CENPES) and the Brazilian Study and Project Financing Institution (FINEP).

Appendix A

Figures A1. A2 and A3, for ATR–W, ATR–Y and ATR–Z, respectively, showed the development of film surface temperature (T_s) as a function of radial position (RD) for different EVT conditions.

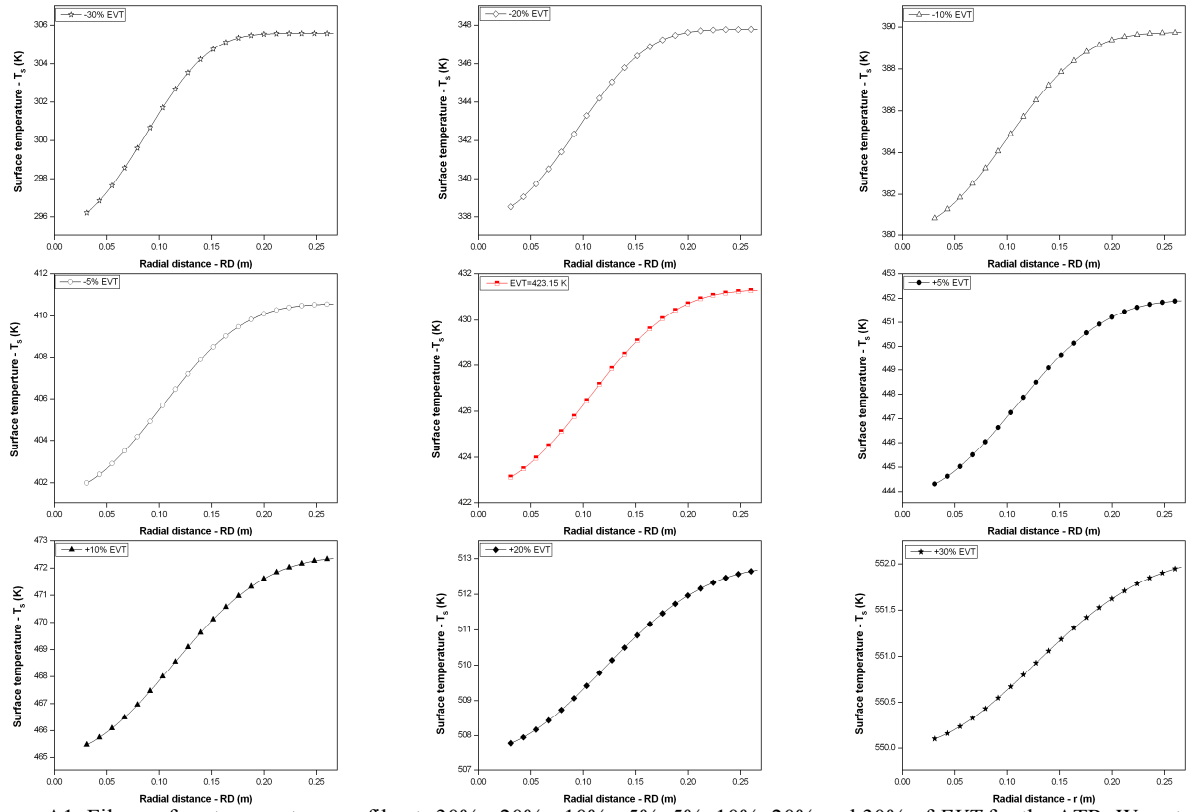


Figure A1. Film surface temperature profile at -30%, -20%, -10%, -5%, 5%, 10%, 20% and 30% of EVT for the ATR-W system.

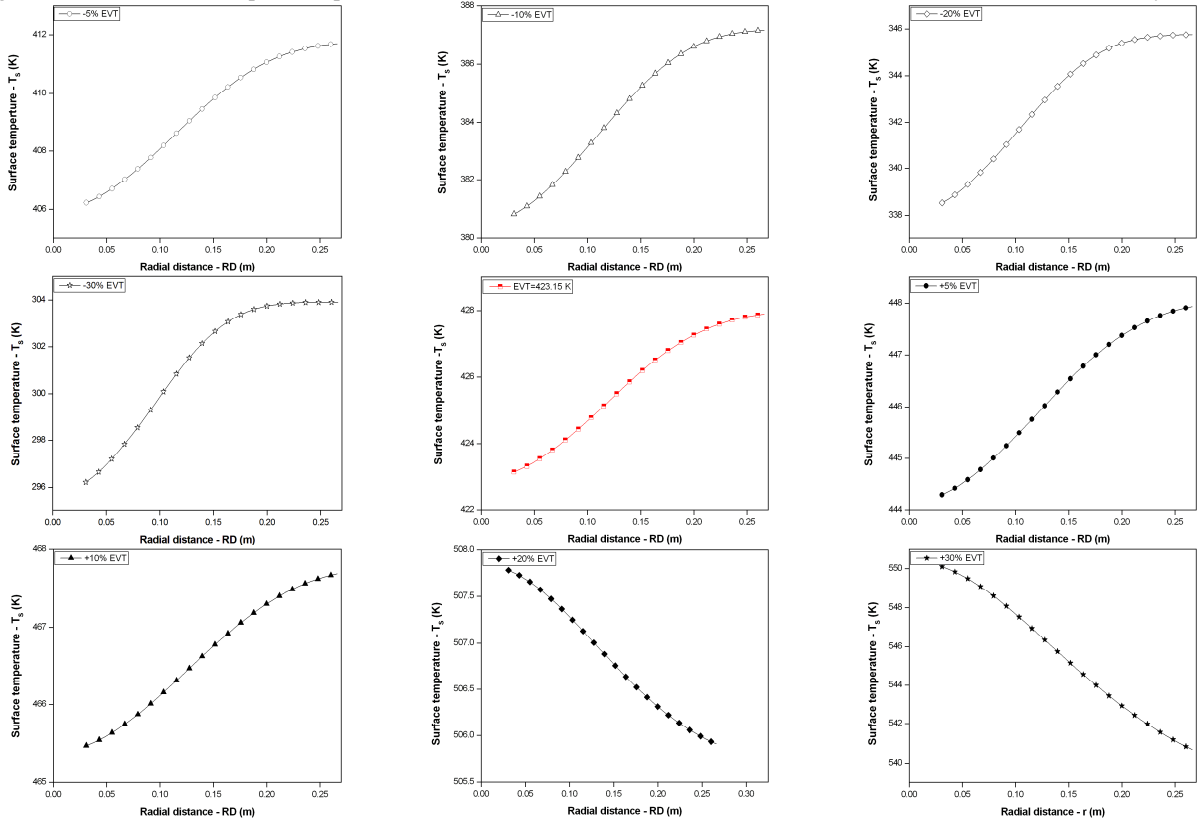


Figure A2. Film surface temperature profile at -30%, -20%, -10%, -4%, 5%, 10%, 20% and 30% of EVT for the ATR-Y system.

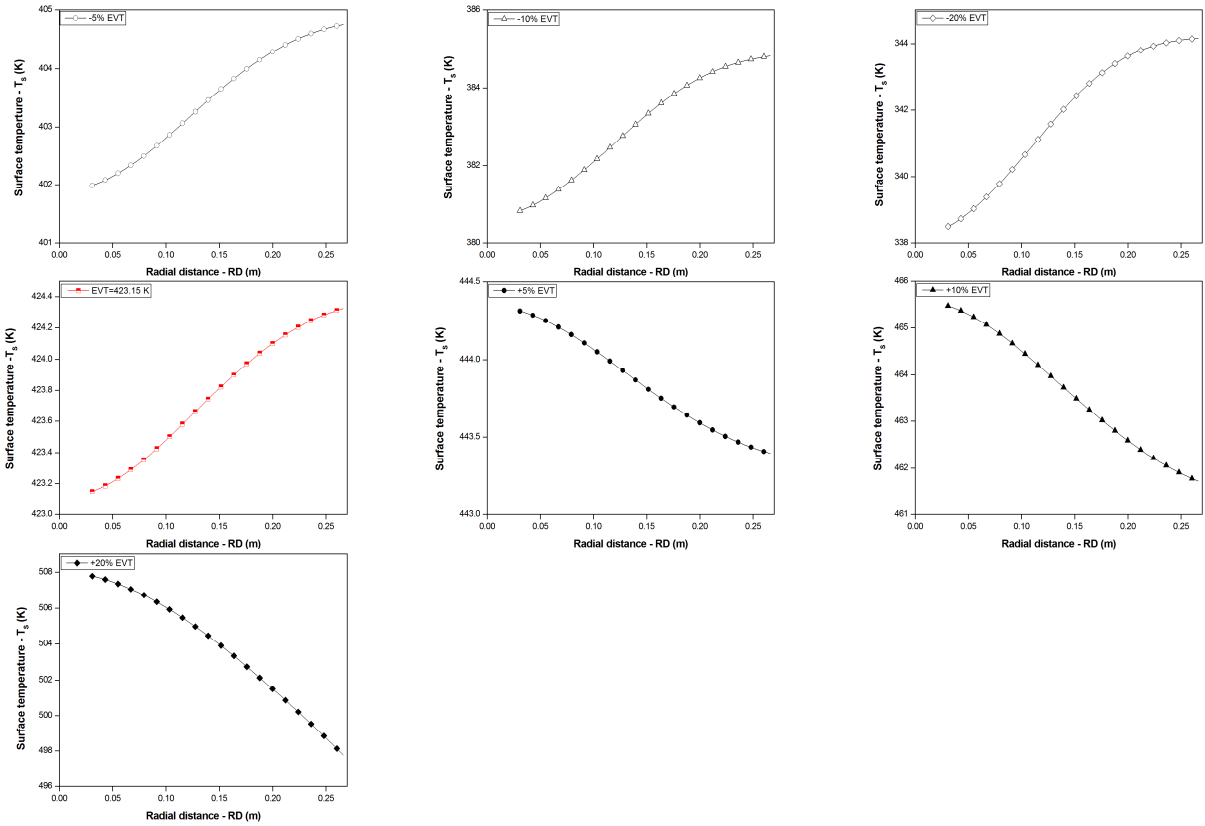


Figure A3. Film surface temperature profile at -30%, -20%, -10%, -5%, 5%, 10%, and 20% of EVT for the ATR-Z system.

Nomenclature

C_p	=	Specific heat capacity	$[\text{J} \cdot \text{kg}^{-1} \cdot \text{K}^{-1}]$
d_e	=	Diameter of evaporation surface curvature	$[\text{m}]$
EVT	=	Evaporator temperature	$[\text{K}]$
G_E	=	Effective evaporation rate	$[\text{kg} \cdot \text{m}^{-2} \cdot \text{s}^{-1}]$
Kn	=	Knudsen number	$[-]$
k^*	=	Anisotropy of vapor phase	$[-]$
L	=	Distance between evaporator and condenser surfaces	$[\text{m}]$
M	=	Molar mass	$[\text{kg} \cdot \text{kmol}^{-1}]$
MFP	=	Mean free path	$[\text{m}]$
n'	=	Number of intermolecular collisions before the vapor reaches isotropic state ($n'=5$)	$[-]$
N_m	=	Number density – number of molecules per unit volume of vapor phase	$[\text{m}^{-3}]$
N_A	=	Avogadro Constant ($6.023 \times 10^{23} \text{ mol}^{-1}$)	$[\text{mol}^{-1}]$
P_s	=	System pressure	$[\text{Pa}]$
Pr	=	Prandtl number	$[-]$
P_{vap}	=	Equilibrium vapor pressure	$[\text{Pa}]$
q_w	=	Heating rate at evaporator wall	$[\text{J} \cdot \text{m}^{-2} \cdot \text{s}^{-1}]$
Q	=	Feed flow rate	$[\text{kg} \cdot \text{h}^{-1}]$
\dot{Q}	=	Volumetric feed flow rate	$[\text{m}^3 \cdot \text{s}^{-1}]$
\dot{Q}_i	=	Volumetric feed flow rate at $r = r_i$	$[\text{m}^3 \cdot \text{s}^{-1}]$

r	=	r – direction of coordinate system	[-]
R	=	Universal gas constant ($8314 \text{ J} \cdot \text{K}^{-1} \cdot \text{kmol}^{-1}$)	$[\text{J} \cdot \text{K}^{-1} \cdot \text{kmol}^{-1}]$
r_i	=	Distance from apex at which liquid enters cone	[m]
r_o	=	Radial position which liquid leaves	
RD	=	Radial distance along evaporator surface	[m]
RS	=	Rotor speed	[rpm]
s	=	s – direction of coordinate system perpendicular to cone surface	[-]
T_s	=	Temperature	[K]
T_s	=	Surface Temperature	[K]
<i>Greek Letter</i>			
β'	=	Half angle of apex of cone radius	[-]
δ	=	Thickness of liquid film	[m]
ΔH	=	Heat of evaporation	$[\text{J} \cdot \text{kg}^{-1}]$
λ	=	Thermal conductivity	$[\text{W} \cdot \text{m}^{-1} \cdot \text{K}^{-1}]$
θ	=	θ – direction of coordinate system	[-]
ρ	=	Average Density and density fraction	$[\text{kg} \cdot \text{m}^{-3}]$
π	=	Pi parameter	[-]
v_r, v_φ, v_θ	=	Thin liquid film velocity in r -, φ – and θ –direction	$[\text{m} \cdot \text{s}^{-1}]$
μ	=	Dynamic viscosity	[Pa.s]
ν	=	Kinematic viscosity	$[\text{m}^2 \cdot \text{s}^{-1}]$
ω	=	Angular velocity of cone	$[\text{s}^{-1}]$
<i>Subscripts</i>			
i	=	inlet	
o	=	Outlet	
E	=	Effective	
<i>Superscripts</i>			
*	=	Dimensionless variable	
+	=	Dimensionless parameter	

References

- American Society for Testing Material, ASTM D 2892. Standard test method for distillation of crude petroleum (15–Theoretical plate column). West Conshohoken, (Pennsylvania): ASTM International, 2005. 32p.
- Badin V., Cvengroš J. (1992) Model of temperature profiles during condensation in a film in a molecular evaporator, *The Chemical Engineering Journal* **49**, 3, 177–180.
- Batistella C. B., Maciel M. R. W. (1996) Modeling, simulation and analysis of molecular distillators: Centrifugal and falling film, *Computers & Chemical Engineering* **20**, supplement 1, S19–S24.
- Batistella C. B., Maciel M. R. W., Maciel Filho R. (2000) Rigorous modeling and simulation of molecular distillators: Development of a simulator under conditions of non ideality of the vapor phase, *Computers & Chemical Engineering* **24**, 2–7, 1309–1315.

- Batistella C. B., Moraes E. B., Maciel Filho R., Wolf-Maciel M. R. (2006) Mathematical development for scaling-up of molecular distillators: Strategy and test with recovering carotenoids from palm oil, *16th European Symposium on Computer Aided Process Engineering*, 1113–1118.
- Bhandarkar M., Ferron J. R. (1991) Simulation of rarefied vapor flows, *Industrial & Engineering Chemistry Research* **30**, 5, 998–1007.
- Bhandarkar M., Ferron J. R. (1988) Transport processes in thin liquid films during high-vacuum distillation, *Industrial & Engineering Chemistry Research* **27**, 6 1016–1024.
- Bose A., Palmer H. J. (1984) Influence of heat and mass transfer resistences on the separation efficiency in molecular distillations, *Industrial & Engineering Chemistry Fundamentals* **23**, 4, 459–465.
- Burrows G. (1973) Notes on some features of high-vacuum distillation, *Vacuum* **23**, 10, 353–358.
- Cvengroš J., Lutišan J., Micov M. (2000) Feed temperature influence on the efficiency of a molecular evaporator, *Chemical Engineering Journal* **78**, 1, 61–67.
- Cvengroš J., Pollák S., Micov M., Lutišan J. (2001) Film wiping in the molecular evaporator, *Chemical Engineering Journal* **81**, 1, 9–14.
- Emslie A. G., Bonner F. T., Peck L. G. (1958) Flow of a viscous liquid on a rotating disk, *Journal of Applied Physics* **29**, 5, 858–862.
- Ferron J. R. (1986) Evaporation and condensation of mixtures under rarefied conditions, *Industrial & Engineering Chemistry Fundamentals* **25**, 4, 594–602.
- Greenberg D. B. (1972) A theoretical and experimental study of the centrifugal molecular still, *AIChE Journal* **18**, 2, 269–276.
- Hickman K. C. D. (1944) High-vacuum Short-path Distillation—A Review, *Chemical Review* **34**, 1, 51–106.
- Hinze J. O., Milborn H. (1950) Atomization of liquid by means of a rotating cup, *Journal of Applied Mechanics* **17**, 2, 145–153.

- Inuzuka M., Sugiyama R., Saito I., Yamada I., Hiraoka S., Ishikawa H., Banno, I. (1986) Analysis of heat and mass transfer in a centrifugal molecular still, *Journal of Chemical Engineering of Japan* **19**, 1, 14–20.
- Inuzuka M., Ishikawa H., Yamada, I., Hiraoka S., Aragaki T., Inukai Y., Erciyes A. T., Kobayashi S. (1989) Vaporization from liquid film of binary mixture in a centrifugal molecular still, *Journal of Chemical Engineering of Japan* **22**, 3, 291–297.
- Kaplon J., Kawala Z., Skoczylas A. (1986) Evaporation rate of a liquid from the surface of a rotating disc in high vacuum, *Chemical Engineering Science* **41**, 3, 519–522.
- Kawala Z., Dakiniewicz P. (2002) Influence of evaporation space geometry on rate of distillation in high–vacuum evaporator, *Separation Science and Technology* **37**, 8, 1877–1895.
- Kawala Z., Stephan K. (1989) Evaporation rate and separation factor of molecular distillation in a falling film apparatus, *Chemical Engineering & Technology* **12**, 1, 406–413.
- Langmuir I. (1916) The characteristics of tungsten filaments as functions of temperature, *Physical review* **7**, 3, 302–330.
- Langmuir I. (1913) The vapor pressure of metallic tungsten, *Physical Review* **2**, 5, 329–342.
- Lutišan J., Cvengroš J. (1995) Mean free path of molecules on molecular distillation, *The Chemical Engineering Journal and the Biochemical Engineering Journal* **56**, 2, 39–50.
- Lutišan J., Cvengroš J., Micov M. (2002) Heat and mass transfer in the evaporating film of a molecular evaporator, *Chemical Engineering Journal* **85**, 2–3, 225–234.
- Lutišan J., Micov M., Cvengroš J. (1998) The influence of entrainment separator on the process of molecular distillation, *Separation Science and Technology* **33**, 1, 83–96.
- Martinello M. A., Bonino F., Gatica E. A., Pramparo M. C. (2003) Modelado y análisis de la destilación molecular de película descendente, *Mécanica Computacional en ENIEF XIII Congreso sobre métodos numéricos y sus aplicaciones* **22**, 1692–1701.
- Mathews J. H., Fink K. K. (2004) *Numerical Methods Using Matlab* (4th edition ed.). New Jersey: Pearson Prentice Hall.
- Micov M., Lutišan J., Cvengroš J. (1997) Balance equations for molecular distillation. *Separation Science and Technology* **32**, 18, 3051–3066.

- Nguyen A. D., Goffic F. L. (1997) Limits of wiped film short-path distiller, *Chemical Engineering Science* **52**, 16, 2261–2666.
- Poling B. E., Prausnitz J. M., O'Connell J. P. *The properties of gases and liquids*. McGraw-Hill, 2004, 707p.
- Rees G. J. (1980) Centrifugal molecular distillation – I: Fluid dynamics, heat transfer and surface evaporation, *Chemical Engineering Science* **35**, 4, 837–840.
- Sales-Cruz M., Gani R. (2006) Computer-Aided modelling of short-path evaporation for chemical product purification, analysis and design, *Chemical Engineering Research and Design* **84**, 7, 583–594.
- Schiesser W. E. *The Numerical Method of Lines*, San Diego, CA: Academic Press, 1991.
- Shao P., Jiang S. T., Ye K. (2007) Influences of feed and condenser temperature on molecular distillation of ideal binary mixtures, *Journal of Scientific & Industrial Research* **66**, 1, 37–46.
- Tovar, Laura Plazas. Modeling and simulation of the centrifugal reactive molecular distillation: Development, assessment and application to upgrade high-boiling-point petroleum fractions. 2012, 442p. Ph. D. Thesis (Doctorate of Chemical Engineering) – School of Chemical Engineering, State University of Campinas, Campinas, 2012.
- Tovar L. P., Wolf Maciel M. R., Maciel Filho R., Batistella C. B., Ariza O. C., Medina L. C. (2011) Overview and computational approach for studying the physicochemical characterization of high-boiling-point petroleum fractions (350 °C+). *Oil & Gas Science and Technology*; doi:10.2516/ogst/2011150.
- Xiang A., Xu S. (2005) Comparison of two turbulent models in simulating evaporating liquid film in a wiped molecular distillator, *Science in China Series B. Chemistry* **48**, 3, 183–188.
- Xubin Z., Chunjian X., Ming Z. (2005) Modeling of falling film molecular distillator, *Separation Science and Technology* **40**, 6, 1371–1386.
- Zuñiga-Liñan L., Nascimento-Lima N. M., Manenti F., Wolf-Maciel M. R., Maciel Filho R., Medina L. C. (2011) Experimental campaign, modeling, and sensitivity analysis for the molecular distillation of petroleum residues 673.15 K⁺, *Chemical Engineering Research and Design* doi:10.1016/j.cherd.2011.07.001.

Source: From Tovar L. P., Winter A., Wolf Maciel M. R., Batistella C. B., Maciel Filho R., Medina L. C. Reliable-based optimization using an experimental factorial design, response surface methodology and mathematical modeling of a centrifugal molecular distillation process to split heavy petroleum fractions. Separation Science and Technology, DOI:10.1080/01496395.2011.644612.

Copyright notice: The content of this manuscript is licensed under the Ethical Guidelines to Publication of Taylor & Francis Group. Please contact credited rights holders directly for permission to reproduce material.

Reliability-based optimization using surface response methodology to split heavy petroleum fractions by centrifugal molecular distillation process

Abstract

The present work aimed to develop an experimental and computational study for optimizing the centrifugal molecular distillation process to split heavy petroleum fractions. On the basis of the balance equations and Langmuir–Knudsen equation, a mathematical model was proposed. The influence of the evaporator temperature (EVT), volumetric feed flow rate (Q) and the interactions between them, on the overall distillate mass flow rate (D) and the distillate yield ($\%D$) was analyzed. A full 2^2 factorial central plus star rotatable ($\alpha=\pm\sqrt{2}$) composite design was performed in the experimental range from 423.15 to 603.15 K for EVT and from 1.473 to 4.418 $\text{kg}\cdot\text{h}^{-1}$ for Q . The optimized conditions, using the response surface methodology, established that the EVT must range from 540 to 600 K and the Q from 1.5 to 3.5 $\text{kg}\cdot\text{h}^{-1}$. The comparison of the experiment results with the predicted model results shows an acceptable qualitative agreement between the experiment and simulated data.

Keywords: Molecular distillation, heavy petroleum fractions, reliability-based optimization, distillate mass flow rate, numerical simulation.

Contents

1. Introduction
2. Mathematical description
 - 2.1. Momentum balance equation
 - 2.2. Velocity profile
 - 2.3. Anisotropic condition and effective rate of evaporation
 - 2.4. Thickness of the evaporating film
 - 2.5. Temperature profile in the liquid film

- 2.6. Overall distillate mass flow rate
- 3. Methods and materials
 - 3.1. The centrifugal molecular distillation experiments
 - 3.2. Physicochemical characterization
 - 3.2.1. Rheological analysis of distillate and residue streams
 - 3.2.2. Analysis of density of distillate and residue streams
 - 3.2.3. Colloidal characterization
 - 3.3. Factorial experiments for optimization
 - 3.4. Response surface methodology
- 4. Results and discussion
 - 4.1. Influence of operating conditions
 - 4.2. Optimization of the experimental conditions and response surface methodology
 - 4.3. Physicochemical characterization of split products
 - 4.4. Analysis of the performance of the centrifugal molecular distillation by simulation
 - 4.4.1. Evaporator temperature influence on centrifugal molecular distillation
 - 4.4.2. Feed flow rate influence on centrifugal molecular distillation
 - 4.4.3. Model validity
- 5. Conclusions
- Acknowledgments
- Nomenclature
- References

1. Introduction

The petroleum industry and research groups have committed efforts to develop and improve process technologies for the upgrading of petroleum residue. The residue is defined as a liquid or semi-liquid product obtained as the residue from the atmospheric and vacuum distillation of petroleum and consisting principally of asphaltic hydrocarbons with a low H/C ratio (1.2–1.4) (1,2).

However, a novel technique based on the molecular distillation process has been developed by the Separation Processes Development Laboratory and the Laboratory of Optimization, Project and Advanced Control (LDPS/LOPCA/UNICAMP) sponsored by the Research Center of Petrobras–Brazil (CENPES/Petrobras) and Brazilian Study and Project Financing Institution (FINEP). It constitutes one of the best non-conventional processes to split and characterize heavy liquid petroleum fractions (3–10).

The molecular distillation process is a Hi-Tech thermal and special liquid-liquid separation technology, in which the good distribution of the liquid in a uniform thin film is guaranteed (10–12). Basically, the principle of molecular distillation is related to the vapor

molecules generated that find a free path between the evaporator and the condenser surfaces under high vacuum conditions. In centrifugal molecular distillation (CMD) process, a type of molecular distillation, the centrifugal force is used to enhance the performance of the process. The rapid flow of the liquid film makes the residence time in the device extremely short, which offers some advantages with respect to the chemical degradation of the products (13–17). Under these conditions, theoretically, the evaporation rate should only be governed by the rate of escape of molecules from the liquid surface, and therefore, phase equilibrium does not exist (5,6,18). The combination of a small distance between the evaporator and the condenser (from 0.02 to 0.08 m) with a high vacuum in the distillation gap results in a specific mass transfer mechanism with evaporation outputs as high as $20 - 40 \text{ g} \cdot \text{m}^{-2} \cdot \text{s}^{-1}$ (15).

Over the last years, the molecular distillation process has been recognized as a multidisciplinary process concerning the feedstock, operating conditions and configuration strategies for the equipment (Table 1). Experimental procedures and theoretical studies have been developed. These studies involved the stripping, separation, concentration and extraction of components from natural products, the separation of mono-, di- and triacylglycerols, extraction of fatty acids and the characterization of petroleum fractions, which are applications related to the food, chemical, pharmaceutical and petrochemical areas (8–10,19–32).

Table 1. Overview of experimental research on molecular distillation process from different feedstock and operating conditions.

Feedstock	Application	Operating conditions			Equipment type	Source
		Pressure system (Pa)	Evaporator temperature (K)	Feed flow (mL·min ⁻¹)		
Deodorized oil from the squid <i>Illex argentinus</i>	Recovery of ω-3 fatty acid ethyl esters	40	273.15 and 393.15 K for the first stage and 393.15 and 413.15 K for the second stage	NA	FFMD	(19)
Cymbopogon citratus essential oil	Purification/ Extraction	5	333.15–393.15	1.5–6.0	CMD	(20)
Fast pyrolysis of biomass	Separation	60	343.15 – 403.15	1	FFMD	(21)
Rapeseed soapstock	Acidification	2.66	323.15 and 393.15	NA	FFMD	(22)
Pyrolysis oil	Separation	60	323.15	1	FFMD	(23)
Palm oil	Purification	0.1	493.15 – 523.15	†0.5–1	FFMD	(24)
Vegetable oils	Purification	2.7–3.3	393.15–513.15	3	CMD	(25)
Decanoic acid in cuphea fatty acids	Purification	0.08–0.40	313.15–383.15	†0.03–0.1122	CMD	(26)
Octacosanol extract from rice bran wax	Purification	66.66	363.15	3	FFMD	(27)
Grape seed oil	Recovery and deacidification	1.25	469.15–497.15	0.3–1.7	FFMD	(28)
Palm fatty acid distillates	Extraction tocotrienols	0.13	393.15 (3 rd stage) and 433.15 (4 th stage)	†0.25	FFMD	(29)
Palm oil distillates	Extraction tocotrienols	0.13	383.15–433.15	†0.1, 0.25 and 0.4	FFMD	(30)
Olive Tree	Isolation	150–200	343.15–463.15	15	FFMD	(31)
Heavy oils (Brazilian vacuum residue)	Characterization oil (extend the true boiling point)	0.1	508.15–613.15	8.33	FFMD	(8-10)
Soya oil	Separation	0.1	373.15 – 433.15	†0.1 – 0.7	FFMD	(18)
Product of vegetable refining edible oil	Recover of tocopherol and fatty acid methyl esters	NA	443.15–503.15	30–150	FFMD	(32)

CMD: Centrifugal molecular distillation; FFMD: Falling film molecular distillation; †: Feed flow rate in kg·h⁻¹; NA: Not available

This work presents the use of the CMD process to split heavy petroleum fractions using both theoretical and experimental studies. In the first part, a central composite factorial design was used to analyze the operating conditions of the centrifugal molecular distillation process with respect to the distillate stream. The independent variables studied were the evaporator temperature (EVT) and the feed flow rate (Q), and the dependent variables were the overall distillate mass flow rate (D) and the yield of distillate stream ($\%D$). The experimental factorial design allowed one to define and to analyze the effect of each independent variable on the dependent variables and to optimize the conditions using the response surfaces and statistical model. All the data were treated with the software Statistica 7.0 from Statsoft Inc (33). The qualities of the fitted models were evaluated by analyzing the variance (ANOVA).

The theoretical study comprised the mathematical description and the numerical results of the centrifugal molecular distillation process to split heavy petroleum fractions. The theoretical study was illustrated for an atmospheric petroleum residue (ATR-W 673.15 K⁺) divided into twenty five pseudocomponents (34). The mathematical model was based on a highly viscous liquid film flow, and hence with small Reynolds numbers, and the velocity profile was fully developed (35–36).

The process under study was modeled according to the mass, momentum and energy balance equations. Computational analyses are based on the Langmuir–Knudsen equation, derived from the kinetic theory of the ideal gas for the effective evaporation rate. The simulations were carried out under steady–state conditions, and the output variables, such as surface temperature (T_s), film thickness (δ), effective evaporation rate (G_E) and distillate mass flow rate (D) profiles were computed. The set of partial differential algebraic equations was solved by a computer aided environment developed in FORTRAN programming language, using the method of lines.

2. Mathematical description

The thin liquid film flowing over the rotating evaporator surface in the centrifugal molecular still is depicted in Fig. 1. The conical surface rotates at angular velocity ω . The liquid is brought up to the cone surface at a radius r_i , which means, that the liquid is fed to the conical surface at radius r_i and left at r_o .

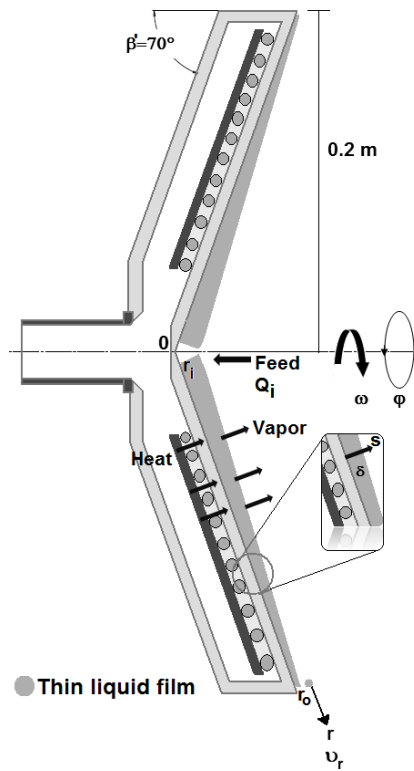


Figure 1. Sketch of the evaporator surface and its coordinate system.

The thin liquid film flowing over conical evaporator surface in the centrifugal molecular distiller obeys the follows assumptions:

- Spherical coordinates system is suited to the model. However some simplifications are made based on the fact that the film is very thin.
- Liquid flow is considered in steady state.
- Liquid film thickness is very small in comparison with the radius of the conical surface.
- Tangential and meridional velocity components are negligibly small in comparison with the radial component.
- The thin liquid film is completely viscous and it is in laminar pattern flow.
- The liquid has the same rotational speed as the rotational surface.
- Gravitational force is negligibly in comparison with the centrifugal force.

- A coordinate s instead of θ is introduced ($-ds = r d\theta$).

The model developed by Inuzuka et al. (36) has been taken to propose a generalized two-dimensional steady state mathematical model of the centrifugal molecular distillation from heavy petroleum fraction. It comprises the temperature, velocity, film thickness, effective evaporation rate and distillate mass flow rate profiles.

2.1. Momentum balance equation

A momentum balance is used below to derive a general differential equation that can be then employed to solve thin film flowing over conical evaporator surface in spherical coordinates. For this, an incompressible liquid film fluid in laminar regime inner a system of radial length, which is at an angle β' to the vertical, is considered (Fig. 1).

The continuity equation can be written as Eq. (1):

$$\rho \frac{d\dot{Q}}{dr} + 2\pi r G_E (\sin \beta') = 0 \quad (1)$$

2.2. Velocity profile

The velocity profile in the liquid film is assumed to be fully developed on the rotating evaporator surface, as presented in the Eq. (2) (35, 36).

$$v_r = \frac{\omega^2 \sin^2 \beta'}{\nu} r \left(\delta s - \frac{s^2}{2} \right) \quad (2)$$

2.3. Anisotropic condition and effective rate of evaporation

The evaporation rate is an important factor in evaluating the efficiency of the molecular distillation process. Evaporation proceeds at a different rate and the vapor phase presents different physical properties as consequences of the fact that the gas behaves like a collection of independent particles. Thus, the appropriate vapor phase dynamic regime is determined by means of the Knudsen number (Kn), Eq. (3), which expresses the ratio of the mean free path (MFP) of the vapor phase to a characteristic length (L), such as the boundary layer thickness, or a molecular distiller device dimension (the distance between the evaporator and the condenser surface) (37).

$$Kn = \frac{MFP}{L} \quad (3)$$

In the case of a molecular distillation process, $Kn > 0.1$ explains the fact that the vapor phase shows anisotropic behavior, which means that, at $Kn > 0.1$ intermolecular collisions in the region of interest (space between the evaporator and the condenser surfaces) are much less frequent than molecular interactions (37). In the other cases, the Knudsen number is less than 0.1, and thus the vapor has isotropic properties and behaves as continuous matter, such that the number of collisions between the molecules increases and the molecules can reach the condenser, but can also return to the evaporator surface and attain equilibrium; not a valid state in the process (37).

Nevertheless, with short distances between the evaporator and the condenser and a low number of collisions, evaporation of the molecules proceeds at the maximal rate described by the Langmuir–Knudsen equation (Eq. 4) (36,38–39).

$$G_T = P_{vap} \sqrt{\frac{M}{2\pi R_g T_s}} \quad (4)$$

Where G_T is the theoretical rate of evaporation, P_{vap} is the equilibrium vapor pressure at the absolute temperature T_s , M is the molar mass of the compound, and R_g is the universal gas constant.

Therefore the molecular distillation process is a function of the molecular species and the surface temperature, that is, the molecular distillation process is a surface phenomenon (40).

The effective rate of evaporation (G_E) of each component is calculated using a modified Langmuir–Knudsen equation, where conditions in the vapor phase, above the thin evaporating liquid film, influence the effective mean free path of the molecules, as described by Eq. (5) (37,41):

$$G_E = G_T f \quad (5)$$

Where the coefficient f represents the fraction of vaporized molecules that reach the condenser and is expressed as follows (37):

$$f = \left[1 - (1 - F) \left(1 - e^{k^* K n} \right)^{n'} \right] \quad (6)$$

Kawala and Stephan (41) stated that the best value for n' is equal to 5, and the degree of anisotropy, k^* , of the vapor phase in the space between the evaporator and the condenser is given by:

$$\log k^* = 0.2F + 1.38(F + 0.1)^4 \quad (7)$$

Where F describes the curvature of the evaporation surface (37):

$$F = \frac{d_e - 2L}{2d_e - 2L} \quad (8)$$

Where d_e is the diameter of the evaporation surface curvature and L is the distance between the evaporator and the condenser. Hence, the effective rate of the evaporation surface takes into account the anisotropic effect of the vapor phase.

2.4. Thickness of the evaporating film

$$\delta = \left[\frac{3\nu}{2\pi\omega^2 r^2 (\sin^3 \beta')} \left(\dot{Q}_i - \frac{1}{\rho} \int_{r_i}^r 2\pi r G_E (\sin \beta') dr \right) \right]^{1/3} \quad (9)$$

2.5. Temperature profile in the liquid film

The thermal balance was described by the equation of conservation of energy as follows (23):

$$\frac{d}{dr} \int_0^\delta \rho C_p r v_r T (\sin \beta') ds = \sin \beta' \left[q_w - (\Delta H + C_p T_s) G_E \right] r \quad (10)$$

With the following boundary conditions:

$$T = T_i \quad \text{at} \quad r = r_i \quad \text{and} \quad 0 \leq s \leq \delta \quad (11)$$

$$-\lambda \frac{\partial T}{\partial s} = q_w = \text{cons} \tan t \quad \text{at} \quad r_i \leq r \leq r_o \quad \text{and} \quad s = 0 \quad (12)$$

$$-\lambda \frac{\partial T}{\partial s} = \Delta H G_E \quad \text{at} \quad r_i \leq r \leq r_o \quad \text{and} \quad s = \delta \quad (13)$$

2.6. Overall distillate mass flow rate

$$D = 3600 \int_{r_i}^{r_o} 2\pi r G_E (\sin \beta') dr \quad (14)$$

3. Methods and materials

Case study: The objective was to split the heavy petroleum atmospheric residue (ATR) 673.15 K⁺ of “W” crude oil. The total residue was divided into twenty five pseudocomponents for the simulating process, and in the simulation environment, the sample was characterized using the computational approach developed by Tovar et al. (34).

3.1. The centrifugal molecular distillation experiments

The equipment used in the experiments was a centrifugal molecular distiller (with an evaporation surface area of 0.1935 m²) built and sponsored by the Laboratory for the Development of Separation Processes (LDPS) and the Laboratory of Optimization, Project and Advanced Control (LOCA) at the School of Chemical Engineering (FEQ) of the State University of Campinas (UNICAMP), the Research Center of Petrobras–Brazil (CENPES/Petrobras) and Brazilian Study and Project Financing Institution (FINEP). The layout of the centrifugal molecular distiller is shown in Fig. 2.

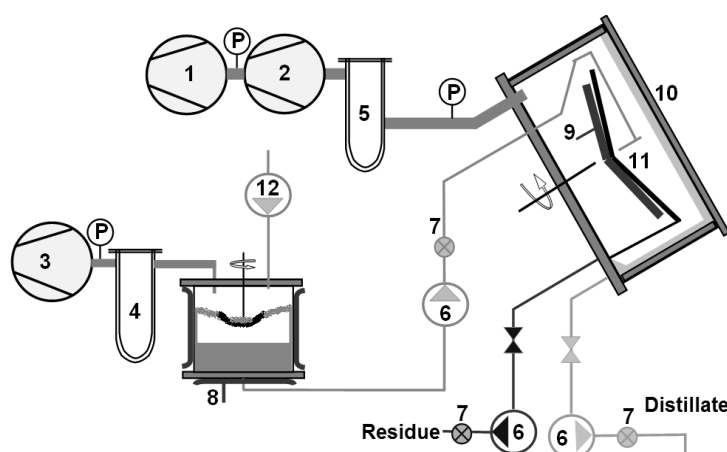


Figure 2. Schematic diagram of the centrifugal molecular distiller. 1. Backing/Roughing vacuum pump (chamber); 2. Diffusion (high vacuum) pump; 3. Rough vacuum pump (degasser); 4. Trap (degasser); 5. Trap (chamber); 6. Liquid transfer pump; 7. Check valve; 8. Degasser heater; 9. Rotor heater; 10. Vacuum chamber/condenser; 11. Rotor; 12. Variable speed liquid transfer pump; P: Vacuum pressure gauge (42).

The centrifugal molecular distiller is formed by the heated evaporator and the cooling–condenser surface with an electrical heating system. It also includes the temperature, pressure and flow rate control units. The module is completed by a vacuum unit composed of two vacuum pumps: a mechanical vacuum pump and another diffuser pump. The centrifugal force allows for the formation of a thin liquid film that passes through the heated disk and makes contact with the condenser surface. The use of the central rotational heated disk is a mechanical way of creating a thin liquid film well distributed over the evaporator surface.

The tests started when the conditions for EVT and Q were defined. The equipment was stabilized and the operational conditions were reached. Approximately 2 h were necessary to stabilize the system. The raw material is driven up to the evaporator by a feed system at the predetermined Q value, where the material is heated (at 353.15 K) and subsequently driven by a tube (kept at 423.15 K) up to the centre of the rotor of the evaporator. The evaporator rotation velocity was 540 rpm, which provides a uniform film throughout the distiller due to the centrifugal force. The typical pressure of the system was 0.4 Pa. The condenser temperature was maintained at 353.15 K.

When the raw material was submitted to the CMD process, two product streams are generated: the distillate stream rich in the molecules that escape from the evaporator and get to the condenser surface; and the residue stream rich in the heavier molecules that remain on the evaporator surface and which did not reach the condenser surface. Non–condensable molecules are exhausted and confined in the trap gap, where they are condensed by a liquid at temperature of 273.15 K. In order to evaluate the liquid yield as function of distillate mass flow rate (D) and residue mass flow rate (R) Eq. 15 was used.

$$\%D = \frac{D}{D + R} * 100 \quad (15)$$

3.2. Physicochemical Characterization

In order to evaluate the success of the process, the fractions (11 distillates and 11 residues) from CMD were assayed by colloidal characterization using size exclusion chromatography (SEC) with UV–absorption detection, for the determination of the molar mass distribution. In addition, physicochemical properties of distillate and residue streams, density, relative density and API gravity, were determined.

3.2.1. Rheological analysis of distillate and residue streams obtained from CMD process

The experimental measurements were performed using a *HAAKE RheoStress 6000–UTC rheometer* (Thermo Electron Corporation, Karlsruhe, Germany), with a plate–plate sensor system constituted by two (02) parallel plates (PP35 and PP60) of 0.035 m of diameter (for ATR–W sample and residue streams) and 0.060 m of diameter (for distillate streams). The flow behavior of the ATR–W and products streams (distillate and residue) obtained from CMD was investigated over a wide range of shear rates at 343.15 K, 363.15 K and 373.15 K for ATR–W; 372.15 K for distillate streams and 423.15 K for residue streams. The test temperature was maintained at a constant value and controlled to allow a maximum deviation of ± 0.1 K with a *HAAKE* universal temperature controller (Thermo Electron Corporation, Karlsruhe, Germany). The rheological measurements referred to the analyses of transition between non–Newtonian and Newtonian behavior obtained from an analysis of the flow curve prepared using the controlled rate mode and at the shear rate range from 10 to 700 s^{-1} with measurements being made every 10 s^{-1} . The dynamic viscosity values were determined from simple linear regression through the set of 70 experimental data since. Regression tool of *HAAKE RheoWin Job Manager* software (Version 3.61.0000) was used. In order to determine the Newtonian behavior, data must obey the general equation (Eq. 16):

$$\tau = \mu\gamma \quad (16)$$

Where τ is the shear stress (Pa), μ is the dynamic viscosity (Pa·s) and γ is the shear rate (s^{-1}). Using experimental data, when τ is plotted against γ , a straight line is obtained. With this linear relation, the μ is calculated from the slope of the straight line.

3.2.2. Analysis of density of distillate and residue streams

The ASTM D 4052 (43) and ASTM D5002 (44) standard methods, for density measurements in the petroleum industry, were used to determine the density and relative density at 293.15 K of the distillate streams obtained from CMD process. The tests were performed through the Density Meter DMA 4500 – Anton Paar. A built–in Peltier thermostat automatically ensured the correct measuring temperature at 293.15 K. The repeatability is not worse than $\pm 3 \times 10^{-4} \text{ g}\cdot\text{cm}^{-3}$. Averages among repetitions (mean value of triplicate determinations) and standard deviation were determined and analyzed. On the other hand, density measurements of

residue streams were analyzed using the pycnometer method following the standard method ASTM D 70 (45).

3.2.3. Colloidal characterization

The chromatographic system, VISCOTEK GPC/SEC TDAmaxTM (Viscotek Corporation, Houston, TX, USA), comprises a VISCOTEK GPCmax (VE2001) solvent/sample module, a VISCOTEK TDA 302 triple detector array, three GPC/SEC Phenogel analytical columns (Phenomenex, Torrance, CA) in series, a VISCOTEK UV detector model 2501 and OmniSEC software (Version 4.5.0.257). The products (distillate and residue streams) were analyzed using size exclusion chromatography on three GPC/SEC Phenogel analytical columns (Phenomenex, Torrance, CA) with different pore sizes (50–100 Å), dimensions of 300 mm x 7.8 mm and packed with spherical styrene divinylbenzene copolymer beads with a particle size of 5 µm. Tetrahydrofuran (THF) (HPLC grade UV, Fisher Scientific, Fair Lawn, New Jersey) was used as the mobile phase at a flow rate of 0.7 mL·min⁻¹, and the column temperature was maintained at 313.15±1 K during the analyses. The samples (distillate and residue streams) were introduced through a 20 µL loop injection valve and detection was by means of UV absorption at 340 nm. The molecular mass distribution with the number and weight average molar masses (*M_n* and *M_w*) and the polydispersity index (PID) were calculated by OmniSEC software (Version 4.5.0.257).

The GPC/SEC Phenogel detectors used for the determination of the molar mass distributions were calibrated for molar mass versus retention volume using several polystyrenes (PS580, PS1300, PS2497, PS5460, PS8864, PS12347, PS16953 and PS28500) and hydrocarbon (naphthalene, tetralin, carbazole, ammonium heptamolybdate) standards. The calibration curve was fitted using a cubic equation (Eq. 17) with a regression square coefficient of 0.98.

$$\log(M_w) = 18.568 - 2.120V_p + 0.093V_p^2 - 1.410 \times 10^{-3}V_p^3 \quad (17)$$

Where *M_w* is the average molar mass (kg·kmol⁻¹) of the products from the CMD and *V_p* is the retention volume (mL).

3.3. Factorial experiments for optimization

The use of molecular distillation to split heavy petroleum fractions was the subject of experimental and theoretical research by (8–10). They evaluated the influence of the operational

conditions of the molecular distillation process, such as the evaporator temperature (*EVT*) and feed flow rate (*Q*), on the dependent variables i.e. overall distillate mass flow rate (*D*) and the distillate yield (%*D*).

Preliminary studies by the author's research group with other systems showed that the variables *EVT* and *Q* were the ones that had the greatest effect on the response variable in the molecular process (9,16). However, in our previous paper, parametric sensitivity of the centrifugal molecular distillation from the high-boiling-point petroleum fraction ATR-W showed that the evaporator temperature (*EVT*) and rotor speed (*RS*) are the main operating variables for this particular process. Thus, in a preceding experimental exercise it was observed that when *RS* variable varied from 700 rpm to 1300 rpm, the evaporator surface device exhibited an oscillation or vibration which made impossible the operation and it does not guarantee a uniform film on the evaporator surface. Hence, the input variables considered for the optimization were the *EVT* and *Q*, setting the rotor speed (*RS*) at 540 rpm.

A central composite factorial design, which takes all the degrees of freedom into account was used. The general form of this factorial design is 2^n plus a star configuration ($\pm\alpha = 2^{n/4}$), with a central point, where n is the number of factors (in this case *EVT* and *Q*) and 2 represents the two levels of work. The levels are identified as the low level (-1) and the high level (+1) and the central point (0), as shown in Table 2. The central point (0) is very important since it represents a set of experimental conditions at which three (03) replicates were run, and is used to calculate the standard deviations. In this study, a 2^2 full-factorial central composite design with 4 axial (star configuration) and 3 central points was used, resulting in 11 experiments.

Table 2. Variables and levels investigated using the central composite factorial experimental design.

Independent variable	Unit	Coded factor	Level				
			$-\alpha=-\sqrt{2}$	-1	0	+1	$+\alpha=\sqrt{2}$
<i>EVT</i>	K	X_1	423.15	449.15	513.15	577.15	603.15
<i>Q</i>	kg·h ⁻¹	X_2	1.473	1.914	2.945	3.976	4.418

EVT: Evaporator temperature; *Q*: Feed flow rate; X_1 , and X_2 , coded factor for *EVT* and *Q*, respectively.

The conditions of the full-factorial central composite design (star configuration) ranged between 423.15 and 603.15 for *EVT* and 1.473 and 4.418 kg·h⁻¹ for *Q*. These values were chosen

based on the formation of a thin film on the evaporator surface, on the thermal conditions required to avoid cracking of the feedstock, and on the operating range of the centrifugal molecular distillation unit. Table 3 shows the design matrix for the 11 experiments. The distillate mass flow rate (D) and the distillate yield ($\%D$) were defined as the dependent variables.

Table 3. Design matrix (real levels in parentheses) and experimental results for the central composite factorial design.

Trial	Coded factor		Dependent variable		
	X_1	X_2	$\%D$ (%wt)	D (kg·h ⁻¹)	R (kg·h ⁻¹)
1	-1 (449.15)	-1 (1.914)	20.512	0.624	2.418
2	-1 (449.15)	1 (3.976)	40.666	0.708	1.033
3	1 (577.15)	-1 (1.914)	58.861	1.296	0.906
4	1 (577.15)	1 (3.976)	45.655	1.584	1.885
5	$-\sqrt{2}$ (423.15)	0 (2.945)	17.883	0.263	1.208
6	$+\sqrt{2}$ (603.15)	0 (2.945)	48.763	1.656	1.740
7	0 (513.15)	$-\sqrt{2}$ (1.473)	37.975	1.080	1.764
8	0 (513.15)	$+\sqrt{2}$ (4.418)	48.889	1.596	1.669
9	0 (513.15)	0 (2.945)	47.794	1.356	1.481
10	0 (513.15)	0 (2.945)	47.418	1.332	1.477
11	0 (513.15)	0 (2.945)	47.602	1.296	1.427

EVT: Evaporator temperature; Q : Feed flow rate; X_1 and X_2 coded factor for *EVT* and Q , respectively; $\%D$: Distillate yield, D : Distillate mass flow rate obtained in the experimental trials and R : Residue mass flow rate obtained in the experimental trials.

3.4. Response surface methodology

Using response surface methodology, non-linear multiple regression models were fitted for the dependent variables (D and $\%D$). Based on the central composite factorial design, independent and dependent variables were fitted to a second-degree polynomial equation (Eq. 18), where D and $\%D$ were the estimated responses, ξ_i the coefficient related to the direct influence of the independent variables, ξ_{ij} the coefficients of the statistical model related to the possible linear interactions amongst the independent variables *EVT* and Q ; and ξ_{ii} and ξ_{jj} the coefficients corresponding to the quadratic influence of the independent variables.

$$D \text{ or } \%D = \xi_0 + \xi_1 \cdot EVT + \xi_2 \cdot Q + \xi_{12} \cdot EVT \cdot Q + \xi_{11} \cdot EVT^2 + \xi_{22} \cdot Q^2 + \text{error observed in the response} \quad (18)$$

The response surfaces and related contour diagrams were calculated for the two experimental factors (*EVT* and Q) using the software Statistica 7.0 from Statsoft Inc (33). Rising ridge behaviors in the quadratic response surfaces were identified.

The qualities of the fitted models were evaluated analyzing the variance (ANOVA), and verifying if the models reproduced the experimental data in the range studied. The F -test and the percentage of explained variance were also checked (46).

4. Results and discussion

4.1. Influence of operating conditions

Table 3 shows the coded factors used for EVT and Q and the experiments that were carried out for the central composite factorial design of the 11 trials. It consisted of a complete 2^2 factorial design (levels -1 and $+1$) plus a star configuration (levels $-\sqrt{2}$ and $+\sqrt{2}$), with a central point (level 0). The repetition at the central point was used to estimate the error. The results for the distillate mass flow rate (D) obtained in the experimental trials and the distillate yield ($\%D$), are presented in the final columns.

The estimated effects of both variables are outlined in Table 4. The significant effects were calculated using the p -value and confidence interval concepts. Accordingly, it was possible to investigate a quadratic polynomial relationship of the independent variables on D and $\%D$. Thus, the statistical analysis showed that, at the 95% confidence interval, the linear factors EVT_l and Q_l and the quadratic factor EVT_q presented significant effects on the variable D (Table 4). On the other hand for the variable $\%D$ the linear factors EVT_l and Q_l , the quadratic factors EVT_q and Q_q and the interactions between the linear factors presented significant effects (Table 4).

Table 4. Main effects and the interaction effect involving the factors for D and $\%D$ independent variables by applying the central composite factorial design.

Independent variable	Factor	Effect	Error	t ^a	p ^b	-95% ^c	+95% ^c
D	Mean*	1.328	0.017	76.166	1.723×10^{-4}	1.253	1.403
	X_{1l} *	0.879	0.021	41.186	5.890×10^{-4}	0.394	0.486
	X_{1q} *	-0.416	0.025	-16.382	3.705×10^{-3}	-0.263	-0.154
	X_{2l} *	0.275	0.021	12.818	5.957×10^{-3}	0.092	0.184
	X_{2q}	-0.038	0.025	-1.490	2.746×10^{-1}	-0.074	0.036
	X_{1l} by X_{2l}	0.102	0.030	3.378	7.759×10^{-2}	-0.014	0.116
$\%D$	Mean*	47.605	0.109	438.550	5.199×10^{-6}	47.138	48.072
	X_{1l} *	21.752	0.133	163.617	3.735×10^{-5}	10.590	11.162
	X_{1q} *	-12.759	0.158	-80.630	1.538×10^{-4}	-6.720	-6.039
	X_{2l} *	5.596	0.133	42.090	5.640×10^{-4}	2.512	3.084
	X_{2q} *	-2.650	0.158	-16.745	3.547×10^{-3}	-1.665	-0.984
	X_{1l} by X_{2l} *	-16.680	0.188	-88.717	1.270×10^{-4}	-8.744	-7.936

D : Distillate mass flow rate; $\%D$: Distillate yield; EVT : Evaporator temperature; Q : Feed flow rate; X_1 , and X_2 , coded factor for EVT and Q , respectively; l : linear effect; q : quadratic effect.

* Statistically significant at a confidence level of 95 %

^a The value of the coefficient of regression for the error, measures how big the effect is with respect to the residual error

^b Probability of significance. At the confidence level of 95 %, a p -value < 0.05 , shows that the result is significant

^c Limits of confidence: The effects are statistically reliable when the limits do not pass zero.

4.2. Optimization of the experimental conditions and response surface methodology

The experimental data were analyzed by non-linear multiple regression using the software Statistica 7.0 from Statsoft Inc (33). The models expressed by Eqs. (19) – (20), in terms of independent variables, were generated, representing the overall distillate mass flow rate (D) and the distillate yield ($\%D$) as a function of the more significant variables as follows:

$$D = b_0 + b_1 \cdot EVT + b_2 \cdot Q + b_{11} \cdot EVT^2 + 9.120 \times 10^{-4} \quad (19)$$

$$\%D = b_0 + b_1 \cdot EVT + b_2 \cdot Q + b_{12} \cdot EVT \cdot Q + b_{11} \cdot EVT^2 + b_{22} \cdot Q^2 + 3.541 \times 10^{-2} \quad (20)$$

Table 5 shows the parameter estimated, the standard error and the confidence interval (95%).

Table 5. Estimates of the parameters for the fitted models.

Equation	Parameter	Estimated value	Standard deviation	Confidence interval	
				Lower limit (-95%)	Upper limit (+95%)
19	b_0	-15.796	0.785	-19.172	-12.420
	b_1	0.058	0.003	0.045	0.071
	b_2	0.133	0.010	0.089	0.177
	b_{11}	-5.005×10^{-5}	0.000	-0.000	-0.000
20	b_0	-663.154	5.735	-687.830	-638.477
	b_1	2.155	0.021	2.067	2.243
	b_2	74.814	0.852	71.147	78.481
	b_{12}	-1.264×10^{-1}	0.001	-0.133	-0.120
	b_{11}	-1.571×10^{-3}	0.000	-0.002	-0.001
	b_{22}	-1.228	0.073	-1.544	-0.913

EVT : Evaporator temperature; Q : Feed flow rate; b_i the coefficient related to the direct influence of the independent variables (EVT and Q), b_{ij} the coefficients of the statistical model related to the possible linear interactions amongst the independent variables EVT and Q ; and b_{ii} , and b_{jj} the coefficients corresponding to the quadratic influence of the independent variables (EVT and Q).

Table 6 shows the ANOVA for the quadratic models. According to the ANOVA, the responses presented high correlation coefficients (>0.96). The qualities of the fitted models were checked. The ratio between the mean square regression (MS_{QR}) and the mean square residual (MS_{QR}), $F\text{-ratio}_{R/r}$, was used to establish if the models were statistically significant. Also, the ratio between the mean square lack of fit (MS_{QLOF}) and the mean square pure error (MS_{QPE}), the $F\text{-ratio}_{LOF/PE}$, was used to evaluate if the models were well adjusted to the observations. High values for the $F\text{-ratio}_{LOF/PE}$ are evidence of a lack of fit of the models. Thus Eq. (19) was predictive for D and statistically significant under the experimental conditions studied, for a high percentage of explained variance (99.99 %), and close to the percentage of explained variance

predicted by the mathematical model (96.52 %). The calculated $F\text{-ratio}_{R/r}$ (64.717) was more than fourteen times higher than the $F\text{-value}_{R/r}$ at a 95 % confidence interval ($F_{0.95;3;7} = 4.347$), which is in good agreement with the practical rule, that establishes that the model has statistical significance when the calculated $F\text{-value}$ is at least three to five times larger than the listed value) (47). Furthermore, Table 6 shows the ANOVA analysis, and the model from Eq. (19) fit the experimental data well, since the calculated $F\text{-ratio}_{LOF/PE}$ (15.048) was lower than the critical $F\text{-value}_{LOF/PE}$ ($F_{0.95;5;2} = 19.295$) in the 95 % confidence interval.

On the other hand, the analysis of variance (ANOVA) for %D model from Eq. (20) is also shown in Table 6. The response has a correlation coefficient (R^2) equal to 0.982 and the $F\text{-test}$ shows that the model was reliable, since the calculated $F\text{-value}$ was 10.74 times larger than the listed $F\text{-value}$, in the 95% confidence level.

Table 6. Analysis of variance (ANOVA) of D and %D fitted to Eqs. (19) – (20).

Source of variation	Eq.	SS	DF	MSq	F-ratio	F-value
R	19	1.954	3	0.651	64.717 ^a	4.347
	20	1518.554	5	303.711	54.239 ^a	5.0503
r	19	0.070	7	0.010	–	–
	20	27.997	5	5.599	–	–
LOF	19	0.069	5	0.014	15.048 ^b	19.295
	20	27.926	3	9.309	262.887 ^b	19.164
PE	19	0.002	2	0.001	–	–
	20	0.071	2	0.035	–	–
$Total$	19	2.024	10			
	20	1546.552	10			
% of explained variance				Eq. (19) (96.5%)		
				Eq. (20) (98.2%)		
% of maximum explainable variance				Eq. (19) (99.9%)		
				Eq. (20) (100.0%)		

R : Regression; r : Residual; LOF : lack of fit; PE : Pure error; SS : Sum of Squares; DF : Degrees of freedom; MSq : Mean Square.

^a $F\text{-ratio}$ (regression/residual). ^b $F\text{-ratio}$ (lack of fit/pure error).

The relationship between the independent and dependent variables is illustrated in a three-dimensional representation of the response surfaces (Figs. 3 – 4) and two-dimensional contour plots (Fig. 5), as generated by the models presented in Eqs. (19) and (20).

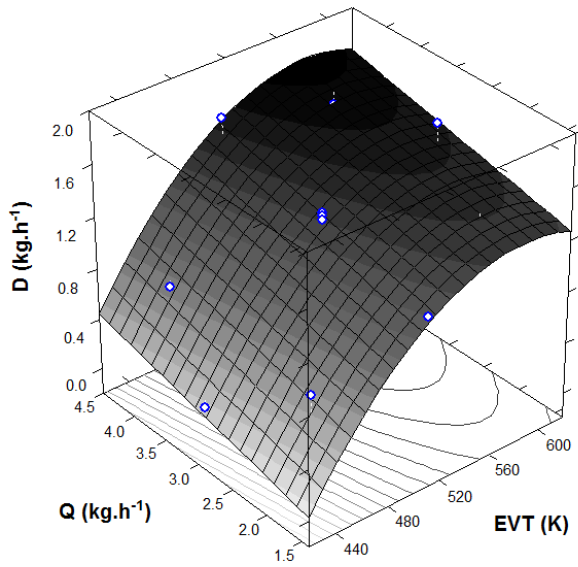


Figure 3. Response surface plot for the distillate mass flow rate (D) using the statistical model presented in Eq. (19).

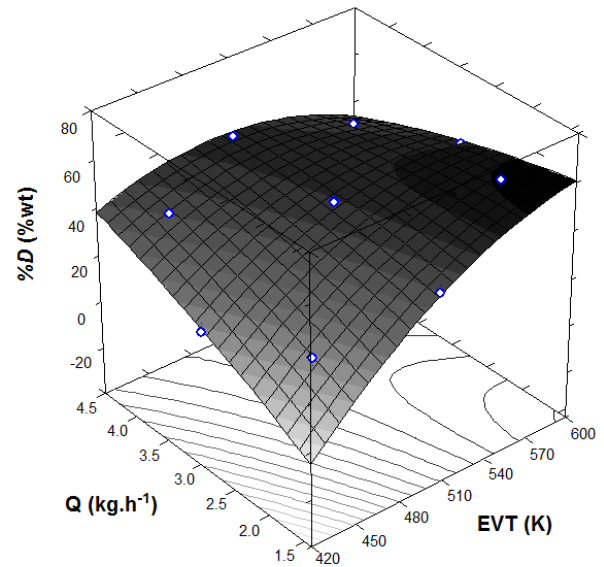


Figure 4. Response surface plot for the distillate yield ($\%D$) using the statistical model presented in Eq. (20).

The models described above are valid for the simulated range described in Table 2. Analyzing the response functions in Figs. 3 – 4, it can be seen that the overall distillate mass flow rate (D) and the distillate yield ($\%D$) were both strongly affected by the molecular distillation temperature (EVT). Similarly, at a fixed feed flow rate (Q), increasing the distillation temperature represents a times six increase in the effective evaporation rate and distillate mass flow rate with respect to the initial value. Therefore, the EVT must be maintained at the highest levels tested. In addition, the assumption related to the high values of Q was confirmed, since the residence time of the molecules on the evaporator surface was low, and the effective evaporation rate not have been enough to evaporate the molecules.

In order to define the shape of the response surfaces, a canonical analysis must be carried out to describe the type of the second order surfaces, the location of the optimum value and the canonical direction.

Analyzing Figs. 5, the contour lines are perpendicular to the EVT axis, indicating relatively little change in the distillate mass flow rate (D) with variation in the feed flow rate (Q), but relatively large shifts in the same variable (D) with changes in EVT . However, the relationship between EVT and Q provides a rising ridge response surface as presented in Fig. 5.

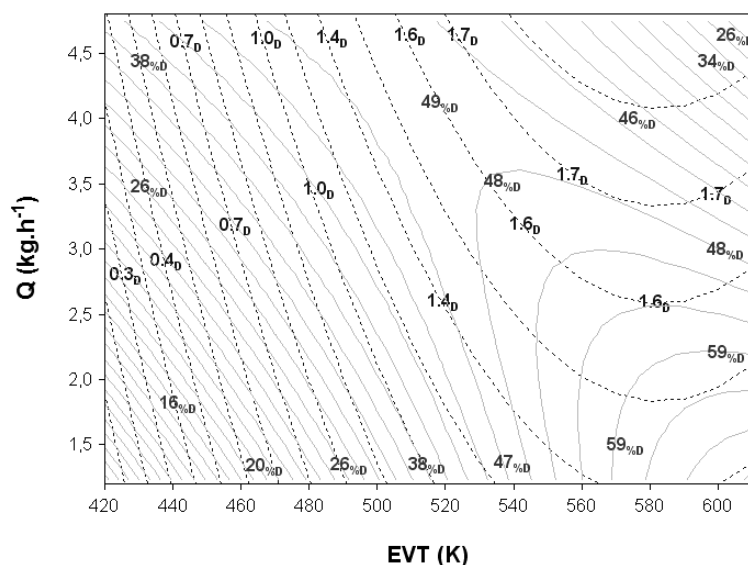


Figure 5. Overlapped contour plots of the distillate mass flow rate (D) and the distillate yield ($\%D$).

No maximum was indicated within the experimental region, but there is a ridge of high values starting at about 495 K and $3.0 \text{ kg} \cdot \text{h}^{-1}$ and rising with increasing EVT and Q , and a steep inclination in D moving from low EVT values (420 K) and low values for Q ($1.5 \text{ kg} \cdot \text{h}^{-1}$) towards the central point of the experimental factorial design.

On the basis of these results, it is reasonable to assume that the input variables indicating the maximum distillate mass flow rate may only be a local maximum on a rising ridge, particularly in the case of EVT , where it is assumed that higher EVT values would give higher distillate mass flow rates (D). However, since the stationary point lies outside the region, it would be difficult to define an optimal point, but it is possible to define a good region to obtain good performance of the centrifugal molecular distillation process (48).

On the other hand, the response surface obtained with Eq. (20) showed a saddle point, at which the two variables, EVT and Q , must be analyzed from two perpendicular directions. For one of these, each vertical slice of the surface shows a maximum value, and for the other, a minimum (see Fig. 5).

A general canonical analysis allowed one to explore and exploit the fitted quadratic response surface, indicating that the predicted response surface would be shaped like a saddle, since the eigenvalues were positive ($\psi_1 = 1.678 \times 10^{-3}$) and negative ($\psi_2 = -1.232$). Similarly, since

one of the eigenvalues is close to zero (ψ_1), then the response surface has one or more ridges (49). Thus, the eigenvalue of 1.678×10^{-3} presented a valley that was less curved than the hill orientation. Hence, the coefficients of the associated eigenvectors showed that the valley was more aligned with Q and the hill with EVT , as depicted in Fig. 5.

In order to facilitate a straightforward examination of the distillate mass flow rate (D) and the distillate yield ($\%D$) generated by varying the evaporator temperature (EVT) and the feed flow rate (Q), the contour plots, constructed using Eqs. (19) – (20), respectively, were overlapped (see Fig. 5).

Analyzing the contour plot related to D , the maximum values of this variable can be seen in the ranges from 520 – 610 K and $2.0 - 4.5 \text{ kg} \cdot \text{h}^{-1}$. The vertical oval shape in the maximum region suggests that the effect of Q on D is less predominant than that of EVT . In contrast, both variables, EVT and Q , show their main effect on $\%D$ in the maximum region, ranging from 540 – 600 K and $1.5 - 3.5 \text{ kg} \cdot \text{h}^{-1}$. Consequently, the maximum values for D and $\%D$ can be obtained in the region delimited by the EVT range from 540 to 600 K and Q range from 1.5 to $3.5 \text{ kg} \cdot \text{h}^{-1}$.

4.3. Physicochemical characterization of split products

In Fig. 6 are shown the rheograms of the distillate and residue streams obtained from CMD.

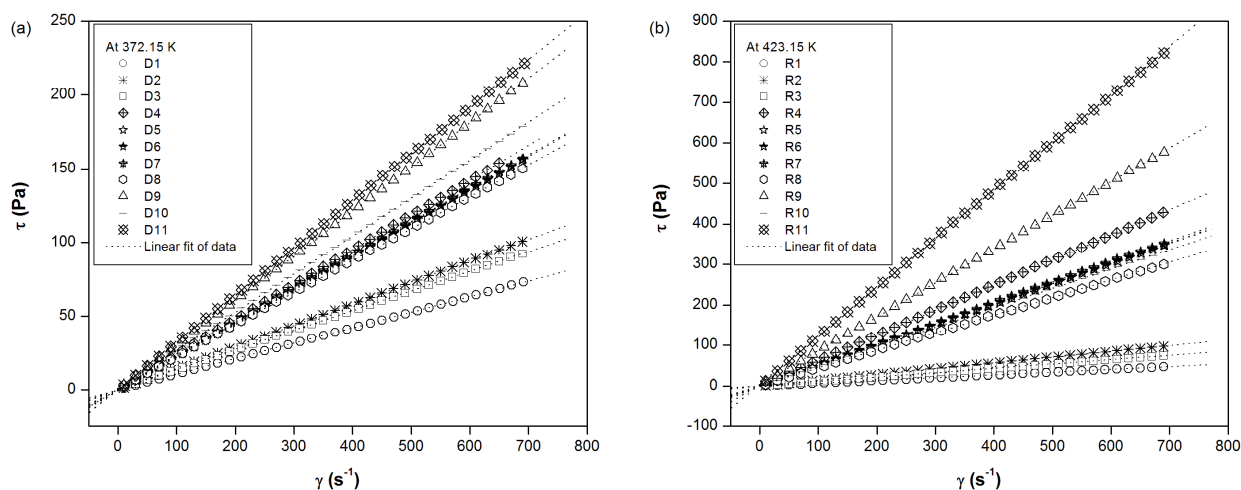


Figure 6. Rheograms of distillate (a) and residue (b) streams obtained by centrifugal molecular distillation from ATR-W 673.15 K⁺.

The behavior of distillate and residue streams in rheological experiments conducted at constant temperature and pressure has the following features: (i) the shear viscosity does not vary with shear rate; (ii) the dynamic viscosity (μ) is constant with respect to the time of shearing; and (iii) the stress in studied samples falls to zero ($\tau=0.000$ Pa) immediately the shearing γ is equal to zero ($\dot{\gamma}=0.000$ s⁻¹). Therefore, with constant pressure and temperature (test temperature), distillate and residue streams exhibit a Newtonian behavior.

The plots of τ versus $\dot{\gamma}$ depicted straight lines, where the slope allows to calculate the dynamic viscosity at test temperature (μ^T). Table 7 presents the μ values of distillate and residue streams at different operating conditions. Good straight line fits was determined since the linear squares correlation varied between 0.9998 and 1.0000.

Dynamic viscosity (μ) is the quantity that describes a fluid of resistance to flow. A high dynamic viscosity (μ) means that the liquid fluid will not flow easily and vice versa. The viscosity values versus shear rate for the residue streams from CMD process displayed a Newtonian behavior in the range of the shear rates and temperature examined at 423.15 K as presented in Table 7. Hence, it is possible to affirm that residue streams are constituted by higher carbon number chains with high viscosity and polarity related to the presence of complex compounds such as resins and asphaltenes (50) when compared to distillate streams which exhibit a Newtonian behavior at a lower temperature (372.15 K) than residue streams.

Table 7 also reports the density at 293.15 K, specific gravity, relative density and API gravity of the distillate and residue streams obtained by CMD. Furthermore, it is possible to confirm that the processing of ATR-W 673.15 K⁺ by CMD allows producing products (distillate streams) with a remarkable difference regarding to initial sample. Hence, the CMD process represents a gain regarding to the decreased of the gravity and the increases of API gravity values of the distillate streams reporting fractions with API gravity higher than 16.

Table 7. Physicochemical and colloidal characterization of the distillate and residue streams obtained by centrifugal molecular distillation from ATR–W 673.15 K⁺.

Stream	Physicochemical characterization									Colloidal characterization		
	<i>EVT</i> (K)	<i>Q</i> (kg·h ⁻¹)	stream name	μ^T (Pa·s)	R ²	$\rho^{293.15\text{ K}}$ (g·cm ⁻³)	$\rho_r^{293.15\text{ K}}$	SG _{20/4}	°API	<i>Mn</i> (kg·kmol ⁻¹)	<i>Mw</i> (kg·kmol ⁻¹)	PDI
-	-	-	ATR–W	3.8359 [†] 0.7799 [‡] 0.4133 [*]	0.9940 0.9998 1.0000	0.9860	0.9878	0.9861	11.9	1017	2956	2.91
Distillate	423.15	2.945	D1	0.1051	1.0000	0.9483±0.0001	0.9500	0.9483	17.6	170	192	1.13
	449.15	1.914	D2	0.1458	1.0000	0.9514±0.0001	0.9531	0.9514	17.1	182	213	1.17
	449.15	3.976	D3	0.1341	1.0000	0.9512±0.0001	0.9529	0.9512	17.2	182	220	1.21
	513.15	1.473	D4	0.2374	1.0000	0.9553±0.0001	0.9570	0.9553	16.5	214	273	1.28
	513.15	2.945	D5	0.2282	0.9998	0.9554±0.0001	0.9571	0.9554	16.5	214	271	1.27
	513.15	2.945	D6	0.2258	1.0000	0.9549±0.0001	0.9566	0.9549	16.6	215	275	1.28
	513.15	2.945	D7	0.2276	1.0000	0.9556±0.0001	0.9573	0.9556	16.5	205	259	1.26
	513.15	4.418	D8	0.2189	0.9998	0.9549±0.0001	0.9566	0.9549	16.6	205	260	1.27
	576.15	1.914	D9	0.3021	1.0000	0.9574±0.0001	0.9591	0.9574	16.2	230	308	1.34
	576.15	3.976	D10	0.2604	0.9998	0.9483±0.0001	0.9500	0.9483	17.6	223	293	1.31
	603.15	2.945	D11	0.3202	1.0000	0.9514±0.0001	0.9531	0.9514	17.1	241	337	1.40
Residue	423.15	2.945	R1	0.0672	0.9998	0.9931	0.9949	0.9934	10.8	1017	2956	2.91
	449.15	1.914	R2	0.1413	1.0000	0.9969	0.9987	0.9971	10.3	376	2931	7.80
	449.15	3.976	R3	0.1072	1.0000	0.9973	0.9991	0.9976	10.2	2733	2590	0.95
	513.15	1.473	R4	0.6228	1.0000	0.9976	0.9994	0.9979	10.2	447	2537	5.68
	513.15	2.945	R5	0.5062	1.0000	1.0007	1.0025	1.0010	9.8	422	2947	6.98
	513.15	2.945	R6	0.5034	1.0000	1.0029	1.0047	1.0031	9.5	271	2613	9.64
	513.15	2.945	R7	0.5125	1.0000	0.9986	1.0004	0.9989	10.1	281	2837	10.10
	513.15	4.418	R8	0.4368	1.0000	1.0040	1.0059	1.0043	9.3	312	2577	8.26
	576.15	1.914	R9	0.8424	0.9998	1.0123	1.0141	1.0125	8.1	428	2544	5.94
	576.15	3.976	R10	0.4815	1.0000	1.0165	1.0183	1.0168	7.6	684	2920	4.27
	603.15	2.945	R11	1.2020	0.9998	1.0192	1.0211	1.0195	7.2	309	3146	10.18

EVT: Evaporator temperature; *Q*: Feed flow rate; *Di*: distillate stream (for i=1,2,...11); *Ri*: residue stream (for i=1,2,...11); μ^T : Dynamic viscosity at test temperature (*T*=372.15 K for distillate streams obtained by centrifugal molecular distillation; *T*=423.15 K for residue streams obtained by centrifugal molecular distillation; [†]*T*=343.15 K; [‡]*T*=363.15 K and ^{*}*T*=373.15 K for ATR–W 673.15 K⁺); R²: linear square correlation for linear fit between shear stress (τ) and shear rate ($\dot{\gamma}$); $\rho^{293.15\text{ K}}$: density data at 293.15 K; $\rho_r^{293.15\text{ K}}$: relative density data at 293.15 K; SG_{20/4}: Specific gravity using Brazilian standard; °API: API gravity data; *Mn*: Number average molar mass; *Mw*: Weight average molar mass and PDI: Polydispersity Index (*Mw/Mn*).

In this sense, the density values in distillate streams are lower than values of this property in the original sample (ATR–W 673.15 K⁺) and residue streams, which satisfy the objective of the CMD process since it is a function of the difference in molar mass of the mixture (the larger the difference in molar mass, the separation will be greater) and depletion of the volatile compounds as the temperature of the film surface increases (51). Nevertheless, the rise of the density in residue streams is due to the components bearing higher structural complexity are concentrated as the evaporator temperature (*EVT*) rises. Therefore, it is expected that the heaviest molecules with greater intermolecular forces and which did not reach the condenser surface are routed to the residue stream.

4.4. Colloidal characterization: Molar mass distribution

Figs. 7 – 8 present the SEC profiles of the ATR–W 673.15 K⁺ and the materials obtained from the CMD process carried out in an *EVT* range from 423.15 K to 603.15 K and *Q* from 1.473 kg·h⁻¹ to 4.418 kg·h⁻¹. The profiles were normalized between 0 – 100% for the UV signals (mV) to permit comparison of the retention volume segments of the curves.

The distillate streams obtained from the CMD process were analyzed using the SEC method to determine the molar mass distribution of the products (Table 7). It was observed that the molar mass distribution of the liquids varied within a wide range. The number average (*M_n*) of the liquid products ranged between 170 kg·kmol⁻¹ and 337 kg·kmol⁻¹ while the weight average (*M_w*) ranged between 192 kg·kmol⁻¹ and 308 kg·kmol⁻¹. Table 7 also shows the polydispersity index (PDI), which reflects the deviations of the molar mass distribution from the Gaussian distribution of an ideal single compound (52).

The polydispersity values (between 1.13 – 1.40) for the distillate streams indicated the presence of a broader range of low carbon number compounds in these streams. Hence, there was a considerable variation in the molar mass of the liquids with increases in the *EVT* and *Q*, under the conditions investigated.

On the other hand, the residue products obtained from the CMD process were found to have values for *M_n* and *M_w* ranging from 376 kg·kmol⁻¹ to 2733 kg·kmol⁻¹ and from 2537 kg·kmol⁻¹ to 3146 kg·kmol⁻¹, respectively. Furthermore, Table 7 presented that the PDI values exhibited a wide range, which means that the number and weight average molar masses (*M_n* and

M_w) of these products were not similar in nature to those of the distillate products, suggesting that the compounds in the residue streams were very different and containing high carbon number chains as resins and asphaltenes.

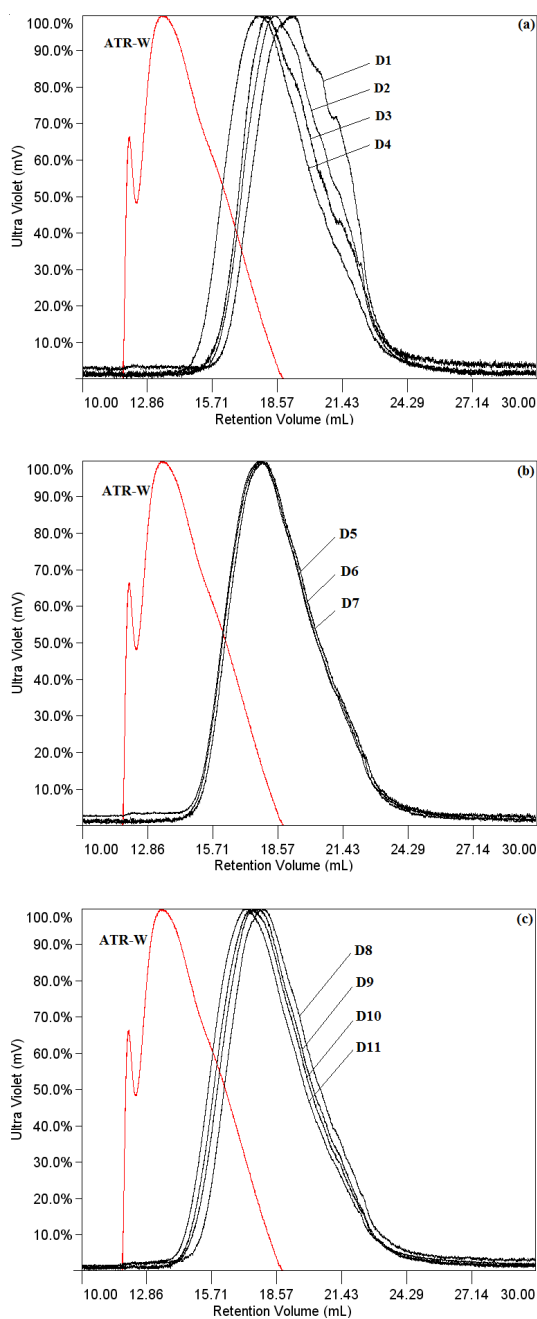


Figure 7. SEC chromatograms of distillate streams obtained by centrifugal molecular distillation from ATR-W 673.15 K⁺. (a) D1 – D4, (b) D5 – D7 and (c) D8 – D11 from Table 7.

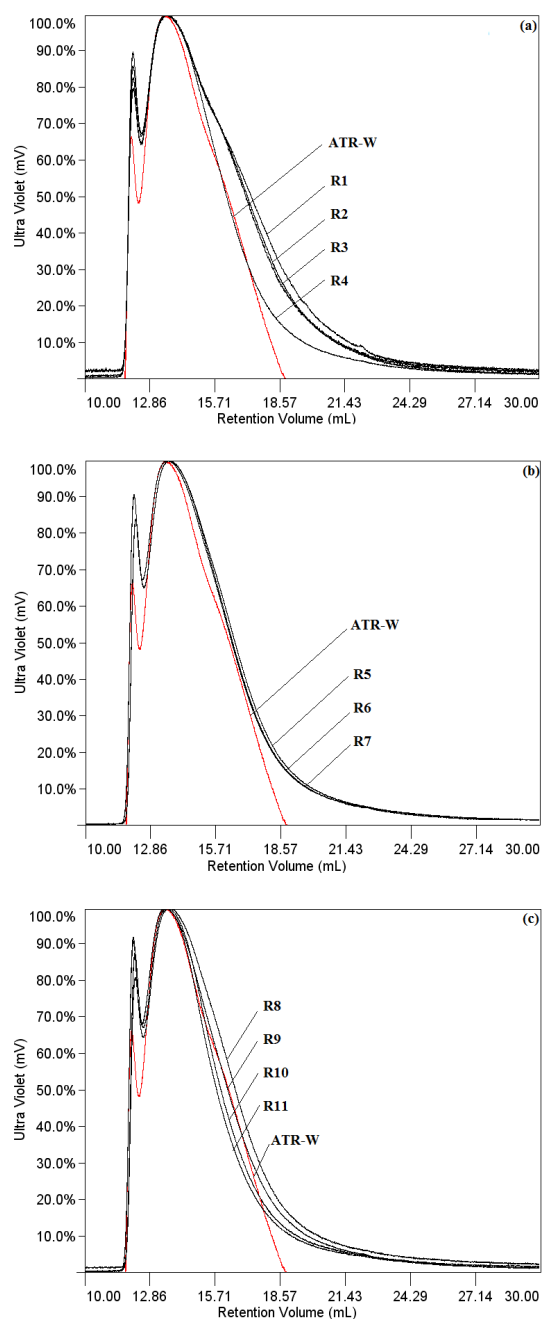


Figure 8. SEC chromatograms of residue streams obtained by centrifugal molecular distillation from ATR-W 673.15 K⁺. (a) R1 – R4, (b) R5 – R7 and (c) R8 – R11 from Table 7.

In this sense, the results presented in Table 7 showed that as evaporator temperature (*EVT*) increases the residue streams exhibited higher values of molar mass than distillate streams since there is higher concentration of non-volatile compounds and a high fraction of compounds with structural complexity.

4.4. Analysis of the performance of the centrifugal molecular distillation by simulation

In this section the numerical results will be presented plus a comparison with the experimental data obtained from the CMD process used to split a heavy petroleum fractions. The modeling and simulation are illustrated for a heavy residue (ATR-W 673.15 K⁺) divided into twenty five pseudocomponents. The physicochemical properties (basic and thermodynamic properties) were estimated using correlations available in the literature as presented by Tovar et al. (34). The thermophysical properties (kinematic viscosity, thermal conductivity, specific heat capacity, evaporation enthalpy, vapor pressure and diffusion coefficient) were estimated as a function of the normal boiling point, specific gravity and temperature (surface temperature of the film), as presented by Tovar et al. (34).

The equipment dimensions and operating conditions are listed in Table 8.

Table 8. Simulated conditions and data.

Variables	Value	Units
<i>Equipment dimensions</i>		
Evaporator radius	0.2662	m
Distance from apex at which liquid enters cone	0.03095	m
Evaporation gap	0.08	m
Half angle of apex of cone radius	70	—
<i>Model parameters</i>		
Number of intermolecular collisions	5	—
<i>Operating conditions</i>		
Feeding temperature	423.15	K
Condenser temperature	353.15	K
Trap cooler temperature	373.55	K
Rotor speed	540	rpm
Feed flow rate	Table 2	kg·h ⁻¹
Evaporator temperature	Table 2	K
Pressure system	0.4	Pa

Numerical results of surface temperature (T_s), effective evaporation rate (G_E), distillate mass flow rate (D) and liquid film thickness (δ) profiles have been analyzed from simulated data obtained with the computational environment through the mathematical model developed by Inuzuka et al. (36) and modified, using the effective evaporation rate. Therefore, it was adopted for discussing the effect of operating condition (EVT and Q) on output variables. Typical results from these computed profiles are presented in Figs. 9 – 12.

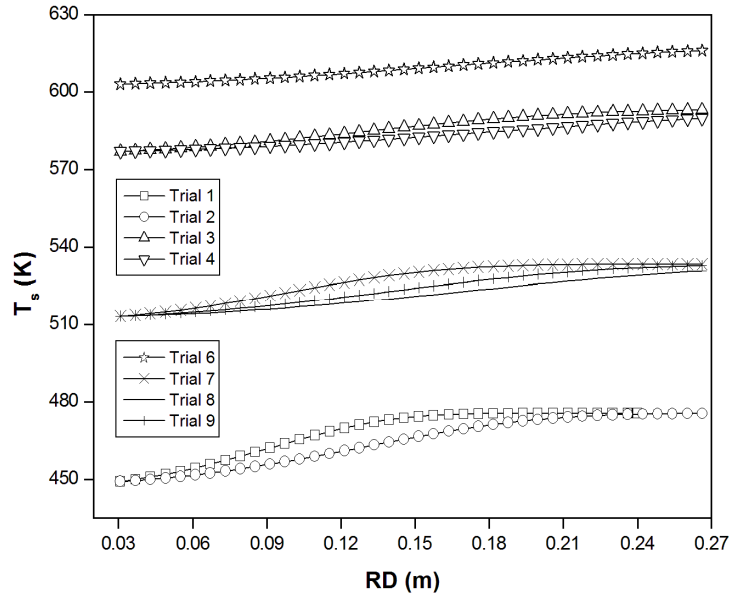


Figure 9. Surface temperature (T_s) profiles of centrifugal molecular distillation from ATR–W 673.15 K⁺.

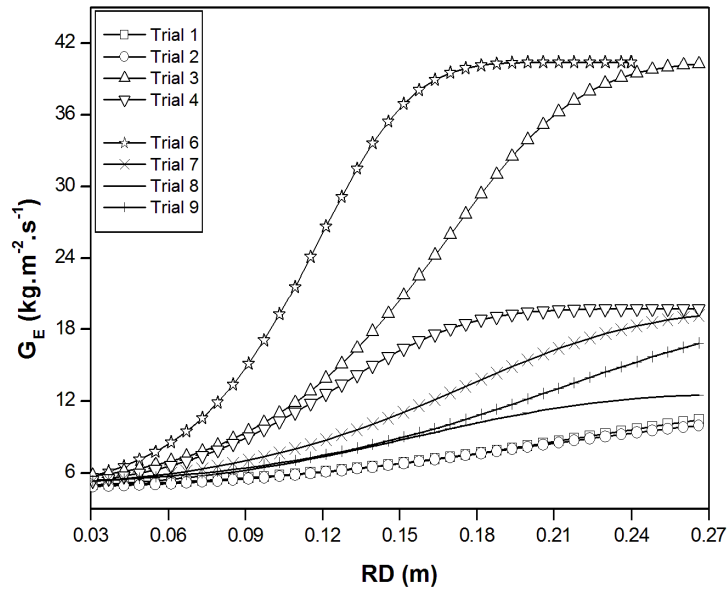


Figure 10. Effective evaporation rate (G_E) profiles of centrifugal molecular distillation from ATR–W 673.15 K⁺.

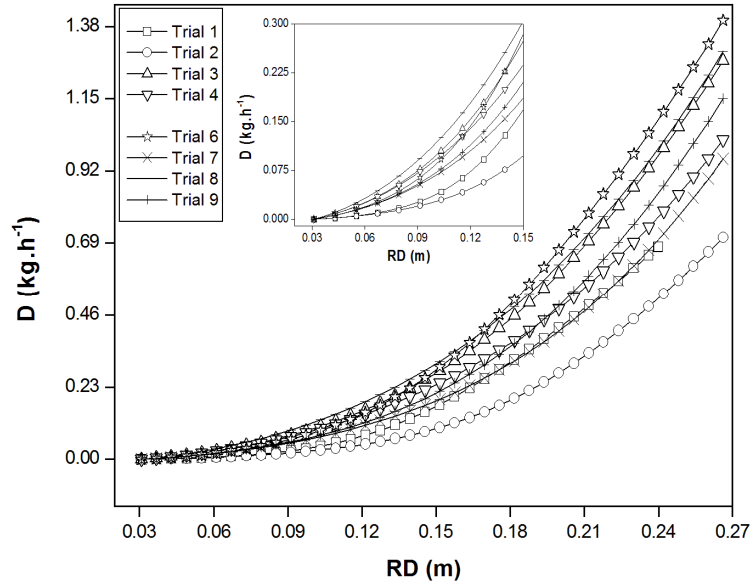


Figure 11. Overall distillate mass flow rate (D) profiles of centrifugal molecular distillation from ATR-W 673.15 K⁺.

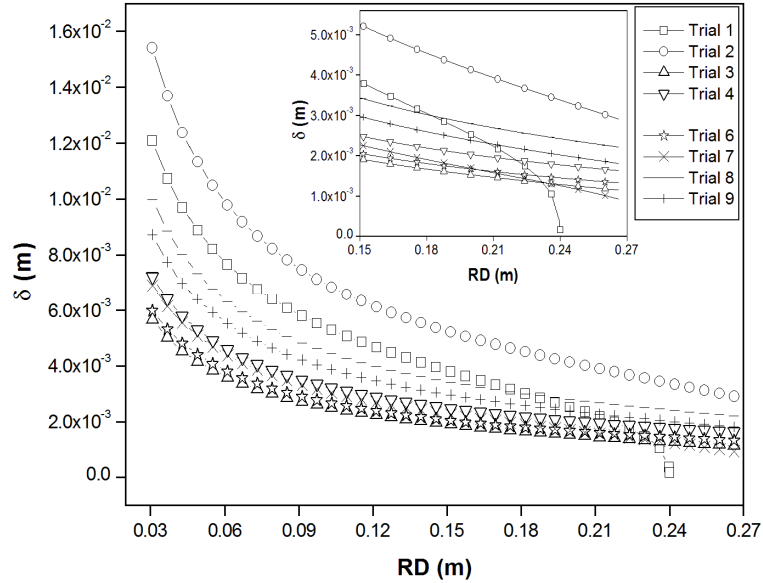


Figure 12. Film thickness (δ) profiles of centrifugal molecular distillation from ATR-W 673.15 K⁺.

4.4.1. Evaporator temperature influence on centrifugal molecular distillation

The EVT is the most important governing condition in the evaporating flow. In Fig. 9, the T_s profiles of the liquid film are shown as a function of the radial distance, RD , along of the evaporator surface. Hence, when a thin liquid film of a multicomponents flows over a heated evaporator surface, under vacuum conditions (i.e. 0.4 Pa), evaporation phenomenon at the free

surface, leads to depletion of the most volatile component or components in the liquid phase, forming a thin liquid film that, evenly, might to condense along the condenser surface. As a result, the distillate flow increases as consequence of: (i) The elevated film surface temperature; (ii) the decrease of the film thickness on the evaporator surface and, (iii) advantageous operating conditions on the centrifugal molecular distillation process.

Furthermore, results showed that the radial thermal gradients inner the thin liquid film produced a significantly change in the G_E and D . Figs. 10 – 11 showed that the G_E and D varied strongly after the center of evaporator surface, representing how fast the front of liquid film flow advances along the evaporator surface and how the fluid flow changes into the vapor state over the evaporator surface, which means that the G_E profiles are greatly influenced by EVT , the concept of relaxation length was applied for understand the effect on this output variable.

On the other hand, the relaxation length concept refers to the radial position at which a given parameter (T_s and G_E) reaches asymptotic value (15). Therefore, in reference to the G_E , the upper limits were $10.4555 \text{ kg}\cdot\text{m}^{-2}\cdot\text{s}^{-1}$ (trial 1 and trial 2 at 0.2662 m), $40.005 \text{ kg}\cdot\text{m}^{-2}\cdot\text{s}^{-1}$ (trial 3 at 0.2541 m), $19.601 \text{ kg}\cdot\text{m}^{-2}\cdot\text{s}^{-1}$ (trial 4 at 0.2119 m), $40.358 \text{ kg}\cdot\text{m}^{-2}\cdot\text{s}^{-1}$ (trial 6 at 0.1938 m), $19.129 \text{ kg}\cdot\text{m}^{-2}\cdot\text{s}^{-1}$, $12.538 \text{ kg}\cdot\text{m}^{-2}\cdot\text{s}^{-1}$ and $16.842 \text{ kg}\cdot\text{m}^{-2}\cdot\text{s}^{-1}$ (trial 7, trial 8 and trial 9 at 0.2662 m). With respect to the heat transfer, two regions can be elucidated: (i) the temperature profile in the entrance section of conical evaporator surface from 0.03095 m to 0.1800 m and, (ii) a fully developed T_s profile from 0.1500 m to 0.2662 m. thus, in the first section, evaporation of liquid was negligible in comparison with the section between 0.180 m and 0.2662 m. In consequence, the efficiency of the CMD process increased along the RD , resulting in the correspondingly exponential increase of the distillate mass flow rate, D , due to the increase of the induced centrifugal force, which is known as the flow driving force in the system (Fig. 11).

In Fig. 12 is presented the δ profile for different values of EVT at range from 423.15 K to 603.15 K and Q from $1.473 \text{ kg}\cdot\text{h}^{-1}$ to $4.418 \text{ kg}\cdot\text{h}^{-1}$. The radial distance, RD , is plotted on the abscissa and the film thickness, δ , on the ordinate. It can be seen that the greatest changes in the film thickness profile occurred in the region between 0.03095 m to 0.1800 m corresponding to the entrance section of the feed material and center section of the evaporator surface. Analyzing the film thickness profiles it was depicted a continuous decrease to $1\times 10^{-3} \text{ m}$ at 603.15 K and $2.945 \text{ kg}\cdot\text{h}^{-1}$. This is explained by depletion of the volatile pseudocomponents due to the increase

in the temperature of the film surface (T_s), the lower viscosity and the higher effective evaporation rates of the evaporating molecules as presented by Zuñiga-Liñan et al. (10).

4.3.2. Feed flow rate influence on centrifugal molecular distillation

In order to provide a qualitative and quantitative physical insight inner the evaporating liquid film over the evaporator surface device, it was extensively performed the study on the flow behavior in terms of the T_s , G_E , D and δ , analyzing the influence of Q .

In Figs. 9 – 12 the relationship of the T_s , G_E , D and δ versus RD are shown with EVT and Q as parameter. Thus, the T_s profiles increase gradually throughout the film length and reach the asymptotic values in correspondence with the relaxation length of 0.1800 m. In the studied range of Q , the temperature difference in the radial direction was very small ($0.05 \text{ K}\cdot\text{m}^{-1}$). These relatively small radial gradients might be ascribed to the low thermal conductivity, about $1.22 \text{ W}\cdot\text{m}^{-1}\cdot\text{K}^{-1}$ for ATR–W 673.15 K^+ , to conduct heat transferred from the evaporator surface to the inner of the liquid film.

The slight rise of the T_s (Fig. 9) and the G_E (Fig. 10) profiles as Q decrease is related mainly to the good mass transfer over the evaporator surface and, consequently, to the increase of evaporation of volatile compounds. In addition, at fixed temperature (i.e. 577.15 K), the liquid film at lower Q values had higher asymptotic profile of G_E and higher relaxation lengths per film thickness unit as along radial distance (RD) when compared to high values of Q . Therefore, Q parameter influenced directly in the liquid film thickness and mass transfer, once, values of Q lower than $1.000 \text{ kg}\cdot\text{h}^{-1}$ may not be high enough to efficient mass and heat transfers. On the other hand, for Q values higher than $2.000 \text{ kg}\cdot\text{h}^{-1}$, the system might operate with low effectiveness because the residence time of the molecules on the evaporator might be too low.

Fig. 12 shows the development of the δ along the evaporator length in r -direction. Given the dependence on the δ in relationship with the Q , the δ profiles were affected by the change of Q condition. Thus, it is noted that lower δ values were reached at the low values of Q , guarantying in this conditions, that a uniform thin film promotes high efficiency in the mass and in the energy transfers. This engages to the fact that the evaporation speed increases when the liquid film over the evaporator surface becomes more uniform at lower values of Q ensuring the

short residence time of the liquid load over the evaporator surface and the distributing in the form of a thin liquid film.

4.3.3. Model validity

The results obtained of distillate mass flow rate (D) and distillate yield ($\%D$) in the simulations and the response surface analyses, were compared with the experimental data as presented in Table 9. Moreover, results were evaluated in terms of the average absolute deviation percent ($AAD\%$) defined as the absolute deviation percent in estimating a quantity divided by its observed value (y_{ref}). The absolute deviation percent is defined as the difference among the observed values (y_{ref}) and the response predicted (y_{cal}) by the modeling approach at each operating condition (Table 9). Consequently, the mathematical and statistical models from Eqs. (19) – (20) gave a good representation of the experimental data related to the overall distillate mass flow rate (D) since, the average absolute deviation ($AAD\%$) were of 12.14% (mathematical model), 14.16% (statistical model from Eq. 19) and; distillate yield ($\%D$) since $AAD\%$ was 4.58% (statistical model form Eq. 20), respectively.

Table 9. Predicted distillate mass flow rate (D) and distillate yield ($\%D$) and absolute deviations percent (%) calculated by mathematical model and statistical models (Eqs. 19 – 20) at various operating conditions.

Operating condition		Experimental data (y_{ref})		Predicted data (y_{cal})			Absolute deviations percent (%)		
EVT (K)	Q (kg·h ⁻¹)			Mathematical model	Statistical model Eq. 19	Statistical model Eq. 20	Mathematical model	Statistical model Eq. 19	Statistical model Eq. 20
		D (kg·h ⁻¹)	$\%D$ (%wt)	D (kg·h ⁻¹)	D (kg·h ⁻¹)	$\%D$ (%wt)			
449.15	1.914	0.624	20.512	0.679	0.413	18.101	8.77	33.76	11.75
449.15	3.976	0.708	40.666	0.708	0.688	40.589	0.06	2.89	0.19
577.15	1.914	1.296	58.861	1.271	1.262	56.592	1.92	2.59	3.85
577.15	3.976	1.584	45.655	1.220	1.537	45.726	22.98	2.99	0.16
423.15	2.945	0.263	17.883	0.302	0.178	19.929	15.12	32.36	11.44
603.15	2.945	1.656	48.763	1.399	1.372	50.605	15.52	17.17	3.78
513.15	1.473	1.080	37.975	0.959	0.984	41.178	11.20	8.88	8.44
513.15	4.418	1.596	48.889	1.301	1.376	49.480	18.48	13.79	1.21
513.15	2.945	1.356	47.794	1.150	1.180	47.992	15.21	12.98	0.41
							$AAD\%=12.14\%$	$AAD\%=14.16\%$	$AAD\%=4.58\%$

EVT : Evaporator temperature; Q : Feed flow rate; D : distillate mass flow rate; $\%D$: Distillate yield

$$AAD\% = (1/n) \sum_{i=1}^n \frac{|y_{i,cal} - y_{i,ref}|}{y_{i,ref}} * 100 \quad \text{Where } n \text{ equals } 9$$

On the other hand, as can be seen, the predicted values with the statistical models (Eqs. 19 – 20) match the experimental values reasonably well with a percent of maximum explainable

variance of 99.9% and a percent of explained variance of 95.6% for response D while for the response $\%D$ the percent of maximum explainable variance was 100% and the percent of explained variance of 98.2%. Figs. 13 – 14 are residual plots for D and $\%D$ in the statistical model. It shows that the distribution of the residual for the response approximately follows the fitted normal distribution and the residuals of the response randomly scatter in the residual plots.

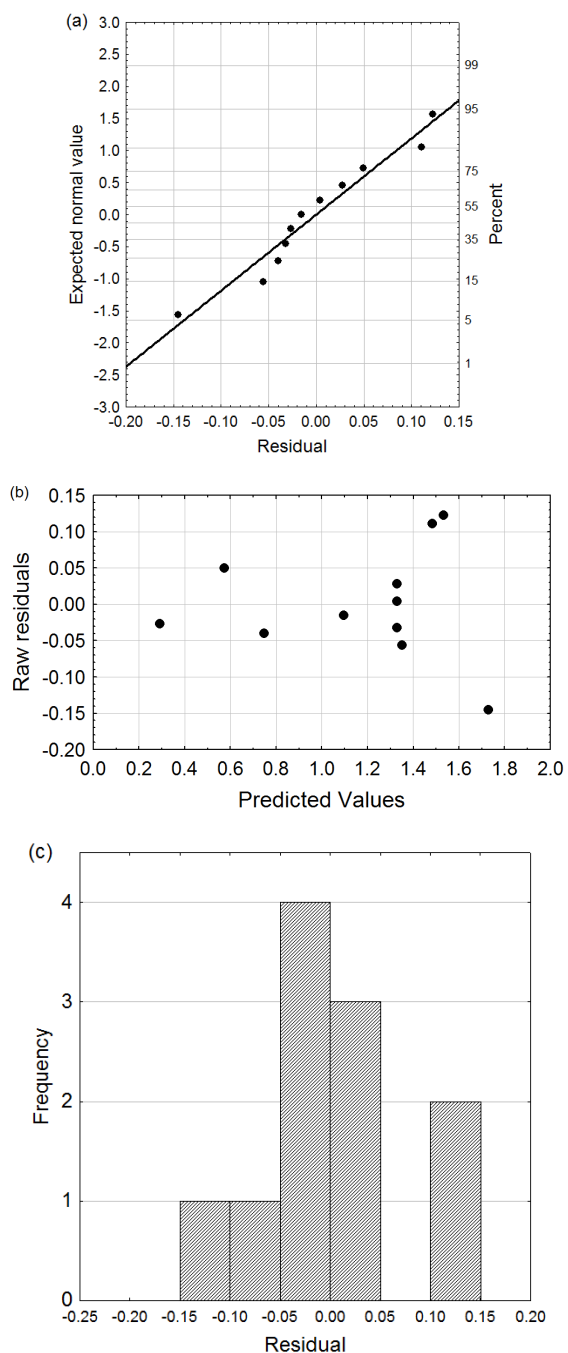


Figure 13. Residual plots for distillate mass flow rate (D) response in the statistical model (Eq. 19).

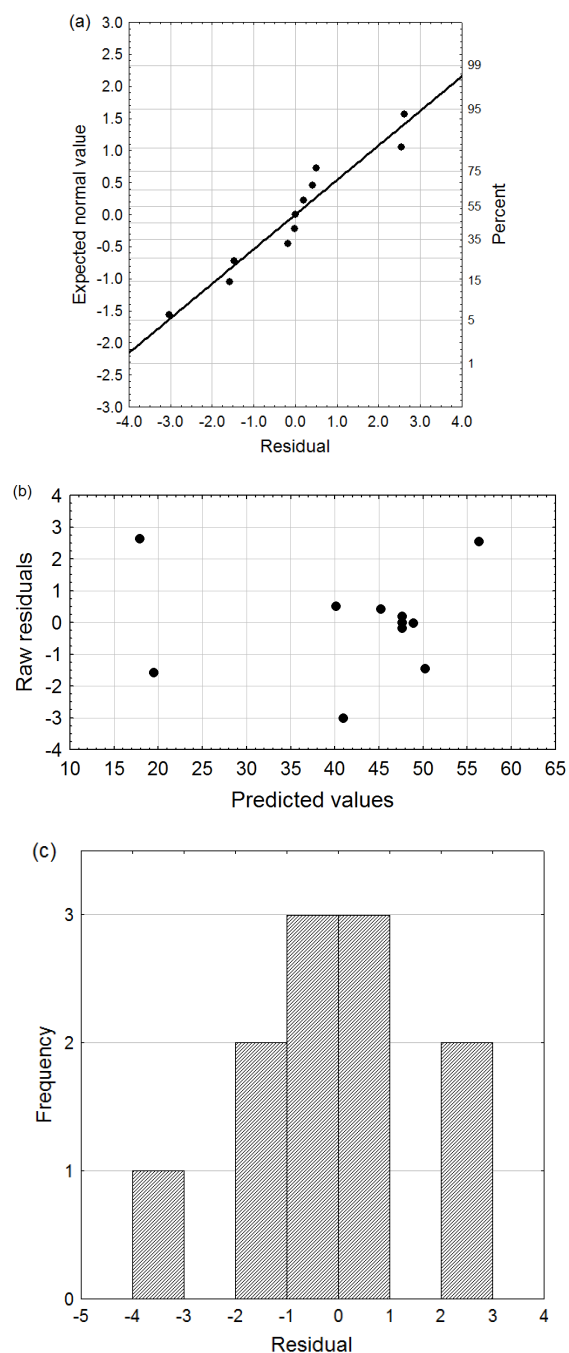


Figure 14. Residual plots for distillate yield ($\%D$) response in the statistical model (Eq. 20).

Conclusions

Response surface methodology was used in conjunction with central composite factorial design to optimize the operating conditions of the centrifugal molecular distillation from a high-boiling-point petroleum fraction (ATR-W 673.15 K⁺). The central composite factorial design technique was shown to be very useful for the analysis of the significant effects on the overall distillate mass flow rate (D) and the distillate yield ($\%D$) in the centrifugal molecular distillation process. The analysis of variance revealed that the main effects of the evaporator temperature (EVT) and the feed flow rate (Q) were the most significant factors that influenced the dependent variable distillate mass flow rate (D), followed by the quadratic effect of evaporator temperature, while the most significant factors that influenced the distillate yield ($\%D$) were the main effects of the evaporator temperature (EVT) and the feed flow rate (Q), followed by the quadratic effects of both operating variables (EVT and Q) and the two-level interaction effect of evaporator temperature (EVT) and feed flow rate (Q).

Regression equations (statistical models from Eqs. 19 – 20) were derived for both the distillate mass flow rate (D) and distillate yield ($\%D$), predicting values in good agreement with experimental values. Therefore, statistical models can be used to predict within the range of evaporator temperature (EVT) and feed flow rate (Q) analyzed in this study. Accordingly, using the response surface methodology it was possible to determine the optimal operating conditions to obtain a high distillate mass flow rate (D) without a loss of yield in the centrifugal molecular distillation process (high values of $\%D$). From the analysis of the response surfaces, the most suitable operating conditions to study the processing (split) of heavy petroleum fractions were determined. Consequently, maximum values for D and $\%D$ can be obtained in the region delimited by ranges for EVT from 540 to 600 K and for Q from 1.5 to 3.5 kg·h⁻¹.

Rheological profiles of the distillate and residue streams obtained by centrifugal molecular distillation process revealed a Newtonian behavior at 372.15 K and 423.15 K, respectively, since the dynamic viscosity (μ) stayed constant in front of the linear increase of the shear stress (τ) as function of the shear rate ($\dot{\gamma}$). On the other hand, it was clear the increase of API gravity data of the distillate streams. This can be explained since the centrifugal molecular distillation process produces distillate streams which have a lower proportion of compounds with

complex molecular structures when compared with residue streams which have compounds with features of resins and asphaltenes.

From the simulated results obtained for the centrifugal molecular distillation processing of the heavy residue ATR–W 673.15 K⁺, it was concluded that the surface temperature, film thickness, effective evaporation rate and overall distillate mass flow rate were strongly affected by the evaporator temperature (*EVT*). Thus, the effectiveness of centrifugal molecular distillation process from ATR–W 673.15 K⁺ was evaluated by minimum film thickness, high distillate mass flow rate and high effective evaporation rate as consequence of the depletion phenomenon of the most volatile compound or compounds (pseudocomponents) and efficient mass and heat transfers inner the evaporating liquid film over the evaporator surface device.

Acknowledgments

This research was supported by the Brazilian National Council for Technological and Scientific Development (CNPq), the Petrobras Research and Development Center (PETROBRAS/CENPES) and the Brazilian Study and Project Financing Institution (FINEP).

Nomenclature

C_p	=	Specific heat capacity	[J·kg ⁻¹ ·K ⁻¹]
d_e	=	Diameter of evaporation surface curvature	[m]
D	=	Distillate mass flow rate	[kg·h ⁻¹]
% D	=	Distillate yield	[%wt]
EVT	=	Evaporator temperature	[K]
G_E	=	Effective evaporation rate	[kg·m ⁻² ·s ⁻¹]
Kn	=	Knudsen number	[-]
k^*	=	Anisotropy condition of vapor phase	[-]
L	=	Distance between evaporator and condenser surfaces	[m]
M	=	Molar mass	[kg·kmol ⁻¹]
MFP	=	Mean free path	[m]
MSq_{LOF}	=	Mean square lack of fit	[-]
MSq_{PE}	=	Mean square pure error	[-]
MSq_R	=	Mean square regression	[-]
MSq_r	=	Mean square residual	[-]
n'	=	Number of intermolecular collisions before the vapor reaches isotropic state ($n'=5$)	[-]
N_m	=	Number of molecules per volume unit of vapor phase	[mol·m ⁻³]
N_A	=	Avogadro Constant (6.023x10 ²³ mol ⁻¹)	[mol ⁻¹]
P_s	=	System pressure	[Pa]
P_{vap}	=	Equilibrium vapor pressure	[Pa]
q_w	=	Heating rate at evaporator wall	[J·m ⁻² ·s ⁻¹]

Q	= Feed flow rate	$[\text{kg} \cdot \text{h}^{-1}]$
\dot{Q}	= Volumetric feed flow rate	$[\text{m}^3 \cdot \text{s}^{-1}]$
\dot{Q}_i	= Volumetric feed flow rate at $r = r_i$	$[\text{m}^3 \cdot \text{s}^{-1}]$
r	= r – direction of coordinate system	$[-]$
R_g	= Universal gas constant ($8314 \text{ J} \cdot \text{K}^{-1} \cdot \text{kmol}^{-1}$)	$[\text{J} \cdot \text{K}^{-1} \cdot \text{kmol}^{-1}]$
r_i	= Distance from apex at which liquid enters cone	$[\text{m}]$
r_o	= Radial position which liquid leaves	
RD	= Radial distance along evaporator surface	$[\text{m}]$
RS	= Rotor speed	$[\text{rpm}]$
s	= s – direction of coordinate system perpendicular to cone surface	$[-]$
T_s	= Surface Temperature	$[\text{K}]$
y_{cal}	= Predicted value	$[\text{kg} \cdot \text{h}^{-1}]$
y_{ref}	= Observed value	$[\text{kg} \cdot \text{h}^{-1}]$

Greek Letter

β^*	= Half angle of apex of cone radius	$[-]$
δ	= Thickness of liquid film	$[\text{m}]$
ΔH	= Heat of evaporation	$[\text{J} \cdot \text{kg}^{-1}]$
λ	= Thermal conductivity	$[\text{W} \cdot \text{m}^{-1} \cdot \text{K}^{-1}]$
ρ	= Density	$[\text{kg} \cdot \text{m}^{-3}]$
π	= Pi parameter	$[-]$
v_r	= Thin liquid film velocity in r -direction (radial velocity)	$[\text{m} \cdot \text{s}^{-1}]$
μ	= Dynamic viscosity	$[\text{Pa} \cdot \text{s}]$
ν	= Kinematic viscosity	$[\text{m}^2 \cdot \text{s}^{-1}]$
ω	= Angular velocity of cone	$[\text{s}^{-1}]$
ξ_i	= Coefficient related to the direct influence of independent variables	$[-]$
ξ_{ij}	= Coefficients statistical model related to the possible linear interactions among the independent variables	$[-]$
ξ_{ii}, ξ_{jj}	= Coefficient corresponding to the quadratic influence of independent variables	$[-]$
ψ_1, ψ_2	= Eigenvalues	$[-]$

Subscripts

i	= inlet
o	= Outlet
E	= Effective
l	= Linear effect
q	= Quadratic effect

Acronyms

ATR	= Residue from conventional atmospheric distillation
CNPq	= Brazilian National Council for Technological and Scientific Development
FINEP	= Brazilian Study and Project Financing Institution
LDPS	= Laboratory of Separation Process Development
LOPCA	= Laboratory of Optimization, Project and Advanced Control
W	= Dummy name for ATR fraction

References

1. Rana, M. S.; Sámano, V.; Ancheyta, J.; Diaz, J. A. I. (2007). A review of recent advances on process technologies for upgrading of heavy oils and residua. *Fuel*, 86 (9): 1216.

2. American Society for Testing Materials, ASTM D 4175. Standard terminology relating to petroleum, petroleum products, and lubricants. West Conshohoken, (Pennsylvania): ASTM International, 2009. 48p.
3. Batistella, C. B.; Maciel, M. R. W. (1996). Modeling, simulation and analysis of molecular distillators: Centrifugal and falling film. *Comput. Chem. Eng.*, 20 (Supplement 1): S19.
4. Batistella, C. B.; Wolf-Maciel, M. R. (1998). Recovery of carotenoids from palm oil by molecular distillation. *Comput. Chem. Eng.*, 22 (Supplement 1), S53.
5. Batistella, C. B.; Maciel, M. R. W.; Maciel Filho, R. (2000). Rigorous modeling and simulation of molecular distillators: development of a simulator under conditions of non ideality of the vapor phase. *Comput. Chem. Eng.*, 24 (2–7): 1309.
6. Batistella, C. B.; Moraes, E. B.; Maciel Filho, R.; Wolf Maciel, M. R. (2002). Molecular distillation: Rigorous modeling and simulation for recovering vitamin E from vegetal oils. *Appl. Biochem. Biotechnol.*, 98–100 (1–9): 1187.
7. Maciel-Filho, R.; Batistella, C. B.; Sbaite, P.; Winter, A.; Vasconelos, C. J.; Wolf-Maciel, M. R.; Gomes, A.; Medina, L.; Kunert R. (2006). Evaluation of atmospheric and vacuum residues using molecular distillation and optimization. *Pet. Sci. Technol.*, 24 (3–7): 275.
8. Sbaite, P.; Batistella, C. B.; Winter, A.; Vasconcelos, C. J. G.; Wolf Maciel, M. R.; Maciel Filho, R.; Gomes, A.; Medina, L.; Kunert R.. (2006). True boiling point extended curve of vacuum residue through molecular distillation. *Pet. Sci. Technol.*, 24 (3–4): 265.
9. Liñan, L. Z.; Lopes, M. S.; Wolf Maciel, M. R.; Lima, N. M. N.; Maciel Filho, R.; Embiruçu, M.; Medina, L. C. (2010). Molecular distillation of petroleum residues and physical–chemical characterization of distillate cuts obtained in the process. *J. Chem. Eng. Data*, 55 (9): 3068.
10. Zuñiga-Liñan L., Nascimento-Lima N. M., Manenti F., Wolf-Maciel M. R., Maciel Filho R., Medina L. C. (2011) Experimental campaign, modeling, and sensitivity analysis for the molecular distillation of petroleum residues 673.15 K+, *Chem. Eng. Res. Des.*, doi:10.1016/j.cherd.2011.07.001.
11. Lee, E. (2009). Simulation of the thin-film thickness distribution for an OLED thermal evaporation process. *Vacuum*, 83 (5): 848.

12. Makarytchev, S. V.; Langrish, T. A. G.; Prince, R. G. H. (2001). Thickness and velocity of wavy liquids films on rotating conical surfaces. *Chem. Eng. Sci.*, 56 (1): 77.
13. Xubin, Z.; Chunjian, X.; Ming, Z. (2005). Modeling of falling film molecular distillator. *Sep. Sci. Technol.*, 40 (6): 1371.
14. Cvengroš, J.; Pollák, Š.; Micov, M.; Lutišan, J. (2001). Film wiping the molecular evaporator. *Chem. Eng. J.*, 81 (1–3): 9.
15. Cvengroš, J.; Lutišan, J.; Micov, M. (2000). Feed temperature influence on the efficiency of a molecular evaporator. *Chem. Eng. J.*, 78 (1): 61.
16. Fregolente, L. V.; Fregolente, P. B. L.; Chicuta, A. M.; Batistella, C. B.; Maciel-Filho, R.; Wolf-Maciel, M. R. (2007). Effect of operating conditions on the concentration of monoglycerides using molecular distillation. *Chem. Eng. Res. Des.*, 85 (11), 1524.
17. Jebson, R. S.; Chen, H.; Campanella, O. H. (2003). Heat transfer coefficients for evaporation from the inner surface of a rotating cone – II. *Food Bioprod. Process.*, 81 (4): 293.
18. Moraes, E. B.; Martins, P. F.; Batistella, C. B.; Alvarez, M. E. T.; Maciel Filho, R.; Wolf Maciel, M. R. (2006). Molecular distillation, a powerful technology for obtaining tocopherols from soya sludge. *Appl. Biochem. Biotechnol.*, 132 (1–3): 1066.
19. Rossi, P. C.; Pramparo, M. C.; Gaich, M. C.; Grosso, N. R.; Nepote, V. (2011) Optimization of molecular distillation to concentrate ethyl esters of eicosapentaenoic (20:5 ω -3) and docosahexaenoic acids (22: 6 ω -3) using simplified phenomenological modeling. *J. Sci. Food Agr.*, 91 (8): 1452.
20. Tovar, L. P.; Wolf-Maciel, M. R.; Ferreira-Pinto, G. M.; Maciel-Filho, R.; Gomes, D. R. (2010). Factorial design applied to concentrate bioactive component of *cymbopogon citratus* essential oil using short path distillation. *Chem. Eng. Res. Des.*, 88 (2A): 239.
21. Wang, S.; Gu, Y.; Liu, Q.; Yao, Y.; Guo, Z.; Luo, Z.; Cen, K. (2009). Separation of bio-oil by molecular distillation. *Fuel Process. Tech.*, 90 (5): 738.
22. Shao, P.; He, J.; Sun, P.; Jiang, S. (2009). Process optimisation for the production of biodiesel from rapeseed soapstock by a novel method of short path distillation. *Biosystems Eng.*, 10 (3): 285.

23. Guo, Z. -G., Wang, S. -R., Zhu, Y. -Y., Luo, Z. -Y., and Cen, K. -F. (2009). Separation of acid compounds for refining biomass pyrolysis oil. *J. Fuel Chem. Technol.*, 37 (1): 49.
24. Lin, S. W.; Yoo, C. K. (2009). Short-path distillation of palm olein and characterization of products. *Eur. J. Lipid Sci. Tech.*, 111(2): 142.
25. Compton, D. L.; Laszlo, J. A.; Eller, F. J.; Taylor, S. L. (2008). Purification of 1,2-diacylglycerols from vegetable oils: Comparison of molecular distillation and liquid CO₂ extraction. *Ind. Crop. Prod.*, 28 (2): 113.
26. Cermak, S. C.; John, A. L.; Evangelista, R. L. (2007). Enrichment of decanoic acid in cuphea fatty acids by molecular distillation. *Ind. Crop. Prod.*, 26 (1): 93.
27. Chen, F.; Wang, Z.; Zhao, G.; Liao, X.; Cai, T.; Guo, L.; Hu, X. (2007). Purification process of octacosanol extracts from rice bran wax by molecular distillation. *J. Food Eng.*, 79 (1): 63.
28. Martinello, M.; Hecker, G.; Pramparo, M. C. (2007). Grape seed oil deacidification by molecular distillation: Analysis of operative variables influence using the response surface methodology. *J. Food Eng.*, 81 (1): 60.
29. Posada, L. R.; Shi, J.; Kakuda, Y.; Xue, S. J. (2007). Extraction of tocotrienols from palm fatty acid distillates using molecular distillation. *Separ. Purif. Tech.*, 57 (2): 220.
30. Shi, J.; Posada, L. R.; Kakuda, Y.; Xue, S. J. (2007). Molecular distillation of palm oil distillates: Evaporation rates, relative volatility and distribution coefficients of tocopherols and other minor components. *Sep. Sci. Tech.*, 42 (14): 3029.
31. Rada, M.; Guinda, A.; Cayuela, J. (2007). Solid/liquid extraction and isolation by molecular distillation of hydroxytyrosol from *Olea europaea* L. leaves. *Eur. J. Lipid Sci. Technol*, 109 (11): 1071.
32. Jiang, S. T.; Shao, P.; Pan, L. J.; Zhao, Y. Y. (2006). Molecular distillation for recovering tocopherol and fatty acid methyl esters from rapessed oil deodorizer distillate. *Biosystems Eng.*, 93 (4): 383.
33. StatSoft Inc., (2004) StatSoft Inc., Statistica for Windows (Computer Program Manual), Statsoft Inc., 2300, East 14th Street, Tulsa, OK, USA (2004).

34. Tovar, L. P.; Wolf-Maciel, M. R.; Maciel-Filho, R.; Batistella, C. B.; Ariza, O. J. C.; Medina, L. C. Overview and computational approach for studying the physicochemical characterization of high-boiling-point petroleum fractions (350 °C+). *Oil Gas Sci. Technol. – Rev. IFP*, doi: 10.2516/ogst/2011150.
35. Hinze, J. O.; Milborn, H. (1950). Atomization of liquid by means of a rotating cup. *J. Appl. Mech.*, 17 (Paper 49–SA–2): 145.
36. Inuzuka, M.; Sugiyama, R.; Saito, I.; Yamada, I.; Hiraoka, S.; Ishikawa, H.; Banno, I. (1986). Analysis of heat and mass transfer in a centrifugal molecular still. *J. Chem. Eng. Jpn.*, 19 (1): 14.
37. Kawala, Z.; Dakiniewicz, P. (2002). Influence of evaporation space geometry on rate of distillation in high-vacuum evaporator. *Sep. Sci. Technol.*, 37 (8): 1877.
38. Langmuir, I. (1913). The vapor pressure of metallic tungsten. *Phys. Rev.*, 2 (5): 329.
39. Lutišan, J.; Cvengroš, J.; Micov, M. (2002). Heat and mass transfer in the evaporating film of a molecular evaporator. *Chem. Eng. J.*, 85 (2–3): 225.
40. Greenberg, D. B. (1972). A theoretical and experimental study of the centrifugal molecular still. *AIChE J.*, 18 (2): 269.
41. Kawala, Z.; Stephan, K. (1989). Evaporation rate and separation factor of molecular distillation in a falling film apparatus. *Chem. Eng. Technol.*, 12 (1): 406.
42. Myers–Vacuum, 2010. Available in: < <http://www.myers-vacuum.com/index.shtml> >. Accessed in: November 10th. 2010.
43. American Society for Testing Material, ASTM D 4052. Standard test method for density, relative density, and API gravity of liquids by digital density meter. West Conshohoken, (Pennsylvania): ASTM International, 2009. 8p.
44. American Society for Testing Materials, ASTM D 5002. Standard test method for density and relative density of crude oils by digital density analyzer. West Conshohoken, (Pennsylvania): ASTM International, 1999. 5p, [Reapproved 2010].

45. American Society for Testing Material, ASTM D 70. Standard test method for density of semo–solid bituminous materials (pynometer method). West Conshohoken, (Pennsylvania): ASTM International, 2009. 4p.
46. Rodrigues, S.; Lona, L. M.; Franco, T. T. (2006). Optimizing panose production by modeling and simulation using factorial design and surface response analysis. *J. Food Eng.*, 75 (3): 433.
47. Kalil, S. J.; Maugeri, F.; Rodrigues, M. I. (2000). Response surface analysis and simulation as a tool for bioprocess design and optimization. *Process Biochem.*, 35 (6): 539.
48. Berry, J. W.; Tucker, H.; Deutschman Jr., J. A. (1963). Starch Vinylation. Determination of optimum conditions by response surface designs. *Ind. Eng. Chem. Process Des. Dev.*, 2 (4), 318.
49. Ankenman, B. E. (2003). Identifying rising ridge behavior in quadratic response surface. *IIE Transactions*, 35 (6): 493.
50. Merdrignac, I.; Espinat, D. (2007). Physicochemical characterization of petroleum fractions: The state of the art. *Oil Gas Sci. Technol. – Rev. IFP*, 62 (1): 7.
51. Tovar, L. P.; Pinto, G. M. F.; Wolf–Maciel, M. R.; Batistella, C. B.; Maciel–filho, R. (2011). Short–Path–Distillation process of lemongrass essential oil: Physicochemical characterization and assessment quality of the distillate and the residue products. *Ind. Eng. Chem. Res.*, 50 (13): 8185.
52. Ahmaruzzaman, M.; Sharma, D. K. (2006). Characterization of liquids products obtained from cocracking of petroleum vacuum residue with plastics. *Energy Fuels*, 20 (6): 2498.

6.3. Considerações finais

Este capítulo apresentou o sistema de equações diferenciais parciais que representa a modelagem matemática do processo de destilação molecular de resíduos de petróleo (ATR-W, ATR-Y e ATR-Z), em um destilador molecular centrífugo. Essa modelagem baseou-se no trabalho apresentado por Inuzuka et al. (1986) introduzindo uma modificação na taxa de evaporação e assumindo ela como a taxa de evaporação efetiva levando em conta os efeitos da geometria do sistema e o grau de anisotropia do sistema, sendo este uma mistura multicomponente.

Em virtude dos resultados obtidos com a ferramenta computacional que abrange a simulação do processo, pôde-se estimar e analisar o comportamento dos perfis das variáveis de interesse, que caracterizam o processo (temperatura da superfície do filme, taxa de destilado, taxa efetiva, espessura do filme e velocidade de escoamento), através da sensibilidade paramétrica das variáveis operacionais: vazão de alimentação, temperatura do evaporador, velocidade do rotor e pressão do sistema.

Resultados da análise de sensibilidade paramétrica apresentaram que as variáveis determinantes e características do processo foram: a temperatura na superfície do filme, a taxa de evaporação, a taxa de destilado e a espessura do filme. Tais variáveis mostraram-se ser fortemente influenciadas pela temperatura da destilação ou temperatura do evaporador. Quando a temperatura da superfície do filme aumenta, o filme sofre uma diminuição na concentração dos componentes (pseudo-componentes) mais voláteis. Em consequência, o perfil da espessura do filme se apresenta como uma queda exponencial onde esse diminui com maior velocidade na região a qual apresenta a maior taxa de aumento da temperatura da superfície do filme.

Todos os desempenhos das variáveis estudadas e analisadas neste capítulo descrevem as características particulares do processo de destilação molecular centrífuga, evidenciando as altas taxas de evaporação e as altas taxas do destilado, satisfazendo, com isso, os princípios do processo referentes a um menor tempo de exposição do material às condições da temperatura de destilação (temperatura do evaporador) e, portanto, um menor efeito térmico. Utilizando a metodologia de superfície de resposta foi possível determinar a condições operacionais ideais para obter altas taxa de destilado (D), sem uma perda de rendimento no processo de destilação

molecular centrífugo (% D). A partir da análise, as condições operacionais mais adequadas estão delimitadas por faixas de EVT 540 – 600 K e Q 1,5 – 3,5 kg.h⁻¹.

Capítulo 7.

Aplicação da calorimetria exploratória diferencial no estudo da cinética de craqueamento em presença de catalisador de frações pesadas de petróleo

7.1. Introdução

Em geral, o início do processo de destilação molecular reativa é detectado pela presença de cadeias carbônicas menores, pela redução na massa molar e pela diminuição na viscosidade, sendo esta última, provocada pela cisão das ligações da cadeia carbônica ou pela perda de grupos laterais, o que gera a formação de radicais livres, que causam uma instabilidade ou craqueamento das moléculas. Por sua vez, a redução na massa molar da fração de petróleo, provocada pelo craqueamento catalítico, por menor que sejam seus efeitos, acarretará uma alteração na conformação estrutural das cadeias de carbono nas frações de petróleo.

Estudos cinéticos envolvendo craqueamento de cargas industriais em um processo catalítico (craqueamento catalítico fluidizado e/ou hidroprocessamento) são complexos, e depende tanto da distribuição dos diversos compostos presentes, quanto dos níveis de conversão desejados.

Adotando-se um modelo, baseado na Lei de Potência, para a cinética de craqueamento aparente, a expressão da taxa de reação ($\frac{d\alpha}{dt}$) pode ser representada pela Equação A como segue:

$$\frac{d\alpha}{dt} = k''(T)f(\alpha) \quad (A)$$

Onde k'' é a constante de velocidade dada pela Lei de Arrhenius, $f(\alpha)$ o mecanismo da reação e α o grau de conversão.

Assim, nesse trabalho, a calorimetria exploratória diferencial, do inglês DSC (*Differential scanning calorimetry*) foi usada com o objetivo de verificar as transições físico-

químicas que aconteceram no processo de craqueamento das frações de petróleo (resíduos atmosféricos ATR–W e ATR–Z). Portanto, esse estudo objetivou analisar a cinética do processo de craqueamento das frações pesadas do petróleo, permitindo, assim, que fosse avaliada a influência da quantidade de catalisador (3, 5 e 10% m/m) durante o processo. Da mesma forma, o estudo cinético não-isotérmico utilizando o método isoconversional de Flynn–Wall–Ozawa, permitiu determinar os parâmetros cinéticos para diferentes frações de massa, sendo capaz de determinar a energia de ativação sem conhecimento prévio do modelo de reação e permitindo avaliar os efeitos de compensação cinética.

7.2. Metodologia de análise

As curvas calorimétricas foram obtidas a partir da célula Mettler–Toledo DSC 823e (Mettler Toledo GmbH, Germany), em atmosfera controlada dinâmica de N₂. Razões de aquecimento linear de 15, 20, 25 e 30 K·min⁻¹ foram utilizadas na faixa de temperatura 303,15 – 823,15 K, com um fluxo de nitrogênio de 50 mL·min⁻¹ controlado através do sistema Mettler–Toledo TS0800GC1. A célula DSC foi calibrada e/ou verificada antes dos ensaios no eixo de temperatura utilizando índio (como padrão) ($T_{fusão} = 429,75 \pm 0,3$ K) com pureza de 99,99%. Para o fluxo de calor empregou-se o $H_{fusão}$ do índio metálico ($28,45 \pm 0,6$ kJ·kg⁻¹). As análises foram realizadas com uma quantidade de amostra de ~10 mg. As amostras foram pesadas em cadinhos de alumínio, hermeticamente fechados e colocados na câmara da porta-amostra do módulo DSC. Como referência foi utilizado um cadinho vazio, idêntico, com um peso igual encontrados dentro de $\pm 0,1$ mg. Os dados foram processados utilizando o software STAR^e (V 9.01).

7.3. Desenvolvimento

- O desenvolvimento deste capítulo é apresentado a seguir, no manuscrito intitulado: *Kinetic study on catalytic cracking of Brazilian high-boiling-point petroleum fractions*, a ser publicado no periódico internacional *Journal of Thermal Analysis and Calorimetry* (publicado on-line em 24 de Novembro de 2011, doi: 10.1007/s10973-011-2068-6).

Source: From Tovar L. P., Wolf Maciel M. R., Araujo A. S., Maciel Filho R., Batistella C. B., Medina L. C. Kinetic study on catalytic cracking of Brazilian high-boiling-point petroleum fractions. Journal of Thermal Analysis and Calorimetry DOI: 10.1007/s10973-011-2068-6.

Copyright notice: The content of this manuscript is licensed under the Ethical Guidelines to Publication of Springer. Please contact credited rights holders directly for permission to reproduce material.

Kinetic study on catalytic cracking of Brazilian high-boiling-point petroleum fractions

Abstract

This work proposed a technique to estimate the kinetic parameters of cracking reaction. High-boiling-point petroleum fractions (>623.15 K) were analyzed. The experiments were performed using a thermal analysis system with a differential scanning calorimetry module at different linear heating rates (15, 20, 25 and 30 K min^{-1}) in the temperature range from 303.15 to 823.15 K. The Arrhenius, Kissinger and Flynn–Ozawa–Wall methods were used to determine the kinetic parameters. The compensation effect and the dependence on the activation energy of the conversion degree were evaluated. The catalyst used was a typical FCC regenerated catalyst containing 48.3 % mass of alumina, and particle size of $67 \mu\text{m}$. The effect of catalyst loading was studied using 3, 5 and 10 % mass. Analysis of the DSC curves showed a major transitional stage between 693.15 and 723.15 K, identified as an endothermic region of high temperature oxidation (HTO). Empirical kinetic models were produced and data were obtained from the kinetic analysis of the HTO region. Under non-isothermal heating conditions higher activation energies were found as the API gravity of the high-boiling-point petroleum fraction decreased. On the other hand, the results showed consistent effects for the dependence of the activation energy on the extent of cracking conversion under non-isothermal conditions, showing a decrease with the extent of conversion. The catalytic loading effect is remarkable, and provides an alternative route for the cracking with lower activation energy with increasing catalyst weight. The kinetic parameters formulated will be used in the mathematical modeling of the reactive molecular distillation process for upgrading high-boiling-point petroleum fractions.

Keywords: Reactive molecular distillation, high-boiling-point petroleum fractions, cracking reaction, catalyst loading, differential scanning calorimetry data, kinetic model.

Contents

1. Introduction
 - 1.1. Kinetic model approach for the cracking reaction
 2. Theoretical background
 - 2.1. Methods for the derivation of kinetic parameters
 - 2.1.1. Kissinger Method
 - 2.1.2. Maximum rate model: Arrhenius model
 - 2.1.3. Kinetic compensation effect (KCE)
 3. Experimental procedure
 - 3.1. Samples
 - 3.2. Differential scanning calorimetry (DSC) measurements
 4. Results and discussion
 - 4.1. Thermal analysis deflection
 - 4.2. Conversion degree of the reaction
 - 4.3. Overall kinetic parameters of the reaction
 - 4.3.1. Arrhenius and Kissinger methods
 - 4.3.2. Aspects of the kinetic compensation effects analysis
 5. Conclusions
- Acknowledgment
Nomenclature
References

1. Introduction

High-boiling-point petroleum fractions (>623.15 K) or heavy petroleum fractions and heavy crude oil include atmospheric and vacuum petroleum residues, coal oil extracts and crude oils extracted from tar sands [1]. They are referred to as "heavy" because their specific gravities are higher than those of light petroleum fractions or light crude oils, which means that the production, transportation and refining operations of these materials present greater challenges than those of light petroleum fractions or light crude oils [2].

The reactive molecular distillation (RMD) process, involving the coupling of molecular distillation (high vacuum separation process) with conversion (reactive process), can be described as an upgraded intensified process for the processing of high-boiling-point petroleum fractions, developed by the Separation Process Development Laboratory (LDPS) and the Optimization, Project and Advanced Control Laboratory (LOPCA) of the Chemical Engineering School of UNICAMP, sponsored by the Research Center of Petrobras-Brazil (CENPES/Petrobras) and Brazilian Study and Project Financing Institution (FINEP). The particular characteristics of RMD configuration (conversion-split) are: (i) the implementation of high vacuum; (ii) the material is

processed above the appropriate temperatures; (iii) the use of short time residence; and (iv) good contact between the sample and the catalyst surface. These factors provide a high effective evaporation rate, high kinetic reaction and, consequently, high rates of conversion–split.

The introduction of an in situ reaction (cracking) in the separation process zone (between separator and condenser) or vice versa, leads to known interactions between the mass transfer rates, diffusion and chemical kinetics. Reactive molecular distillation (RMD) is a combination of reaction (cracking) and molecular distillation (high vacuum) in a single operation, which enjoys specific advantages over the conventional sequential approach of reaction followed by separation process, with effective use of reaction heat and transformation of ultra-heavy and heavy oil into lighter oil, ensuring better flow and processing. It allows the material to be submitted to adequate temperatures to provide a high reaction rate and short exposure time of the material, allowing a controlled reaction, and even, providing an alternative for difficult separations (Fig. 1).

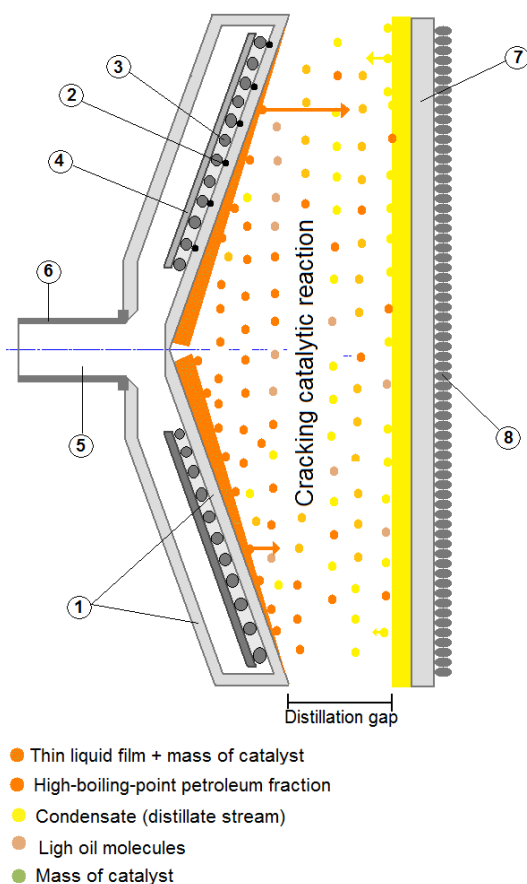


Figure 1. Schematic side view of RMD process. 1. Evaporator surface; 2. Termocouple; 3. Electrical resistance; 4. Support resistance; 5. Shaft hole; 6. Axis; 7. Condenser surface; 8. Cooling coils.

The eqs. (1) – (4) show the model that described the RMD process in a liquid evaporating film. Under steady-state conditions, a one-dimensional mathematical model and a number of assumptions (laminar flow, very thin liquid film thickness, negligible normal and tangential velocity components as compared to the radial component), liquid film processes can be studied in the evaporator system, including fundamental equations for film flow, equations for diffusion and the governing equation for mass, continuity and energy balance. A sketch of the coordinate system is presented in Fig. 2.

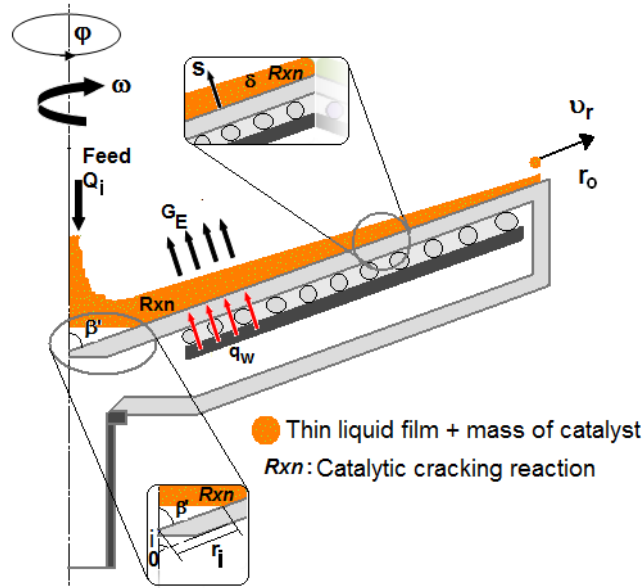


Figure 2. Sketch of coordinate system of rotor in reactive molecular distiller.

The continuity equation for the overall mass balance can be presented as [3]:

$$\frac{1}{3600} \frac{dQ'}{dr} + 2\pi r G_E (\sin \beta') = 0 \quad (1)$$

Where the effective evaporation rate under high vacuum conditions, G_E , is given by the surface composition of each component and the surface temperature by Eq. 2 [3]:

$$G_E = \sum_i x_{s_{NPSE_i}} G_{E_{NPSE_i}} \quad (2)$$

Where $x_{s_{NPSE_i}}$ is the molar fraction at the evaporating surface. $G_{E_{NPSE_i}}$ is the effective evaporation rate of the i -th pseudocomponent.

The energy equation is

$$\rho(T)C_p(T)v_r(r)\frac{\partial T(r,s)}{\partial r} = \lambda(T)\frac{\partial^2 T(r,s)}{\partial s^2} - \rho(T)(\Delta H_r)_{i,m,n}r_{NPSE_i} \quad (3)$$

The equation for diffusion of the i–th pseudocomponent is given by Eq. 4:

$$v_r(r)\frac{\partial x_{NPSE_i}(r,s)}{\partial r} = \mathbf{D}_{NPSE_i,mix}\frac{\partial^2 x_{NPSE_i}(r,s)}{\partial s^2} - r_{NPSE_i} \quad (4)$$

One important attribute of these equations is that they are all in the form:

$$\left\{ \begin{matrix} Entity \\ increase \end{matrix} \right\} = \left\{ \begin{matrix} Entity \\ addition \\ net rate \end{matrix} \right\} + \left\{ \begin{matrix} rate of \\ entity \\ production \end{matrix} \right\} \quad (5)$$

Each governing equation is the avowal of a conservation law, in which entity refers to mass, momentum or energy, respectively. The rates of entity production come from the chemical reactions in Eq, (4) and from the external force field in Eqs. (1) – (3). From an observation of the reaction term in the RMD model (see Eq. 4), the need for substantial attention in order to expand the domain of RMD processes to complex chemical system, i.e. high–boiling–point petroleum fractions (>623.15 K), is evident. Thus, the chemical reaction kinetic is an important aspect in the context of the RMD process, and consequently the kinetics parameters must be estimated from the kinetic approach.

The cracking reaction of the high–boiling–point petroleum fractions is extremely complex, but if appropriate generalizations are made the chemical kinetics can be represented. In the present work, a kinetic representation was formulated, adequate to combine with the flow, energy and diffusion equations to predict the in–situ reaction in the RMD process of high–boiling–point petroleum fractions. Non–isothermal kinetic analyses by differential scanning calorimetry (DSC) were performed in order to understand and study the transitional stage identified as cracking reactions in the endothermic region of high temperature oxidation (HTO).

1.1. Kinetic model approach for the cracking reaction

In the present work, catalytic cracking denotes the transition of a complex substance in presence of catalyst, where high–boiling–point petroleum fractions are converted into better quality products, that is, petroleum molecules are broken into shorter molecules to extract low–boiling fractions with reduced molar mass [4, 5]. Ebrahimi et al. [6] and Gupta [7] developed a

model based on the pseudocomponent approach. It is assumed that when one mole of a pseudocomponent cracked gives one mole each of two other pseudocomponents and some amount of coke may also form as described in Eq. (6).



Where i , m , and n are pseudocomponents numbers, $\zeta_{i,m,n}$ is the amount of coke formed when a i th pseudocomponent ($NPSE_i$) cracks to produces m th and n th pseudocomponents ($NPSE_m$ and $NPSE_n$). Therefore, the intensive kinetics for the cracking reaction can be written as the rate of the kinetic process, as follows:

$$\frac{d\alpha}{dt} = k''(T)f(\alpha) \quad (7)$$

Furthermore, the dependence of the reaction rate on temperature is manifested by the temperature dependence of the rate constant (k'') according to the Arrhenius equation as follows:

$$\frac{d\alpha}{dt} = A \exp\left(-\frac{E}{RT}\right)f(\alpha) \quad (8)$$

Where, α is the conversion degree, E the activation energy of the reaction, R the gas constant, A the pre-exponential factor, and T the temperature.

2. Theoretical background

Kinetic parameters have been determined by isothermal and dynamic experiments using thermal analytical methods such as thermogravimetry/derivate thermogravimetry (TG/DTG) and differential scanning calorimetry (DSC). K k and Keskin [8] investigated the thermal characteristics and combustion kinetics of three crude oils (13 – 27  API) using DSC and TG/DTG, identifying three reaction regions as low temperature oxidation (LTO), fuel deposition (FD) and high temperature oxidation (HTO) using a first order kinetic model. K k [9] determined the combustion kinetics of light crude oils with and without FeCl₃ solution as catalyst (1 – 1.5 % mol/mol), using TG/DTA. The activation energy was shown to be between 59.8 and 49.8 kJ mol⁻¹ with 1 – 1.5 % mol/mol of catalyst. When the experiments were carried out without the catalyst, the activation energy was 94.7 kJ mol⁻¹.

Other researchers applied thermal analyses (DSC and TG) to medium and heavy petroleum fractions (with high asphaltene contents) [10] and distillation residues [11], in order to

characterize the thermal behavior, and the endothermic behavior and melting temperature of the asphaltenes. Recently, Sánchez-Jiménez et al. [12] applied the methodology in the thermal analysis using the dynamic heating rate to carry out a study with the Kissinger method to determine the kinetic parameters. The apparent kinetic study carried out by Guo et al. [13] using thermogravimetry (TG), showed that during the thermal cracking/coking of Jinzhou residue and its fractions, the cracking reaction followed a first order reaction in two different temperature zones with activation energies of 75–120 kJ mol⁻¹ and 130–210 kJ mol⁻¹. On the other hand, Silva et al. [14] used TG/DTG techniques to study the catalytic degradation of heavy oil (15.4 °API) over silica-based MCM-41 mesoporous molecular sieve, determining the activation energy for oil degradation decreased from 128 to 69 kJ mol⁻¹ for PET/MCM-41 applying the kinetic method of Vyazovkin. Furthermore, Kök and Gundogar [15] studied non-isothermal combustion and kinetic analysis of crude oil in limestone matrix was studied with different clay concentrations by thermogravimetry (TG/DTG). In TG/DTG experiments, three distinct reaction regions were identified in all of the crude oil + limestone mixture known as low temperature oxidation (LTO), fuel deposition (FD) and high temperature oxidation (HTO) respectively.

Discussions about reaction kinetics focus on the reaction model, since it is independent of the heating rate, but the activation energy is dependent on the conversion were presented by Açıkalın [16]. Considering the kinetic compensation effects (KCEs) due to differences in the physicochemical properties of the samples under the experimental conditions, different methods have been used to analyze the experimental kinetic data [17]. The occurrence of the KCEs and the E -dependence on α can generate large deviations in the prediction of the reaction rate. Hence, researchers have carried out experimental work under non-isothermal and isothermal conditions to evaluate the E -dependence on α of diverse feedstock. The existence of the KCEs has been presented in published literature for several researchers of heterogeneous reactions [18]. Joraid [19] and, Vyazovkin and Sbirrazzuoli [20] evaluated the E -dependence for non-isothermal crystallization. The first researcher analyzed two regions (between 471.15 – 479.15 K and 481.15 – 491.15 K) and attributed the E -dependence to changes in the crystallization kinetics as the polymer melted; and the second group of researchers presented the variation in activation energy (from 128.7 to 77.8 kJ mol⁻¹) as a consequence of sample morphology.

In this work, cracking reaction of two different high-boiling-point petroleum fractions were investigated in order to obtain the overall kinetic parameters (activation energy (E) and

frequency factor (A)). In order to study the kinetic compensation effects (KCE) and activation energy dependence on the degree of conversion, the Flynn–Ozawa–Wall (FWO) method was used. The procedure was applied to two high-boiling-point petroleum fractions (atmospheric distillation residues –ATRs) from crude oil with different API gravities (between 12 – 25 °API).

2.1. Methods for the derivation of kinetic parameters

Differential scanning calorimetry (DSC) provides both qualitative and quantitative information about material transitions (reactions). Most published kinetic methods using DSC data are based on the enthalpy change, where the gradient dH/dt is directly proportional to the reaction rate $d\alpha/dt$, as shown in Eq. (9) [21].

$$\frac{d\alpha}{dt} = \frac{1}{\Delta H} \left(\frac{dH}{dt} \right) \quad (9)$$

Thus the application of calorimetry techniques has been used to obtain complete qualitative and quantitative information about the cracking reaction for high-boiling-point petroleum fractions, determining the reaction order (n), activation energy (E), frequency factor (A), conversion degree (α) and rate constants at different temperatures.

2.1.1. Kissinger Method

The kinetic parameters determined by the Kissinger method are based on the study of the rate equation at the maximum reaction rate, which means that $d^2\alpha/dt^2$ is equal to zero (see Eq.10) [13, 21, 22].

$$\frac{d^2\alpha}{dt^2} = \left(\frac{E\beta}{RT_m^2} + Af'(\alpha_m) \exp\left(-\frac{E}{RT_m}\right) \right) \left(\frac{d\alpha}{dt} \right)_m = 0 \quad (10)$$

Where T_m is the temperature at the maximum peak on the DSC curve, α_m is the conversion degree at T_m , $d\alpha/dt_m$ is the maximum reaction rate and β is the heating rate.

Considering a reaction order of $n=1$, the Kissinger method is given as Eq. 11:

$$\ln\left(\frac{\beta}{T_m^2}\right) = \ln\left(\frac{AR}{E}\right) - \frac{E}{R T_m} \quad (11)$$

Where, the activation energy (E) is determined from the DSC data at different heating rates by liner regression of the $\ln\left(\frac{\beta}{T_m^2}\right)$ versus T_m^{-1} plot, and the activation energy (E) is calculated from the slope of the resulting straight line.

2.1.2. Maximum rate model: Arrhenius model

This approach assumes Arrhenius behavior and first-order reaction kinetics, and is based on the maximum rate of heat absorption during the analysis at constant heating rates (see Eq. 12).

$$\frac{E}{RT_m^2} = \frac{A}{\beta} \exp\left(\frac{-E}{RT_m}\right) \quad (12)$$

A plot of $\ln(\beta^{-1})$ versus T_m provides the information required to calculate the activation energy (E) from the slope, and the pre-exponential factor (A) from the intercept of the straight [23].

2.1.3. Kinetic compensation effect (KCE)

The kinetic compensation effect (KCE) suggests that the pre-exponential factor A varies with the activation energy E according to Eq. (13) [24, 25]:

$$\ln A = a^* E + b^* \quad (13)$$

Where a^* and b^* are constant coefficients and act as compensation parameters.

The evaluation of the activation E -dependence on α is based on the following assumptions:

The activation energy (E) and pre-exponential factor (A) do not depend on the heating rate (β) and are correlated by Eq. (13).

The kinetic compensation effects are evaluated in the following range of conversion degrees $0.2 < \alpha < 0.9$ to lessen the effects of transition.

The E -dependence on α is given as:

$$E = E_0 + E_1 \left(\frac{1}{\alpha}\right) \quad (14)$$

Where E_0 and E_1 are constants.

An approximate differential method for determining the E –dependence on α is based on the method developed by Flynn–Ozawa–Wall (FWO) (see Eq. 15), based on the fact that to evaluate the kinetic parameters it is not necessary to know the reaction order or the conversional function $F(\alpha)$ [26, 27].

$$\ln F(\alpha) = \ln\left(\frac{EA}{R}\right) - \ln(\beta) - 5.3305 - 1.0516 \frac{E}{RT} \quad (15)$$

Where $F(\alpha)$ is the conversion functional relationship; A is the pre-exponential factor; E is the activation energy; R is the general gas constant; β is the heating rate and T is the absolute temperature.

Reorganizing Eq. (15), the activation energy of the cracking reaction can be obtained from multiple constant heating based on Eq. (16):

$$\ln \beta \cong -1.0516 \frac{E}{RT} + \left(\ln \frac{EA}{RT} - \ln F(a) - 5.3305 \right) \quad (16)$$

Considering that the mechanism of cracking is independent of the heating rate, $F(a)$ is constant for the iso-conversional case, the plot of $\ln \beta$ versus T^I , obtained from the curves recorded during multiple constant heating, should be a straight line whose slope can be used to evaluate the activation energy (approximately $-1.0516E/R$).

In order to determine the reaction order (n) and pre-exponential factor (A), the Avrami's theory has been used, extended to describe non-isothermal cases (see Eq. 17) [28].

$$\ln[-\ln(1-\alpha)] = \ln A - \frac{E}{RT} - n \ln \beta \quad (17)$$

Hence, a plot of $\ln[-\ln(1-\alpha)]$ versus $\ln \beta$ provided some straight lines, of which the slope corresponded to the reaction order (n), and from the value of the intercept $\ln A - \frac{E}{RT}$, it was possible to determine the pre-exponential factor value since E was evaluated using the FWO method for every value of α . Thus the values for $\ln A$ corresponding to various values for E and α were obtained. Finally, the plotting of $\ln A$ versus E should be linear as required by the existence of the KCEs (see Eq. 13).

3. Experimental procedure

3.1. Samples

For the cracking reaction study, Brazilian crude oils with different API gravities (12 – 25 °API) from several sources were distilled by conventional atmospheric distillation [29], resulting in two atmospheric distillation residues (ATR–W and ATR–Z). They were supplied by the Petrobras Research and Development Center (CENPES–Brazil) and the properties of the high-boiling-point petroleum fractions are shown in Table 1.

Table 1 Properties of the atmospheric petroleum distillation residues (high-boiling-point petroleum fractions) studied.

Feedstock	API feedstock	API source crude oil	Asphaltene content/ % mass
ATR–W	11.9	16.8	9.15
ATR–Z	N.A.	28.3	>1.1

N.A.: Not available

The most promising aspects related to the efficiency of the catalytic RMD process listed before are related to accomplishment of operational temperatures and pressures (below 50 Pa), depending on the characteristics of the reactants, a lower amount of catalyst and the products desired. In this sense, the influence of adding catalyst to the high-boiling-point petroleum fractions at 3, 5 and 10 % mass of catalyst was also studied, using the zeolite-based catalyst CR–1 (regenerated catalyst used for FCC technology), and its primary properties are listed in Table 2.

Table 2 Properties of CR–1 FCC catalyst

Property	Value
Micro Activity testing/%	69
Surface area/m ² g ⁻¹	53
Particle size distribution/μm	67
Al ₂ O ₃ / % mass	48.3
Rare earth oxide RE ₂ O ₃ (RE = Y, Gd, Nd and La)/ % mass	2.85
Carbon/% mass	0.08

3.2. Differential scanning calorimetry (DSC) measurements

Thermal experiments were carried out on the high-boiling-point petroleum fractions using a Mettler–Toledo DSC 823e thermal analysis system (Mettler Toledo GmbH, Germany), and liquid nitrogen was used for cooling. The DSC module was calibrated with indium with indium standard (it had a certified fusion temperature of 156.6 ± 0.3 °C and heat flow calibration of 28.45 ± 0.6 J g⁻¹). The experiments were carried out with a sample size of ~10 mg. The samples were weighed into open aluminum pans, hermetically sealed and then placed in the sample chamber of the DSC module. The reference was an identical, empty pan, with an equal weight matched within ± 0.1 mg. Linear heating rates of 15, 20, 25 and 30 K min⁻¹ were used over the temperature range from 303.15 to 823.15 K, with a nitrogen flow of 50 mL min⁻¹ controlled by a gas control system (Mettler–Toledo TS0800GC1). The STARe (V 9.01) software Instrument Software was used to provide an estimate of the enthalpy (ΔH) and the heat flow calculated from the DSC transition curve. In order to evaluate the repeatability of the measurement, the relative standard deviation (%RSD) with respect to the mean signal of each measurement, calculated over three (03) consecutive repetitions of Indium standard was examined. The value obtained was lower than 8.53%.

4. Results and discussion

The thermal analyses used to estimate the kinetic parameters of the two high-boiling-point petroleum fractions: ATR–W, and ATR–Z, and their mixtures with added catalyst (3, 5 and 10 % mass of catalyst) are presented in this work.

4.1. Thermal analysis deflection

The thermal analyses carried out using DSC showed the changes in the properties of the high-boiling-point petroleum fractions studied occurring with temperature. In Fig. 3, the heat flow rate signal (DSC signal) is internally calculated from the temperature difference between the sample material and the reference pan, showing the endothermic region where the cracking reaction took place, and thus the changes in heat content and properties of the samples are indicated by a peak and/or deflection. Thus the reaction rate, $d\alpha/dt$, rises to a maximum value when the temperature is increased, while the reaction occurs. The maximum rate occurs at a temperature, T_m , where the peak differential thermal analysis deflection occurs.

In the DSC experiments, one transition region was detected on the curves. This region occurred between 693 and 723 K and was called the high temperature oxidation (HTO) region where hydrocarbons were fully oxidized by atmosphere surrounding the sample and the presence of a catalyst. During the course of this process, hydrocarbons were continuously converted to other types of hydrocarbons, which makes the conversion process mainly attributed to cracking due to the effect of heat and the catalyst. In this region, complex organic molecules are broken down into simple molecules, and as a result, the C–C, C–H and C–heteroatom bonds are broken, producing reactive free radicals [30].

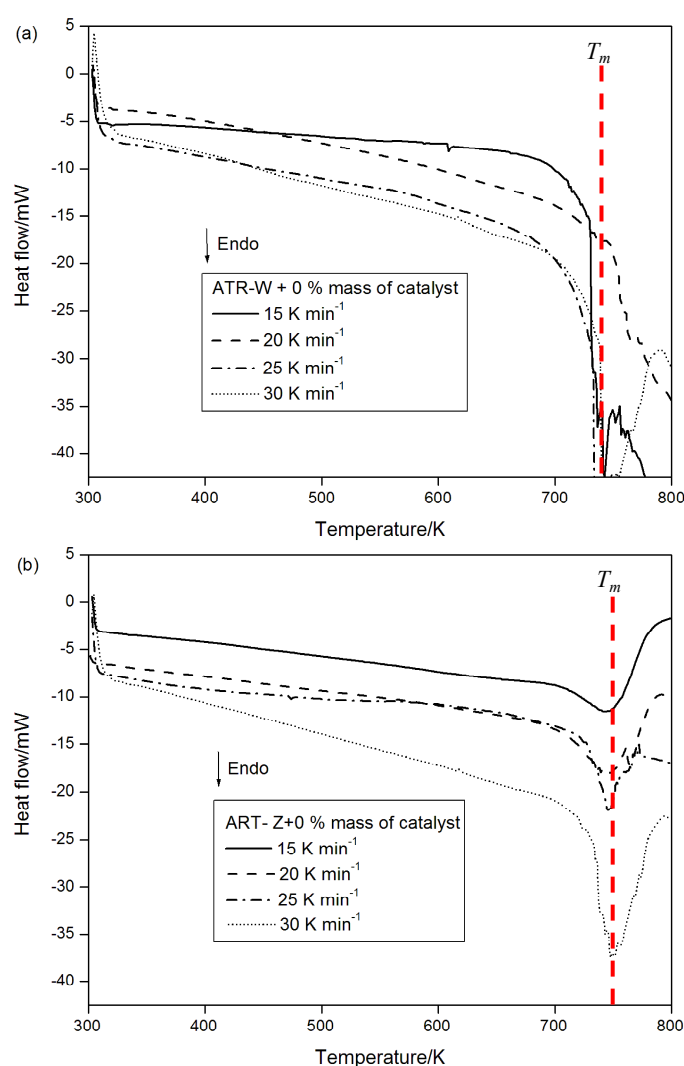


Figure 3. Curve at non-isothermal heating conditions of: a) ATR–W and b) ATR–Z.

Under non-isothermal heating conditions, the DSC curves (Fig. 3) gave heat flow rates showing that the ATR–W generated greater heat flow than the ATR–Z. As a consequence, as the

API gravity decreased, so the heat flow during the transition stage (HTO) increased. However, the rise in the heat flow rates is also associated with the amount of asphaltenes in the samples. K  k and Karacan [31] explained in their paper that when the asphaltene content in the crude oil increased, so the heating value of the cracking reaction increased, and this proposition concords with the results obtained in the present work.

Table 3 shows the dependence of heat production on the heating rate and the maximum peak temperatures for the different materials. Using four different heating rates (15, 20, 25 and 30 K min⁻¹), the results demonstrated that all the peaks or deflections shifted towards higher reaction temperatures (T_m) and heat flows at higher heating rates, even in the presence of the catalyst, as summarized in Table 3. However, results indicated that the colloidal composition of high-boiling-point petroleum fractions, as well as the transferability, impurities around the sample and heat transfer characteristics, does not have a pronounced influence on the heat evolved in the HTO region.

Table 3. Heat properties of high-boiling-point petroleum fractions obtained from DSC curves.

Feedstock	Catalyst/% mass	Peak temperature, T_m /K				Heat evolved, HTO/J Kg ⁻¹			
		Heating rate/K min ⁻¹				Heating rate/K min ⁻¹			
		15	20	25	30	15	20	25	30
ATR-W	0	742.54	742.99	743.88	745.38	-21275	-70.32	-22752	-13404
	3	754.62	756.94	756.94	759.57	-7050	-12008	-9006	-4398
	5	747.25	750.64	748.47	756.20	-6165	-31432	-24261	-5925
	10	742.16	747.35	762.39	767.89	-6770	-6196	-8163	-19335
ATR-Z	0	743.55	744.82	745.78	747.40	-5785	-7252	-6567	-11247
	3	740.46	747.57	753.58	758.55	-6350	-12028	-20808	-3276
	5	743.60	745.70	761.90	768.26	-5475	-15204	-5079	-11727
	10	745.00	746.82	769.36	779.48	-4465	-30896	-10335	-8793

4.2. Conversion degree of the reaction

The quantitative kinetic analysis began with the determination of the conversion-temperature data determined by the STARe (V 9.01) software linked with the Mettler-Toledo DSC 823e thermal analysis system. Hence, when the conversion degree was plotted against the temperature, the kinetics was shown to obey sigmoid curves (Figs. 4 and 5). From the experiments carried out, it can be seen that although the T_m changed when the heating rate was increased, the conversion degree (α) remained nearly the same, as seen in Figs. 4 and 5, for ATR-W and ATR-Z, respectively.

In order to study the catalytic effect on the cracking reaction of the high-boiling-point petroleum fractions, the effect of adding 3, 5 and 10 % mass of catalyst on the conversion of the high-boiling-point petroleum fractions at heating rates of 15, 20, 25 and 30 K min⁻¹, was studied.

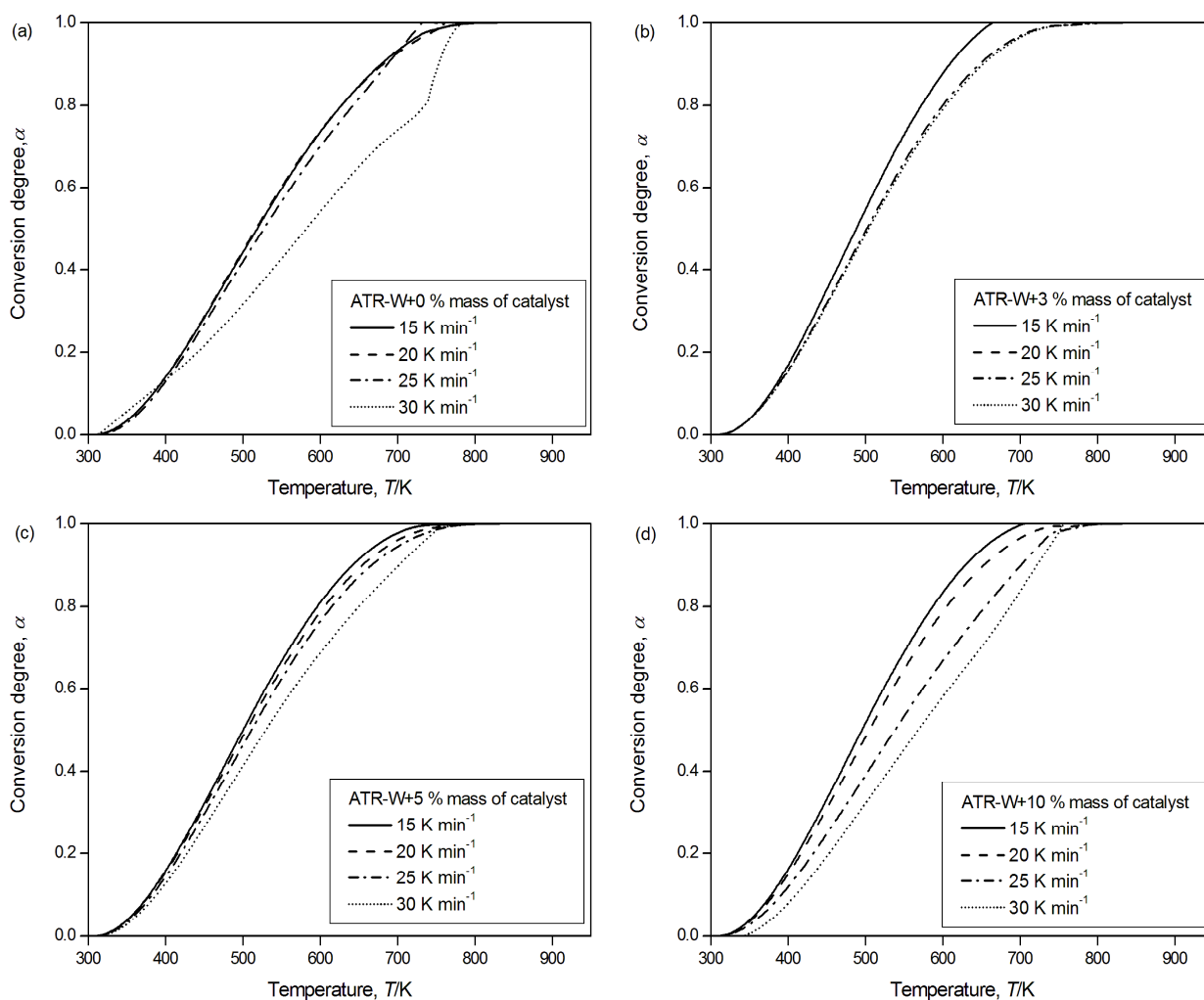


Figure 4. Conversion degree as a function of temperature and heating rate (15, 10, 25 and 30 K min⁻¹) for different systems: a) ATR-W+0 % mass of catalyst, b) ATR-W+3 % mass of catalyst, c) ATR-W+5 % mass of catalyst and d) ATR-W+10 % mass of catalyst.

In the α versus T curves, three zones were identified. The initial region that starts from 303 K up to 400 K, depending on the high-boiling-petroleum fraction, characterized by a low velocity conversion not being bigger than 18%. In the ATR-W and ATR-Z high-boiling-point petroleum fractions (Figs. 4a and 5a, respectively), the velocity conversion, in the range 693–723 K, is bigger than for the rest of the range, which is basically due to the process whereby complex

organic molecules or hydrocarbons with high molar mass are broken down into simpler molecules (hydrocarbons with lower molar mass), by the breaking of C–C bonds in the precursors, reaching conversion degree values from 18 to 90%. The third stage of these curves is understood at 723 K. In this stage is assumed that the cracking is almost complete since the variation of the conversion with temperature is the lowest.

Then, Figs. 4 and 5 suggest that the cracking reaction is possible in a catalytic process in the same three stages, and the rate of cracking and the end products are strongly dependent on the temperature and the presence of catalysts.

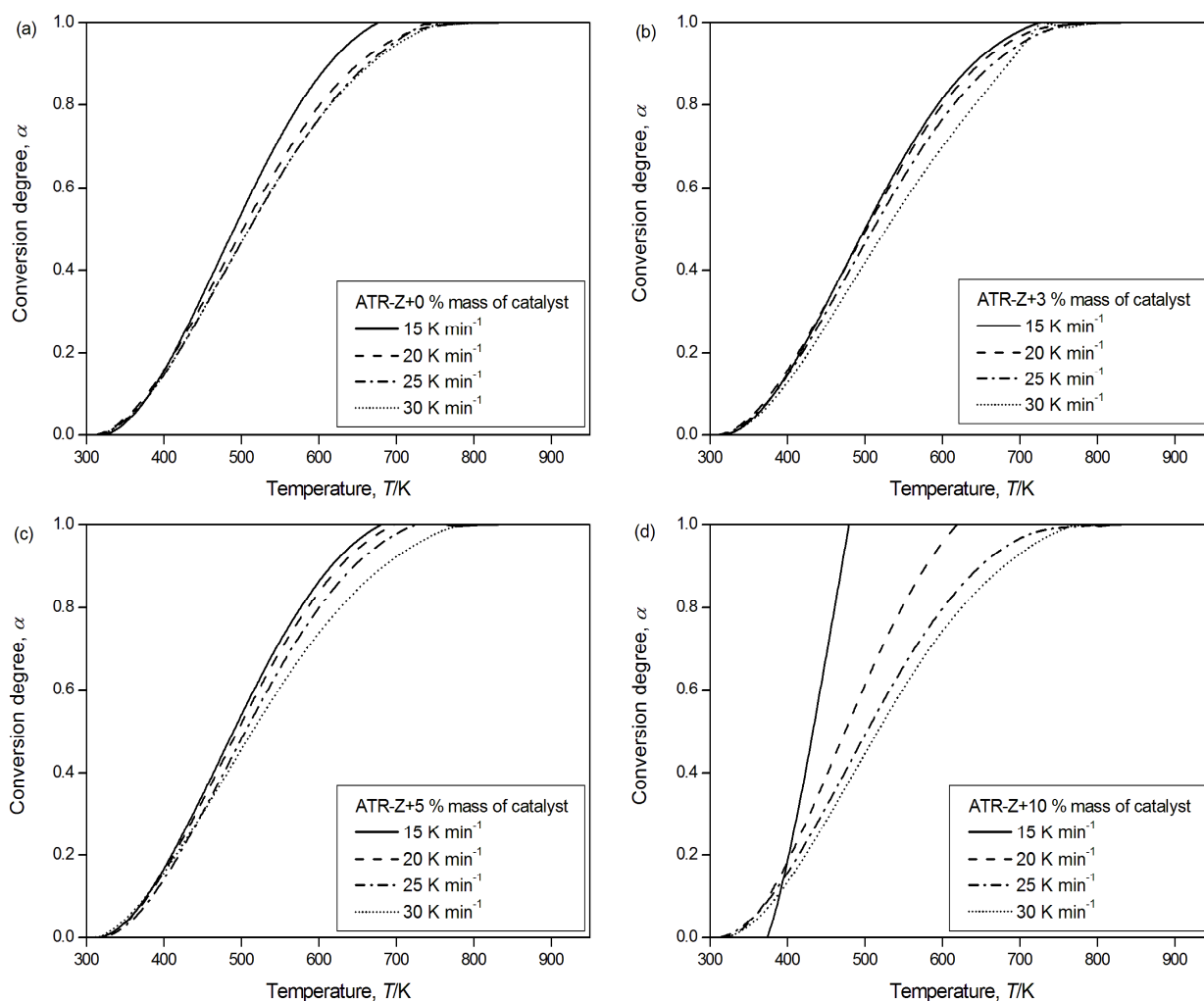


Figure 5. Conversion degree as a function of temperature and heating rate (15, 10, 25 and 30 K min⁻¹) for different systems: a) ATR–Z+0 % mass of catalyst, b) ATR–Z+3 % mass of catalyst, c) ATR–Z+5 % mass of catalyst and d) ATR–Z+10 % mass of catalyst.

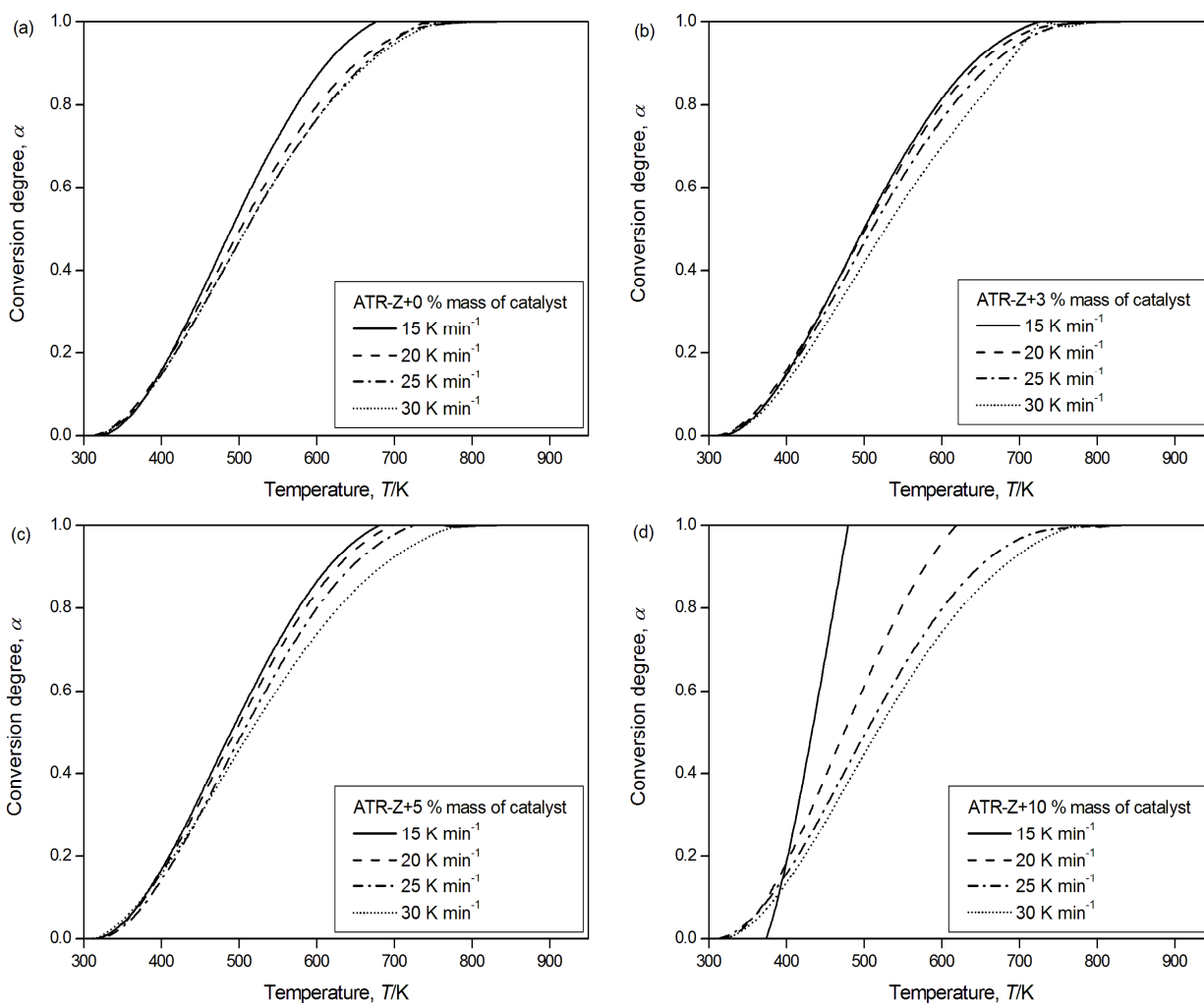


Figure 5. Conversion degree as a function of temperature and heating rate (15, 10, 25 and 30 K min⁻¹) for different systems: a) ATR-Z+0 % mass of catalyst, b) ATR-Z+3 % mass of catalyst, c) ATR-Z+5 % mass of catalyst and d) ATR-Z+10 % mass of catalyst.

Therefore, in Figs. 4 and 5 the variation of conversion with the temperature, α versus T , is shown for the mixtures with catalyst up to 10% in mass, and three stages are observed as follows: (i) The first stage corresponds to the formation of the first radicals, which is a period when the cracking reaction velocity is slow and in consequence the conversion degree is low. (ii) In the second stage, the free-radical mechanism accelerates to cause scission of hydrocarbon C–C bonds and a reduction in molar mass of heavier hydrocarbons compounds. (iii) In the last stage, the reaction velocity slows down, since catalyst activity declines. Nevertheless, α versus T curve at 15 K min⁻¹, in Fig. 5d, had different effects based on the type of curve shift introduced. Hence, for ATR-Z+10% mass of catalyst case study, the amount of the lost substances at the first stage is rather due to the evaporation than to the formation of the first radical. Accordingly, the α versus T curve

for ATR–Z+10% mass of catalyst presents two well–defined steps, before and after 400 K, which can be easily recognized in the α versus T curve (Fig. 5d) identified as non–formation of free radicals (attributed to the evaporation process) followed by the complete catalytic cracking of heavier compounds, respectively.

4.3. Overall kinetic parameters of the cracking reaction

4.3.1. Arrhenius and Kissinger methods

The unity models proposed by Arrhenius and Kissinger to calculate the activation energy and pre–exponential factor from DSC data at constant heating rates (15, 20, 25 and 30 K min^{–1}) were studied. The kinetic data were obtained from the HTO region of the DSC curves, assuming a first–order cracking reaction for the high–boiling–point petroleum fractions. According to this assumption, the plots of $\ln(\beta^{-1})$ versus T_m^{-1} (Arrhenius model) and $\ln\left(\frac{\beta}{T_m^2}\right)$ versus T_m^{-1} (Kissinger model) should be straight lines, where the slope allows one to calculate the activation energy. These plots were constructed for the high–boiling–point petroleum fractions of different API gravity with the addition of catalyst (at 3, 5 and 10 % mass of catalyst) (Figs. 6 and 7).

In the HTO region, higher activation energies were found as the API gravity of the ATR samples decreased (Table 4). These values are comparable to the activation energies of 128.3 kJ mol^{–1} and 142.3 kJ mol^{–1} calculated for crude Raman (°API=18.7) and Bati Raman (°API=12.9) oils, respectively, by K  k [32], using similar methodology.

Table 4. DSC–derived kinetic parameters through Arrhenius and Kissinger method with first–order reaction.

Feedstock	Catalyst /mass %	Arrhenius method				Kissinger method			
		$E/\text{kJ mol}^{-1}$	A/min^{-1}	SD	R ²	$E/\text{kJ mol}^{-1}$	A/min^{-1}	SD	R ²
ATR–W	0	1113.10	7.81×10^{78}	0.15	0.91	1100.73	1.04×10^{78}	0.15	0.91
	3	662.36	1.54×10^{46}	0.12	0.89	649.77	2.04×10^{45}	0.12	0.88
	5	274.10	1.56×10^{19}	0.31	0.84	261.60	2.01×10^{18}	0.31	0.60
	10	113.02	3.45×10^7	0.09	0.94	100.47	4.15×10^6	0.09	0.93
ATR–Z	0	837.84	2.05×10^{59}	0.06	0.97	825.44	2.73×10^{58}	0.07	0.91
	3	178.64	2.3×10^{12}	0.01	1.00	166.18	2.91×10^{11}	0.01	0.88
	5	110.51	2.26×10^7	0.12	0.89	97.95	2.99×10^6	0.12	0.60
	10	79.32	1.02×10^5	0.13	0.88	66.63	1.16×10^4	0.13	0.93

E : Activation energy; A : Pre–exponential factor; SD: Standard deviation; R²: Squared correlation coefficient; ATR: Atmospheric petroleum residue.

However, it can be seen that the activation energy calculated for the peak in the HTO region was also related to the asphaltene content, because the activation energies of ATR–W was significantly higher than that of ATR–Z, which had a low asphaltene content, inhibiting the

cracking process with 5 and 10 % mass of catalyst. The activation energy data calculated were statistically analyzed to find the degree of reliability, and the results are presented in Table 4.

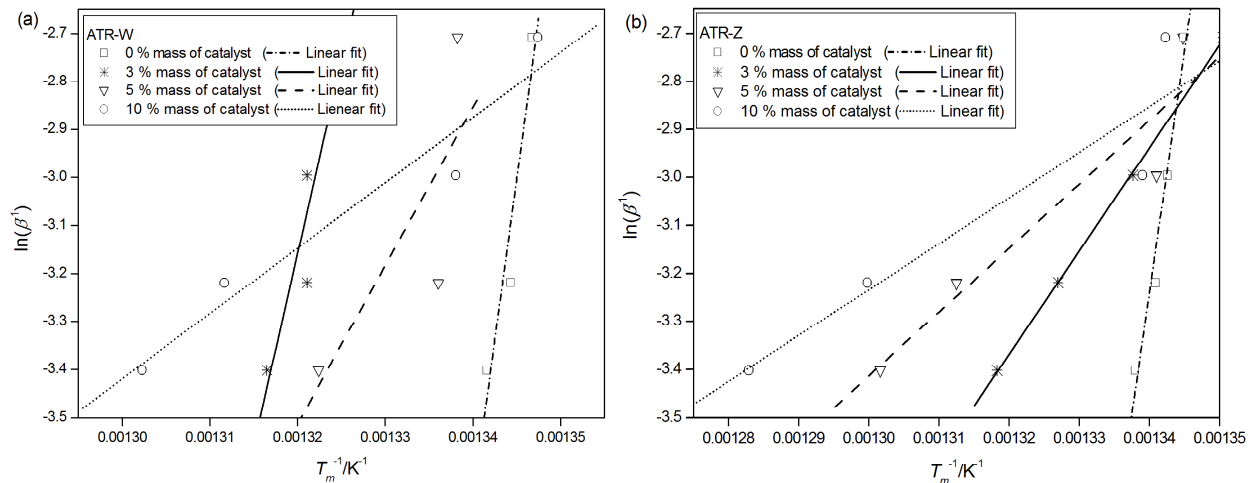


Figure 6. Arrhenius plot of the values of $\ln(\beta^{-1})$ as a function of T_m^{-1} . a) ATR-W samples and b) ATR-Z samples.

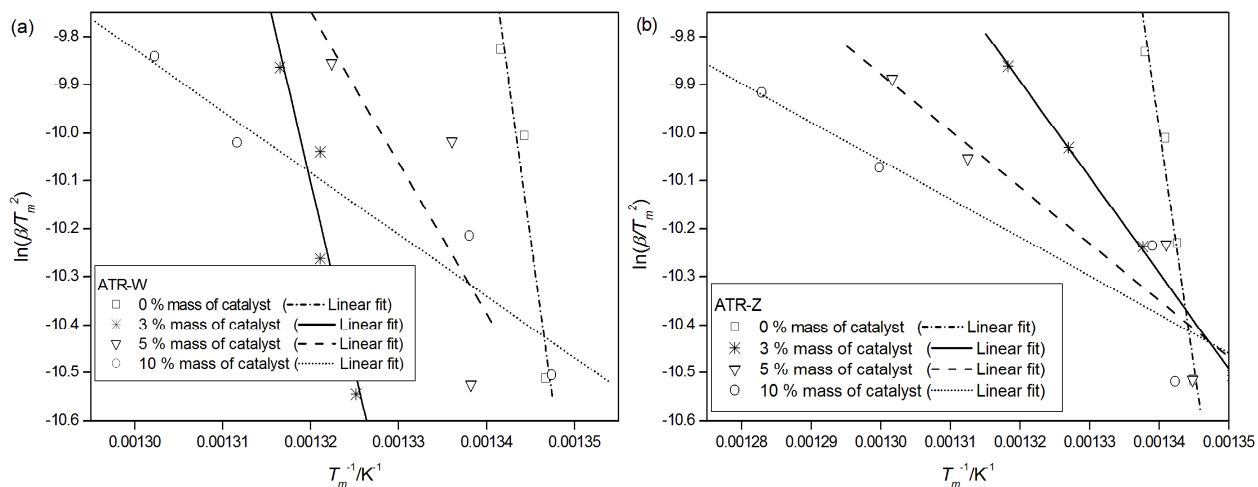


Figure 7. Kissinger plot of the values of $\ln(\beta/T_m^2)$ as a function of T_m^{-1} . a) ATR-W samples and b) ATR-Z samples.

Discussions about reaction kinetics tend to be focused on the activation energy parameter due to the following: i) the influence of temperature on the reaction rate is mainly determined by the activation energy, while the pre-exponential factor has the responsibility of a scale parameter; and ii) the pre-exponential factor is calculated from the intercept of the linear

regression, which could produce a large variation in the value of the pre-exponential factor from a small deviation in the value of the intercept [33].

Non-isothermal differential scanning calorimetry is often used to determine the activation energy of cracking kinetics. Regarding the estimation of the activation energy, it is clear that: i) it is a positive value; ii) it depends on the reaction mechanism, and iii) it is dependent on the addition of catalyst. The activation energies calculated for the cracking of the high-boiling-point petroleum fractions varied over a wide range. Similar results were reported by Yang et al. [34] for a Chinese vacuum residue whose activation energy values were between 82.13 and 149.3 kJ mol⁻¹ using a first-order rate.

Despite the wide range of activation energies, the calculations demonstrated a general trend with respect to the API gravity. As the high-boiling-point petroleum fractions got heavier (decrease in API gravity) so the cracking activation energy increased. The cracking activation energy also showed a general trend with respect to asphaltene content. Thus, as the API gravity of the high-boiling-point petroleum fractions decreased and the asphaltene content increased, so the activation energy showed an increment.

4.3.2. Aspects of the kinetic compensation effects analysis

The kinetic representation for the cracking reaction, used to establish the DSC curves for the ATR-W+% mass catalyst and ATR-Z+% mass catalyst samples, were recorded at four different heating rates (15, 20, 25 and 30 K min⁻¹) in the temperature range studied, applying the FWO method. The Figs. 8 – 9 shows the estimates for the activation energy, determined using the FWO method, for the whole set of α values used in the linear plot. The slope of the lines changes with increasing conversion degree because the side reaction becomes more important. Table 5 gives an overview of the values obtained for the E of the cracking reaction, calculated between $0.2 < \alpha < 0.9$ from the slopes of the straight lines in Figs. 8 and 9.

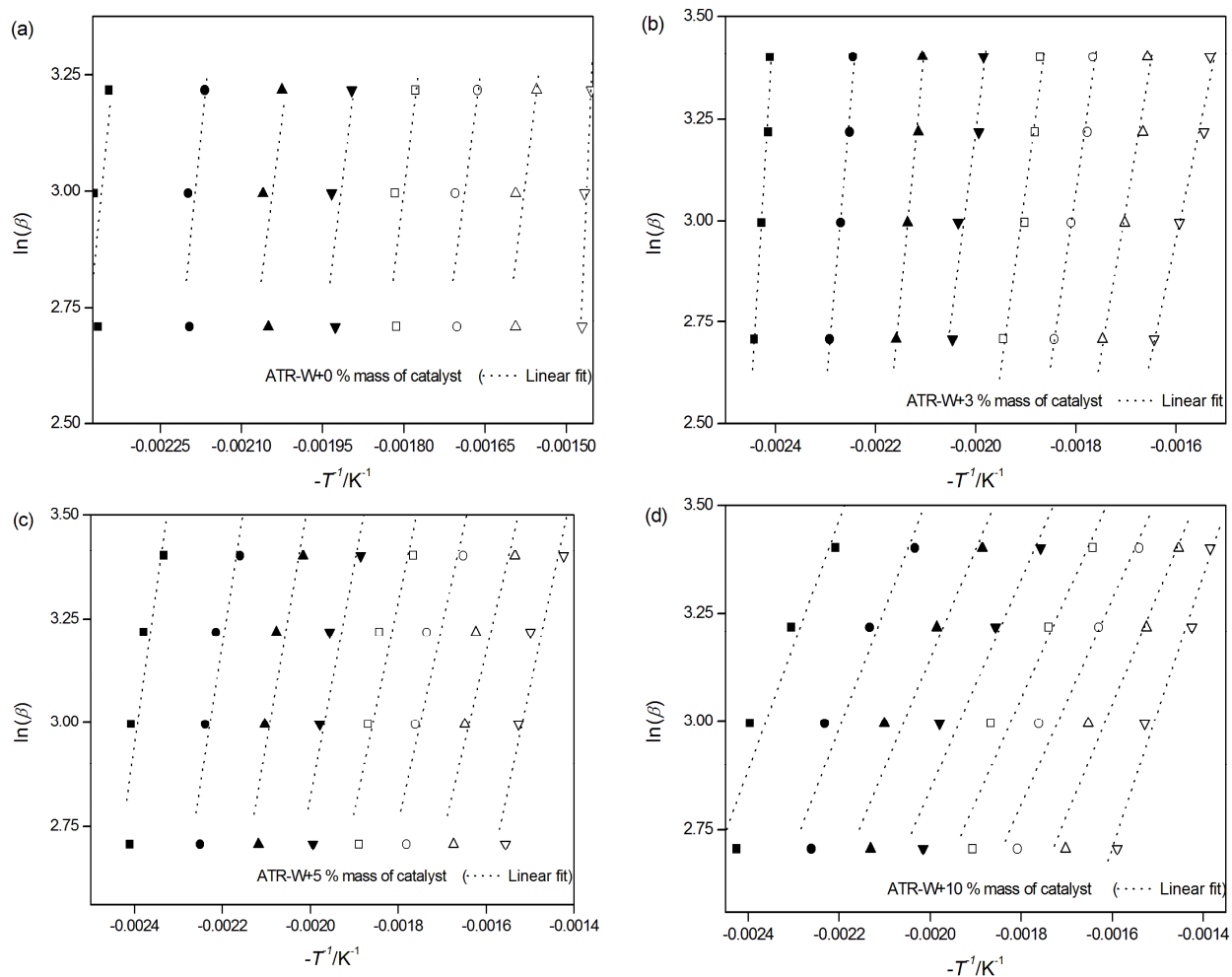


Figure 8. Flynn–Wall–Ozawa plot for the cracking reaction at heating rate of 15, 10, 25 and 30 K min⁻¹ and at conversion degree of (■) $\alpha=0.2$; (●) $\alpha=0.3$; (▲) $\alpha=0.4$; (▼) $\alpha=0.5$; (□) $\alpha=0.6$; (○) $\alpha=0.7$; (△) $\alpha=0.8$; and (▽) $\alpha=0.9$ for different systems: a) ATR–W+0 % mass of catalyst, b) ATR–W+3 % mass of catalyst, c) ATR–W+5 % mass of catalyst and d) ATR–W+10 % mass of catalyst.

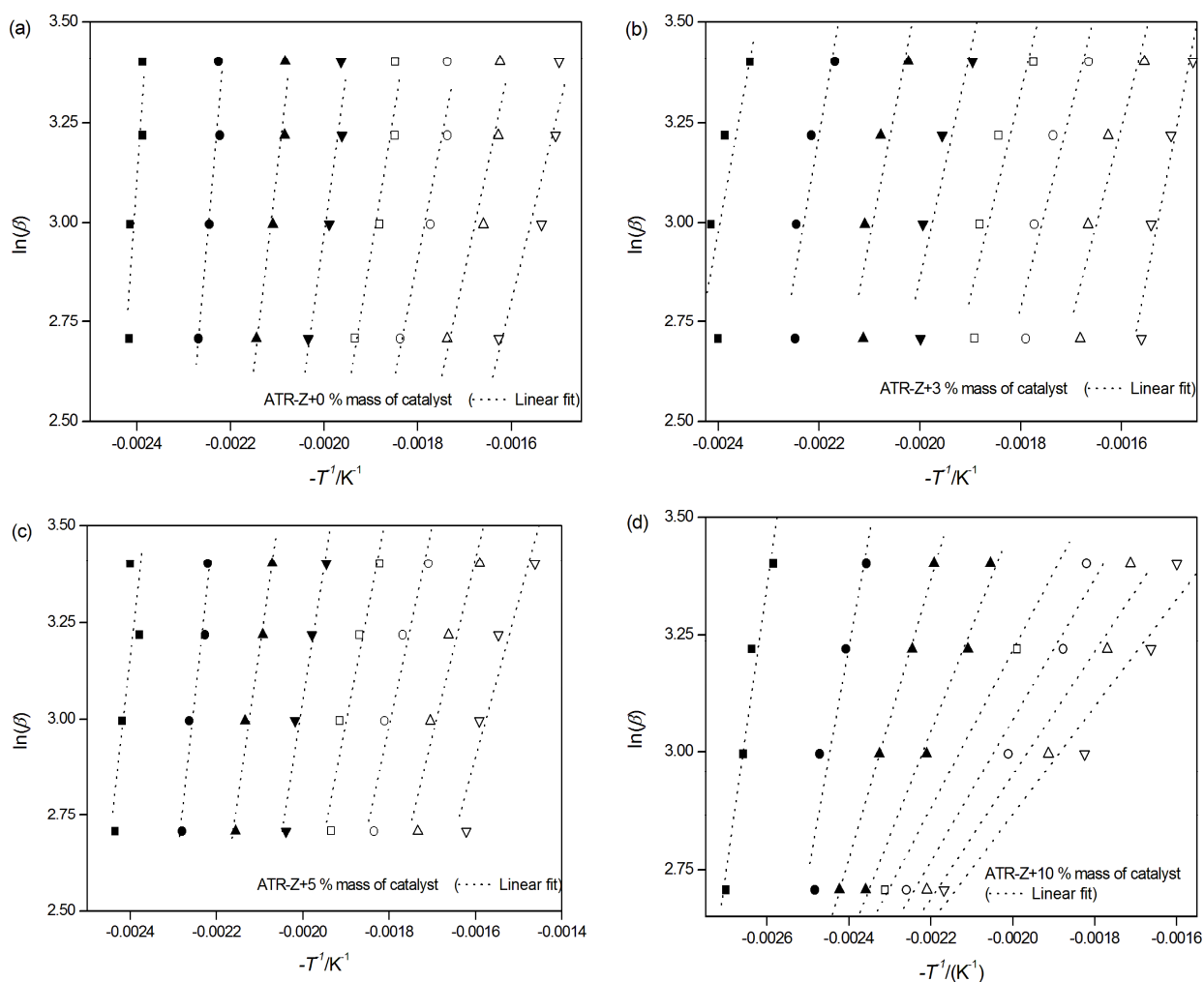


Figure 9. Flynn–Wall–Ozawa plot for the cracking reaction at heating rate of 15, 10, 25 and 30 K min⁻¹ and at conversion degree of (■) $\alpha=0.2$; (●) $\alpha=0.3$; (▲) $\alpha=0.4$; (▼) $\alpha=0.5$; (□) $\alpha=0.6$; (○) $\alpha=0.7$; (△) $\alpha=0.8$; and (▽) $\alpha=0.9$ for different systems: a) ATR–Z+0 % mass of catalyst, b) ATR–Z+3 % mass of catalyst, c) ATR–Z+5 % mass of catalyst and d) ATR–Z+10 % mass of catalyst.

An inspection of Figs. 8 and 9 allowed one to estimate the values for the activation energy (E) (Table 5). The coefficient of determination (R^2) corresponding to the straight line of $\ln \beta$ versus $-T^1$ had a value higher than 0.92. According to these results, the value for E decreased from 214.71 kJ mol⁻¹ (at $\alpha=0.2$) to 75.08 kJ mol⁻¹ (at $\alpha=0.9$) for ATR–W+0 % mass; from 161.19 kJ mol⁻¹ (at $\alpha=0.2$) to 45.93 kJ mol⁻¹ (at $\alpha=0.9$) for ATR–W+3 % mass; from 59.21 (at $\alpha=0.2$) to 39.06 kJ mol⁻¹ (at $\alpha=0.9$) for ATR–W+5 % mass and from 24.84 kJ mol⁻¹ (at $\alpha=0.2$) to 20.17 kJ mol⁻¹ (at $\alpha=0.9$) for ATR–W+10 % mass.

Table 5 Activation energy (E) and natural logarithm of the pre-exponential factor ($\ln A$) values obtained by the FWO method.

Catalyst/% mass	Conversion, α	ATR-W	ATR-Z	ATR-W	ATR-Z
		Activation energy, $E/\text{kJ mol}^{-1}$		$\ln(A)/\text{min}^{-1}$	
0	0.2	214.71 \pm 0.12	134.39 \pm 0.16	58.83 \pm 7.00 $\times 10^{-3}$	37.33 \pm 6.00 $\times 10^{-3}$
	0.3	93.77 \pm 0.28	105.70 \pm 0.11	23.20 \pm 4.00 $\times 10^{-3}$	27.46 \pm 5.00 $\times 10^{-3}$
	0.4	91.86 \pm 0.22	79.07 \pm 0.09	21.40 \pm 6.00 $\times 10^{-3}$	19.36 \pm 5.00 $\times 10^{-3}$
	0.5	72.05 \pm 0.28	67.15 \pm 0.11	15.83 \pm 2.00 $\times 10^{-3}$	15.69 \pm 3.00 $\times 10^{-3}$
	0.6	74.62 \pm 0.25	56.47 \pm 0.10	15.63 \pm 4.00 $\times 10^{-3}$	12.67 \pm 6.00 $\times 10^{-3}$
	0.7	75.42 \pm 0.22	47.40 \pm 0.11	15.04 \pm 2.00 $\times 10^{-3}$	10.29 \pm 5.00 $\times 10^{-3}$
	0.8	69.62 \pm 0.23	42.68 \pm 0.11	13.25 \pm 4.77 $\times 10^{-3}$	9.02 \pm 2.00 $\times 10^{-3}$
	0.9	75.08 \pm 0.20	37.62 \pm 0.12	13.76 \pm 1.00 $\times 10^{-2}$	7.83 \pm 5.00 $\times 10^{-3}$
3	0.2	161.19 \pm 0.06	54.13 \pm 0.23	45.47 \pm 2.00 $\times 10^{-3}$	14.03 \pm 7.00 $\times 10^{-3}$
	0.3	111.83 \pm 0.05	57.33 \pm 0.16	29.40 \pm 6.39 $\times 10^{-4}$	14.33 \pm 1.00 $\times 10^{-2}$
	0.4	101.42 \pm 0.04	50.69 \pm 0.17	25.28 \pm 3.00 $\times 10^{-3}$	12.02 \pm 2.00 $\times 10^{-3}$
	0.5	74.97 \pm 0.10	44.69 \pm 0.16	17.75 \pm 2.00 $\times 10^{-3}$	10.18 \pm 5.00 $\times 10^{-3}$
	0.6	70.99 \pm 0.07	40.67 \pm 0.15	16.13 \pm 1.36 $\times 10^{-4}$	8.96 \pm 3.00 $\times 10^{-3}$
	0.7	67.41 \pm 0.04	39.40 \pm 0.14	14.74 \pm 4.00 $\times 10^{-3}$	8.44 \pm 4.00 $\times 10^{-3}$
	0.8	57.23 \pm 0.06	38.53 \pm 0.14	12.11 \pm 2.00 $\times 10^{-3}$	8.05 \pm 3.00 $\times 10^{-3}$
	0.9	45.93 \pm 0.06	50.56 \pm 0.10	9.52 \pm 2.00 $\times 10^{-3}$	10.06 \pm 3.00 $\times 10^{-3}$
5	0.2	59.21 \pm 0.16	78.59 \pm 0.22	15.48 \pm 1.00 $\times 10^{-2}$	21.28 \pm 2.00 $\times 10^{-3}$
	0.3	53.21 \pm 0.15	79.76 \pm 0.09	13.16 \pm 4.00 $\times 10^{-3}$	20.54 \pm 6.00 $\times 10^{-3}$
	0.4	48.20 \pm 0.15	60.67 \pm 0.06	11.38 \pm 1.00 $\times 10^{-3}$	14.76 \pm 2.00 $\times 10^{-3}$
	0.5	44.26 \pm 0.16	55.71 \pm 0.08	10.04 \pm 4.00 $\times 10^{-3}$	13.01 \pm 2.00 $\times 10^{-3}$
	0.6	40.01 \pm 0.15	45.40 \pm 0.10	8.78 \pm 2.00 $\times 10^{-3}$	10.21 \pm 5.00 $\times 10^{-3}$
	0.7	37.62 \pm 0.16	41.03 \pm 0.11	8.03 \pm 2.00 $\times 10^{-3}$	9.24 \pm 1.00 $\times 10^{-3}$
	0.8	35.45 \pm 0.15	36.19 \pm 0.11	7.39 \pm 1.00 $\times 10^{-3}$	7.76 \pm 3.00 $\times 10^{-3}$
	0.9	39.06 \pm 0.13	32.26 \pm 0.12	7.89 \pm 8.95 $\times 10^{-4}$	6.88 \pm 3.00 $\times 10^{-3}$
10	0.2	24.84 \pm 0.11	48.00 \pm 0.08	5.48 \pm 9.00 $\times 10^{-3}$	12.55 \pm 1.70 $\times 10^{-2}$
	0.3	22.89 \pm 0.11	38.07 \pm 0.12	4.94 \pm 3.00 $\times 10^{-3}$	9.49 \pm 1.10 $\times 10^{-3}$
	0.4	21.77 \pm 0.11	23.48 \pm 0.01	4.64 \pm 6.00 $\times 10^{-3}$	5.51 \pm 9.00 $\times 10^{-3}$
	0.5	19.97 \pm 0.10	17.57 \pm 0.04	4.21 \pm 3.00 $\times 10^{-3}$	4.04 \pm 5.00 $\times 10^{-3}$
	0.6	19.17 \pm 0.10	13.25 \pm 0.03	4.04 \pm 3.00 $\times 10^{-3}$	3.09 \pm 3.00 $\times 10^{-3}$
	0.7	18.82 \pm 0.09	11.89 \pm 0.07	4.00 \pm 3.00 $\times 10^{-3}$	2.92 \pm 1.00 $\times 10^{-3}$
	0.8	18.75 \pm 0.08	10.38 \pm 0.08	4.05 \pm 3.00 $\times 10^{-3}$	2.75 \pm 2.00 $\times 10^{-3}$
	0.9	20.17 \pm 0.06	9.06 \pm 0.08	4.44 \pm 2.00 $\times 10^{-3}$	2.73 \pm 1.200 $\times 10^{-2}$

On the other hand, analyzing the kinetic function, $E=E(\alpha)$, for ATR-Z case study, it was possible to report a decreases from 134.39 kJ mol^{-1} (at $\alpha=0.2$) to 37.62 kJ mol^{-1} (at $\alpha=0.9$) for ATR-Z+0 % mass; from 54.13 kJ mol^{-1} (at $\alpha=0.2$) to 50.56 kJ mol^{-1} (at $\alpha=0.9$) for ATR-Z+3 % mass; from 78.59 kJ mol^{-1} (at $\alpha=0.2$) to 32.26 kJ mol^{-1} (at $\alpha=0.9$) for ATR-Z+5 % mass and from 48.00 kJ mol^{-1} (at $\alpha=0.2$) to 9.06 kJ mol^{-1} (at $\alpha=0.9$) for ATR-Z+10 % mass.

According to the FWO method, corresponding to various degrees in the range $0.2 < \alpha < 0.9$, Table 5 shows the values of $\ln A$ for different values of α . Considering that the E -dependence on α described by Eq. (14), the values for E_0 and E_I were found (Table 6). The linear E -dependence on $1/\alpha$ is justified by the results shown in Table 5, where the values calculated using Eq. (14) presented a deviation below 0.28. From the intercept of the linear regression according to Eq. (13), the values of $\ln A$ for each value of E were obtained (Table 6). The

coefficient of determination (R^2) corresponding to the straight line of $\ln A$ versus E had a value higher than 0.98. The Fig. 10 shows the straight lines corresponding to the compensation effect for the ATR–W and ATR–Z with catalyst. The linearity observed for several $\ln A$ and E values indicated that the proposed kinetic representation might be used to evaluate the cracking reaction of the ATR–W+% mass catalyst samples, with the compensation parameters a^* (between 0.24 and 0.34) and b^* (between -7.75 and -0.45) and for ATR–Z +% mass catalyst samples using compensation parameters around 0.30 mol $\text{kJ}^{-1} \cdot \text{min}^{-1}$ for a^* and between -4.32 min^{-1} and -0.13 min^{-1} for b^* .

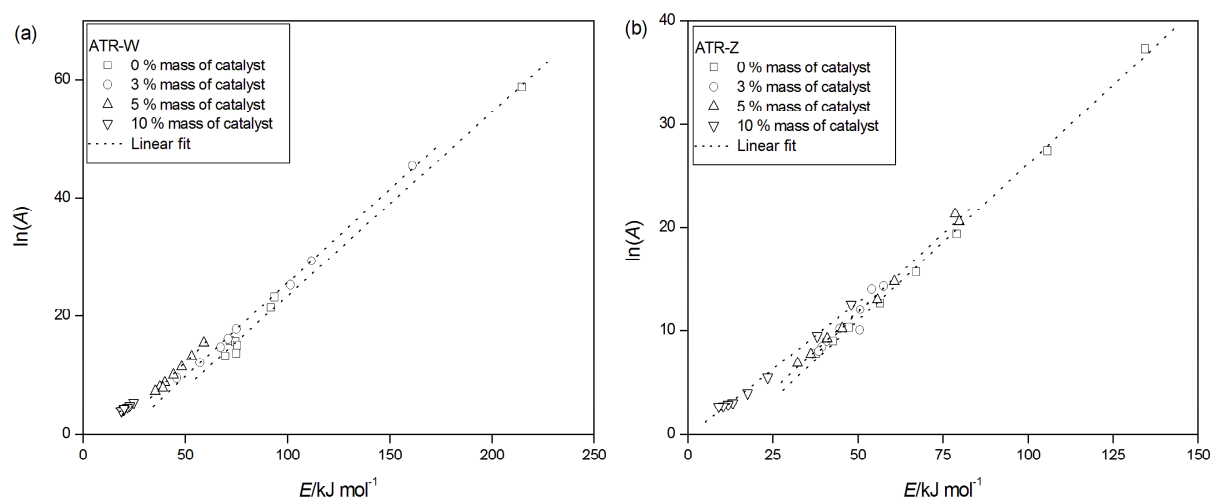


Figure 10. Kinetic compensation effect plotting $\ln A$ versus E for (a) ATR–W and (b) ATR–Z with (□) 0 % mass of catalyst; (○) 3 % mass of catalyst; (△) 5 % mass of catalyst and (▽) 10 % mass of catalyst.

Table 6. Kinetic compensation parameters and E –dependence on the conversion degree (α) parameters for ATR–W+% mass of catalyst and ATR–Z+% mass of catalyst.

Feedstock	Catalyst/% mass	Equation 13			Equation 14		
		b^* / min^{-1}	$a^* / \text{mol kJ}^{-1} \text{min}^{-1}$	R^2	$E_0 / \text{kJ mol}^{-1}$	$E_I / \text{kJ mol}^{-1}$	R^2
ATR–W	0	-7.75	0.31	0.99	19.09	33.59	0.83
	3	-6.02	0.32	1.00	22.52	27.93	0.99
	5	-5.10	0.34	0.99	30.65	6.11	0.94
	10	-0.45	0.24	0.98	17.20	1.58	0.90
ATR–Z	0	-4.24	0.30	1.00	13.26	25.40	0.98
	3	-4.32	0.32	0.89	38.22	3.85	0.50
	5	-3.25	0.30	0.99	24.55	12.75	0.84
	10	-0.17	0.26	0.99	-3.03	10.71	0.97

In this sense, this paper described a methodology for the modeling reaction term involved in the diffusion equation for the set of governing equations in the RMD modeling, to describe the kinetic schemes for the in-situ reaction of high-boiling-point petroleum fractions.

Various methods (Arrhenius, Kissinger and Flynn–Ozawa–Wall) have been developed for determining the kinetic parameters (E , A and $f(\alpha)$). These methods allow one to obtain the dependence of the activation energy (E –dependence) on the conversion degree (α) by means of a function $E=E(\alpha)$ and the change of activation energy, E , compensated by the same change in temperature or in the logarithm of the pre–exponential factor.

Conclusions

This work provided information about the cracking behavior of two high–boiling–point petroleum fractions from Brazilian crude oils and the effect of adding a catalyst on the kinetic reaction. Three methods were used to calculate the kinetic parameter (activation energy, pre–exponential factor and reaction rate), from the DSC data analyses obtained with the non–isothermal method (linear heating rate). The study showed that the cracking rates of the high–boiling–point petroleum fractions were temperature dependent between 693.15 and 723.15 K, and an endothermic region of high temperature oxidation (HTO) was identified.

In the methods studied, the kinetic parameters were determined from the slope and intercept, respectively, of the linear regression equation. Both the Arrhenius and Kissinger equations allowed for the simultaneous determination of the activation energy and pre–exponential factor for several increasing linear temperature experiments. On the other hand, the cracking of the samples studied can be considered as a first–order reaction for the kinetic term in the reactive molecular distillation modeling. The kinetic parameters of the high–boiling–point petroleum fractions samples showed that higher activation energy values were obtained in the HTO region as the API gravity of the high–boiling–point petroleum fractions decreased. The activation energy also showed a trend to increase with increasing asphaltene content. The effect of adding catalyst (at 3, 5 and 10 % mass of catalyst) on the kinetic parameters was also studied. The addition of catalyst increased the reaction rates by providing another pathway (a new mechanism) that presented exponential decay activation energy for the cracking reaction in all the systems studied.

Considering the fact that the kinetic parameters exhibit compensation effects, $\ln A$ was correlated by the linear kinetic compensation equation (see Eq. 13). Hence, it is to be expected that the $\ln A$ values increase with increasing E value, and this effect results in a change in one of the Arrhenius parameters, which is compensated by a corresponding change in the other by

means of the compensation parameters (a^* and b^*). On the other hand, when one considers the effect of adding a catalyst, the different treatments with catalyst (addition of 3, 5 and 10 % mass of catalyst) resulted in a change in the calculated E -dependence, but with no corresponding change in the reaction rate, showing that the E values were strongly dependent on conversion. The results showed a decrease in the E -dependence on α with increasing catalyst content, providing an alternative mechanism involving a different transition state and lower activation energy.

Acknowledgement

The authors acknowledge financial support of this research from the National Technological and Scientific Development Council (CNPq) and from the National Plan for the Science and Technology of Petroleum and Natural Gas (CTPETRO).

Nomenclature

A	=	Pre-exponential factor	$[\text{min}^{-1}]$
C_p	=	Specific heat capacity	$[\text{J kg}^{-1}\text{K}^{-1}]$
$D_{NPSE_i, \text{mix}}$	=	Difussion coefficient	$[\text{m}^2\text{s}^{-1}]$
E	=	Activation energy	$[\text{kJ mol}^{-1}]$
G_E	=	Effective evaporation rate	$[\text{kg m}^{-2}\text{s}^{-1}]$
H	=	Enthalpy	$[\text{J kg}^{-1}]$
$k'' = k_{i,m,n}$	=	Kinetic constant	$[\text{s}^{-1}]$
n	=	Reaction order	$[-]$
Q	=	Feed flow rate	$[\text{kg h}^{-1}]$
Q'	=	Flow rate over the evaporator surface	$[\text{kg h}^{-1}]$
Q_i	=	Feed flow rate at $\theta = 0$	$[\text{kg h}^{-1}]$
r	=	r – direction of coordinate system	$[-]$
R	=	Universal gas constant ($8.314 \text{ J K}^{-1}\text{mol}^{-1}$)	$[\text{J K}^{-1}\text{mol}^{-1}]$
$-r_{NPSE_i}$	=	the rate of disappearance of i -th pseudocomponent	$[\text{s}^{-1}]$
r_i	=	Distance from apex at which liquid enters cone	$[\text{m}]$
r_o	=	Radial position which liquid leaves	$[\text{m}]$
S	=	Shape index S of the conversion curve	$[-]$
s	=	s – direction of coordinate system perpendicular to cone surface	$[-]$
t	=	Time	$[\text{s}]$
T	=	Temperature	$[\text{K}]$
T_m	=	Temperature at the maximum peak on the DSC curve	$[\text{K}]$
T_s	=	Surface Temperature	$[\text{K}]$
x_{NPSE_i}	=	Molar fraction of i -th pseudocomponent ($NPSE_i$)	$[-]$
x_{sNPSE_i}	=	Molar fraction of i -th pseudocomponent ($NPSE_i$) at the evaporating surface	$[-]$
<i>Greek Letter</i>			
α	=	Conversion degree	$[-]$
β	=	Heating rate	$[\text{K min}^{-1}]$

β'	=	Half angle of apex of cone radius	[–]
δ	=	Thickness of liquid film	[m]
$(\Delta H_r)_{i,m,n}$	=	Heat of reaction	[J kg ⁻¹]
φ	=	φ – direction of coordinate system	[–]
λ	=	Thermal conductivity	[W m ⁻¹ K ⁻¹]
θ	=	θ – direction of coordinate system	[–]
ρ	=	Average Density and density fraction	[kg m ⁻³]
π	=	Pi parameter	[–]
v_r	=	Thin liquid film velocity in r–direction (radial velocity)	[m s ⁻¹]
ω	=	Angular velocity of cone	[s ⁻¹]
$\zeta_{i,m,n}$	=	Amount of coke formed when a <i>ith</i> pseudocomponent (<i>NPSE_i</i>) cracks to produces <i>mth</i> and <i>nth</i> pseudocomponents (<i>NPSE_m</i> and <i>NPSE_n</i>)	[kg h ⁻¹]
<i>Acronyms</i>			
KAS	=	Kissinger–Akahira–Sonase method	
FWO	=	Flynn–Ozawa–Wall method	
HTO	=	High temperature oxidation region	
RMD	=	Reactive molecular distillation process	

References

1. Merdrignac I, Espinat D. Physicochemical characterization of petroleum fractions: The state of the art. *Oil Gas Sci Technol.* 2007;62:7–32.
2. Tovar LP, Wolf Maciel MR, Maciel Filho R, Batistella CB, Ariza OC, Medina LC. Overview and computational approach for studying the physicochemical characterization of high-boiling-point petroleum fractions (350 °C+). *Oil Gas Sci Technol.* 2011; doi:10.2516/ogst/2011150.
3. Inuzuka M, Ishikawa H, Yamada, I, Hiraoka S, Aragaki T, Inukai Y, Erciyes AT, Kobayashi S. Vaporization from liquid film of binary mixture in a centrifugal molecular still. *J Chem Eng Jpn.* 1989;22:291–7.
4. Hernández–Barajas JR, Vázquez–Román R, Félix–Flores MaG. A comprehensive estimation of kinetic parameters in lumped catalytic cracking reaction models. *Fuel.* 2009;88:169–78.
5. Gupta RK, Kumar V, Srivastava VK. A new generic approach for modeling of fluid catalytic cracking (FCC) riser reactor. *Chem Eng Sci.* 2007;62:4510–28.
6. Ebrahimi S, Moghaddas JS, Razavi Aghjeh MK. Study on thermal cracking behavior of petroleum residue. *Fuel.* 2008;87:1623–7.
7. Gupta SR. Modeling and simulation of fluid catalytic cracking unit. Thesis (Doctor of Philosophy) – Department of Chemical Engineering, Deemed University, India, 2006.

8. K k MV, Keskin C. Comparative combustion kinetics for in situ combustion process. *Thermochim Acta*. 2001;369:143–7.
9. K k MV. Effect of metal oxide on light oil combustion. *J Therm Anal Calorim*. 2003;73:241–6.
10. Gonalves MLA, Barreto JRC, Cerqueira WV, Teixeira AMRF. Effect of zeolite, kaolin and alumina during cracking of heavy petroleum residue evaluated by thermogravimetry. *J Therm Anal Calorim*. 2009;97:515–9.
11. Yasar M, Akmaz S, Gurkaynak MA. Investigation of glass transition temperatures of Turkish asphaltenes. *Fuel*. 2007;86:1737–48.
12. S nchez–Jim nez PE, Criado JM, P rez–Maqueda LA. Kissinger kinetic analysis of data obtained under different heating schedules. *J Therm Anal Calorim*. 2008;94:427–32.
13. Guo A, Zhang X, Wang Z. Simulated delayed coking characteristics of petroleum residues and fractions by thermogravimetry. *Fuel Process Technol*. 2008;89:643–50.
14. Silva EFB, Ribeiro MP, Coriolano ACF, Melo ACR, Santos AGD, Fernandes VJ, Araujo AS. Kinetic study of degradation of heavy oil over MCM–41. *Therm Anal Calorim*. 2011; doi:10.1007/s10973–011–1543–4.
15. K k MV, Gundogar AS. Effect of different clay concentrations on crude oil combustion kinetics by thermogravimetry. *J Therm Anal Calorim*. 2010;99:779–83.
16. Aıkalin K. Thermogravimetric analysis of walnut shell as pyrolysis feedstock. *J Therm Anal Calorim*. 2011;105:145–50.
17. Kobelnik M, Ribeiro CA, Dias DS, Almeida S, Crespi MS, Capela JMV. Study of the thermal behavior of the transition phase of Co(II)–diclofenac compound by non–isothermal method. *J Therm Anal Calorim*. 2011;105: 467–71.
18. Crespi MS, Hikosada MY, Amaral GCA, Ribeiro CA. Kinetic parameters obtained for thermal decomposition of acrylic resins present in commercial paint emulsions. *J Therm Anal Calorim*. 2007;88:669–72.
19. Joraid AA. Estimating the activation energy for the non–isothermal crystallization of an amorphous $\text{Sb}_{9.1}\text{Te}_{20.1}\text{Se}_{70.8}$ alloy. *Thermochim Acta*. 2007;456:1–6.

20. Vyazovkin SV, Sbirrazzuoli N. Estimating the activation energy for non-isothermal crystallization of polymer melts. *J Therm Anal Calorim.* 2003;72:681–6.
21. Perošević S, Rašković L. Correlation of reaction kinetic parameters in two component polyurethane systems. *Facta Univ, Ser: Work Living Environ Prot* 1. 2000;1:69–79.
22. Kissinger H. Reaction kinetics in differential thermal analysis. *Anal Chem.* 1957;29: 1702–6.
23. Skala D, Kopsch H, Sokić M, Neumann H, Jovanović J. Thermogravimetrically and differential scanning calorimetrically derived kinetics of oil pyrolysis. *Fuel.* 1987;66:1185–91.
24. Khawam A., Flanagan DR. Role of isoconversional methods in varying activation energies of solid–state kinetics I. isothermal kinetic studies. *Thermochim Acta.* 2005;429:93–102.
25. Galwey AK, Brown ME. Arrhenius parameters and compensation behaviour in solid–state decompositions. *Thermochim Acta.* 1997;300:107–15.
26. Flynn JH, Wall LA. A quick, direct method for the determination of activation energy from thermogravimetric data. *J Polym Sci Pol Lett.* 1966;4:323–8.
27. Ozawa T. Kinetic analysis of derivative curves in thermal analysis. *J Therm Anal Calorim.* 1970;2:301–24.
28. Moreno RMB, Medeiros de ES, Ferreira FC, Alves N, Gonçalves PS, Mattoso LHC. Thermogravimetric studies of decomposition kinetics of six different IAC *Hevea* rubber clones using Flynn–Wall–Ozawa approach. *Plast Rubber Compos.* 2006;35:15–21.
29. American Society for Testing Materials– ASTM D 2892. Standard test method for distillation of crude petroleum (15–Theoretical plate column). West Conshohoken, (Pensylvania): ASTM International, 2005. 32p.
30. Del Bianco A, Panariti N, Anelli M, Beltrame PL, Carniti P. Thermal cracking of petroleum residues: 1. Kinetic analysis of the reaction. *Fuel.* 1993;72:75–80.
31. Kök MV, Karacan O. Pyrolysis analysis and kinetics of crude oils. *J Therm Anal Calorim.* 1998;52:781–8.
32. Kök MV. Use of thermal equipment to evaluate crude oils. *Thermochim Acta.* 1993;214:315–24.

33. Gao Z, Amasaki I, Kaneko T, Nakada M. Assessment of the error of the pre-exponential factor obtained from the isoconversional plot and the single heating rate plot for dynamic thermogravimetric measurement of polymer degradation. *Polym Degrad Stab.* 2004;83:67–70.
34. Yang J, Chen J, Sun Z, Fan Y. Kinetic behavior for the non-isothermal coking of four chinese vacuum residua. *Pet Sci Technol.* 1993;11:909–21.

7.4. Considerações finais

O presente trabalho permitiu estabelecer positivamente a verificação do fato de que a técnica termoanalítica (DSC) leva a informações úteis e importantes sobre as características térmicas dos resíduos pesados de petróleo, em um curto período de tempo. Por conseguinte, a caracterização do comportamento térmico dos resíduos de destilação (atmosférica e/ou a vácuo) do petróleo, por DSC, pode ser o passo inicial para uma avaliação mais consistente dos mesmos.

A equação da taxa de reação foi assumida como sendo de primeira ordem levando em conta o efeito do catalisador. Os parâmetros cinéticos foram determinados usando calorimetria diferencial de varredura avaliando o efeito da compensação cinética, possibilitando bons ajustes com os dados experimentais.

A mudança na energia de ativação da reação de craqueamento não mostrou alteração significativa com as taxas de aquecimento testadas.

A presença do catalisador aumentou a velocidade de uma reação de craqueamento, atuando como promotor de uma nova rota de reação com uma menor energia de ativação. O catalisador acelera a reação, pois diminui a energia de ativação das moléculas, mas não participa da reação, ou seja, não ocorre nenhuma mudança nos elementos químicos da reação.

A determinação dos parâmetros cinéticos também foi realizada utilizando-se a análise do efeito de compensação cinética, a qual foi verificada pela existência linear entre o logaritmo neperiano do fator pré-exponencial e a energia de ativação.

Capítulo 8.

Destilação molecular reativa (tipo centrífuga): Modelagem e simulação

8.1. Introdução

O processo de destilação molecular reativa (DMR), no qual ocorre o acoplamento de destilação molecular e reação química simultaneamente, pode ser qualificado como um processo híbrido e também como um processo intensificado.

Os desenvolvimentos em níveis computacional (modelagem e simulação) e experimental do processo de destilação molecular reativa, no qual ocorre o acoplamento de destilação molecular e conversão (reação química) simultaneamente, é apresentado nos capítulos subsequentes. Entretanto, dadas as configurações do equipamento e as condições operacionais que viabilizam a implementação de alto vácuo pode-se submeter o material a temperaturas adequadas, em um curto espaço de tempo operacional, garantindo, assim, um contato mais intenso da amostra com a superfície catalítica. Esses fatores devem proporcionar alta taxa de evaporação e alta cinética de reação e, conseqüentemente, elevadas taxas de conversão/evaporação, permitindo, com isso, altas taxas de processamento.

Com respeito à modelagem do destilador molecular reativo, essa estará baseada na modelagem desenvolvida para o processo de destilação molecular centrífuga de frações de petróleo pesado (Tovar et al., 2012). Essa modelagem será devidamente adaptada, com o objetivo de fazer estudos de predição e também de avaliação do processo, acarretando, com isso, a condução de trabalhos experimentais em condições já otimizadas, possibilitando, assim, a verificação dos resultados que seriam conseguidos com uma aplicação experimental.

A modelagem matemática compreende equações de balanço de massa, energia e momento. A taxa de evaporação é a efetiva de Langmuir que considera os efeitos da fase vapor e o grau de anisotropia do sistema. A equação da taxa de reação foi assumida como sendo de primeira ordem levando em conta o efeito do catalisador. Os parâmetros cinéticos foram

determinados usando calorimetria exploratória diferencial avaliando o efeito da compensação cinética, possibilitando bons ajustes com os dados experimentais.

A modelagem do processo descrita neste capítulo assume que:

- O sistema é estabelecido em coordenadas esféricas.
- O material apresenta um comportamento característico dos fluidos newtonianos, altamente viscoso com número de Reynolds baixo característico de um sistema em regime laminar.
- Considerou-se nas simulações deste trabalho um sistema multicomponente, no qual o fluido simulado tem propriedades físicas em função do perfil de temperatura na no filme líquido que escoar sobre a superfície do evaporador.
- O filme líquido é considerado incompressível, distribuído uniformemente na superfície do evaporador garantindo uma boa transferência de massa.
- A superfície do evaporador é cônica e internamente aquecida através de resistências térmicas.
- A espessura do filme é considerada muito menor quando comparada com o raio da superfície cônica.
- Com a tentativa de obter a solução numérica para o fluxo em estado estacionário sobre a superfície do evaporador, a força gravitacional é desprezível em comparação com a força centrífuga.
- A superfície cônica gira a velocidade angular ω , e o fluxo apresenta simetria axial em relação à coordenada φ , o que implica que a velocidade na direção θ é muito menor do que a velocidade na direção $-\varphi$ e a velocidade na direção $-r$. No entanto, baseado no trabalho desenvolvido por Medina et al., (2010) apenas o vetor da velocidade na direção radial ($-r$) apresenta variação apreciável com as condições operacionais do processo da destilação molecular.
- Não – ondas , re-evaporação no filme.

Para a simulação, foi considerado como caso de estudo o processamento de um resíduo atmosférico do petróleo “W” (ATR-W) 673,15 K⁺, em um destilador molecular centrífugo

reativo aquecido, onde a superfície do evaporador constitui uma superfície cônica. O resíduo atmosférico total foi dividido em 02 pseudo-componentes, os quais foram caracterizados utilizando dados de propriedades físico-químicas geradas pelo simulador desenvolvido por Tovar et al. (2011).

O conjunto de $(11+18N)$ equações diferenciais parciais e algébricas e $(27+19N)$ variáveis foi incorporado no ambiente computacional, denominado DESTMOL-R, desenvolvido na linguagem FORTRAN-90 usando o compilador Compaq Visual Fortran (*professional edition* 6.6). O sistema de equações formuladas no filme, ao longo da superfície cônica do evaporador, foi resolvido numericamente através do método das linhas. Condições de temperatura do evaporador entre 473.15 e 523.15 K e de porcentagem de catalisador entre 3 e 5% m/m foram avaliadas. Realizando as simulações do processo, foi possível analisar o comportamento dos perfis das variáveis de interesse através da análise das variáveis de entrada (que são a temperatura do evaporador e a porcentagem de catalisador) sob os perfis característicos do processo: Temperatura na superfície do filme (T_s), espessura do filme (δ), taxa de evaporação efetiva (G_E), taxa de destilado (D), perfil de velocidade (v_r), taxa de reação e conversão (α).

Em relação ao desenvolvimento experimental, ensaios foram desenvolvidos entre 473.15 e 523.15 K considerando na carga do processo 1, 3 e 5% m/m de catalisador, constituindo um processo em catálise heterogênea (termo que descreve a catálise quando o catalisador está em uma fase diferente (ou seja sólido) aos reactantes). Como resultados foram obtidos quinze cortes de destilados e quinze de resíduos do processo de destilação molecular centrífuga reativa, cujas propriedades de massa molar, viscosidade, massa específica e °API foram avaliadas utilizando técnicas cromatográficas (SEC do inglês size-exclusion chromatography), análises reológicas e métodos padronizados (ASTM D 4052, ASTM D 5002 e ASTM D 70).

A complexidade química e a identificação estrutural foram analisadas utilizando a cromatografia por destilação simulada a elevadas temperaturas (HT-SimDis GC) (ASTM D 7169).

8.2. Desenvolvimento

O desenvolvimento deste capítulo é apresentado a seguir, nos manuscritos intitulados:

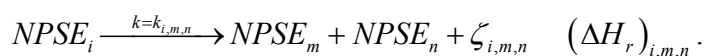
- *Reactive centrifugal molecular distillation: An intensified process–Part I. Mathematical modeling and simulation of the centrifugal reactive–molecular distillation process: Screening design using Plackett–Burman and 2_{IV}^{4-1} factorial designs*, a ser submetido no periódico internacional *Industrial & Engineering Chemistry Research*.
- *Centrifugal reactive–molecular distillation: An intensified process–Part II. Key operating variables and their effects on the performance of the centrifugal reactive–molecular distillation process*, publicado nos anais, respectivamente, como *High–boiling–point petroleum fractions upgrading using the centrifugal reactive–molecular distillation process over catalyst: Mathematical modeling and simulation including experimental validation* no *European Symposium on Computer Aided Process Engineering – ESCAPE 22*; University College London, UK; 17–20 June 2012.
- *Centrifugal reactive–molecular distillation: An intensified process–Part III. Heavy petroleum residue upgrading using the centrifugal reactive–molecular distillation process over catalyst: High–temperature simulated distillation for the evaluation of converted products (distillate and residue streams)*, a ser submetido no periódico internacional *Industrial & Engineering Chemistry Research*.

Centrifugal reactive–molecular distillation: An intensified process–Part I

Mathematical modeling and simulation of the centrifugal reactive–molecular distillation process of high–boiling–point petroleum fractions (>623.15 K): Screening design using Plackett–Burman and 2_{IV}^{4-1} factorial designs

Abstract

Reactive molecular distillation process (RMD), in which the molecular distillation process and reactive process occur simultaneously, can be characterized as an intensified and hybrid process. The modeling of the reactive molecular distillation process (centrifugal type – CRMD) to upgrade high–boiling–point petroleum fractions is presented in this work. The mathematical model involves equations for the evaluation of the physicochemical properties, macroscopic variables (mean free path and Knudsen number), heat, continuity and material balances. In the in–situ cracking reaction, it can be assumed that one mole of a cracked pseudocomponent ($NPSE_i$) gives one mole each of two other pseudocomponents ($NPSE_m, NPSE_n$) and a certain amount of coke ($\zeta_{i,m,n}$) may also be formed (Gupta, 2006):



The mathematical model was numerically solved by the numerical method of lines, applying centered finite difference to obtain its discretization. A set of $(11+18N)$ equations classified as PDEs, ODEs and AEs and $(27+19N)$ variables were processed by the computational program named DESTMOL–R, developed in FORTRAN–90 language using Compaq Visual Fortran compiler (professional edition 6.6). The modeling was described under steady–state conditions. A case study is illustrated for an atmospheric petroleum residue (>673.15 K) of “W” crude oil. In this paper, a screening approach, involving the use of the Plackett–Burman and fractional factorial designs (2_{IV}^{4-1}), permitted the evaluation of the effects of the operating conditions (evaporator temperature, feed flow rate, percent weight of catalyst, feed temperature, condenser temperature, rotor speed and system pressure) on the relevant process variables, such as film thickness, surface evaporation rate, distillate mass flow rate, concentration profiles and velocity profiles.

The results showed that the inlet variables, such as the evaporator temperature, the percent weight of catalyst and the feed flow rate were the most relevant operational conditions for the final composition of the condensate flow. The concentration of the pseudocomponent “a” shrank in both the s - and r - directions, due to the rapid temperature rise in the thin liquid film. Consequently, the thickness of the film rapidly decreased in this region, whereas the amount of distillate mass flow rate from the split molecules continuously increased throughout the evaporator under the selected operational conditions.

Keywords: Centrifugal reactive–molecular distillation, mathematical modeling, heavy petroleum residue, DESTMOL–R, method of lines, Plackett–Burman design, fractional factorial design.

Contents

1. Introduction
 2. Non–conventional heavy residue upgrading technology
 - 2.1. The molecular distillation technology
 - 2.2. Reactive molecular distillation process
 - 2.2.1. Centrifugal reactive–molecular distiller operation
 3. Mathematical description
 - 3.1. Overall mass balance
 - 3.2. Velocity profile of the liquid film
 - 3.3. Thickness of the evaporating film
 - 3.4. Overall distillate mass flow rate
 - 3.5. Effective evaporation rate
 - 3.6. Temperature profile in the liquid film
 - 3.7. Concentration profile in the liquid film
 - 3.8. Approximate reaction equation for the catalytic reaction term
 - 3.8.1. Kinetic parameters
 4. Physical modeling
 5. Computational tool
 - 5.1. Numerical solution strategy
 - 5.2. Model evaluation
 - 5.2.1. Plackett–Burman design
 - 5.2.2. Fractional factorial screening design
 6. Results and discussion
 - 6.1. Screening of the significant variables using the Plackett–Burman design
 - 6.2. Screening of the significant variables using a fractional factorial design
 7. Conclusions and outlook
- Acknowledgements
 Nomenclature
 References

1. Introduction

Petroleum processing and refining involves a series of steps to convert the crude oil into products with the desired properties and qualities. Every day, the processing of crude oil produces important quantities of cuts and heavy petroleum residues (high-boiling-point petroleum fractions >623.15 K). Heavy petroleum residues present specific characteristics in relation to their compositions, such as low H/C ratios, high sulfur and metal contents and are constituted of complex hydrocarbons such as paraffins, naphthenes and aromatic compounds (Rana et al., 2007). However, there are two types of residue, depending on the source: an atmospheric residue, designated as the material at the bottom of the atmospheric distillation tower, with an atmospheric equivalent boiling point (AET) above 616.15 K, and a vacuum residue, which refers to the material at the bottom of the vacuum distillation tower, with an AET above 838.15 K, obtained at 3.33 – 13.33 kPa (Rana et al., 2007; Reddy et al., 1998).

The upgrading of the residue, basically, involves thermal and catalytic cracking, which implies the breaking of large molecules into smaller molecules. These technologies can be classified into two main routes as shown in Table 1. However, the processing of heavy crude oil and heavy petroleum fractions by the conventional methods listed in Table 1, restricts their use to a few applications. Thus, they must be converted into more valuable products.

Table 1. Classification of petroleum residue upgrading.

	Process	Temperature (K)	Pressure (MPa)	Source
Non-catalytic process	Solvent deasphalting			Sattarin et al., 2006.
	Gasification	>1273.15	–	Rana et al., 2007; Pindoria et al., 1997.
	Delayed coking	753.15–788.15	0.61	Guo et al., 2008; Rana et al., 2007; Rodríguez-Reinoso et al., 1998.
	Thermal	Fluid coking	753.15–838.15	Rana et al., 2007.
		Flexicoking	1103.15–1273.15	Rana et al., 2007; Furimsky, 2000;
		Visbreaking	723.15–783.15	Rana et al., 2007; Bozzano et al., 2005; Omole et al., 1999
Catalytic processes	Residue of fluid catalytic cracking			Wang et al., 2008; Rana et al., 2007.
	Fluid catalytic cracking			Bollas et al., 2007
	Hydroprocessing	Fixed bed hydrotreating	623.15–703.15	Verstraete et al., 2007; Marroquín-Sánchez and Ancheyta-Juárez, 2001; Rana et al., 2007.
		Fixed bed hydrocracking	703.15–723.15	Ali et al., 2002; Rana et al., 2007; Zhou, 2003.
		Slurry hydrocracking	~713.15	Zhang et al., 2007; Rana et al., 2007.
		Ebullated bed	653.15–723.15	Rana et al., 2007.
		hydrotreating		
		Ebullated bed	*668.15–713.15	Martínez et al., 2010; Rana et al., 2007.
	hydrocracking		†658.15–723.15	

*LC-Fining process; †H-Oil process

A technology known as molecular distillation has been largely used in several applications in the Separation Process Development Laboratory (LDPS) of the State University of Campinas (UNICAMP, Brazil), and appears to be one of the best alternatives to split and to characterize heavy liquid petroleum cuts and high-boiling-point petroleum fractions (Zuñiga-Liñan et al., 2011; Zuñiga et al., 2009; Sbaite et al., 2006; Batistella et al., 2000). Recently, the same research group developed the reactive molecular distillation technique sponsored by the Petrobras Research Center–Brazil (CENPES/Petrobras) and the Brazilian Study and Project Financing Institution (FINEP). In this process, the molecular distillation and the reactive process take place simultaneously.

2. Non-conventional heavy residue upgrading technology

2.1. The molecular distillation technology

The molecular distillation (MD) process is a high-tech thermal separation technique, operating at pressures in the range from 0.1 to 10 Pa (Tovar, 2012). The potential of MD is due to the fact that it is appropriate for the separation and purification of heat sensitive products with high-boiling points, since the process occurs under high vacuum at lower temperatures (Zuñiga-Liñan et al., 2011; Zuñiga et al., 2009; Tovar et al., 2011; Tovar et al., 2010; Xubin et al., 2005; Sales-Cruz and Gani, 2006; Batistella et al., 2002; Cvengroš et al., 2000). In the MD process, the vapor molecules must find a free path between the evaporator and the condenser, the pressure must be low and the width of the distillation gap must be comparable with the mean free path of the evaporating molecules. Under these conditions, phase equilibrium does not exist (Hickman, 1944).

2.2. Reactive molecular distillation process

Many authors define process intensification as a term used to describe a revolutionary strategy for any process or plant design to reduce the size of the chemical plant needed, to achieve a given production objective, to provide a chemical process with the precise environment it needs, and to provide processes which are safer, cleaner, smaller and cheaper (Keil, 2007; Stankiewicz and Moulijn, 2002). Keil (2007) presents an overview of the equipment and strategies established for process intensification (Figure 1), which achieve reductions in investment, energy costs and waste production.

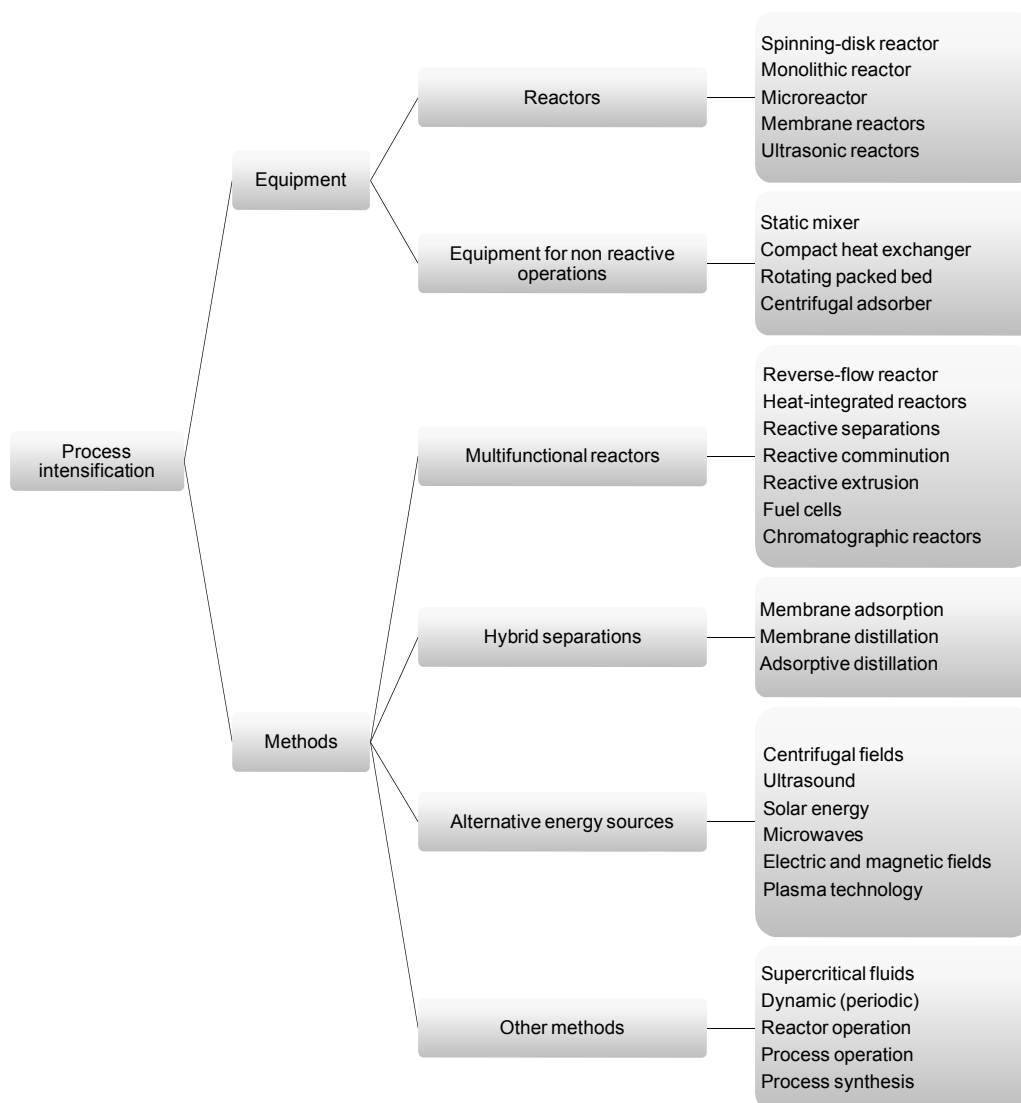


Figure 1. Tools for process intensification. *Source:* Keil, 2007.

The reactive molecular distillation (RMD) process can be considered as an intensified/hybrid process, in which molecular distillation (high vacuum) and reactive process are carried out simultaneously. The particular features of the configuration of RMD equipment facilitate the implementation of a high vacuum with lower temperatures than used in the conventional process, maintain the material inside the equipment for a shorter operational residence time, and achieve a very intensive contact between the sample and the catalytic surface. These advantages should provide high rates of cracking / split, allowing for high processing rates and relatively high conversion degrees.

This study describes the mathematical modeling of the RMD (centrifugal type– CRMD) for high-boiling-point fractions. Accordingly, the RMD process will be represented by the temperature, concentration, velocity, effective evaporation rate, distillate mass flow rate, film thickness and reaction rate profiles, supporting both the operational analysis and the process design at the same time.

The mathematical model comprises equations for the evaluation of the physicochemical properties in order to characterize the reaction and distillation mixtures. Heat and material balances involve a system of partial differential and algebraic equations (PDAEs). The set of PDAEs was solved by a computer aided environment (DESTMOL–R) developed in FORTRAN–90 language using Compaq Visual Fortran compiler (professional edition 6.6), using the numerical method of lines.

The simulations were carried out under steady-state conditions. The output variables, such as the surface temperature (T_s), film thickness (δ), effective evaporation rate (G_E), distillate mass flow rate (D), radial velocity (v_r), concentration of pseudocomponent “a” (X_a) and the conversion degree (α) profiles, were computed by analyzing the effects of the operational conditions (the evaporator temperature (EVT), feed flow rate (Q), percent weight of catalyst (%CAT), feed temperature (T_{feed}), condenser temperature (T_{cond}), rotor speed (RS) and the system pressure (P_s)). The variables were screened using a 16-run Plackett–Burman design followed by a fractional factorial design (2_{IV}^{4-1}), since this allowed for the simultaneous consideration of several variables at different levels (upper limits and lower limits), using a reduced number of simulations. The higher order interactions were negligible. All the data were treated using the software Statistica 7.0 from Statsoft Inc (2004).

2.2.1. Centrifugal reactive–molecular distiller operation

The centrifugal reactive–molecular distillation (CRMD) process, a type of RMD process, represents the coupling of the in-situ catalytic reaction and the centrifugal molecular distillation process, in which the evaporating liquid film is formed due to the centrifugal force. The introduction of the reaction into the separation process zone leads to know interactions between the mass transfer rates, diffusion and chemical kinetics .

The reactive centrifugal molecular distiller has a rapidly rotating spinning cone to create a rapidly spreading and moving film of liquid. When the rotating cone is heated, the

reaction/evaporation takes place (Figure 2a). The CRMD unit consists of a heated spinning rotor housed in a vacuum chamber (Figure 2b).

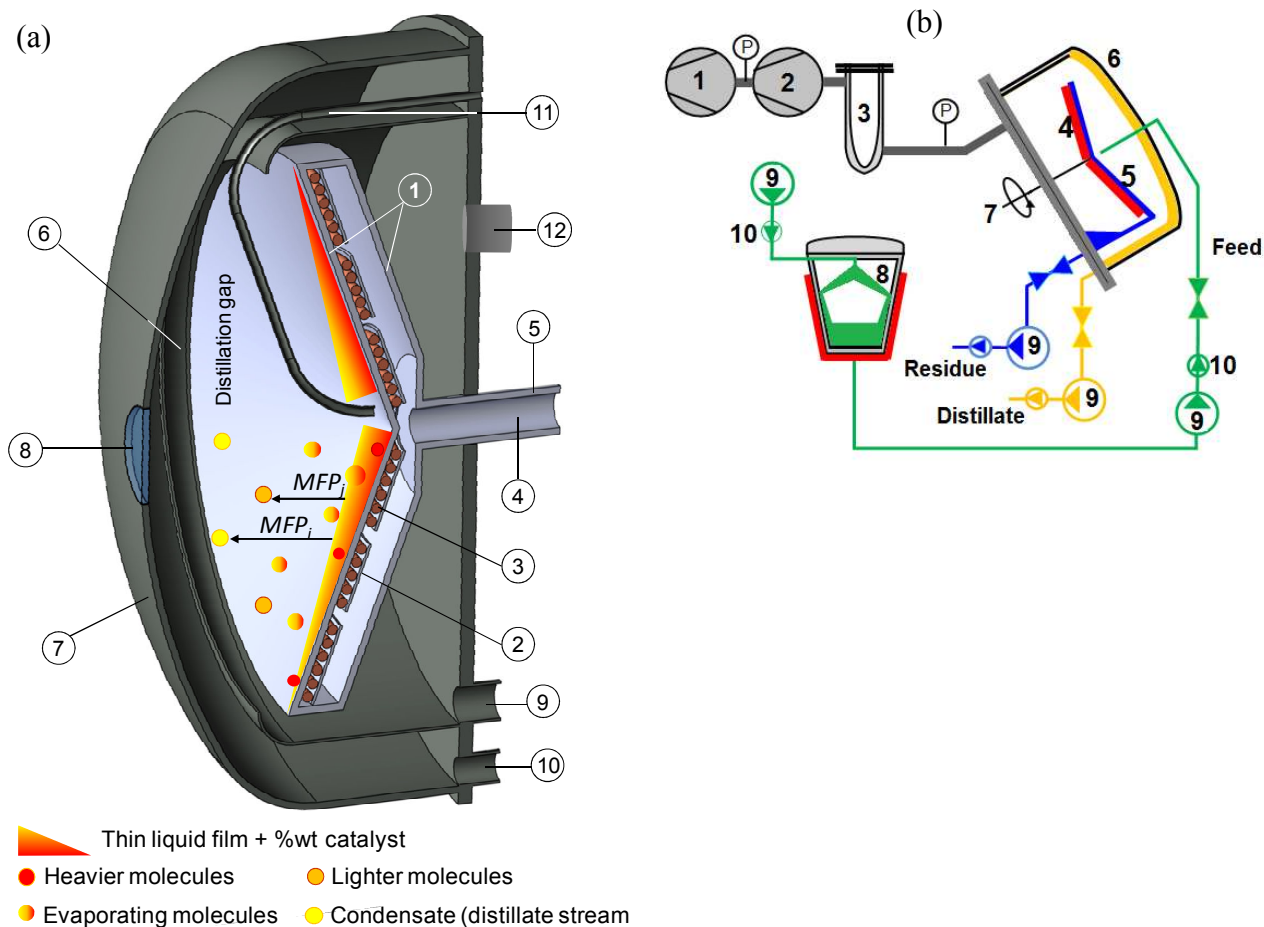


Figure 2. (a) Schematic side view of the evaporator–condenser device of the centrifugal reactive molecular distiller. 1. Evaporator surface; 2. Support resistance; 3. Thermocouple/resistance; 4. Shaft hole; 5. Axis; 6. Cooling camera; 7. Dome; 8. Viewfinder; 9. Residue pipe connection; 10. Distillate pipe connection; 11. Feeding tube; 12. Vacuum tube.

Figure 2. (b) Scheme of the centrifugal reactive–molecular distiller. 1. Backing/Roughing Vacuum Pump; 2. Diffusion Ejector Pump (High vacuum); 3. Chamber trap; 4. Heater rotor; 5. Evaporator surface; 6. Dome condenser; 7. Rotor; 8. Feed storage; 9. Liquid Transfer Pump; and 10. Check Valve Rotor. Modified Myers–Vacuum (2010).

The material, constituted of a high-boiling-point petroleum fraction plus catalyst (heterogeneous catalysis), is pumped into the center of the heated rotating disk, and the feedstock is spread over the inside of the chamber by the centrifugal force. By way of a careful control of the heater temperature, the molecules are cracked on the rotor (by the effect of the high vacuum and low temperatures) into lower molar mass molecules, which evaporate and condense on the cooled condenser. The lighter distillate molecules (cracked molecules) are pumped from the

system via the distillate collect valve into the distillate collector. The portion which does not distill (called the residue stream) is pumped from the CRMD unit via the collect valve into the collector system.

The mathematical description is based on the modeling of the centrifugal molecular distillation process proposed by Tovar (2012), Kawala and Stephan (1989), Bruin (1969), Inuzuka et al. (1989) and Inuzuka et al. (1986) as a starting point to develop a specific modeling of the CRMD process for high-boiling-point petroleum fractions. The following assumptions were made to develop the generalized two-dimensional steady state mathematical model of the CRMD process:

$$-ds = r d\theta \quad (1)$$

Figure 3. Sketch of the coordinate system of the rotor in the reactive molecular distiller (Tovar et al., 2011).

- The flow over the evaporator surface is in the form of a thin liquid film. The pattern itself is essentially stationary. The flow is laminar and practically no waves are formed on the surface of the thin film. Furthermore, the liquid film is considered to be incompressible and uniformly distributed on the evaporator wall, guaranteeing excellent mass transfer.
- The liquid film thickness is very small in comparison with the radius of the conical surface. It is assumed to be a Newtonian fluid. The evaporated liquid is highly viscous, and hence the Reynolds numbers are small.
- Re-evaporation and splashing phenomena are both neglected, and the diffusion process in the θ -direction is also neglected.
- Gravitational force is negligibly in comparison with the centrifugal force.
- The velocity components in the θ - and φ -directions, respectively, are negligible when compared with the radial velocity component (in the r -direction).
- The thermophysical properties (specific heat capacity, thermal conductivity, kinematic viscosity, vapor pressure, effective evaporation rate and evaporation enthalpy), are functions of the temperature (at the evaporator wall) and the surface temperature (T_s) profile on the inside of the thin liquid film.

3.1. Overall mass balance

The continuity equation can be written as follows (Inuzuka et al., 1986):

$$\frac{1}{3600} \frac{dQ'}{dr} + 2\pi r G_E (\sin \beta') = 0 \quad (2)$$

The velocity profile in the liquid film is assumed to be fully developed on the rotating evaporator surface, as presented by Hinze and Milborn (1950), Inuzuka et al. (1989) and Inuzuka et al. (1986).

$$\mu \frac{\partial^2 v_r(r)}{\partial s^2} + \rho (\sin^2 \beta') r \omega^2 = 0 \quad (3)$$

The boundary conditions for $Q(r)$ and $v_r(r)$ are given as:

$$Q'(r) = Q_i(r) \quad \text{at} \quad r = r_i \quad (4)$$

$$v_r(r) = 0 \quad \text{at} \quad s = 0 \quad \text{At the wall} \quad (5)$$

$$\frac{\partial v_r(r, s)}{\partial s} = 0 \quad \text{at} \quad s = \delta(s) \quad \text{At the free surface} \quad (6)$$

3.2. Velocity profile of the liquid film

Mathematically, the velocity profile in the liquid film is expressed by Equation (3), and from the integration with Equations (5) and (6), it is possible to obtain an expression for determining the velocity profile as a function of the thickness of the liquid film in the s -direction, as follows:

$$v_r(r) = \frac{\omega^2 \sin^2 \beta'}{\nu} r \left(\delta s - \frac{s^2}{2} \right) \quad (7)$$

3.3. Thickness of the evaporating film

The film thickness (δ) is fundamental to evaluate the velocity profile (Equation 7). This varies with radial distance along the evaporator surface, due to the axial and radial gradients of the temperature in the liquid film. Substituting Equation (7) in the volumetric flow rate equation (Equation 2), and solving the continuity equation with the corresponding boundary conditions, the film thickness is given by Equation (8) (Inuzuka et al., 1986):

$$\delta(r) = \left[\frac{3\nu}{2\pi\omega^2 r^2 \rho (\sin^3 \beta')} \left(\frac{Q_i - D}{3600} \right) \right]^{1/3} \quad (8)$$

3.4. Overall distillate mass flow rate

The overall distillate mass flow rate (D) is defined as the sum of the local distillate mass flow rates, and therefore presents variations in the r -direction, as already discussed by Inuzuka et al. (1986), as follows:

$$D(r) = 3600 \int_{r_i}^{r_o} 2\pi (\sin \beta') r G_E \, dr \quad (9)$$

3.5. Effective evaporation rate

The effective evaporation rate (G_E) is calculated using the modified Langmuir–Knudsen equation described by Equation (10), which takes the anisotropic properties of the vapor into account (Tovar, 2012; Kawala and Dakiniewicz, 2002; Kawala and Stephan, 1989; Langmuir, 1913; Lutišan et al., 2002).

$$G_E = \sum_{i=1}^{NPSE} \left(P_{vap_{NPSE_i}} \sqrt{\frac{M_{NPSE_i}}{2\pi R T_s}} \right) \left[1 - \left(1 - \left(\frac{d_e - 2L}{2d_e - 2L} \right) \right) \left(1 - e^{k^* K n_{NPSE_i}} \right)^{n'} \right] \quad NPSE_i = 1, \dots, N \quad (10)$$

Where P_{vap} is the vapor pressure at the absolute temperature T_s , M is the molar mass of the compound, Kn is the Knudsen number, defined as the ratio of the mean free path (MFP) of the vapor phase to the characteristic length (L) (Equation 11), R is the universal gas constant and n' represents the number of intermolecular collisions before the vapor reaches the isotropic state ($n'=5$) (Kawala and Stephan, 1989) and the degree of anisotropy k^* of the vapor phase in the space between the evaporator and the condenser is given by Equation (12) (Kawala and Dakiniewicz, 2002).

$$Kn_{NPSE_i} = \frac{MFP_{NPSE_i}}{L} \quad NPSE_i = 1, \dots, N \quad (11)$$

$$\log k^* = 0.2 \left[\frac{d_e - 2L}{2d_e - 2L} \right] + 1.38 \left[\left(\frac{d_e - 2L}{2d_e - 2L} \right) + 0.1 \right]^4 \quad (12)$$

Where d_e is the diameter of the evaporation surface curvature and L the distance between the evaporator and the condenser (equals 0.08 m). Hence, the effective evaporation rate surface takes into account the anisotropic effect of the vapor phase.

The mean free path (MFP) is defined as (Lutišan and Cvengroš, 1995):

$$MFP_{NPSE_i} = \frac{1}{\sqrt{2} \pi \sigma_{NPSE_i}^2 N_m} \quad (13)$$

$$N_m = \frac{N_A P_s}{RT(r, s)} \quad (14, 15)$$

Where, $NPSE_i = 1, \dots, N$ (Poling et al., 2004)

$$\sigma_{NPSE_i} = 8.09 \times 10^{-11} V_c^{1/3} \quad (16)$$

Where MFP is the mean free path (m); σ is the molecule diameter (m); N_m is the number density – number of molecules per unit volume of vapor phase (m^{-3}); T is the temperature (or evaporator temperature) (K); P_s is the pressure system (Pa); R is the universal gas constant ($8.314 \text{ J} \cdot \text{K}^{-1} \cdot \text{mol}^{-1}$), N_A is the Avogadro constant ($6.023 \times 10^{23} \text{ mol}^{-1}$); and V_c is the critical volume ($\text{cm}^3 \cdot \text{mol}^{-1}$).

3.6. Temperature profile in the liquid film

In the case of a heated evaporator surface, there is heat exchange between the inner surface and the liquid film. Reaction/evaporation phenomena take place at the free surface of the liquid and the heat required is supplied from the deeper layers by conduction, forced convection and heat reaction. Consequently, temperature gradients in the liquid film are generated and are defined by Equation (16).

$$\rho(T)C_p(T)v_r(r)\frac{\partial T(r,s)}{\partial r} = \lambda(T)\frac{\partial^2 T(r,s)}{\partial s^2} - \rho(T)\sum_{i=1}^{NPSE}(\Delta H_r)_{i,m,n}r_{NPSE_i} \quad (16)$$

The initial and boundary conditions are:

$$T(r,s) = T_{feed} \quad \text{at} \quad r = r_i \text{ and } 0 \leq s \leq \delta \quad (17)$$

$$-\lambda(T)\frac{\partial T(r,s)}{\partial s} = q_w = \text{const} \quad \text{at} \quad r_i \leq r \leq r_o \text{ and } s = 0 \quad (18)$$

$$-\lambda(T)\frac{\partial T(r,s)}{\partial s} = \sum_{i=1}^{NPSE} X_{s_{NPSE_i}}(r,s)\Delta H_{NPSE_i}(T)G_{E_{NPSE_i}} \quad \text{at} \quad r_i \leq r \leq r_o \text{ and } s = \delta \quad (19)$$

3.7. Concentration profile in the liquid film

The concentrations of the pseudocomponents in the liquid film vary in the s - and r -directions according to the kinetic reaction rate and effective evaporation rate on the film surface, and can be expressed by the following equations.

$$v_r(r)\frac{\partial X_{NPSE_i}(r,s)}{\partial r} = \mathbf{D}_{NPSE_i,mix}\frac{\partial^2 X_{NPSE_i}(r,s)}{\partial s^2} - r_{NPSE_i} \quad NPSE_i = 1, \dots, N \quad (20)$$

The initial and boundary conditions are:

$$X_{NPSE_i}(r,s) = X_{0_{NPSE_i}} \quad \text{at} \quad r = r_i \text{ and } 0 \leq s \leq \delta \quad (21)$$

$$\frac{\partial X_{NPSE_i}(r,s)}{\partial s} = 0 \quad \text{at} \quad r_i \leq r \leq r_o \text{ and } s = 0 \quad (22)$$

$$X_{NPSE_i}(r,s) = X_{s_{NPSE_i}} \quad \text{at} \quad r_i \leq r \leq r_o \text{ and } s = \delta \quad (23)$$

Where the mole fraction of the i -th pseudocomponent ($NPSE_i$) at the evaporating surface, $X_{s_{NPSE_i}}$, is initially unknown, but should satisfy the following mass balance:

$$\rho \frac{d}{dr} \int 2\pi(\sin \beta')rv_r(r)X_{NPSE_i}(r,s)ds + 2\pi r(\sin \beta')X_{s_{NPSE_i}}(r,s)G_E = 0 \quad NPSE_i = 1, \dots, N \quad (24)$$

The constitutive model used to estimate the properties of the pseudocomponents was the approach presented by Tovar et al. (2011), here the thermophysical properties are calculated from a temperature-dependent relationship. Table 2 summarizes the equations used in the model.

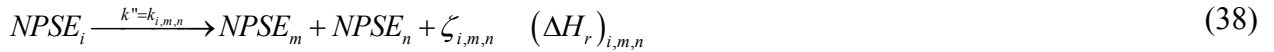
Table 2. Summary of the basic, thermodynamic and thermophysical properties (Tovar et al., 2011).

Property	Equation	Source	Equation N°.
Density	$\rho_{NPSE_i} = 1215.253 \left(T_{bi}^{1/3} / K_w \right)$	Miquel and Castells, 1993	(25)
Characterization factor	$K_w = K_{OUP} = \left(\sqrt[3]{1.8 T_b / SG} \right)$	Watson and Nelson, 1933	(26)
Molar mass	$M = 42.965 \left[\exp \left(2.097 \times 10^{-4} T_b - 7.78712 (SG) + 2.08476 \times 10^{-3} (T_b SG) \right) \right] T_b^{1.26007} SG^{-4.98308}$	Riazi and Daubert, 1980	(27)
Critical temperature	$T_c = 35.9413 \left[\exp \left(-6.9 \times 10^{-4} T_b - 1.4442 (SG) + 4.91 \times 10^{-4} (T_b SG) \right) \right] T_b^{0.7293} SG^{1.2771}$	Riazi and Daubert, 1980	(28)
Critical Pressure	$P_c = 10^5 \left\{ 6.9575 \left[\exp \left(-1.35 \times 10^{-2} T_b - 0.3129 (SG) + 9.174 \times 10^{-3} (T_b SG) \right) \right] T_b^{0.6791} SG^{-0.6807} \right\}$	Riazi and Daubert, 1980	(29)
Critical volume	$V_c = \left\{ \frac{83.14 T_c}{P_c \left[3.72 + 0.26 (\alpha_R - 7.00) \right]} \right\} \quad \alpha_R = 5.811 + 4.919 \omega_{ac}$	API, 1997	(30)
Acentric factor	$\omega_{ac} = \frac{-\ln P_t - 5.92714 + 6.09648 / T_{b_r} + 1.28862 \ln T_{b_r} - 0.169347 T_{b_r}^6}{15.2518 - 15.6875 / T_{b_r} - 13.4721 \ln T_{b_r} + 0.43577 T_{b_r}^6}$	Lee and Kesler, 1975	(31)
Thermal conductivity	$\lambda = 2.540312 (SG/T)^{0.5} - 0.014485$	Aboul-Seoud and Moharam, 1999b	(32)
Specific heat capacity	$C_p = A_1 + A_2 T + A_3 T^2$ $A_1 = \left[-4.90383 + (0.099319 + 0.104281 SG) K_w + \frac{4.81407 - 0.194833 K_w}{SG} \right] (10^3)$ $A_2 = (10^{-1}) (7.53624 + 6.214610 K_w) \left(1.12172 - \frac{0.27634}{SG} \right)$ $A_3 = -(10^{-4}) (1.35652 + 1.11863 K_w) \left(2.9027 - \frac{0.70958}{SG} \right)$	Kesler and Lee, 1976	(33)
Kinematic viscosity	$\ln \ln \left[v(10^{-6}) + 0.8 \right] = a_1 + a_2 \ln(T)$ $a_1 = 4.3414 (T_b SG)^{0.2} + 6.6913 \quad a_2 = -3.7$	Aboul-Seoud and Moharam, 1999a	(34)
Heat of evaporation	$\Delta H = T_b \left(9.549 + 14.811 \left[\ln(T_b) \right] + 12.346 \left(\frac{T_b}{M} \right) - 0.06662 \left(\frac{T_b^2}{M} \right) + 7.833 \times 10^{-5} \left(\frac{T_b^3}{M} \right) + 19.334 \ln(SG) \right)$	Fang et al., 2003	(35)
Vapor Pressure	$\log_{10} (1 \times 10^5 P_{vap}) = 3.2041 \left[1 - 0.998 \left(\frac{T_b - 41}{T - 41} \right) \left(\frac{1393 - T}{1393 - T_b} \right) \right]$	Riazi, 2004	(36)
Diffusivity	$D_{NPSE_i_mis} = 7.4 \times 10^{-8} \frac{(f_{asc} M)^{1/2} T}{\eta V_{m_NPSE_i}^{0.6}} \quad f_{asc} M = \sum_{j=1}^N x_j f_{ascj} M_j$	Poling et al., 2004	(37)

Where, T_b : Normal boiling point; and for whole petroleum fraction is the mean average boiling point ($MeABP$) (K); SG : Ratio of its density (ρ) to the density of the water (ρ_{water}) at 288.75 K (15.6 °C or 60 °F); K_w : Watson characterization factor; K_{UOP} : Universal Oil Products Company (UOP) characterization factor; T_c : Critical Temperature (or T_{cNPSE} : pseudocritical temperature) (K); P_c : critical pressure (or P_{cNPSE} : pseudocritical critical) (Pa); M : molar mass (or M_{NPSE} : molar mass of pseudocomponents) ($\text{kg} \cdot \text{kmol}^{-1}$). For V_c : Critical volume (or V_{cNPSE} : pseudocritical volume) ($\text{cm}^3 \cdot \text{mol}^{-1}$); P_c : critical pressure (or P_{cNPSE} : pseudocritical critical) (bar). ω_{ac} : Acentric factor (or ω_{ac_NPSE} pseudoacentric factor); v : Kinematic viscosity ($\text{m}^2 \cdot \text{s}^{-1}$); C_p : Specific heat capacity ($\text{J} \cdot \text{kg}^{-1} \cdot \text{K}^{-1}$); λ : Thermal conductivity ($\text{W} \cdot \text{m}^{-1} \cdot \text{K}^{-1}$); P_{vap} : Vapor pressure (Pa); ΔH : Heat of evaporation ($\text{J} \cdot \text{mol}^{-1} \cdot \text{K}^{-1}$); D_{NPSE_mis} : Diffusion coefficient for pseudocomponent i in the mixture ($\text{cm}^2 \cdot \text{s}^{-1}$), f_{asc} : Factor equals 1 for hydrocarbon mixtures; η : Dynamic viscosity of the mixture (cP), x_j : Mole fraction of pseudocomponent j (different from pseudocomponent i), $V_{m_NPSE_i}$: Molar volume of pseudocomponent i ; M : Molar mass of pseudocomponent j and $NPSE_i$: pseudocomponent i .

3.8. Approximate reaction equation for the catalytic reaction term

A heterogeneous catalytic system was assumed using the zeolite-based catalyst CR-1 (regenerated catalyst used for FCC technology containing 48.3 % mass of alumina, and particle size of 67µm). The catalyst CR-1 was assumed mixed with the high-boiling-point petroleum fraction, constituting the load to the CRMD process. The approach to the catalytic reaction carried out in the evaporation zone during the CRMD process was already presented in a previous paper (Tovar et al., 2011). The pseudocomponent-based approach for simulating the CRMD process of a high-boiling-point petroleum fraction is highly successful if it is assumed that when one mole of a pseudocomponent is cracked it gives one mole each of two other pseudocomponents, and a certain amount of coke may also be formed as described in Equation (38) (Gupta, 2006).



Where i , m and n are the numbers of the pseudocomponents, $\zeta_{i,m,n}$ is the amount of coke formed when the i^{th} pseudocomponent ($NPSE_i$) cracks to produce the m^{th} and n^{th} pseudocomponents ($NPSE_m$ and $NPSE_n$).

By defining $NPSE_i$ as the species reacting, W_c as the weight of catalyst, n_{NPSE_i} as the number of moles of $NPSE_i$ present, $n_{NPSE_i}^0$ as the initial number of moles of $NPSE_i$, k_j as the constant ($j= 1, 2, \dots, j$), N_T as the total moles of material present, $n_{NPSE,c}$ as the number of moles of n_{NPSE_i} on the catalyst in the reactive situation, P_s as the system pressure, t as the time, α as the fraction of $NPSE_i$ converted (conversion degree) and Q as the mass of sample to be processed per hour; it is possible to define the rate of reaction. The theoretical kinetic scheme presented in this paper assumes that the cracking reaction is of first order (pseudo first order reaction), and for a pseudo first-order reaction, it should be possible to represent the rate of disappearance of the i^{th} pseudocomponent ($-r_{NPSE_i}$) by a relatively simple expression, as follows (Blanding, 1953):

$$-r_{NPSE_i} = -\frac{dn_{NPSE_i}}{dt} = k_1 n_{NPSE_i} \quad (39)$$

Nevertheless, Blanding (1953) presented the influence of the catalyst on the reaction rate as being a proportional relationship with some power of the partial pressure of the reactant surrounding the catalyst, as follows:

$$n_{NPSE_i c} = k_2 W_c \left[\frac{P_s n_{NPSE_i}}{N_T} \right]^{k_3} \quad (40)$$

Thus, Equation (39) can be written as:

$$-r_{NPSE_i} = -\frac{dn_{NPSE_i c}}{dt} = \frac{k_4 W_c n_{NPSE_i c}^{k_3} P_s^{k_3}}{N_T^{k_3}} \quad (41)$$

Based on the fact that the reactants are used up in the reaction, the moles produced per mole of reactant increase considerably due to the secondary reactions, as follows (Blanding, 1953):

$$\frac{n_{NPSE_i}}{N_T} = k_5 \left(\frac{n_{NPSE_i}}{n_{NPSE_{i0}}} \right)^2 \quad (42)$$

Thus, Equation (41) can be written as:

$$-r_{NPSE_i} = -\frac{dn_{NPSE_i}}{dt} = k_6 \left(\frac{n_{NPSE_i}}{n_{NPSE_{i0}}} \right)^{2k_3} P_s^{k_3} W_c \quad (43)$$

The experimental data published in Blanding (1953) showed that the term k_3 in Equation (43) is approximately equal to 1.0. Thus, the reaction rate of the CRMD process can be defined according to Equation (43):

$$-r_{NPSE_i} = -\frac{dn_{NPSE_i}}{dt} = k'' \left(\frac{n_{NPSE_i}}{n_{NPSE_{i0}}} \right)^2 P_s W_c \quad (44)$$

3.8.1. Kinetic parameters

The reaction rate constant, k'' , is assumed to follow the Arrhenius equation in terms of the kinetic parameters (pre-exponential factor, A and the activation energy, E). The kinetic parameters used in this study were determined in a previous work (Tovar et al., 2011) based on the kinetic compensation effect (KCE), where the pre-exponential factor, A , varied with the activation energy, E , according to Equation (45) (Khawam, 2007):

$$\ln A = a^* E + b^* \quad (45)$$

Where a^* and b^* are constant coefficients and act as compensation parameters.

And the E -dependence on α is given as:

$$E = E_0 + E_1 \left(\frac{1}{\alpha} \right) \quad (46)$$

Where E_0 and E_1 are constants

Table 3 summarizes the kinetic compensation parameters calculated for 3, 5 and 10 %wt of zeolite-based catalyst CR-1 (regenerated catalyst used for FCC technology) (Tovar et al., 2011).

Table 3. Summary of the kinetic compensation parameters (KCE) for ATR-W (Tovar et al., 2011).

KCE parameters	Weight percent of catalyst (%wt)		
	3	5	10
E_0 (kJ·mol ⁻¹)	22.52	30.65	17.20
E_I (kJ·mol ⁻¹)	27.93	6.11	1.58
b^* (min ⁻¹)	-6.02	-5.10	-0.45
a^* (mol·kJ ⁻¹ ·min ⁻¹)	0.32	0.34	0.24

E_0 , E_I , b^* and a^* : Kinetic compensation parameters.

4. Physical modeling

In order to simulate the processing of a high-boiling-point petroleum fraction >673.15 K of “W” crude oil by the CRMD process, the total residue was divided into two pseudocomponents based on a previous sensibility analysis of concentration profiles, which were characterized using the correlations from Table 2 as presented in Table 4.

Table 4. Basic properties of the constituent pseudocomponents of the feed.

i	NPSE _i	x_{NPSE}	Tb_i (K)	ρ (kg·m ⁻³)	Tc (K)	Pc (MPa)	V_c (cm ³ ·mol ⁻¹)	ω_{ac}	Kw
1	“a”	0.9762	812.5	927.6	957.1	0.869	1819.64	1.2347	12.22
2	“b”	0.0238	2199.0	1292.7	1937.6	0.188	11232.13	3.2467	12.22

NPSE: Pseudocomponent; x_{NPSEi} : Weight of the fraction of the component (or pseudocomponent i); T_{bi} : Normal boiling point of pseudocomponent i ; ρ : Density; Kw : Watson characterization factor; $MeABP$: Mean average boiling point; M : Molar mass; Pc : Critical pressure; Tc : Critical temperature; Vc : Critical volume; ω_{ac} : acentric factor.

Table 5 summarizes the list of variables and parameters used in the model. The degrees of freedom of the model were determined in a way similar to that used in the analysis carried out by Sales-Cruz and Gani (2006). The CRMD model described above, consisting of Equation (2) – (46), is a PDAE system with (11+18 N) equations classified as: (1+ N) PDEs (Equations 16 and 20), (2) ODE (Equations 2 and 9) and (8+17 N) AEs (Equations 7 – 8, 10 – 15, 25 – 37, 44 – 46 and the Arrhenius equation). The total number of variables (27+19 N) are classified as: (10+ N) known, (6) parameters, (9+16 N) explicit and (2+2 N) dependent. Hence the degrees of freedom are (16+ N), which means that some of the variables must be specified as: three (3) fixed variables (R_g , N_A and P_i), five (5) geometrical parameters (RD , r_0 , L , β' , de), seven (7+ N) operational conditions (EVT , Q , P_s , RS , T_{feed} , T_{cond} , %CAT, X_{NPSEi}) and one (1) model parameter (n').

Table 5. Variables used in the mathematical model of the centrifugal reactive–molecular distillation.

Variable	Type of variable	Number of variables
<i>Constants</i>		
Avogadro Constant	Known	1
Universal gas constant	Known	1
Pi	Known	1
<i>Geometrical parameters</i>		
Evaporator radius	Parameter	1
Distance from apex at which liquid enters cone	Parameter	1
Distillation gap	Parameter	1
Half angle of apex of cone radius	Parameter	1
<i>Model parameters</i>		
Number of intermolecular collisions	Parameter	1
Mean free path	Explicit	N
Knudsen number	Explicit	N
Diameter of evaporation surface curvature	Parameter	1
Anisotropy degree of vapor phase	Explicit	1
Number of molecules per unit volume of vapor phase	Explicit	1
Molecular diameter	Explicit	N
<i>Physicochemical properties</i>		
Molar mass	Explicit	N
Thermal conductivity	Explicit	N
Specific heat capacity	Explicit	N
Vapor pressure	Explicit	N
Kinematic viscosity	Explicit	N
Density	Explicit	N
Heat of evaporation	Explicit	N
Characterization factor	Explicit	N
Diffusivity	Explicit	N
Critical temperature	Explicit	N
Critical Pressure	Explicit	N
Critical volume	Explicit	N
Acentric factor	Explicit	N
<i>Output variables</i>		
Temperature profile	Dependent	1
Velocity profile	Explicit	1
Distillate mass flow rate of each pseudocomponent	Dependent	N
Overall distillate mass flow rate profile	Dependent	1
Effective evaporation rate profile	Explicit	1
Liquid film thickness profile	Explicit	1
Concentration profiles of pseudocomponents	Dependent	N
Conversion degree profile	Explicit	1

5. Computational tool

In the previous section the CRMD model obtained was presented in three stages: (i) The first step refers to the model definition, where the modeling assumptions were established; (ii) in

the second step the specific model was derived from the evaluation of the physicochemical properties, macroscopic variables (mean free path and Knudsen number), heat, continuity and material balances and the diffusion equation, and (iii) The degrees of freedom. These three stages have been implemented in the computational aid named DESTMOL–R, developed in FORTRAN–90 language using Compaq Visual Fortran compiler (professional edition 6.6).

5.1. Numerical solution strategy

In order to solve the CRMD model represented by a set of PDAEs, the method of lines is used to obtain its discretization form in one dimension (s –direction), and the semi–discrete problem then integrated as a system of ODEs and DAEs, which are then solved using ODE solvers (Schiesser, 1991). The space derivatives are discretized in the DESTMOL–R computational tool (see basic structure of DESTMOL–R in Figure 4), by applying second order centered finite difference. In particular, considering $F(r,s)$ as the functions, the PDEs can be approximated as follows:

$$f_r(r,s) \cong \frac{F(r+\Delta r,s) - F(r-\Delta r,s)}{2\Delta r} \quad (47)$$

$$f_s(r,s) \cong \frac{F(r,s+\Delta s) - F(r,s-\Delta s)}{2\Delta s} \quad (48)$$

$$f_{ss}(r,s) \cong \frac{F(r,s+\Delta s) - 2F(r,s) + F(r,s-\Delta s)}{\Delta s^2} \quad (49)$$

In the present study using the evaporator model in the CRMD process, discretization is carried out for the film thickness in the s –direction (with a minimum value of 11 points) and along the r –direction (with a minimum value of 101 points); which gives a trade–off between higher–accuracy discretization, with a reasonable number of equations and good computational time. In Figure 5, each bullet stands for a discretization point, where the original PDE behavior is approximated by an ODE. The resulting system of ODEs and DAEs were solved using the DESOLV and RKF45 (fifth/fourth order Runge Kutta Fehlberg with adaptive step sizing (Mathews and Fink, 2004)) subroutines available in the FORTRAN–90 code.

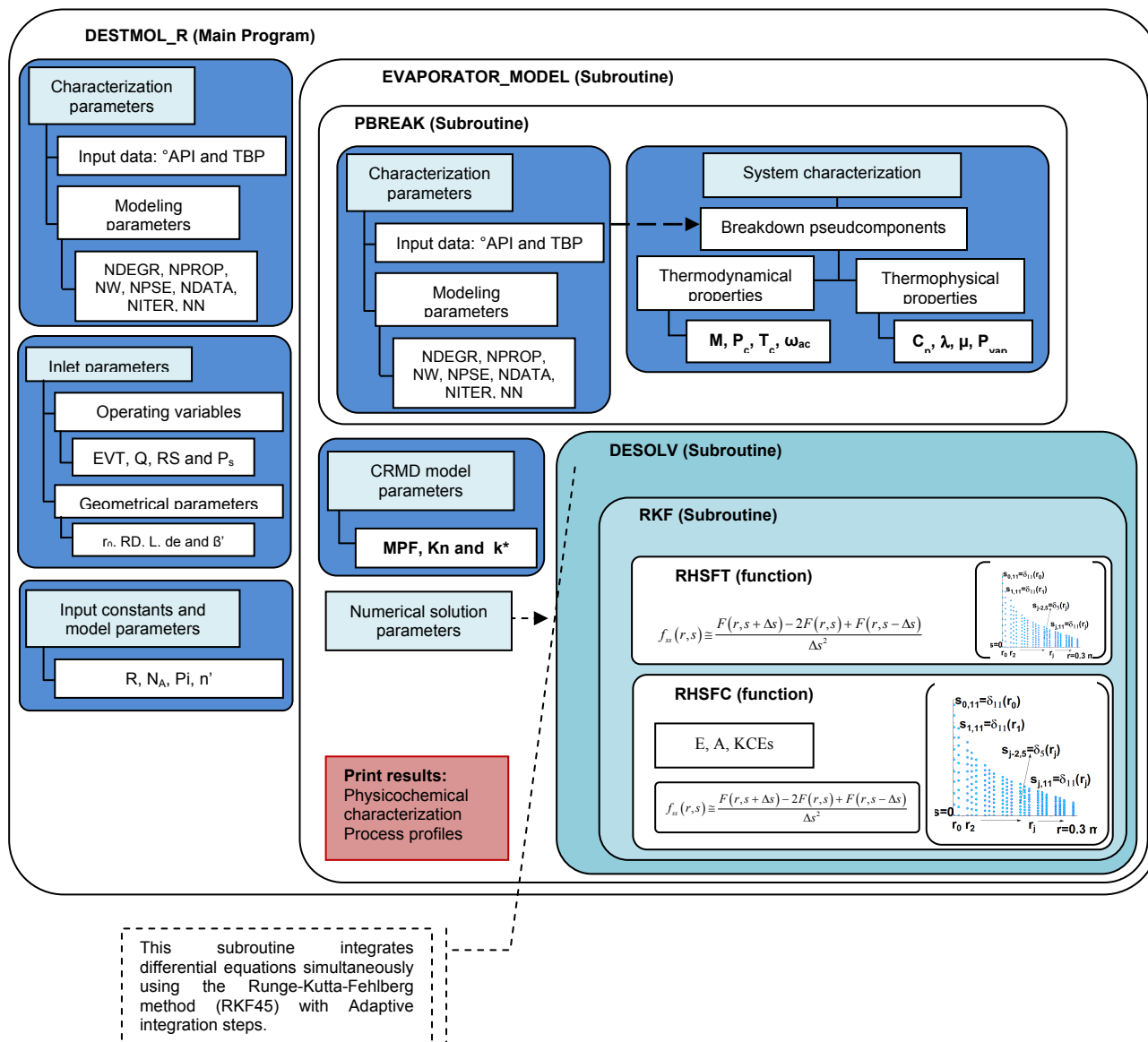


Figure 4. DESTMOL–R Computational aided environment to obtain the numerical solution.

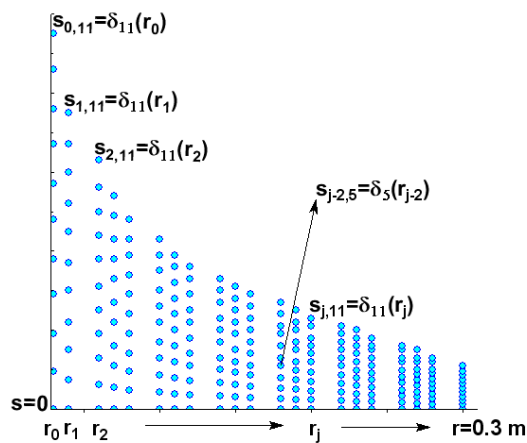


Figure 5. Discretization scheme.

5.2. Model evaluation

The model was evaluated by analyzing the effects of each independent variable (EVT , $\%CAT$, Q , RS , T_{cond} , T_{feed} and P_s) on the dependent variables (T_s , δ , D , G_E , v_r , x_a and α). The statistical analysis was carried out using the software Statistica 7.0 from Statsoft Inc (2004). Dependent variables were evaluated at the radial position (r_o) equals 0.3 m related to the distance from apex at which the thin liquid film gets out evaporator surface.

5.2.1. Plackett–Burman design

This paper aims to provide a sensitivity analysis to determine the sensitivity of the response variables (output variables) of the model due to changes in the input variables. The Plackett–Burman design (Plackett and Burman, 1946) was used in the present study to screen the most important process variables that significantly influenced the yield in the centrifugal reactive–molecular distillation process (CRMD): the conversion degree (α), the concentration of the final products (X_a), the effective evaporation rate (G_E), the film thickness (δ), the radial velocity (v_r) and the surface temperature (T_s) profiles. In this study, a 16–run Plackett–Burman design plus a central point was applied to evaluate seven factors, namely the evaporator temperature (EVT), feed flow rate (Q), pressure system (P_s), percent weight of catalyst ($\%CAT$), feed temperature (T_{feed}), condenser temperature (T_{cond}) and rotor speed (RS). Thus a total of seven variables was selected, and each variable examined at two levels: +1 for the upper level and –1 for the lower level (Table 6) plus eight dummy variables, giving a total of 16 trials plus a central point, as shown in Table 7.

Table 6. Variables and levels investigated using the Plackett–Burman design.

Independent variable	Unit	Coded factor	Level		
			-1	0	+1
EVT	K	x_1	473.15	513.15	553.15
Q	kg·h ⁻¹	x_2	1.473	1.841	2.209
$\%CAT$	%wt	x_3	3	5	10
T_{feed}	K	x_4	393.15	408.15	423.15
T_{cond}	K	x_5	353.15	373.15	393.15
RS	rpm	x_6	800	1000	1200
P_s	Pa	x_7	40	50	100

EVT : Evaporator temperature; Q : Feed flow rate; $\%CAT$: Percentage weight of catalyst; T_{feed} : Feed temperature; T_{cond} : Condenser temperature; RS : Rotor speed; P_s : System pressure, x_1 , x_2 , x_3 , x_4 , x_5 , x_6 and x_7 , coded factor for EVT , Q , $\%CAT$, T_{feed} , T_{cond} , RS and P_s , respectively.

Table 7: Plackett–Burman design generated by fractional rotation of a full factorial design where x_1, \dots, x_7 are independent variables and D1, \dots , D8 are dummy variables.

Run order	x_1	x_2	x_3	x_4	x_5	x_6	x_7	D1	D2	D3	D4	D5	D6	D7	D8	$^{\dagger}D$ ($\text{kg} \cdot \text{h}^{-1}$)	$^{\dagger}G_E$ ($\text{kg} \cdot \text{m}^{-2} \cdot \text{s}^{-1}$)	$^{\dagger}\delta$ (m)	$^{\dagger}u_r$ ($\text{m} \cdot \text{s}^{-1}$)	$^{\dagger}X_a$	$^{\dagger}\alpha$
1	-1	-1	-1	-1	1	1	1	1	1	1	-1	-1	-1	-1	1	1.27	6.076	8.100×10^{-5}	13.90	0.700	0.222
2	1	-1	-1	-1	-1	-1	-1	1	1	1	1	1	1	-1	-1	1.16	5.555	8.700×10^{-5}	20.05	0.446	0.504
3	-1	1	-1	-1	-1	1	1	-1	-1	1	1	1	-1	1	-1	1.27	6.076	8.100×10^{-5}	13.90	0.66	0.267
4	1	1	-1	-1	1	-1	-1	-1	-1	1	-1	-1	1	1	1	1.16	5.555	8.700×10^{-5}	20.05	0.441	0.510
5	-1	-1	1	-1	1	-1	1	-1	1	-1	1	-1	1	1	-1	1.27	6.076	1.800×10^{-4}	29.84	0.732	0.187
6	1	-1	1	-1	-1	1	-1	-1	1	-1	-1	1	-1	1	1	1.16	5.555	1.000×10^{-4}	59.34	0.568	0.369
7	-1	1	1	-1	-1	-1	1	1	-1	-1	-1	1	1	-1	1	1.27	6.076	1.800×10^{-4}	29.84	0.689	0.234
8	1	1	1	-1	1	1	-1	1	-1	-1	1	-1	-1	-1	-1	1.16	5.555	1.000×10^{-5}	59.34	0.562	0.376
9	-1	-1	-1	1	1	1	-1	1	-1	-1	-1	1	1	1	-1	1.27	6.076	8.100×10^{-5}	13.90	0.700	0.222
10	1	-1	-1	1	-1	-1	1	1	-1	-1	1	-1	-1	1	1	1.16	5.555	8.700×10^{-5}	20.05	0.446	0.504
11	-1	1	-1	1	-1	1	-1	-1	1	-1	1	-1	1	-1	1	1.27	6.076	8.100×10^{-5}	13.90	0.660	0.267
12	1	1	-1	1	1	-1	1	-1	1	-1	-1	1	-1	-1	-1	1.16	5.555	8.400×10^{-5}	20.05	0.441	0.510
13	-1	-1	1	1	1	-1	-1	-1	-1	1	1	1	-1	-1	1	1.27	6.076	1.800×10^{-4}	29.84	0.732	0.187
14	1	-1	1	1	-1	1	1	-1	-1	1	-1	-1	1	-1	-1	1.16	5.555	1.000×10^{-4}	59.34	0.568	0.369
15	-1	1	1	1	-1	-1	-1	1	1	1	-1	-1	-1	1	-1	1.27	6.076	1.800×10^{-4}	29.84	0.689	0.234
16	1	1	1	1	1	1	1	1	1	1	1	1	1	1	1	1.16	5.555	1.000×10^{-4}	59.34	0.562	0.376
17	0	0	0	0	0	0	0	0	0	0	0	0	0	0	0	1.21	5.798	0.00	32.22	0.634	0.296

† : Dependent variables at the radial position, equals 0.3 m. *EVT*: Evaporator temperature; *Q*: Feed flow rate; %*CAT*: Percentage weight of catalyst; T_{feed} : Feed temperature; T_{cond} : Condenser temperature; *RS*: Rotor speed; P_s : Pressure system, $x_1, x_2, x_3, x_4, x_5, x_6$ and x_7 , coded factor for *EVT*, *Q*, %*CAT*, T_{feed} , T_{cond} , *RS* and P_s , respectively.

5.2.2. Fractional factorial screening design

The next step in the formulation of the variables shown to be the most important one in the CRMD process (*EVT*, *Q*, *RS* and %*CAT*) with respect to the response variables, was to carry out a $2_{IV}^{(4-1)}$ fractional factorial design. This means that 04 factors will be studied (the first number in parentheses), although 01 of these factors (the second number in parentheses) was generated from the interactions of a full $2^{((4-1)=3)}$ factorial design. As a result, the design does not give full resolution; that is, some factors and each interaction are totally confounded with one of the main effects. In this resolution IV design, the main effects of the factors examined are not confounded with any other interaction of an order less than $4-1=3$. Also, two-way interactions are not confounded with any other interaction of an order less than $4-2=2$ (Loukas, 1998). Each variable was ranked as -1 and +1 corresponding to the lower and upper levels, respectively, as shown in Table 8. A central point (0) run was also added. Table 9 shows the design for the total of nine (09) runs at the -1 and +1 levels (at $P_s=40$ Pa; $T_{feed}=393.15$ K and $T_{cond}=353.15$ K).

Table 8. Variables and levels investigated using the fractional factorial design $2_{IV}^{(4-1)}$.

Independent variable	Unit	Coded factor	Level		
			-1	0	+1
<i>EVT</i>	K	x_1	473.15	513.15	553.15
<i>Q</i>	$\text{kg} \cdot \text{h}^{-1}$	x_2	1.473	1.841	2.209
% <i>CAT</i>	%wt	x_3	3	5	10
<i>RS</i>	rpm	x_6	800	1000	1200

EVT: Evaporator temperature; *Q*: Feed flow rate; %*CAT*: Percentage weight of catalyst and *RS*: Rotor speed, x_1, x_2, x_3 and x_6 , coded factor for *EVT*, *Q*, %*CAT* and *RS*, respectively.

Table 9. The factors included in the $2_{IV}^{(4-1)}$ fractional factorial design.

Run order	x_1	x_2	x_3	x_6	$^\dagger D$ ($\text{kg} \cdot \text{h}^{-1}$)	$^\dagger G_E$ ($\text{kg} \cdot \text{m}^{-2} \cdot \text{s}^{-1}$)	$^\dagger \delta$ (m)	$^\dagger v_r$ ($\text{m} \cdot \text{s}^{-1}$)	$^\dagger \alpha$	$^\dagger X_a$
1	-1	-1	-1	-1	1.27	6.076	1.100×10^{-4}	10.60	0.268	0.659
2	1	-1	-1	1	1.17	5.555	8.700×10^{-5}	20.05	0.510	0.441
3	-1	1	-1	1	1.27	6.076	1.800×10^{-4}	29.84	0.234	0.689
4	1	1	-1	-1	1.16	5.555	1.300×10^{-4}	45.29	0.417	0.525
5	-1	-1	1	1	1.27	6.076	9.100×10^{-5}	12.31	0.286	0.642
6	1	-1	1	-1	1.16	5.555	7.500×10^{-5}	23.27	0.474	0.473
7	-1	1	1	-1	1.27	6.076	1.500×10^{-4}	34.62	0.167	0.750
8	1	1	1	1	1.16	5.555	1.100×10^{-4}	52.55	0.397	0.543
9	0	0	0	0	1.21	5.798	1.200×10^{-4}	30.03	0.308	0.623

† : Dependent variables at radial positions equal 0.3 m. *EVT*: Evaporator temperature; *Q*: Feed flow rate; %*CAT*: Percentage weight of catalyst and *RS*: Rotor speed, x_1 , x_2 , x_3 , and x_6 are coded factors for *EVT*, *Q*, %*CAT* and *RS*, respectively.

6. Results and discussion

6.1. Screening of the significant variables using the Plackett–Burman design

A total of seven (07) variables were analyzed with regard to their effects on the yield of the CRMD process as a function of the distillate mass flow rate (*D*), the concentration of final product (X_a), the effective evaporation rate (G_E), the film thickness (δ), radial velocity (v_r) and surface temperature (T_s) profiles, using the Plackett–Burman design. The design matrix selected for the screening of significant variables is shown in Table 7. Factors evidencing *p*-values less than 0.05 were considered to have significant effects on the response, and were therefore selected for further screening studies.

Distillate mass flow rate (D) and effective evaporation rate (G_E) responses: The evaporator temperature (*EVT*), a variable associated with the x_1 factor, with a probability value of 3.180×10^{-16} and 2.091×10^{-17} , respectively for *D* and G_E , was shown to be the most significant factor (Table 10). The lower probability values indicate the most significant factors with respect to the responses *D* and G_E .

Film thickness (δ) and radial velocity (v_r): The feed flow rate (*Q*), associated with the x_2 factor, with a probability of 8.021×10^{-16} and 1.077×10^{-15} , respectively for δ and v_r , was shown to be the most significant factor, followed by the variables of rotor speed (*RS*) and evaporator temperature (*EVT*). Two of the three significant variables screened, *EVT* and *RS*, exerted negative effects on δ (Table 10).

Table 10. Main effects of EVT , $\%CAT$, Q , T_{feed} , T_{cond} , RS and P_s according to the Plackett–Burman design.

Response	Factor	Effect	Error	t ^a	p ^b	-95% ^c	+95% ^c
D	Mean*	1.215	0.000	3097.500	1.940x10 ⁻²⁸	1.214	1.216
	x_1 *	-0.110	0.001	-136.062	3.180 x10 ⁻¹⁶	-0.056	-0.054
	x_2	0.000	0.001	0.000	1.000 x10 ⁰	-0.001	0.001
	x_3	0.000	0.001	0.000	1.000 x10 ⁰	-0.001	0.001
	x_4	0.000	0.001	0.000	1.000 x10 ⁰	-0.001	0.001
	x_5	0.000	0.001	0.000	1.000 x10 ⁰	-0.001	0.001
	x_6	0.000	0.001	0.000	1.000 x10 ⁰	-0.001	0.001
	x_7	0.000	0.001	0.000	1.000 x10 ⁰	-0.001	0.001
G_E	Mean*	5.814	0.001	4236.257	1.159 x10 ⁻²⁹	5.811	5.818
	x_1 *	-0.521	0.003	-184.126	2.091 x10 ⁻¹⁷	-0.264	-0.257
	x_2	0.000	0.003	0.000	1.000 x10 ⁰	-0.003	0.003
	x_3	0.000	0.003	0.000	1.000 x10 ⁰	-0.003	0.003
	x_4	0.000	0.003	0.000	1.000 x10 ⁰	-0.003	0.003
	x_5	0.000	0.003	0.000	1.000 x10 ⁰	-0.003	0.003
	x_6	0.000	0.003	0.000	1.000 x10 ⁰	-0.003	0.003
	x_7	0.000	0.003	0.000	1.000 x10 ⁰	-0.003	0.003
δ	Mean*	1.117 x10 ⁻⁴	2.228 x10 ⁻⁷	501.471	2.539 x10 ⁻²¹	1.112 x10 ⁻⁴	1.122 x10 ⁻⁴
	x_1 *	-3.738 x10 ⁻⁵	4.592 x10 ⁻⁷	-81.387	3.232 x10 ⁻¹⁴	-1.921 x10 ⁻⁵	-1.817 x10 ⁻⁵
	x_2	-3.750 x10 ⁻⁷	4.592 x10 ⁻⁷	-0.817	4.352 x10 ⁻¹	-7.069 x10 ⁻⁷	3.319 x10 ⁻⁷
	x_3 *	5.638 x10 ⁻⁵	4.592 x10 ⁻⁷	122.762	8.021 x10 ⁻¹⁶	2.767 x10 ⁻⁵	2.871 x10 ⁻⁵
	x_4	-3.750 x10 ⁻⁷	4.592 x10 ⁻⁷	-0.817	4.352 x10 ⁻¹	-7.069 x10 ⁻⁷	3.319 x10 ⁻⁷
	x_5	-3.750 x10 ⁻⁷	4.592 x10 ⁻⁷	-0.817	4.352 x10 ⁻¹	-7.069 x10 ⁻⁷	3.319 x10 ⁻⁷
	x_6 *	-4.263 x10 ⁻⁵	4.592 x10 ⁻⁷	-92.820	9.914 x10 ⁻¹⁵	-2.183 x10 ⁻⁵	-2.079 x10 ⁻⁵
	x_7	-3.750 x10 ⁻⁷	4.592 x10 ⁻⁷	-0.817	4.352 x10 ⁻¹	-7.069 x10 ⁻⁷	3.319 x10 ⁻⁷
ν_r	Mean*	30.867	0.113	273.777	5.890 x10 ⁻¹⁹	30.612	31.122
	x_1 *	17.825	0.232	76.690	5.515 x10 ⁻¹⁴	8.650	9.175
	x_2	0.000	0.232	0.000	1.000 x10 ⁰	-0.263	0.263
	x_3 *	27.615	0.232	118.810	1.077 x10 ⁻¹⁵	13.545	14.070
	x_4	0.000	0.232	0.000	1.000 x10 ⁰	-0.263	0.263
	x_5	0.000	0.232	0.000	1.000 x10 ⁰	-0.263	0.263
	x_6 *	11.675	0.232	50.230	2.465 x10 ⁻¹²	5.575	6.100
	x_7	0.000	0.232	0.000	1.000 x10 ⁰	-0.263	0.263
X_a	Mean*	0.602	0.003	223.509	3.655 x10 ⁻¹⁸	0.596	0.608
	x_1 *	-0.191	0.006	-34.412	7.295 x10 ⁻¹¹	-0.102	-0.089
	x_2 *	-0.023	0.006	-4.234	2.194 x10 ⁻³	-0.018	-0.005
	x_3 *	0.076	0.006	13.693	2.484 x10 ⁻⁷	0.032	0.044
	x_4	0.000	0.006	0.000	1.000 x10 ⁰	-0.006	0.006
	x_5 *	0.018	0.006	3.243	1.011 x10 ⁻²	0.003	0.015
	x_6 *	0.045	0.006	8.198	1.821 x10 ⁻⁵	0.016	0.029
	x_7	0.000	0.006	0.000	1.000 x10 ⁰	-0.006	0.006
α	Mean*	0.331	0.003	112.200	1.802 x10 ⁻¹⁵	0.325	0.338
	x_1 *	0.212	0.006	34.856	6.505 x10 ⁻¹¹	0.099	0.113
	x_2 *	0.026	0.006	4.311	1.959 x10 ⁻³	0.006	0.020
	x_3 *	-0.084	0.006	-13.836	2.271 x10 ⁻⁷	-0.049	-0.035
	x_4	0.000	0.006	0.000	1.000 x10 ⁰	-0.007	0.007
	x_5 *	-0.020	0.006	-3.243	1.010 x10 ⁻²	-0.017	-0.003
	x_6 *	-0.050	0.006	-8.252	1.726 x10 ⁻⁵	-0.032	-0.018
	x_7	0.000	0.006	0.000	1.000 x10 ⁰	-0.007	0.007

EVT : Evaporator temperature; Q : Feed flow rate; $\%CAT$: Percentage weight of catalyst; T_{feed} : Feed temperature; T_{cond} : Condenser temperature; RS : Rotor speed; P_s : Pressure system, x_1 , x_2 , x_3 , x_4 , x_5 , x_6 and x_7 , coded factors for EVT , Q , $\%CAT$, T_{feed} , T_{cond} , RS and P_s , respectively.

* Statistically significant at a level of confidence of 95 %; ^a Value of the coefficient of regression for the error, which measures how great the effect is with respect to the residual error; ^b Probability of significance. At a confidence level of 95 %, a p -value <0.05 means that the result is significant; ^c Limits of confidence: The effects are statistically reliable when the limits do not pass zero.

Concentration of pseudocomponent “a” (X_a) and conversion degree (α) responses: The evaporator temperature (EVT), associated with x_1 , with a probability value of 7.295×10^{-11} and 6.505×10^{-11} , respectively, for X_a and α , was shown to be the most significant factor, followed by the feed flow rate (Q), rotor speed (RS), weight percent of catalyst ($\%CAT$) and condenser temperature (T_{cond}). The lower probability values indicate the more significant factors with respect to X_a and α . Two of the five significant variables screened, EVT and $\%CAT$, exerted a negative effect on X_a . On the other hand, three of the five significant variables screened, Q , T_{cond} and RS , exerted a negative effect on α . In other words, when EVT and $\%CAT$ were raised, X_a decreased; and similarly, when Q , T_{cond} and RS were raised, α decreased (Table 10).

Of the significant variables identified, T_{cond} was excluded from the process analyses and fixed at the lowest level (353.15 K). The condenser temperature (T_{cond}) ingoing the peripheral of the conical evaporation surface of a centrifugal reactive–molecular evaporator corresponds to an important operational parameter. Practical experience over many years with the operation of centrifugal molecular evaporator, developed in our research laboratories, has shown that the optimum temperature of the condenser (T_{cond}) should differ at least 50 K lower from the working temperature (evaporator temperature) inside the evaporator, pointing to the advantages from the first moment the distilled liquid gets onto the evaporation surface, reaching higher effective evaporation rate to the operation temperature, since, the most volatile molecules reach the condenser surface and the intermolecular collisions in the region of interest (space between the evaporator and the condenser surfaces) are much less frequent than molecular interactions. In this sense, in the CRMD process, in which the coupling of the centrifugal molecular distillation and catalytic chemical reaction (in heterogeneous catalysis) takes place simultaneously, setting the condenser temperature (T_{cond}) at 353.15 K is guaranteed higher effective evaporation rate to the operation temperature keeping a substantial temperature difference between wall temperature (evaporator temperature, EVT) and the condenser temperature (T_{cond}) even under steady–state conditions. On the other hand, the other insignificant variables were also ignored (T_{feed} and P_s), and fixed at 393.15 K and 40 Pa, respectively. The screening levels of the four variables, (EVT , Q , RS and $\%CAT$) were further analyzed using a $(2_{IV}^{(4-1)})$ fractional factorial design .

6.2. Screening of the significant variables using a fractional factorial design

In this case the CRMD process could be influenced by multiple variables (*EVT*, *Q*, %*CAT* and *RS*). The statistical factorial design has been shown to be a powerful tool for determining the effects of the operating conditions on the dependent variables. A four factor, two-level 2_{IV}^{4-1} fractional factorial design was used, which means carrying out nine (09) simulations. The (2_{IV}^{4-1}) fractional factorial design can cover the main and interaction effects of the parameters within the range of selected variables, but higher order interactions are negligible. In other words, interactions such as two and three-factor ones are considered to be residual. The effects of the parameters studied are presented comparatively in Table 11.

Table 11. Main effects of *EVT*, *Q*, %*CAT* and *RS* when applying the fractional factorial design.

Response	Factor	Effect	Error	t^a	p^b	-95% ^c	+95% ^c
<i>D</i>	Mean*	1.215	0.001	1113.255	3.906×10^{-12}	1.212	1.218
	x_1^*	-0.108	0.002	-46.860	1.241×10^{-6}	-0.057	-0.051
	x_2	-0.002	0.002	-0.648	5.524×10^{-1}	-0.004	0.002
	x_3	-0.002	0.002	-0.648	5.524×10^{-1}	-0.004	0.002
	x_6	0.001	0.002	0.648	5.524×10^{-1}	-0.002	0.004
<i>G_E</i>	Mean*	5.814	0.003	2114.128	3.003×10^{-13}	5.806	5.821
	x_1^*	-0.521	0.006	-89.314	9.421×10^{-8}	-0.269	-0.252
	x_2	0.000	0.006	0.000	1.000×10^0	-0.008	0.008
	x_3	0.000	0.006	0.000	1.000×10^0	-0.008	0.008
	x_6	0.000	0.006	0.000	1.000×10^0	-0.008	0.008
δ	Mean*	1.170×10^{-4}	3.401×10^{-6}	3.440×10^1	4.262×10^{-6}	1.076×10^{-4}	1.264×10^{-4}
	x_1^*	-3.225×10^{-5}	7.215×10^{-6}	-4.470×10^0	1.108×10^{-2}	-2.614×10^{-5}	-6.108×10^{-6}
	x_2^*	5.175×10^{-5}	7.215×10^{-6}	7.172×10^0	2.001×10^{-3}	1.586×10^{-5}	3.589×10^{-5}
	x_3^*	-2.025×10^{-5}	7.215×10^{-6}	-2.806×10^0	4.849×10^{-2}	-2.014×10^{-5}	-1.084×10^{-7}
	x_6	7.500×10^{-7}	7.215×10^{-6}	1.039×10^{-1}	9.222×10^{-1}	-9.642×10^{-6}	1.039×10^{-5}
ν_r	Mean*	28.729	0.932	30.839	6.587×10^{-6}	26.142	31.315
	x_1^*	13.448	1.976	6.805	2.437×10^{-3}	3.980	9.467
	x_2^*	24.017	1.976	12.154	2.630×10^{-4}	9.265	14.752
	x_3	4.242	1.976	2.147	9.833×10^{-2}	-0.622	4.865
	x_6	0.243	1.976	0.123	9.083×10^{-1}	-2.622	2.865
<i>X_a</i>	Mean*	28.729	0.932	30.839	6.587×10^{-6}	26.142	31.315
	(1) x_1^*	13.448	1.976	6.805	2.437×10^{-3}	3.980	9.467
	(2) x_2^*	24.017	1.976	12.154	2.630×10^{-4}	9.265	14.752
	(3) x_3	4.242	1.976	2.147	9.833×10^{-2}	-0.622	4.865
	(6) x_6	0.243	1.976	0.123	9.083×10^{-1}	-2.622	2.865
α	Mean*	0.594	0.006	91.947	8.388×10^{-8}	0.576	0.612
	x_1^*	-0.190	0.014	-13.830	1.584×10^{-4}	-0.114	-0.076
	x_2^*	0.073	0.014	5.328	5.974×10^{-3}	0.017	0.056
	x_3	0.024	0.014	1.715	1.615×10^{-1}	-0.007	0.031
	x_6	-0.023	0.014	-1.679	1.685×10^{-1}	-0.031	0.008

EVT: Evaporator temperature; *Q*: Feed flow rate; %*CAT*: Percentage weight of catalyst; and *RS*: Rotor speed; x_1 , x_2 , x_3 , and x_6 are the coded factors for *EVT*, *Q*, %*CAT* and *RS*, respectively.

* Statistically significant at a level of confidence of 95 %; ^a Value of the regression coefficient for the error, which measures how big the effect is with respect to the residual error.

^b Probability of significance. At a confidence level of 95 %, a *p-value* <0.05 means that the result is significant.

^c Limits of confidence: The effects are statistically reliable when the limits do not pass zero.

An analysis of the effects of the principal factors showed that *EVT*, *Q* and *RS* caused significant variation in the responses, *EVT* being the most important variable. According to the negative effect of this parameter, the results showed that as the *EVT* rises, so the distillate mass flow rate (*D*) may decrease as a consequence of the reduction in mass transfer within the thin film, because the density of the evaporating molecules increases during the reactive process, within the evaporating gap. Hence, with higher *EVT* and %*CAT* values, low *MFP* values are obtained, because the density of the molecules rises in the distillation gap, and the motion of the particles in the distillation gap causes isotropic behavior. Under these conditions, the evaporation rate of the molecule with the lowest vapor pressure was lower than the molecule with the lowest vapor pressure in the non-catalytic process, and, in consequence, a lower evaporation rate values were reported. Qualitatively, this result is in agreement with the CRMD process, and it is related to the successive cracking of heavier molecules inner the thin liquid film into lighter molecules raising the molecular collisions in the distillation gap.

Moreover, the variable %*CAT* should be included in the analysis since it has a direct influence on the reaction process, such that, kinetically, the catalytic reaction that occurs during the CRMD process is characterized by the frequency of contact between the species with the inner reacting surface of the thin film and the heated surface of the evaporator. Similarly, in heterogeneous catalysis, the diffusion of these species and the diffusion of products from these surfaces becomes the determining step of the reaction rate.

Furthermore, the mathematical model of the CRMD process allows for the prediction of the entire profiles of the variables studied along the radial position (*RD*) over the evaporator surface and thin film thickness, as shown in Figures 6 – 14, considering a value for *RS* equal to 800 rpm. The results presented in Figures 6 – 14 confirm that at lower values of the variable *RS*, it is possible to maintain the efficiency of the reaction, followed by the separation stage, obtaining results for the degree of conversion of about 42% and 48%, respectively.

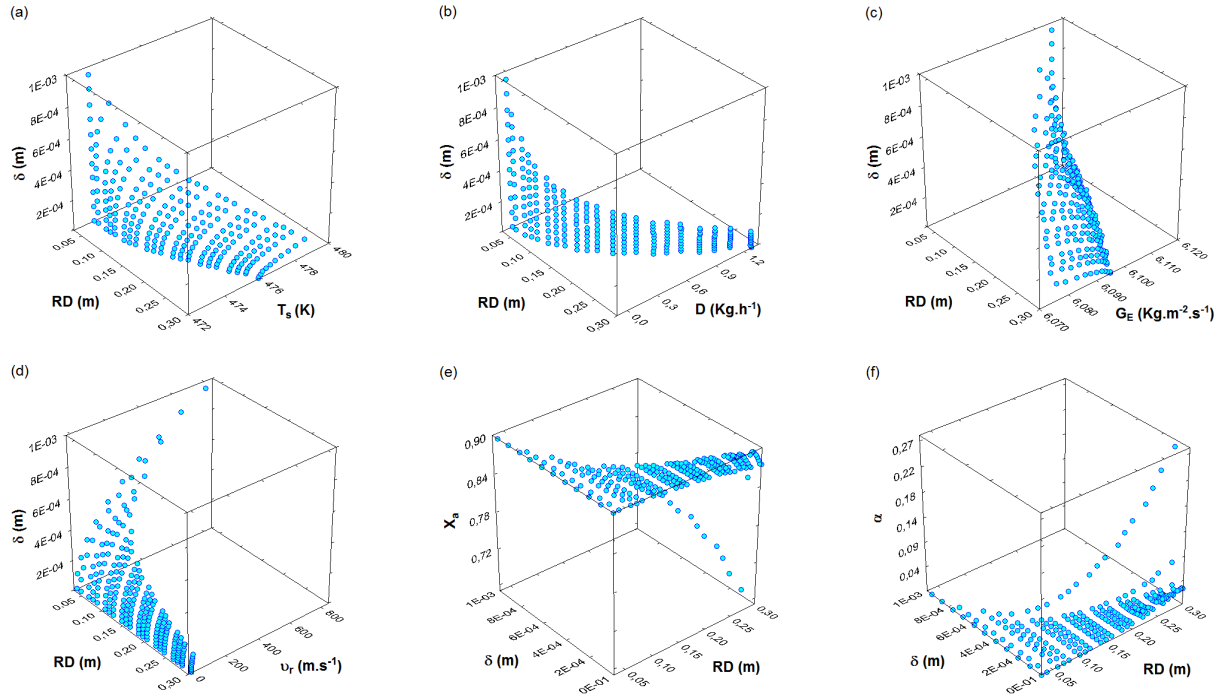


Figure 6. CRMD profiles for run 1 of the 2_{IV}^{4-1} fractional factorial design.

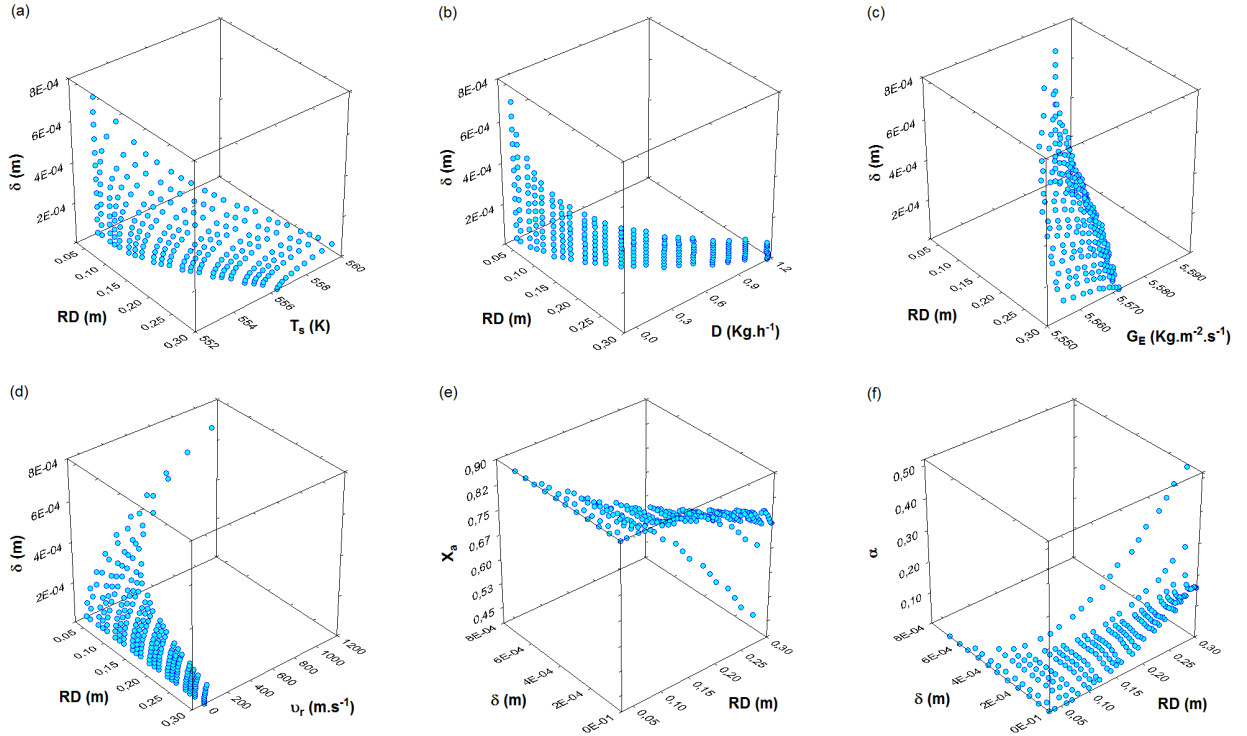


Figure 7. CRMD profiles for run 2 of the 2_{IV}^{4-1} fractional factorial design.

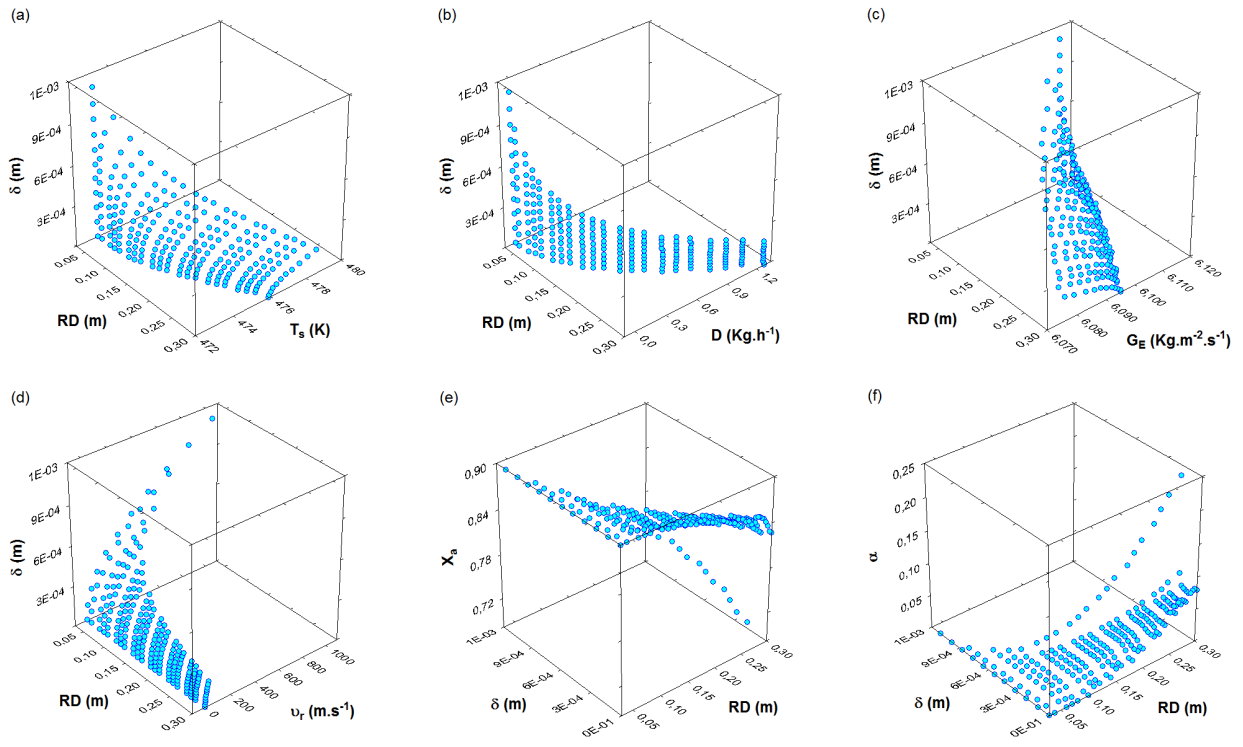


Figure 8. CRMD profiles for run 3 of the 2_{IV}^{4-1} fractional factorial design.

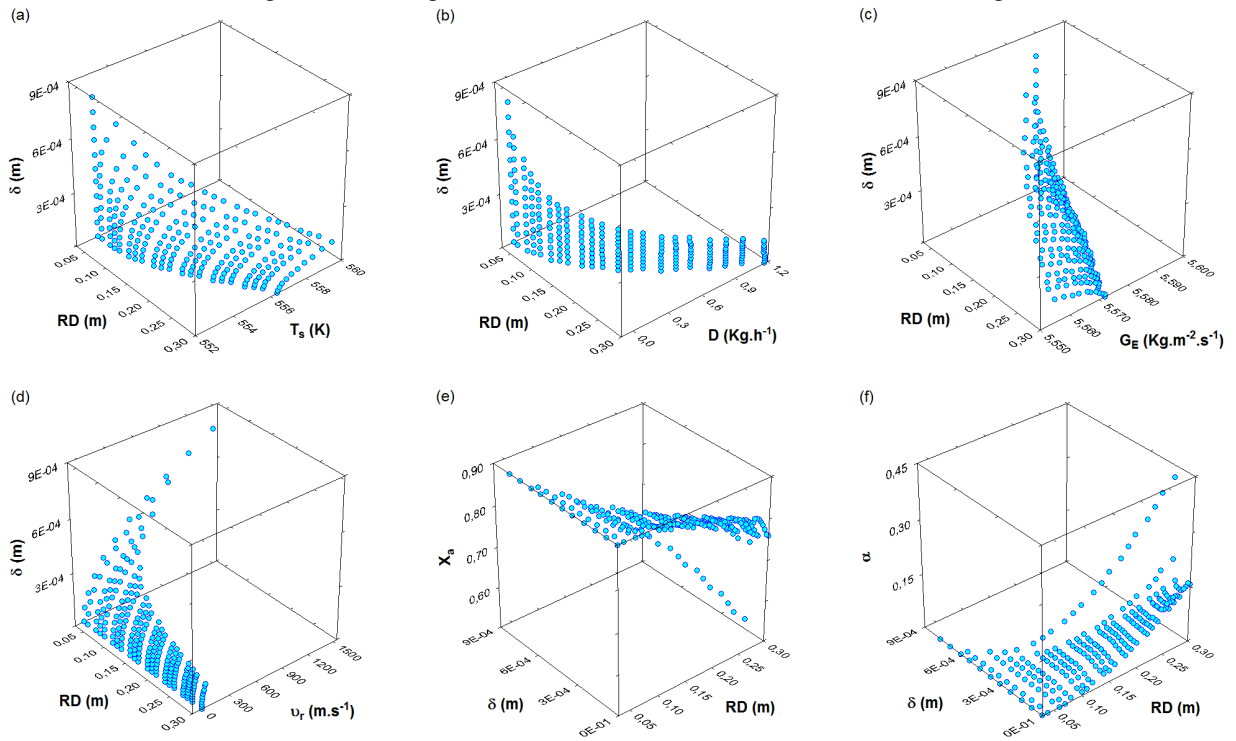


Figure 9. CRMD profiles for run 4 of the 2_{IV}^{4-1} fractional factorial design.

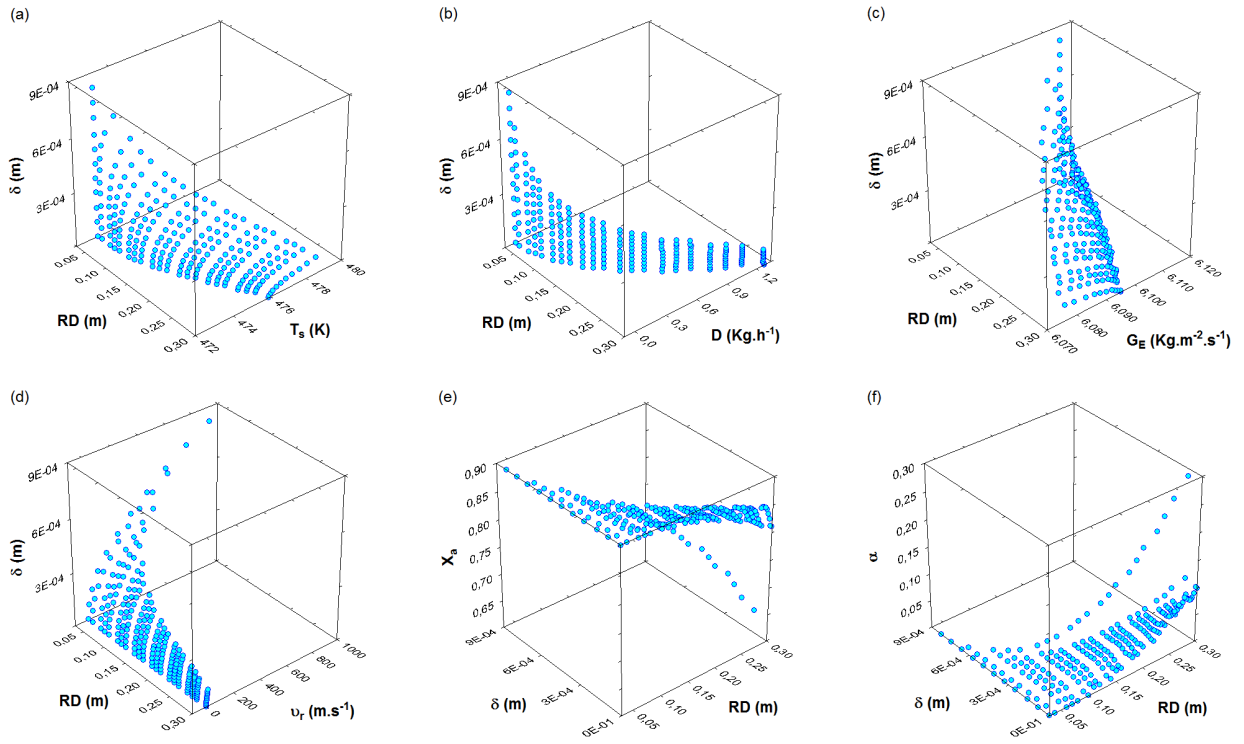


Figure 10. CRMD profiles for run 5 of the 2_{IV}^{4+1} fractional factorial design.

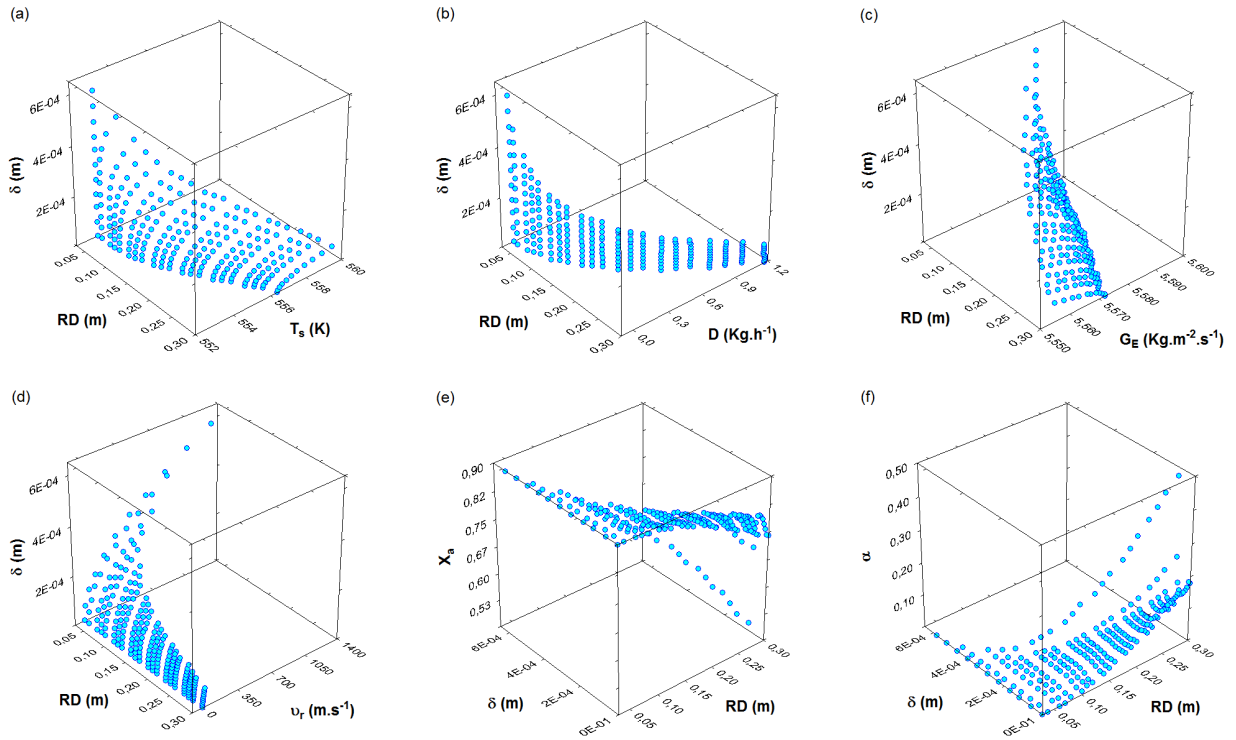


Figure 11. CRMD profiles for run 6 of the 2_{IV}^{4+1} fractional factorial design.

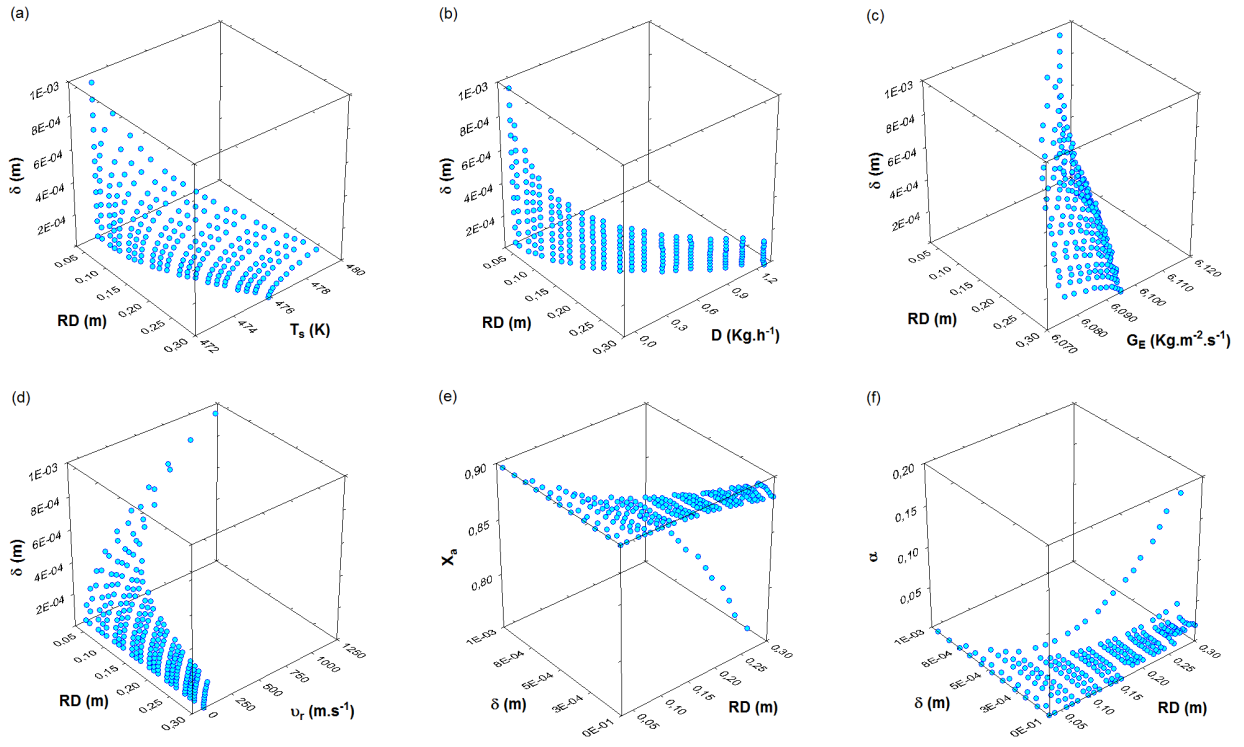


Figure 12. CRMD profiles for run 7 of the 2_{IV}^{4+1} fractional factorial design.

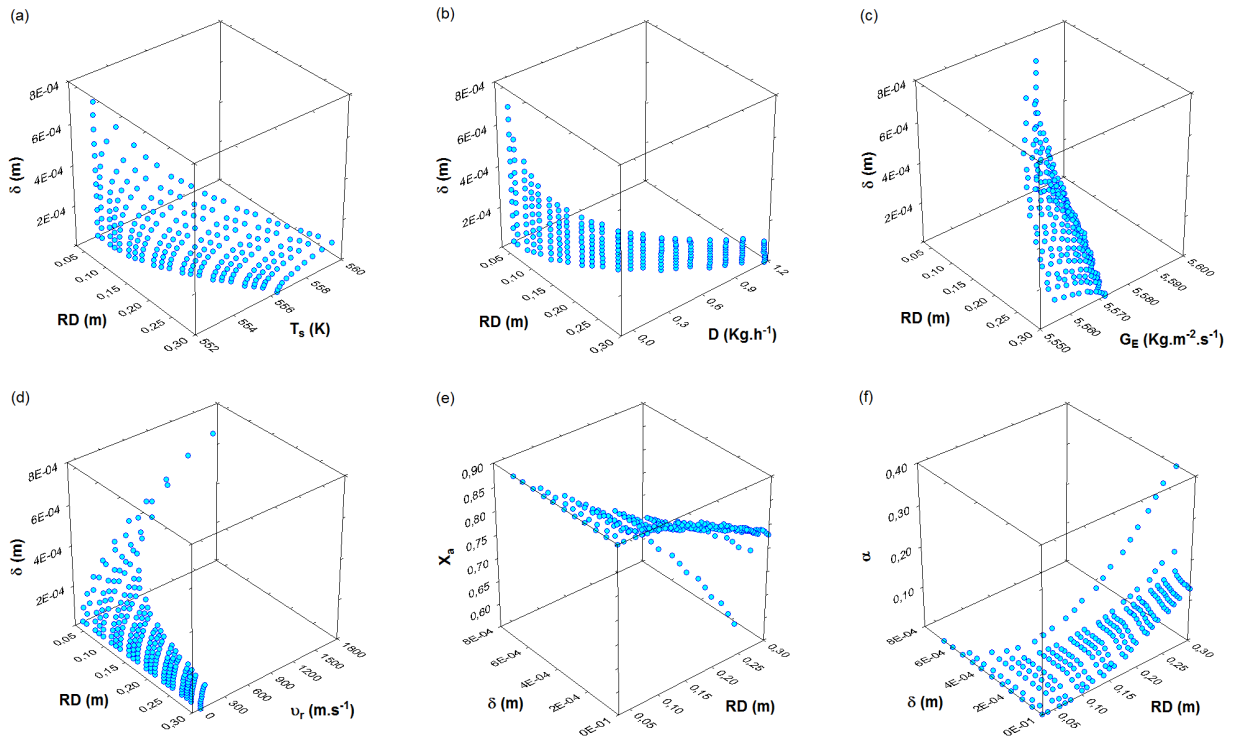


Figure 13. CRMD profiles for run 8 of the 2_{IV}^{4+1} fractional factorial design.

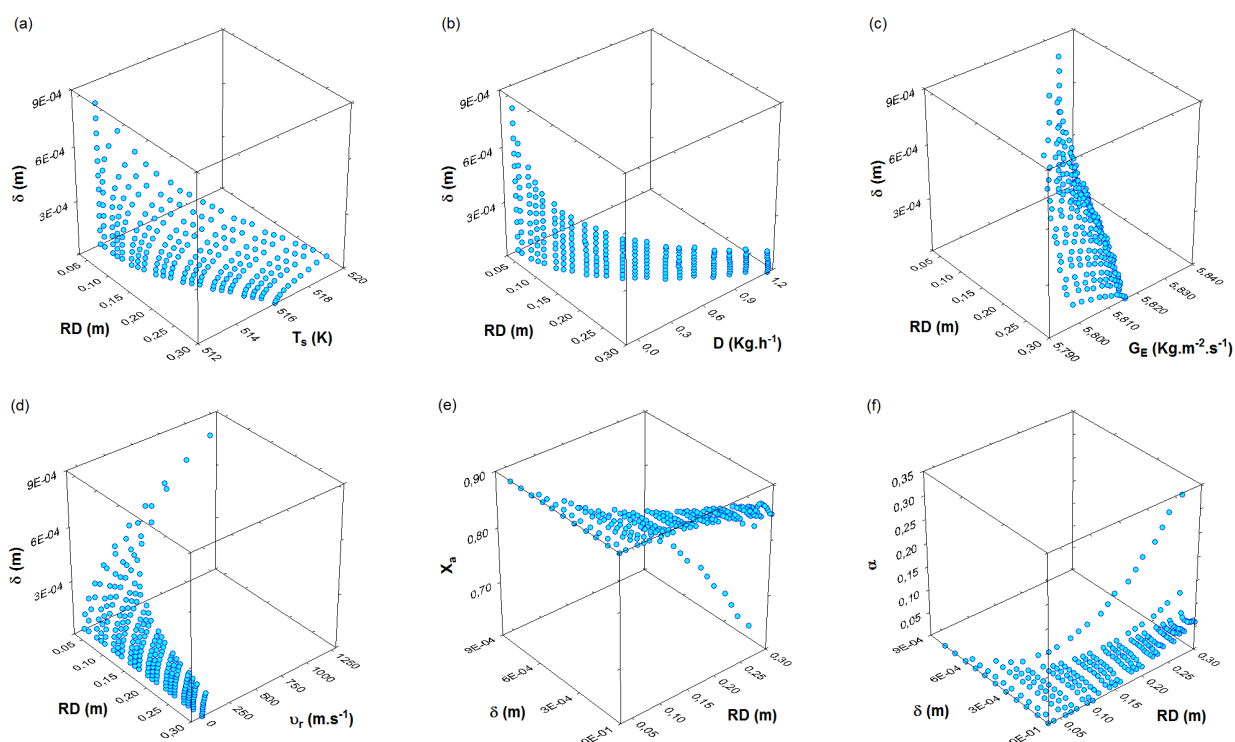


Figure 14. CRMD profiles for run 9 of the 2_{IV}^{4+1} fractional factorial design.

The profiles depicted in Figures 6 – 14 show that the surface temperature (T_s), distillate mass flow rate (D), effective evaporation rate (G_E), film thickness (δ), radial velocity, concentration of pseudocomponent “a” (X_a) and conversion degree (α) all vary continuously along the radial position (RD) and are highly influenced by the *EVT*. Thus, the *EVT* is one of the important operating parameters, which determines the rate of evaporation governing the separation process. On the other hand, both the variables *EVT* and %*CAT* determine the continuous decreasing of the concentration of heavier molecules in the thin liquid film, governing the in-situ catalytic reactive process.

Considering that the catalytic reaction involves breaking complex hydrocarbons (heavier molecules) into simpler molecules (lighter molecules), in order to increase the quality and quantity of the final product, obtaining a more desirable product, the concentration of the products and the conversion degree (α) are sensitive to changes in the selected parameters such as the feed flow rate (Q), the evaporator temperature (*EVT*) and the weight percent of catalyst (%*CAT*). Thus the upgrading of high-boiling-point petroleum fractions by the CRMD process may involve the rearrangement of the molecular structure of the hydrocarbon compounds to

convert heavy hydrocarbon feedstock into lighter petroleum fractions. In fact, from the initial mixture, pseudocomponent “a” is the main compound that reacts, evaporates and condenses, and products are obtained in both the distillate and residue streams (Figures 6e – 14e). Thus a rise in surface temperature (T_s) is related to an increase in the evaporation rate of the products generated from the in-situ catalytic reaction in the separation zone, which confirms the fact that the most significant variables in the CRMD process are the EVT and the $\%CAT$, enhancing the reaction and the separation process in the same process unit.

7. Conclusions and outlook

The goal of this study was to present the modeling of the reactive molecular distillation (centrifugal type)–CRMD process. The set of PDAEs (11+18*N*) for the generalized model was constituted of: material and energy balance equations, physical properties, kinetic model, velocity equation and liquid film thickness, overall distillate mass flow rate, effective evaporation rate and concentration profile of the fluid over the evaporator surface.

The general reactive molecular distillation (centrifugal type) model offered the possibility of studying a large range of operating conditions. The new features of the general model regarding the centrifugal molecular distillation model, includes the reaction term. Therefore, a computer aided environment (DESTMOL–R), which facilitates the solution of different simulation problems, was built up. The computational approach helped to obtain qualitative and quantitative results, to improve the design and to identify the operational conditions for a given case study.

The Plackett–Burman and fractional factorial designs were carried out to identify the predominant variables affecting the response variables (T_s , D , G_E , δ , v_r , X_a and α). The factorial designs were carried out at two levels of the operating variables (EVT , Q , $\%CAT$, T_{feed} , T_{cond} , RS and P_s). This set of simulations focused mainly on screening out the variables that could enhance the CRMD process with respect to higher conversion of the reactants, higher evaporation rates and higher distillate mass flow rates.

Consequently, the evaluation of the steady state model showed that the film surface temperature, the evaporation rate, the overall distillate mass flow rate and the conversion degree were strongly affected by the operating conditions (evaporator temperature, EVT ; feed flow rate, Q ; rotor speed, RS and percentage weight of catalyst, $\%CAT$). However, the feed flow rate (Q)

and rotor speed (RS) could be fixed at low levels of around $1.473 \text{ kg}\cdot\text{h}^{-1}$ and 800 rpm, respectively, in future experimental trials.

The current and future studies are related to experimental work developed in the LDPS/LOPCA research laboratories at UNICAMP, in order to validate the DESTMOL-R tool and check the performance of the CRMD process.

Acknowledgements

This research was supported by the Brazilian National Council for Technological and Scientific Development (CNPq), the Petrobras Research and Development Center (PETROBRAS/CENPES) and the Brazilian Study and Project Financing Institution (FINEP).

Nomenclature

a^*	= Compensation effect in Equation (45)	$[\text{mol}\cdot\text{kJ}^{-1}\cdot\text{min}^{-1}]$
A	= Pre-exponential factor	$[\text{min}^{-1}]$
b^*	= Compensation effect in Equation (45)	$[\text{min}^{-1}]$
C_p	= Specific heat capacity	$[\text{J}\cdot\text{kg}^{-1}\cdot\text{K}^{-1}]$
d_e	= Diameter of the evaporation surface curvature	$[\text{m}]$
D	= Distillate mass flow rate	$[\text{kg}\cdot\text{h}^{-1}]$
$D_{NPSE_i, \text{mix}}$	= Diffusion coefficient	$[\text{m}^2\cdot\text{s}^{-1}]$
E	= Activation energy	$[\text{kJ}\cdot\text{mol}^{-1}]$
E_0	= E -dependence in Equation (46)	$[\text{kJ}\cdot\text{mol}^{-1}]$
E_1	= E -dependence in Equation (46)	$[\text{kJ}\cdot\text{mol}^{-1}]$
EVT	= Evaporator temperature	$[\text{K}]$
G_E	= Effective evaporation rate	$[\text{kg}\cdot\text{m}^{-2}\cdot\text{s}^{-1}]$
$k'' = k_{i,m,n}$	= Kinetic constant	$[\text{s}^{-1}]$
Kn	= Knudsen number	$[-]$
K_{OUP}	Universal Oil Products Company characterization factor	$[-]$
K_w	Watson characterization factor	$[-]$
k^*	= Anisotropy of vapor phase	$[-]$
L	= Distance between evaporator and condenser surfaces	$[\text{m}]$
M	= Molar mass	$[\text{kg}\cdot\text{kmol}^{-1}]$
MFP	= Mean free path	$[\text{m}]$
n'	= Number of intermolecular collisions before the vapor reaches the isotropic state ($n'=5$)	$[-]$
n_{NPSE_i}	= Number of moles of $NPSE_i$	$[\text{mol}]$
n_{NPSE_0}	= Number of moles of $NPSE_i$ at $\theta=0$	$[\text{mol}]$
$n_{NPSE_i,c}$	= Number of moles of n_{NPSE_i} on catalyst in reactive situation	$[\text{mol}]$
N	= Total number of pseudocomponents	$[-]$
N_m	= Number of molecules per unit volume of vapor phase	$[\text{mol}\cdot\text{m}^{-3}]$
N_A	= Avogadro Constant ($6.023\times 10^{23} \text{ mol}^{-1}$)	$[\text{mol}^{-1}]$
N_T	= Total number of moles	$[\text{mol}]$

P_c	Critical pressure	[Pa]
P_s	= System pressure	[Pa]
P_{vap}	= Equilibrium vapor pressure	[Pa]
q_w	= Heating rate at evaporator wall	[J·m ⁻² ·s ⁻¹]
Q	= Feed flow rate	[kg·h ⁻¹]
Q'	= Flow rate over the evaporator surface	[kg·h ⁻¹]
Q_i	= Feed flow rate at $\theta = 0$	[kg·h ⁻¹]
r	= r – direction of coordinate system	[-]
R	= Universal gas constant (8314 J·K ⁻¹ ·kmol ⁻¹)	[J·K ⁻¹ ·kmol ⁻¹]
$-r_{NPSE_i}$	= the rate of disappearance of i th pseudocomponent	[s ⁻¹]
r_i	= Distance from apex at which liquid enters cone	[m]
RD	= Radial distance	[m]
RS	= Rotor speed	[rpm]
s	= s – direction of coordinate system perpendicular to cone surface	[-]
SG	Specific gravity	[-]
t	= Time	[s]
T	= Temperature	[K]
T_{bi}	= Normal boiling point	[K]
T_c	= Critical temperature	[K]
T_{cond}	= Condenser temperature	[K]
T_{feed}	= Feed temperature	[K]
T_s	= Surface Temperature	[K]
V_c	= Critical volume	[cm ³ ·mol ⁻¹]
W_c	= Amount of catalyst	[kg]
X_a	= Molar fraction of pseudocomponent “a”	[-]
X_{NPSE_i}	= Molar fraction of i^{th} pseudocomponent ($NPSE_i$)	[-]
X_{sNPSE_i}	= Molar fraction of i^{th} pseudocomponent ($NPSE_i$) at the evaporating surface	[-]
X_{0NPSE_i}	= Molar fraction of i^{th} pseudocomponent ($NPSE_i$) at $\theta = 0$	[-]
%CAT	= Weight percent of catalyst	[%wt]
Greek Letter		
α	= Conversion degree	[-]
β'	= Half angle of apex of cone radius	[-]
δ	= Thickness of liquid film	[m]
(ΔH_{NPSE_i})	= Heat of evaporation of pseudocomponent i	[J·kg ⁻¹]
$(\Delta H_r)_{i,m,n}$	= Heat of reaction	[J·kg ⁻¹]
φ	= φ – direction of coordinate system	[-]
λ	= Thermal conductivity	[W·m ⁻¹ ·K ⁻¹]
θ	= θ – direction of coordinate system	[-]
ρ	= Average Density and density fraction	[kg·m ⁻³]
σ	= Molecule diameter	[m]
π	= Pi parameter	[-]
v_r	= Thin liquid film velocity in r –direction (radial velocity)	[m·s ⁻¹]
μ	= Dynamic viscosity	[Pa·s]
ν	= Kinematic viscosity	[m ² ·s ⁻¹]
ω	= Angular velocity of cone	[s ⁻¹]
ω_{ac}	= Acentric factor	[-]

$\zeta_{i,m,n}$	= Amount of coke formed when the i^{th} pseudocomponent ($NPSE_i$) cracks to produce the m^{th} and n^{th} pseudocomponents ($NPSE_m$ and $NPSE_n$)	[kg·h ⁻¹]
<i>Subscripts</i>		
i	= Inlet	
o	= Outlet	
$NPSE_i$	= i^{th} pseudocomponent	

References

- Aboul-Seoud A.-L., Moharam H. M. (1999a) A generalized viscosity correlation for undefined petroleum fractions, *Chemical Engineering Journal* **72**, 3, 253–256.
- Aboul-Seoud A.-L., Moharam H. M. (1999b) A simple thermal conductivity–temperature correlation for undefined petroleum and coal liquid fractions, *Chemical Engineering Research and Design* **77**, 3, 248–252.
- Ali M. A., Tatsumi T., Masuda T. (2002) Development of heavy oil hydrocracking catalysts using amorphous silica–alumina and zeolites as catalyst supports, *Applied Catalysis A: General* **233**, 1, 77–90.
- API (1997). API Technical Data book–petroleum refining. In: T. E. Daubert, and R. P. Danner, *API Technical Data book–petroleum refining* (6th ed.). Washington, DC, USA: American Petroleum Institute (API).
- Batistella C. B., Maciel M. R. W., Maciel Filho R. (2000) Rigorous modeling and simulation of molecular distillators: Development of a simulator under conditions of non ideality of the vapor phase, *Computers & Chemical Engineering* **24**, 2, 1309–1315.
- Batistella C. B., Moraes E. B., Maciel Filho R., Wolf Maciel M. R. (2002) Molecular distillation: Rigorous modeling and simulation for recovering vitamin E from vegetal oils, *Applied Biochemistry and Biotechnology* **98–100**, 1–9, 1187–1206.
- Blanding F. H. (1953) Reaction rates in catalytic cracking of petroleum, *Industrial & Engineering Chemistry* **45**, 6, 1186–1197.
- Bollas G. M., Vasalos I. A., Lappas A. A., Iatridis D. K., Voutetakis S. S., Papadopoulou S. A. (2007) Integrated FCC riser–regenerator dynamics studied in a fluid catalytic cracking pilot plant, *Chemical Engineering Science* **62**, 7, 1887–1904.
- Bozzano G., Dente M., Carlucci F. (2005) The effect of naphthenic components in the visbreaking modeling, *Computers & Chemical Engineering* **29**, 6, 1439–1446.

- Bruin S. (1969) Velocity distributions in a liquid film flowing over a rotating conical surface, *Chemical Engineering Science* **24**, 11, 1647–1654.
- Cvengroš J., Lutišan J., Micov M. (2000) Feed temperature influence on the efficiency of a molecular evaporator, *Chemical Engineering Journal* **78**, 1, 61–67.
- Fang W., Lei Q., Lin R. (2003) Enthalpies of vaporization of petroleum fractions from vapor pressure measurements and their correlation along with pure hydrocarbons. *Fluid Phase Equilibria* **205**, 1, 149–161.
- Furimsky E. (2000), Characterization of cokes from fluid/flexi-coking of heavy feeds, *Fuel Processing Technology* **67**, 3, 205–230.
- Guo A., Zhang X., Wang Z. (2008) Simulated delayed coking characteristics of petroleum residues and fractions by thermogravimetry, *Fuel Processing Technology* **89**, 7, 643–650.
- Gupta, Rajkumar Satyapal. Modeling and simulation of fluid catalytic cracking unit. 2006, 142p. Thesis (Doctor of Philosophy) – Department of Chemical Engineering, Deemed University, India, 2006.
- Hickman K. C. D. (1944) High-vacuum Short-path Distillation—A Review, *Chemical Review* **34**, 1, 51–106.
- Hinze J. O., Milborn H. (1950) Atomization of liquid by means of a rotating cup, *Journal of Applied Mechanics* **17**, 2, 145–153.
- Inuzuka M., Sugiyama R., Saito I., Yamada I., Hiraoka S., Ishikawa H., Banno, I. (1986) Analysis of heat and mass transfer in a centrifugal molecular still, *Journal of Chemical Engineering of Japan* **19**, 1, 14–20.
- Inuzuka M., Ishikawa H., Yamada, I., Hiraoka S., Aragaki T., Inukai Y., Erciyas A. T., Kobayashi S. (1989) Vaporization from liquid film of binary mixture in a centrifugal molecular still, *Journal of Chemical Engineering of Japan* **22**, 3, 291–297.
- Khawam, Ammar. Application of solid-state kinetics to desolvation reactions. 2007, 347p. Thesis (Doctor of Philosophy degree in Pharmacy) – Graduate College, University of Iowa, Iowa, 2007.

- Kawala Z., Dakiniewicz P. (2002) Influence of evaporation space geometry on rate of distillation in high-vacuum evaporator, *Separation Science and Technology* **37**, 8, 1877–1895.
- Kawala Z., Stephan K. (1989) Evaporation rate and separation factor of molecular distillation in a falling film apparatus, *Chemical Engineering & Technology* **12**, 1, 406–413.
- Keil F. J. *Modeling of Process Intensification*, Wiley-VCH Verlag GmbH & Co. KGaA, Weinheim (2007).
- Kesler M. G., Lee B. I. (1976) Improve prediction of enthalpy of fractions, *Hydrocarbon Processing* **55**, 3, 153–158.
- Langmuir I. (1913) The vapor pressure of metallic tungsten, *Physical Review* **2**, 5, 329–342.
- Lee B. I., Kesler M. G. (1975) A generalized thermodynamic correlation based on three-parameter corresponding states, *AIChE Journal* **21**, 3, 510–527.
- Loukas Y. L. (1998) A computer-based expert system designs and analyzes a 2(k–p) fractional factorial design for the formulation optimization of novel multicomponent liposomes, *Journal of Pharmaceutical and Biomedical Analysis* **17**, 1, 133–140.
- Lutišan J., Cvengroš J. (1995) Mean free path of molecules on molecular distillation, *The Chemical Engineering Journal and the Biochemical Engineering Journal* **56**, 2, 39–50.
- Lutišan J., Cvengroš J., Micov M. (2002) Heat and mass transfer in the evaporating film of a molecular evaporator, *Chemical Engineering Journal* **85**, 2–3, 225–234.
- Marroquín-Sánchez G., Ancheyta-Juárez J. (2001) Catalytic hydrotreating of middle distillates blends in a fixed-bed pilot reactor, *Applied Catalysis A: General* **207**, 1, 407–420.
- Martínez J., Sánchez J. L., Ancheyta J., Ruiz R. S. (2010) A review of process aspects and modeling of ebullated bed reactors for hydrocracking of heavy oil, *Catalysis Reviews: Science and Engineering* **52**, 1, 60–105.
- Mathews, J. H., and Fink, K. K. (2004). *Numerical methods using Matlab* (4th edition ed.). New Jersey: Pearson Prentice Hall.
- Miquel J., Castells F. (1993) Easy characterization of petroleum fractions (part 1), *Hydrocarbon Processing* **72**, 12, 101–105.

- Myers–Vacuum, 2010. Available in: < <http://www.myers-vacuum.com/index.shtml> >. Accessed in: November 10th. 2010.
- Omole O., Olieh M. N., Osinowo, T. (1999) Thermal visbreaking of heavy oil from the Nigerian tar sand, *Fuel* **78**, 12, 1489–1496.
- Pindoria R. V., Megaritis A., Chatzakis I. N., Vasanthakumar L. S., Zhang S. –F., Lazaro M. –J., Herod A. A., Garcia X. A., Gordon A. L., Kandiyoti, R. (1997) Structural characterization of tar from a coal gasification plant: Comparison with a coke oven tar and a crude oil flash–column residue, *Fuel* **76**, 2 101–113.
- Plackett R. L., Burman J. P. (1946) The design of optimum multifactorial experiments, *Biometrika* **33**, 4, 305–325.
- Poling B. E, Prausnitz J. M., O’Connell J. P. *The properties of gases and liquids*. McGraw–Hill, 2004, 707p.
- Rana M. S., Sámano V., Ancheyta J., Diaz J. A. I. (2007) A review of recent advances on process technologies for upgrading of heavy oils and residua, *Fuel* **86**, 9, 1216–1231.
- Reddy K. M., Wei B., Song C. (1998) High–temperature simulated distillation GC analysis of petroleum resids and their products from catalytic upgrading over Co–Mo/Al₂O₃ catalyst, *Catalysis Today* **43**, 3–4, 187–202.
- Riazi M. R. Characterization and properties of petroleum fractions. ASTM International Standards Worldwide, 2004. 407p.
- Riazi M. R., Daubert T. E. (1980) Simplify property predictions, *Hydrocarbon Processing* **59**, 3, 115–116.
- Rodríguez–Reinoso F., Santana P., Romero–Palazon E., Diez M. –A., Marsh H. (1998) Delayed coking: Industrial and laboratory aspects, *Carbon* **36**, 1–2, 105–116.
- Sales–Cruz M., Gani R. (2006) Computer–Aided modelling of short–path evaporation for chemical product purification, analysis and design, *Chemical Engineering Research and Design* **84**, 7, 583–594.
- Sattarin M., Modarresi H., Talachi H., Teymori M. (2006) Solvent deasphalting of vacuum residue in a bench–scale unit, *Petroleum & Coal* **48**, 3, 14–19.

- Sbaite P., Batistella C. B., Winter A., Vasconcelos C. J. G., Wolf-Maciel M. R., Maciel-Filho R., Gomes A., Medina L., Kunert R. (2006) True boiling point extended curve of vacuum residue through molecular distillation, *Petroleum Science and Technology* **24**, 3–4, 265–274.
- Schiesser W. E. *The numerical method of lines*, San Diego, CA: Academic Press, 1991.
- Stankiewicz A., Moulijn J. A. (2002) Process intensification, *Industrial and Engineering Chemistry Research* **41**, 8, 1920–1924.
- StatSoft Inc., (2004) StatSoft Inc., Statistica for Windows (Computer Program Manual), Statsoft Inc., 2300, East 14th Street, Tulsa, OK, USA (2004).
- Tovar, Laura Plazas. Modeling and simulation of the centrifugal reactive molecular distillation: Development, assessment and application to upgrade high-boiling-point petroleum fractions. 2012, 442p. Ph. D. Thesis (Doctorate of Chemical Engineering) – School of Chemical Engineering, State University of Campinas, Campinas, 2012.
- Tovar L. P., Pinto G. M. F., Wolf-Maciel M. R., Batistella C. B., Maciel-Filho R. (2011) Short-path-distillation process of lemongrass essential oil: Physicochemical characterization and assessment quality of the distillate and the residue products, *Industrial and Engineering Chemistry Research* **50**, 13, 8185–8194.
- Tovar L. P., Wolf Maciel M. R., Araujo A. S., Maciel Filho R., Batistella C. B., Medina L. C. (2011) Kinetic study on catalytic cracking of Brazilian high-boiling-point petroleum fractions. *Journal of Thermal Analysis and Calorimetry*; doi: 10.1007/s10973-011-2068-6.
- Tovar L. P., Wolf Maciel M. R., Maciel Filho R., Batistella C. B., Ariza O. C., Medina L. C. (2011) Overview and computational approach for studying the physicochemical characterization of high-boiling-point petroleum fractions (350 °C+). *Oil & Gas Science and Technology*; doi:10.2516/ogst/2011150.
- Tovar L. P., Wolf-Maciel M. R., Ferreira-Pinto G. M., Maciel-Filho R., Gomes D. R. (2010) Factorial design applied to concentrate bioactive component of *cymbopogon citratus* essential oil using short path distillation, *Chemical Engineering Research and Design* **88**, 2, 239–244.
- Verstraete J. J., Le Lannic K., Guibard I. (2007) Modeling fixed-bed residue hydrotreating processes, *Chemical Engineering Science* **62**, 18–20, 5402–5408.

- Wang G., Yang G. -F., Xu C. -M, Gao J. -S. (2008) A novel conceptional process for residue catalytic cracking and gasoline reformation dual-reactions mutual control, *Applied Catalysis A: General* **341**, 1–2, 98–105.
- Watson K. M., Nelson E. F. (1933) Improved methods for approximating critical and thermal properties of petroleum fractions, *Industrial & Engineering Chemistry* **25**, 8, 880–887.
- Xubin Z., Chunjian X., Ming Z. (2005) Modeling of falling film molecular distillator, *Separation Science and Technology* **40**, 6, 1371–1386.
- Zhang S., Liu D., Deng W., Que G. (2007) A review of slurry-phase hydrocracking heavy oil technology, *Energy & Fuels* **21**, 6, 3057–3062.
- Zhou J. (2003) High conversion slurry bed hydrocracking process for producing high octane gasoline and high cetane diesel simultaneously from vacuum gas oil, *Preprints of Papers–American Chemical Society, Division of Fuel Chemistry* **48**, 2, 668–669.
- Zuñiga-Liñan L., Nascimento-Lima N. M., Manenti F., Wolf-Maciel M. R., Maciel Filho R., Medina L. C. (2011) Experimental campaign, modeling, and sensitivity analysis for the molecular distillation of petroleum residues 673.15 K+, *Chemical Engineering Research and Design* **90**, 2, 243–258.
- Zuñiga L. L., Lima N. M. N., Wolf-Maciel M. R., Maciel Filho R., Batistella C. B., Manca D., Manenti F., Medina L. C. (2009) Modeling and simulation of molecular distillation process for a heavy petroleum cut, *Chemical Engineering Transaction* **17**, n.a., 1639–1644.

Source: From Tovar L. P., Wolf-Maciel M. R., Batistella C. B., Winter A., Maciel-Filho R., Medina L. C. (manuscript accepted in 2012) High-boiling-point petroleum fractions upgrading using the centrifugal reactive-molecular distillation process over catalyst: Mathematical modeling and simulation including experimental validation. European Symposium on Computer Aided Process Engineering – ESCAPE 22; University College London, UK; 17–20 June 2012.

Copyright notice: The content of this manuscript is licensed under the Ethical Guidelines to Publication of Elsevier B.V.p. Please contact credited rights holders directly for permission to reproduce material.

Centrifugal reactive-molecular distillation: An intensified process-Part II

Key operating variables and their effects on the performance of the centrifugal reactive-molecular distillation process

Abstract

In an earlier paper, the reactive molecular distillation process was presented with the main purpose of upgrading the high-boiling-point petroleum fractions. A steady-state model for describing the catalytic molecular distillation process was established, and solved with the method of lines.

In this work, a computational study was developed using the DESTMOL-R tool developed in FORTRAN-90 language using Compaq Visual Fortran compiler (professional edition 6.6) in order to evaluate the effects of the operating conditions (evaporator temperature and weight percent of catalyst) on the performance of the centrifugal reactive-molecular distillation process (CRMD) in terms of the film thickness, surface evaporation rate, distillate rate, concentration profiles, velocity and the conversion profiles. The simulations were carried out at the steady-state conditions. The influence of adding a catalyst (3 and 5 %wt) was examined. The process temperature (evaporator temperature) range was from 473.15 K to 523.15 K and the constant feed flow rate was $1.473 \text{ kg}\cdot\text{h}^{-1}$.

The results showed that the inlet variables: the evaporator temperature and the percent weight of catalyst were relevant operational conditions for the performance of the CRMD process reaching an conversion of the feedstock about 65% in the distillate stream and 48% in the residue stream with 3 and 5 weight percent of catalyst.

The objective of the experimental work was not only to validate the profiles estimation but also characterize the 20 fractions (10 distillates and 10 residues) obtained from CRMD process under the operating conditions. Because of the complex composition of products obtained by CRMD, high-temperature simulated distillation using gas chromatography (HT-SimDis GC) based on ASTM D 7169 was used in order to evaluate the extent conversion and to characterize converted products.

The experimental results agreed well with those obtained from the theoretical simulation calculations, indicating the accuracy and reliability of the mathematical model, since the average absolute deviation (*AAD%*) was no larger than 6.82%, 9.39% and 14.92% for the distillate mass flow rate and the extent of conversion in the distillate and the residue stream, respectively. Finally, the CRMD model can provide theoretical guidance for the further experimental runs and process optimization.

Keywords: Centrifugal reactive-molecular distillation, DESTMOL-R, distillate mass flow rate, degree of conversion, upgrading high-boiling-point petroleum fraction.

Contents

1. Introduction
 2. Modeling approach
 - 2.1. Chemical system and reaction kinetics
 - 2.2. Thermodynamics and physical properties
 - 2.3. Solution strategy
 3. Experimental set-up of the CRMD
 4. Results and discussion
 - 4.1. Model results
 - 4.2. Mathematical model verification
 5. Conclusions
- Acknowledgments
Nomenclature
References

1. Introduction

In an earlier work, the centrifugal reactive-molecular distillation (CRMD) process was presented as a technique developed and implemented by the Separation Process Development Laboratory (LDPS) and the Optimization, Project and Advanced Control Laboratory (LOPCA) of the Chemical Engineering School of UNICAMP, sponsored by the Petrobras Research Center(CENPES/Petrobras, Brazil) and Brazilian Study and Project Financing Institution

(FINEP), and aimed at enhancing the performance of the heavy petroleum fractions and heavy petroleum crude oil.

The CRMD process, in which the coupling of the centrifugal molecular distillation and catalytic chemical reaction (in heterogeneous catalysis) takes place simultaneously, might be considered as one of the most important concepts for the upgrading of residues in the petroleum industry. This process has attracted considerable attention because of its remarkable advantages, principally its in-situ reaction, which occurs in the reaction and separation zones or evaporation gap (distance between the evaporator and the condenser surface of the CRMD unit). The most promising aspects related to the efficiency and operating conditions of the catalytic CRMD process are listed below:

- The integration of the reaction and separation processes, simultaneously, leads to a reduction in the number of variables influencing the process (evaporator temperature and weight percent of catalyst), and in the response variables measured and quantified (exit flow rates and conversion degree of the reaction).
- Operation in the presence of small amounts of catalyst.
- Accomplishment of operational temperatures and pressures (below 50 Pa), depending on the characteristics of the reactants, the amount of catalyst and the products desired.
- High rates of reaction–evaporation–split, allowing for high processing rates and relatively high conversion degrees.
- Lower exposure time of the reactants with the catalyst and the process conditions.
- Optimum configuration of the reaction and separation zones in the CRMD unit.

Thus, the CRMD process results in a so-called hybrid, intensified process (Tovar, 2012; Winter, 2011). In a catalytic CRMD process, the reaction–evaporation, condensation–diffusion couplings in the thin liquid film, flowing over the evaporator surface (which is a multi-component system), implies in heat and mass transfer processes. As a consequence, Tovar (2012) proposed a modeling approach, taking into account the momentum, and the mass and energy balance equations, including the reaction term, as well as the Langmuir–Knudsen equation derived from the kinetic theory for the ideal gas to describe the effective evaporation rate, which takes into account the anisotropic properties of the vapor.

A computational study was developed using the DESTMOL–R computational tool in order to evaluate the operating conditions (evaporator temperature, feed flow rate, weight percent of catalyst, feed temperature, condenser temperature, rotor speed and system pressure) on the relevant process variables, such as film thickness, surface evaporation rate, distillate mass flow rate, concentration profiles, velocity and conversion profiles (Tovar, 2012).

The aim of this paper was to provide a comprehensive overview of the use of the DESTMOL–R computational environment to model and simulate the CRMD under key operating conditions (*EVT* and %*CAT*). The theoretical study was illustrated for the upgrading of a high-boiling-point petroleum fraction (atmospheric residue of 673.15 K⁺ of “W” crude oil), divided into two (02) pseudocomponents. In the simulation of the process, a thin liquid film, a heated evaporator surface and a very low pressure system were considered.

The CRMD process was modeled according to the mass, momentum and energy balance equations. The simulations were carried out under steady-state conditions, and the output variables, such as surface temperature (T_s), film thickness (δ), effective evaporation rate (G_E), distillate rate (D), reactant concentrations (X_{NPSEi}) and conversion (α) profiles were computed. A steady-state model was then used to describe the catalytic molecular distillation process and solved with the numerical method of lines. Simulations were carried out in the evaporator temperature range (*EVT*) from 473.15 K to 523.15 K, with the feed flow rate (Q) fixed at 1.473 kg·h⁻¹. The influence of adding a catalyst (3 and 5 %wt) was examined, and different experimental runs were used to validate the model. The derived results related to the distillate mass flow rate and conversion degree were validated using the experimental data obtained previously from a pilot plant, and presented in Tovar (2012) and Winter (2011). Accordingly, the performance of the CRMD process was examined in two ways: (i) evaluation of the conversion degree of the feedstock (ATR–W) at the outlet section of the evaporator surface, and (ii) identification of the products (distillate and residue streams) and quantification of their yields.

2. Modeling approach

The mathematical description is based on the modeling of the centrifugal molecular distillation process proposed by Tovar (2012), Kawala and Stephan (1989), Bruin (1969), Inuzuka et al. (1986) and Inuzuka et al. (1989), and adapted to include the kinetic reaction term.

To develop the generalized two-dimensional steady state mathematical model of the CRMD process, the following assumptions were made: (i) the model uses a spherical coordinate system, adopting the relationship $-ds = r d\theta$; (ii) the liquid flow is considered to be steady state; (iii) the liquid film thickness is very small in comparison with the radius of the conical surface; (iv) the velocity components in φ - and θ - directions are negligible in comparison with the velocity component in r -direction; (v) the thin liquid film is completely viscous and is in a laminar regime; (vi) the liquid has the same rotational speed as the rotating surface; (vii) the gravitational force is negligible in comparison with the centrifugal force; (viii) the evaporator is assumed to have a conical shape and it is heated internally, attaining a constant temperature called the evaporator temperature (EVT); and (ix) the condensing surface is maintained at a constant temperature, T_{cond} .

The CRMD model used in this paper is based on the thin liquid film and consists of the material and energy balances over the evaporator surface (see Figure 1). The steady-state component balances and algebraic equations related to the effective evaporation rate for the liquid system are presented as follows:

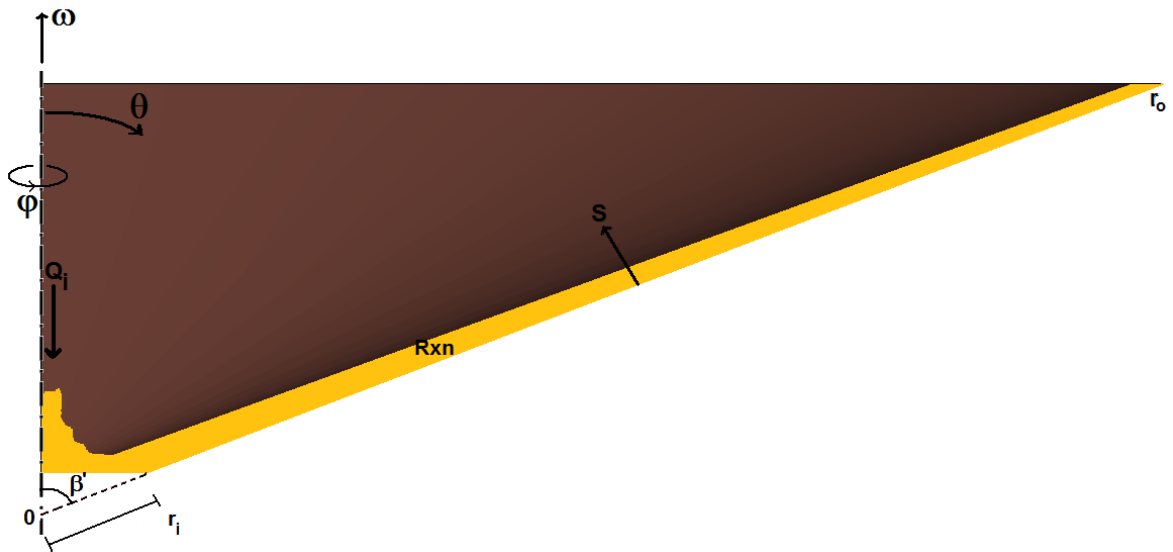


Figure 1. Schematic picture of a thin liquid film flowing on a rotating conical evaporator surface

Overall mass balance

$$\frac{1}{3600} \frac{dQ'}{dr} + 2\pi r G_E (\sin \beta') = 0 \quad (1)$$

$$\mu \frac{\partial^2 v_r(r)}{\partial s^2} + \rho (\sin^2 \beta') r \omega^2 = 0 \quad (2)$$

The boundary conditions for $\dot{Q}(r)$ and $v_r(r)$ are given as:

$$Q'(r) = Q_i(r) \quad \text{At} \quad r = r_i \quad (3)$$

$$v_r(r) = 0 \quad \text{At} \quad s = 0 \quad \text{At wall} \quad (4)$$

$$\frac{\partial v_r(r, s)}{\partial s} = 0 \quad \text{At} \quad s = \delta(s) \quad \text{At free surface} \quad (5)$$

Thickness of the evaporating film

$$\delta(r) = \left[\frac{3\nu}{2\pi\omega^2 r^2 \rho (\sin^3 \beta')} \left(\frac{Q_i - D}{3600} \right) \right]^{1/3} \quad (6)$$

Overall distillate mass flow rate

$$D(r) = 3600 \int_{r_i}^{r_o} 2\pi (\sin \beta') r G_E dr \quad (7)$$

Effective evaporation rate

$$G_E = \sum_{i=1}^{NPSE} \left(P_{vap, NPSE_i} \sqrt{\frac{M_{NPSE_i}}{2\pi RT_s}} \right) \left[1 - \left(1 - \left(\frac{d_e - 2L}{2d_e - 2L} \right) \right) \left(1 - e^{k^* K n_{NPSE_i}} \right)^{n'} \right] \quad (8)$$

$$NPSE_i = 1, \dots, N$$

Temperature profile in the liquid film

$$\rho(T) C_p(T) v_r(r) \frac{\partial T(r, s)}{\partial r} = \lambda(T) \frac{\partial^2 T(r, s)}{\partial s^2} - \rho(T) \sum_{i=1}^{NPSE} (\Delta H_r)_{i, m, n} r_{NPSE_i} \quad (9)$$

The initial and boundary conditions are:

$$T(r, s) = T_{feed} \quad \text{At} \quad r = r_i \quad \text{and} \quad 0 \leq s \leq \delta \quad (10)$$

$$-\lambda(T) \frac{\partial T(r, s)}{\partial s} = q_w = \text{const} \quad \text{At} \quad r_i \leq r \leq r_o \quad \text{and} \quad s = 0 \quad (11)$$

$$-\lambda(T) \frac{\partial T(r, s)}{\partial s} = \sum_{i=1}^{NPSE} X_{s, NPSE_i}(r, s) \Delta H_{NPSE_i}(T) G_{E, NPSE_i} \quad \text{At} \quad r_i \leq r \leq r_o \quad \text{and} \quad s = \delta \quad (12)$$

Concentration profile in the liquid film

$$v_r(r) \frac{\partial X_{NPSE_i}(r, s)}{\partial r} = \mathbf{D}_{NPSE_i, mix} \frac{\partial^2 X_{NPSE_i}(r, s)}{\partial s^2} - r_{NPSE_i} \quad (13)$$

The initial and boundary conditions are:

$$X_{NPSE_i}(r, s) = X_{0, NPSE_i} \quad \text{at} \quad r = r_i \quad \text{and} \quad 0 \leq s \leq \delta \quad (14)$$

$$\frac{\partial X_{NPSE_i}(r, s)}{\partial s} = 0 \quad \text{at} \quad r_i \leq r \leq r_o \text{ and } s = 0 \quad (15)$$

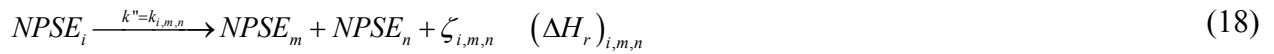
$$X_{NPSE_i}(r, s) = X_{s_{NPSE_i}} \quad \text{at} \quad r_i \leq r \leq r_o \text{ and } s = \delta \quad (16)$$

Where the molar fraction of the i^{th} pseudocomponent ($NPSE_i$) at the evaporating surface, $X_{s_{NPSE_i}}$, is initially unknown, but should satisfy the following mass balance:

$$\rho \frac{d}{dr} \int 2\pi (\sin \beta') r v_r(r) X_{NPSE_i}(r, s) ds + 2\pi r (\sin \beta') X_{s_{NPSE_i}}(r, s) G_E = 0 \quad (17)$$

2.1. Chemical system and reaction kinetics

A heterogeneous catalytic system was assumed using the zeolite-based catalyst CR-1 (regenerated catalyst used for FCC technology containing 48.3 % mass of alumina, and particle size of 67 μm). The catalyst CR-1 was mixed with the atmospheric petroleum residue, constituting the load to the CRMD process. The cracking reaction is an endothermic reaction and it is explained in Tovar et al. (2011). In the cracking catalytic reaction, it is assumed that the cracking of one mole of a pseudocomponent produces one mole each of two other pseudocomponents, and also a certain amount of coke may be formed, as described in Equation (18) (Gupta, 2006).



Therefore, assuming that the amount of material on the catalyst in the reactive process (during the CRMD process) is an adsorbed layer, the reaction term can be written as (Blanding, 1953):

$$-r_{NPSE_i} = -\frac{dn_{NPSE_i}}{dt} = k'' \left(\frac{n_{NPSE_i}}{n_{NPSE_0}} \right)^2 P_s W_c \quad (19)$$

The temperature dependence of the reaction rate constant (k'') is expressed by the Arrhenius equation as a function of the effective compensation effects (Tovar et al., 2011). Table 1 shows all the reaction kinetic parameters, taking into account the compensation effects.

Table 1. Parameter set for reaction kinetics model (Tovar et al., 2011).

Parameters	%wt of catalyst	
	3	5
E_0 (kJ·mol ⁻¹)	22.52	30.65
E_I (kJ·mol ⁻¹)	27.93	6.11
b^* (min ⁻¹)	-6.02	-5.10
a^* (mol·kJ ⁻¹ ·min ⁻¹)	0.32	0.34

E_0 , E_I , b^* and a^* : Parameters of the kinetic compensation effects

2.2. Thermodynamics and physical properties

The physical properties such as densities, viscosities and thermal conductivities were calculated by the methods studied in Tovar et al., (2011).

2.3. Solution strategy

For the numerical solution, a careful analysis of the appropriate variables was carried out (Tovar, 2012). The mathematical model presented above comprises a system of partial differential algebraic equations (PDAEs) solved numerically using the method of lines. The film thickness was discretized at 11 points along the radial distance (*RD*) of 101 points. With this discretization, good simulation performance was guaranteed. Furthermore, all the model equations were implemented into the DESTMOL–R computational environment, developed in FORTRAN–90 language using Compaq Visual Fortran compiler (professional edition 6.6) to solve the overall system using the DESOLV and RKF45 (fifth/fourth order Runge Kutta Fehlberg with adaptive step sizing (Mathews and Fink, 2004)) subroutines.

3. Experimental set-up of the CRMD

The experiments were carried out in the CRMD pilot plant shown in Figure 2. The series 316 stainless steel CRMD unit has an evaporator with an inner diameter of 400 mm and a conical shape with a half angle of 70°. The operating pressure lies between 40 and 50 Pa and the operating temperature is up to 523.15 K. A detailed description of the CRMD unit and the experimental methodology can be found in Winter (2011).

All process data such as temperatures (evaporator, outlet stream, trap and cooling system), system pressure, flow rates (feed and outlet streams) and rotor speed are displayed and monitored by a process control system. Liquid outlet samples (distillate and residue streams) are collected in a gutter surrounding the rotor, and then flow down to the collector vessel. The samples (converted products) were analyzed by high-temperature simulated distillation using gas chromatography (HT–SimDis GC) based on ASTM D 7169 (2011), with a capillary column (Tovar, 2012). The experimental trial and simulation of the process for high-boiling-point petroleum fraction (ATR–W) upgrading, were based on theoretical studies of the parameters to determine the appropriate operating ranges for both variables, the evaporator temperature (*EVT*) and the percent weight of catalyst (*%CAT*) (Tovar, 2012).

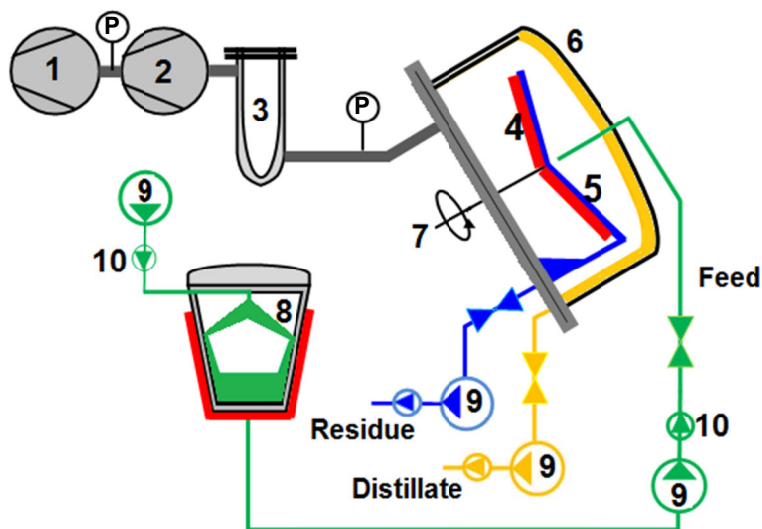


Figure 2. Flow diagram of the CRMD pilot plant. Schematic diagram of CMD:

1. Backing/Roughing Vacuum Pump; 2. Diffusion Ejector Pump (high Vacuum); 3. Chamber Trap; 4. Heater rotor; 5. Evaporator surface; 6. Dome condenser; 7. Rotor; 8. Feed storage; 9. Liquid Transfer Pump; and 10. Check Valve Rotor. Modified Myers–Vacuum (2010).

4. Results and discussion

The upgrading of the high-boiling-point petroleum fraction (atmospheric residue of 673.15 K⁺ of “W” crude oil, ATR–W) was considered. The total residue was divided into two (02) pseudocomponents and Table 2 presents the basic and thermodynamic properties, whereas Table 3 lists the equipment dimensions and operating conditions.

Table 2. Basic properties of the constituent feed pseudocomponents

i	NPSE _i	x_{NPSE}	T_{b_i} (K)	M (kg·kmol ⁻¹)	ρ (kg·m ⁻³)	T_c (K)	P_c (MPa)	V_c (cm ³ ·mol ⁻¹)	ω_{ac}	Kw
1	“a”	0.9762	812.5	440.1	927.6	957.1	0.869	1819.64	1.2347	12.22
2	“b”	0.0238	2199.0	2797.2	1292.7	1937.6	0.188	11232.13	3.2467	12.22

NPSE: Pseudocomponent; x_{vi} : Volume fraction of component (or pseudocomponent i); x_{wi} : Weight fraction of component (or pseudocomponent i); T_{bi} : Normal boiling point of pseudocomponent i ; ρ : Density at evaporator temperature; Kw: Watson characterization factor; $MeABP$: Mean average boiling point; M : Molar mass; P_c : Critical pressure; T_c : Critical temperature; V_c : Critical volume; ω_{ac} : acentric factor.

Table 3. Simulated conditions and data

Variables	Value	Units
<i>Constants</i>		
Universal gas constant	8314	J·kmol ⁻¹ ·K ⁻¹
Pi	3.1416	-
<i>Equipment dimensions</i>		
Evaporator radius	0.297	m
Distance from apex at which liquid enters cone	0.03095	m
Evaporation gap	0.08	m
Half angle of apex of cone radius	70	-
<i>Model parameters</i>		
Number of intermolecular collisions	5	-
<i>Operating conditions</i>		
Feed temperature	423.15	K
Condenser temperature	353.15	K
Trap cooler temperature	273.15	K
Rotor speed	540	rpm
Feed flow rate	1.473	kg·h ⁻¹
Evaporator temperature	473.15	K
	483.15	K
	498.15	K
	503.15	K
	523.15	K
Weight percent catalyst	3	%wt
	5	%wt
System pressure	At 3 %wt of catalyst the vacuum system reached 41.6 Pa	
	At 5 %wt of catalyst the vacuum system reached 50.0 Pa	

4.1. Model results

The solution of the evaporator model for the upgrading of the atmospheric petroleum residue ATR–W provides simulated values for the output variables such as surface temperature (T_s), film thickness (δ), effective evaporation rate (G_E), distillate rate (D), concentration of reactant (X_{NPSEi}) profiles and conversion (α) profiles, both in the distillate and residue streams, as shown in Figures 3 – 9 against the evaporator length (radial distance, RD) on the horizontal axis. According to these results, the ATR–W was upgraded well, as shown by an analysis of the performance of the liquid film.

As already mentioned in a previous manuscript (Tovar, 2012), the film surface temperature, T_s , represents the determining factor in the CRMD process. Thus, the film surface temperature was determined along the RD as a function of the evaporator temperature and weight percent of catalyst (3 and 5 %wt of catalyst), at constant liquid load (1.473 kg·h⁻¹) and a constant liquid feed temperature (423.15 K). The temperature of the film surface, (T_s), increases gradually along the film length, and reaches an asymptotic value corresponding to the outlet region of the evaporator, as shown in Figure 3. Furthermore, T_s increases with the evaporator temperature

(*EVT*, evaporator wall temperature) and establishes a temperature gradient inside the film, where the reaction of the heaviest pseudocomponent occurs, followed by evaporation of the more volatile pseudocomponent.

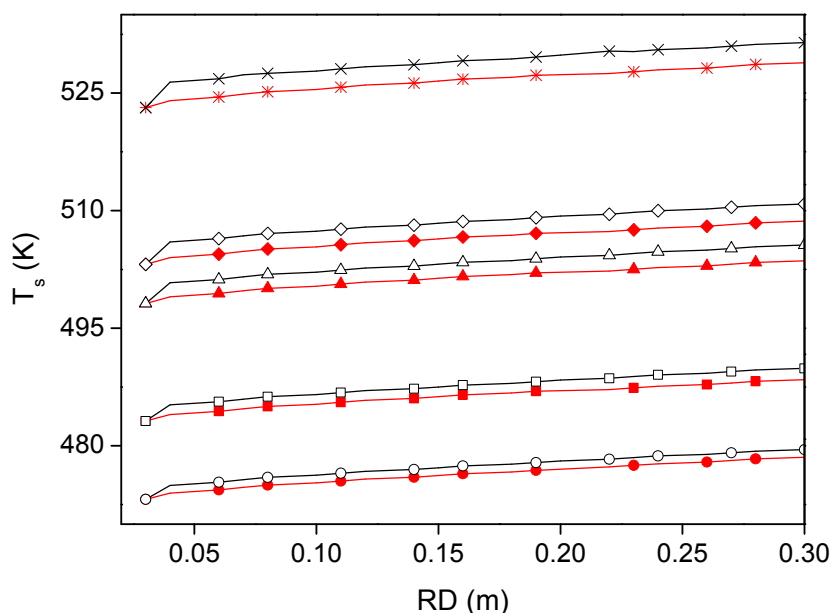


Figure 3. Surface temperature film (T_s) profiles.
 Upgrading over 3% wt of catalyst: —●— 473.15 K; —■— 483.15 K; —▲— 498.15 K; —◆— 503.15 K; —×— 523.15 K
 Upgrading over 5% wt of catalyst: —○— 473.15 K; —□— 483.15 K; —△— 498.15 K; —◇— 503.15 K; —×— 523.15 K

Furthermore, the *EVT* was the most important governing condition in the reaction and evaporation process. Hence, when a thin liquid film of a multicomponents flows over a heated evaporator surface, under vacuum conditions (Table 3), the reaction inner the film and evaporation phenomenon at the free surface lead to cracking of heavier molecules and the depletion of the most volatile component or components in the liquid phase, forming a thin liquid film that, evenly, might to condense along the condenser surface. As a result, the distillate flow increases as consequence of: (i) High amount of molecules with low molar mass; (ii) the elevated film surface temperature; (iii) the decrease of the film thickness on the evaporator surface and, (iv) advantageous operating conditions on the centrifugal reactive molecular distillation process.

Moreover, results showed that the radial thermal gradients inner the thin liquid film produced a significantly change in the distillate mass flow rate (D) profiles. Figure 4 showed that

D varied strongly after the center of evaporator surface, representing how fast the front of liquid film flow advances along the evaporator surface and how the fluid flow changes into the vapor state over the evaporator surface, which means that the G_E and δ profiles are greatly influenced by EVT as operating condition.

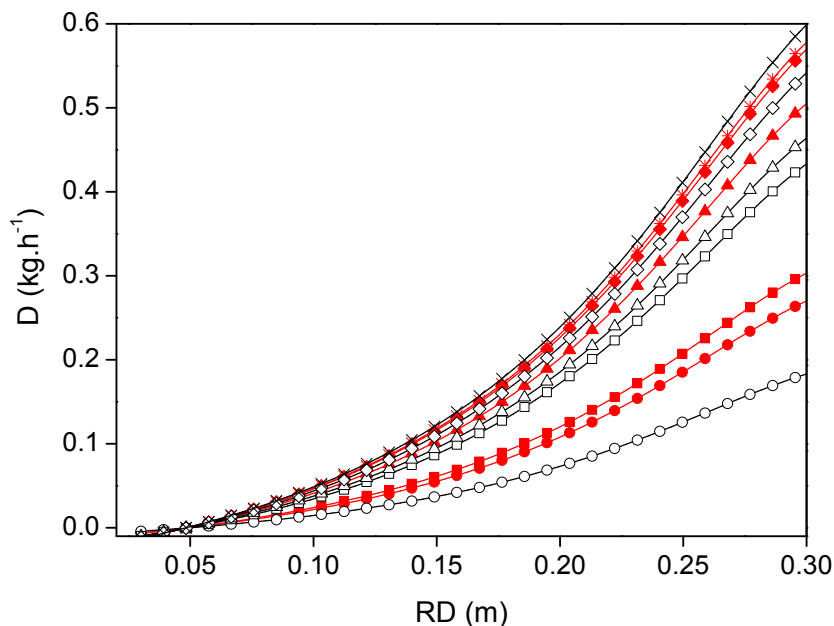


Figure 4. Distillate mass flow rate (D) profiles.
 Upgrading over 3% wt of catalyst: —●— 473.15 K; —■— 483.15 K; —▲— 498.15 K; —◆— 503.15 K; —*— 523.15 K
 Upgrading over 5% wt of catalyst: —○— 473.15 K; —□— 483.15 K; —△— 498.15 K; —◇— 503.15 K; —×— 523.15 K

However, in our previous paper was described that with higher EVT and % CAT values caused a larger molecule density and the distillate mass flow rate (D) may decrease as a consequence of the reduction in mass transfer within the thin film (Tovar, 2012). Nevertheless, in the evaporator temperature (EVT) range studied in the present work the split process is governed by the rise of EVT while the cracking process is driven at the cracking temperature between 473.15 K and 483.15 K when considered 3 – 5 wt% of catalyst and 40 – 50 Pa, respectively. Thus, when considered at EVT between 483.15 and 523.15 K the evaporation phenomenon at the free surface, leads to depletion of the most volatile component in the liquid phase, forming a thin liquid film and D varied strongly after the center of evaporator surface, representing how fast the front of liquid film flow advances along the evaporator surface and how the fluid flow changes into the vapor state over the evaporator surface.

On the other hand, the effective evaporation rate (G_E) was studied as a function of RD for various EVT values at a fixed feed flow rate (Figure 5). In this case, the functional path was as expected, following a relaxation length (0.15 m) corresponding to the center zone of the evaporator surface. Nevertheless, Figure 5 shows that the behavior of the effective evaporation rate (G_E) follows downward as a function of RD under different EVT conditions. Qualitatively, this result is in agreement with the CRMD process, and it is related to the temperature gradients, because the density of the molecules rises in the distillation gap, and the motion of the particles in the distillation gap might causes isotropic behavior due to successive cracking of heavier molecules inner the thin liquid film.

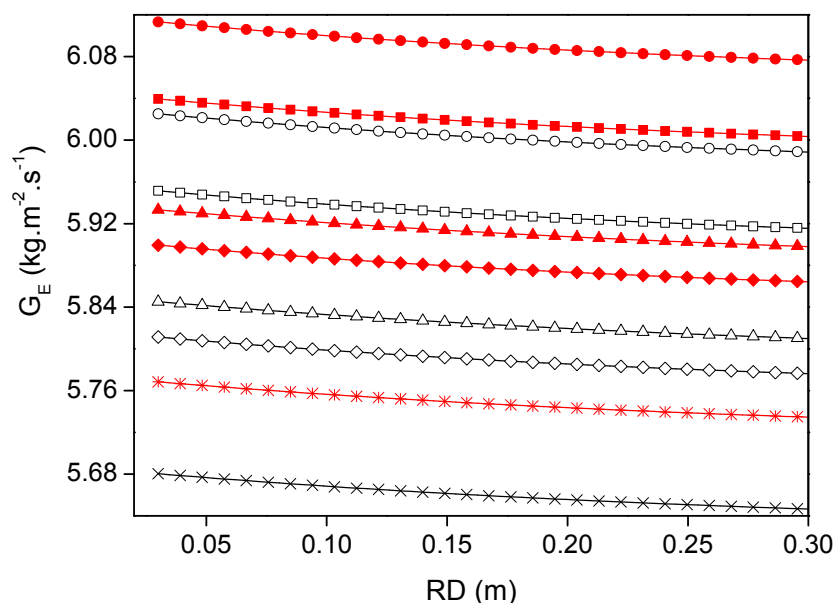


Figure 5. Effective evaporation rate (G_E) profiles.

Upgrading over 3% wt of catalyst: —●— 473.15 K; —■— 483.15 K; —▲— 498.15 K; —◆— 503.15 K; —*— 523.15 K
Upgrading over 5% wt of catalyst: —○— 473.15 K; —□— 483.15 K; —△— 498.15 K; —◇— 503.15 K; —×— 523.15 K

In Figure 6, it is presented the δ profile for different values of EVT at range from 423.15 K to 523.15 K and Q equal to $1.473 \text{ kg} \cdot \text{h}^{-1}$. The radial distance, RD , is plotted on the abscissa and the film thickness, δ , on the ordinate. It can be seen that the greatest changes in the film thickness profile occurred in the region between 0.03095 m to 0.1800 m corresponding to the entrance section of the feed material and center section of the evaporator surface. Analyzing the film

thickness profiles it was depicted that it decreases considerably with an increment in EVT , due to both the temperature dependence of the liquid viscosity and the effects of evaporation.

Analyzing the film thickness profiles, it was depicted a continuous decrease to 1×10^{-4} m. This is explained by the in-situ reaction of the heavier pseudocomponents, the depletion of the most volatile of the pseudocomponents produced, and the temperature gradient in the liquid film, caused by the heat exchange between the inner surface of the evaporator, the reaction heat and the evaporation heat.

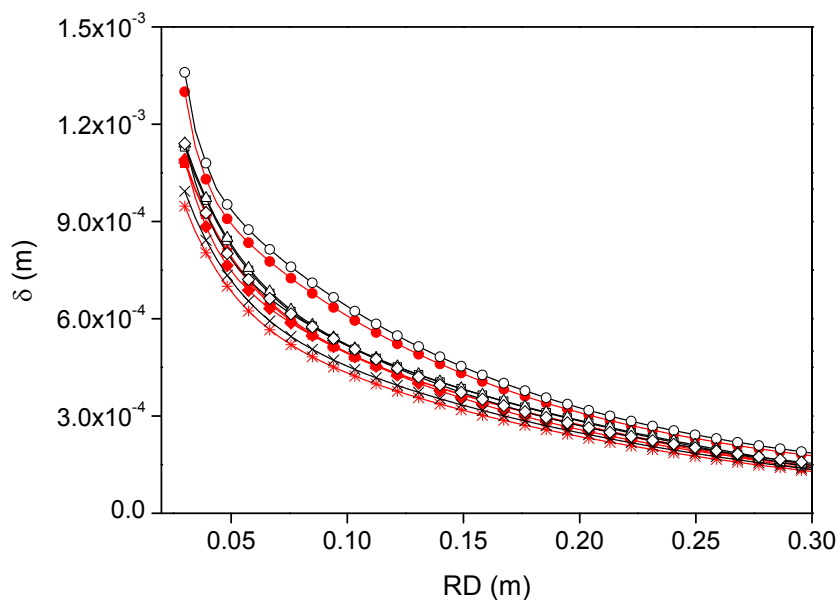


Figure 6. film thickness (δ) profiles in the evaporating liquid film.
Upgrading over 3% wt of catalyst: —●— 473.15 K; —■— 483.15 K; —▲— 498.15 K; —◆— 503.15 K; —*— 523.15 K
Upgrading over 5% wt of catalyst: —○— 473.15 K; —□— 483.15 K; —△— 498.15 K; —◇— 503.15 K; —×— 523.15 K

Figure 7 shows the variation in velocity at the evaporating surface. It can be seen that as the film thickness decreases at the outlet section of the evaporator, so the velocity decreases greatly. Figure 7 shows the development of the v_r along the evaporator length in r -direction. Given the dependence on the δ in relationship with the v_r , the v_r profiles were affected by the presence of catalyst in the system. Thus, it is noted that low v_r values were reached at the outlet of the evaporator surface. However, along the radial distance, it is guarantying in this conditions, that a uniform thin film promotes high efficiency in the mass and in the energy transfers.

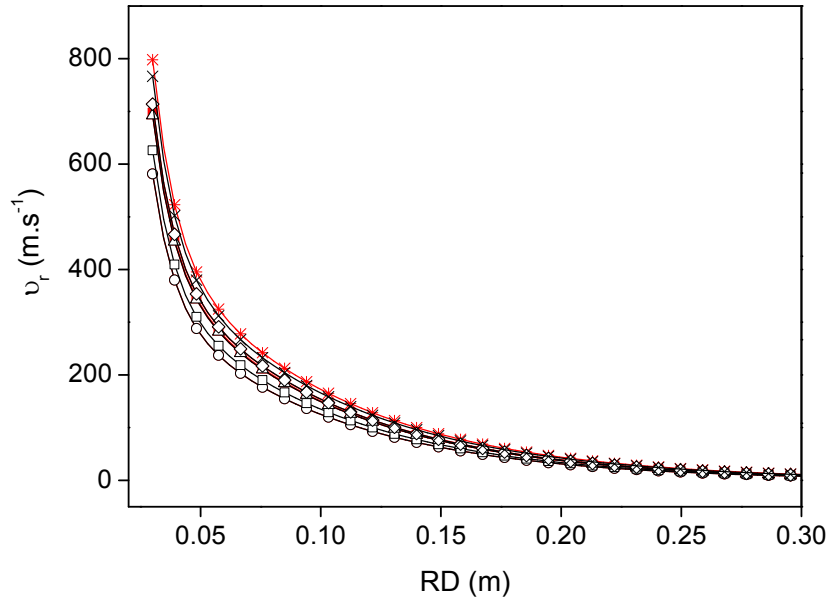


Figure 7. Velocity (v_r) profiles at the evaporating surface.
 Upgrading over 3% wt of catalyst: —●— 473.15 K; —■— 483.15 K; —▲— 498.15 K; —◆— 503.15 K; —*— 523.15 K
 Upgrading over 5% wt of catalyst: —○— 473.15 K; —□— 483.15 K; —△— 498.15 K; —◇— 503.15 K; —×— 523.15 K

Figure 8 shows the simulated liquid concentrations under the different operational conditions between 423.15 K and 523.15 K, for the case studies with 3 and 5 %wt of catalyst. Consequently, the concentration gradient driving the diffusion of pseudocomponent “a” from the evaporator surface into the bulk decreases rapidly, and the reaction inside the liquid film becomes the predominant pathway for the consumption of pseudocomponent “a”, such that the molar fraction of the products formed (X_{NPSEb}) increases.

Analyzing Figure 8b for pseudocomponent “b”, the highest gradient concentration can be seen when EVT is equal to 483.15 K, which is associated with the cracking temperature at 3 and 5 percent weight of catalyst. To illustrate the conversion of the pseudocomponents, Figures 9a – 9b show that, under the operational conditions of the CRMD, the pseudocomponents “a” and “b” reacted and evaporated along the entire length of the liquid film over the evaporator surface. A gradually decrease in the concentration of pseudocomponent “a” occurred in the liquid film (Figure 8b). Pseudocomponent “b” reacted in the presence of the catalyst, and its concentration increased in the liquid film as shown in Figure 8b. This behavior indicates that both pseudocomponents “a” and “b” continue changing during the CRMD process, and are present in both the distillate and residue streams.

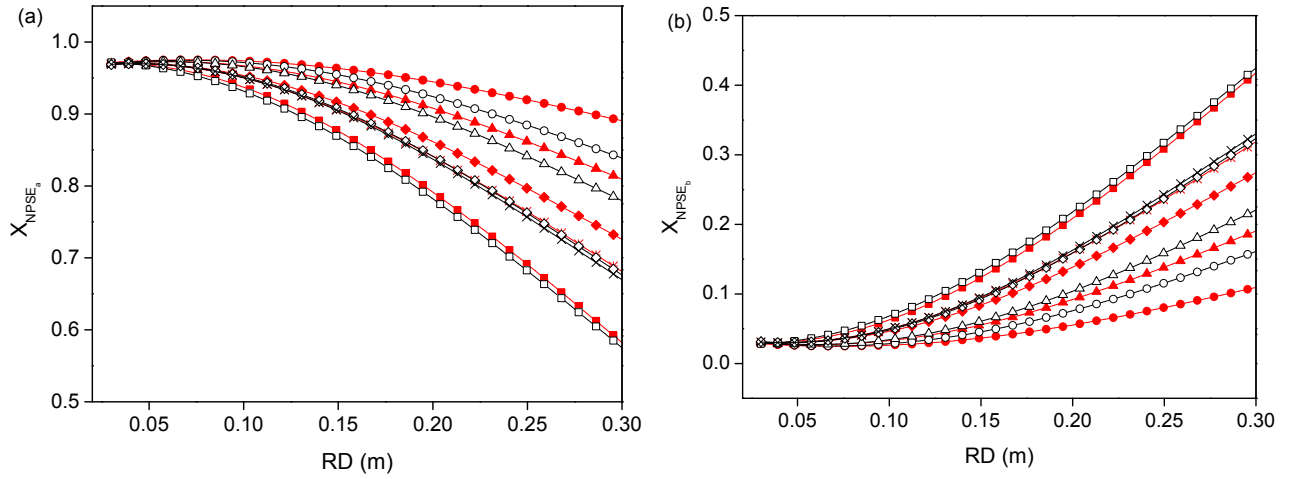


Figure 8. Composition profiles of pseudocomponents “a” and “b” in the evaporating film.
 Upgrading over 3% wt of catalyst: —●— 473.15 K; —■— 483.15 K; —▲— 498.15 K; —◆— 503.15 K; —*— 523.15 K
 Upgrading over 5% wt of catalyst: —○— 473.15 K; —□— 483.15 K; —△— 498.15 K; —◇— 503.15 K; —×— 523.15 K

In the particular case of the upgrading of high-boiling-point petroleum fractions using the CRMD process, one can consider that the conversion of the feedstock (ATR–W) into lighter products per unit of feed at the outlet section of the evaporator surface, may be expected to vary inversely (for the distillate stream) and directly (for the residue stream) with the radial distance (RD) along the evaporator surface. In this sense, the extent of conversion (α_D) of the ATR–W in the distillate stream can be defined as:

$$\alpha_D = 100 \left[1 - \frac{X_{NPSE_a}}{X_{NPSE_{a_F}}} \right] \quad (20)$$

Where $X_{NPSE_{a_F}}$ is the molar fraction of the $NPSE_a$ in the feedstock.

The extent of conversion (α_R) of the ATR–W in the residue stream can be expressed approximately as 100 minus the conversion in the distillate stream (α_D).

Figures 9a – 9b show the profiles of the extent of conversion for five different evaporator temperatures (EVT). It is clear that, in the residue stream, the cracking reaction advances during the CRMD process (as the RD increases), and consequently the molar fraction of pseudocomponent “b” increases. The conversion in the distillate stream expressed the increase in the amount of reactants ($NPSE_a$) consumed as the RD increased.

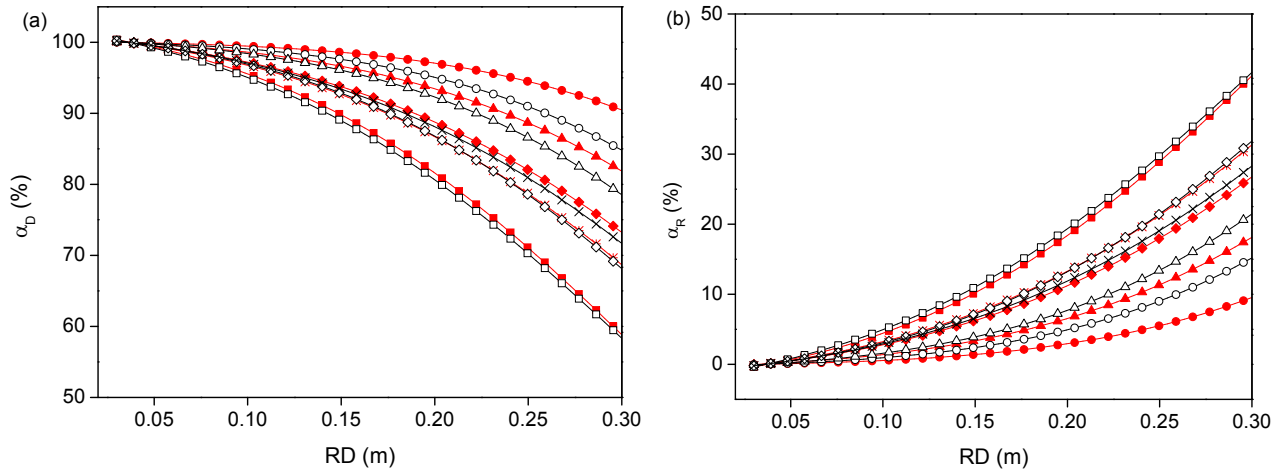


Figure 9. Conversion profiles in the evaporating film: (a) the distillate stream (α_D) and (b) the residue stream (α_R).
 Upgrading over 3% wt of catalyst: —●— 473.15 K; —■— 483.15 K; —▲— 498.15 K; —◆— 503.15 K; —*— 523.15 K
 Upgrading over 5% wt of catalyst: —○— 473.15 K; —□— 483.15 K; —△— 498.15 K; —◇— 503.15 K; —×— 523.15 K

4.2. Mathematical model verification

Experimental trials were carried out to investigate the liquid yield and conversion in the distillate and residue streams (Tovar, 2012; Winter, 2011). Table 4 shows the conversions in the distillate and residue streams as well as the experimental and simulated flow rates of the distillate stream, and it can be seen that the model is able to predict the key parameters such as the outlet flow rates and conversion degree quite satisfactorily.

Taking into account that the modeling approach is not exact, but approximate, its inaccuracy was evaluated by its approximation to the experimental data (Tovar, 2012; Winter, 2011) (Table 4). The results were evaluated in terms of average absolute deviation ($AAD\%$) which is defined as a relation among the absolute deviation of a predicted quantity divided by its experimental value ($y_{i,ref}$). The absolute deviation is defined as the difference between the experimental value ($y_{i,ref}$) and the response predicted by the modeling approach at each operating condition ($y_{i,cal}$) as follows:

$$AAD\% = (1/m) \sum_{i=1}^m \frac{|y_{i,cal} - y_{i,ref}|}{y_{i,ref}} * 100 \quad (21)$$

Table 4. Verification of the CRMD mathematical model.

Stream	Operating condition		Experimental data (y_{ref})		Predicted data (y_{cal})		Absolute deviations percent (%)	
	%CAT	EVT (K)	Mass flow rate (kg·h ⁻¹)	α	Mass flow rate (kg·h ⁻¹)	α	Mass flow rate (kg·h ⁻¹)	α
Distillate	3.0	473.15	0.28	94.0	0.270	84.8	0.036	0.098
	3.0	483.15	0.32	65.6	0.304	58.4	0.063	0.110
	3.0	498.15	0.54	83.4	0.505	78.6	0.065	0.058
	3.0	503.15	0.47	73.3	0.520	68.2	0.106	0.070
	3.0	523.15	0.59	77.0	0.570	67.5	0.034	0.123
	5.0	473.15	0.14	97.5	0.160	90.4	0.143	0.073
	5.0	483.15	0.41	64.3	0.434	59.1	0.059	0.081
	5.0	498.15	0.43	89.1	0.464	81.9	0.079	0.081
	5.0	503.15	0.50	83.8	0.542	73.2	0.080	0.126
	5.0	523.15	0.59	78.0	0.600	68.7	0.017	0.119
							AAD%=6.82%	AAD%=9.39%
Residue	3.0	473.15	2.35	12.5	NA	15.2	NA	0.216
	3.0	483.15	0.32	49.6	NA	41.6	NA	0.161
	3.0	498.15	1.95	21.1	NA	21.4	NA	0.014
	3.0	503.15	0.80	37.0	NA	31.8	NA	0.141
	3.0	523.15	1.49	29.4	NA	32.5	NA	0.105
	5.0	473.15	2.24	8.00	NA	9.6	NA	0.200
	5.0	483.15	0.36	53.1	NA	40.9	NA	0.230
	5.0	498.15	2.18	15.8	NA	18.1	NA	0.146
	5.0	503.15	1.67	22.4	NA	26.8	NA	0.196
	5.0	523.15	1.47	28.9	NA	31.3	NA	0.083
							AAD%= NA	AAD%=14.32

EVT: Evaporator temperature; %CAT: Percent weight of catalyst; NA: Not available.

$$AAD\% = (1/m) \sum_{i=1}^m \frac{|y_{i,cal} - y_{i,ref}|}{y_{i,ref}} * 100 \quad \text{Where } m \text{ equals } 10.$$

Consequently, the mathematical model gave a good representation of the experimental data related to the overall distillate mass flow rate (D) in the reactive centrifugal molecular distillation process since, the average absolute deviation ($AAD\%$) was of 6.82% . On the other hand, the extent conversion in the distillate stream (α_D) and the extent conversion in the residue stream (α_R) reported an average absolute deviation ($AAD\%$) of 9.39% and 14.32%, respectively.

The results presented here clearly demonstrated that the mathematical model proposed was able to predict the performance and steady-state behavior of the CRMD process, presenting good agreement with the experimental data at the outlet section and providing theoretical guidance for the further experimental runs and process optimization.

5. Conclusions

Verification of the mathematical model of the catalytic centrifugal reactive molecular-distillation process was discussed in this contribution. Extensive pilot plant experiments for the

upgrading of a petroleum residue (ATR–W) were used to validate the performance of the centrifugal reactive–molecular distillation process in the outlet section of the evaporator surface. The results presented in this work clearly demonstrated the accuracy and reliability of the mathematical model proposed, since the average absolute deviation (*AAD%*) was no larger than 6.82%, 9.39% and 14.32% for the distillate mass flow rate, the extent conversion in the distillate stream and in the residue stream, respectively.

The simulation of the centrifugal reactive–molecular distillation process led to the prediction of the characteristic profiles in the thin liquid film in terms of the variables evaporator temperature (*EVT*) and percent weight of catalyst (*%CAT*). Simulated data showed the presence of temperature and concentration gradients in the radial direction. The higher distillate mass flow rates were obtained at the higher evaporator temperatures. Nevertheless, an increase in the evaporator temperature caused a distinct decrease in the effective evaporation rate. The performance of the CRMD process was checked by the degree of conversion of the feedstock (ATR–W), determined by the overall rate of the cracking reaction of the reactants in the liquid film. It was shown that the concentration of pseudocomponent “a” decreased and the concentration of pseudocomponent “b” increased along the flow path.

The influence of the catalyst was analyzed. The results obtained showed that at 3 percent weight of catalyst, the centrifugal reactive–molecular distillation process worked under good operational conditions with a pressure of 41.6 Pa. Simulated data indicated a conversion equal to 49.6% of feedstock in the residue stream and 65.6% of feedstock in the distillate stream when considered 3 wt% of catalyst and a evaporator temperature (*EVT*) equals 483.15 K.

Acknowledgements

This research was supported by the Brazilian National Council for Technological and Scientific Development (CNPq), the Petrobras Research and Development Center (PETROBRAS/CENPES) and the Brazilian Study and Project Financing Institution (FINEP).

Nomenclature

a^*	= Compensation effect in Equation (46)	$[\text{mol} \cdot \text{kJ}^{-1} \cdot \text{min}^{-1}]$
A	= Pre–exponential factor	$[\text{min}^{-1}]$
b^*	= Compensation effect in Equation (46)	$[\text{min}^{-1}]$
C_p	= Specific heat capacity	$[\text{J} \cdot \text{kg}^{-1} \cdot \text{K}^{-1}]$
d_e	= Diameter of evaporation surface curvature	$[\text{m}]$

D	= Distillate mass flow rate	$[\text{kg} \cdot \text{h}^{-1}]$
$\mathbf{D}_{NPSE_i, \text{mix}}$	= Diffusion coefficient	$[\text{m}^2 \cdot \text{s}^{-1}]$
E	= Activation energy	$[\text{kJ} \cdot \text{mol}^{-1}]$
E_0	= E -dependence in Equation (47)	$[\text{kJ} \cdot \text{mol}^{-1}]$
E_1	= E -dependence in Equation (47)	$[\text{kJ} \cdot \text{mol}^{-1}]$
EVT	= Evaporator temperature	$[\text{K}]$
G_E	= Effective evaporation rate	$[\text{kg} \cdot \text{m}^{-2} \cdot \text{s}^{-1}]$
$k'' = k_{i,m,n}$	= Kinetic constant	$[\text{s}^{-1}]$
Kn	= Knudsen number	$[-]$
K_{OUP}	Universal Oil Products Company characterization factor	$[-]$
K_w	Watson characterization factor	$[-]$
k^*	= Anisotropy of vapor phase	$[-]$
L	= Distance between evaporator and condenser surfaces	$[\text{m}]$
M	= Molar mass	$[\text{kg} \cdot \text{kmol}^{-1}]$
MFP	= Mean free path	$[\text{m}]$
n'	= Number of intermolecular collisions before the vapor reaches the isotropic state ($n'=5$)	$[-]$
n_{NPSE_i}	= Number of moles of $NPSE_i$	$[\text{mol}]$
n_{NPSE_0}	= Number of moles of $NPSE_i$ at $\theta=0$	$[\text{mol}]$
$n_{NPSE_i, c}$	= Number of moles of n_{NPSE_i} on the catalyst in the reactive situation	$[\text{mol}]$
N	= Total number of pseudocomponents	$[-]$
N_m	= Number of molecules per volume unit of vapor phase	$[\text{mol} \cdot \text{m}^{-3}]$
N_A	= Avogadro Constant ($6.023 \times 10^{23} \text{ mol}^{-1}$)	$[\text{mol}^{-1}]$
N_T	= Total number of moles	$[\text{mol}]$
P_c	Critical pressure	$[\text{Pa}]$
P_s	= System pressure	$[\text{Pa}]$
P_{vap}	= Equilibrium vapor pressure	$[\text{Pa}]$
q_w	= Heating rate at evaporator wall	$[\text{J} \cdot \text{m}^{-2} \cdot \text{s}^{-1}]$
Q	= Feed flow rate	$[\text{kg} \cdot \text{h}^{-1}]$
Q'	= Flow rate over the evaporator surface	$[\text{kg} \cdot \text{h}^{-1}]$
Q_i	= Feed flow rate at $\theta = 0$	$[\text{kg} \cdot \text{h}^{-1}]$
r	= r - direction of coordinate system	$[-]$
R	= Universal gas constant ($8314 \text{ J} \cdot \text{K}^{-1} \cdot \text{kmol}^{-1}$)	$[\text{J} \cdot \text{K}^{-1} \cdot \text{kmol}^{-1}]$
$-r_{NPSE_i}$	= the rate of disappearance of the i^{th} pseudocomponent	$[\text{s}^{-1}]$
r_i	= Distance from the apex at which the liquid enters the cone	$[\text{m}]$
RD	= Radial distance	$[\text{m}]$
RS	= Rotor speed	$[\text{rpm}]$
s	= s - direction of coordinate system perpendicular to cone surface	$[-]$
SG	Specific gravity	$[-]$
t	= Time	$[\text{s}]$
T	= Temperature	$[\text{K}]$
T_{bi}	= Normal boiling point	$[\text{K}]$
T_c	= Critical temperature	$[\text{K}]$
T_{cond}	= Condenser temperature	$[\text{K}]$
T_{feed}	= Feed temperature	$[\text{K}]$
T_s	= Surface temperature	$[\text{K}]$

V_c	= Critical volume	$[\text{cm}^3 \cdot \text{mol}^{-1}]$
W_c	= Amount of catalyst	$[\text{kg}]$
X_a	= Molar fraction of pseudocomponent “a”	$[-]$
X_{NPSE_i}	= Molar fraction of i^{th} pseudocomponent ($NPSE_i$)	$[-]$
X_{sNPSE_i}	= Molar fraction of i^{th} pseudocomponent ($NPSE_i$) at the evaporating surface	$[-]$
X_{0NPSE_i}	= Molar fraction of i -th pseudocomponent ($NPSE_i$) at $\theta = 0$	$[-]$
$\%CAT$	= Percent weight of catalyst	$[\%wt]$
α	= Conversion degree	$[-]$
β'	= Half angle of the apex of the cone radius	$[-]$
δ	= Thickness of liquid film	$[\text{m}]$
(ΔH_{NPSE_i})	= Heat of evaporation of pseudocomponent i	$[\text{J} \cdot \text{kg}^{-1}]$
$(\Delta H_r)_{i,m,n}$	= Heat of reaction	$[\text{J} \cdot \text{kg}^{-1}]$
φ	= φ – direction of coordinate system	$[-]$
λ	= Thermal conductivity	$[\text{W} \cdot \text{m}^{-1} \cdot \text{K}^{-1}]$
θ	= θ – direction of coordinate system	$[-]$
ρ	= Average density and density fraction	$[\text{kg} \cdot \text{m}^{-3}]$
σ	= Molecule diameter	$[\text{m}]$
π	= Pi parameter	$[-]$
v_r	= Thin liquid film velocity in r -direction (radial velocity)	$[\text{m} \cdot \text{s}^{-1}]$
μ	= Dynamic viscosity	$[\text{Pa} \cdot \text{s}]$
ν	= Kinematic viscosity	$[\text{m}^2 \cdot \text{s}^{-1}]$
ω	= Angular velocity of cone	$[\text{s}^{-1}]$
ω_{ac}	= Acentric factor	$[-]$
$\zeta_{i,m,n}$	= Amount of coke formed when the i^{th} pseudocomponent ($NPSE_i$) cracks to produce the m^{th} and n^{th} pseudocomponents ($NPSE_m$ and $NPSE_n$)	$[\text{kg} \cdot \text{h}^{-1}]$
<i>Subscripts</i>		
i	= Inlet	
o	= Outlet	
$NPSE_i$	= i^{th} pseudocomponent	

References

- American Society for Testing Materials, ASTM D 7169. Standard test method for boiling point distribution of samples with residues such as crude oils and atmospheric and vacuum residues by high temperature gas chromatography. West Conshohocken, (Pennsylvania): ASTM International, 2011. 17p.
- Blanding F. H. (1953) Reaction rates in catalytic cracking of petroleum, *Industrial & Engineering Chemistry* **45**, 6, 1186–1197.
- Bruin S. (1969) Velocity distributions in a liquid film flowing over a rotating conical surface, *Chemical Engineering Science* **24**, 11, 1647–1654.

- Gupta , Rajkumar Satyapal. Modeling and simulation of fluid catalytic cracking unit. 2006, 142p. Thesis (Doctor of Philosophy) – Department of Chemical Engineering, Deemed University, India, 2006.
- Inuzuka M., Sugiyama R., Saito I., Yamada I., Hiraoka S., Ishikawa H., Banno, I. (1986) Analysis of heat and mass transfer in a centrifugal molecular still, *Journal of Chemical Engineering of Japan* **19**, 1, 14–20.
- Inuzuka M., Ishikawa H., Yamada, I., Hiraoka S., Aragaki T., Inukai Y., Erciyes A. T., Kobayashi S. (1989) Vaporization from liquid film of binary mixture in a centrifugal molecular still, *Journal of Chemical Engineering of Japan* **22**, 3, 291–297.
- Kawala Z., Stephan K. (1989) Evaporation rate and separation factor of molecular distillation in a falling film apparatus, *Chemical Engineering & Technology* **12**, 1, 406–413.
- Mathews, J. H., and Fink, K. K. (2004). *Numerical methods using Matlab* (4th edition ed.). New Jersey: Pearson Prentice Hall.
- Myers–Vacuum, 2010. Available in:< <http://www.myers-vacuum.com/index.shtml> >. Accessed in: November 10th. 2010.
- Tovar, Laura Plazas. Modeling and simulation of the centrifugal reactive molecular distillation: Development, assessment and application to upgrade high-boiling-point petroleum fractions. 2012, 442p. Ph. D. Thesis (Doctorate of Chemical Engineering) – School of Chemical Engineering, State University of Campinas, Campinas, 2012.
- Tovar L. P., Wolf Maciel M. R., Araujo A. S., Maciel Filho R., Batistella C. B., Medina L. C. (2011) Kinetic study on catalytic cracking of Brazilian high-boiling-point petroleum fractions. *Journal Thermal Analysis and Calorimetry*; doi: 10.1007/s10973-011-2068-6.
- Tovar L. P., Wolf Maciel M. R., Maciel Filho R., Batistella C. B., Ariza O. C., Medina L. C. (2011) Overview and computational approach for studying the physicochemical characterization of high-boiling-point petroleum fractions (350 °C+). *Oil & Gas Science and Technology*; doi:10.2516/ogst/2011150.
- Winter, Alessandra. Development of reactive molecular distillation technology : design and construction of the unit. 2011, 166p. Ph. D. Thesis (Doctorate of Chemical Engineering) – School of Chemical Engineering, State University of Campinas, Campinas, 2011.

Centrifugal reactive–molecular distillation: An intensified process–Part III

High–boiling–point petroleum fraction upgrading using the centrifugal reactive–molecular distillation process with a catalyst: high–temperature simulated distillation to evaluate the conversion products (distillate and residue streams)

Abstract

Centrifugal reactive–molecular distillation (CRMD), an intensified process using reactive and hybrid separations, was developed and implemented by LDPS/LOPCA/UNICAMP, sponsored by PETROBRAS/FINEP. This work deals with the development of experimental methodology to accomplish the upgrading of a heavy petroleum residue by centrifugal reactive–molecular distillation (CRMD). The experimental case study illustrated was a 673.15 K⁺ high–boiling–point petroleum fraction of “W” crude oil (atmospheric residue ATR–W). The influence of adding a catalyst (1, 3 and 5 %wt) was examined. In this process, 30 fractions (15 distillates and 15 residues) were obtained under different operating conditions: the process temperature (evaporator temperature) range was from 473.15 K to 523.15 K and the constant feed flow rate was 1.473 kg·h⁻¹.

Due to the complex composition of the products obtained by CRMD, high–temperature simulated distillation gas chromatography (HT–SimDis GC), based on ASTM D 7169 using a capillary column, played an important role as an analytical technique to evaluate the extent of conversion and to characterize the converted products. The analysis of the AEBP distribution as a function of the evaporator temperature (or CRMD temperature) revealed that the CRMD process with added 1, 3 and 5 percent by weight of catalyst, produced lighter fractions in the distillate stream and generated important changes in the >613.15 K analytical fraction when compared to the ATR–W feedstock (673.15 K⁺ high–boiling–point petroleum fraction). Significant changes were found in the >613.15 K and >813.15 K fractions of the residue streams, reaching an conversion of the feedstock of about 50% when using 3 and 5 percent by weight of catalyst.

Keywords: Centrifugal reactive–molecular distillation, simulated distillation gas chromatography, distillation temperature distribution, conversion, converted products.

Contents

1. Introduction
 - 1.1. High-temperature simulated distillation GC
2. Experimental
 - 2.1. Sample and catalyst
 - 2.2. Centrifugal reactive-molecular distillation experiments
 - 2.2.1. Centrifugal reactive-molecular still assembly
 - 2.2.2. The centrifugal reactive-molecular distiller operation
 - 2.3. High-temperature simulated distillation GC and ATR-W conversion
 - 2.3.1. Calibration of retention time scale
 - 2.3.2. Quantitation
 - 2.3.3. Repeatability test of HT-SimDis GC
 - 2.3.4. Feedstock conversion
3. Results and discussion
 - 3.1. Analysis of upgrading products
4. Conclusions
- Acknowledgment
- References

1. Introduction

According to the literature and the Brazilian National Agency of Petroleum (ANP), crude oil and oil fractions with an API gravity above 31 are considered “light”, between 22 and 31 are considered “middle”, between 10 and 22 are considered “heavy” and below 12 are considered “extra-heavy” (Canziani et al., 2009). Specifically, heavy and extra-heavy oils are characterized by a low H/C ratio, a viscosity larger than that of water, high molar mass hydrocarbons (asphaltenes and resins) and metals (Canziani et al., 2009; Rana et al., 2007).

In view of this, there is a growing interest in the petroleum industry for research and development into alternative technologies for upgrading heavy feedstock (HF) (high-boiling-point petroleum fractions and heavy oils) into high quality lower boiling point products with lower API gravity values, as well as a dynamic viscosity and molar masses of the lighter oil fractions as compared to HF, favoring the flow and transport properties.

In this context, the reactive molecular distillation (CRMD) process has been developed by the Separation Process Development Laboratory (LDPS) and the Optimization, Project and Advanced Control Laboratory (LOPCA) of the Chemical Engineering School of UNICAMP, sponsored by the Research Center of Petrobras-Brazil (CENPES/Petrobras) and Brazilian Study

and Project Financing Institution (FINEP), aiming to improve the upgrading of heavy petroleum fractions and heavy petroleum crude oil.

The CRMD process was presented in an earlier manuscript (Tovar, 2012), and in addition the modeling and simulation of the process were developed. The simulation provided useful data about the thin liquid film flowing over the conical evaporator surface inside the centrifugal reactive–molecular distiller, data used in the present study (Tovar, 2012). The CRMD process can be described as a hybrid intensified process, since it offers the “hardware” configuration and operating conditions which permit one to obtain a high vacuum, allowing the material to react at appropriate temperatures with short operating times, and ensuring very intensive contact with the surface of the catalyst. Therefore, according to the classification of Keil (2007) for intensified processes, the CRMD process can be introduced into this category as a consequence of the following features:

- Operations at lower temperatures, leading to a better control of the desired products.
- Higher rates of mass transfer due to the ability to expose the reactants to contact with the catalyst and to the process conditions.
- Operating conditions favoring the cracking reaction in a single step process involving reaction– evaporation–condensation.
- Flexibility of operating temperatures and pressures depending on the characteristics of the reactants, catalyst and products desired.
- Multidisciplinary approach, which considers the coupling of both the separation processes and cracking.

Using these special features, the CRMD process was applied in order to convert HF into lower boiling point products (corresponding to the distillate and residue streams), resulting from the subsequent catalytic reaction and evaporated compounds. Since not much information about processing high–boiling–point petroleum fractions using the CRMD process is available in the scientific literature, this work constitutes a great contribution to a better understanding of the CRMD process and its operating conditions. In this work, the experiments were carried out in the range of evaporator temperatures (*EVT*) from 473.15 K to 523.15 K, and the feed flow rate (*Q*) was fixed at 1.473 kg·h⁻¹. The influence of adding a catalyst (1, 3 and 5 % by wt) was examined.

The main purpose of adding the catalyst was to accelerate the cracking reaction process, taking advantage of the high vacuum conditions. A heterogeneous catalytic system was assumed, this being a system where the catalyst phase differs from that of the reactants involved. In this process, fifteen (15) distillate fractions and fifteen (15) reactive–molecular distillation residues were obtained. In order to evaluate the efficiency of the CRMD process, they were characterized by high–temperature simulated distillation GC (HT–SimDis GC).

1.1. High–temperature simulated distillation GC

Several methods have been applied to characterize and to determine the boiling point distribution (atmospheric equivalent boiling point, AEBP, distribution) of these materials (Adam et al., 2010; Boczkaj et al., 2011; Carbognani et al., 2007; Espinosa–Peña et al., 2004; Reddy et al., 1998). The distillation procedures, standardized by the American Society for Testing and Materials (ASTM) are summarized in Table 1.

Table 1. Summary of ASTM physical and simulated distillation procedures

Method	Scope	
ASTM D1160 (2006)	Distillation of petroleum products at reduced pressure	It covers the determination at pressures as low as 133.32 Pa, applied to fractions with final boiling points up to 773.15 K
ASTM D 2892 (2005)	Distillation of crude petroleum (15–theoretical plate column)	It covers the distillation of stabilized crude petroleum to a final cut temperature of 773.15 K atmospheric equivalent temperature (AET).
ASTM D 2887 (1997)	Boiling range distribution of petroleum fractions by gas chromatography	It covers the determination of the boiling range distribution of petroleum products and fractions having a boiling point between 328.65 K and 811.15 K.
ASTM D 3710 (1995)	Boiling range distribution of gasoline and gasoline fractions by gas chromatography	It covers the determination of the boiling range distribution of petroleum products and fractions with a final boiling point of 533.15 K or lower.
ASTM D 5236 (2003)	Distillation of heavy hydrocarbon mixtures (vacuum potstill method)	It covers the distillation of mixtures with initial boiling points greater than 423.15 K, such as heavy crude oils, bitumens, residues or synthetic mixtures. A temperature up to 838.15 K can be attained.
ASTM D 5307 (2007)	Determination of boiling range distribution of crude petroleum by gas chromatography	This method covers the determination of the boiling range distribution of water–free crude petroleum up to 811.15 K and reports material above this temperature as a residue. It is applicable to whole crude oils that can be dissolved in CS ₂ .
ASTM D 6352 (2009)	Boiling range distribution of petroleum distillates in the boiling range from 174 to 700°C by gas chromatography	This method covers the determination of the boiling range distribution of petroleum distillate fractions with initial temperature above 447.15 K and final boiling point below 973.15 K.
ASTM D7169 (2011)	Boiling point distribution of samples with residues such as crude oils and atmospheric and vacuum residues by high temperature gas chromatography	This method covers the boiling range distribution of crude oils and residues with a final boiling point of 993.15 K or lower, using an external standard. This method essentially extends the applicability of ASTM D 6352 to samples which do not completely elute from the GC column.

The HT–SimDis GC analyses carried out in this work were based on ASTM D 7169 (2011), which is applicable to petroleum products having a final boiling point of 993.15 K or

lower. The HT–SimDis analysis data were processed and reported according to the cut point ranges proposed by Altgelt and Boduszonski (1994), assuming that the FBP (final boiling point) was higher than 973.15 K (Table 2).

Table 2. Boiling point ranges proposed by Altgelt and Boduszonski (1994).

Fraction	Atmospheric equivalent boiling point distribution, AEBP		
	°C	K	°F
Light naphtha	IBP (°C)–130	IBP (K)–403.15	IBP(°F)–266
Heavy naphtha	130–220	403.15–493.15	266–428
Atmospheric gas oil	220–340	493.15–613.15	428–644
Light gas oil	340–450	613.15–723.15	644–842
Heavy vacuum gas oil	450–540	723.15–813.15	842–1004
Extra heavy gas oil	540–720	813.15–993.15	1004–1328
Non-distillable residue	>720	>993.15	>1328

2. Experimental

2.1. Sample and catalyst

For the experimental study, a Brazilian crude oil with an API gravity lower than 16 °API was distilled by conventional atmospheric distillation (ASTM D 2892, 2005), producing an atmospheric distillation residue (ATR–W). Thus, an atmospheric petroleum residue (11.9 °API, 3.8359 at 343.15 K Pa.s) of “W” crude oil constituted the raw material used in the CRMD process, and was supplied by the Petrobras Research and Development Center (CENPES–Brazil)

A heterogeneous catalytic system (refers to the form of catalysis where the phase of the catalyst differs from that of the reactants) was assumed using the zeolite–based catalyst CR–1 (regenerated catalyst used for FCC technology containing 48.3 %wt of alumina, and particle size of 67µm). The influence of adding a catalyst at 1, 3 and 5 % by wt was also studied. The primary properties of CR–1 are listed in Table 3.

Table 3. Properties of CR–1 catalyst.

Property	Value
Micro Activity testing, %	69
Surface area, m ² ·g ^{−1}	53
Particle size distribution, µm	67
Al ₂ O ₃ , %wt	48.3
Rare earth oxide RE ₂ O ₃ (RE = Y, Gd, Nd and La), %wt	2.85
Carbono, %wt	0.08

2.2. Centrifugal reactive–molecular distillation experiments

2.2.1. Centrifugal reactive–molecular still assembly

Figure 1a shows the device used for the CRMD process. A more detailed description of the experimental pilot plant was presented in Winter (2011). The centrifugal reactive–molecular still consists of the evaporator itself (Figure 1b) with an electric heating system and a cooling–condensation system (dome). Two display glass ports are disposed in the condenser dome. Both the evaporator (reaction/evaporation surface) and condenser systems were constructed in series 316 stainless steel.

The conical surface rotates at an angular velocity of ω and the liquid is brought up to the cone surface along the radial length. The evaporator has a conical shape and the rotational movement is conferred on it by an electric motor. The use of the central rotational heated disk is a mechanical way of creating a thin liquid film uniformly distributed over the evaporator surface. The better half cone angle of the rotor was 70° , information obtained experimentally by Myers–Vacuum (Myers–vacumm, 2010). This angle allows for good spreading of the liquid on the surface of the rotor, allowing for the formation of a thin liquid film that passes through the heated disk and makes contact with the condenser surface.

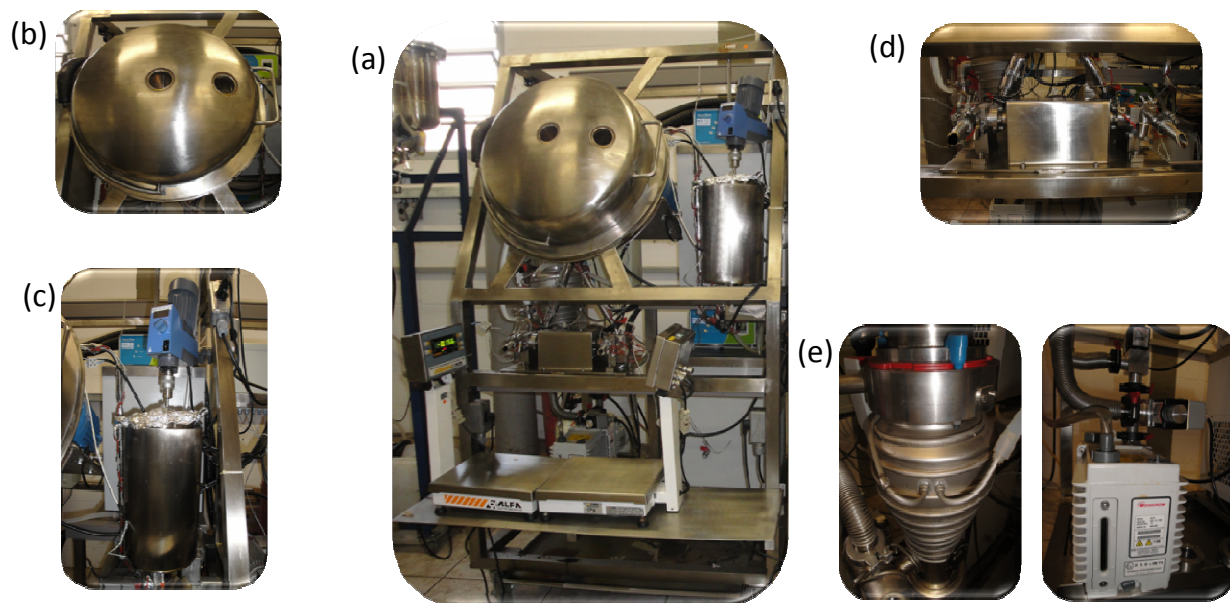


Figure 1: a) Centrifugal molecular distiller module; (b) molecular distillation device (evaporator–condenser); (c) Feeding and stirring systems; (d) Collector system; and (e) Vacuum system: diffusion pump (left) and mechanical pump (right).

The construction parameters and operating conditions such as rotor speed, evaporator radius (defined as 0.26 m), distance between the evaporator and condenser (defined as 0.08 m); ratio between the condenser and evaporator areas, and condenser temperature (related to evaporation efficiency) were studied in Winter (2011).

The module was completed by a vacuum system composed of a combination of several vacuum pumps in series, consisting of a mechanical pump (40 Pa) and a diffusion pump (0.1 Pa) (Figure 1e). The vacuum configuration contained valves and a trap system to retain volatile molecules arising during the process.

The operational capacity was from 05 to 40 liters per hour and the temperature range between 298.15 K and 623.15 K. The feed and distillate product lines (distillate and residue streams) were made from series 316 stainless steel, equipped with check valves to allow for continuous feed/discharge of the materials.

2.2.2. The centrifugal reactive–molecular distiller operation

The centrifugal reactive–molecular distiller operates in a continuous and steady state. After setting the flow conditions (Q) and evaporator temperature (EVT), the tests were started. The equipment was first operated using the control panel to reach the desired operational conditions, and approximately 2 hours were necessary to stabilize the system. The experiments were carried out based on the operational conditions described by simulated the results obtained previously using the DESTMOL–R (computational tool developed in FORTRAN–90 language using Compaq Visual Fortran compiler developed by Tovar (2012)). Figure 2 shows a sketch of the operation of the CRMD unit, and Table 4 describes the experimental conditions for upgrading the ATR–W using the CRMD where the catalyst CR–1 was mixed with the atmospheric petroleum residue, constituting the load to the CRMD process (a heterogeneous catalytic system).

The steps of the distillation process can be described as follows:

Feeding stage: The catalyst CR–1 was assumed mixed with the high–boiling–point petroleum fraction, constituting the load to the CRMD process. The material, which is kept in a storage tank with a heating system, is fed to the center of the evaporator at a pre–established flow rate using a gear pump. The evaporator rotates at a fixed velocity of 540 rpm, and the centrifugal force is responsible for forming a uniform thin liquid film that flows over the evaporator surface, set at the pre–established temperature (evaporator temperature, EVT).

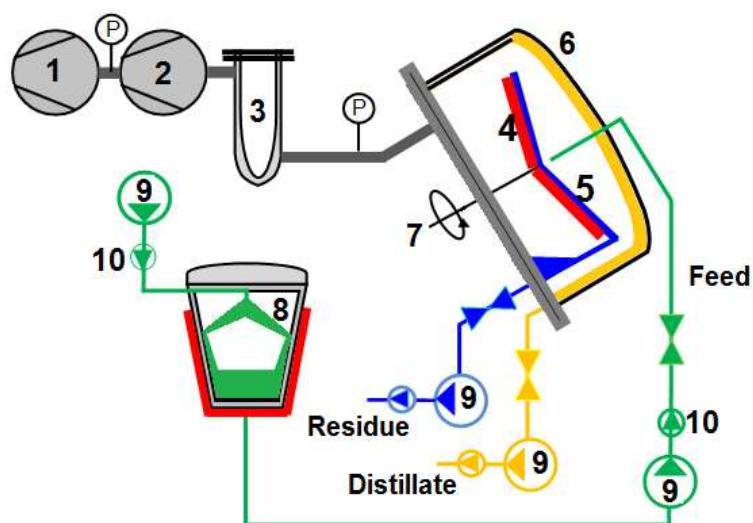


Figure 2. Scheme of the centrifugal reactive-molecular distiller. 1. Backing/Roughing Vacuum Pump; 2. Diffusion Ejector Pump (high Vacuum); 3. Chamber Trap; 4. Heater rotor; 5. Evaporator surface; 6. Dome condenser; 7. Rotor; 8. Feed storage; 9. Liquid Transfer Pump; and 10. Check Valve Rotor. Modified Myers-Vacuum (2010).

Table 4. Operational conditions established to processing the ATR-W sample by CRMD process.

Operating conditions						
Feeding temperature		423.15 K				
Condenser temperature		353.15 K				
Trap cooler temperature		273.15 K				
Rotor speed		540 rpm				
Stream products temperature (D/R)		353.15K / 423.15 K				
Process	%CAT (%wt)	EVT (K)	Q (kg·h ⁻¹)	P_s (Pa)	Distillate stream name	Residue stream name
Reactive centrifugal-molecular distillation (CRMD)	1	473.15	1.473	28.6	D1-1%	R1-1%
		483.15		(pressure reached after adding the zeolite-based catalyst)	D2-1%	R2-1%
		498.15			D3-1%	R3-1%
		503.15			D4-1%	R4-1%
		523.15			D5-1%	R5-1%
	3	473.15		41.6	D1-3%	R1-3%
		483.15		(pressure reached after adding the zeolite-based catalyst)	D2-3%	R2-3%
		498.15			D3-3%	R3-3%
		503.15			D4-3%	R4-3%
		523.15			D5-3%	R5-3%
	5	473.15		50.0	D1-5%	R1-5%
		483.15		(pressure reached after adding the zeolite-based catalyst)	D2-5%	R2-5%
		498.15			D3-5%	R3-5%
		503.15			D4-5%	R4-5%
		523.15			D5-5%	R5-5%

%CAT: Percentage weight of catalyst; EVT: Evaporator temperature; Q : Feed flow rate; P_s : Pressure inside the vacuum chamber (pressure inside the evaporator surface); D: distillate stream; R: Residue stream.

Conditioning vacuum stage: The high vacuum in the centrifugal reactive–molecular still is attained using a mechanical pump. The system uses a bath to cool and condense the molecules in a collector system located behind the mechanical pump. Furthermore, the influx of the molecules of components evaporated into the free film surface occurs quickly as a result of high vacuum in the system (<50 Pa). However, two types of molecules contribute to increase the pressure therein; these are molecules of the residual gas formed by atmospheric air which seeps into the catalyst, and any other gas which may be dissolved in the distilled mixture originally and the molecules of steam distilled. In this sense, the processing of a high-boiling-point petroleum fraction (ATR–W 673.15 K⁺) in a heterogeneous catalytic system with an ultimate goal of developing practical catalytic system for specific chemical transformations, causes a increases in the pressure system from 0.4 Pa to 28.6 Pa when it is added 1 %wt of a zeolite–based catalyst, from 0.4 Pa to 41.6 Pa when it is added 3 %wt of a zeolite–based catalyst, and from 0.4 Pa to 50.0 Pa when it is added 5 %wt of a zeolite–based catalyst.

Film formation and reaction–vaporization–condensation stage: The film is formed as a result of the distribution of the liquid sample on the conical surface of the evaporator, reaching a characteristic thickness of about 1×10^{-4} m. Having satisfied the essential conditions of the CRMD process (high vacuum conditions, thin film thickness and a distance between the evaporator and condenser to the same order of magnitude as the mean free path), the catalytic cracking reaction takes place and the phenomenon of vaporization of the volatile molecules begins. In heterogeneous catalysis, the reactants diffuse to the catalyst surface and adsorb onto it, via the formation of chemical bonds. After, the products desorb from the surface and diffuse away. On the other hand, the evaporated molecules travel through the evaporation gap to the surface of the condenser.

Collection of the products stage: The products obtained (distillate and residue streams) are collected in a gutter concentric to the rotor and removed from the distiller. There is no need to break the vacuum to collect the products. The heaviest non–evaporated residue slides off the rotor into a collecting gutter.

2.3. High–temperature simulated distillation GC and ATR–W conversion

The HT–SimDis GC analyses were performed using an Agilent Technologies 7890A gas chromatograph (GC) equipped with a temperature cool on–column injector and flame ionization

detector (FID). The suitable column temperature program and flame ionization detector temperature were established after several tests. The GC conditions used in this work were as follows: initial oven temperature, 313.15 K; rate, 10 K·min⁻¹; final temperature, 703.15 K; final time, 5 min; total run time, 44 min. A FID system set at 703.15 K was used for detection. The H₂, air and N₂ (make up) flows were, respectively, 35, 350 and 30 mL·min⁻¹. The temperature of the column was programmed from 323.15 K to 703.15 K at 15 K·min⁻¹.

The products (distillate and residue streams obtained from the CRMD process) were diluted with carbon disulfide (CS₂) at a concentration of approximately 2.0% by wt. High purity CS₂ (purchased from *Vetec*, Rio de Janeiro – Brazil) was used as the solvent because of its miscibility with the samples, low boiling point and low response factor in the FID (Falla et al., 2006). The samples were injected with an automatic injector (Agilent Technologies 7683 B Series) to maximize reproducibility. 1 µL of this solution was injected into a high-temperature silica capillary column (stationary phase of polydimethylsiloxane, 6 m in length, i.d. of 530 µm, and 0.15 µm of film thickness; from Wasson KC100). The analyses were carried out with a constant helium flow of 22.5 mL·min⁻¹. The velocity of the carrier gas was 160.57 cm·s⁻¹.

A computer-based chromatography data system (Agilent GC ChemStation software, B.03.02) was used for the data acquisition. The SimDis curves were obtained using the algorithm defined in the ASTM D 7169 (2011) standard method using the SimDis software (AscentSimDis for netCDF A06.01 V1.012409) provided by Wasson–ECE Instrumentation.

2.3.1. Calibration of retention time scale

Calibration of the standards in the range from C5 to C110 was carried out using a *n*-paraffins mixture (C5 – C24) (Agilent technologies batch no. CE-1983, Catalogue n°. 5080-8716), and poliwx (Poliwax 1000, Resket Corporation batch n°. A067718, Catalogue n°. 36227). The standards, obtained from commercial suppliers, were dissolved in CS₂ to about 2% by wt. The calibration curve was verified using a reference standard (Reference gas oil ASTM D 2887, Agilent technologies batch n°. 248873). The resulting chromatograms are presented in Figure 3.

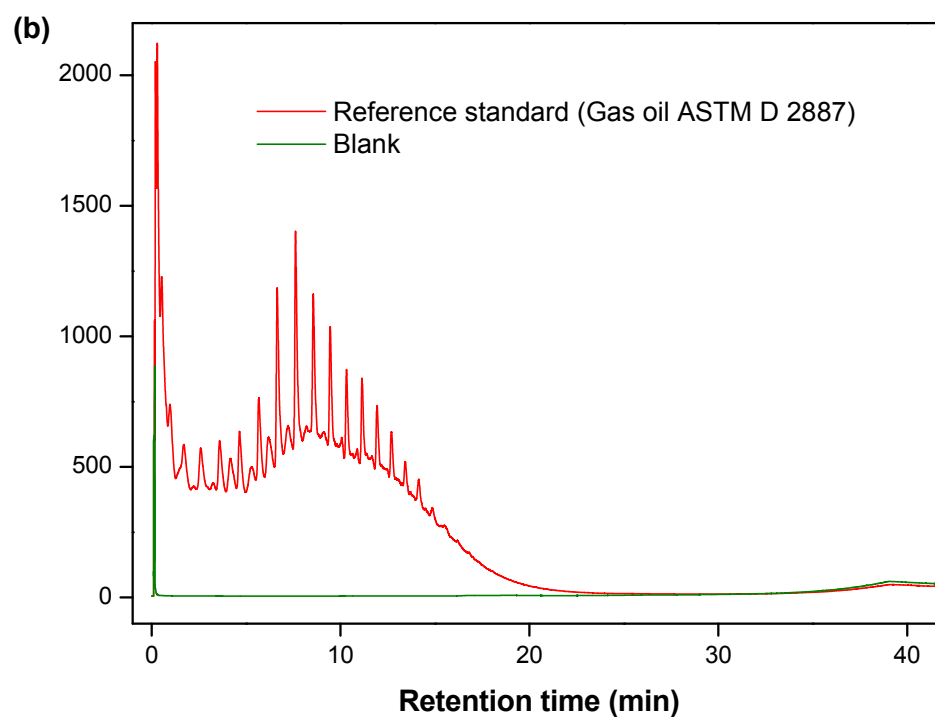
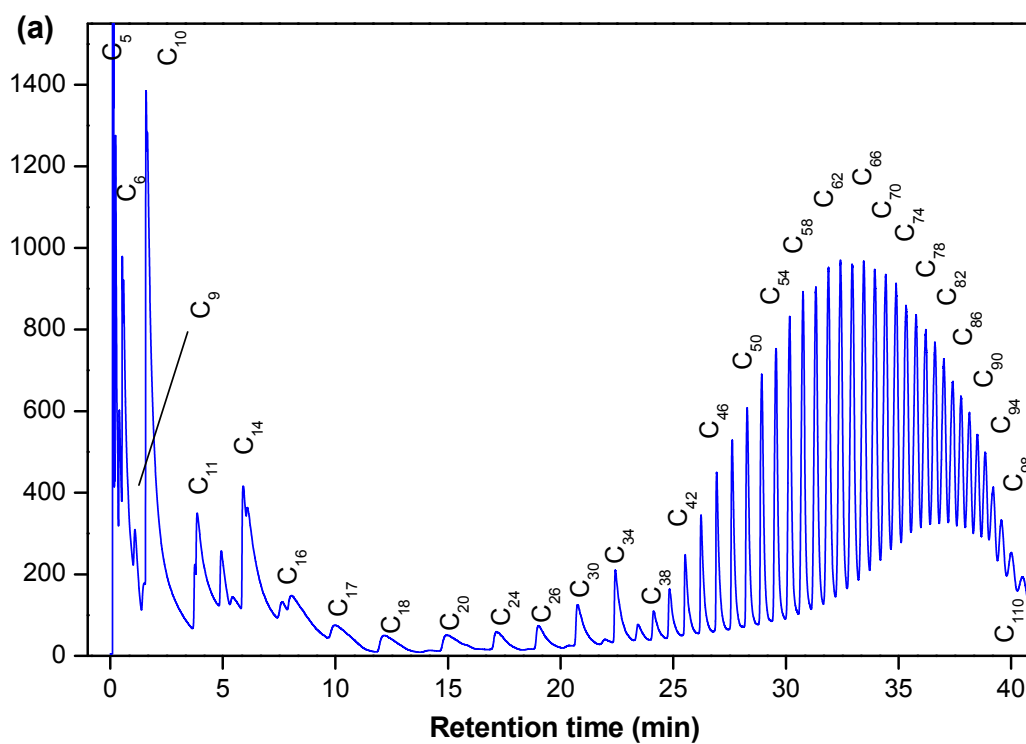


Figure 3. HT-SimDis gas chromatograms of (a) the Poliwax standard (Poliwax 1000, Resket Corporation batch no. A067718, Catalogue n°. 36227); (b) blank and reference standard (Reference gas oil ASTM D 2887, Agilent technologies batch no. 248873).

2.3.2. Quantitation

For quantification, the detector signal was integrated every 0.1 min. The blank analysis was carried out under the same conditions, and repeated periodically because of the habitual chromatographic baseline instability existing from sample to sample. The signal corresponding to the blank run was subtracted in the data processing using the SimDis software (AscentSimDis for netCDF A06.01 V1.012409).

2.3.3. Repeatability test of HT–SimDis GC

In order to evaluate the repeatability of the group peak, the relative standard deviation (% RSD) with respect to the mean signal of each peak, calculated from three (03) consecutive repetitions of the Poliwax standard, ATR–W sample, D3–3% (distillate stream obtained from the CRMD process) and R3–3% (residue stream obtained from the CRMD process) was examined. The values obtained, corresponding to the Poliwax standard, ATR–W, D3–3% and R3–3%, were lower than 5.8%.

2.3.4. Feedstock conversion

The feedstock (ATR–W) conversion using the CRMD process was calculated from the fractions with boiling points of >613.14 K and >813.15 K, based on the yields for the liquid distillate (% D_{yield}) and liquid residue (% R_{yield}) (Reddy et al., 1998). Based on the work developed by Blanding (1953), the conversion, defined on these bases (% D_{yield} and % R_{yield}), is equivalent to 100 minus the mass percent of liquid material with boiling points above 613.15 K and 813.15 K according to the simulated distillation curve, obtained by HT–SimDis GC, as presented in Equations (1) – (2).

$$\alpha_{>613.15} = 100 - \frac{(\%D_{yield} \text{ or } \%R_{yield}) * \%product, \text{ based on feed, above } 613.15 \text{ K}}{100 - \% \text{ below } 613.15 \text{ K in feed}} \quad (1)$$

$$\alpha_{>813.15} = 100 - \frac{(\%D_{yield} \text{ or } \%R_{yield}) * \%product, \text{ based on feed, above } 813.15 \text{ K}}{100 - \% \text{ below } 813.15 \text{ K in feed}} \quad (2)$$

3. Results and discussion

3.1. Analysis of upgrading products

The HT-SimDis gas chromatograms of the ATR-W 673.15 K⁺ high-boiling-point petroleum fraction contained two major peaks (Figure 4). The first and second peaks corresponded to AEBPs of about 740.37 K and 981.23 K, respectively.

Figures 5a – 5b compare the HT-SimDis gas chromatograms of the distillate and residue products obtained using 3 % by wt of catalyst at an evaporator temperature between 473.15 K and 523.15 K. As compared to that of the ATR-W feedstock, the chromatogram of the distillate products had much lighter compounds, whilst the second GC peak, corresponding to the heavy fractions, had disappeared.

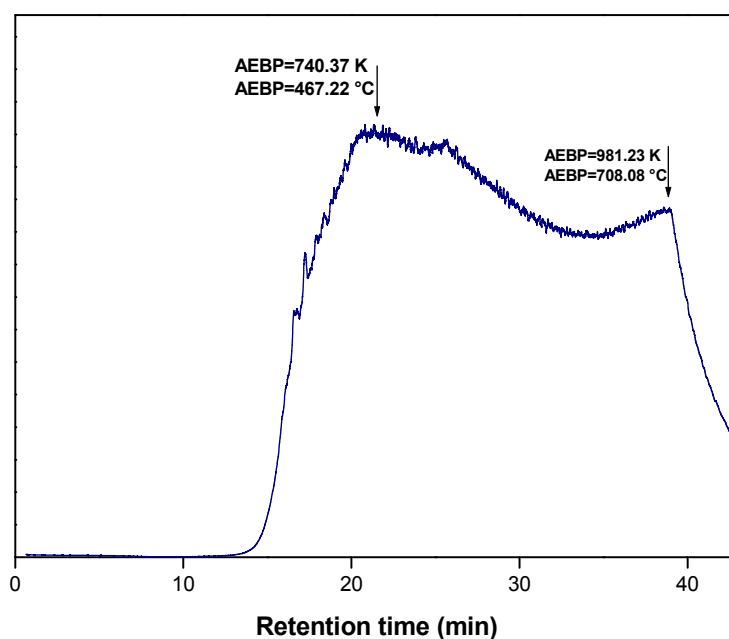


Figure 4. HT-SimDis gas chromatograms of ATR-W.

The HT-SimDis gas chromatograms of D1-3%, D2-3%, D3-3%, D4-3% and D5-3% only showed one major peak, corresponding to AEBPs of about 616.15 K, 620.15 K, 628.15 K, 629.15 K and 630.15 K, respectively.

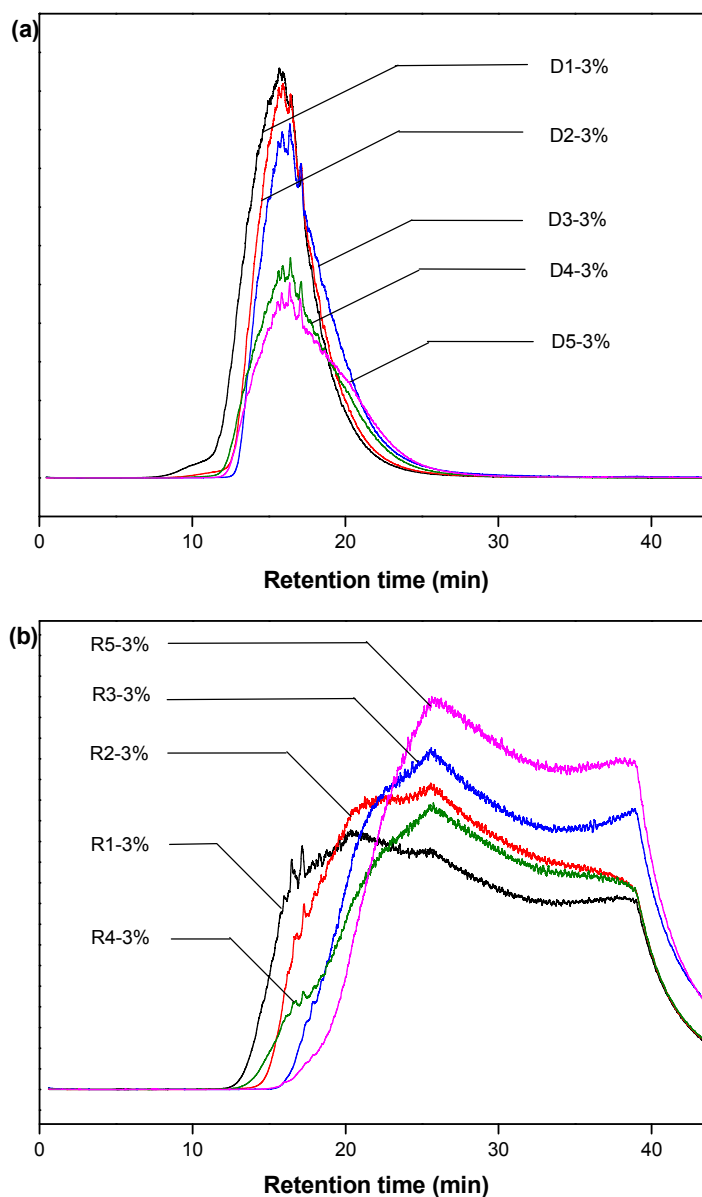


Figure 5. HT-SimDis gas chromatograms of the products from the CRMD upgrading process with 3% by wt of catalyst at an evaporator temperature between 473.15 K and 523.15 K. (a) Distillate streams and (b) Residue streams.

One interesting aspect can be observed in the residue chromatograms presented in Figure 5b; the shape of the HT-SimDis gas chromatogram suggests that two regions can be considered. The first one, spanning from the injection point up to about 18.5 min, corresponds to lighter products. The other region (heavier compounds) starts at about 18.5 min and ends at approximately 38 min. Considering this paramount, the chromatogram of the residue products has lighter compounds and the second GC peak corresponds to the heavy compounds, eluting at a lower temperature when compared to the ATR-W HT-SimDis gas chromatograms (Figure 4).

Thus the HT-SimDis gas chromatograms of the R1–3%, R2–3%, R3–3%, R4–3% and R5–3% residue products (Table 4) contain two major peaks (Figure 5b). The first peak corresponds to AEBPs between 704.15 K and 815.15 K, and the second peak corresponds to AEBPs between 981.15 K and 982.15 K. In the same way, analogous HT-SimDis gas chromatograms were obtained with 1 and 5 % by wt of catalyst, and similar trends were observed.

Table 5 shows the AEBP distribution of the ATR–W and of the converted products (distillates and residues) obtained using HT-SimDis, and classified according to their boiling point ranges. The AEBP distribution in Table 5 reveals that both the distillate and residue products presented lower boiling point temperatures. Furthermore, in the case of the distillate products, most of the 813.15 K fraction was converted, reaching 100 % of conversion when compared to the products from the residue streams. Consequently, in the distillate products, the fractions between IBP (K)–613.15 K and 613.15–723.15 K increased significantly during the CRMD processing of the ATR–W between 473.15 K and 523.15 K (operational temperature, *EVT*). It is worth mentioning that the distillate products are clearly different from the feedstock. Nevertheless the residue products are also different from the feed, although at first sight, present similarities. Analyzing the distillate streams, it can be seen that between 473.15 and 498.15 K there is a significant change in the >813.15 K fraction, and in addition, an increase in *EVT* led to a significant conversion of the IBP(K)–613.15 K and 613.15–723.15 K AEBP material fractions into lighter fractions, when compared with the feedstock (ATR–W).

Furthermore, it was revealed that the *EVT* (CRMD temperature or evaporator temperature) had a significant effect on the distribution of the residue products, particularly on the >813.15 K fractions. An evaporator temperature below 523.15 K led to a significant conversion (around 50%) of the 813.15–973.15 K AEBP materials, which means that increasing the *EVT* to between 473.15 K and 523.15 K leads to the production of considerable amounts of lighter fractions from the ATR–W feedstock. Hence, it was also possible to obtain the scenario for the CRMD experiments. The data from Table 5 show two interesting aspects with respect to the analyses: (i) some particular fractions such as: <723.15 K, 723.15–813.15 K and >813.15 K can represent heavy, medium and light fractions, respectively; and (ii) cracking effects are induced by the catalytic reaction and evaporator temperatures (*EVT*). Thus the most favorable conditions for upgrading the ATR–W by CRMD must be carried out between 473.15 K and 498.15 K using 3 % by wt of catalyst.

Table 5. HT-SimDis GC analysis of products obtained by the ATR-W processed using CRMD over catalyst.

Sample	Atmospheric equivalent boiling point distribution (wt%)					Liquid yield (wt%)	Conversion of fractions (%)	
	IBP(K)-613.15	613.15-723.15	723.15-813.15	813.15-973.15	973.15-FBP(K)		>613.15	>813.15
ATR-W	0.8	20.4	23.2	49.0	6.6			
D1-1%	31.1	62.9	6.0	0.0	0.0	10.1	93.0	100.0
D2-1%	36.2	57.0	6.9	0.0	0.0	16.5	89.4	100.0
D3-1%	24.2	67.6	8.1	0.0	0.0	21.7	83.4	100.0
D4-1%	20.7	67.8	10.7	0.9	0.0	24.8	80.2	99.6
D5-1%	16.9	65.0	16.3	1.9	0.0	30.8	74.2	99.0
D1-3%	43.3	53.7	3.0	0.0	0.0	10.5	94.0	100.0
D2-3%	31.7	64.3	4.0	0.0	0.0	50.0	65.6	100.0
D3-3%	24.0	68.2	7.8	0.0	0.0	21.7	83.4	100.0
D4-3%	28.3	62.5	9.2	0.0	0.0	36.9	73.3	100.0
D5-3%	23.6	62.8	12.6	0.9	0.0	29.9	77.0	99.5
D1-5%	57.6	40.2	2.2	0.0	0.0	5.9	97.5	100.0
D2-5%	33.6	60.2	6.2	0.0	0.0	53.5	64.3	100.0
D3-5%	34.0	60.5	5.6	0.0	0.0	16.4	89.1	100.0
D4-5%	30.0	62.7	7.3	0.0	0.0	23.0	83.8	100.0
D5-5%	24.1	62.2	13.2	0.5	0.0	28.8	78.0	99.7
R1-1%	0.0	22.0	23.6	49.1	5.3	89.9	9.5	12.1
R2-1%	0.0	15.6	24.8	53.6	6.0	83.5	15.8	10.5
R3-1%	0.0	11.8	25.1	56.7	6.4	78.3	21.1	11.3
R4-1%	0.0	7.9	24.0	59.8	8.3	75.2	24.2	8.0
R5-1%	0.0	1.7	22.1	68.4	7.9	69.2	30.3	5.2
R1-3%	3.0	24.0	21.8	45.4	5.8	89.5	12.5	17.7
R2-3%	0.0	19.4	22.1	52.9	5.6	50.0	49.6	47.4
R3-3%	0.0	10.4	24.8	57.1	7.6	78.3	21.1	8.9
R4-3%	1.0	13.4	23.8	55.6	6.3	63.1	37.0	29.8
R5-3%	0.0	5.1	22.8	63.6	8.5	70.1	29.4	9.1
R1-5%	3.0	23.9	21.3	45.9	5.9	94.1	8.0	12.4
R2-5%	0.0	16.1	55.9	21.5	6.5	46.6	53.1	76.5
R3-5%	0.0	17.3	23.9	52.5	6.3	83.6	15.8	11.6
R4-5%	0.0	11.1	24.7	57.4	6.8	77.0	22.4	11.1
R5-5%	1.0	0.3	21.2	70.8	6.8	71.2	28.9	0.7

FBP: Final boiling point: 993.15 K; IBP: Initial boiling point.

4. Conclusions

The HT–SimDis GC method was successfully applied to analyze the AEBP distribution of a heavy feedstock and of its conversion products after upgrading by centrifugal reactive–molecular distillation (distillate and residue streams). The HT–SimDis GC analysis of the CRMD products and feedstock indicated that the centrifugal reactive–molecular distillation of ATR–W caused significant changes in the AEBP distribution of the >613.15 K and >813.15 K fractions.

In the trials using 3 and 5 % by wt of catalyst, the yield in products with AEBP from 813.15 to 973.15 K changed drastically in the distillate stream. The conversion of the fraction with an AEBP above 613.15 K decreased, reaching 65.6% (at 3 %wt of catalyst) and 64.3% (at 5 %wt of catalyst), while the fraction with an AEBP above 813.15 K remained approximately constant when process temperatures between 473.15 and 523.15 K were used, reaching about 100% of conversion. In the residue streams, the same fraction did not report any trend in the *EVT* range. At an *EVT* equal to 483.15 K, the fraction with an AEBP above 613.15 K was converted significantly, attaining about 49.6% (at 3 %wt of catalyst) and 53.1% (at 5 %wt of catalyst) of conversion. With such fractions, the CRMD process could be considered as an interesting option for high–boiling–point petroleum fraction upgrading, since it allows for a reduction in the boiling point of high–boiling–point petroleum fractions and presents high conversion rates under relatively mild conditions of about 483.15 K and 40 Pa.

Acknowledgements

This research was supported by the Brazilian National Council for Technological and Scientific Development (CNPq), the Petrobras Research and Development Center (PETROBRAS/CENPES) and the Brazilian Study and Project Financing Institution (FINEP).

References

- Adam F., Thiébaud D., Bertoncini F., Courtiade M., Hennion M. (2010) Supercritical fluid chromatography hyphenated with twin comprehensive two–dimensional gas chromatography for ultimate analysis of middle distillates, *Journal of Chromatography A* **1217**, 8, 1386–1394.
- Altgelt K. H., Boduszynski M. M. (1994) Composition and analysis of heavy petroleum fractions. New York: Marcel Dekker, Inc.

- American Society for Testing Materials, ASTM D 1160. Distillation of petroleum products at reduced pressure. West Conshohoken, (Pennsylvania): ASTM International, 2006. 18p.
- American Society for Testing Material, ASTM D 2887. Standard test method for boiling range distribution of petroleum fractions by gas chromatography. West Conshohoken, (Pennsylvania): ASTM International, 2008. 20p.
- American Society for Testing Material, ASTM D 2892. Standard test method for distillation of crude petroleum (15–Theoretical plate column). West Conshohoken, (Pennsylvania): ASTM International, 2005. 32p.
- American Society for Testing Material, ASTM D 3710. Standard test method for boiling range distribution of gasoline and gasoline fractions by gas chromatography. West Conshohoken, (Pennsylvania): ASTM International, 1995. 12p, [Reapproved 2009].
- American Society for Testing Materials, ASTM D 5236. Standard test method for distillation of heavy hydrocarbon mixtures (vacuum potstill method). West Conshohoken, (Pennsylvania): ASTM International, 2003. 18p, [Reapproved 2007].
- American Society for Testing Materials, ASTM D 5307. Standard test method for determination of boiling range distribution of crude petroleum by gas chromatography. West Conshohoken, (Pennsylvania): ASTM International, 1997. 7p, [Reapproved 2007].
- American Society for Testing Materials, ASTM D 6352. Standard test method for boiling range distribution of petroleum distillates in boiling range from 174 to 700 °C by gas chromatography. West Conshohoken, (Pennsylvania): ASTM International, 2004. 16p, [Reapproved 2009].
- American Society for Testing Materials, ASTM D 7169. Standard test method for boiling point distribution of samples with residues such as crude oils and atmospheric and vacuum residues by high temperature gas chromatography. West Conshohoken, (Pennsylvania): ASTM International, 2011. 17p.
- Blanding F. H. (1953) Reaction rates in catalytic cracking of petroleum, *Industrial & Engineering Chemistry* **45**, 6, 1186–1197.

- Boczka G., Przyjazny A., Kamiński M. (2011) A new procedure for the determination of distillation temperature distribution of high-boiling petroleum products and fractions, *Analytical and Bioanalytical Chemistry* **399**, 9, 3253–3260.
- Canziani D., Ndiaye P. M., Franceschi E., Corazza M. L., Oliveira J. V. (2009) Phase behaviour of heavy petroleum fractions in pure propane and n-butane and with methanol as co-solvent, *The Journal of Chemical Thermodynamics* **41**, 8, 966–972.
- Carbognani L., Lubkowitz J., Gonzalez M. F., Pereira-Almao P. (2007) High temperature simulated distillation of Athabasca vacuum residue fractions: Bimodal distributions and evidence for secondary "on-column" cracking of heavy hydrocarbons, *Energy & Fuels* **21**, 5, 2831–2839.
- Espinosa-Peña M., Figueroa-Gómez Y., Jiménez-Cruz F. (2004) Simulated distillation yield curves in heavy crude oils: A comparison of precision between ASTM D-5307 and ASTM D-2892 physical distillation, *Energy & Fuels* **18**, 6, 1832–1840.
- Falla F. S., Larini C., Le Roux G. A. C., Quina F. H., Moro L. F. L., Nascimento C. A. O. (2006). Characterization of crude petroleum by NIR, *Journal of Petroleum Science and Engineering* **51**, 1–2, 127–137.
- Keil F. J. *Modeling of Process Intensification*, Wiley-VCH Verlag GmbH & Co. KGaA, Weinheim (2007).
- Myers-Vacuum, 2010. Available in: < <http://www.myers-vacuum.com/index.shtml> >. Accessed in: November 10th. 2010.
- Rana M. S., Sámano V., Ancheyta J., Diaz J. A. I. (2007) A review of recent advances on process technologies for upgrading of heavy oils and residua, *Fuel* **86**, 9, 1216–1231.
- Reddy K. M., Wei B., Song C. (1998) High-temperature simulated distillation GC analysis of petroleum resids and their products from catalytic upgrading over Co-Mo/Al₂O₃ catalyst, *Catalysis Today* **43**, 3–4, 187–202.
- Tovar, Laura Plazas. Modeling and simulation of the centrifugal reactive molecular distillation: Development, assessment and application to upgrade high-boiling-point petroleum fractions. 2012, 442p. Ph. D. Thesis (Doctorate of Chemical Engineering) – School of Chemical Engineering, State University of Campinas, Campinas, 2012.

Winter, Alessandra. Development of reactive molecular distillation technology : design and construction of the unit. 2011, 166p. Ph. D. Thesis (Doctorate of Chemical Engineering) – School of Chemical Engineering, State University of Campinas, Campinas, 2011.

8.3. Considerações finais

A modelagem do processo de destilação molecular reativa (tipo centrífuga–CRMD) está baseada na modelagem desenvolvida para o processo de destilação molecular centrífuga, previamente apresentada nessa Tese de Doutorado (Capítulo 6), porém sem consideração de reação química. A modelagem foi devidamente adaptada, com objetivo de fazer estudos de predição e também de avaliação do processo em estudo (CRMD), levando, com isso, à condução de trabalhos experimentais em condições já otimizadas e mesmo possibilitando, a priori, a verificação dos resultados que seriam conseguidos com uma aplicação experimental. Equações de transferência de massa, energia e momento foram consideradas nessa modelagem. A taxa de evaporação considerada foi a de Langmuir modificada levando em consideração a geometria do equipamento e o grau de anisotropia do sistema.

O termo cinético reativo foi incorporado ao modelo e a equação da taxa de reação foi assumida como cinética de primeira ordem, tendo em conta, a influência do catalisador no sistema. Ainda assim, os parâmetros cinéticos foram determinados pela técnica termoanalítica, usando calorimetria exploratória diferencial (do inglês *DSC–differential scanning calorimeter*).

Esta modelagem deu origem a um ambiente computacional, designado DESTMOL–R, capaz de prever todas as variáveis do processo como: perfis de temperatura na superfície do filme, espessura do filme, taxa de evaporação efetiva, taxa de destilado, perfil de velocidade e taxa de reação. Em virtude da simulação do processo de destilação molecular centrífuga reativa pôde-se analisar o comportamento dos perfis das variáveis de interesse, através da manipulação das variáveis de entrada, da vazão de alimentação (Q), da temperatura do evaporador (EVT) e da porcentagem de catalisador ($\%CAT$). O processo em estado estacionário mostrou que a temperatura do filme escoando na superfície (T_s), a taxa de evaporação (G_E) e a taxa de destilado (D) são fortemente influenciadas pela temperatura do evaporador (EVT). Toda a energia consumida pelos pseudo–componentes que reagem e evaporam é suprida continuamente pelo calor fornecido na superfície do evaporador.

Resultados obtidos das simulações apresentaram uma conversão da carga de 58% no destilado e de 42% no resíduo, considerando uma porcentagem de 3% m/m de catalisador na carga inicial e uma temperatura de processo de 483,15 K. As predições oriundas da simulação foram comparadas com os dados experimentais e indicaram um desvio relativo percentual médio

menor do que 6,82%; 9,39% e 14,92% para a taxa global de destilado, conversão na corrente de destilado e conversão na corrente de resíduo, respectivamente.

Dados experimentais foram gerados através de uma metodologia experimental direcionada para processar (*upgrading*) um resíduo de petróleo pesado (ATR-W). A influência da adição de um catalisador (1, 3 e 5% m/m) foi examinada. Em este processo 30 frações (15 e 15 de destilados resíduos) foram obtidas em diferentes condições operacionais: a temperatura do processo (evaporador faixa de temperatura) de 473,15 K a 523,15 K, a vazão de alimentação taxa de 1,473 kg·h⁻¹.

Utilizando o método padronizado de análise por destilação simulada (ASTM D 7169, 2011), foi possível analisar a distribuição de pontos de ebulição equivalente da matéria-prima, bem como seus produtos convertidos da destilação molecular centrífuga reativa (destilados e resíduos) e o grau de conversão destes com respeito à carga inicial no processo, existindo mudanças apreciáveis nas frações definidas como >613,15 K e >813,15 K.

Para os testes experimentais utilizando 3 e 5% m/m de catalisador, o rendimento e conversão dos produtos na fração de 813,15 a 973,15 K muda drasticamente na corrente de destilado. Assim sendo, a conversão da fração maior de 613,15 K atinge uma conversão de 65,6% quando considerado uma temperatura de 483,15 K e 3 %m/m de catalisador, e uma conversão de 64,3% quando considerado uma temperatura de 483,15 K e 5 %m/m de catalisador. Por outra parte, a fração com distribuição de ponto de ebulição superior a 813,15 K quando considerado temperaturas do processo entre 473,15K e 523,15 K, atinge cerca de 100% de conversão. Na corrente de resíduo, não se apresenta uma tendência definida da conversão. Mas resultados importantes foram alcançados, conseguindo conversões entre 12 e 49,6% quando considerado temperaturas do processo entre 473,15K e 523,15 K e 3 %m/m de catalisador.

Capítulo 9.

Caracterização dos produtos obtidos por destilação molecular centrífuga reativa de um resíduo atmosférico de 673.15 K⁺

9.1. Introdução

A caracterização físico-química dos produtos obtidos do processamento de petróleo e frações pesadas resulta em uma difícil tarefa dada a complexidade das amostras e as limitações que apresentam as técnicas analíticas disponíveis. Entretanto, a caracterização precisa ser realizada para avaliar a eficiência do processo e a qualidade dos produtos (Merdrignac e Espinat, 2007).

Numerosos estudos têm apresentado diversas abordagens relacionadas às técnicas analíticas usadas para a caracterização de produtos de petróleo. Assim, Zuñiga-Liñan et al. (2011) e Merdrignac e Espinat (2007) apresentam uma revisão destes métodos resumidos na Tabela A.

Tabela A. Métodos de análise físico-químicos usados para a caracterização de cortes pesados de petróleo.

Procedimento de caracterização	Método	Informação fornecida
Fracionamento preparativo	Destilação simulada.	Definição das temperaturas de ebulição dos produtos (ASTM D 7169, 2011).
Caracterização por classe química	Desasfaltação	Precipitação de asfaltenos ASTM 6560 (2000)
	Separação SAR	Composição de componentes saturados, aromáticos e resinas polares utilizando cromatografia líquida preparativa (<i>flash chromatography</i>), cromatografia analítica (<i>high performance liquid chromatography and thin layer chromatography</i>)
	Fracionamento <i>ABAN</i>	Este método é usado para separar amostras em frações ácidas, básicas, anfotéricas e neutras (hidrocarbonetos saturados e aromáticos).
	Solubilidade	Relação entre a solubilidade e a estrutura molecular. Aplicado para avaliar a solubilidade dos asfaltenos a qual está relacionada com o grau de aromaticidade, alifaticidade e a polaridade.

Tabela A continua. Métodos de análise físico-químicos usado para a caracterização de cortes pesados de petróleo.

Procedimento de caracterização	Método	Informação fornecida
Caracterização química	Pirólise – Cromatografia Gasosa– Espectrometria de massa (Py–GC;MS)	Composição de asfaltenose hidrocarbonetos
	Cromatografia Líquida de Alta Performance (HPLC)	Análise de compostos poliaromáticos presentes em produtos pesados de petróleo.
	Ressonância Magnética Nuclear ^{13}C (NMR)	Estrutura molecular e grupos funcionais presentes em frações de petróleo.
	Espectroscopia IR e transformada de Fourier	Informação detalhada de grupos funcionais (CH_n , OH, NH, CO).
	Espectroscopia de Foto-elétron de Raios X (XPS)	Funcionalidade química do enxofre, nitrogênio e elementos metálicos.
	Raios X de estrutura fina entendida (EXAFS)	
	Espectroscopia de Absorção de Raios X (XANES)	
Caracterização coloidal	Osmometria de Pressão de Vapor (VPO).	Massa molar de produtos entre 500 – 10.000 $\text{kg}\cdot\text{kmol}^{-1}$.
	Cromatografia Exclusiva por Tamanho (SEC).	Massa molar de produtos entre 1000 – 10.000 $\text{kg}\cdot\text{kmol}^{-1}$ e distribuição do volume molecular.
	Espectrometria de Massa (MS).	Massa molar de produtos entre 500 – 1000 $\text{kg}\cdot\text{kmol}^{-1}$.
Caracterização físico-química	Massa específica (ASTM D 7042 e ASTM D 70)	Massa específica e densidade.
	Viscosidade (Reômetro)	Características reológicas.
	Composição elementar CHN	Composição dos elementos carbono, hidrogênio, oxigênio e enxofre.

Como parte desta Tese de Doutorado, foram realizadas ensaios analíticos para os produtos obtidos do *upgrading* do resíduo de petróleo ATR–W por destilação molecular centrífuga reativa, pertencentes a cada um dos grupos descritos na Tabela A. As análises foram realizadas nos Laboratórios LDPS e LOPCA da FEQ e no Laboratório da central analítica do IQ, ambos da UNICAMP.

9.2. Desenvolvimento

O desenvolvimento deste capítulo é apresentado a seguir, nos manuscritos intitulados:

- *Characterization of converted products (distillate and residue streams) obtained from a petroleum residue upgrading using centrifugal reactive molecular distillation process: Rheological behavior, density, relative density and API gravity*, a ser submetido em congresso ou periódico internacional.
- *Colloidal characterization of the fractions split using centrifugal reactive–molecular distillation of a Brazilian atmospheric residue 673.15 K^+* , a ser submetido em congresso ou periódico internacional.

**Characterization of converted products (distillate and residue streams)
obtained from a petroleum residue upgrading using centrifugal reactive
molecular distillation process: Rheological behavior, density, relative density
and API gravity**

Abstract

The objective of this work was to accomplish the evaluation of the centrifugal reactive molecular distillation (CRMD) process as alternative technique for upgrading of high-boiling-point petroleum fractions and heavy crude oils. Experimental study is illustrated for an atmospheric petroleum residue (ATR-W 673.15 K⁺) within the process temperature (evaporator temperature) range from 473.15 K to 523.15 K at feed flow rate of 1.473 kg·h⁻¹. The influence of adding catalyst to ATR-W at 1, 3 and 5 %wt was also studied. It was obtained 15 distillate and 15 residues streams by CRMD process. They were characterized through rheological measurements. The experimental measurements were performed using a HAAKE RheoStress 6000-UTC rheometer, with plate-plate sensor system constituted by two (02) parallel plates (PP35 and PP60) of 0.035 m and 0.060 m, respectively. Transition between non-Newtonian and Newtonian viscous flow was analyzed by flow curves at the shear rate range from 10 to 700 s⁻¹. Density, relative density and API gravity were determined by ASTM D 4052 (2009), ASTM D 5002 (1999) and ASTM D 70 (2009) standard methods.

Experimental results of products from CRMD process were compared with characterization performed for products obtained from centrifugal molecular distillation process (CMD) known as a non-catalytic process. In this sense, products obtained from CRMD process were found to exhibit Newtonian behavior at 333.15 K (distillate streams) and 393.15 K (residue streams) when compared to CMD products which exhibited a Newtonian behavior at 372.15 K and 423.15 K, respectively. Furthermore, it was clear the increase of API gravity data of the distillate streams. This can be explained since the CRMD process produces distillate streams which have a lower proportion of compounds with complex molecular structures when compared with residue streams which have compounds with features of resins and asphaltenes.

Keywords: Centrifugal reactive molecular distillation; heavy petroleum residue; density; viscosity; Newtonian behavior; API gravity.

Contents

1. Introduction
 2. Experimental Methodology
 - 2.1. Centrifugal molecular distillation and centrifugal reactive–molecular distillation experiments
 - 2.2. Viscosity Analysis of distillate and residue streams obtained from CMD and CRMD processes
 - 2.3. Analysis of density of distillate streams
 - 2.4. Analysis of density of residue streams
 3. Results and discussion
 4. Conclusions
- Acknowledgment
- References

1. Introduction

Upgrading heavy crude oil and high-boiling-point petroleum fractions (bottom product from the atmospheric and vacuum distillation units) is essential in the petroleum industry. The heavy crude oils and high-boiling-point petroleum fractions exhibit API gravity lesser than 20° API, kinematic viscosity at 20 °C >20 cSt ($20 \text{ mm}^2 \cdot \text{s}^{-1}$), high dynamic viscosity from 100 to 10,000 mPa·s and corresponding density >950 kg·m⁻³ and can not be pipelined without previous treatment (Tovar et al., 2011; Martínez-Palou et al., 2011; Rana et al., 2007; Dehkissia et al., 2004; Lai and Smith, 2001).

A hybrid and intensified process, named as centrifugal reactive–molecular distillation (CRMD) process, was developed and implemented by the Separation Process Development Laboratory (LDPS) and the Optimization, Project, and Advanced Control Laboratory (LOPCA) at the Chemical Engineering School of UNICAMP, sponsored by the Research Center of Petrobras–Brazil (CENPES/Petrobras) and Brazilian Study and Project Financing Institution (FINEP) (Tovar 2012; Winter, 2011). This technique, in which the molecular distillation and reactive processes are carried out concomitantly, is suitable for upgrading by mean of the cracking and split heavy crude oil and heavy petroleum residue with specific characteristic in relation with their low H/C ratio, sulfur and metals contents and complex hydrocarbon mixtures, as paraffins, naphthenes and aromatics.

The CRMD, defined as intensified process, refers to the development of processing technology to generate new products which could not be produced by conventional process technology due to its special operating conditions: lower pressure, lower temperatures, shorter residence times of the distilled liquid over the thermally exposed surface, a sufficiently small space between evaporator and condenser surfaces and more intensive contact between the sample and the catalytic surface than conventional catalytic process (Tovar 2012; Winter, 2011).

In this process, two streams are generated: distillate stream (condensed molecules) and residue stream (non-evaporated molecules). Characterization of these materials, in terms of rheological behavior and density data will help to evaluate the performance of the upgrading process in front of different operational conditions as well as significance information in reference to application, and the optimum conditions for the efficient operation of centrifugal reactive molecular distillation unit.

Thus, the objective of this study was to accomplish the evaluation of the centrifugal reactive molecular distillation (CRMD) process as alternative technique for processing high-boiling-point petroleum fractions and heavy crude oils. The CRMD from an atmospheric petroleum residue (ATR-W 673.15 K⁺) was carried out at process temperature (evaporator temperature) range from 473.15 K to 523.15 K at feed flow rate of 1.473 kg·h⁻¹. The influence of adding catalyst to ATR-W 673.15 K⁺ at 1, 3 and 5 %wt was studied (Tovar, 2012; Winter, 2011). In order to evaluate the efficiency of the technique, products obtained from CRMD process, the distillate and residue streams, were characterized through rheological measurements and density, relative density and API gravity by ASTM D 4052 (2009), ASTM D5002 (1999) and ASTM D 70 (2009) standard methods.

On the other hand, characterization of the distillate and residue streams from CRMD (catalytic process) was compared with the characterization presented for distillate and residue streams obtained by centrifugal molecular distillation (CMD) process described as a non-catalytic process (Tovar, 2012). This comparison held assessing whether or not CRMD might be considered as a total or partial upgrading process of the heavy petroleum fractions and heavy crude oils into products (distillate and residue streams) with lower viscosity and density. Rheological and density data could be used to provide a strategy in reference to the transportation and exploitation of heavy crude oil and processing of heavy petroleum fractions.

2. Experimental Methodology

A Brazilian crude oil (W) with API gravity, approximately, 16 °API was processed by conventional atmospheric distillation (ASTM D 2892, 2005). Bottom product or atmospheric distillation residue (ATR–W 673.15 K⁺) constituted the high-boiling-point petroleum fraction (feedstock) processed by CMD and CRMD processes (Tovar, 2012; Winter, 2011).

2.1. Centrifugal molecular distillation and centrifugal reactive–molecular distillation experiments

The equipment used in the experiments was the pilot plant with an evaporation surface area of 0.1935 m² built up and available at the Laboratory of Development of Separation Processes (LDPS) and Laboratory of Optimization, Design and Advanced Control (LOPCA), at the School of Chemical Engineering, State University of Campinas. A sketch of centrifugal reactive molecular distiller unit is presented in Figure 1. Table 1 describes the experimental conditions established to CMD (non–catalytic) and CRMD (catalytic) processes of the ATR–W 673.15 K⁺. The distiller unit is basically comprised by a spinning rotor (540 rpm) with a disk in a high vacuum chamber. The evaporation occurs from the inner surface of the evaporator towards the external surface of the condenser. The distance between the evaporator surface and condenser surface is of 0.08 m. Centrifugal force spreads the material rapidly over the heated evaporator surface homogenizing the film that is formed and allowing an easier heat and mass transfer from the inner layers (in contact with the evaporator surface) to the free film liquid surface.

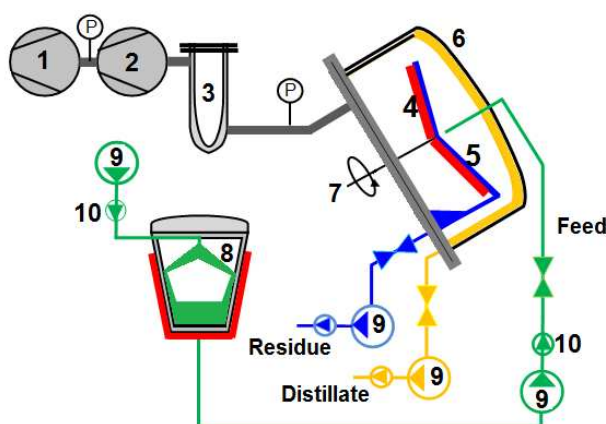


Figure 1. (b) Scheme of the centrifugal reactive–molecular distiller. 1. Backing/Roughing Vacuum Pump; 2. Diffusion Ejector Pump (High vacuum); 3. Chamber trap; 4. Heater rotor; 5. Evaporator surface; 6. Dome condenser; 7. Rotor; 8. Feed storage; 9. Liquid Transfer Pump; and 10. Check Valve Rotor. Modified Myers–Vacuum (2010).

Table 1. Operational conditions established to processing the ATR–W 673.15 K⁺ sample by CMD and CRMD processes.

Operating conditions						
Feeding temperature		423.15 K				
Condenser temperature		353.15 K				
Trap cooler temperature		273.15 K				
Rotor speed		540 rpm				
Stream products temperature (D/R)		353.15K / 423.15 K				
Process	% wt catalyst	EVT (K)	Q (kg·h ⁻¹)	Ps (Pa)	Distillate stream name	Residue stream name
Centrifugal molecular distillation (CMD)	0	423.15	2.945	0.4	D1	R1
		449.15	1.914		D2	R2
		449.15	3.976		D3	R3
		513.15	1.473		D4	R4
		513.15	2.945		D5	R5
		513.15	2.945		D6	R6
		513.15	2.945		D7	R7
		513.15	4.418		D8	R8
		576.15	1.914		D9	R9
		576.15	3.976		D10	R10
		603.15	2.945		D11	R11
Reactive centrifugal molecular distillation (CRMD)	1	473.15	1.473	28.6 (pressure reached after adding the zeolite-based catalyst)	D1–1%	R1–1%
		483.15			D2–1%	R2–1%
		498.15			D3–1%	R3–1%
		503.15			D4–1%	R4–1%
		523.15			D5–1%	R5–1%
	3	473.15	1.473	41.6 (pressure reached after adding the zeolite-based catalyst)	D1–3%	R1–3%
		483.15			D2–3%	R2–3%
		498.15			D3–3%	R3–3%
		503.15			D4–3%	R4–3%
		523.15			D5–3%	R5–3%
	5	473.15	1.473	50.0 (pressure reached after adding the zeolite-based catalyst)	D1–5%	R1–5%
		483.15			D2–5%	R2–5%
		498.15			D3–5%	R3–5%
		503.15			D4–5%	R4–5%
		523.15			D5–5%	R5–5%

%wt catalyst: Percentage weight of catalyst; *EVT*: Evaporator temperature; *Q*: Feed flow rate; *P_s*: Pressure inside the vacuum chamber (pressure inside the evaporator surface); *D*: distillate stream; *R*: Residue stream.

Collector samples of CMD and CRMD are constituted by two vessels. Two product streams were generated: distillate streams rich in lighter molecules that escape from the evaporator and get the condenser surface; and the residue streams rich in the heavier molecules and remain in the evaporator surface. The vacuum system is a combination of several vacuum pumps in series; In the case of CMD process, this system consists of an auxiliary pump and a diffusion pump. On the other hand, in the CRMD process the mechanical pump is enough to attain the vacuum conditions. The vacuum configuration contains valves and a trap system to retain volatile molecules from process. In the experiments, a typical pressure reached in the CMD

process was in the order of 0.4 Pa and in the CRMD process the reached vacuum pressure was function of the weight percent of catalysts used in the experiments. Hence, typical pressure was between 29 Pa and 50 Pa (Tovar, 2012).

2.2. Viscosity analysis of distillate and residue streams obtained from CMD and CRMD processes

The experimental measurements were performed using a HAAKE RheoStress 6000–UTC rheometer (Thermo Electron Corporation, Karlsruhe, Germany), with a plate–plate sensor system constituted by two (02) parallel plates (PP35 and PP60) of 0.035 m of diameter (for ATR–W 673.15 K⁺ sample and residue streams obtained by CRMD) and 0.060 m of diameter (for distillate streams obtained by CRMD). Characteristics of plate–plate sensor systems are presented in Table 2.

Table 2. Plate–plate sensor system characteristic (Thermo Scientific, 2007).

Sensor	PP35	PP60
Inertia (kg·m ²) x10 ⁻⁶	1.7	17
Material	Titan	Titan
Inlet radius (mm)	17.5	30
± delta inlet radius (mm)	0.0035	0.006
Gap (mm)	1	1
External radius (mm)	18.0	30.5
± delta external radius (mm)	0.0025	0.0025
Sample volume (cm ³)	1.0	3.0
Maximum temperature (K)	623.15	623.15

The rheological measurements refers to the analyses of transition between non–Newtonian and Newtonian behavior obtained from an analysis of the flow curve prepared using the controlled rate mode and at the shear rate range from 10 to 700 s⁻¹ with measurements being made every 10 s⁻¹. All experiments were carried out using compressed air as an oxidizing atmosphere. Measurements were defined and controlled through *HAAKE RheoWin Job Manager software* (Version 3.61.0000).

The procedure carried out in the rheological analyses is described in five (05) steps as follows (Tovar et al., 2011; Liñan et al., 2010):

Step 1. *Setting temperature of analyze*. The flow behavior of the ATR–W 673.15 K⁺ and products streams (distillate and residue) was investigated over a wide range of shear rates at:

(i) 343.15 K, 363.15 K and 373.15 K for ATR–W 673.15 K⁺; (ii) 372.15 K for distillate streams and 423.15 K for residue streams from CMD process; and (iii) 333.15 K for distillate streams and 393.15 K for residue streams from CRMD process. The test temperature was maintained at a constant value and controlled to allow a maximum deviation of ± 0.1 K with a *HAAKE* universal temperature controller (Thermo Electron Corporation, Karlsruhe, Germany).

Step 2. *Temperature stabilization system*. The temperature must be kept constant during a time of 300 seconds, while the shear rate reached 10.00 s^{-1} . This procedure allows a uniform allocation of the samples over the titan plate.

Step 3. *CS/CR–rotation step*. The analyses were conducted in the CS/CR–Rotation Ramp tool available in the *HAAKE RheoWin Job Manager software* (Version 3.61.0000). The shear rate was increased continuously at a constant temperature from 0.00 s^{-1} to 700 s^{-1} .

Step 4. *Rheogram*. Typical rheogram in terms of shear stress and shear rate is depicted through *HAAKE RheoWin Job Manager software* (Version 3.61.0000). Then, the shear– and time–dependent rheology of samples can be determined and utilized to predict their behavior (Newtonian and non–Newtonian).

Step 5. *Evaluation data*. The dynamic viscosity values were determined from simple linear regression through the set of 70 experimental data since they exhibit a linear relationship between shear stress and shear strain. Regression tool of *HAAKE RheoWin Job Manager software* (Version 3.61.0000) was used. In order to determine the Newtonian behavior, data must obey the general equation:

$$\tau = \mu \frac{\partial u}{\partial y} \quad (1)$$

Hence, through this method, the relation between the shear stress τ and the velocity gradient $\frac{\partial u}{\partial y}$ defined as shear rate can be obtained by Equation (2).

$$\tau = \mu \gamma \quad (2)$$

Where τ is the shear stress (Pa), μ is the dynamic viscosity (Pa·s) and γ is the shear rate (s^{-1}). Using experimental data, when τ is plotted against γ , a straight line is obtained. With this linear relation, the μ is calculated from the slope of the straight line.

2.3. Analysis of density of distillate streams

The ASTM D 4052 (2009) and ASTM D 5002 (1999) standard method, for density measurements in the petroleum industry, were used to determine the density and relative density at 20 °C (293.15 K) of the distillate streams obtained from CMD and CRMD processes.

The tests were performed through the Density Meter DMA 4500 – Anton Paar. A built-in Peltier thermostat automatically ensured the correct measuring temperature at 293.15 K. A minimum of 1.5 mL is required. Each sample required only 40 seconds for measurement and the results are automatically displayed.

2.4. Analysis of density of residue streams

Experimental analyses were carried out using the pycnometer method follows the standard method ASTM D 70 (2009). Density (ρ^T) and relative density (ρ_r) of samples (residue streams obtained from CRMD process) were determined at 293.15 K. Density ($\rho^{293.15\text{ K}}$) and relative density ($\rho_r^{293.15\text{ K}}$) of residue streams were calculated with Equations (3) – (4) as described in ASTM D 70 (2009).

$$\rho_r^{293.15\text{ K}} = (C - A) / [(B - A) - (D - C)] \quad (3)$$

$$\rho^{293.15\text{ K}} = \rho_r^{293.15\text{ K}} * W_T \quad (4)$$

Where A is the mass of pycnometer (plus stopper); B is the mass of pycnometer filled with water; C is the mass of pycnometer partially filled with; D is the mass of pycnometer plus sample plus water, and W_T is the density of water at the test temperature (Perry et al., 1999).

3. Results and discussion

Distillate and residue streams from CMD (non-catalytic process) and CRMD (catalytic process) may be change from Newtonian at high temperatures to non-Newtonian behavior at low temperatures due to paraffins, asphaltene and other compounds. Hence, the basic parameter to be investigated in the rheological behavior is the dynamic viscosity (μ). The flow properties of the samples are usually illustrated using rheograms defined as plots of shear stress (τ) and viscosity as a function of shear rate ($\dot{\gamma}$).

The dynamic viscosity (μ) of the ATR-W 673.15 K⁺ sample was measured isothermally at a fixed temperature of 343.15 K, 363.15 K and 373.15 K and the results were recorded and

fitted to the Newtonian model (Equation 2). Hence, ATR-W 673.15 K⁺ found to follow Newtonian behavior based on the yield stress of the sample at 363.15 K and 373.15 K (Figure 2). It can be observed that the shear stress is proportional to the shear rate (Newtonian behavior) which mean that the dynamic viscosity (μ) is constant and independent from the shear rate at constant temperature (test temperature). Under these conditions, at 363.15 K and 373.15 K, the ATR-W 673.15 K⁺ sample has Newtonian behavior with values of μ of 0.7799 Pa·s and 0.4132 Pa·s, respectively (Figure 3).

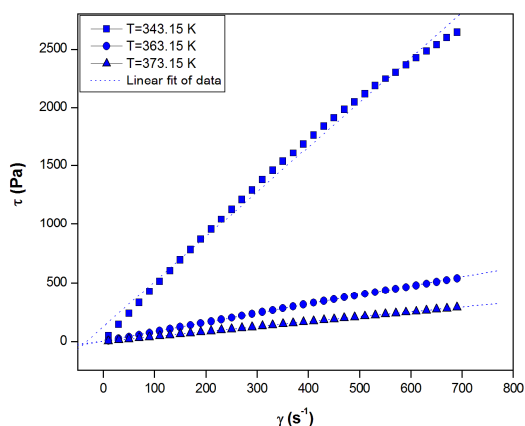


Figure 2. Shear rate (γ) and shear stress (τ) relationship for ATR-W 673.15 K⁺ sample at 343.15K, 363.15 K and 373.15K.

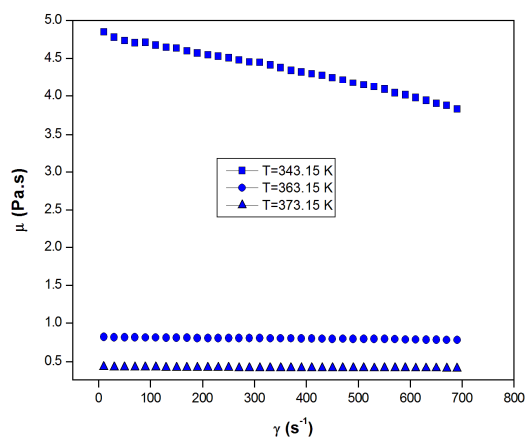


Figure 3. Effect of shear rate (γ) on the dynamic viscosity (μ) of the ATR-W 673.15 K⁺ sample at 343.15K, 363.15 K and 373.15K.

In Figures 4 – 5 are shown the rheograms of the distillate and residue streams obtained from CMD (non-catalytic process) and CRMD (catalytic process). The behavior of distillates streams obtained from CMD and CRMD (Figure 4) in experiments conducted at constant temperature and pressure has the following features: (i) the shear viscosity does not vary with shear rate; (ii) the dynamic viscosity (μ) is constant with respect to the time of shearing; and (iii) the stress in studied samples falls to zero ($\tau=0.000$ Pa) immediately the shearing γ is equal to zero ($\gamma=0.000$ s⁻¹). Therefore, with constant pressure and temperature (test temperature), distillate streams (both, catalytic and non-catalytic processes) exhibit a Newtonian behavior.

The plots of τ versus γ depicted straight lines, where the slope allows to calculate the dynamic viscosity at test temperature (μ^T). Table 3 presents the μ values of each distillate stream obtained by catalytic and non-catalytic processes. Good straight line fits was determined since the linear squares correlation varied between 0.9998 and 1.0000.

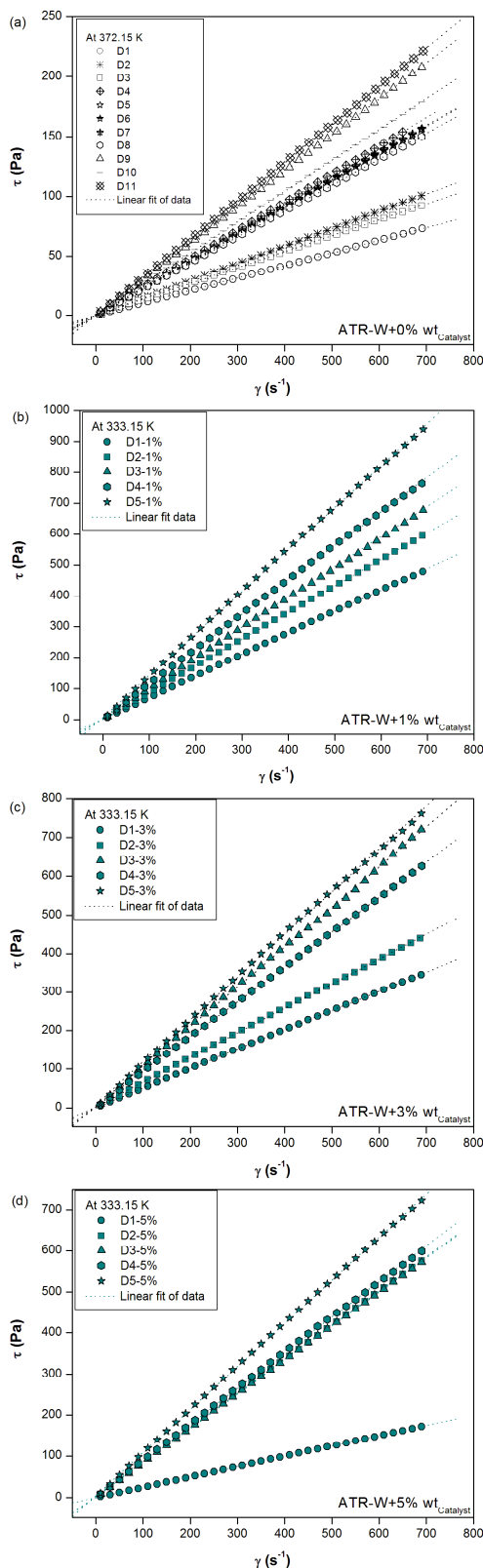


Figure 4. Rheograms of distillate streams obtained by (a) CMD (non-catalytic) process and CRMD (catalytic process) at (b) 1%wt, (c) 3%wt and (d) 5%wt of catalyst.

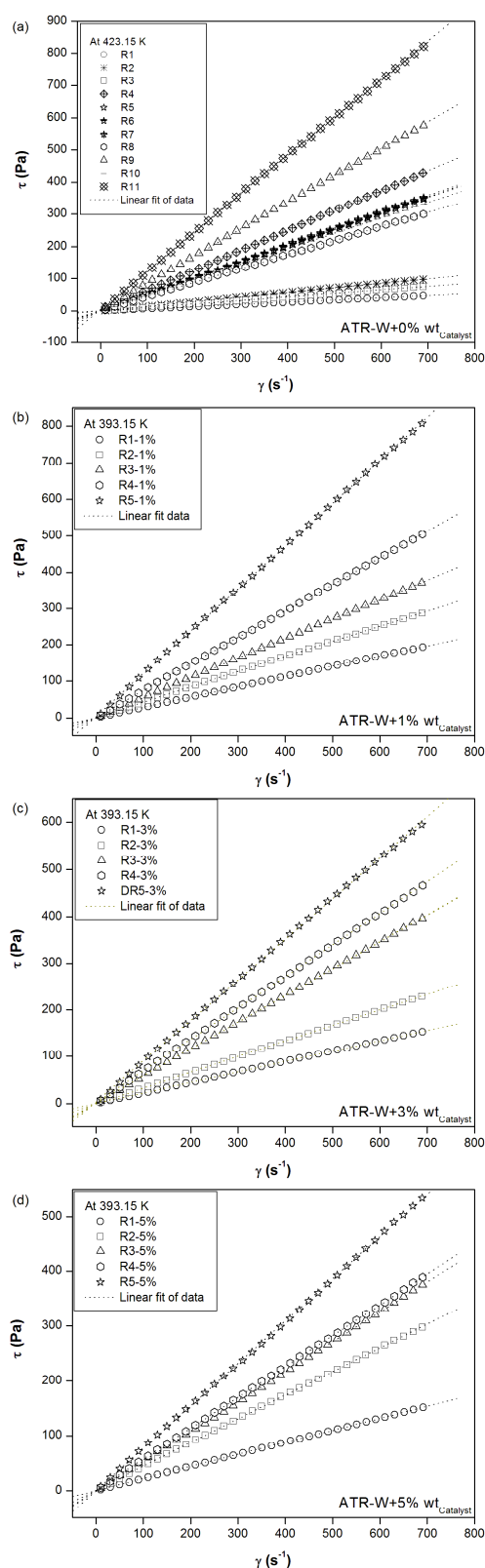


Figure 5. Rheograms of residue streams obtained by (a) CMD (non-catalytic) process and CRMD (catalytic process) at (b) 1%wt, (c) 3%wt and (d) 5%wt of catalyst.

Table 3. Dynamic viscosity at test temperature and density data at 293.15 K for distillate streams obtained by CMD (non-catalytic process) and CRMD (catalytic process).

Process	% wt catalyst	EVT (K)	Q (kg·h ⁻¹)	stream name	μ^T (Pa·s)	R ²	$\rho^{293.15\text{ K}}$ (g·cm ⁻³)	$\rho_r^{293.15\text{ K}}$	SG _{20/4}	°API
–	–	–	–	ATR–W	3.8359 [†] 0.7799 [‡] 0.4133 [*]	0.9940 0.9998 1.0000	0.9860	0.9878	0.9861	11.9
Centrifugal molecular distillation (CMD)	0	423.15	2.945	D1	0.1051	1.0000	0.9483±0.0001	0.9500	0.9483	17.6
		449.15	1.914	D2	0.1458	1.0000	0.9514±0.0001	0.9531	0.9514	17.1
		449.15	3.976	D3	0.1341	1.0000	0.9512±0.0001	0.9529	0.9512	17.2
		513.15	1.473	D4	0.2374	1.0000	0.9553±0.0001	0.9570	0.9553	16.5
		513.15	2.945	D5	0.2282	0.9998	0.9554±0.0001	0.9571	0.9554	16.5
		513.15	2.945	D6	0.2258	1.0000	0.9549±0.0001	0.9566	0.9549	16.6
		513.15	2.945	D7	0.2276	1.0000	0.9556±0.0001	0.9573	0.9556	16.5
		513.15	4.418	D8	0.2189	0.9998	0.9549±0.0001	0.9566	0.9549	16.6
		576.15	1.914	D9	0.3021	1.0000	0.9574±0.0001	0.9591	0.9574	16.2
		576.15	3.976	D10	0.2604	0.9998	0.9483±0.0001	0.9500	0.9483	17.6
		603.15	2.945	D11	0.3202	1.0000	0.9514±0.0001	0.9531	0.9514	17.1
Reactive centrifugal molecular distillation (CRMD)	1	473.15	1.473	D1–1%	0.6999	1.0000	0.9463±0.0001	0.9480	0.9463	17.9
		483.15		D2–1%	0.8649	1.0000	0.9462±0.0001	0.9479	0.9462	17.9
		498.15		D3–1%	0.9816	0.9998	0.9474±0.0001	0.9491	0.9474	17.7
		503.15		D4–1%	1.1260	0.9996	0.9483±0.0002	0.9500	0.9483	17.6
		523.15		D5–1%	1.3740	0.9996	0.9488±0.0001	0.9505	0.9488	17.5
	3	473.15	1.473	D1–3%	0.5043	1.0000	0.9384±0.0003	0.9401	0.9384	19.2
		483.15		D2–3%	0.6447	0.9998	0.9440±0.0001	0.9457	0.9440	18.3
		498.15		D3–3%	1.0420	0.9996	0.9454±0.0039	0.9471	0.9454	18.1
		503.15		D4–3%	0.9112	0.9998	0.9465±0.0001	0.9482	0.9465	17.9
		523.15		D5–3%	1.1220	0.9994	0.9483±0.0001	0.9500	0.9483	17.6
	5	473.15	1.473	D1–5%	0.2496	1.0000	0.9273±0.0008	0.9290	0.9273	21.0
		483.15		D2–5%	0.8379	1.0000	0.9450±0.0009	0.9467	0.9450	18.1
		498.15		D3–5%	0.8332	1.0000	0.9445±0.0007	0.9462	0.9445	18.2
		503.15		D4–5%	0.8776	0.9996	0.9462±0.0006	0.9479	0.9462	17.9
		523.15		D5–5%	1.0580	0.9998	0.9373±0.0096	0.9390	0.9373	19.4

%wt catalyst: Percentage weight of catalyst; *EVT*: Evaporator temperature; *Q*: Feed flow rate; *D*: distillate stream; μ^T : Dynamic viscosity at test temperature (T=372.15 K for distillate streams obtained by CMD and T=333.15 K for distillate streams obtained by CRMD process; [†]T=343.15 K; [‡]T=363.15 K and ^{*}T=373.15 K); R²: linear square correlation for linear fit between shear stress (τ) and shear rate ($\dot{\gamma}$); $\rho^{293.15\text{ K}}$: density data at 293.15 K (pycnometric method); $\rho_r^{293.15\text{ K}}$: relative density data at 293.15 K (ASTM D 70, 2009); SG_{20/4}: Specific gravity using Brazilian standard; °API: API gravity data.

When distillate streams from CRMD and CMD processes are compared, results indicated a decreasing in the test temperature to exhibit a Newtonian behavior. This indicated that the CRMD process has great influence on the properties of the products. In this sense, distillate streams from CRMD presented a Newtonian behavior at 333.15 when compared to distillate streams obtained from CMD which exhibited Newtonian behavior at 372.15 K.

Dynamic viscosity (μ) is the quantity that describes a fluid of resistance to flow. A high dynamic viscosity (μ) means that the liquid fluid will not flow easily and vice versa. The viscosity values (Pa·s) versus shear rate (s⁻¹) for the residue streams from CRMD and CMD processes displayed a Newtonian behavior in the range of the shear rates and temperature examined at 393.15 (for CRMD) and 423.15 K (for CMD) as presented in Table 4. Hence, it is

possible to affirm that residue streams are constituted by higher carbon number chains as discussed by Merdrignac and Espinat (2007) who confirmed that the high viscosity and polarity in petroleum samples may be related to the presence of complex compounds such as resins and asphaltenes.

Table 4. Dynamic viscosity at test temperature and density data at 293.15 K for residue streams obtained by CMD (non-catalytic process) and CRMD (catalytic process).

Process	% wt catalyst	EVT (K)	Q (kg·h ⁻¹)	stream name	μ^T (Pa·s)	R ²	$\rho^{293.15\text{ K}}$ (g·cm ⁻³)	$\rho_r^{293.15\text{ K}}$	SG _{20/4}	°API
–	–	–	–	ATR–W	3.8359 [†] 0.7799 [‡] 0.4133 [*]	0.9940 0.9998 1.0000	0.9860	0.9878	0.9861	11.9
Centrifugal molecular distillation (CMD)	0	423.15	2.945	R1	0.0672	0.9998	0.9931	0.9949	0.9934	10.8
		449.15	1.914	R2	0.1413	1.0000	0.9969	0.9987	0.9971	10.3
		449.15	3.976	R3	0.1072	1.0000	0.9973	0.9991	0.9976	10.2
		513.15	1.473	R4	0.6228	1.0000	0.9976	0.9994	0.9979	10.2
		513.15	2.945	R5	0.5062	1.0000	1.0007	1.0025	1.0010	9.8
		513.15	2.945	R6	0.5034	1.0000	1.0029	1.0047	1.0031	9.5
		513.15	2.945	R7	0.5125	1.0000	0.9986	1.0004	0.9989	10.1
		513.15	4.418	R8	0.4368	1.0000	1.0040	1.0059	1.0043	9.3
		576.15	1.914	R9	0.8424	0.9998	1.0123	1.0141	1.0125	8.1
		576.15	3.976	R10	0.4815	1.0000	1.0165	1.0183	1.0168	7.6
		603.15	2.945	R11	1.2020	0.9998	1.0192	1.0211	1.0195	7.2
Reactive centrifugal molecular distillation (CRMD)	1	473.15	1.473	R1–1%	0.2811	1.0000	0.9965	0.9983	0.9965	10.4
		483.15		R2–1%	0.4195	1.0000	0.9968	0.9986	0.9968	10.3
		498.15		R3–1%	0.5423	1.0000	0.9971	0.9989	0.9971	10.3
		503.15		R4–1%	0.7338	0.9998	0.9975	0.9993	0.9975	10.3
		523.15		R5–1%	1.1790	0.9998	0.9978	0.9996	0.9978	10.2
	3	473.15	1.473	R1–3%	0.2195	1.0000	0.9858	0.9876	0.9858	11.9
		483.15		R2–3%	0.4343	0.9998	0.9857	0.9875	0.9857	11.9
		498.15		R3–3%	0.5420	0.9998	0.9868	0.9886	0.9868	11.8
		503.15		R4–3%	0.5648	1.0000	0.9874	0.9892	0.9874	11.7
		523.15		R5–3%	0.7731	0.9998	0.9874	0.9892	0.9874	11.7
	5	473.15	1.473	R1–5%	0.2223	1.0000	0.9893	0.9911	0.9893	11.4
		483.15		R2–5%	0.3332	1.0000	0.9894	0.9912	0.9894	11.4
		498.15		R3–5%	0.5776	1.0000	0.9901	0.9919	0.9901	11.3
		503.15		R4–5%	0.6788	1.0000	0.9917	0.9935	0.9917	11.1
		523.15		R5–5%	0.8768	0.9996	0.9923	0.9941	0.9923	11.0

%wt catalyst: Percentage weight of catalyst; *EVT*: Evaporator temperature; *Q*: Feed flow rate; *R*: Residue stream; μ^T : Dynamic viscosity at test temperature (T=423.15 K for residue streams obtained by CMD and T=393.15 K for residue streams obtained by CRMD process; [†]T=343.15 K; [‡]T=363.15 K and ^{*}T=373.15 K); R²: linear square correlation for linear fit between shear stress (τ) and shear rate ($\dot{\gamma}$); $\rho^{293.15\text{ K}}$: density data at 293.15 K (pycnometric method); $\rho_r^{293.15\text{ K}}$: relative density data at 293.15 K (ASTM D 70, 2009); SG_{20/4}: Specific gravity using Brazilian standard; °API: API gravity data.

Distillate and residue streams, obtained from CRMD process, were found to exhibit Newtonian behavior at 333.15 K and 393.15, respectively, when compared to CMD products which exhibited Newtonian behavior at 372.15 K and 423.15 K, correspondingly.

As expected, the Newtonian behavior can be significantly affected by variables such as temperature and shear rate (Figures 4 – 5), as well as it is affected by molecular structure and molar mass distribution. It was found that CRMD process produces a progressive decrease in the

temperature which is reflected in the Newtonian behavior of the materials. This indicates that the amount of catalyst in the process has a significant effect on rheological profile.

Table 3 and 4 also register the density at 293.15 K, specific gravity (Brazilian standard), relative density and API gravity of the distillate and residue streams obtained by catalytic process (CMD) and non-catalytic process (CRMD). It is possible to confirm that the processing of ATR-W 673.15 K⁺ through CRMD allows producing products with a remarkable difference regarding to products generated from CMD.

Related to the density and API gravity, it is possible to observe a small variation of such property with the evaporator temperature and the weight percent of catalyst. Even though an increases in weight percent of catalyst stands for a difference in the density values and carbon number chains. Hence, the CRMD process represents a gain regarding to the increases of API gravity values when compared to the distillate and residue streams obtained from CMD process. Analyzing trials with 3 %wt of catalyst, it is clear that the complexity of mixtures is decreasing which might be ascribed to removal of higher molar mass species as confirmed in Tovar (2012). Nevertheless, results demonstrated that the components bearing a higher structural complexity are concentrated to the highest evaporator temperature (*EVT*), since the viscosity and the density data increased as the *EVT* rises.

In this sense, the density values in distillate streams are lower than values of this property in the original sample (ATR-W 673.15 K⁺) and residue streams, which satisfy the objective of the CRMD process since it is a function of conversion degree and the difference in molar mass of the mixture (the larger the difference in molar mass, the separation will be greater) and depletion of the volatile compounds as the temperature of the film surface increases (Tovar et al., 2011). Nevertheless, the rise of the density in residue streams is due to the components bearing higher structural complexity are concentrated as the evaporator temperature (*EVT*) rises. Therefore, it is expected that the heaviest molecules with greater intermolecular forces and which did not reach the condenser surface are routed to the residue stream.

4. Conclusions

Rheological profiles of the distillate streams obtained from CMD and CRMD process revealed a Newtonian behavior at 372.15 K and 333.15 K, respectively. Residue streams obtained by CMD and CRMD processes exhibited a Newtonian behavior over the temperature 423.15 K

and 393.15 K, respectively, since the dynamic viscosity (μ) stayed constant in front of the linear increase of the shear stress (τ) as function of the shear rate ($\dot{\gamma}$).

Concerning the density data of the distillate streams obtained by CRMD process, it was evident the low variation of these data with the process temperature (evaporator temperature). Nevertheless, significant differences were noticeable in the API gravities exhibiting an increase when the amount of catalyst rises. Under this assumption it is possible to affirm that the CRMD process might be performed to generate products (distillate streams) with carbon number chains lower than the initial sample with a noticeable improve in the physicochemical properties (density, molar mass and rheological properties). Although in residue streams the effects over the density data were not major, when compared with the distillate stream, it was clear a slight increase of API gravity data of the residue streams obtained by CRMD when compared with the residue streams obtained by CMD and initial sample (ATR–W 673.15 K⁺).

In this sense, the CRMD process might be considered as a suitable strategy to partially upgrade heavy petroleum fractions and heavy crude oil due to: (i) the reduction in the temperature range in which products from CRMD evidenced a Newtonian behavior; (ii) the significant effects of the amount of catalysts in the density data of the distillate streams obtained by CRMD and, (iii) the minor increase of the API with the process temperature (evaporator temperature) when compared with values obtained for residue streams from CMD process and ATR–W 673.15 K⁺ sample.

Acknowledgements

This research was supported by the Brazilian National Council for Technological and Scientific Development (CNPq), the Petrobras Research and Development Center (PETROBRAS/CENPES) and the Brazilian Study and Project Financing Institution (FINEP).

References

American Society for Testing Material, ASTM D 70. Standard test method for density of semi-solid bituminous materials (pycnometer method). West Conshohocken, (Pennsylvania): ASTM International, 2009. 4p.

- American Society for Testing Materials– ASTM D 2892. Standard test method for distillation of crude petroleum (15–Theoretical plate column). West Conshohoken, (Pennsylvania): ASTM International, 2005. 32p.
- American Society for Testing Material, ASTM D 4052. Standard test method for density, relative density, and API gravity of liquids by digital density meter. West Conshohoken, (Pennsylvania): ASTM International, 2009. 8p.
- American Society for Testing Materials, ASTM D 5002. Standard test method for density and relative density of crude oils by digital density analyzer. West Conshohoken, (Pennsylvania): ASTM International, 1999. 5p, [Reapproved 2010].
- Dehkissia S., Larachi F., Rodrigue D., Chornet E. (2004) Characterization of Doba–Chad heavy crude oil in relation with the feasibility of pipeline transportation, *Fuel* **83**, 16, 2157–2168.
- Lai W. –C., Smith K. J. (2001) Heavy oil microfiltration using ceramic monolith membranes, *Fuel* **80**, 8, 1121–1130.
- Liñan L. Z., Lopes M. S., Wolf Maciel M. R., Lima N. M. N., Maciel Filho R., Embiruçu M., Medina L. C. (2010) Molecular distillation of petroleum residues and physical–chemical characterization of distillate cuts obtained in the process, *Journal of Chemical Engineering and Data*, **55**, 9, 3068–3076
- Martínez–Palou R., Mosqueira M. de L., Zapata–Rendón B., Mar–Juárez E., Bernal–Huicochea C., Clavel–López J. de C., Aburto J. (2011) Transportation of heavy and extra–heavy crude oil by pipeline: A review, *Journal of Petroleum Science and Engineering* **75**, 3–4, 274–282.
- Merdrignac I., Espinat D. (2007) Physicochemical characterization of petroleum fractions: The state of the art, *Oil & Gas Science and Technology* **62**, 1, 7–32.
- Myers–Vacuum, 2010. Available in:< <http://www.myers-vacuum.com/index.shtml> >. Accessed in: November 10th. 2010.
- Perry R. H., Green, D.W. and Maloney, J.O., Editors, Perry's chemical engineers' handbook, McGraw–Hill Companies Inc., New York (1999).
- Rana M. S., Sámano V., Ancheyta J., Diaz J. A. I. (2007) A review of recent advances on process technologies for upgrading of heavy oils and residua, *Fuel* **86**, 9, 1216–1231.

- Thermo Scientific, Thermo scientific viscometers, Falling ball viscometer, HAAKE RheoStress 6000, Thermo Fisher Scientific Inc, Karlsruhe, 2007.
- Tovar L. P., Wolf Maciel M. R., Maciel Filho R., Batistella C. B., Ariza O. C., Medina L. C. (2011) Overview and computational approach for studying the physicochemical characterization of high-boiling-point petroleum fractions (350 °C+). *Oil & Gas Science and Technology*; doi:10.2516/ogst/2011150.
- Tovar L. P., Pinto G. M. F., Wolf-Maciel M. R., Batistella C. B., Maciel-Filho R. (2011) Short-path-distillation process of lemongrass essential oil: Physicochemical characterization and assessment quality of the distillate and the residue products, *Industrial and Engineering Chemistry Research* **50**, 13, 8185–8194.
- Tovar, Laura Plazas. Modeling and simulation of the centrifugal reactive molecular distillation: Development, assessment and application to upgrade high-boiling-point petroleum fractions. 2012, 442p. Ph. D. Thesis (Doctorate of Chemical Engineering) – School of Chemical Engineering, State University of Campinas, Campinas, 2012.
- Winter, Alessandra. Development of reactive molecular distillation technology : design and construction of the unit. 2011, 166p. Ph. D. Thesis (Doctorate of Chemical Engineering) – School of Chemical Engineering, University of Campinas, Campinas, 2011.

Colloidal characterization of the fractions split using centrifugal reactive–molecular distillation of a Brazilian atmospheric residue 673.15 K⁺

Abstract

Reactive–molecular distillation is presented as an alternative technique for the catalytic cracking and split of high–boiling–point petroleum fraction and heavy crude oils. The process was carried out in a stationary state using a pilot plant, obtaining two streams: the distillate and the residue streams. The technique was used so as to obtain 30 fractions with, from an atmospheric residue 673.15 K⁺ (high–boiling–point petroleum fraction) with 1, 3 and 5% by weight of the catalyst, under different operating conditions (Tovar, 2012).

In order to evaluate the effectiveness of the process, the fractions (15 distillates and 15 residues) were assayed by colloidal characterization using size exclusion chromatography (SEC) with UV–absorption detection, for the determination of the molar mass distribution (in the distillate and residue streams) and for the fractionation of asphaltene (in residue streams).

The SEC analyses indicated a monomodal distribution of the fractions obtained by centrifugal reactive–molecular distillation (catalytic process), with a weight average molar mass (M_w) in the distillate stream ranging from 210 to 245 kg·kmol⁻¹ with 1% by weight of catalyst, from 206 to 244 kg·kmol⁻¹ with 3% by weight of catalyst and from 215 to 243 kg·kmol⁻¹ with 5% by weight of catalyst. On the other hand, the M_w in the residue stream varied from 2554 to 2753 kg·kmol⁻¹ with 1% by weight of catalyst, from 2570 to 2908 kg·kmol⁻¹ with 3% by weight of catalyst and from 2750 to 2806 kg·kmol⁻¹ with 5% by weight of catalyst. The data were compared with those obtained for the fractions produced using molecular distillation (non–catalytic process), where the M_w ranged from 192 to 337 kg·kmol⁻¹ in the distillate streams and from 2537 to 3146 kg·kmol⁻¹ in the residue streams. The results showed that the reactive–molecular distillation process, involving the introduction of an in situ reaction in the separation process zone, led to the breakdown of the larger molecules into smaller molecules with lower molar mass. However, the weight average molar mass (M_w) and the asphaltene content (%A) increased with increase in the reactive–molecular distillation temperature (evaporator temperature). Such behavior demonstrated that the components with greater structural complexity were concentrated at the higher process temperatures.

Keywords: Size exclusion chromatography, molar mass distribution, asphaltene content, breaking of large molecules, reactive–molecular distillation process.

Contents

1. Introduction
 2. Experimental section
 - 2.1. Experiments with the centrifugal molecular distillation process
 - 2.2. Experiments with the centrifugal reactive–molecular distillation process
 - 2.3. Samples
 - 2.4. Size exclusion chromatography (SEC)
 - 2.5. Asphaltene determination by the gravimetric method
 3. Results and discussion
 - 3.1. Characterization by SEC of the distillate and residue streams
 - 3.2. Molar mass distribution of the products obtained using centrifugal reactive–molecular
 - 3.3. Molar mass distribution of the products obtained using centrifugal molecular distillation
 - 3.4. Fractionation of the asphaltene compounds
 4. Conclusions
- Acknowledgment
References

1. Introduction

High-boiling-point petroleum fraction are characterized by containing molecules with more than 25 carbon atoms (C₂₅), presenting structural complexity which increases as the boiling point, molar mass, specific mass, viscosity and polarity increase (Merdrignac and Espinat, 2007).

The centrifugal reactive molecular distillation (CRMD) technique was developed and implemented by the Separation Process Development Laboratory (LDPS) and the Optimization, Project and Advanced Control Laboratory (LOPCA) of the Chemical Engineering School of UNICAMP, sponsored by the Research Center of Petrobras–Brazil (CENPES/Petrobras) and Brazilian Study and Project Financing Institution (FINEP), aimed at enhancing the performance of the heavy petroleum fractions and heavy petroleum crude oil (Tovar 2012; Winter, 2011). Centrifugal reactive molecular distillation (CRMD) is a catalytic–separation technique which uses high vacuum, reduced temperatures and short exposition of the material at the operating temperature (evaporator temperature). During the CRMD process, the liquid film is evenly distributed on the inner surface of the evaporator surface in the shape of a very thin film in which the thickness depends on the viscosity of the mixture and the feed flow rate. The breakage of the molecule (cracking process) takes places due to the very intensive contact between the sample

and the catalytic surface under the conditions of high vacuum and lower operating temperature in comparison with the conventional cracking process (>658.15 K) as described by Tovar et al. (2011).

Thus, the CRMD process represents the coupling of the cracking reaction and the centrifugal molecular distillation (CMD) process, in which the evaporating liquid film is formed due to the centrifugal force. The reactive centrifugal molecular distiller has a fast rotating spinning cone to create a fast spreading and moving film of liquid. When the rotating cone is heated, reaction/evaporation takes place.

The cracking and separation of the compounds in the mixture inside the evaporator is carried out in five basic stages: (i) Transport of the evaporated molecules from the feeding section to the evaporator wall; (ii) simultaneously breaking down of the heavier molecules into lighter molecules and distillation of the mixture; (iii) transport of the broken down and evaporated molecules through the distillation gap (space between the evaporator and condenser surfaces); (iv) condensation of the evaporated molecules and (v) the flow downwards of the distillate and residue streams towards the collector system (Zuñiga-Liñan et al., 2011; Liñan et al., 2010; Sbaite et al., 2006; Batistella et al., 2000; Batistella and Wolf-Maciel, 1996, 1998).

In order to analyze the breakdown of the heavier molecules into lighter molecules carried out by the CRMD process, as a function of the evaporator temperature (EVT) and the weight percent of catalyst (1, 3 and 5%), colloidal characterization was required. This refers to the dispersion of the entities (lighter and heavier molecules) in the distillate and residue streams obtained from the CRMD process. The main parameters that can define the colloidal structure are the molecular size and/or the molar mass distribution and the asphaltene content ($\%A$), as determined by several techniques (Merdrignac and Espinat, 2007).

Colloidal characterization with respect to the determination of molar mass has been carried out by vapor pressure osmometry (Liñan et al., 2010; Stubington et al., 1995), membrane osmometry (Zengin et al., 2007) and size exclusion chromatography (SEC). However some authors reported the number average molar mass (M_n) and others the weight average molar mass (M_w). With respect to SEC, this technique provides information about the molar mass distribution of the compounds by way of calibration curves prepared using standards of the molecules found in the petroleum samples, and hence the weight average molar mass (M_w) and

the heterogeneity index (M_w/M_n), defined as the polydispersity index, can be determined (Evans et al., 1986; Bartle et al., 1984).

Size exclusion chromatography (SEC), also referred to as gel permeation chromatography (GPC), separates molecules according to their linear molecular size, based on their distribution between a stationary phase of controlled pore size distribution and a liquid mobile phase (Philip and Anthony, 1982). In SEC the retention is governed by the portioning (or exchange) of the molecules between the mobile phase (the eluent flowing through the column) and the stationary liquid phase that occupies the interior of the pores. Hence, longer molecules elute faster than shorter molecules (Meunier, D. M. In Settle, F.A., 1997). This technique has been used for synthetic polymers (Im et al., 2009; Karaca et al., 2009; Šimeková and Berek, 2005), in the separation and fractionation of coal and coal-tar bitumen (Champagne et al., 1985), the separation of asphaltenes (Sato and Takanohashi, 2005; Evans et al., 1986; Bockrath et al., 1979) and in the characterization of petroleum derivatives (Morgan et al., 2010; Berruoco et al., 2008; Al-Muhareb et al., 2007; Paul-Dauphin et al., 2007; Al-Muhareb et al., 2006).

Accordingly, the present work aimed to develop a methodology based on SEC to characterize the distillate and residue streams obtained from the CRMD process in terms of colloidal parameters such as the asphaltene content and molar mass distribution, using conventional polystyrene standards and hydrocarbon standards structurally similar to the compounds present in the samples studied. The distillate and residue streams produced in the CRMD process were obtained in an evaporator temperature range (EVT) from 473.15 to 523.15 K with 1, 3 and 5% by weight of catalyst, at a feed flow rate (Q) of 1.473 kg·h⁻¹. Furthermore, the colloidal characterization of the products obtained from the CRMD process was compared with the results obtained for the 22 fractions (11 distillates and 11 residues) produced during the centrifugal molecular distillation process (CMD) carried out under optimized conditions in the experimental range from 423.15 to 603.15 K for the evaporator temperature (EVT) and from 1.473 to 4.418 kg·h⁻¹ for the feed flow rate (Q) (Tovar, 2012).

The results allowed for the confirmation of the success of the CRMD process, since it led to the breakage of the larger molecules into smaller molecules with lower molar mass in the distillate and residue streams, as compared to the initial ATR-W sample and the products (distillate and residue streams) obtained from CMD (non-catalytic process).

2. Experimental section

A Brazilian crude oil (W) with a gravity of approximately 16 °API was distilled by conventional atmospheric distillation (ASTM D 2892, 2005), resulting in an atmospheric distillation residue (ATR–W). This ATR–W constituted the high-boiling-point petroleum fraction (raw material) processed by the CMD and CRMD processes (Tovar, 2012; Winter, 2011).

2.1. Experiments with the centrifugal reactive–molecular distillation process

The experiments carried out with the CRMD process are described in detail in Tovar (2012) and Winter (2011). The equipment used in those experiments was the pilot centrifugal molecular distiller (with an evaporation surface area of 0.1935 m²) available in the Laboratory of Development of Separation Processes (LDPS) and Laboratory of Optimization, Design and Advanced Control (LOPCA) of the School of Chemical Engineering, State University of Campinas, Brazil (Figure 1a). The centrifugal molecular distiller is basically comprised of a spinning rotor (540 rpm) with a rotational disk in a high vacuum chamber (Figure 1b). The distance between the evaporator surface and the condenser surface is to the order of 0.08 m. The feeding system consists of a storage tank with heating facilities and a feed flow controller. A feed pump was used to control Q at 1.473 kg·h⁻¹.

The module has independent temperature controllers, which control the feed, evaporator, condenser and stream process (distillate and residue) temperatures. Accordingly, the EVT was controlled by an electrical heater system from 423.15 to 603.15 K, while the condenser temperature was controlled by thermostatic baths at 353.15 K. The sample collector of the CRMD process is constituted of two tube liners, one for each stream (distillate and residue), connected to two vessels. The vacuum system is a combination of several vacuum pumps in series, consisting of a mechanical pump and a diffusion pump. The vacuum configuration contains valves and a trap system to retain volatile molecules from the process. In the experiments, the typical pressures (28.6; 41.6 and 50.0 Pa) were function of the amount of catalyst used (1, 3 and 5% by weight), were obtained using a vacuum system consisting only of the mechanical pump.

2.2. Experiments with the centrifugal molecular distillation process

Centrifugal molecular distillation process from ATR–W was carried out in the unit available in our research laboratories (Figure 1). The process is described in detail in Tovar (2012). However, some important features of the experiments are briefly presented in this work:

- The evaporator temperature (*EVT*) was controlled by an electrical heater system from 423.15 to 603.15 K. The experiments were carried out at feed flow rate range between 1.473 and 4.418 kg·h⁻¹ and the condenser temperature was controlled by thermostatic baths at 353.15 K.
- In the experiments, a typical pressure of 0.4 Pa was obtained by the vacuum system.

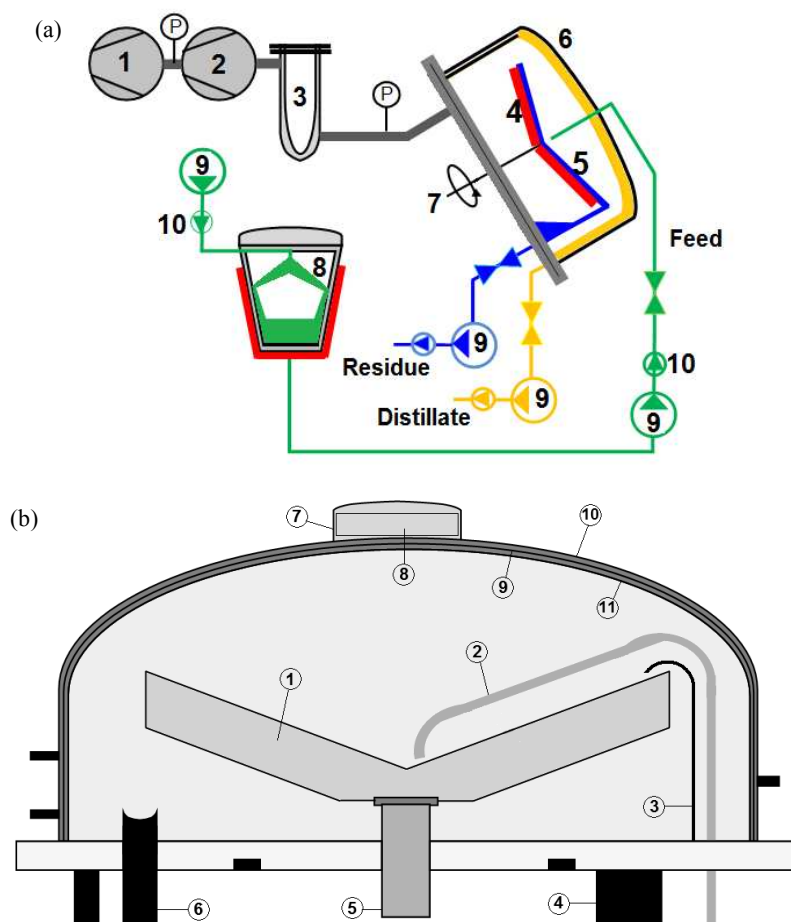


Figure 1: (a) Centrifugal molecular distiller module. 1. Backing/Roughing Vacuum Pump; 2. Diffusion ejector pump (high Vacuum); 3. Chamber Trap; 4. Heater rotor; 5. Evaporator surface; 6. Dome condenser; 7. Rotor; 8. Feed storage; 9. Liquid Transfer Pump; and 10. Check Valve Rotor. Modified Myers–Vacuum (2010); (b) molecular distillation device (evaporator–condenser) . 1. Thermocouple; 2. Evaporator surface; 3. Electrical resistance; 4. Support resistance; 5. Region of electrical cables and thermocouples; 6. Axis; and 7. Shaft hole.

Both the CMD and CRMD processes generated two product streams named as: distillate (rich in the molecules that escape from the evaporator and reach the condenser surface) and residue (rich in the heavier molecules). Different operating conditions were studied.

2.4. Size exclusion chromatography (SEC)

Apparatus

The chromatographic system (VISCOTEK GPC/SEC TDAmTM) consisted of a VISCOTEK GPCmax VE2001 solvent/sample module, a VISCOTEK TDA 302 triple detector array, three GPC/SEC Phenolgel analytical columns (Phenomenex, Torrance, CA) in series, a UV detector (filter at 340 nm) and OmniSEC software.

Method

The products (distillate and residue streams) were analyzed using size exclusion chromatography on three GPC/SEC Phenolgel analytical columns (Phenomenex, Torrance, CA) with different pore sizes (50–100 Å), dimensions of 300 mm x 7.8 mm and packed with spherical styrene divinylbenzene copolymer beads with a particle size of 5 µm. Tetrahydrofuran (THF) was used as the mobile phase at a flow rate of 0.7 mL·min⁻¹, and the column temperature was maintained at 313.15±1 K during the analyses. The samples were introduced through a 20 µL loop injection valve and detection was by means of UV absorption at 340 nm. The flow rate was measured continuously using a sensor and the detector interfaced to a data acquisition system. The SEC samples were prepared by dissolving each sample into THF and filtering the obtained solution by a Teflon membrane filter (pore size 0.45 µm). The molecular mass distribution with the number and weight average molar masses (M_n and M_w) and the polydispersity index (PID) were calculated by OmniSEC software. The environmental temperature was stabilized to prevent any changes in viscosity of the solvent. For this test, the laboratory was air-conditioned at 291.15 K.

Calibration

The GPC/SEC analytical detectors used for the determination of the molar mass distributions were calibrated for molar mass versus retention volume using several polystere (PS580, PS1300, PS2497, PS5460, PS8864, PS12347, PS16953 and PS28500) and hydrocarbon (naphthalene, tetralin, carbazole, ammonium heptamolybdate) standards. Figure 2 shows the

calibration curve of Log (M_w) against retention volume for these compounds using THF as the mobile phase.

This curve was fitted using a cubic equation (Equation 1) with a regression square coefficient of 0.989.

$$\log(M_w) = 18.568 - 2.120V_p + 0.093V_p^2 - 1.410 \times 10^{-3}V_p^3 \quad (1)$$

Where M_w is the average molar mass ($\text{kg} \cdot \text{kmol}^{-1}$) of the products from the CMD and CRMD processes and V_p is the retention volume (mL).

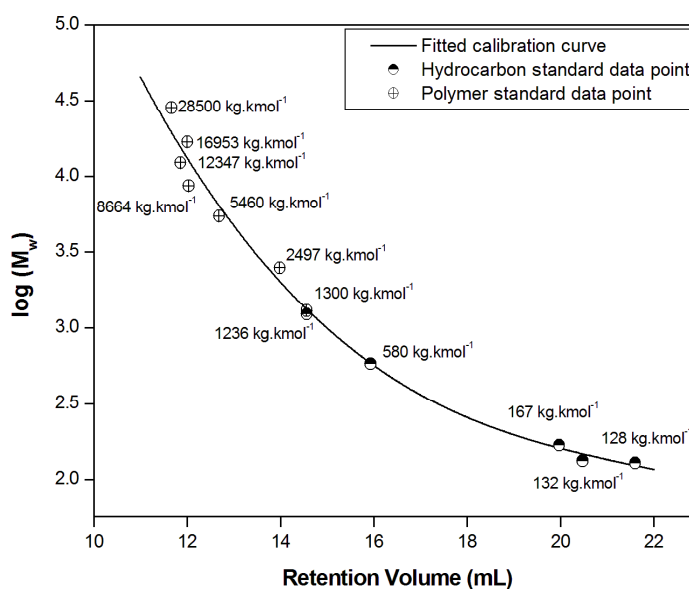


Figure 2. SEC calibration curve.

2.5. Asphaltene determination by the gravimetric method

The ATR–W asphaltene sample was precipitated from a ATR–W atmospheric petroleum residue 673.15 K⁺ by the addition of a 40:1 (v/v) excess of *n*–heptane, based on a modification of the ASTM 6560 (2000) standard test method (Gordillo et al., 2011). Briefly, 5 g of sample were mixed with *n*–heptane (150 mL), the suspension stirred with a magnetic mixer and boiled under reflux for 1 h, then allowed to settle and stored in a dark cupboard for 2 h, and finally filtered. The precipitated asphaltene, waxy substances and inorganic material were collected on the filter paper. After filtration, the thimble containing the filter cake was extracted in a Soxhlet apparatus (extractor system). The waxy substances were removed by washing with hot *n*–heptane in an extractor under vacuum at a rate of 2 to 4 drops per second. In practice, the extraction was run

for 3 h, or until the wash was only slightly colored. The asphaltene dried in an oven at 373.15 K for 30 min.

3. Results and discussion

Figures 3 – 6 present the SEC profiles of the ATR–W and the products obtained from the CMD process carried out in an *EVT* range from 423.15 K to 603.15 K and Q from 1.473 kg·h⁻¹ to 4.418 kg·h⁻¹, and from the CRMD process carried out in an *EVT* range from 473.15 K to 523.15 K (at 1.473 kg·h⁻¹) with the addition of 1, 3 and 5% by weight of catalyst. The profiles were normalized between 0 – 100% for the UV signals (mV) to permit comparison of the retention volume segments of the curves.

3.1. Characterization by SEC of the distillate and residue streams

The samples were dissolved in THF to give a final concentration of 1mg·mL⁻¹. The SEC chromatograms of the distillate and residue samples obtained from the CMD process and normalized by area are shown in Figures 3 – 4 (Tovar, 2012). The eluent used on the GPC/SEC Phenolgel analytical columns was THF, with detection by UV–absorbance at 340 nm.

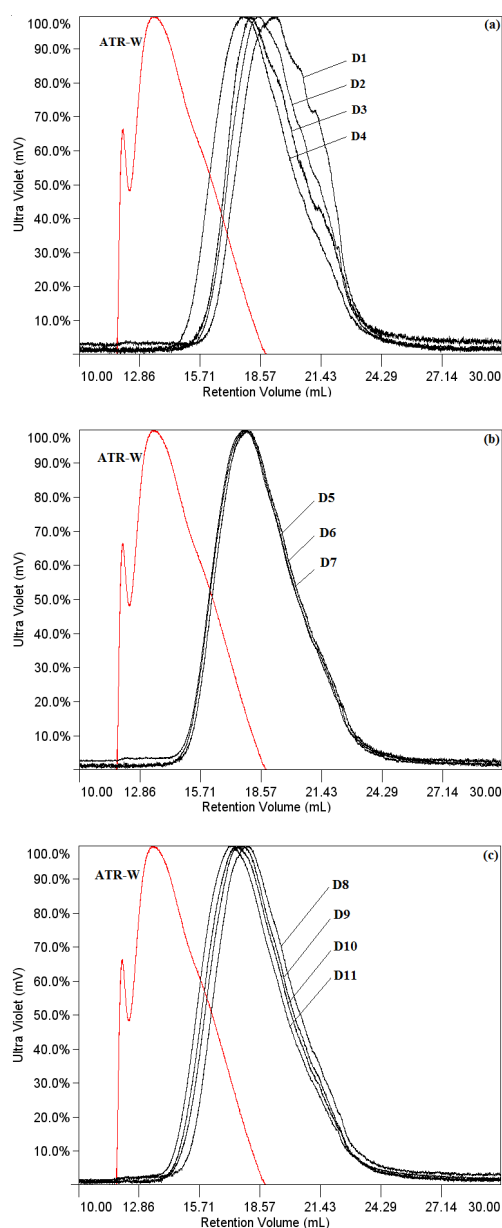


Figure 3. SEC chromatograms of distillate streams obtained from the CMD process. (a) D1 – D4, (b) D5 – D7 and (c) D8 – D11 as described in Table 1.

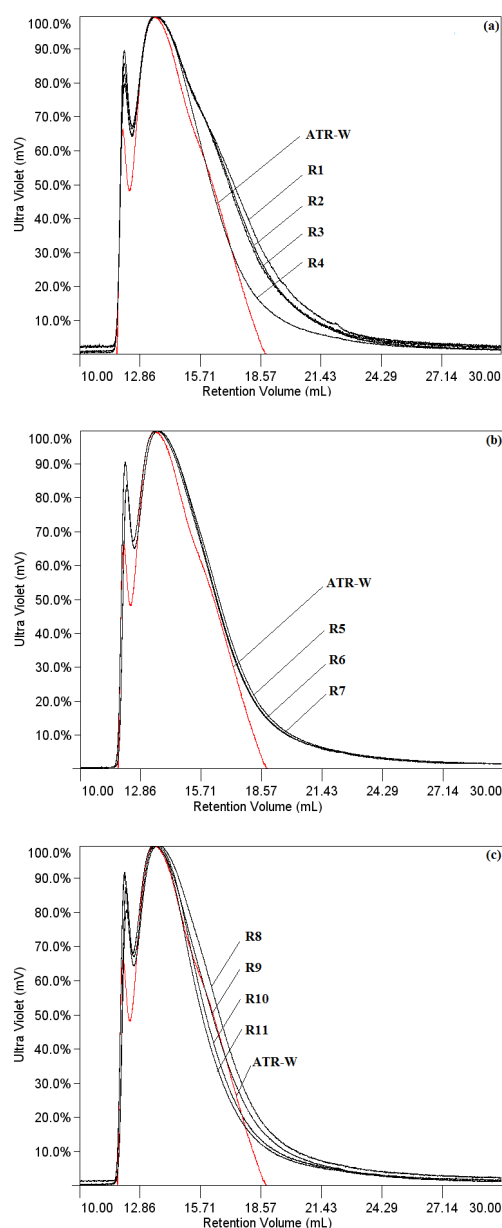


Figure 4. SEC chromatograms of residue streams obtained from CMD. (a) R1 – R4, (b) R5 – R7 and (c) R8 – R11 as described in Table 1.

Figures 5 – 6 present analogous chromatograms for the distillate and residue samples obtained from the CRMD process using the same system of columns. In general, the distillate streams were presented as unfractionated samples, while the residue streams were presented as samples fractionated into asphaltene and non-asphaltene peaks, eluting both products with small retention volumes.

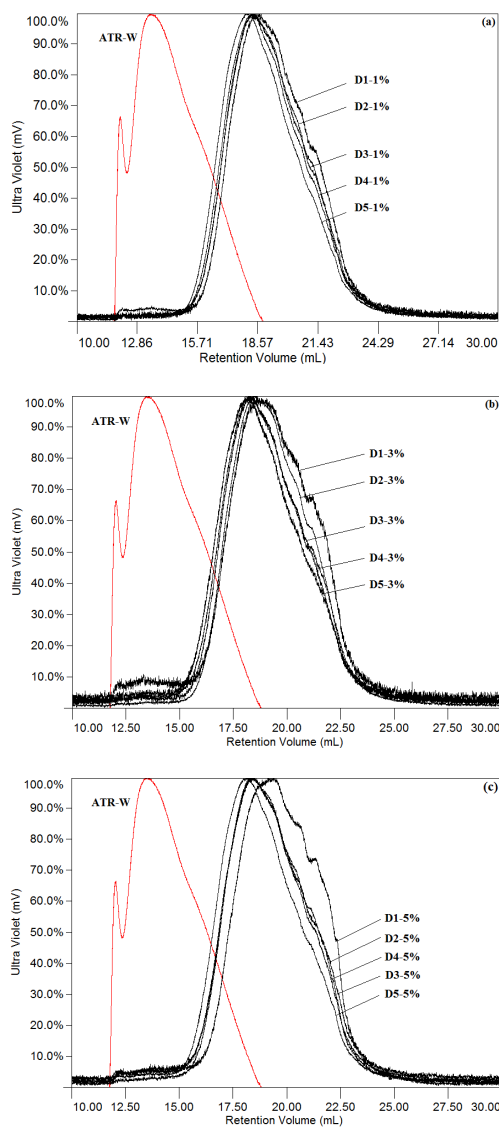


Figure 5. SEC chromatograms of distillate streams obtained from the CMD process with (a) 1% by wt catalyst, (b) 3% by wt catalyst and (c) 5% by wt catalyst.

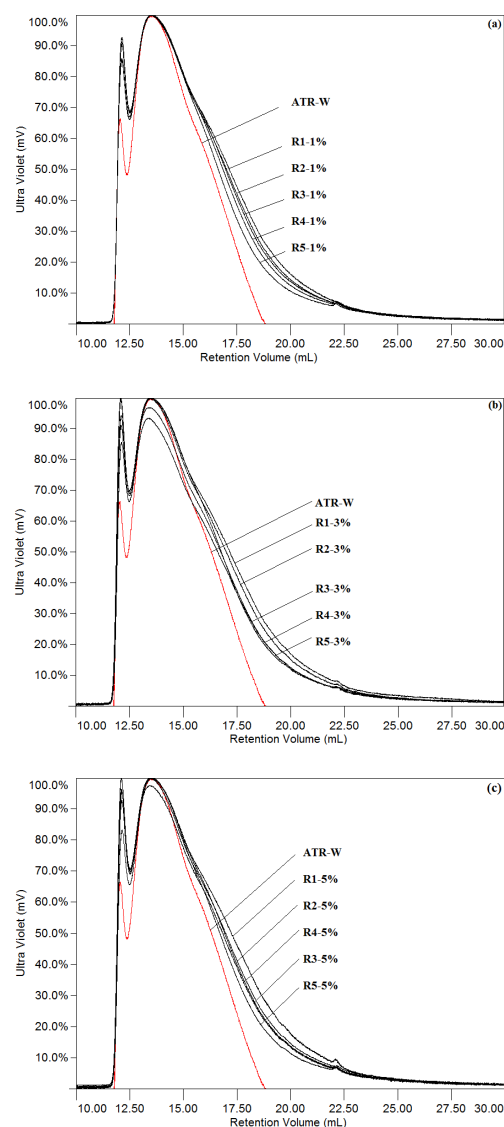


Figure 6. SEC chromatograms of residue streams obtained from the CRMD process with (a) 1% by wt catalyst, (b) 3% by wt catalyst and (c) 5% by wt catalyst.

Figures 4 and 6 present the SEC chromatograms obtained for the residue streams. These diagrams clearly show how the fractionation process was effective in fractionating the larger molar mass material (asphaltene compounds) excluded by the column porosity. Furthermore, the earlier eluting SEC peak was shifted by approximately 12 mL (retention volume).

3.2. Molar mass distribution of the products obtained from molecular distillation

The distillate streams obtained from the CMD process in an *EVT* range from 423.15 K to 603.15 K and *Q* from 1.473 kg·h⁻¹ to 4.418 kg·h⁻¹ were analyzed using the SEC method to determine the molar mass distribution of the products (Table 1). It was observed that the molar mass distribution of the liquids varied within a wide range. The number average (*Mn*) and weight average (*Mw*) molar masses of the liquid products ranged between 170 kg·kmol⁻¹ and 241 kg·kmol⁻¹ and between 192 kg·kmol⁻¹ and 337 kg·kmol⁻¹, respectively. Table 1 also shows the polydispersity index (PDI), which reflects the deviations of the molar mass distribution from the Gaussian distribution of an ideal single compound (Ahmaruzzaman and Sharma, 2006).

Table 1. Molar mass distributions of the distillate and residue streams obtained from ATR–W by the CMD process under different operating conditions.

EVT (K)	Q (kg·h ⁻¹)	Distillate streams from CMD				Residue streams from CMD			
		Sample	<i>Mn</i> (kg·kmol ⁻¹)	<i>Mw</i> (kg·kmol ⁻¹)	PDI	Sample	<i>Mn</i> (kg·kmol ⁻¹)	<i>Mw</i> (kg·kmol ⁻¹)	PDI
-	-	ATR–W*	1017	2956	2.91	ATR–W*	1017	2956	2.91
423.15	2.945	D1	170	192	1.13	R1	376	2931	7.80
449.15	1.914	D2	182	213	1.17	R2	2733	2590	0.95
449.15	3.976	D3	182	220	1.21	R3	447	2537	5.68
513.15	1.473	D4	214	273	1.28	R4	422	2947	6.98
513.15	2.945	D5	214	271	1.27	R5	271	2613	9.64
513.15	2.945	D6	215	275	1.28	R6	281	2837	10.10
513.15	2.945	D7	205	259	1.26	R7	312	2577	8.26
513.15	4.418	D8	205	260	1.27	R8	428	2544	5.94
576.15	1.914	D9	230	308	1.34	R9	684	2920	4.27
576.15	3.976	D10	223	293	1.31	R10	391	2939	7.52
603.15	2.945	D11	241	337	1.40	R11	309	3146	10.18

*: ATR–W before processing by the CMD process; *EVT*: Evaporator temperature; *Q*: Feed flow rate; *Mn*: Number average molar mass; *Mw*: Weight average molar mass and PDI: Polydispersity Index (*Mw/Mn*).

On the other hand, the residue products obtained from the CMD process were found to have values for *Mn* and *Mw* ranging from 281 kg·kmol⁻¹ to 2733 kg·kmol⁻¹ and from 2537 kg·kmol⁻¹ to 3146 kg·kmol⁻¹, respectively. Furthermore, Table 1 presented that the PDI values exhibited a wide range, which means that the number and weight average molar masses (*Mn* and *Mw*) of these products were not similar in nature to those of the distillate products, suggesting that the compounds in the residue streams were very different and containing high carbon number chains.

3.3. Molar mass distribution of the products obtained using centrifugal reactive–molecular distillation

The SEC chromatograms obtained are important to define the change in UV signal against molecular size in relation to molar mass. Each SEC chromatogram (Figures 5 – 6) was shown as a unique profile, depending mainly on the evaporator temperature (*EVT*) and the percentage weight of catalyst (% wt catalyst). The molar mass distribution data obtained by SEC for the distillate and residue streams generated by the CRMD process can be seen in Table 2.

The molar mass distribution range for all the distillate streams was characterized by the non–polar asphaltenes materials. The experimental data showed that the non–polar asphaltenes corresponded to relatively small molecules with values for M_w between 210 kg·kmol⁻¹ and 245 kg·kmol⁻¹ with 1% wt of catalyst, between 206 kg·kmol⁻¹ and 244 kg·kmol⁻¹ at 3% wt of catalyst, and between 215 kg·kmol⁻¹ and 243 kg·kmol⁻¹ at 5% wt of catalyst. The number molar mass averages (M_n) can be seen in Table 2.

Table 2. Molar mass distribution of the distillate and residue streams obtained from ATR–W using the CRMD process under different operating conditions.

Catalyst (%wt)	EVT (K)	Distillate streams from CRMD				Residue streams from CRMD			
		Sample	M_n (kg·kmol ⁻¹)	M_w (kg·kmol ⁻¹)	PDI	Sample	M_n (kg·kmol ⁻¹)	M_w (kg·kmol ⁻¹)	PDI
ATR–W*	-	-	1017	2956	2.91	-	1017	2956	2.91
1	473.15	D1–1%	181	210	1.16	R1–1%	367	2554	6.96
	483.15	D2–1%	188	218	1.16	R2–1%	373	2555	6.85
	498.15	D3–1%	191	225	1.18	R3–1%	313	2635	8.42
	503.15	D4–1%	193	230	1.19	R4–1%	274	2642	9.64
	523.15	D5–1%	200	245	1.23	R5–1%	284	2753	9.69
3	473.15	D1–3%	177	206	1.16	R1–3%	349	2570	7.36
	483.15	D2–3%	182	213	1.17	R2–3%	428	2712	6.34
	498.15	D3 ₁ –3%	188	226	1.20	R3 ₁ –3%	406	2714	6.68
	498.15	D3 ₂ –3%	193	233	1.21	R3 ₂ –3%	405	2786	6.88
	498.15	D3 ₃ –3%	191	225	1.18	R3 ₃ –3%	405	2880	7.11
	503.15	D4–3%	191	229	1.20	R4–3%	481	2764	5.75
	523.15	D5–3%	200	244	1.22	R5–3%	370	2908	7.86
5	473.15	D1–5%	170	215	1.26	R1–5%	356	2764	7.76
	483.15	D2–5%	185	222	1.20	R2–5%	379	2750	7.26
	498.15	D3–5%	183	230	1.26	R3–5%	242	2601	10.75
	503.15	D4–5%	183	234	1.28	R4–5%	385	2762	7.17
	523.15	D5–5%	198	243	1.23	R5–5%	563	2806	4.98

*: ATR–W before processing by the CRMD process; *EVT*: Evaporator temperature; M_n : Number average molar mass; M_w : Weight average molar mass and PDI: Polydispersity Index (M_w/M_n).

The SEC chromatograms indicated that the distillate streams obtained from CRMD eluted later than the distillate streams obtained from CMD, indicating that these samples consisted of compounds with lower molar masses, which decreased as the sample elution proceeded. Furthermore, with respect to the CRMD process, it can be seen that the maximum chromatography peak moved from a high elution volume (19.087 mL) to a low elution volume

(18.156 mL) due to the removal and breakage of heavier molecules into lighter molecules, as compared to the distillate streams obtained from the CMD process. Thus, the decrease in molar mass may be ascribed to the removal of more and higher molar mass compounds.

Interestingly, the distillate streams from CRMD were found to show a range of PDI values from 1.16 to 1.28, higher than those shown by the distillate streams obtained from CDM, which means greater differences between the minimum and maximum values for the molar masses in the former, presenting a wider variation in molar mass of the constituent molecules in the distillate streams obtained from the CRMD process as compared to those obtained from the CDM process. On the other hand, Figures 6a – 6c compare the SEC chromatograms of the fractionated residue streams obtained from CRMD with 1, 3 and 5% wt of catalyst, acquired using THF as the eluent with a GPC/SEC Phenolgel column and detection by UV-absorbance at 340 nm. The sets of chromatograms excluded one peak from the samples, whose signal was found to be from a high molar mass compound ($>12000 \text{ kg}\cdot\text{kmol}^{-1}$) present in the samples. This peak was due to the presence of asphaltene-materials as described in the next section.

The molar mass range for all the residue streams was defined by the asphaltene and non-asphaltene materials. The experimental data showed that the values for M_w ranged from $2554 \text{ kg}\cdot\text{kmol}^{-1}$ to $2753 \text{ kg}\cdot\text{kmol}^{-1}$ with 1% wt of catalyst, from $2570 \text{ kg}\cdot\text{kmol}^{-1}$ to $2908 \text{ kg}\cdot\text{kmol}^{-1}$ with 3% wt of catalyst and from $2750 \text{ kg}\cdot\text{kmol}^{-1}$ to $2806 \text{ kg}\cdot\text{kmol}^{-1}$ with 5% wt of catalyst. The number average molar mass values are shown in Table 2.

Furthermore, the average weight molar mass (M_w) data were compared with that of the initial ATR-W sample (before processing by CRMD). The results showed that the complex organic molecules were broken down into simpler molecules by breaking the carbon-carbon bonds in the precursors, since the values for M_w were lower than those of the ATR-W (M_w equal to $2956 \text{ kg}\cdot\text{kmol}^{-1}$) and of the residue streams obtained from the CMD processes, as presented in Table 2. Thus, on the basis of these results, it is reasonable to assume that the input variables, the evaporator temperature (EVT) and the weight percent of catalyst (% wt catalyst), had a great influence on the CRMD process from the point of view of the molar mass distribution.

3.4. Fractionation of the asphaltene compounds

Asphaltenes were isolated from the ATR-W obtained by the atmospheric distillation of a crude oil (W). Figure 7 shows a representative SEC chromatogram of the isolated asphaltene,

carried out using the above described series of GPC/SEC Phenolgel analytical columns. The elution volume corresponding to the maximum detector response was around 12.024 mL, and the average weight molar mass (M_w) of the asphaltene material isolated was 12,274 kg·kmol⁻¹.

On the basis of the SEC analysis of the asphaltene isolated from the ATR–W, the residue streams obtained from the CMD and CRMD processes (Figures 4 and 6) and the initial ATR–W sample were fractionated into two corresponding peaks, eluted using THF as the mobile phase, as shown in the SEC chromatograms in Figures 4 and 6.

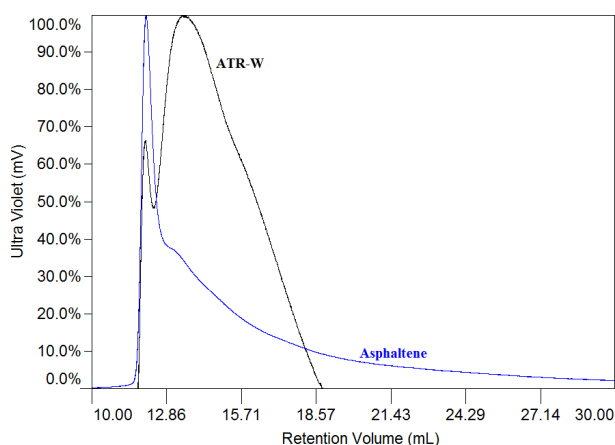


Figure 7: Area normalized SEC chromatogram of the asphaltene isolated from the ATR–W sample.

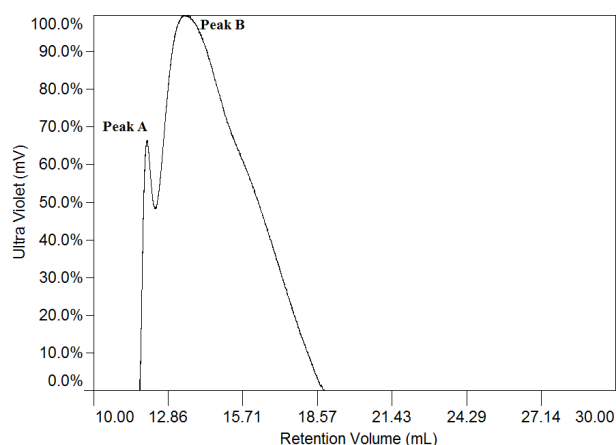


Figure 8: SEC chromatogram of the ATR–W before processing by the CMD and CRMD processes. Peak A: asphaltene material; Peak B: non-asphaltene material.

An analysis of the ATR–W sample shows that a clear fractionation of the asphaltene compound being a composite of the peaks A and B, defined, respectively, as asphaltene and non-asphaltene materials, as shown in the SEC chromatogram (Figure 8). The first peak at a retention volume (V_p) of around 12.024 mL, corresponding to a value for M_w of 12,274 kg·kmol⁻¹. The second peak at a V_p of around 13.000 mL, corresponded to an M_w of 1624 kg·kmol⁻¹ (Table 3). Analogous chromatograms were depicted for the residue streams obtained by the CMD and CRMD processes (Figures 4 and 6, respectively).

Therefore, size exclusion chromatography provided a suitable technique for the quantitative and qualitative analyses of the asphaltene content, comparing the initial ATR–W sample with the residue streams: 15 fractions obtained from the CRMD and 11 fractions obtained from the CMD processes. The experimental data showed that the non-asphaltene material corresponded to relatively small molecules with M_w values of approximately 1,700 kg·kmol⁻¹

(Table 3), which constituted the largest fraction of the residue stream, usually between 89 and 92% by weight.

On the other hand, the Mw values of the asphaltene material varied between 10,955 and 12,050 $\text{kg}\cdot\text{kmol}^{-1}$ in the residue streams obtained from the CMD process; and between 11,638 and 11,882 $\text{kg}\cdot\text{kmol}^{-1}$ in the CRMD process, depending on the weight percent of catalyst used. The asphaltenes constituted between 8 and 11 % by weight of the residue stream (Table 3). It is clear that the fractionation of the residue streams into asphaltene and non-asphaltene compounds must be used as a parameter to assess the effectiveness of the CRMD process as compared with the CMD process and with the asphaltene composition of the initial ATR-W (raw material), since it varies with the evaporator temperature, feed flow rate (in the CMD process) and the percentage weight of catalyst (in the CRMD process).

Table 3: Amount of asphaltene sub-fractions present in the initial ATR-W sample and in the residue streams obtained using the CMD and CRMD processes.

% wt cat	EVT (K)	Q ($\text{kg}\cdot\text{h}^{-1}$)	Sample	Asphaltene peak			Non-Asphaltene peak			%A
				V_p (mL)	Mn ($\text{kg}\cdot\text{kmol}^{-1}$)	Mw ($\text{kg}\cdot\text{kmol}^{-1}$)	V_p (mL)	Mn ($\text{kg}\cdot\text{kmol}^{-1}$)	Mw ($\text{kg}\cdot\text{kmol}^{-1}$)	
-	-	-	ATR-W*	12.024	12,467	12,274	13.414	949	2,190	9.15
0	423.15	2.945	R1	12.070	11,473	11,934	13.475	344	1,624	8.21
	449.15	1.914	R2	12.075	11,293	11,753	13.550	1905	1,694	8.39
	449.15	3.976	R3	12.068	11,606	12,050	13.538	414	1,673	8.05
	513.15	1.473	R4	12.066	11,356	11,835	13.54	384	1,869	10.44
	513.15	2.945	R5	12.143	10,498	10,921	13.617	241	1,710	9.53
	513.15	2.945	R6	12.068	11,349	11,831	13.552	256	1,795	10.07
	513.15	2.945	R7	12.140	10,551	10,971	13.704	291	1,690	9.26
	513.15	4.418	R8	12.150	10,558	10,955	13.664	393	1,704	8.82
	576.15	1.914	R9	12.138	10,608	11,022	13.524	608	1,899	10.80
	576.15	3.976	R10	12.066	11,357	11,834	13.47	347	1,851	10.43
	603.15	2.945	R11	12.066	11,294	11,780	13.508	1285	1,973	11.54
1	473.15	1.473	R1-1%	12.080	11,317	11,780	13.652	333	1,632	8.57
	483.15		R2-1%	12.066	11,278	11,768	13.442	338	1,662	9.49
	498.15		R3-1%	12.073	11,331	11,798	13.463	278	1,676	9.23
	503.15		R4-1%	12.082	11,227	11,692	13.459	248	1,681	9.66
	523.15		R5-1%	12.080	11,237	11,702	13.466	263	1,740	9.89
3	473.15	1.473	R1-3%	12.063	11,407	11,879	13.468	320	1,623	8.93
	483.15		R2-3%	12.068	11,410	11,882	13.414	389	1,689	9.56
	498.15		R3-3%	12.068	11,359	11,831	13.498	370	1,721	9.50
	503.15		R4-3%	12.054	11,310	11,831	13.377	427	1,726	9.80
	523.15		R5-3%	12.082	11,298	11,748	13.503	340	1,727	10.26
5	473.15	1.473	R1-5%	12.073	11,267	11,748	13.461	324	1,593	9.11
	483.15		R2-5%	12.061	11,367	11,871	13.379	347	1,680	10.03
	498.15		R3-5%	12.075	11,223	11,702	13.505	215	1,619	9.40
	503.15		R4-5%	12.087	11,336	11,782	13.300	356	1,692	10.32
	523.15		R5-5%	12.075	11,146	11,638	13.435	506	1,744	10.57

*: ATR-W before processing by the CMD and CRMD processes; % wt cat: Percentage weight of catalyst; EVT: Evaporator temperature; Q: Feed flow rate; V_p : Retention volume; Mn : Number average molar mass; Mw : Weight average molar mass and % A: percentage weight of asphaltene in the residue streams obtained by the CMD and CRMD processes.

4. Conclusions

The SEC method developed presented a great potential for the characterization of the distillate and residue streams obtained from the CMD and CRMD processes. The simplicity and accuracy of this technique make it suitable for the colloidal characterization by way of the parameters of molar mass distribution and asphaltene content.

A significant reduction in molar mass was found in the distillate and residue streams obtained from the CRMD process as compared to the products obtained from the CMD process and that of the initial ATR–W sample before processing. The average weight molar masses (M_w) of the distillate streams from the CRMD process were found to be between $210 \text{ kg}\cdot\text{kmol}^{-1}$ and $245 \text{ kg}\cdot\text{kmol}^{-1}$ with 1% by weight of catalyst, between $206 \text{ kg}\cdot\text{kmol}^{-1}$ and $244 \text{ kg}\cdot\text{kmol}^{-1}$ with 3% wt of catalyst and between $215 \text{ kg}\cdot\text{kmol}^{-1}$ and $243 \text{ kg}\cdot\text{kmol}^{-1}$ with 5% wt of catalyst, as compared with a M_w range between $192 \text{ kg}\cdot\text{kmol}^{-1}$ and $337 \text{ kg}\cdot\text{kmol}^{-1}$ in the distillate stream from the CMD process. On the other hand, the M_w values for the residue streams obtained from the CRMD process ranged from 2554 to $2753 \text{ kg}\cdot\text{kmol}^{-1}$ with 1% wt of catalyst, from 2570 to $2908 \text{ kg}\cdot\text{kmol}^{-1}$ with 3% wt of catalyst and from 2750 to $2806 \text{ kg}\cdot\text{kmol}^{-1}$ with 5% wt of catalyst. These data were compared with the results determined for the residue streams obtained by the CMD process, which ranged between $2931 \text{ kg}\cdot\text{kmol}^{-1}$ and $3146 \text{ kg}\cdot\text{kmol}^{-1}$. The higher polydispersity for the distillate and residue streams indicated a broader range of compounds of low and high carbon numbers, respectively.

The SEC chromatograms showed that the residue streams from the CRMD and CMD processes contain asphaltene compounds, $<10.57\%$ by weight for the CRMD process and $<11.54\%$ by weight for the CMD process. However, the asphaltene sub-fraction in the CRMD process was lower than that in the CMD process, which constitutes an indication of the cracking of higher molecules into lighter molecules.

Acknowledgements

This research was supported by the Brazilian National Council for Technological and Scientific Development (CNPq), the Petrobras Research and Development Center (PETROBRAS/CENPES) and the Brazilian Study and Project Financing Institution (FINEP).

References

- Ahmaruzzaman M., Sharma D. K. (2006) Characterization of liquids products obtained from cocracking of petroleum vacuum residue with plastics, *Energy & Fuels* **20**, 6, 2498–2503.
- Al-Muhareb E. M., Karaca F., Morgan T. J., Herod A. A., Bull I. D., Kandiyoti R. (2006) Size exclusion chromatography for the unambiguous detection of aliphatics in fractions from petroleum vacuum residues, coal liquids, and standard materials, in the presence of aromatics, *Energy & Fuels* **20**, 3, 1165–1174.
- Al-Muhareb E., Morgan T. J., Herod A. A., Kandiyoti R. (2007) Characterization of petroleum asphaltenes by size exclusion chromatography, UV–fluorescence and mass spectrometry. *Petroleum Science and Technology* **25**, 1–2, 81–91.
- American Society for Testing Material, ASTM D 2892. Standard test method for distillation of crude petroleum (15–Theoretical plate column). West Conshohoken, (Pennsylvania): ASTM International, 2005. 32p.
- American Society for Testing Materials, ASTM D 6560. Standard test method for determination of asphaltenes (heptanes insolubles) in crude petroleum and petroleum products. West Conshohoken, (Pennsylvania): ASTM International, 2000. 5p, [Reapproved 2005].
- Bartle K. D., Mulligan M. J., Taylor N., Martin T. G., Snape C. E. (1984) Molecular mass calibration in size–exclusion chromatography of coal derivatives, *Fuel* **63**, 11, 1556–1560.
- Batistella C. B., Maciel M. R. W. (1996) Modeling, simulation and analysis of molecular distillators: Centrifugal and falling film, *Computers & Chemical Engineering* **20**, supplement 1, S19–S24.
- Batistella C. B., Wolf–Maciel M. R. (1998) Recovery of carotenoids from palm oil by molecular distillation, *Computers & Chemical Engineering* **22**, supplement 1, S53–S60.
- Batistella C. B., Maciel M. R. W., Maciel Filho R. (2000) Rigorous modeling and simulation of molecular distillators: Development of a simulator under conditions of non ideality of the vapor phase, *Computers & Chemical Engineering* **24**, 2, 1309–1315.
- Berrueco C., Venditti S., Morgan T. J., Álvarez P., Millan M., Herod A. A., Kandiyoti R. (2008), Calibration os size–exclusion chromatography columns with 1–Methyl–2–pyrrolidinone

- (NMP)/Chloroform mixtures as eluent: Applications to petroleum-derived samples, *Energy & Fuels* **22**, 5, 3265–3274.
- Bockrath B. C., Schroeder K. T., Steffgen W. F. (1979) Characterization of asphaltenes isolated from a coal-derived liquid, *Analytical Chemistry* **51**, 8, 1168–1172.
- Champagne P. J., Manolakis E., Ternan M. (1985) Molecular weight distribution of Athabasca bitumen, *Fuel* **64**, 3, 423–425.
- Evans N., Haley T. M., Mulligan M. J., Thomas K. M. (1986) An investigation of the use of size exclusion chromatography for the determination of molar mass distributions and fractionation of coal tars, *Fuel* **65**, 5, 694–703.
- Gordillo C. A., Macias C. M., Sbaite P., Claudete B. H., Koroishi E. T., Maciel-Filho R. (2010). Caracterização de asfaltenos obtidos a partir de frações ultrapesadas de petróleo por meio de GPC e DLS. *Rio Oil & Gas Expo and Conference 2010*, (IBP2668_10-1–IBP2668_10-7). Rio de Janeiro, Brazil.
- Im K., Park H. -W., Lee S., Chang T. (2009), Two-dimensional liquid chromatography analysis of synthetic polymers using fast size exclusion chromatography at high column temperature, *Journal of Chromatography A* **1216**, 21, 4606–4610.
- Karaca F., Morgan T. J., George A., Bull I. D., Herod A. A., Millan M., Kandiyot R. (2009) Molecular mass ranges of coal tar pitch fractions by mass spectrometry and size-exclusion chromatography, *Rapid Communications in Mass Spectrometry* **23**, 13, 2097–2098.
- Liñan L. Z., Lopes M. S., Wolf Maciel M. R., Lima N. M. N., Maciel Filho R., Embiruçu M., Medina L. C. (2010) Molecular distillation of petroleum residues and physical-chemical characterization of distillate cuts obtained in the process, *Journal of Chemical Engineering Data*, **55**, 9, 3068–3076.
- Merdrignac I., Espinat D. (2007) Physicochemical characterization of petroleum fractions: The state of the art, *Oil & Gas Science and Technology* **62**, 1, 7–32.
- Meunier D. M. In: Chapter 46: Molecular Weight determinations. Settle, F.A. Editor, Handbook of Instrumental Techniques For Analytical Chemistry Prentice Hall PTR, Upper Saddle River, NJ (1997).

- Morgan T. J., George A., Alvarez-Rodriguez P., Millan M., Herod A. A., and Kandiyoti, R. (2010) Estimating molecular masses of petroleum-derived fractions: High mass (>2000 u) materials in maltenes and asphaltenes from Maya crude oil, *Journal of Chromatography A* **1217**, 24, 3804–3818.
- Myers–Vacuum, 2010. Available in: < <http://www.myers-vacuum.com/index.shtml> >. Accessed in: November 10th. 2010.
- Paul–Dauphin S., Karaca F., Morgan T. J., Millan–Agorio M., Herod A. A., Kandiyoti R. (2007) Probing size exclusion mechanisms of complex hydrocarbon mixtures: The effect of altering eluent compositions, *Energy & Fuels* **21**, 6, 3484–3489.
- Philip C. V., Anthony R. G. (1982) Separation of coal-derived liquids by gel permeation chromatography, *Fuel* **61**, 4, 357–363.
- Sato S., Takanohashi T. (2005) Molecular weight calibration of asphaltenes using gel permeation chromatography/mass spectrometry, *Energy & Fuels* **19**, 5, 1991–1994.
- Sbaite P., Batistella C. B., Winter A., Vasconcelos C. J., Wolf–Maciel M. R., Maciel–Filho R., Gomes A., Medina L., Kunert R. (2006) True boiling point extended curve of vacuum residue through molecular distillation, *Petroleum Science Technology* **24**, 3–4, 265–274.
- Šimeková M., Berek D. (2005) Studies on high–performance size–exclusion chromatography of synthetic polymers: I. Volume of silica gel column packing pores reduced by retained macromolecules, *Journal of Chromatography A* **1084**, 1–2, 167–172.
- Stubington J. F., Sergeant G. D., Barrett D., Do P. T. D. H., Raval K. A. (1995) Molecular weight determination in the study of the lubricating oil potential of shale oils, *Fuel* **74**, 1, 79–82.
- Tovar, Laura Plazas. Modeling and simulation of the centrifugal reactive molecular distillation: Development, assessment and application to upgrade high–boiling–point petroleum fractions. 2012, 442p. Ph. D. Thesis (Doctorate of Chemical Engineering) – School of Chemical Engineering, State University of Campinas, Campinas, 2012.
- Tovar L. P., Wolf Maciel M. R., Araujo A. S., Maciel Filho R., Batistella C. B., Medina L. C. (2011) Kinetic study on catalytic cracking of Brazilian high–boiling–point petroleum fractions. *Journal Thermal Analysis and Calorimetry*; doi: 10.1007/s10973–011–2068–6.

- Winter, Alessandra. Development of reactive molecular distillation technology : design and construction of the unit. 2011, 166p. Ph. D. Thesis (Doctorate of Chemical Engineering) – School of Chemical Engineering, State University of Campinas, Campinas, 2011.
- Zengin H., Spencer H. G., Zenguin G., Gregory R. V. (2007) Studies of solution properties of polyaniline by membrane osmometry, *Synthetic Metals* **157**, 2–3, 147–154.
- Zuñiga-Liñan L., Nascimento-Lima N. M., Manenti F., Wolf-Maciel M. R., Maciel Filho R., Medina L. C. (2011) Experimental campaign, modeling, and sensitivity analysis for the molecular distillation of petroleum residues 673.15 K+, *Chemical Engineering Research and Design* doi:10.1016/j.cherd.2011.07.001.

9.3. Considerações finais

Neste capítulo foram apresentados os resultados da caracterização físico-química realizadas nos produtos obtidos do processo de destilação molecular centrífuga reativa do resíduo atmosférico ATR–W 673.15 K⁺. Esta caracterização foi comparada com os dados obtidos para a amostra inicial e os produtos obtidos do processo não catalítico (destilação molecular centrífuga apresentada no Capítulo 6).

A caracterização compreendeu as seguintes análises:

- Fracionamento preparativo: Análises de destilação simulada foram realizadas para avaliar a conversão dos produtos.
- Físico-química: Foram realizadas análises reológicas avaliando a faixa do comportamento newtoniano e determinação da massa específica e grau API para as correntes de destilado e resíduo.
- Caracterização coloidal: Determinação da distribuição de massa molar pela técnica de cromatografia de permeação em gel (GPC), tanto para os cortes de destilado, como para os resíduos.

Logo, o processo em estudo apresentou uma tecnologia de *upgrading* para óleo cru pesado e frações pesadas de petróleo provenientes da destilação atmosférica e a vácuo dado que: (i) foi reportado a redução da faixa de temperatura em que os produtos do processo evidenciaram um comportamento newtoniano, (ii) a diminuição considerável na massa específica dos destilados e leve diminuição nos valores de massa específica dos resíduos incluindo os efeitos significativos da quantidade de catalisador (3 e 5 % em massa), (iii) o leve aumento do grau API (e por tanto a diminuição da densidade) das amostras coletadas no resíduo quando comparados com os valores obtidos para os resíduos provenientes do processo não-catalítico (destilação molecular centrífuga) e com a amostra inicial (alimentação) e (iv) a redução significativa na massa molar encontrada nos destilados e nos resíduos obtidos pelo processo de destilação molecular centrífuga reativa quando comparado com os produtos obtidos com processo não-catalítico e a amostra inicial.

Capítulo 10.

Conclusões e sugestões

10.1. Conclusões

As conclusões específicas sobre os conteúdos característicos de cada capítulo foram descritas ao final de cada um deles e no desenvolvimento do mesmo (manuscrito(s) a ser submetido(s), aceito e/ou apresentado(s)). Consequentemente, a seguir apresentam-se as conclusões gerais inerentes aos desenvolvimentos descritos neste relatório.

Foram desenvolvidas duas abordagens para a caracterização de frações pesadas baseadas nos conceitos de pseudocomponente e da termodinâmica contínua através de uma modelagem computacional na linguagem FORTRAN, visando seu acoplamento na modelagem matemática e a simulação do processo de destilação molecular reativa. A implementação computacional para a caracterização de frações de petróleo apresentou um resultado bastante condizente com o esperado, tendo inclusive boa predição com um desvio médio menor do que 10%.

Nos capítulos subsequentes foi apresentada uma profunda revisão de conceitos inerentes ao processo de destilação molecular. Portanto, foi realizada uma descrição teórica do processo de destilação molecular baseada nas variáveis que descrevem a fase vapor tais como: o livre percurso médio, o número de *Knudsen* e a taxa de evaporação efetiva, envolvendo as condições operacionais da destilação molecular (temperatura do evaporador e pressão do sistema). A simulação numérica destes parâmetros mostrou que as principais características da destilação molecular estão relacionadas com a distância entre as superfícies do evaporador e do condensador e a pressão do sistema. A última inferência está relacionada com o número de *Knudsen* ($0,01 < Kn < 3$), e os resultados das simulações demonstraram que para distâncias entre o evaporador e o condensador de 0,08 m e 0,05 m, se estabelece um padrão de fluxo similar ao fluxo molecular característico desse processo.

Utilizando a fluidodinâmica computacional (do inglês *computational fluid dynamics* – CFD), foi realizada a caracterização em termos do regime de fluxo e das condições operacionais do processo. Foi analisado o escoamento do filme de líquido que se encontrava distribuído

uniformemente na parede interna da superfície de evaporador de acordo com o processo de destilação molecular centrífuga. As equações do modelo foram resolvidas no software comercial ANSYS CFX (de Ansys Inc., EUROPE). Para isso, considerações foram baseadas nas equações de continuidade, de Navier–Stokes e equações de modelos de turbulência (k – ϵ e *Shear Stress Transport* k – ω). No entanto, pequenas diferenças entre os resultados obtidos com modelos de turbulência e laminar foram encontrados. Assim, o modelo de fluxo laminar é aceitável para a modelagem do processo de destilação molecular centrífugo.

Dando continuidade ao desenvolvimento da tese, foi desenvolvida uma ferramenta computacional para auxiliar na modelagem e simulação do processo de destilação molecular centrífugo. O modelo desenvolvido foi baseado na contribuição feita por Inuzuka et al. (1986), Inuzuka et al. (1989) e Bruin (1969). No desenvolvimento da modelagem foi considerada a taxa de evaporação efetiva descrita pela equação modificada de *Langmuir–Knudsen* no trabalho de Kawala e Dakiniewicz (2002).

Com os resultados da simulação do processo, apresentou-se que as variáveis de saída como a temperatura do filme na superfície do evaporador, a taxa de vaporização efetiva, a taxa de destilado e a espessura do filme, foram fortemente influenciadas pela temperatura do evaporador (temperatura da destilação). Assim, constatou-se que existe uma diminuição da concentração de componentes voláteis no filme com o aumento da taxa de evaporação efetiva em direção radial (raio do evaporador) e, portanto, se tem uma diminuição na espessura do filme na mesma direção.

Uma vez definida a parte de modelagem sem reação, necessitou-se implementar uma modelagem que levasse em conta a reação de craqueamento. Assim, adaptou-se a modelagem do processo de destilação molecular centrífugo incluindo o termo cinético. Finalmente, equações de transferência de massa, energia, momento e a equação de difusão do componente i -th foram consideradas nesta modelagem. A taxa de evaporação avaliada para essa modelagem foi a efetiva de Langmuir, levando em consideração os efeitos da fase vapor e o grau de anisotropia do sistema. A equação da taxa de reação foi assumida como sendo de primeira ordem levando em conta o efeito do catalisador.

A calorimetria exploratória diferencial, técnica termoanalítica, do inglês DSC (*Differential scanning calorimetry*) foi usada com o objetivo de verificar as transições físico-químicas que acontecem no processo de craqueamento das frações de petróleo (resíduos

atmosféricos ATR–W e ATR–Z). Também foi estudado o efeito da adição de um catalisador nos parâmetros cinéticos (energia de ativação, fator pré-exponencial e ordem da reação).

Foram utilizados métodos para calcular os parâmetros cinéticos a partir da análise dos dados obtidos com a técnica termoanalítica, a calorimetria exploratória diferencial (DSC). O estudo mostrou que as taxas de craqueamento das frações pesadas foram dependentes da temperatura entre 693,15 e 723,15 K, identificando uma região endotérmica. O método de Kissinger e o método de Arrhenius foram aplicados para calcular os parâmetros cinéticos. Estes parâmetros foram determinados a partir da inclinação e interceptação da equação de regressão linear. Os métodos de Arrhenius e Kissinger permitiram a determinação simultânea de energia de ativação, o fator pré-exponencial considerando uma ordem de reação $n=1$. Portanto, conclui-se que a reação de craqueamento a ser incluída no termo cinético da modelagem reativa pode ser considerada como uma reação de primeira ordem (pseudo-reação de primeira ordem).

Neste estudo, o efeito da adição de catalisador (3, 5 e 10% m/m) nos parâmetros cinéticos também foi estudado. A adição de catalisador aumentou as taxas de reação e forneceu um outro mecanismo reacional, estabelecendo um decaimento exponencial da energia de ativação para a reação de craqueamento em todos os sistemas estudados.

A determinação de parâmetros cinéticos também foi avaliada utilizando a análise do efeito de compensação cinética, que se verificou pela existência linear entre o logaritmo do fator pré-exponencial e a energia de ativação. Considerando o fato de que os parâmetros cinéticos exibem efeitos de compensação, foi avaliada a dependência da energia de ativação com a conversão α , ($E = E(\alpha)$). Com isso, é de se esperar que os valores do logaritmo Neperiano do fator pré-exponencial ($\ln A$) se incremente devido ao incremento da energia de ativação (E). Este efeito resulta então na mudança dos parâmetros de Arrhenius, que é compensado pela mudança correspondente dos parâmetros de compensação (a^* e b^*).

Nesta fase do trabalho, também foi desenvolvida uma ferramenta computacional na linguagem FORTRAN no qual foram incorporadas a modelagem e a simulação do processo de destilação molecular centrífuga reativa. O modelo matemático esteve constituído por 11+18N equações diferenciais parciais e algébricas conformado por equações de balance de massa, energia, quantidade de movimento, equação de difusão e a taxa de evaporação efetiva de Langmuir (para representar o fenômeno de evaporação). A equação da taxa de reação foi

assumida como sendo de primeira ordem levando em conta o efeito do catalisador. O modelo matemático foi resolvido utilizando o método numérico chamado método das linhas. Portanto, permitiu-se determinar a influência das variáveis de entrada do processo como temperatura do evaporador, de alimentação, velocidade do rotor, temperatura de alimentação, temperatura do condensador e porcentagem de catalisador sob a taxa de destilado e o grau de conversão no destilado e no resíduo.

Análises e estudos estatísticos foram realizados com o objetivo de avaliar a influência das variáveis operacionais do processo de destilação molecular centrífuga reativa. Assim, foi realizada uma série de simulações projetadas num planejamento de *Placket Burman* – PB 16 e num planejamento fracionário de resolução IV (2_{IV}^{4-1}), com os que se conseguiram definiram as variáveis de maior influência (*EVT*, %*CAT*) nas variáveis respostas.

A simulação do processo de destilação molecular centrífuga reativa permitiu descrever o efeito da temperatura do evaporador e da porcentagem de catalisador. Dados simulados apresentaram a presença de gradientes de temperatura e concentração ao longo da distancia radial do evaporador. A taxa de destilado aumenta conforme a temperatura do evaporador aumenta. No entanto, o incremento na temperatura do evaporador causa a diminuição da taxa de evaporação efetiva como consequência da contínua e rápida transformação de compostos pesados em compostos mais leves aumentando a quantidade destes.

O processo em estudo foi avaliado em termos do grau de conversão da mistura reacional, determinada pela taxa global de craqueamento dos reagentes no filme de líquido escoando sobre a superfície do evaporador. Neste sentido, os pseudo-componentes “a” e “b” reagem e evaporam ao longo da superfície cônica do evaporador. Analisando os perfis dos componentes, conclui-se que a concentração do pseudo-componente “a” decresce gradualmente no filme de líquido destilante. Por outra parte, o pseudo-componente “b” reage e evapora em presença do catalisador e sua concentração se incrementa, estando presente em maior proporção na corrente de resíduo do processo. Portanto, os perfis dos pseudo-componentes “a” e “b” permanecem cambiando continuamente durante o processo de destilação molecular centrífuga reativa, constituindo as duas correntes principais: o destilado e o resíduo.

A influência do catalisador também foi analisada. Os resultados apresentaram que utilizando 3% em massa de catalisador, é possível atingir condições favoráveis para o processo de

destilação molecular reativa favorecendo-se a conversão da alimentação. Dados experimentais e simulados indicaram que as melhores condições, para atingir uma conversão entre 15.2% e 41.6% na corrente de resíduo e entre 58.4% e 84.9% na corrente de destilado do processo de destilação molecular centrífuga reativa são: uma temperatura de processo (temperatura do evaporador) entre 473,15 K e 483,15 K; 3% m/m de catalisador e $1,473 \text{ kg}\cdot\text{h}^{-1}$. Logo, o alto vácuo (entre 29 Pa e 50 Pa) e a presença do catalisador (entre 3 %m/m e 5% m/m de catalisador) aumenta a velocidade da reação de craqueamento, atuando como promotor de uma nova rota de reação com uma menor energia de ativação.

O desenvolvimento de um modelo validado utilizando a ferramenta computacional (DESTMOL-R) projetada para complementar o processo de destilação molecular centrífugo reativo, se realizou através da avaliação dos produtos convertidos obtidos no processo (os destilados e os resíduos) em diferentes condições operacionais. Assim, o método padronizado de análise por destilação simulada (ASTM D 7169, 2011) foi aplicada com sucesso para analisar a distribuição de pontos de ebulição equivalente da matéria-prima, bem como seus produtos de processamento de destilação reativa centrífuga molecular (destilados e resíduos) e o grau de conversão destes com respeito à carga inicial no processo.

As predições oriundas da simulação foram comparadas com os dados experimentais e indicaram um desvio relativo percentual médio menor do que 6,82%; 9,39% e 14,92% para a taxa global de destilado, conversão na corrente de destilado e conversão na corrente de resíduo, respectivamente, o que é valioso, considerando-se a complexidade do processo e da mistura sendo tratada. Assim, conclui-se que o modelo desenvolvido mostrou-se adequado para descrever os processos de reação – separação na destilação molecular reativa fornecendo orientação teórica para o desenvolvimento experimental e a futura otimização do processo.

O alcance do processo de destilação molecular centrífuga reativa foi confirmado com as posteriores caracterizações realizadas nos produtos obtidos. Assim, o processo em estudo apresenta uma rota de processamento efetiva para óleo cru pesado e frações pesadas de petróleo provenientes da destilação atmosférica e a vácuo dado que: (i) foi reportada a redução da faixa de temperatura em que os produtos do processo evidenciaram um comportamento newtoniano, (ii) a diminuição considerável na massa específica dos destilados e leve diminuição nos valores de massa específica dos resíduos incluindo os efeitos significativos da quantidade de catalisador (3 e

5 % em massa), (iii) o leve aumento do grau API (e por tanto a diminuição da massa específica) das amostras coletadas no resíduo quando comparados com os valores obtidos para os resíduos provenientes do processo não-catalítico (destilação molecular centrífuga) e com a amostra inicial (alimentação).

O método cromatográfico por exclusão de tamanho (com siglas em inglês SEC – *Size exclusion chromatography*) apresentou-se como de grande potencial para a caracterização dos destilados e dos resíduos obtidos dos processos catalíticos e não-catalíticos apresentados nesta tese. A simplicidade e precisão desta técnica o tornam adequado para a caracterização coloidal por meio dos parâmetros da distribuição de massa molar e teor de asfaltenos. Uma redução significativa na massa molar foi encontrada nos destilados e nos resíduos obtidos pelo processo de destilação molecular centrífuga reativa em relação aos produtos obtidos a partir do processo não-catalítico e da amostra inicial.

10.2. Sugestões para trabalhos futuros

As sugestões apresentadas para continuidade do trabalho estão descritas para o desenvolvimento teórico (modelagem e simulação) e experimental do processo de destilação molecular centrífuga reativa, como segue:

Desenvolvimento computacional

- Desenvolver a modelagem do processo de destilação molecular centrífuga reativa em catálise homogênea.
- Desenvolver a modelagem do processo de destilação molecular de filme descendente (em catálise homogênea e heterogênea).
- Definir um termo de reação mais robusto com o intuito de prever a conversão de diferentes frações.
- Avaliar e introduzir na modelagem o efeito da pressão residual na taxa de evaporação efetiva (G_E)

Desenvolvimento experimental

- Estudar o processo de destilação molecular em catálise homogênea e heterogênea, na configuração de filme descendente.

- Desenvolver outros resíduos pesados de petróleo com características diversas (composição, °API, propriedades reológicas).
- Estudar o processo de destilação molecular centrífuga reativa com adição de solventes (tetralina, decano, nafteno e metil nafteno) permitindo a desagregação dos asfaltenos e como consequência os resíduos de petróleo sofrerão alterações físico químicas. O desenvolvimento desse trabalho está sendo realizado pela Dr^a. Melina Savioli Lopes (Pós-doutoranda).

Projeto do equipamento

- Dispor de um mecanismo de alimentação direto sob a parte central da superfície do evaporador aproveitando o efeito da força gravidade.
- Modificar o controlador da pressão da bomba mecânica.
- Incluir um sistema de agitação com múltiplas turbinas de pás inclinadas no tanque de alimentação.

Capítulo 11.

Referências

- American Society for Testing Material, ASTM D 2892. Standard test method for distillation of crude petroleum (15–Theoretical plate column). West Conshohoken, (Pennsylvania): ASTM International, 2005. 32p.
- American Society for Testing Materials, ASTM D 4175. Standard terminology relating to petroleum, petroleum products, and lubricants. West Conshohoken, (Pennsylvania): ASTM International, 2009. 48p.
- American Society for Testing Materials, ASTM D 5236. Standard test method for distillation of heavy hydrocarbon mixtures (vacuum potstill method). West Conshohoken, (Pennsylvania): ASTM International, 2003. 18p, [Reapproved 2007].
- American Society for Testing Materials, ASTM D 6560. Standard test method for determination of asphaltenes (heptanes insolubles) in crude petroleum and petroleum products. West Conshohoken, (Pennsylvania): ASTM International, 2000. 5p, [Reapproved 2005].
- American Society for Testing Materials, ASTM D 7169. Standard test method for boiling point distribution of samples with residues such as crude oils and atmospheric and vacuum residues by high temperature gas chromatography. West Conshohoken, (Pennsylvania): ASTM International, 2005. 17p.
- ANP, 2011. Anuário estatístico brasileiro do petróleo, gás natural e biocombustíveis 2011, ANP, Rio de Janeiro, ISSN: 1983–5884, 231p (http://www.anp.gov.br/?pg=57890#Se__o_2 >. Acesso em 06/12/2011) ou (<http://www.anp.gov.br/?pg=36235&m=anuario&t1=&t2=anuario&t3=&t4=&ar=0&ps=1&cachebust=1288827791294>).
- Badin V., Cvengroš J. (1992) Model of temperature profiles during condensation in a film in a molecular evaporator, *The Chemical Engineering Journal* **49**, 3, 177–180.

- Barber R. W., Emerson D. R. (2002) The influence of Knudsen number on the hydrodynamic development length within parallel plate micro-channels. In: *Advances in Fluid Mechanics IV*, *Advances in fluid mechanics series* (p. 207–216). WIT Press, Southampton: UK
- Batistella, César Benedito. Modelagem e simulação de destiladores moleculares de filme descendente e centrífugo. 1996. 176p. Dissertação (Mestrado em Engenharia Química) – Faculdade de Engenharia Química, Universidade Estadual de Campinas, Campinas, 1996.
- Batistella C. B., Maciel M. R. W. (1996) Modeling, simulation and analysis of molecular distillators: Centrifugal and falling film, *Computers & Chemical Engineering* **20**, supplement 1, S19–S24.
- Batistella C. B., Wolf–Maciel M. R. (1998) Recovery of carotenoids from palm oil by molecular distillation, *Computers & Chemical Engineering* **22**, supplement 1, S53–S60.
- Batistella C. B., Maciel M. R. W., Maciel Filho R. (2000) Rigorous modeling and simulation of molecular distillators: Development of a simulator under conditions of non ideality of the vapor phase, *Computers & Chemical Engineering* **24**, 2, 1309–1315.
- Batistella C. B., Moraes E. B., Maciel Filho R., Wolf Maciel M. R. (2002) Molecular distillation: Rigorous modeling and simulation for recovering vitamin E from vegetal oils, *Applied Biochemistry and Biotechnology* **98–100**, 1–9, 1187–1206.
- Benito A. M., Martínez M. T., Fernández I., Miranda J. L. (1995). Visbreaking of an asphaltenic coal residue, *Fuel* **74**, 6, 922–927.
- Bozzano G., Dente M., Carlucci F. (2005) The effect of naphthenic components in the visbreaking modeling, *Computers & Chemical Engineering* **29**, 6, 1439–1446.
- Bruin S. (1969) Velocity distributions in a liquid film flowing over a rotating conical surface, *Chemical Engineering Science* **24**, 11, 1647–1654.
- Bueno, Aeronon Ferreira. Caracterização de petróleo por espectroscopia no infravermelho próximo. 2004, 122p. Dissertação (Mestrado em Química) – Instituto de Química, Universidade Estadual de Campinas, Campinas, 2004.
- Burrows G. (1973) Notes on some features of high–vacuum distillation, *Vacuum* **23**, 10, 353–358.

- Catalogo UIC GmbH, 2010. Disponível em:< <http://www.UIC-GmbH.de/>>. Acesso em: 10/12/2010.
- Coats K. H. (1985) Simulation of gas condensate reservoir performance, *Journal of Petroleum Technology* **37**, 10, 1870–1886.
- Cotterman R. L., Prausnitz J. M. (1985) Flash calculations for continuous or semicontinuous mixtures using an equation of state, *Industrial & Engineering Chemistry Process Design and Development* **24**, 2, 434–443.
- Cotterman R. L., Bender R., Prausnitz J. M. (1985) Phase equilibria for mixtures containing very many components. Development and application of continuous thermodynamics for chemical process design, *Industrial & Engineering Chemistry Process Design and Development* **24**, 1, 194–203.
- Cross W. T., Ramshaw C. (1986) Process intensification: laminar flow heat transfer, *Chemical Engineering Research and Design* **64**, 4, 293–301.
- Cvengroš J., Lutišan J., Micov M. (2000) Feed temperature influence on the efficiency of a molecular evaporator, *Chemical Engineering Journal* **78**, 1, 61–67.
- Danesh A. (1998). PVT and phase behavior of reservoir fluids. In: *Developments in Petroleum Science*. New York: Elsevier.
- Daubert T. E., Danner R. P., Sibul H. M., Stebbins C. C., Oscarson J.L., Zundel N., Marshall T.L., Adams M.E., Wilding W. V. (2000) *Physical and Thermodynamic Properties of Pure Chemicals: DIPPR: Data Compilation*. (10th ed.). Taylor and Francis.
- Dente M., Bozzano G., Bussani G. (1997) A comprehensive program for visbreaking simulation: product amounts and their properties prediction, *Computers & Chemical Engineering* **21**, 10, 1125–1134.
- Du P. C., Mansoori G. A. (1986) Phase equilibrium computational algorithms of continuous mixtures, *Fluid Phase Equilibria* **30**, n.d., 57–64.
- Eckert E., Vaněk T. (2005) New approach to the characterisation of petroleum mixtures used in the modelling of separation processes, *Computers & Chemical Engineering* **30**, 2, 343–356.

- Equipe Petrobras. Processos de refino. Adaptado do material original de Elie Abadie. Curitiba: Petrobras / Abastecimento UN's: Repar, Regap, Replan, Refap, RPBC, Recap, SIX, Revap, 2002.
- Erthal, Raul Henrique. Modelagem e simulação dinâmica de um conversor de craqueamento catalítico. 2003, 138p. Dissertação (Mestrado em Engenharia Mecânica e de Materiais) — Faculdade de Engenharia Mecânica e de Materiais, Centro Federal De Educação Tecnológica do Paraná, Curitiba, 2003.
- Fregolente L. V., Fregolente P. B. L., Chicuta A. M., Batistella C. B., Maciel-Filho R., Wolf-Maciel M. R. (2007) Effect of operating conditions on the concentration of monoglycerides using molecular distillation, *Chemical Engineering Research and Design* **85**, 11, 1524–1528.
- Fregolente L. V., Batistella C. B., Maciel-Filho R., Wolf-Maciel M. R. (2005) Response surface methodology applied to optimization of distilled monoglycerides production. *Journal of the American Oil Chemists' Society* **82**, 9, 673–678.
- Furimsky E. (2000), Characterization of cokes from fluid/flexi-coking of heavy feeds, *Fuel Processing Technology* **67**, 3, 205–230.
- Guimarães R. C.; Pinto, U. B. Curso de Caracterização e Análise de Petróleo. CENPES/PDP/TPAP – PETROBRAS, Rio de Janeiro, RJ, 2007. 99 p.
- Guo A., Zhang X., Wang Z. (2008) Simulated delayed coking characteristics of petroleum residues and fractions by thermogravimetry, *Fuel Processing Technology* **89**, 7, 643–650.
- Hernández, Julie Ballesteros. Estudo e caracterização de frações pesadas de petróleo btidas da destilação molecular e definição das propriedades físico-químicas para a modelagem deste processo. 2009, 154p. Dissertação (Mestrado em Engenharia Química) – Faculdade de Engenharia Química, Universidade Estadual de Campinas, Campinas, 2009.
- Hernández J. A. B, Liñan L. Z., Jardini A. L., Wolf-Maciel M. R., Maciel Filho R., Medina L. C. (2008) Determinação do calor específico de derivados ultrapesados de petróleo. Proceedings of Rio Oil & Gas Expo and Conference 2008, Rio Oil & Gas 2008, 15–18 Setember 2008, Riocentro, Rio de Janeiro, RJ–Brazil.
- Holló, J., Kurucz, E. E Boródi, A. The applications of molecular distillation. 210 Seiten, 36 Abb., 25 Tab. im Text, 9 Tab. im Anhang. Akadémiai Kiadó, Budapest, 1971.

- Hu S., Zhu F. X. X. (2001) A general framework for incorporating molecular modelling into overall refinery optimisation, *Applied Thermal Engineering* **21**, 13–14, 1331–1348.
- Inuzuka M., Sugiyama R., Saito I., Yamada I., Hiraoka S., Ishikawa H., Banno, I. (1986) Analysis of heat and mass transfer in a centrifugal molecular still, *Journal of Chemical Engineering of Japan* **19**, 1, 14–20.
- Inuzuka M., Ishikawa H., Yamada, I., Hiraoka S., Aragaki T., Inukai Y., Erciyes A. T., Kobayashi S. (1989) Vaporization from liquid film of binary mixture in a centrifugal molecular still, *Journal of Chemical Engineering of Japan* **22**, 3, 291–297.
- Kawala Z., Dakiniewicz P. (2002) Influence of evaporation space geometry on rate of distillation in high–vacuum evaporator, *Separation Science and Technology* **37**, 8, 1877–1895.
- Kehlen H., Rätzsch M. T., Bergmann J. (1985) Continuous thermodynamics of multicomponent systems, *AIChE Journal* **31**, 7, 1136–1148.
- Keil F. J. Modeling of process intensification, Wiley–VCH Verlag GmbH & Co. KGaA, Weinheim (2007).
- Langmuir I. (1913) The vapor pressure of metallic tungsten, *Physical Review* **2**, 5, 329–342.
- de Lima R. S., Schaeffer R. (2011) The energy efficiency of crude oil refining in Brazil: A Brazilian refinery plant case, *Energy* **36**, 5, 3101–3112.
- Lima N. M. N., Liñan L. Z., Manenti F., Maciel–Filho R., Wolf–Maciel M. R., Embiruçu M., Medina L. C. (2011) Fuzzy cognitive approach of a molecular distillation process, *Chemical Engineering Research and Design* **89**, 4, 471–479.
- Liñan L. Z., Lima N. M. N., Hernández J. A. B., Tovar L. P., Rocha R. S., Batistella C. B., Wolf–Maciel M. R., Maciel–Filho R., Medina L. C. (2007) Simulation of molecular distillation process. 1. Formulation of generalized correlation for predicting heavy liquid petroleum fractions properties of brazilian oil petroleum. Proceedings of The eighth International Conference on Chemical & Process Engineering, 8th ICheaP, 24–27 June 2007, Ischia Island, Gulf of Naples.
- Lopes, Melina Savioli. Caracterização das correntes do processo de destilação molecular aplicado a frações pesadas de petróleo e desenvolvimento de correlações da curva PEV. 2008, 85p.

- Dissertação (Mestrado em Engenharia Química) – Faculdade de Engenharia Química, Universidade Estadual de Campinas, Campinas, 2008.
- Lopes M. S., Winter A., Batistella C. B., Maciel-Filho R., Wolf-Maciel M. R., Medina L. C. (2007) Análise estatística das frações pesadas de petróleo processadas através da destilação molecular. Anais 4º Congresso Brasileiro de Pesquisa e Desenvolvimento em Petróleo e Gás, 4º PDPETRO, 21–24 de Outubro 2007, Campinas – SP, Brasil.
- Lutišan J., Cvengroš J. (1995) Effect of inert gas pressure on the molecular distillation process, *Separation Science and Technology* **30**, 17, 3375–3389.
- Lutišan J., Cvengroš J., Micov M. (2002) Heat and mass transfer in the evaporating film of a molecular evaporator, *Chemical Engineering Journal* **85**, 2–3, 225–234.
- Maciel-Filho R., Batistella C. B., Sbaite P., Winter A., Vasconelos C. J., Wolf-Maciel M. R., Gomes A., Medina L., Kunert R. (2006) Evaluation of atmospheric and vacuum residues using molecular distillation and optimization, *Petroleum Science and Technology* **24**, 3–4, 275–283.
- Maciel-Filho R., Lima-Silva N., Batistella C. B., Wolf-Maciel M. R., Winter A., Sbaite P., Medina L. (2006) Biodiesel production, lubricant fractionating and development of a new true boiling point curve through molecular distillation. Distillation & Absorption Symposium 2006, DA2006, 4–6 September 2006, London – UK / Ed. Eva Sorensen – ISBN 9780852955055, p. 142–151.
- Mansoori G. A., Du P. C., Antoniadis E. (1989) Equilibrium in multiphase polydisperse fluids, *International Journal of Thermophysics* **10**, 6, 1181–1204.
- Martins P. F., Batistella C. B., Maciel-Filho R., Wolf-Maciel M. R. (2006) Comparison of two different strategies for tocopherols enrichment using a molecular distillation process, *Industrial & Engineering Chemistry Research* **45**, 2, 753–758.
- Martins P. F., Ito V. M., Batistella C. B., Maciel M. R. W. (2006) Free fatty acids separation from vegetables oil deodorizer distillate using molecular distillation process, *Separation and Purification Technology* **48**, 1, 78–84.
- Martínez-Palou M. de L. M., Zapata-Rendón B., Mar-Juárez E. Bernal-Huicochea C., Clavel-López J. de la C., Aburto J. (2011) Transportation of heavy and extra-heavy crude oil by pipeline: A review, *Journal of Petroleum Science and Engineering* **75**, 3–4, 274–282.

- Medina L. C., Tovar L. P., Wolf Maciel M. R., Batistella C. B., Maciel Filho R. (2010) CFD-based analysis of the flow regime in the centrifugal molecular distillation of a petroleum atmospheric residue. Conference Proceedings; 2010 AIChE Annual Meeting, 10AIChE; Salt Lake City, UT; 7 November 2010 through 12 November 2010. ISBN/ISSN: 978-081691065-6.
- Merdrignac I., Espinat D. (2007) Physicochemical characterization of petroleum fractions: The state of the art, *Oil & Gas Science and Technology* **62**, 1, 7–32.
- Miquel J., Castells F. (1993) Easy characterization of petroleum fractions (part 1), *Hydrocarbon Processing* **72**, 12, 101–105.
- Miquel J., Castells F. (1994) Easy characterization of petroleum fractions (part 2), *Hydrocarbon Processing* **73**, 1, 99–103.
- Moraes E. B., Martins P. F., Batistella C. B., Alvarez M. E., Maciel-Filho R., Wolf-Maciel M. R. (2006) Molecular distillation: A powerful technology for obtaining tocopherols from soya sludge, *Applied Biochemistry and Biotechnology* **129–132**, 1–3, 1066–1076.
- Omole O., Olieh M. N., Osinowo, T. (1999) Thermal visbreaking of heavy oil from the Nigerian tar sand, *Fuel* **78**, 12, 1489–1496.
- Pagani, Adriana Siveiro. Estudo cinético do craqueamento catalítico de moléculas modelo de hidrocarbonetos em catalisadores de FCC. 2009, 170p. Tese (Doutorado em Engenharia Química) – Faculdade de Engenharia Química, Universidade Estadual de Campinas, Campinas, 2009.
- Parisotto, Graciele. Determinação do Número de Acidez Total em Resíduo de Destilação Atmosférica e de Vácuo do Petróleo Empregando a Espectroscopia no Infravermelho (ATR-FTIR) e Calibração Multivariada. 2007. 85p. Dissertação (Mestrado em Química), Departamento de Química – Universidade Federal de Santa Maria, Santa Maria, 2007.
- Peixoto, F., Platt, G., and Pessôa, F. (2000). Vapor-Liquid equilibria of multi-indexed continuous mixtures using an equation of state and group contributions methods. *Chemical Engineering Journal*, **77**, 3, 179–187.
- Quann R. J., Jaffe S. B. (1992) Structure-oriented lumping: Describing the chemistry of complex hydrocarbon mixtures, *Industrial & Engineering Chemistry Research* **31**, 11, 2483–2497.

- Rana M. S., Sámano V., Ancheyta J., Diaz J. A. I. (2007) A review of recent advances on process technologies for upgrading of heavy oils and residua, *Fuel* **86**, 9, 1216–1231.
- Rätzsch M. T., Kehlen H. (1983) Continuous thermodynamics of complex mixtures, *Fluid Phase Equilibria* **14**, n.d., 225–234.
- Riazi M. R. Characterization and properties of petroleum fractions. ASTM International Standards Worldwide, 2004. 407p.
- Riazi M. R. (1989) Distribution model for properties of hydrocarbon-plus fractions, *Industrial & Engineering Chemistry Research* **28**, 11, 1731–1735.
- Riazi M. R., Al-Sahhaf T. A. (1996) Physical properties of heavy petroleum fractions and crude oils, *Fluid Phase Equilibria* **117**, 1–2, 217–224.
- Ribeiro, Pleycienne Trajano. Modelagem e controle de unidades de craqueamento catalítico – FCC. 2007, 215p. Dissertação (Mestrado em Engenharia Química) – Faculdade de Engenharia Química, Universidade Estadual de Campinas, Campinas, 2007.
- Rocha E. R. L., Lopes M. S., Wolf-Maciel M. R., Maciel-Filho R., Batistella C. B., Medina L. C. (2011) Application of Molecular Distillation Process to Extend the True Boiling Point Curve of Petroleum Residues 400 °C⁺, *Journal of Chemistry and Chemical Engineering* **5**, n.a., 116–120.
- Rocha E. R. L., Wolf-Maciel M. R., Maciel-Filho R., Batistella C. B., Medina L. C. (2009a) Special molecular distillation prototype to characterization petroleum residue, *Chemical Engineering Transactions* **17**, n.a., 1603–1608.
- Rocha E. R. L., Wolf-Maciel M. R., Maciel-Filho R., Batistella C. B., Medina L. C. (2009b) Valoração de petróleo pesado utilizando destilador molecular nacional, *Petro & Química* **316**, n.a., 49–53.
- Rocha, Erica Roberta Lovo. Utilização de protótipo nacional de destilador molecular para caracterização de frações pesadas de petróleo. 2009, 101p. Dissertação (Mestrado em Engenharia Química) – Faculdade de Engenharia Química, Universidade Estadual de Campinas, Campinas, 2009.

- Rocha, Rodrigo Santos. Determinação experimental de correntes do processo de destilação molecular de resíduos de petróleo e extensão da curva PEV. 2008, 168p. Dissertação (Mestrado em Engenharia Química) – Faculdade de Engenharia Química, Universidade Estadual de Campinas, Campinas, 2008.
- Rocha R. S., Hernández J. A. B., Batistella C. B., Maciel-Filho R., Wolf-Maciel M. R., Medina L. C. (2007) Purificação de óleos lubrificantes especiais através do processo de destilação molecular. Anais do 4º Congresso Brasileiro de Pesquisa e Desenvolvimento em Petróleo e Gás, 4º PDPETRO, 21–24 de Outubro 2007, Campinas – SP, Brasil.
- Rocha R. S., Batistella C. B., Wolf-Maciel M. R., Maciel-Filho R., Medina L. C. (2008a) Extensão da curva de destilação de petróleos pesados através do processo de destilação molecular e da correlação FRAMOL. Anais do XVII Congresso Brasileiro de Engenharia Química 2008, COBEQ2008; 14–17 Setembro 2008, Recife, PE–Brazil.
- Rocha R. S., Batistella C. B., Wolf-Maciel M. R., Maciel-Filho R., Medina L. C. (2008b) Extensão da curva PEV de petróleos extrapesados por destilação molecular e ampliação da caracterização. Proceedings of Rio Oil & Gas Expo and Conference 2008, Rio Oil & Gas 2008, 15–18 September 2008, Riocentro, Rio de Janeiro, RJ–Brazil.
- Rodríguez-Reinoso F., Santana P., Romero-Palazon E., Diez M. –A., Marsh H. (1998) Delayed coking: Industrial and laboratory aspects, *Carbon* **36**, 1–2, 105–116.
- Sbaite P., Batistella C. B., Winter A., Vasconcelos C. J. G., Wolf-Maciel M. R., Maciel-Filho R., Gomes A., Medina L., Kunert R. (2006) True boiling point extended curve of vacuum residue through molecular distillation, *Petroleum Science Technology* **24**, 3–4, 265–274.
- Sbaite, Paula Santos Duarte. Extensão da curva do ponto de ebulição verdadeiro para petróleos pesados nacionais através do processo de destilação molecular. 2005, 187p. Tese (Doutorado em Engenharia Química) – Faculdade de Engenharia Química, Universidade Estadual de Campinas, Campinas, 2005.
- Sbaite P., Batistella C. B., Winter A., Wolf-Maciel M. R., Maciel-Filho R., Gomes A., Medina L. C., Kunert R., Pontes-Bittencourt C., Mathias-Leite L. F. (2005) Characterization of residue stream obtained through molecular distillation of heavy oil petroleum. Proceedings of

- The seventh International Conference on Chemical & Process Engineering, 7th ICheaP, 15–18 May 2005, Giardini Di Naxos, Taormina, Italy.
- Sbaite P., Vasconcelos C. J. G., Batistella C. B., Wolf–Maciel M. R., Maciel–Filho R., Medina L. C., Kunert R. (2003) Evaluation of some kinds of lubricants through molecular distillation and optimization. Proceedings of 53rd Canadian Chemical Engineering Conference, CSCHE 2003, 26–29 October 2003, Hamilton, Ontario – Canada.
- Silva, 2010. Disponível em: < <http://www.agais.com/simula.htm> >. Acesso em: 18/11/2010.
- Shibata S. K., Sandler S. I., Behrens R. A. (1987) Phase equilibrium calculations for continuous and semicontinuous mixtures, *Chemical Engineering Science* **42**, 8, 1977–1988.
- Souza M. J. B., Fernandes F. A. N., Pedrosa A. M. G., Araujo A. S. (2008) Selective cracking of natural gasoline over HZSM–5 zeolite, *Fuel Processing Technology* **89**, 9, 819–827.
- Souza, Marcelo José Bairros de. Beneficiamento da fração C5⁺ do pólo de Guamaré a partir de reações de craqueamento catalítico sobre zeólitas ácidas. 2001, 164p. Dissertação (Mestrado em Engenharia Química) – Faculdade de Engenharia Química, Universidade Federal do Rio Grande do Norte, Natal, 2001.
- Stankiewicz A., Moulijn J. A. Process intensification. (2002) *Industrial and Engineering Chemistry Research* **41**, 8, 1920–1924.
- Thomas J. E. (2004). *Fundamentos de engenharia de petróleo*. Editora Interciência 2 ed, Rio de Janeiro, RJ.
- Tovar, Laura Plazas. Modelagem e simulação do processo de destilação molecular centrífuga reativa: Desenvolvimento, Avaliação e Aplicação para o “Upgrading” de Frações Pesadas de Petróleo. 2012, 442p. Tese (Doutorado em Engenharia Química) – Faculdade de Engenharia Química, Universidade Estadual de Campinas, Campinas, 2012.
- Tovar L. P., Winter A., Wolf Maciel M. R., Batistella C. B., Maciel Filho R., Medina L. C. (2012) Reliable–based optimization using an experimental factorial design, response surface methodology and mathematical modeling of a centrifugal molecular distillation process to split heavy petroleum fractions. *Separation Science and Technology*; doi:10.1080/01496395.2011.644612.

- Tovar L. P., Wolf Maciel M. R., Araujo A. S., Maciel Filho R., Batistella C. B., Medina L. C. (2011) Kinetic study on catalytic cracking of Brazilian high-boiling-point petroleum fractions. *Journal Thermal Analysis and Calorimetry*; doi: 10.1007/s10973-011-2068-6.
- Tovar L. P., Wolf Maciel M. R., Maciel Filho R., Batistella C. B., Ariza O. C., Medina L. C. (2011) Overview and computational approach for studying the physicochemical characterization of high-boiling-point petroleum fractions (350 °C⁺). *Oil & Gas Science and Technology*; doi:10.2516/ogst/2011150.
- Tovar L. P., Pinto G. M. F., Wolf-Maciel M. R., Batistella C. B., Maciel-Filho R. (2011) Short-path-distillation process of lemongrass essential oil: Physicochemical characterization and assessment quality of the distillate and the residue products, *Industrial and Engineering Chemistry Research* **50**, 13, 8185–8194.
- Tovar L. P., Wolf-Maciel M. R., Ferreira-Pinto G. M., Maciel-Filho R., Gomes D. R. (2010) Factorial design applied to concentrate bioactive component of *cymbopogon citratus* essential oil using short path distillation, *Chemical Engineering Research and Design* **88**, 2, 239–244.
- Vakili-Nezhaad G. R., Modarress H., Mansoori G. A. (2001) Continuous thermodynamics of petroleum fluids fractions, *Chemical Engineering and Processing* **40**, 5, 431–435.
- Vieria, William Gonçalves. FCC: Controle preditivo e identificação via redes neurais. 2002, 201p. Tese (Doutorado em Engenharia Química) – Faculdade de Engenharia Química, Universidade Estadual de Campinas, Campinas, 2002.
- Whitson C. H. (1983) Characterizing hydrocarbon plus fractions, *SPE Journal* **23**, 4, 683–694.
- Winter, Alessandra. Caracterização de frações ultra pesadas de petróleo nacional por meio do processo de destilação molecular. 2007, 116p. Dissertação (Mestrado em Engenharia Química) – Faculdade de Engenharia Química, Universidade Estadual de Campinas, Campinas, 2007.
- Winter, Alessandra. Desenvolvimento de tecnologia de destilação molecular reativa: Projeto e construção da unidade. 2011, 166p. Tese (Doutorado em Engenharia Química) – Faculdade de Engenharia Química, Universidade Estadual de Campinas, Campinas, 2011.
- Winter A., Batistella C. B., Wolf-Maciel M. R., Maciel-Filho R., Medina L. C. (2009) A true boiling point curve through molecular distillation using Framol correlation. Proceedings of The

ninth International Conference on Chemical & Process Engineering, 9th ICheaP, 10–13 May 2009, Rome, Italy.

Winter A., Batistella C. B., Wolf–Maciel M. R., Maciel–Filho R., Lopes M. S., Medina L. C. (2007) A true boiling point curve through molecular distillation using Framol correlation. Proceedings of The eight International Conference on Chemical & Process Engineering, 8th ICheaP, 24–27 June 2007, Ischia Island, Gulf of Naples, Italy.

Winter A., Liñan L. Z., Batistella C. B., Wolf–Maciel M. R., Maciel–Filho R., Medina L. C. (2006) Split fraction of basic lubricant oils by falling film molecular distiller. Proceedings of The 17th International Congress of Chemical And Process Engineering, CHISA 2006, 27–31 August 2006, Prague, Czech Republic.

Winter A., Sbaite P., Batistella C. B., Maciel–Filho R., Wolf–Maciel M. R., Medina L. C., Gomes A., Kunert R., Mathias–Leite L. F., Pontes–Bittencourt C. (2004) Caracterização de correntes de resíduos pesados de petróleo obtidas pelo processo de destilação molecular. Anais do 3º Congresso Brasileiro de P&D em Petróleo e Gás, 3º PDPETRO, 2–5 de Outubro 2004, Salvador – BA, Brasil.

Zuñiga–Liñan, Lamia. Modelagem e simulação do processo de destilação molecular e determinação experimental aplicado a resíduos pesados de petróleo. 2009, 325p. Tese (Doutorado em Engenharia Química) – Faculdade de Engenharia Química, Universidade Estadual de Campinas, Campinas, 2009.

Zuñiga–Liñan L., Nascimento–Lima N. M., Manenti F., Wolf–Maciel M. R., Maciel Filho R., Medina L. C. (2011) Experimental campaign, modeling, and sensitivity analysis for the molecular distillation of petroleum residues 673.15 K⁺, *Chemical Engineering Research and Design* doi:10.1016/j.cherd.2011.07.001.

Zuñiga L. L., Lima N. M. N., Wolf–Maciel M. R., Maciel Filho R., Batistella C. B., Manca D., Manenti F., Medina L. C. (2009) Modeling and simulation of molecular distillation process for a heavy petroleum cut, *Chemical Engineering Transaction* **17**, n.a., 1639–1644.

Zuñiga L. L., Lima N. M. N., Batistella C. B., Wolf–Maciel M. R., Maciel Filho R., Medina L. C. (2009) Correlação para prever as massas moleculares de cortes pesados de petróleo, *Revista Petro & Química Maio*, n.a., 67–72.

